Amélioration des outils géochimiques pour l'investigation des paléoenvironnements

François Fourel

Université de Lyon

Ecole doctorale : Evolution, Ecosystèmes, Microbiologie, Modélisation

Thèse de doctorat
Sciences de l'Univers

François FOUREL

Amélioration des Outils Géochimiques pour l'Investigation des Paléoenvironnements.

Comment l'évolution des outils de mesure des isotopes stables permet de répondre à de nouvelles interrogations scientifiques

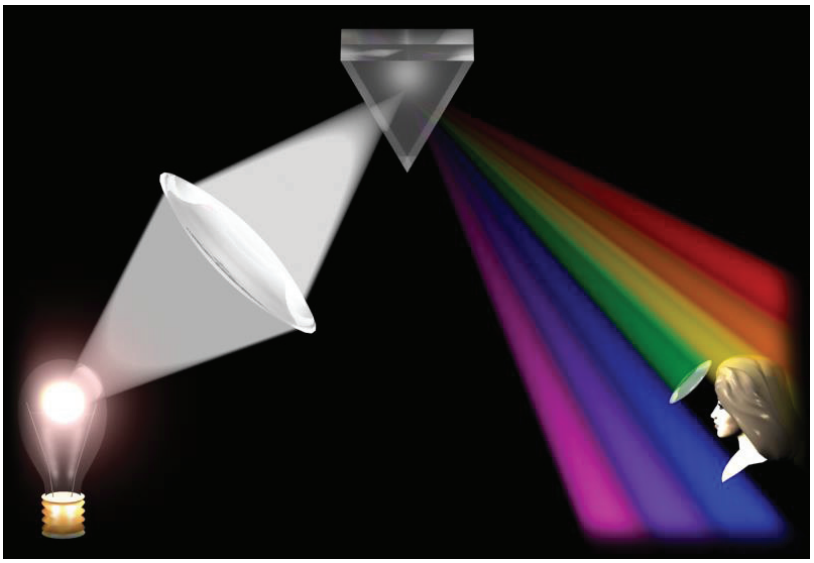

Thèse dirigée par : Christophe Lécuyer

Soutenue le 23 Octobre 2014

Jury :

M. Tony Fallick (Rapporteur)
M. Christian France-Lanord (Rapporteur)
M. Christophe Lécuyer
M. Bruno Malaizé
M. André Mariotti
M. Bruno Reynard
Mme Federica Tamburini

UNIVERSITE CLAUDE BERNARD - LYON 1

Président de l'Université	**M. François-Noël GILLY**
Vice-président du Conseil d'Administration	M. le Professeur Hamda BEN HADID
Vice-président du Conseil des Etudes et de la Vie Universitaire	M. le Professeur Philippe LALLE
Vice-président du Conseil Scientifique	M. le Professeur Germain GILLET
Directeur Général des Services	M. Alain HELLEU

COMPOSANTES SANTE

Faculté de Médecine Lyon Est – Claude Bernard	Directeur : M. le Professeur J. ETIENNE
Faculté de Médecine et de Maïeutique Lyon Sud – Charles Mérieux	Directeur : Mme la Professeure C. BURILLON
Faculté d'Odontologie	Directeur : M. le Professeur D. BOURGEOIS
Institut des Sciences Pharmaceutiques et Biologiques	Directeur : Mme la Professeure C. VINCIGUERRA
Institut des Sciences et Techniques de la Réadaptation	Directeur : M. le Professeur Y. MATILLON
Département de formation et Centre de Recherche en Biologie Humaine	Directeur : Mme. la Professeure A-M. SCHOTT

COMPOSANTES ET DEPARTEMENTS DE SCIENCES ET TECHNOLOGIE

Faculté des Sciences et Technologies	Directeur : M. F. DE MARCHI
Département Biologie	Directeur : M. le Professeur F. FLEURY
Département Chimie Biochimie	Directeur : Mme Caroline FELIX
Département GEP	Directeur : M. Hassan HAMMOURI
Département Informatique	Directeur : M. le Professeur S. AKKOUCHE
Département Mathématiques	Directeur : M. Georges TOMANOV
Département Mécanique	Directeur : M. le Professeur H. BEN HADID
Département Physique	Directeur : M. Jean-Claude PLENET
UFR Sciences et Techniques des Activités Physiques et Sportives	Directeur : M. Y.VANPOULLE
Observatoire des Sciences de l'Univers de Lyon	Directeur : M. B. GUIDERDONI
Polytech Lyon	Directeur : M. P. FOURNIER
Ecole Supérieure de Chimie Physique Electronique	Directeur : M. G. PIGNAULT
Institut Universitaire de Technologie de Lyon 1	Directeur : M. C. VITON
Ecole Supérieure du Professorat et de l'Education	Directeur : M. A. MOUGNIOTTE
Institut de Science Financière et d'Assurances	Directeur : M. N. LEBOISNE

Dédicace :

Ce travail est dédié à la mémoire de mon père.

Remerciements :

A l'issue de ce travail je tiens à exprimer mes remerciements à ceux qui l'ont rendu possible :

- Tout d'abord je tiens à remercier Christophe Lécuyer, professeur à l'Université Claude Bernard Lyon 1et responsable du groupe ISOSTAB qui fut à l'origine de ce projet, qui l'a dirigé et qui l'a soutenu constamment ;
- Je remercie Christian France-Lanord et Tony Fallick d'avoir bien voulu être les rapporteurs de ce mémoire de doctorat.
- Je remercie André Mariotti, Bruno Reynard d'avoir accepté de faire partie du jury de ce travail de doctorat.
- Je voudrais également associer François Martineau IR1-CNRS et « isotopiste » au sein du groupe ISOSTAB de l'UMR5276 LGL-TPE avec qui j'ai travaillé quotidiennement au cours de ces années passées ;
- Je tiens également à exprimer ma gratitude envers Magali Seris technicienne dans le groupe ISOSTAB de l'UMR5276 LGL-TPE avec qui j'ai travaillé quotidiennement.
- Je me dois de remercier mon employeur la DR7 du CNRS, qui m'a autorisée à accomplir ce travail en parallèle de mon activité d'ingénieur de recherche ;
- Je remercie la direction et l'administration de l'école doctorale E2M2 de l'Université Claude Bernard Lyon 1 pour son aide dans les méandres des démarches administratives ;
- Je voudrais également avoir une pensée pour Eric Jautée et Dominique Barbe dont j'ai apprécié la disponibilité, le professionnalisme et la joie de vivre malgré tout ;
- Il va sans dire, que le soutien des membres de ma famille fut prépondérant pour l'accomplissement de cette tâche.

Titre en français : Amélioration des Outils Géochimiques pour l'Investigation des Paléoenvironnements.

Résumé en français:

L'histoire des isotopes stables débute en 1913 avec les travaux de Frederick Soddy. Dès lors les techniques analytiques dans ce domaine vont constamment évoluer, leur permettant de répondre à des questions scientifiques de plus en plus élaborées et d'investir petit à petit de plus en plus de domaines où leur capacité de traceur devient aujourd'hui indispensable.

Ce travail présente d'abord une partie décrivant l'évolution des techniques de mesures des rapports isotopiques au cours des décennies, insistant sur l'apport fondamental du flux continu et en particulier de l'analyse élémentaire. Dans la deuxième partie nous allons illustrer l'importance des analyses isotopiques dans le domaine des reconstructions paléoenvironnementales afin de mieux appréhender l'histoire climatique de la Terre et de ses habitants à diverses époques. Ceci principalement au moyen des analyses $^{18}O/^{16}O$ sur des matrices phosphatées ou carbonatées. La troisième partie est consacrée à l'utilisation des isotopes stables comme traceurs de certaines réaction métaboliques fondamentales sur des échantillons fossiles mais également sur du matériel actuel. Dans ce dernier cas, nous nous sommes également servis de la capacité des isotopes stables à être utilisés comme traceurs en abondance naturelle mais également en utilisant le marquage isotopique. Pour ce faire nous avons utilisé les signatures isotopiques $^{18}O/^{16}O$ sur du matériel phosphaté mais également les rapports isotopiques $^{13}C/^{12}C$ et $^{15}N/^{14}N$ de la matière organique.

La quatrième partie est consacrée plus particulièrement à des travaux de développement analytiques dans divers domaines. Tout d'abord nous nous sommes intéressés aux analyses isotopiques D/H et $^{18}O/^{16}O$ des eaux. Nous proposons de nouveaux paramètres de correction des analyses isotopiques sur des eaux de salinités supérieures à l'eau de mer. Puis nous avons travaillé sur les analyses isotopiques $^{13}C/^{12}C$ et $^{18}O/^{16}O$ des carbonates en proposant de nouveaux paramètres pour le fractionnement isotopique de l'oxygène entre les carbonates d'apatites et l'eau, les fractionnements isotopiques du carbone et de l'oxygène entre aragonite et calcite sur des organismes vivants actuels. Nous avons également développé une technique semi-automatique pour déterminer les signatures isotopiques en carbone et en oxygène de la calcite et de la dolomite dans des mélanges de proportions variables. Enfin nous avons tenté de quantifier la variabilité naturelle et la variabilité instrumentale des analyses isotopiques du carbone et de l'oxygène sur des microfossiles. Puis, nous nous sommes intéressés à un

domaine représentant une part importante de notre travail analytique sur les analyses isotopiques $^{18}O/^{16}O$ des phosphates biogéniques. En collaboration avec les fabricants d'instruments nous avons développé un nouveau système afin d'améliorer la qualité des analyses, de les automatiser le plus possible et de réduire la taille de la prise d'essai dans le but d'accéder à des échantillons de taille plus réduite. Enfin nous avons développé les analyses isotopiques du soufre toujours en collaboration avec les fabricants d'instrumentation, d'une part pour évaluer la capacité d'un nouveau système analytique à produire des analyses fiables sur des quantités limitées au sein de matrices complexes, et d'autre part, la capacité du même système à produire des analyses multi-isotopiques fiables sur les trois éléments N, C, S. Dans la conclusion de ce travail, nous revenons sur la contribution de nos divers travaux à l'évolution des techniques isotopiques en essayant d'évaluer dans l'avenir les nouveaux champs d'investigation de ces techniques tout juste centenaires.

Mots clés en français : Paléoenvironnements, climat, réactions métaboliques, phosphates, carbonates, isotopes stables, spectrométrie de masse, flux continu, analyse élémentaire, oxygène, hydrogène, carbone, azote, soufre.

Titre en anglais : Improvements of geochemical tools for palaeoenvironment investigations.

Résumé en anglais:

THe history of stable isotopes began in 1913 with the work of Frederick Soddy. Since then, analytical techniques in that domain have been in constant evolution, providing answers to more and more elaborated scientific questions and spreading into various application fields where their tracing abilities have become extremely useful today.

This work first describes the evolution of those analytical techniques through time and especially the fundamental step forward with continuous flow techniques especially through elemental analysis.

For the second part we illustrate the importance of stable isotope analyses for paleoenvironmental reconstructions to better understand the climatic history of the Earth and its inhabitants from different periods. This is mainly based on $^{18}O/^{16}O$ analyses from phosphatic or carbonaceous matrices.

The third part is dedicated to the use of stable isotopes as tracers of various fundamental metabolic pathways from both fossil and actual samples. For this latter case we have used the capacity of stable isotopes to be used at natural abundance as well as artificially labelled. We have used $^{18}O/^{16}O$ isotopic signatures from phosphatic samples as well as $^{13}C/^{12}C$ and $^{15}N/^{14}N$ from organic matter.

The fourth part is dedicated to analytical developments covering several domains. First we investigated D/H and $^{18}O/^{16}O$ measurements from waters. We are proposing new correction parameters for isotopic measurements from waters with salinity higher than sea water. Then we have dealt with $^{13}C/^{12}C$ and $^{18}O/^{16}O$ isotopic analyses from carbonates and we suggest new parameters to constrain oxygen isotopic fractionation between carbonates from apatite and water as well as carbon and oxygen isotopic fractionation between calcite and aragonite from actual living organisms. We have also developed a new semi-automated technique to measure carbon and oxygen isotopic signatures from calcite and dolomite mixtures with various proportions. Then we have attempted to quantify the natural and instrumental variability of oxygen and carbon isotopic analyses from microfossils. An important part of this analytical work has been dedicated to $^{18}O/^{16}O$ isotopic analyses from biogenic phosphate material. In collaboration with instrument manufacturers we have developed a new system to improve both quality and automation of those measurements as well as reduce the aliquot sizes in order to get access to smaller samples. Eventually we have developed sulfur isotopic analyses in

collaboration with instrument manufacturers to evaluate the capacities of a new analytical setup to generate reliable N, C, S multi- isotopic analyses.

Last, we summarize the contribution of this work to the evolution of stable isotope techniques and we try to evaluate the future fields of investigation for those techniques just over one hundred years old.

Mots clés en anglais : Paléoenvironements, climate, metabolic pathways, phosphates, carbonates, stable isotopes, mass spectrometry, continuous flow, elemental analyses, oxygen, hydrogen, carbon, nitrogen, sulfur.

Laboratoire de rattachement:

Laboratoire de Géologie de Lyon: Terre, Planètes Environnement

UMR CNRS 5276 – Université Claude Bernard Lyon 1 – ENS Lyon

Université Claude Bernard Lyon 1, Campus de La Doua, bâtiment Géode

2, rue Raphaël Dubois, 69622 VILLEURBANNE CEDEX

Table des matières

INTRODUCTION

Depuis ses origines, l'homme a été habité par une insatiable soif de comprendre l'environnement dans lequel il évolue. En commençant par l'observation, puis, en développant petit à petit des outils lui permettant d'aller plus loin dans cette quête. Si le point de départ est toujours ce désir de repousser les frontières du possible, c'est cette constante interaction réciproque entre l'imagination et la technique qui fait progresser la science depuis des millénaires.

Dans ce contexte global, l'utilisation des isotopes stables comme « outil scientifique » peut être considérée comme très récente puisqu'elle commence au milieu du vingtième siècle. Le terme même d'isotope ayant été défini par Frederick Soddy dans une publication de février 1913. Cependant, basée sur des techniques de mesures de haute technologie par spectrométrie de masse, cette discipline a su profiter du formidable bond en avant de ces technologies au cours de ces trente dernières années pour étendre ses champs d'investigations, répondre à de nombreuses questions scientifiques et en poser de nouvelles. Initiée par les géochimistes qui en jetèrent les bases, cette discipline a envahi aujourd'hui de vastes domaines de la recherche scientifique comme la médecine, l'environnement, la répression des fraudes ou encore l'archéologie etc…

C'est modestement ce que ce travail de doctorat va tenter d'illustrer à travers l'une des thématiques du Laboratoire de Géologie de Lyon utilisant les mesures isotopiques pour l'étude des paléoenvironnements. Comprendre le fonctionnement de l'environnement de notre planète afin de pouvoir en prédire le futur nécessite de s'intéresser aux enregistrements passés contenus dans les formations géologiques à la fois sur le plan qualitatif, mais le plus possible également, en essayant de quantifier les phénomènes observés. La géochimie des isotopes stables fournit un certain nombre de systèmes isotopiques ($^{13}C/^{12}C$, $^{15}N/^{14}N$, $^{34}S/^{32}S$, D/H…) pouvant être utilisés comme traceurs des phénomènes impliqués dans les diverses réactions physico-chimiques régissant notre environnement. Le degré d'information que nous pouvons obtenir de ces différents traceurs est proportionnel à la précision avec laquelle nous pouvons les mesurer et quantifier leurs variations. Améliorer l'outil isotopique en améliorant les

techniques d'analyse n'obéit donc pas simplement à un souci technique mais également à une volonté de répondre au mieux à de véritables questions scientifiques.

Dans ce manuscrit nous présenterons d'abord un chapitre reprenant l'évolution des techniques de mesures des rapports isotopiques et notamment l'apport décisif des techniques de flux continu par rapport aux techniques de double inlet en détaillant en particulier le système d'analyseur élémentaire. Nous parlerons également de l'automatisation de certaines méthodes d'analyse en mode double inlet. Puis nous nous intéresserons à l'utilisation des isotopes stable pour les études paléoenvironnementales. Nous montrerons en particulier des exemples utilisant les analyses isotopiques des eaux, des carbonates ainsi que des phosphates. Ensuite nous aborderons l'utilisation des isotopes pour comprendre certains mécanismes physiologiques actuels et fossiles avant de détailler les développements méthodologiques que nous avons réalisés afin d'améliorer l'outil isotopique notamment dans le domaine de l'analyse des phosphates.

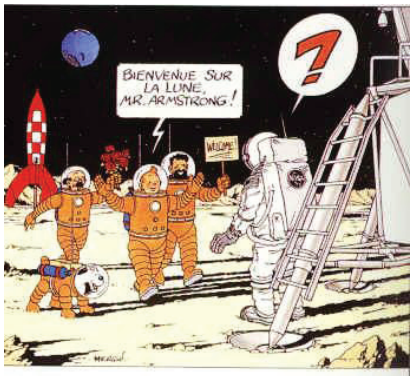

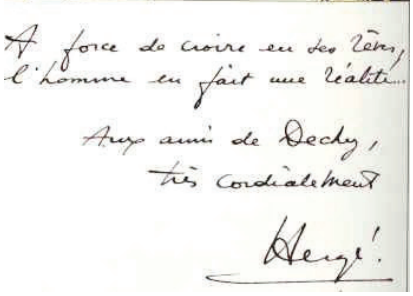

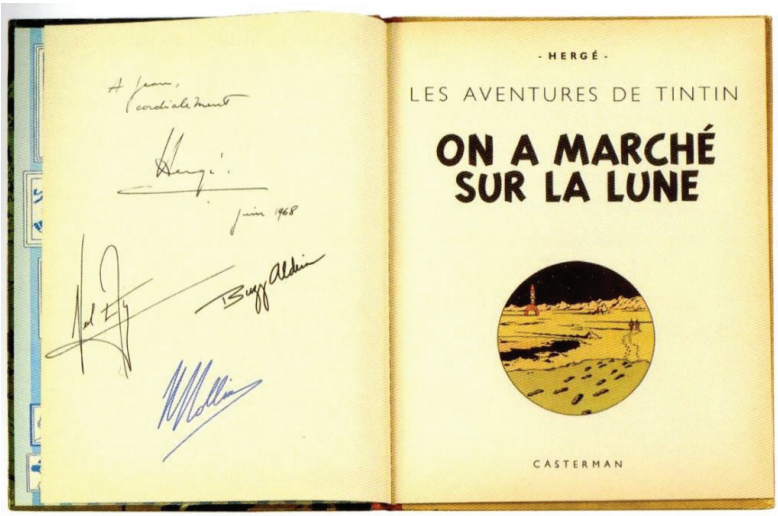

"L'histoire, je le crains, ne nous permet guère de prévoir, mais, associée à l'indépendance d'esprit, elle peut nous aider à mieux voir."
Paul. Valéry

CHAPITRE 1 : Un peu d'histoire

C'est en 1913, c'est-à-dire il y a exactement cent ans que le terme d'isotope est utilisé dans une publication scientifique par le chercheur Britannique Frederick Soddy[1,2] dont les travaux seront récompensés en 1922 par le prix Nobel de chimie.

Figure 1.1 : Portrait de Frederick Soddy.

Les débuts de la chimie des isotopes seront plus tournés vers les isotopes radiogéniques fournissant aux géologues les premiers chronomètres absolus. En ce qui concerne les isotopes

stables, si pendant longtemps les rapports entre les différents isotopes d'un même élément ont été considérés comme constants, l'amélioration des techniques de mesure a permis de faire évoluer cette notion jusqu'à utiliser les mesures de ces variations afin de comprendre et quantifier certains phénomènes physico-chimiques. Si les pionniers de ces découvertes de la structure intime de la matière s'intéressaient principalement aux isotopes radiogéniques, le sujet qui nous préoccupe dans ces travaux s'intéressera aux isotopes stables dits « conventionnels » c'est-à-dire les isotopes stables des éléments légers que sont C, H, O, N et S.

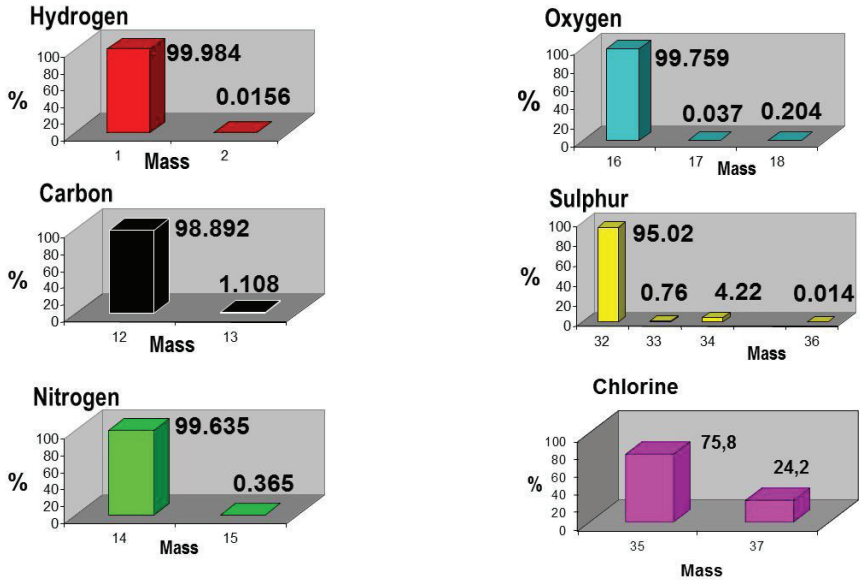

Figure 1.2 : Abondance naturelle des isotopes stables les plus communément analysés par IRMS

La figure 1.2 représente les abondances naturelles des divers éléments les plus communément analysés par les techniques d'IRMS. On constate aisément que tous les systèmes isotopiques ne présentent pas le même degré de difficulté analytique en fonction des écarts d'abondance entre l'isotope majeur et le ou les isotopes mineurs. Par exemple l'hydrogène présente un isotope mineur avec un rapport de 156 ppm quand le soufre 34 représente plus de 4% du soufre total.

La principale technique de mesure utilisée pour quantifier les variations des rapports isotopiques de ces différents éléments est la spectrométrie de masse à source gazeuse par impact électronique. Cette technique obéit toujours aujourd'hui aux mêmes principes que ceux utilisés par Nier[3,4,5] à la fin des années 40 pour son propre instrument de mesure. L'évolution technologique a permis d'améliorer la qualité des analyses, mais les principes de bases sont aujourd'hui identiques.

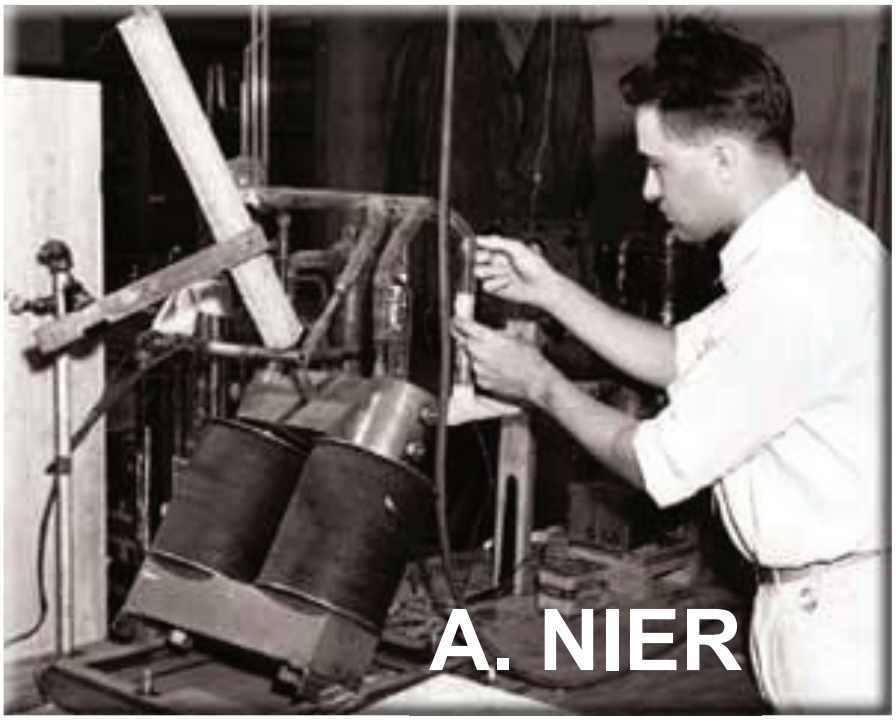

Figure 1.3 : Spectromètre de masse de Nier fin des années 50.

Sans vouloir entrer dans les détails de cette évolution, c'est à Urey[6,7,8]que l'on doit les fondements de la géochimie isotopique dans les années trente. Puis Nier, dans les années 40 va mettre en pratique ces principes en développant son spectromètre de masse (voir figure 1.3). Dans les années 50 Epstein et Mac Kinney[9] vont améliorer considérablement les techniques en bâtissant à leur tour leur propre spectromètre de masse dans leur laboratoire de Caltech à Pasadena-Californie. Dans le même temps Craig[10,11,12] développait tout un aspect de la théorie des analyses isotopiques encore utilisé aujourd'hui. Les années 60-70 ont vu une

véritable explosion des techniques de mesures par spectrométrie de masse aussi bien en ce qui concerne les spectromètres de masse à source gazeuse que la thermo-ionisation ainsi que les sources à plasma avec un développement accru de ce que l'on appelle la spectrométrie de masse organique qui est rapidement devenue un outil indispensable d'identification des molécules. C'est au cours des années 80 que la spectrométrie de masse de rapport isotopiques (généralement appelée IRMS) va connaître un tournant majeur avec l'arrivée des techniques de flux continu qui mérite quelques explications.

Jusqu'alors, le principe de base de notre discipline était le suivant : d'un côté nous devons analyser un échantillon qui peut être sous forme solide (carbonate), liquide (eau) ou gazeuse (air) et de l'autre un spectromètre de masse qui n'est compatible qu'avec des gaz, et de plus un nombre restreint d'espèces gazeuses. Il convient donc d'opérer une étape de préparation de l'échantillon pour le rendre compatible avec notre appareil de mesure qui doit être équipé d'un système d'introduction adéquat. (Voir schéma figure 1.4)

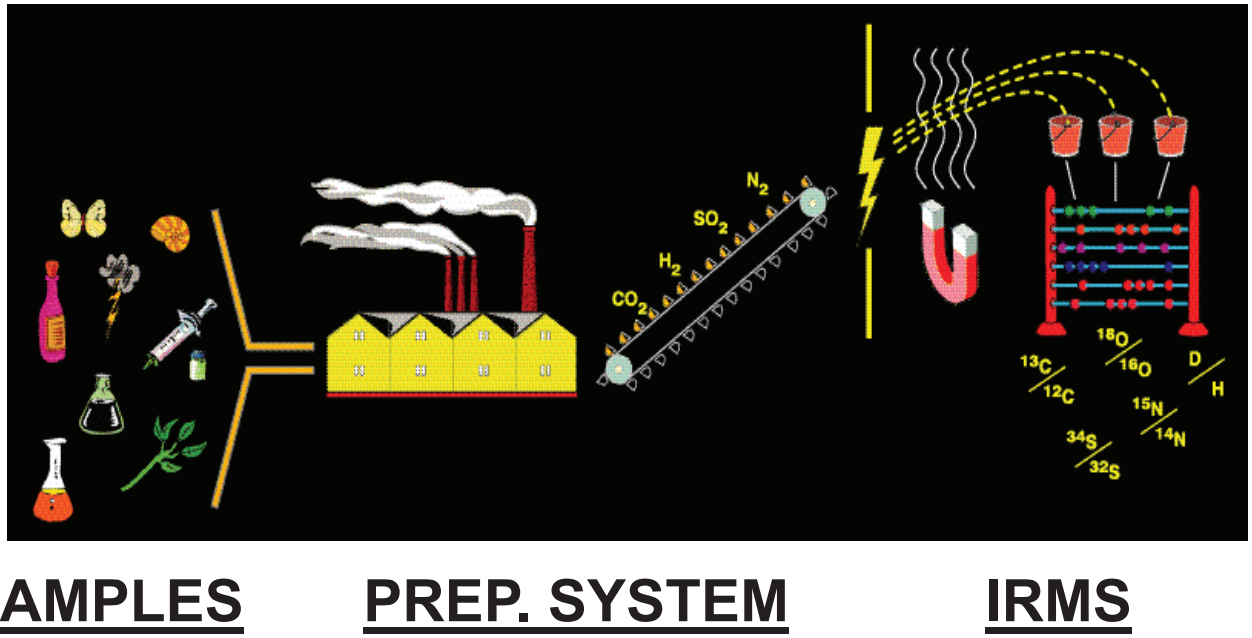

Figure 1.4 : Schéma de principe de l'IRMS

Jusqu'au milieu des années 80 la préparation de l'échantillon se faisait hors-ligne dans des laboratoires équipés de lignes sous ultra-vide, puis le gaz échantillon à analyser était introduit dans la source du spectromètre de masse par un système d'introduction simple d'abord, puis double (double introduction, ou double inlet) ensuite afin d'effectuer de manière continue des comparaisons entre un gaz échantillons inconnu et un gaz de référence de valeur isotopique calibrée.

Partant des travaux de Matthews and Hayes[13], c'est en 1985 que Preston et Owens[14], ouvrent un nouveau champ d'investigations aux isotopes stables en permettant de coupler en ligne un système de préparation automatisé sous flux d'hélium avec un spectromètre de masse sous vide par l'intermédiaire d'un système d' « open split ». Ceci va permettre d'automatiser la préparation des échantillons en utilisant des systèmes automatiques déjà existant comme les analyseurs élémentaires ou les appareils de chromatographie en phase gazeuse. Mais cela va permettre également de simplifier la technique de mesure des isotopes stables de la rendre moins onéreuse et de la faire sortir des laboratoires de recherche pour être utilisée dans l'industrie. Les premières mesures isotopiques en flux continu vont concerner les analyses $^{13}C/^{12}C$ au moyen d'un analyseur élémentaire. Puis ce sera le tour des analyses $^{15}N/^{14}N$ [15]. Au début des années 90 apparaîtrons les premiers systèmes de chromatographie en phase gazeuse en ligne avec un IRMS (technique connu sous le nom de GC-IRMS) d'abord pour les rapports $^{13}C/^{12}C$ [16], puis le $^{15}N/^{14}N$ [17]. Dans le même temps les analyses en mode double inlet bénéficient également d'évolutions technologiques allant vers de plus en plus d'automatisation comme par exemple les systèmes de préparation automatique des carbonates ainsi que des eaux [18]. A la fin des années 90 et au début des années 2000 le flux continu va être accessible pour d'autres systèmes isotopiques comme la mesure des rapports $^{18}O/^{16}O$ et D/H avec le développement des techniques de pyrolyse en ligne d'abord pour l'analyse élémentaire puis pour la chromatographie en phase gazeuse [19,20].

Au cours des années 2000 commencent à apparaître les premiers systèmes de couplage en ligne de la chromatographie en phase liquide (HPLC) avec des spectromètres de masse de rapports isotopiques (technique appelée LC-IRMS) [21]. Cette technique est en effet extrêmement prometteuse puisqu'elle donnerait accès à toutes les molécules non compatibles avec le chromatographie en phase gazeuse avec en particulier les molécules utilisées dans l'industrie pharmaceutique qui pourrait ainsi avantageusement remplacer les traceurs radioactifs par des traceurs d'isotopes stables. Pour l'instant ces systèmes ne sont compatibles qu'avec H_2O comme phase mobile ce qui limite leur utilisation, mais trouver une interface LC-IRMS compatible avec d'autres phases mobiles organiques est certainement un défi d'avenir pour cette discipline. Au cours des années 2000 apparaît également une innovation majeure dans le domaine des techniques IRMS avec l'apparition du couplage en ligne d'un nouveau type d'analyseurs élémentaires utilisant la technique du « purge and trap » sur lequel nous reviendrons dans le chapitre 4 de ce manuscrit. Enfin au début des années 2010 apparaissent pour la première fois des techniques permettant d'analyser des combinaisons d'isotopomères présentant deux isotopes mineurs : $^{13}C^{16}O^{18}O$ connues sous le nom de « clumped isotopes » [22]. Ces techniques, quoique prometteuses, n'en sont qu'à leurs débuts et il faudra attendre qu'elles se généralisent un peu avant de pouvoir les appliquer à des cas réels dans le domaine des paléoenvironnements.

La spectrométrie de masse en général a aujourd'hui envahi non seulement les laboratoires de recherche dans bien des disciplines, mais également l'industrie et notamment l'industrie pharmaceutique. Cette évolution en termes d'applications a été étroitement liée à l'évolution technologique des systèmes analytiques depuis les techniques classiques en mode double inlet vers les systèmes en flux continu. Ce changement a été fondamental dans l'évolution des techniques isotopiques.

Comme nous l'avons brièvement indiqué le premier exemple publié d'analyses isotopiques en flux continu revient à Preston et Owens en 1985 [14] qui constitue un article fondateur des analyses isotopiques en flux continu :

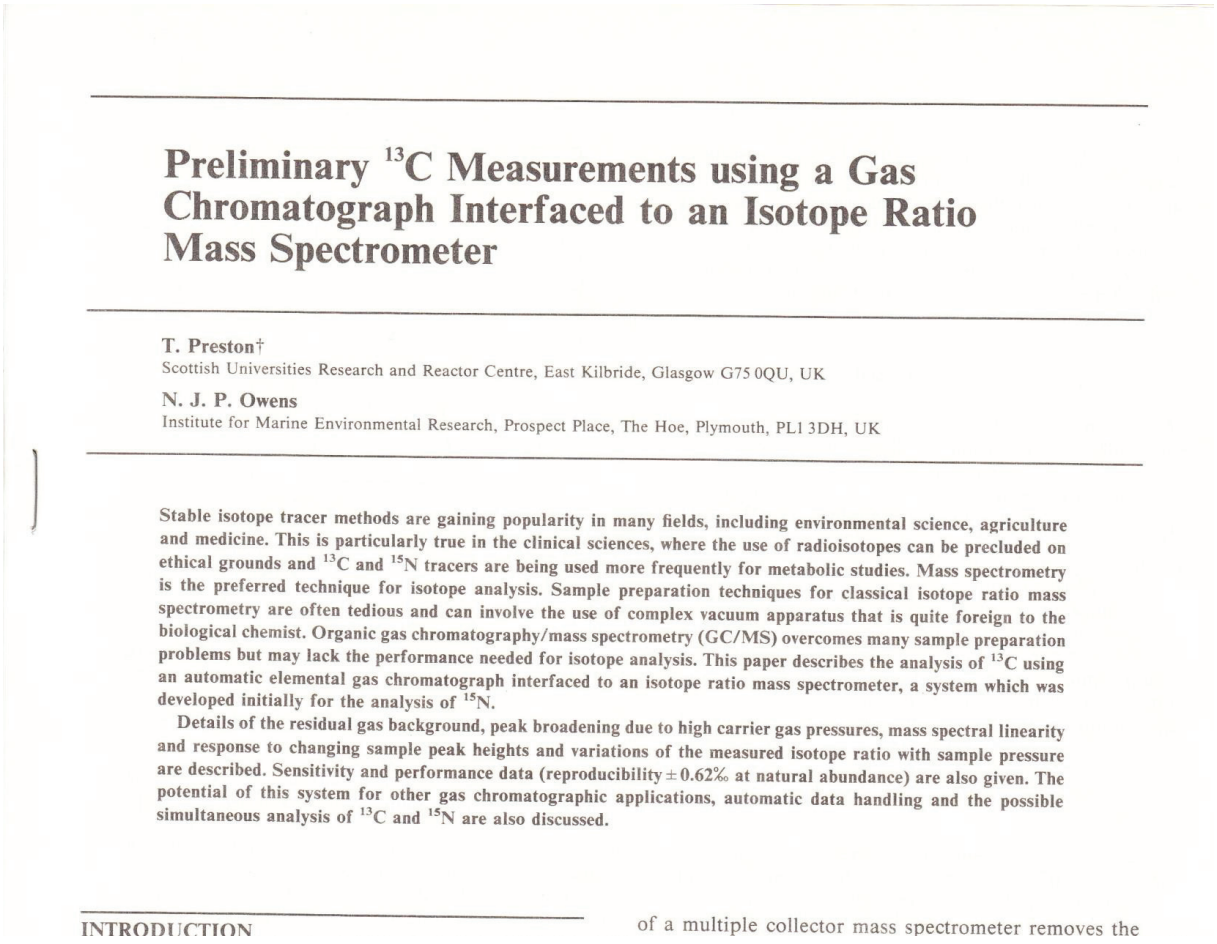

Preliminary ^{13}C Measurements using a Gas Chromatograph Interfaced to an Isotope Ratio Mass Spectrometer

T. Preston†
Scottish Universities Research and Reactor Centre, East Kilbride, Glasgow G75 0QU, UK

N. J. P. Owens
Institute for Marine Environmental Research, Prospect Place, The Hoe, Plymouth, PL1 3DH, UK

Stable isotope tracer methods are gaining popularity in many fields, including environmental science, agriculture and medicine. This is particularly true in the clinical sciences, where the use of radioisotopes can be precluded on ethical grounds and ^{13}C and ^{15}N tracers are being used more frequently for metabolic studies. Mass spectrometry is the preferred technique for isotope analysis. Sample preparation techniques for classical isotope ratio mass spectrometry are often tedious and can involve the use of complex vacuum apparatus that is quite foreign to the biological chemist. Organic gas chromatography/mass spectrometry (GC/MS) overcomes many sample preparation problems but may lack the performance needed for isotope analysis. This paper describes the analysis of ^{13}C using an automatic elemental gas chromatograph interfaced to an isotope ratio mass spectrometer, a system which was developed initially for the analysis of ^{15}N.

Details of the residual gas background, peak broadening due to high carrier gas pressures, mass spectral linearity and response to changing sample peak heights and variations of the measured isotope ratio with sample pressure are described. Sensitivity and performance data (reproducibility ± 0.62% at natural abundance) are also given. The potential of this system for other gas chromatographic applications, automatic data handling and the possible simultaneous analysis of ^{13}C and ^{15}N are also discussed.

INTRODUCTION

of a multiple collector mass spectrometer removes the

Figure 1.5 : Première publication IRMS en flux continu.

Le système utilisé par Preston et Owens est représenté sur la figure 1.6.

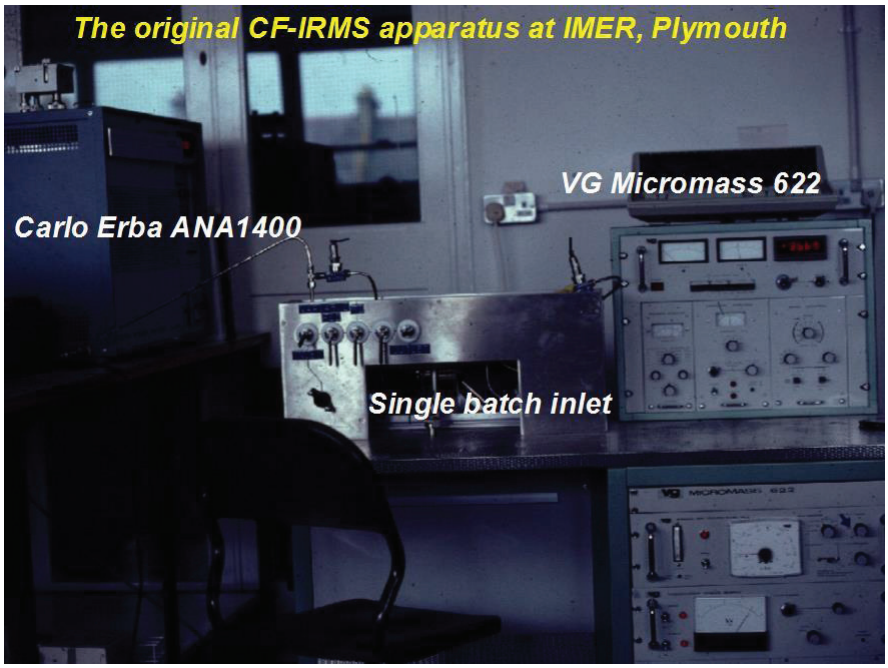

Figure 1.6 : Système utilisé par Preston et Owens pour leur travail initial sur les analyses IRMS en flux continu (communication personnelle de Tom Preston).

Le grand défi des analyses en flux continu, que ce soit pour la spectrométrie de masse dite « organique » ou la spectrométrie de masse isotopique, est de combiner un système d'introduction opérant sous un flux de gaz vecteur (généralement de l'hélium) avec un système de mesure fonctionnant sous vide, et ce sans perturber l'analyse. Le résumé de cette histoire est présenté ici grâce à la courtoisie de Tom Preston. Les premiers exemples de systèmes GC-MS utilisant des spectromètres de masse à quadripôle datent du milieu des années 70. Matthews et Hayes avaient initié un travail sur les analyses isotopiques par quadrupole en flux continu à la fin des années 70 mais pour les isotopes du carbone, les précisions n'étaient pas meilleures que 5‰. Différents systèmes de connexion entre systèmes sous flux d'hélium et système sous vide ont alors été expérimentés. Parmi les plus courants l'on peut citer : Jet Separator, Membrane Separator, Direct inlet, Open split. Les résultats préliminaires souffraient du manqué de précision qui pouvaient être attribués aux problèmes inhérents à l'analyse en collecteur unique à savoir des variations de débit dans le système de

split ou le séparateur, variations de la production d'ions dans la source, la nature même de la forme des pics chromatographiques, le temps de réponse des détecteurs, les faibles vitesses de balayage des détecteurs, l'optimisation des gains des systèmes de détection… Ainsi les principales limitations des analyses en flux continu furent la linéarité faible due à des pressions de gaz trop élevées pour les systèmes de détection ainsi que le faible nombre de comparaison à cause du manque de vitesse des systèmes d'acquisition. Une des façons de résoudre ce problème fut l'utilisation de la multi-collection et la comparaison systématique avec un gaz de calibration de même nature que le gaz analyte. Ainsi, à la suite des travaux de Preston et Owens les techniques d'analyses isotopiques en flux continu se sont développées pour générer des systèmes d'analyses plus simples que les conventionnels systèmes en double inlet comme l'illustre la figure 1.7 :

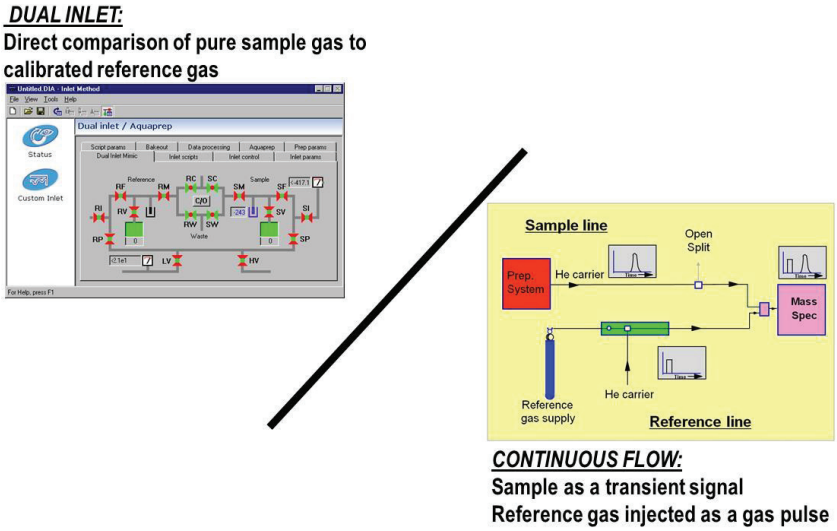

Figure 1.7 : Schéma comparatif des systèmes d'introduction en mode dual inlet et en mode flux continu.

En effet on voit sur la figure 1.7 que les systèmes d'introduction en mode double inlet fonctionnant sous vide nécessitent l'utilisation de systèmes de vannes complexes résistants

aux vides secondaires ainsi que des systèmes de moteurs pas à pas afin de régler les pressions de gaz à analyser qui confèrent à de tels systèmes un coût de fabrication ainsi qu'un degré de complexité qui limitent leur utilisation. En revanche les systèmes en flux continu qui fonctionnent avec un gaz vecteur qui est généralement l'hélium, offrent une alternative plus simple par le nombre réduit de vannes, moins cher à la fabrication puisque ces vannes ne sont plus des vannes à vide et, de plus, ils permettent un plus grand nombre d'analyses pour une période de temps donnée. Dans certains cas la sensibilité des analyses flux continu est même meilleure que leur alternative en double inlet [20]. De plus, l'utilisation du mode d'introduction en flux continu pour les analyses isotopiques a permis de donner accès aux développements qui avaient été préalablement effectués sur des techniques telles que l'analyse élémentaire ou la chromatographie en phase gazeuse.

L'apparition des techniques flux continu pour la spectrométrie de masse de rapports isotopiques a donc représenté une méthode plus simple, plus rapide et moins chère que les techniques traditionnelles en mode dual inlet. A partir du milieu des années 80 ces techniques de flux continu ont été en constante évolution. Les étapes principales peuvent être ainsi résumées :

1986 Un système de chromatographie en phase gazeuse (GC) est interface à un IRMS pour des analyses $^{13}C/^{12}C$.

1989 Premier système de diagnostic médical utilisant les isotopes stables avec le test d'Helicbacter-pylori.

1994 Possibilité d'analyser les isotopes du soufre par EA-IRMS.

1995 Possibilité des mesurer les rapports isotopiques $^{15}N/^{14}N$ par GC-IRMS. Apparition de la technique de réduction au chrome (Chrom-HD) pour les analyses D/H en flux continu.

1997 Apparition de systèmes automatisés pour les analyses isotopiques des gaz atmosphériques à l'état de trace: N_2O et CH_4.

1999 Apparition de systèmes de filtres électrostatiques permettant les analyses isotopiques D/H en flux continu en présence d'hélium.

2000 Apparition des premiers systèmes de pyrolyse à haute température pour la mesure des isotopes de l'oxygène et de l'hydrogène par EA-IRMS.

2000 Apparition des premiers systèmes d'analyses isotopiques de l'eau en flux continu par équilibration.

2001 Développement des analyses isotopiques D/H des eaux par EA-IRMS utilisant la technique du Chrom-HD. Premier exemple où les analyses en flux continu offrent des précisions et des justesses meilleures que les analyses équivalentes effectuées en mode dual inlet.

2008 Apparition de la technique de "Purge and Trap" pour les analyses EA-IRMS.

Tout au long de cette évolution, les techniques d'analyses en mode flux continu ont bénéficié des améliorations technologiques survenues sur les spectromètres de masse eux-mêmes. Au fur et à mesure de l'évolution de ces techniques analytiques, le nombre d'applications s'est étendu à des domaines très variés tels que la répression des fraudes [23] dans le domaine alimentaire [24], la lutte contre le dopage [25], les études environnementales [26], le diagnostic médical [27] ou le domaine médico-légal [28].

Il est à signaler qu'au cours de cette évolution riche en développements analytiques, il est une technique de préparation qui est demeurée prépondérante par rapport aux autres et à laquelle nous nous sommes particulièrement intéressés dans ce travail notamment dans le chapitre 4, il s'agit de l'Analyse Elémentaire couplée à la spectrométrie de masse de rapports isotopiques

(EA-IRMS). En effet, aujourd'hui encore, sous ces formes variées (haute ou basse température, pyrolyse ou combustion, chromatographie ou purge and trap…) les systèmes EA-IRMS représentent la majorité des systèmes de préparation automatiques couplés à des IRMS. Ceci s'explique aisément par la faculté d'accéder à de multiples signatures isotopiques à partir de même système de base puisqu'un système complet permet d'accéder aux signatures isotopiques de N, C, O, H et S. Sous certaines conditions, comme nous le verrons dans le chapitre 4 il est même possible d'accéder à plusieurs signatures isotopiques de manière simultanée à partir de la même aliquote d'échantillon. De plus l'analyseur élémentaire proprement calibré permet également d'accéder aux concentrations de l'échantillon en ces différents éléments. C'est pourquoi la contribution de ce travail à l'amélioration de l'outil isotopique pour les analyses EA-IRMS a concentré une part importante de nos recherches.

References Chapitre 1

(1) F. Soddy (1913) *Chem. News*, **107**:97; *Jahrb. Radioaktiv.,* **10**: 188.

(2) F. Soddy (1922) *Nobel lecture December 12 1922*: 371-399.

(3) A.O. Nier & E.E. Hanson (1936) *Phys. Rev*., **50** :722-726.

(4) A.O. Nier (1940) *Rev. Sci. Instr.,***11** :212-216.

(5) A.O. Nier (1947) *Rev. Sci. Instr.,***18** :398-411.

(6) H.C. Urey & D. Rittenberg (1933) *J. Chem. Phys.,* 1(2): 137-143.

(7) H.C. Urey (1947) *J. Chem. Soc.,* **69**:562-581.

(8) H.C. Urey, H. Lowenstam, S. Epstein & C.R. McKinney (1951) *Geol.Soc. Am.Bull.,* **62**:399-416.

(9) C.R. Mc Kinney, J.M. Mc Crea, S. Epstein, H.A. Allen & H.C. Urey (1950) *Rev. Sc; Instr.*, **21**:724.

(10) H. Craig (1953) *Geochim. Cosmochim. Acta*, **56**: 497-504.

(11) H.Craig (1957) *Geochim. Cosmochim. Acta*, **12**: 133-149.

(12) H.Craig (1961) *Science*, **133**: 1833-1834.

(13) Matthews & Hayes (1978) *Anal Chem* **50**: 1465

(14) Preston &Owens (1985) *Biomadical Mass Spect*. **12**: 510

(15) R. B. Marshall & J.N. Whiteway (1985) Analyst, 110: 867-871.

(16) A. Barrie, J. Bricout & J. Koziet (1984) *Biomed. Mass Spectrom.,* **11**: 583.

(17) M. Desage, R. Guilluy, J.L. Brazier, H. Chaudron, J. Girard, H. Cherpin & J. Jumeau (1991) *Anal. Chim. Acta*, **247** : 249-254.

(18) J. Horita, A. Ueda, K. Mizukami & I. Takatori (1989) *Appl. Radiat. Isot.,* **40** : 801-805.

(19) A. Hilkert, C.B. Douthitt, H.J. Schlüter & W. Brandt (1999) *Rapid Commun. Mass Spectrom.,* **13**: 1226-1230.

(20) J. Morrison, T. Brockwell, T. Merren, F. Fourel & A. Phillips (2001) *Anal. Chem.,* **73**: 3570-3575

(21) F.P. Abramson (1994) *Mass Spectrom. Rev.,* **13**: 341-356.

(22) J.M. Eiler (2007) *Earth and Planet. Sci. Let.,* **262**: 309-325.

(23) O. Breas, F. Fourel & G.J. Martin (1994) *Analusis*, **22** : 268-272.

(24) B. Salmon, G.J. Martin, G. Reamud & F. Fourel (1996) *Flav. and Frag. Journal*, **11**: 353-359.

(25) R. Aguilera, D.H. Catlin, M. Becchi, A. Phillips, C. Wang, R. S. Swerdloff, H.G. Pope & C.K. Hatton (1999) *J. Chromatogr. B*, **727**: 95-105.

(26) D. Widory, S. Roy, Y. LeMoullec, G. Goupil, A. Cocherie & C. Guerrot (2004) *Atmos. Envir.,* **28**: 953-961.

(27) H.M. Crews, V. Ducros, J. Eagles, F.A. Mellon, P. Kastenmayer, J.B. Luten & B.A. McGraw (1994) Analyst, 119 : 2491-2513.

(28) V. Dufey, L. Dujourdy, F. Besacier & H. Chaudron (2007) *Forens. Sci. Intern.,* **169** : 108-117.

« L'existence animale dépend, non seulement de l'environnement, mais aussi de la connaissance de l'environnement. Tout progrès de la connaissance profite à l'action, tout progrès de l'action profite à la connaissance. »

Edgar Morin

CHAPITRE 2 : Isotopes et études paléo-environnementales

Les études paléoenvironnementales ont utilisé ces dernières années de plus en plus les analyses isotopiques de l'oxygène, particulièrement venant des phosphates biogéniques. Dans la nature, le phosphore apparaît principalement dans les processus biologiques sous forme de PO_4^{3-} que l'on peut trouver à la fois dans les eaux, les minéraux et la matière organique. Or il a été démontré que la composition isotopique de l'oxygène des phosphates est liée par des équations empiriques simples à la composition isotopique en oxygène des eaux du milieu de vie ainsi qu'à la température [1-13]. Il se trouve, de plus, que les fractionnements isotopiques pour le système phosphate-eau de tissus fortement minéralisés comme l'émail dentaire semblent mieux préservés des phénomènes d'altération secondaire que dans le système classique calcite-eau [14-20]. Ainsi, les analyses isotopiques de l'oxygène des phosphates sont devenues indispensables pour l'étude, par exemple, des variations de température des océans dans le passé, la thermo physiologie de vertébrés aujourd'hui disparus.

Dans ce chapitre nous présentons des résultats d'études publiées auxquelles j'ai contribué en tant qu'analyste et chercheur utilisant les analyses isotopiques en lien avec des reconstructions paléo-environnementales principalement en analysant les rapports $^{18}O/^{16}O$ des phosphates de l'émail dentaire ou des os de matériel fossilisé, en relation avec les rapports $^{18}O/^{16}O$ des eaux

environnementales ingérées par ces organismes. Ceci fournit de précieuses indications sur les paléoclimats et leurs évolutions, ainsi que sur les différentes stratégies écologiques des divers êtres vivants analysés.

Ainsi dans la publication 2.1 les analyses isotopiques du carbone et de l'oxygène sur des échantillons de coquilles carbonatées d'organismes invertébrés datées du Pléistocène de Grèce ont permis de mettre en évidence que les changements écologiques rapides identifiés dans ces formations de Rhodes sont à relier plus probablement à des changements de salinité qu'à des changements de températures.

Figure 2.1 : Vue des côtes de l'île de Rhodes (Grèce)

Un autre exemple est illustré dans la publication 2.2 où nous avons analysés les rapports $^{18}O/^{16}O$ sur des dents de poissons prélevées en Afrique centrale (Tchad) et datées du Néogène. Cette étude a permis de révéler des changements du cycle de l'eau dans cette région à cette époque avec une tendance générale à la sécheresse entrecoupée par des épisodes successifs plus humides.

Dans la publication 2.3 nous avons réussi à mettre en évidence des variations saisonnières de température durant le Pléistocène supérieur du Jura Français grâce aux analyses isotopiques $^{18}O/^{16}O$ de l'émail dentaire d'ongulés tels que des chevaux et des cerfs. Dans cette étude nous avons également mis en évidence des températures moyennes hivernales inférieures à celles

d'aujourd'hui, responsables de l'étendue plus large de la couverture neigeuse en hiver avec des conséquences sur les ressources alimentaires de ces grands ongulés qui servaient de proies aux Néanderthaliens.

La publication 2.4 nous a permis de mettre en évidence un habitat semi-aquatique dans la famille des théropodes spinosaures grâce aux analyses $^{18}O/^{16}O$ de la partie phosphatique de leurs fossiles en les comparant aux analyses sur des restes phosphatiques de théropodes terrestres ainsi que de restes de crocodiliens et de tortues qui coexistaient avec eux. Ces résultats illustrent la répartition des niches écologiques entre tous ces grands dinosaures prédateurs permettant de coexister à la même époque en réduisant la compétition pour la nourriture et donc les territoires.

Dans la publication 2.5 nous avons à la fois travaillé sur des variations saisonnières de température comme dans la publication 2.3 mais également sur les stratégies alimentaires des vertébrés du Mésozoïque. Nous avons analysé les rapports $^{18}O/^{16}O$ sur des restes phosphatiques provenant de vertébrés terrestres tels que des tortues, des crocodiliens des théropodes ainsi que des sauropodes provenant de site de Thaïlande et couvrant la période du Jurassique supérieur au Crétacé inférieur. Ces données nous ont permis de mettre en évidence un passage entre un climat aride et un climat plus humide. Nos données nous ont également permis de mettre en évidence des stratégies différentes de gestion de l'eau de la part de ces divers vertébrés continentaux et en particulier de mettre en évidence chez Siamosaurus une stratégie proche de celle des vertébrés aquatiques tels que les crocodiliens ou les tortues d'eau douce.

La publication 2.6 s'intéresse également aux variations de paléo températures. Dans ce travail nous avons analysé les rapports isotopiques $^{18}O/^{16}O$ de l'émail dentaire de *Bison Priscus* provenant du site de Coudoulous dans le sud de la France et daté du Pléistocène moyen à supérieur. Les analyses par micro forages effectuées sur plusieurs dents de bisons nous ont

permis de reconstituer des variations sinusoïdales des rapports $^{18}O/^{16}O$ en relation avec les variations saisonnières de la température ambiante mettant en évidence des températures estivales comparables à celles d'aujourd'hui dans cette zone géographique mais des températures hivernales significativement plus basses.

Dans la publication 2.7 nous nous sommes intéressés à des phénomènes climatiques plus globaux. Dans cette étude nous avons mesurés les rapports isotopiques $^{18}O/^{16}O$ sur des parties phosphatiques de fossiles de vertébrés marins de la formation de Pisco au Pérou datés du Miocène moyen à supérieur. Les échantillons provenaient de dauphins, phoques, requins, baleines et pingouins. Les différences de $\delta^{18}O_p$ entre les différentes espèces nous permettent de caractériser des différences écologiques et physiologiques entre ces différents animaux. Mais au-delà, en comparant les résultats obtenus sur nos échantillons avec ceux d'autres localités il nous a été permis de suggérer que les mesures isotopiques des spécimens de Pisco résultent d'une combinaison de phénomènes climatiques locaux et globaux comme la mise en place du désert d'Atacama, du courant froid de Humboldt ou les phases de variations des calottes polaires.

On voit bien à la lecture de ces publications la capacité unique des isotopes stables à fournir des indices sur les conditions paléoenvironnementales qui est illustrée par la variété des types d'échantillons et donc du type d'analyses, permettant de répondre à plusieurs types de questions liées aux conditions de vie. En effet nous avons utilisé les analyses isotopiques $^{13}C/^{12}C$ et $^{18}O/^{16}O$ à partir de coquilles de mollusques carbonatées. Nous avons analysé les rapports isotopiques $^{18}O/^{16}O$ sur de l'émail dentaire de vertébrés terrestres ou marins, sur des os, des carapaces de tortues ou des arêtes de poissons. Nous avons étudié du matériel fossile provenant de site localisé à des latitudes variables provenant de sites du monde entier (Thaïlande, Europe, Amérique du sud ou Afrique centrale. Enfin le matériel étudié couvrait des périodes allant du Mésozoïque au Néogène. Malgré cette diversité d'échantillonnage, la

maîtrise de notre outil isotopique nous a permis de répondre à des questions aussi fondamentales que des alternances paléo climatiques entre des périodes de sècheresse et des périodes d'humidité, mais aussi les amplitudes de variations saisonnières de température, mais aussi de caractériser les stratégies alimentaires et écologiques d'espèces cohabitant à des époques diverses.

On constate au travers de ces différents travaux combien les signatures des isotopes stables peuvent être riches en informations paléoenvironnementales répondant à plusieurs types de questions scientifiques fondamentales pour comprendre l'histoire de la Terre et des êtres vivants qui l'ont habitée. Il est à remarquer ici que la majorité des informations présentées dans ce chapitre ont été obtenues principalement avec les signatures isotopiques $^{18}O/^{16}O$ sur du matériel phosphaté ou carbonaté. Il n'est donc pas interdit de penser que l'utilisation de l'approche multi isotopique, par exemple en mesurant les signatures isotopiques D/H des hydroxy apatites en les combinant aux données $^{18}O/^{16}O$, ou bien les analyses $^{34}S/^{32}S$ à partir des tissus phosphatés lorsque cela est possible serait sans nul doute une autre source d'informations essentielles dans ce domaine.

References Chapitre 2

(1) A. Longinelli & S. Nuti (1973a) *Earth Planet. Sci. Lett.,* **19**: 373-376.

(2) Y. Kolodny, B. Luz & O. Navon (1983) *Earth Planet. Sci. Lett.,* **64**: 298-404.

(3) B. Luz, Y. Kolodny & J. Kovach (1984) *Earth Planet. Sci. Lett.,* **69**: 255-262.

(4) J. Kharu & S. Epstein (1986) *Geochim. Cosmochim. Acta*, **50**: 1745-1756.

(5) Y. Kolodny & M. Raab (1988) *Palaeogeogr., Palaeoclimatol., Palaeoecol.,* **64**: 59-67.

(6) D. D'Angela & A. Longinelli (1990) *Chem. Geol. (Isot. Geosci. Sect.),* **86** : 75-82.

(7) C. Lécuyer, P. Grandjean, J.R. O'Neil, H. Capette & F. Martineau (1993) *Palaeogeogr., Palaeoclimatol., Palaeoecol.,* **105**: 235-243.

(8) H.C. Fricke, J.R. O'Neil & N. Lynnerup (1995) *Geology*, **23**: 869.

(9) H.C. Fricke, W.C. Clyde, J.R. O'Neil & P. D. Gingerich (1998a) *Earth Planet. Sci. Let*., **160**: 193.

(10) H.C. Fricke, W.C. Clyde, J.R. O'Neil & P.D. Gingerich (1998b) *Geochim. Cosmochim. Acta*., **62**: 1839.

(11) L. Genoni, P. Iacumin, V. Nikolaev, Y. Gribchenko & A. Longinelli (1998) *Earth Planet. Sci. Let*., **160**: 587-592.

(12) S. Picard, J.P. Garcia, C. Lécuyer, S.M.F. Sheppard, H. Capetta & C.C. Emig (1998) *Geology*, **26(11)** : 975-978.

(13) T.W. Vennemann & E. Egner (1998) *Palaeogeogr., Palaeoclimatol., Palaeoecol.,* **142**: 107-121.

(14) A. Longinelli (1966) *Nature*, 211: 923-927.

(15) J.M. McArthur, M.L. Coleman & J.M. Bremner (1980) *J. Geol. Soc. London,* **137**: 669-673.

(16) J.M. McArthur & A. Herczeg (1990) *In: Phosphorite research and development. A.J.G. Notholt & I. Jarvis Eds. Geol. Soc. Am*., **52**: 119-124.

(17) A. Shemesh (1990) *Geochim. Cosmochim. Acta*., **54**: 2433-2438.

(18) B. Sanchez Chillon, M.T. Alberdi, G. Leone, F. Bonadonna, B. Stenni & A. Longinelli (1994) *Palaeogeogr., Palaeoclimatol., Palaeoecol.,* **107**: 317-328.

(19) Y. Kolodny, B. luz, M. Sander & W.A. Clemens (1996) *Palaeogeogr., Palaeoclimatol., Palaeoecol.,* **126**: 161-171.

(20) Z.D. Sharp, V. Atudorei & H. Furrer (2000) *Am. J. Sci.,* **300**: 222-237.

Palaeogeography, Palaeoclimatology, Palaeoecology 350–352 (2012) 39–48

Contents lists available at SciVerse ScienceDirect

Palaeogeography, Palaeoclimatology, Palaeoecology

journal homepage: www.elsevier.com/locate/palaeo

Stable carbon and oxygen isotope compositions of invertebrate carbonate shells and the reconstruction of paleotemperatures and paleosalinities—A case study of the early Pleistocene of Rhodes, Greece

Christophe Lécuyer [a,*], Valérie Daux [b], Pierre Moissette [a], Jean-Jacques Cornée [c], Frédéric Quillévéré [a], Efterpi Koskeridou [d], François Fourel [a], François Martineau [a], Bruno Reynard [a]

[a] Laboratoire de Géologie de Lyon, UMR CNRS 5276, Université Lyon 1 et Ecole Normale Supérieure de Lyon, 69622 Villeurbanne, France
[b] Laboratoire des Sciences du Climat et de l'Environnement, UMR8212, IPSL/CEA/CNRS/UVSQ, Bat 701, L'Orme des Merisiers, CEA Saclay, 91191 Gif-sur-Yvette Cedex, France
[c] Géosciences Montpellier, UMR 5243, CC 60, Université Montpellier 2, Place E. Bataillon, 34095 Montpellier, France
[d] Department of Historical Geology-Paleontology, University of Athens, Panepistimiopolis, Zografou, 15784 Athens, Greece

ARTICLE INFO

Article history:
Received 21 June 2011
Received in revised form 1 June 2012
Accepted 12 June 2012
Available online 29 June 2012

Keywords:
Stable isotope
Pleistocene
Rhodes
Mediterranean
Temperature
Salinity
Mollusc

ABSTRACT

The coastal sediments of Rhodes in the eastern Mediterranean have recorded transgression–regression cycles that took place during the early Pleistocene. The sedimentary deposits from the Kritika Member of the Rhodes Formation consist in conglomerates, sandstones, siltstones and clays deposited in brackish to shallow marine environments. Faunal associations are dominated by molluscs and reveal rapid ecological changes. Carbon and oxygen isotope ratios of aquatic skeletal carbonates show that these ecological changes were most likely driven by large salinity changes while water temperature remained rather constant at about 22.0 ± 1.5 °C. The tectonic activity of the island rather than glacio-eustatic variations of climatic origin is advocated to be responsible for the ecological and salinity changes and sea-level variations recorded in the sedimentary sequence.

1. Introduction

Coastal environments are prone to large changes in water temperature and salinity through time. Tectonic activity and climate control the coastline geometry where the mixing of waters depends on bathymetry, shelf morphology, rate of freshwater input and current activity. Drastic changes in water temperature and salinity potentially have deep impacts upon aquatic ecosystems (e.g. Hart et al., 1990; Regier and Holmes, 1990; Håkanson, 2006). Rapid ecological changes are commonly recorded in Cenozoic and Quaternary coastal sediments (e.g. Graham et al., 2003; Cripps et al., 2005; Kowalke, 2005), yet deciphering the respective roles of temperature and salinity remains an uphill task due to the lack of adequate quantitative proxies in most cases.

In the coastal environments, salinity is a key parameter of the aquatic environment as it is very sensitive to the water balance between fresh and marine water inputs. Salinity controls the changes in biodiversity that are recorded in the regression–transgression sedimentary cycles. If co-existing freshwater and marine species are preserved in coastal sedimentary sequences, salinities can be theoretically deduced from their $\delta^{13}C$ values because fresh waters are ^{13}C-depleted by several ‰ relative to marine waters (Klein et al., 1996; Hendry and Kalin, 1997; Aucour et al., 1999; Hendry et al., 2001). However, the mass balance approach requires the knowledge of the relative abundance of dissolved carbon (DC) in the two mixing aqueous reservoirs. The ratio of the DC content of the two aqueous reservoirs varies consequently according to the environment (estuary, mangrove, lagoon) and cannot be inferred easily from the sedimentary record. Oxygen is equally shared between aqueous reservoirs, and once the water temperature is estimated, the $\delta^{18}O$ values of both freshwater and marine end-members can be calculated by using the isotopic fractionation equation between aragonite and water (Grossman and Ku, 1986; Kim et al., 2007) or calcite and water (O'Neil et al., 1969; Kim and O'Neil, 1997). Then, salinities can be theoretically deduced from a mass balance equation combining the compositions of these two aquatic end-members.

Temperature and salinity recorded in carbonate shells are influenced by biological factors. If growth of shell is slow enough, calcium carbonate is precipitated in oxygen isotope equilibrium with seawater (McConnaughey, 1989; Auclair et al., 2003). However, the skeletal calcification can be temperature-dependent, which means that the temperature and salinity conditions under which the shell has been formed may differ significantly from their yearly mean values (e.g. Romanek et al., 1987; Cornu et al., 1993; Elliot et al., 2003). Shell growth can also be disturbed through predator injuries, and also

* Corresponding author at: Institut Universitaire de France, France.
E-mail address: clecuyer@univ-lyon1.fr (C. Lécuyer).

0031-0182/$ – see front matter © 2012 Elsevier B.V. All rights reserved.
doi:10.1016/j.palaeo.2012.06.009

during periods of gametogenesis or severe restrictions in food supply. For recent geological periods, the oxygen isotope compositions of fossil molluscs can be corrected from the growth-dependent temperature factor by using the $\delta^{18}O$ values of modern counterparts (at the genus or species level) for which the temperature and isotopic composition where they live are measured. Salinity is not easily recorded in the chemical composition of fossil skeletons as it is indirectly related to the oxygen isotope composition of ambient water. Even though several attempts were made to decipher temperature and salinity parameters that are imbricated in the oxygen isotope composition of biominerals (e.g. Williams and Thunell, 1979; Thunell and Williams, 1989; Lécuyer et al., 1996; Emeis et al., 2000; Scheurle and Hebbeln, 2003), an innovative strategy is proposed and that consists in a multi-taxa geochemical approach. Stable carbon and oxygen isotope ratios were measured in specimens belonging to a faunal assemblage made of gastropods, bivalves and foraminifera, all of them being characterized by specific ecological preferences that were partly revealed by the geochemical analysis. Temperature and salinity variations through time were therefore determined in a coastal environment submitted to sea level changes whose causes could have been either eustatic or tectonic in origin. The late Pliocene–middle Pleistocene sedimentary sequences outcropping in Rhodes, Greece, offer an interesting opportunity to test this multi-taxa geochemical approach constrained by the well-known ecology of studied aquatic invertebrate fauna.

2. Geological setting

The north-eastern part of Rhodes (Fig. 1) consists in transgressive Pliocene–Pleistocene sediments resting upon a deformed and deeply eroded, mainly calcareous, Mesozoic 'Hellenic' basement (Mutti et al., 1970; Lekkas et al., 2001). The faulting of this basement created a series of horsts and grabens, which were filled in with detrital, mainly marine, sediments (Mutti et al., 1970; Meulenkamp et al., 1972; Hanken et al., 1996). The Kritika Member stands at the base of this lithographic unit, in the Rhodes Formation. Its facies is mostly siliciclastic and it consists in conglomerates, sandstones, siltstones, clays and a few lignite beds which were deposited in brackish to shallow marine environments (Keraudren, 1970; Broekman, 1972; Meulenkamp et al., 1972; Hanken et al., 1996; Hajjaji et al., 1998; Benali-Baitich, 2003).

The age of the Kritika sediments was estimated by biostratigraphic correlation with the Pliocene–Pleistocene boundary section occurring at Vrica–Crotone, Italy (Thomsen et al., 2001). Calcareous nanofossils suggest that the mainly brackish deposits are of early Pleistocene age. The Kritika Member is of Gelasian age (1.89–2.58 Ma) (Cornée et al., 2006a,2006b). The Kritika Member overlies the Upper Pliocene fluvio-lacustrine Damatria Formation and is separated from the overlying Rhodes Formation by an erosional unconformity. The Rhodes Formation includes several facies groups including the Lindos Bay clay characterized by deep-water faunas (bryozoans and pteropods) according to Moissette and Spjeldnaes (1995). All the sediments and fossils examined in this study belong to the Kritika Member that has been deposited during a tectonically controlled sedimentary cycle (Cornée et al., 2006a,2006b). The Kritika Member is organized into transgressive–regressive sedimentary sub-cycles bounded by beachrocks, prograding beach conglomerates, and lower shoreface deposits (Ferry et al., 2001). The duration of the sedimentary cycles cannot be determined because of a lack of precise dating.

Even though the siliciclastic Kritika Member is poorly fossiliferous, some marine beds contain abundant rhodoliths, foraminifers, solitary corals, molluscs, bryozoans and ostracodes, indicating beach to lower shoreface depositional environments (Hajjaji et al., 1998; Benali-Baitich, 2003; Maillet, 2003). Minor influxes of freshwater organisms are also recorded (Benali-Baitich, 2003; Maillet, 2003). Carbonate facies are scarce and principally consist of communities of skeletal organisms developed on drowned beachrocks: red algae, hermatypic corals (*Cladocora caespitosa*), serpulids, bivalves (oysters, spondylids), and bryozoans (Ferry et al., 2001). Freshwater to brackish characean and dasycladacean algae, benthic foraminifers, molluscs, and ostracodes occur in some beds and are particularly common at the top of the Formation.

One of the best exposures of this Formation occurs in Northeastern Rhodes, in the Faliraki area (N36°22.34′, E28°13.57′; Fig. 1) where it was deposited in large embayments open to the East (Mutti et al., 1970). We studied two sections, Faliraki1 (F1) and Faliraki2 (F2), 35 and 50 m thick, respectively, which outcrop along the main road leading to the village of Faliraki (Fig. 2). Beachrock beds occur in each section; they indicate temporary emersions and are considered as sequence boundaries. The two sections were correlated in the field by mapping index beds. They are composed of decameter-thick sedimentary sequences organized in a repetitive pattern with, from bottom to top:

- a dismembered conglomeratic beachrock bed, which shows one meter long 3D-dunes and contains well rounded pebbles from the metamorphic basement;
- beachrock beds encrusted by continuous red algal, bryozoan and serpulid rich bindstones which grew on and covered the dismembered underlying blocks, and in some cases, colonies of the zooxanthellate coral *Cladocora caespitosa*;
- silty to sandy marls with fossils from open marine (bivalves, especially *Glycymeris*, red algae, foraminifers), brackish (coal interbeds, molluscs), or fresh-water environments (*Planorbis*) in the marly levels;
- sandstones with hummocky cross-stratifications, cross-trough stratification and ripple-marks changing upward into dismembered conglomerates.

3. Material and method

A sampling campaign took place in May 2007. Fifty-eight samples of fossil bivalves, gastropods and bryozoans (4 to 12 individuals of a given genus or species per sedimentary sample), and nine samples

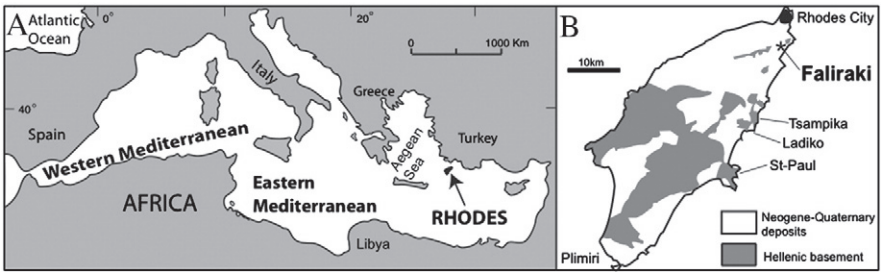

Fig. 1. Location map of the island of Rhodes in the eastern Mediterranean relative to the subduction context of the Aegean arc. The studied early Pleistocene sedimentary sequence outcrops at Faliraki in the northeastern part of the island.

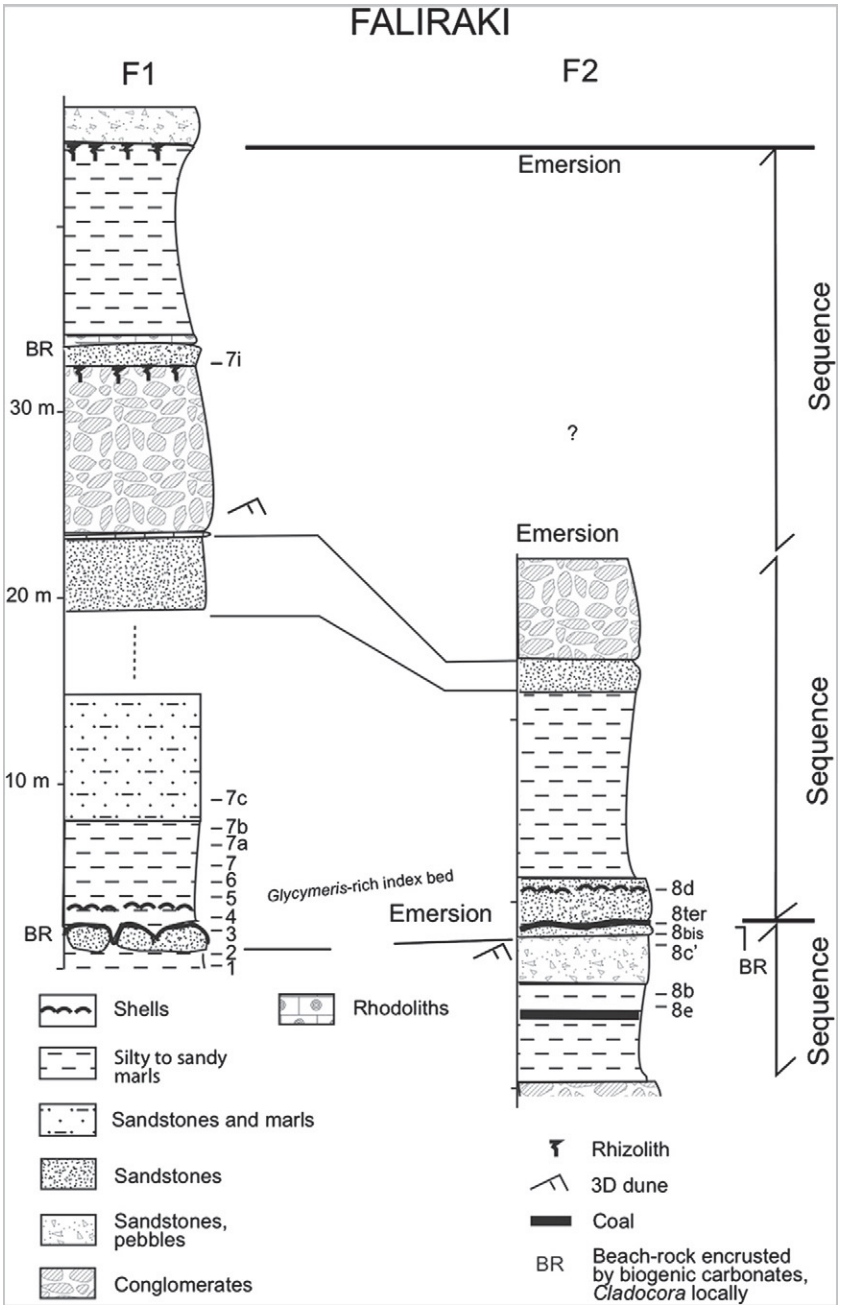

Fig. 2. Correlation between the two lithostratigraphic sequences studied at Faliraki, Rhodes.

of benthic foraminifera (*Elphidium*; 6 to 16 individuals per sample) were collected at various levels in F1 and F2 outcrops.

Three present-day gastropods and ten bivalves were sampled at Plimiri beach (Fig. 1; N35°54′16″, E27°49′16″) at ca. 1 m depth. Foraminifera were collected at Faliraki (N36°22′11″, E28°13′26″) at ca. 4 m depth. Three marine waters were collected at Tsampika (N36°12′53″, E28°08′39″), Ladiko (N36°19′12″, E28°12′21″) and Saint-Paul's bay (N36°05′11″, E28°05′20″) at 1 m depth (Fig. 1). A resurgent fresh water sample was collected at Tsampika. A present-day *Glycymeris* was also collected off Marseille, France (N43°17′42″, E5°21′31″).

3.1. Carbon and oxygen isotope analyses of carbonate skeletons

The sedimentary particles and the organic matter were removed from the carbonate skeletons of the individual fossil and present-day molluscs, bryozoans and foraminifera by using ultrasonic waves then H_2O_2 10% during 12 h, respectively. After washing with deionized water, the samples were dried at ambient temperature. Stable isotope analysis was performed on one complete valve for large shells including *Glycymeris*, whole shells for other molluscs and several individuals for foraminifera (Table 1). Foraminifera were pooled according to their taxonomy and stratigraphic position and crushed in an agate mortar until a fine powder was obtained. The carbon and oxygen isotope ratios were determined using an auto sampler MultiPrep™ system coupled to a dual-inlet GV Isoprime™ isotope ratio mass spectrometer (IRMS). For each sample, an aliquot of about 100–200 μg of calcium carbonate was reacted with anhydrous oversaturated phosphoric acid at 90 °C during 20 min. Isotopic compositions are quoted in the delta notation in ‰ relative to V-PDB. SMOW–PDB conversions were applied using the equation proposed by Coplen (1994). All sample measurements were triplicated and adjusted to the international reference NIST NBS19. External reproducibility is ±0.1‰ for $\delta^{18}O$ values and ±0.05 for $\delta^{13}C$

Table 1
Taxonomy, environment and stable isotope (C and O) compositions of calcareous aquatic invertebrates from the early Pleistocene sediments of Rhodes.

Sample	Section	Environment	Class	Taxon	Mineralogy	$\delta^{13}C$ (‰) (V-PDB)	$\delta^{18}O$ (‰) (V-PDB)
Fal7i-1	Faliraki1	Brackish	Foraminifera	*Elphidium* sp.	Low-Mg calcite	0.82	−0.72
Fal7i-2	Faliraki1	Brackish	Bivalvia	*Cardium* sp.	n.d.	−3.51	−0.48
Fal7i-3	Faliraki1	Brackish	Gastropoda	*Planorbis planorbis*	Aragonite	−8.73	−3.57
Fal7i-4	Faliraki1	Brackish	Gastropoda	*Theodoxus rhodiensis*	Aragonite + minor calcite	−2.44	−4.63
Fal7i-5	Faliraki1	Brackish	Gastropoda	*Potamides* cf. *girondicus*	Aragonite + minor calcite	−1.98	0.46
Fal7i-6	Faliraki1	Brackish	Gastropoda	*Ventrosia ventrosa*	Aragonite	−2.90	−1.29
Fal7i-7	Faliraki1	Brackish	Gastropoda	*Melanopsis sporadum*	Aragonite	−4.57	−4.43
Fal7c-Bi	Faliraki1	Brackish	Bivalvia	n.d.	n.d.	−1.25	1.28
Fal7b-Bi	Faliraki1	Brackish	Bivalvia	*Tellina* sp.	n.d.	0.10	0.32
Fal7a-For	Faliraki1	Brackish	Foraminifera	*Elphidium* sp.	Low-Mg calcite	0.86	−0.20
Fal7a-Gas	Faliraki1	Brackish	Gastropoda	*Obtusella macillenta*	n.d.	0.64	−5.89
Fal7-Bi	Faliraki1	Brackish	Bivalvia	n.d.	n.d.	−3.36	−2.50
Fal6-Bi	Faliraki1	Brackish	Bivalvia	*Nucula sulcata* (embryo)	n.d.	0.48	1.65
Fal5-Bi	Faliraki1	Marine	Bivalvia	*Nucula* sp.	n.d.	0.62	2.07
Fal5-Gas	Faliraki1	Marine	Gastropoda	*Cerithium* sp.	n.d.	1.82	1.19
Fal8d-1	Faliraki2	Marine	Bivalvia	*Glycymeris* sp.	Aragonite	1.27	1.39
Fal8d-2	Faliraki2	Marine	Bivalvia	*Abra* cf. *alba*	Aragonite	1.21	0.21
Fal8d-3	Faliraki2	Marine	Foraminifera	*Elphidium* sp.	n.d.	0.74	−0.93
Fal8d-4	Faliraki2	Marine	Gastropoda	*Acinopsis cancellata*	Aragonite	1.16	−0.42
Fal8d-5	Faliraki2	Marine	Gastropoda	*Bittium lacteum*	Aragonite	1.55	−0.24
Fal8d-6	Faliraki2	Marine	Bivalvia	*Glycymeris* sp.	Aragonite	1.21	0.53
Fal8d-7	Faliraki2	Marine	Bivalvia	*Glycymeris* sp.	Aragonite	1.38	−0.21
Fal4-2	Faliraki1	Marine	Foraminifera	*Elphidium* sp.	n.d.	1.11	−0.02
Fal4-3	Faliraki1	Marine	Bivalvia	*Nucula* sp.	n.d.	1.03	1.85
Fal4-4	Faliraki1	Marine	Decapoda	n.d.	n.d.	−3.75	1.86
Fal4-5	Faliraki1	Marine	Bivalvia	*Acanthocardia paucicostata* *Parvicardium scriptum*	n.d.	1.95	1.56
Fal3-1	Faliraki1	Marine	Foraminifera	*Elphidium* sp.	Low-Mg calcite	0.38	−0.26
Fal3-2	Faliraki1	Marine	Pteropoda	*Creseis* sp.	n.d.	1.07	1.92
Fal3-3	Faliraki1	Marine	Bryozoa	*M. moniliferum*	n.d.	−0.23	0.42
Fal3-4	Faliraki1	Marine	Bryozoa	*I. atlantica*	n.d.	−1.56	0.19
Fal3-5	Faliraki1	Marine	Bryozoa	*Crisia* spp.	n.d.	−1.32	0.37
Fal3-6	Faliraki1	Marine	Bryozoa	*M. cereoides*	n.d.	0.61	0.74
Fal3-7	Faliraki1	Marine	Corallinacea	n.d.	n.d.	−0.06	0.45
Fal3-8	Faliraki1	Marine	Bivalvia	*Arca* sp. *Juvenile*	Aragonite	2.32	1.54
Fal3-9	Faliraki1	Marine	Bivalvia	*Plagiocardium papillosum*	Aragonite	1.70	1.09
Fal3-10	Faliraki1	Marine	Polyplacophora	*Chiton corallinus*	n.d.	−0.50	1.00
Fal3-11	Faliraki1	Marine	Gastropoda	*Jujubinus exasperatus*	n.d.	2.40	0.83
Fal3-12	Faliraki1	Marine	Gastropoda	*Acinopsis cancellata*	Aragonite	1.51	1.17
Fal3-13	Faliraki1	Marine	Gastropoda	*Bittium latreilli*	n.d.	2.06	1.11
Fal8ter-1	Faliraki2	Marine	Gastropoda	*Bittium lacteum*	Aragonite	1.95	1.25
Fal8ter-2	Faliraki2	Marine	Bryozoa	*M. cereoides*	Aragonite	0.35	0.08
Fal8ter-3	Faliraki2	Marine	Corallinacea	n.d.	Mg-calcite	−2.15	1.07
Fal8ter-4	Faliraki2	Marine	Gastropoda	n.d.	n.d.	1.43	1.13
Fal8ter-5	Faliraki2	Marine	Bivalvia	*Abra* cf. *alba*	Aragonite	1.16	1.46
Fal8bis-1	Faliraki2	Marine	Gastropoda	*Pusillina marginata*	Aragonite	−0.71	0.33
Fal8bis-2	Faliraki2	Marine	Gastropoda	*Cerithidium submamillatum*	Aragonite	1.64	1.26
Fal8bis-3	Faliraki2	Marine	Bivalvia	*Abra* cf. *alba*	Aragonite	1.52	0.93
Fal8bis-4	Faliraki2	Marine	Bivalvia	*Acar* sp. *Juvenile*	Aragonite	2.34	2.13
Fal8bis-5	Faliraki2	Marine	Bivalvia	*Glycymeris* sp.	Aragonite	2.04	0.65
Fal2-1	Faliraki1	Marine	Foraminifera	*Elphidium* sp.	Low-Mg calcite	0.83	−0.15
Fal2-2	Faliraki1	Marine	Corallinacea	n.d.	n.d.	1.85	0.86
Fal2-3	Faliraki1	Marine	Decapoda	n.d.	n.d.	−0.28	1.79
Fal2-4	Faliraki1	Marine	Bivalvia	*Acanthocardia* sp.	Aragonite	2.05	1.75
Fal2-5	Faliraki1	Marine	Polyplacophora	n.d.	n.d.	0.43	1.23
Fal2-6	Faliraki1	Marine	Gastropoda	*Jujubinus* sp.	n.d.	2.30	0.94
Fal2-7	Faliraki1	Marine	Gastropoda	*Gibbula guttadauri*	n.d.	1.84	1.18
Fal2-8	Faliraki1	Marine	Gastropoda	*Bittium lacteum*	n.d.	2.20	1.01
Fal2-9	Faliraki1	Marine	Bivalvia	*Arca noae*	Aragonite	2.33	1.62
Fal2-10	Faliraki1	Marine	Gastropoda	*Acinopsis cancellata*	Aragonite	1.28	1.01
Fal2-11	Faliraki1	Marine	Bryozoa	*M. cereoides*	n.d.	0.93	0.71
Fal2-12	Faliraki1	Marine	Bryozoa	*S. cervicornis*	n.d.	0.51	0.55
Fal2-13	Faliraki1	Marine	Bryozoa	*M. moniliferum*	n.d.	0.86	0.25
Fal8c′-1	Faliraki2	Marine	Bryozoa	*M. cereoides*	Aragonite	0.39	0.15
Fal8c′-2	Faliraki2	Marine	Gastropoda	*Bittium lacteum*	Aragonite	1.60	0.04
Fal8c′-3	Faliraki2	Marine	Gastropoda	*Turboella lia*	Aragonite	−1.29	−0.15
Fal8c′-4	Faliraki2	Marine	Foraminifera	*Elphidium* sp.	n.d.	0.41	−0.66
Fal1	Faliraki1	Brackish	Bivalvia	n.d.	n.d.	−0.79	0.21
Fal8b-1	Faliraki2	Brackish	Gastropoda	*Pusillina marginata*	Aragonite	−0.89	0.41
Fal8b-2	Faliraki2	Brackish	Bivalvia	*Divaricella divaricata*	n.d.	−0.31	−0.02
Fal8b-3	Faliraki2	Brackish	Gastropoda	*Hydrobia* sp.	Aragonite	−0.11	−3.51
Fal8b-4	Faliraki2	Brackish	Gastropoda	*Cerithidium submamillatum*	Aragonite	−0.66	0.25
Fal8b-5	Faliraki2	Brackish	Foraminifera	*Elphidium* sp.	n.d.	−0.55	−0.51
Fal8b-6	Faliraki2	Brackish	Bivalvia	*Parvicardium scriptum*	Aragonite	−0.71	0.20

Table 1 (*continued*)

Sample	Section	Environment	Class	Taxon	Mineralogy	$\delta^{13}C$ (‰) (V-PDB)	$\delta^{18}O$ (‰) (V-PDB)
Fal8ε-1	Faliraki2	Brackish	Bivalvia	*Acanthochitona fascicularis*	Aragonite	−0.41	0.33
Fal8ε-2	Faliraki2	Brackish	Foraminifera	*Elphidium* sp.	n.d.	−0.97	−0.23
Fal8ε-3	Faliraki2	Brackish	Gastropoda	*Planorbis planorbis*	Aragonite	−4.37	−4.92
Fal8ε-4	Faliraki2	Brackish	Gastropoda	*Cerithium* sp.	Aragonite	0.43	0.96
Fal8ε-5	Faliraki2	Brackish	Gastropoda	*Ventrosia ventrosa*	Aragonite	−0.88	−2.63

values (1σ). The $\delta^{18}O$ and $d^{13}C$ values of skeletal carbonates are reported in Tables 1 and 2.

3.2. Oxygen isotope analysis of marine waters from Rhodes

The oxygen isotope ratios of marine and fresh water samples were determined according to the CO_2 equilibration technique developed by Horita et al. (1989). Aliquots of 200 μL of water were automatically equilibrated with CO_2 and analyzed using a MultiPrep™ system online with a GVI IsoPrime™ dual inlet IRMS. Reproducibility was typically ±0.03‰ (Table 3).

3.3. Raman spectroscopy

Raman spectra were collected using a LabRam™ HR spectrometer and excitation provided by the 514.53 nm line of a Spectra-Physics™ Ar laser on untreated shells to determine the polymorphs of calcium carbonate. Different parts of the shells were probed at the micrometer scale in backscattering geometry through an Olympus™ microscope. Laser power varied from 0.1 to 10 mW in order to prevent local heating and transformation especially for the absorbing black pigment-bearing parts of some shells. Recording times ranged from 1 to 10 min depending on laser power.

4. Results

4.1. Carbon and oxygen isotope compositions of early Pleistocene carbonate skeletons

Oxygen and carbon isotope compositions of the bulk carbonate skeletons from the early Pleistocene littoral environment of Rhodes range, respectively from –5.9‰ to 2.1‰ and from –8.7‰ to 2.4‰ (Table 1). These large variations of composition reflect the large spectrum of studied taxa that lived in fresh (*Planorbis planorbis, Melanopsis sporadum* and *Theodoxus rhodiensis*), brackish (Gastropoda, Bivalvia) and marine (Gastropoda, Bivalvia, Foraminifera and Bryozoa) aquatic environments (Table 4). As a general tendency, the skeletons of the fresh water fauna have the lowest $\delta^{18}O$ and $\delta^{13}C$ values, those of the marine water the highest, and those from the brackish the intermediate ones (Fig. 3). The inter-species differences in stable isotope compositions can be sizable. The greatest heterogeneities are observed in the brackish water fauna in which inter-species differences in $\delta^{18}O$ and $\delta^{13}C$ are, indeed, respectively as high as 6.9‰ and 9.3‰ for gastropods (1.7‰ and 3.7‰ in marine environments, m.e. hereafter), 3.8‰ and 4.0‰ for bivalves (2.3‰ and 1.7‰ in m.e.) and 0.5‰ and 1.8‰ for foraminifera (0.9‰ and 0.7‰ in m.e.). These large inter-species differences may reflect quick and important environmental changes in an area at the convergence of marine and continental influences, thus prone to variations in salinity and temperature.

In marine sediments (Fig. 4), *Abra* cf. *alba* of Fal8d ($\delta^{18}O = 0.21$‰) excepted, bivalves (n = 14) have $\delta^{18}O$ and $\delta^{13}C$ values which range from −0.21‰ to 2.13‰ and from 0.62‰ to 2.34‰, respectively. Most gastropods (10 out of 15) have positive $\delta^{18}O$ and $\delta^{13}C$ values that range from 0.83‰ to 1.26‰ and from 1.28‰ to 2.40‰, respectively. However, *Acinopsis cancellata*, *Bittium lacteum* and *Turboella lia* from layer Fal8d (see the isotopic composition of *Abra* above) Fal8ter and Fal8c′ are characterized by $\delta^{18}O$ values negative or close to 0‰. It is noteworthy that *Pusillina marginata* from sample Fal8bis has both low $\delta^{18}O$ and low $\delta^{13}C$ values comparable to those measured in specimens of the same taxa collected in brackish sediment Fal8b. The nine samples (five species) of bryozoans, exclusively marine, have positive $\delta^{18}O$ values ranging from 0.08‰ to 0.74‰ and exhibit large variations in $\delta^{13}C$ values from −1.56‰ to 0.93‰. The correlations between the two variables are not significant. Foraminifera are represented by the genus *Elphidium* sp. (n = 9). The benthics collected in sediments of marine origin have positive $\delta^{18}O$ and $\delta^{13}C$ values (0.08‰ to 0.74‰ and 0.41‰ to 1.11‰), in contrast with those of the brackish sediments (−0.72‰ to −0.23‰ and −0.97‰ to 0.82‰). *Glycymeris* shells have $\delta^{18}O$ values that range from −0.21 to 1.39 with

Table 2
Taxonomy, location and stable isotope (C and O) compositions of present-day marine invertebrates from the eastern coast of Rhodes.

Sample	# specimens	Environment	Location	Class	Taxon	Mineralogy	$\delta^{13}C$ ‰ (V-PDB)	$\delta^{18}O$ ‰ (V-PDB)	T (°C) $\delta^{18}O$ sw = 1.8‰ (V-SMOW)
GM	1	5 m	Marseille, France	Bivalvia	*Glycymeris pilosa*	Aragonite	2.29	1.44	15[a]
FalBR	13	−4 m	Faliraki beach	Foraminifera	*Elphidium*	Low-Mg calcite	0.51	−0.40	22
RH-1	1	−2 m	Plimiri beach	Gastropoda	*Monodonta turbinata*	Aragonite	0.69	1.42	17
RH-2	1	−2 m	Plimiri beach	Gastropoda	*Strombus decorus raybardii*	Aragonite	0.46	0.99	19
RH-3	1	−2 m	Plimiri beach	Gastropoda	*Strombus decorus raybardii*	Aragonite	0.54	0.88	18
RH-4	1	−2 m	Plimiri beach	Bivalvia	*Glycymeris pilosa*	Aragonite	2.32	1.02	19
RH-5	1	−2 m	Plimiri beach	Bivalvia	*Glycymeris pilosa*	Aragonite	2.77	1.14	18
RH-6	1	−2 m	Plimiri beach	Bivalvia	*Glycymeris pilosa*	Aragonite	2.30	1.52	16
RH-7	1	−2 m	Plimiri beach	Bivalvia	*Glycymeris pilosa*	Aragonite	2.08	0.85	20
RH-8	1	−2 m	Plimiri beach	Bivalvia	*Glycymeris pilosa*	Aragonite	2.25	0.90	19
RH-9	1	−2 m	Plimiri beach	Bivalvia	*Glycymeris pilosa*	Aragonite	2.27	0.98	21
RH-10	1	−2 m	Plimiri beach	Bivalvia	*Glycymeris pilosa*	Aragonite	2.32	0.72	20
RH-11	1	−2 m	Plimiri beach	Bivalvia	*Acanthocardia tubercolata*	Aragonite	1.49	1.16	18
RH-12	1	−2 m	Plimiri beach	Bivalvia	*Acanthocardia tubercolata*	Aragonite	1.16	0.25	23
RH-13	1	−2 m	Plimiri beach	Bivalvia	*Barbatia barbata*	Aragonite	1.77	1.05	19

[a] Temperature calculated with a $\delta^{18}O$ of water = 1.5‰ (V-SMOW) off Marseille (Pierre, 1999).

Table 3
Oxygen isotope compositions of fresh and marine waters from Rhodes.

Sample	Location	Water	$\delta^{18}O$ (H_2O) ‰ (V-SMOW)
TSA-SW	Tsampika	Marine	1.91
TSA-FW	Tsampika	Fresh	−2.96
LAD-SW	Ladiko	Marine	1.70
SPB-SW	Saint-Paul's Bay	Marine	1.69

a mean value of 0.59 ± 0.66‰. The three freshwater species (*Planorbis planorbis*, *Melanopsis sporadum* and *Theodoxus rhodiensis*) have the lowest $\delta^{18}O$ (−4.63‰ to −3.57‰) and $\delta^{13}C$ values (−8.73‰ to −2.44‰).

4.2. Carbon and oxygen isotope compositions of present-day bulk carbonate skeletons

Among Rhodes molluscs, oxygen isotope ratios range from 0.25‰ to 1.52‰ whereas $\delta^{13}C$ values can be considered as genus-dependent with the highest values measured in *Glycymeris* shells (2.77‰) and the lowest in gastropods shells (0.46‰ to 0.69‰) (Table 2). *Glycymeris* shells have a mean $\delta^{18}O$ value of 1.02 ± 0.26‰. The foraminifera sample (*Elphidium*), has a $\delta^{18}O$ value of −0.40‰ and a $\delta^{13}C$ value of 0.51‰ (Table 2).

Table 4
Taxa and ecology of aquatic invertebrates from the early Pleistocene sediments of Rhodes.

Taxa	Ecology
Bivalvia	
Abra cf. *alba*	0–100 m (optimum: intertidal and lagoons, brackish water)
Acanthocardia paucicostata	Eurybathyal (optimum: intertidal) tropical–subtropical to temperate
Acanthocardia sp.	Littoral–infralittoral
Acar sp.	Normal marine
Arca noae	Normal marine, littoral to infralittoral, warm water
Arca sp.	Littoral–infralittoral
Cardium sp.	Littoral–circalittoral
Divaricella divaricata	Littoral–circalittoral (optimum: littoral–infralittoral)
Glycymeris	Littoral–infralittoral
Nucula sp.	Infralittoral
Parvicardium scriptum	Infralittoral
Plagiocardium papillosum	Eurybathyal (optimum: 0–15 m)
Tellina sp.	Infralittoral
Gastropoda	
Acinopsis cancellata	2–100 m (optimum: 50 m)
Bittium lacteum	Eurybathyal (optimum: 0–40 m)
Bittium latreilli	Eurybathyal (optimum: 0–40 m)
Cerithidium submamillatum	0–50 m
Cerithium sp.	0–50 m
Gibbula guttadauri	0–50 m
Hydrobia sp.	Brackish water (optimum: lagoons)
Jujubinus exasperatus	0–50 m (optimum: 30–50 m)
Obtusella macillenta	Normal marine (0–250 m)
Potamides cf. *girondicus*	Brackishwater
Planorbis planorbis	Freshwater
Pusillina marginata	Normal marine
Melanopsis sporadum	Fresh and brackish water
Theodoxus rhodiensis	Fresh and brackish water
Turboella lia	Infralittoral (optimum: 0–20 m)
Bryozoa	
Crisia spp.	Mostly shallow-water genus
Idmidronea atlantica	10–850 m (optimum 40–400 m)
Margaretta cereoides	10–90 m (optimum 10–50 m)
Metrarabdotos moniliferum	*Metrarbdotos* is an extant warm-water genus
Smittina cervicornis	30–110 m (optimum 40–60 m)

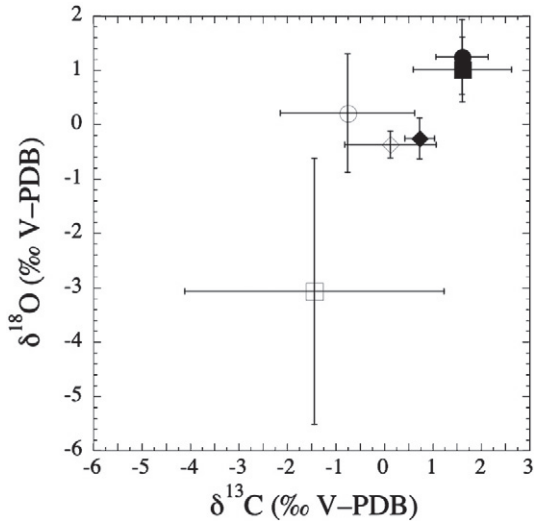

Fig. 3. Distribution of early Pleistocene freshwater, brackish and marine fauna in a $\delta^{18}O$–$\delta^{13}C$ space. Filled circles: marine bivalves; filled squares: marine gastropods; filled diamonds: marine foraminifers; open squares: brackish gastropods; open circles: brackish bivalves; and open diamonds: brackish foraminifers. Errors bars illustrate standard deviations (2σ).

4.3. Oxygen isotope compositions of waters

The marine waters sampled in the northeastern shore of Rhodes are ^{18}O-enriched relative to SMOW, with $\delta^{18}O$ values of 1.69‰ to 1.91‰ (Table 3). These compositions are in agreement with the systematic isotopic study of the Mediterranean seawater performed by Pierre (1999). The resurgent fresh water sampled at Tsampika beach (Fig. 1) has a negative $\delta^{18}O$ value of −2.96‰ which lies in the upper range of meteoric water compositions in Rhodes (IAEA/WMO, 2006).

4.4. Mineralogy of carbonate skeletons

Shell mineralogy was determined from the Raman spectra. Different peak positions and numbers for aragonite and calcite allow straightforward recognition (Gillet et al., 1993). Low-and high-Mg biogenic calcites can also be distinguished by the width of Raman lines, which are much broader in high-Mg calcite due to disordering

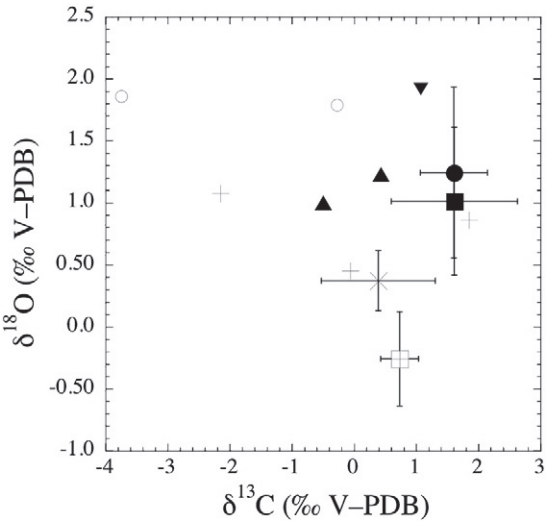

Fig. 4. Distribution of early Pleistocene marine fauna in a $\delta^{18}O$–$\delta^{13}C$ space. Filled circles: bivalves; filled squares: gastropods; plus in square: foraminifers; cross: bryozoans; plus: Corallinacea; filled triangles: chitons; open circles: decapods; and inverted filled triangles: pteropods. Errors bars illustrate standard deviations (2σ).

of the structure by cationic substitution (Lécuyer et al., 2004). Mineralogical determination of shells is reported in Table 1. Fluorescence and specific bands from pigments were also observed on the outer parts of several shells. All bivalves and gastropods are characterized by aragonitic shells whereas the test of foraminifera *Elphidium* is made of low-Mg calcite (Loeblich and Tappan, 1987).

5. Discussion

5.1. State of preservation of fossil carbonate shells

The widespread occurrence of pigments and metastable aragonite attests to the good preservation of the original structure of the biogenic carbonate. The presence of minor calcite on the outer side of some gastropods is likely not a mark of diagenetic transformation but a mark of the original mineralogy observed on living species (Lécuyer et al., 2004).

5.2. Calcareous aquatic invertebrates and the environmental isotopic record

Bivalvia and gastropods occur in fresh, brackish or marine sediments and their carbon and oxygen isotope compositions reflect changes in isotopic composition of dissolved carbon and in water salinity. As illustrated in Fig. 4, the $\delta^{13}C$ and $\delta^{18}O$ values in bivalves and gastropods, which are close to each other, are the highest of the marine taxa (Fig. 4). This result is in agreement with Lécuyer et al. (2004) who showed that gastropods and bivalves fractionate oxygen isotopes in a similar way and close to the equilibrium with tropical seawater. The few Corallinacea, chiton, decapod and pteropod samples have $\delta^{18}O$ values similar to those of bivalves and gastropods. The scattering of their $\delta^{13}C$ values (Fig. 4) could be explained by a combination of factors such as diet or kinetics (growth rate) as well as metabolic (respiration) processes.

Bryozoans have $\delta^{18}O$ values about 1‰ lower than those recorded in mollusc shells (Fig. 4). Their preserved aragonite mineralogy suggests that the studied fossil samples were not affected by a strong diagenetic alteration. Lower oxygen isotope ratios compared to molluscs may suggest that they grew in warmer waters. However, even though several species, which are not those studied here, are known to precipitate their aragonitic or magnesian calcitic skeleton in oxygen isotope equilibrium with seawater (Machiyama et al., 2003; Smith and Key, 2004), other species indicated significant disequilibrium oxygen isotope fractionation during calcification (Crowley and Taylor, 2000).

5.3. Seawater temperature during the early Pleistocene

Water temperatures are calculated on the basis of the oxygen isotope fractionations that were experimentally determined for inorganic low-Mg calcite (Kim and O'Neil, 1997) and inorganic aragonite (Kim et al., 2007). The mean 'isotopic temperature of 19 °C' calculated with the $\delta^{18}O$ values obtained for the present-day *Glycymeris* of Rhodes are close to the measured yearly mean temperature of 20 °C for the surface waters (Levitus 94, 1994). The mean $\delta^{18}O$ value of the modern adult *Glycymeris* (sample GM) shell from Marseille indicates an "isotopic temperature" of 15 °C using a seawater $\delta^{18}O$ value of 1.5‰ (Pierre, 1999). This temperature is 3 °C lower than the average seawater temperature of 18 °C off Marseille (Levitus 94, 1994). The temperature calculated from present-day *Glycymeris* shells induces a negative temperature bias of 2 ± 1 °C relative to oceanographic data which most likely results from a temperature-dependent growth mode already known for other molluscs (e.g. Romanek et al., 1987; Cornu et al., 1993; Elliot et al., 2003).

Elphidium oxygen isotope ratios lead to overestimate water temperatures by 3 °C, corresponding to a negative isotopic offset of 0.7‰ relative to the expected isotopic 'equilibrium' values (use of equation determined by Kim and O'Neil, 1997). This offset suggests that the shell of *Elphidium* is precipitated out of isotopic equilibrium with the environmental water, a result in agreement with previous studies (Erlenkeuser and von Grafenstein, 1999; Polyak et al., 2003; Bauch et al., 2004). Despite a rather constant $\delta^{18}O$ value of -0.43 ± 0.3‰ throughout the Faliraki sedimentary sequence, *Elphidium* isotopic composition does not help to distinguish between brackish and marine environments (Fig. 5A), a result that is at variance with the observations made by Diz et al. (2009). However, this mean $\delta^{18}O$ value compares well with the present-day value of −0.4‰, suggesting that marine water temperatures during the Pleistocene were rather similar. The oxygen isotope offset between *Elphidium* and its living water is known to be species-dependent but can also be influenced by ecological parameters that cannot be inferred from the Pleistocene sedimentary deposits of Rhodes. *Glycymeris*, which is known to be strictly marine, seems more appropriate as a proxy of past water temperatures because several specimens in the present-day waters of Rhodes can be compared to those occurring in the Pleistocene marine sediments. To a first approximation, we can apply to the fossil *Glycymeris* shells the same temperature bias as above, leading to an estimation of the mean seawater temperature of 22.0 ± 1.5 °C if the $\delta^{18}O$ of seawater off Rhodes during the early Pleistocene is assumed to be identical to the present-day value of 1.8‰ (Pierre, 1999). Indeed, the studied sediments have ages comprising between 1.89 and 2.58 Ma and were deposited during a period characterized by rather constant warm marine waters according to the $\delta^{18}O$ of worldwide benthic foraminifera (Zachos et al., 2001). Considering that the water exchange between the Atlantic Ocean and the Mediterranean Sea were already limited and within a geographic configuration close to present-days, a $\delta^{18}O$ value of seawater close to the present-day value of +1.8‰ can be considered as a robust working hypothesis. However, if the development of ice caps remained limited, calculated temperatures would be considered as maximal estimates. This calculated temperature of 22.0 ± 1.5 °C for Pleistocene seawater is slightly higher but remains comparable to the present-day average seawater temperature off Rhodes of 20 °C (Levitus 94, 1994). This result suggests that the studied *Glycymeris* lived in a warm water mass compatible with the climatic conditions of an interglacial phase.

5.4. Variations in water temperature or salinity?

Bivalves, gastropods and foraminifera are numerous enough throughout the Faliraki sedimentary sequence so that water temperature or salinity changes can be tracked. Carbon and oxygen isotope compositions of these three groups are reported as a function of the lithostratigraphy in Fig. 5.

The $\delta^{18}O$ and $\delta^{13}C$ values *of Elphidium* do not show significant changes along the sequence. Except sample Fal7, the highest $\delta^{13}C$ and $\delta^{18}O$ in bivalves correspond to the middle part of the sedimentary sequence where the marine levels associated with the beachrock and sandy deposits occur. However, the isotopic variability between the freshwater–brackish and the marine facies does not exceed 2‰ (Fig. 5). The gastropods with the lowest isotopic ratios occur in the bottom and top parts of the sedimentary sequence ($\delta^{13}C$ and $\delta^{18}O$ as low as about −9‰ and −6‰ resp.) in the freshwater–brackish environments. The highest $\delta^{13}C$ (up to 2.5‰) and $\delta^{18}O$ (about 1‰) of gastropod shells correspond to samples from the beachrocks and marine sandstones.

5.5. Calculation of water salinities throughout the Faliraki sequence

The temperature of the water mass (22.0 ± 1.5 °C) is well assessed on the basis of the rather constant oxygen isotope compositions of bivalves, particularly *Glycymeris*, for which the isotopic bias resulting from its temperature-dependent growth has been determined with the composition of modern shells. A rather constant water temperature is supported by the near constant $\delta^{18}O$ value of *Elphidium* throughout the

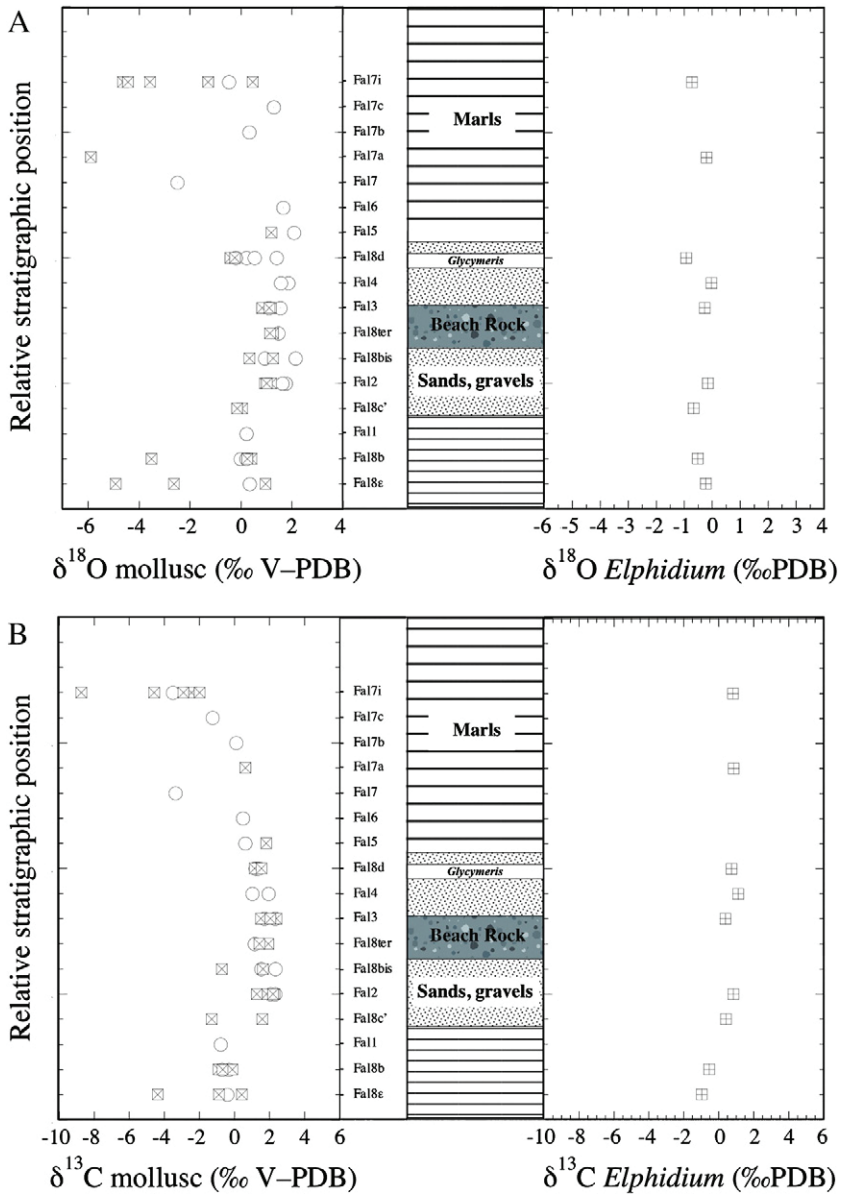

Fig. 5. Variations of oxygen (A) and carbon (B) isotope compositions of molluscs (open circles: bivalves; squares with a cross: gastropods) compared to the foraminifer *Elphidium* reported as a function of the synthetic early Pleistocene lithostratigraphy at Faliraki, Rhodes.

sedimentary sequence. Calculated water temperatures are indeed close to those inferred from the $\delta^{18}O$ values of *Glycymeris* associated with the beach rocks. Changes in both salinity and $\delta^{18}O$ of waters are only detected by the isotopic analysis of various gastropod species of distinct ecology. It is therefore most likely that *Planorbis* lived under the same water temperature conditions. Assuming that *Planorbis* ($\delta^{18}O$ values $= -3.6‰$ and $-4.9‰$) lived under the same temperature conditions, the oxygen isotope composition of the fresh water can be calculated with the aragonite–water fractionation equation determined by Kim et al. (2007). The values of the $\delta^{18}O$ of the early Pleistocene fresh water range from $-3.7 \pm 0.5‰$ to $-2.3 \pm 0.5‰$ (mean $= -3.0 \pm 1‰$ for $S = 0$). This value is bracketed by the oxygen isotope compositions of present-day meteoric waters in Rhodes. Indeed, the monthly and yearly values in the island range from $-6‰$ to $-3‰$ (IAEA/WMO, 2006, monthly). It is also in agreement with our measurement of a pinpoint sample ($\delta^{18}O = -3‰$; Table 3). The $\delta^{18}O$ of the marine end-member is assumed to be close to the present-day value of $+1.8 \pm 0.2‰$ for a salinity of 40‰ ($g.kg^{-1}$) according to the following equation: $\delta^{18}O$ seawater $= 0.25\ S - 8.2$ (Pierre, 1999). The $\delta^{18}O$ and salinity values of the two end-members (marine and fresh water) being estimated, the salinities of brackish waters can be calculated from the $\delta^{18}O$ values of bivalves and gastropods throughout the Faliraki sequence (Fig. 6). Changes in faunal assemblages can be influenced by parameters such as the water depth, the light intensity and the composition of the substrate. However, a near constant water temperature associated with large variations in salinity argue in favor of rapid ecological and environmental changes forced by regional tectonics rather than by global glacio-eustasy.

6. Concluding remarks

Stable carbon and oxygen isotope compositions of various species of gastropod and bivalves can be used as powerful proxies of temperature and water salinity in coastal environments. The temperature calculated from present-day *Glycymeris* shells from Rhodes, Greece, and Marseille, France, induces a positive temperature bias of 2.0 ± 1.5 °C relative to oceanographic data which most likely results from a temperature-dependent growth mode. This temperature bias

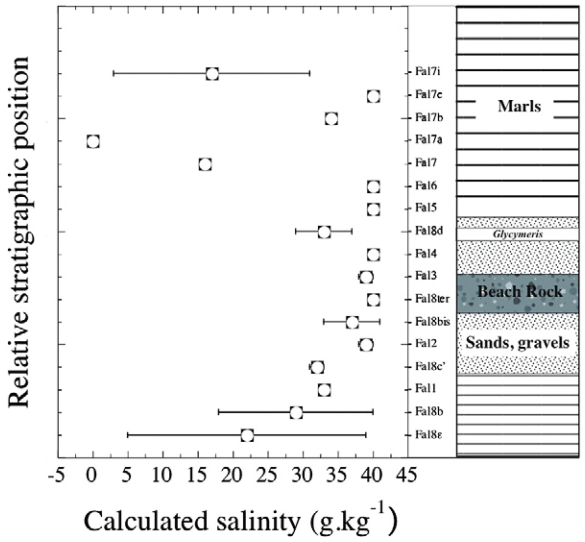

Fig. 6. Variations of 'model salinity' as a function of the early Pleistocene lithostratigraphic succession at Faliraki, Rhodes. Water salinity calculation was performed by using a mass balance equation using the following end-member values: 'model salinity' and we provide in the legend of the artwork the assumptions behind the model that concern the end-member values. Seawater end-member: $\delta^{18}O = 1.8‰$ and $S = 40‰$; freshwater end-member: $\delta^{18}O = -3.75 \pm 1.0‰$ and $S = 0$. See Section '5.5' for more explanations.

was applied to early Pleistocene *Glycymeris* shells from Rhodes, Greece, leading to an estimation of mean seawater temperature of 22.0 ± 1.5 °C. This temperature is slightly higher but remains comparable to the present-day average seawater temperature off Rhodes of 20 °C. This result suggests that the studied *Glycymeris* lived in a warm water mass compatible with the climatic conditions of an interglacial phase.

The isotopic compositions of the various assemblages of aquatic skeletal carbonates from the early Pleistocene of Rhodes show that the observed ecological changes were most likely driven by large salinity variations ranging from 0 to 40 ± 1 g.kg^{-1}. The tectonic activity of the island rather than glacio-eustatic variations of climatic origin is advocated to be responsible for the ecological and salinity changes and sea-level variations recorded in the sedimentary sequence.

Acknowledgments

The authors thank P. Desvignes for her help in the Laboratory. CL is grateful to J.P. Suc for a better knowledge of the biostratigraphy of the Pleistocene sedimentary deposits of Rhodes. This study was funded by both French CNRS and 'Institut Universitaire de France' (CL).

References

Auclair, A.C., Joachimski, M.M., Lécuyer, C., 2003. Deciphering kinetic, metabolic and environmental controls on stable isotope fractionations between seawater and the shell of *Terebratalia transversa* (Brachiopoda). Chemical Geology 202, 59–78.

Aucour, A.M., Sheppard, S.M.F., Guyomar, O., Wattelet, J., 1999. Use of ^{13}C to trace origin and cycling of inorganic carbon in the Rhône river system. Chemical Geology 159, 87–105.

Bauch, H.A., Erlenkeuser, H., Bauch, D., Mueller-Lupp, T., Taldenkova, E., 2004. Stable oxygen and carbon isotopes in modern benthic foraminifera from the Laptev Sea shelf: implications for reconstructing proglacial and profluvial environments in the Arctic. Marine Micropaleontology 51, 285–300.

Benali-Baitich, S., 2003. Paléobiocoenoses d'ostracodes dans les coupes Faliraki I et II de la Formation de Kritika (Pliocène supérieur, Rhodes, Grèce). Unpublished MSc Thesis, University of Lyon 1, 50 pp.

Broekman, J.A., 1972. Sedimentation and paleoecology of Pliocene lagoonal-shallow deposits on the island of Rhodos (Greece). Unpublished Ph.D. Thesis, Rijksuniversitet Utrecht, 132 pp.

Coplen, T.B., 1994. Reporting of stable hydrogen, carbon, and oxygen isotopic abundances. Pure and Applied Chemistry 66, 273–276.

Cornée, J.J., Moissette, P., Joannin, S., Suc, J.-P., Quillévéré, F., Krijgsman, W., Hilgen, F., Koskeridou, E., Münch, P., Lécuyer, C., Desvignes, P., 2006a. Tectonic and climatic controls on coastal sedimentation: the late Pliocene–middle Pleistocene of northeastern Rhodes, Greece. Sedimentary Geology 187, 159–181.

Cornée, J.J., Münch, P., Quillévéré, F., Moissette, P., Vasiliev, I., Krijgsman, W., Verati, C., Lécuyer, C., 2006b. Timing of late Pliocene to middle Pleistocene tectonic events in Rhodes (Greece) inferred from magneto-biostratigraphy and $^{40}Ar/^{39}Ar$ dating of a volcaniclastic layer. Earth and Planetary Science Letters 250, 281–291.

Cornu, S., Pätzold, J., Bard, E., Meco, J., Cuerda-Barcelo, J., 1993. Paleotemperature of the last interglacial period based on $\delta^{18}O$ of *Strombus bubonius* from the western Mediterranean Sea. Palaeogeography, Palaeoclimatology, Palaeoecology 103, 1–20.

Cripps, J.A., Widdowson, M., Spicer, R.A., Jolley, D.W., 2005. Coastal ecosystem responses to late stage DEccan Trap volcanism: the post K–T boundary (Danian) palynfacies of Mumbai (Bombay), west India. Palaeogeography, Palaeoclimatology, Palaeoecology 216, 303–332.

Crowley, S.F., Taylor, P.D., 2000. Stable isotope composition of modern bryozoan skeletal carbonate from the Otago Shelf, New Zealand. New Zealand Journal of Marine and Freshwater Research 34, 331–351.

Diz, P., Jorissen, F.J., Reichart, G.J., Poulain, C., Dehairs, F., Leorri, E., Paulet, Y.M., 2009. Biogeosiences 6, 2549–2560.

Elliot, M., deMonecal, P.B., Braddock, K.L., Howe, S.S., 2003. Environmental controls on the stable isotopic composition of *Mercenaria mercenaria*: potential application to paleoenvironmental studies. Geochemistry Geophysics Geosystems 4, 1056. http://dx.doi.org/10.1029/2002GC000425.

Emeis, K.C., Struck, U., Schulz, H.M., Rosenberg, R., Bernasconi, S., Erlenkeuser, H., Sakamoto, T., Martinez–Ruiz, F., 2000. Temperature and salinity variations of Mediterranean Sea surface waters over the last 16,000 years from records of planktonic stable oxygen isotopes and alkenone unsaturation ratios. Palaeogeography Palaeoclimatology Palaeoecology 158, 259–280.

Erlenkeuser, H., von Grafenstein, U., 1999. Stable oxygen isotope ratios in benthic carbonate shells of ostracoda, foraminifera, and bivalvia from surface sediments of the Laptev Sea, summer 1993 and 1994. In: Kassens, H., Bauch, H., Dmitrenko, I., Eicken, H., Hubberten, H.W., Melles, M., Thiede, J., Timokhov, L. (Eds.), Land–Ocean Systems in the Siberian Arctic: Dynamics and History. Springer, Berlin. 503-514 pp.

Ferry, S., Moissette, P., Suc, J.P., 2001. Le Plio-Pléistocène de Rhodes (Grèce). Field Guide, 1. University of Lyon, pp. 1–72.

Gillet, P., Biellmann, C., Reynard, B., McMillan, P.F., 1993. Raman spectroscopic studies of carbonates. Part 1: high-pressure and high-temperature behaviour of calcite, magnesite, dolomite, aragonite. Physics and Chemistry of Minerals 20, 1–18.

Graham, M.H., Dayton, P.K., Erlandson, J.M., 2003. Ice ages and ecological transitions on temperate coasts. Trends in Ecology and Evolution 18, 33–40.

Grossman, E.L., Ku, T.L., 1986. Oxygen and carbon isotope fractionation in biogenic aragonite: temperature effects. Chemical Geology (Isotope Geoscience Section) 59, 59–74.

Hajjaji, M., Bodergat, A.M., Moissette, P., Prieur, A., Rio, M., 1998. Signification écologique des associations d'ostracodes de la coupe de Kritika (Pliocène supérieur, Rhodes, Grèce). Revue de Micropaléontologie 41, 211–233.

Håkanson, L., 2006. The relationship between salinity, suspended particulate matter and water clarity in aquatic systems. Ecological Research 21, 75–90.

Hanken, N.M., Bromley, R.G., Miller, J., 1996. Plio-Pleistocene sedimentation in coastal grabens, north-east Rhodes, Greece. Geological Journal 31, 271–296.

Hart, B.T., Bailey, P., Edwards, R., Hortle, K., James, K., McMahon, A., Meredith, C., Swadling, K., 1990. Effects of salinity on river, stream and wetland ecosystems in Victoria, Australia. Water Research 24, 1103–1117.

Hendry, J.P., Kalin, R., 1997. Are oxygen and carbon isotopes of mollusc shells reliable palaeosalinity indicators in marginal marine environments? A case study from the middle Jurassic of England. Geological Society of London Journal 154, 321–333.

Hendry, J.P., Perkins, W.T., Bane, T., 2001. Short-term environmental change in a Jurassic lagoon deduced from geochemical trends in aragonite bivalve shells. Geological Society of America Bulletin 113, 790–798.

Horita, J., Ueda, A., Mizukami, K., Takatori, I., 1989. Automatic δD and $\delta^{18}O$ analyses of multi-water samples using H_2- and CO_2–water equilibration methods with a common equilibration set-up. International Journal of Radiation Applications and Instrumentation. Part A. Applied Radiation and Isotopes 40, 801–805.

IAEA/WMO, 2006. Global network of isotopes in precipitation. The GNIP Database. Retrieved August 2008 at: http://isohis.iaea.org.

Keraudren, B., 1970. Les formations quaternaires marines de la Grèce. Bulletin du Musée d'Anthropologie préhistorique de Monaco 6, 5–153.

Kim, S.T., O'Neil, J.R., 1997. Equilibrium and nonequilibrium oxygen isotope effects in synthetic carbonates. Geochimica et Cosmochimica Acta 61, 3461–3475.

Kim, S.-T., O'Neil, J.R., Hillaire-Marcel, C., Mucci, A., 2007. Oxygen isotope fractionation between synthetic aragonite and water: influence of temperature and Mg^{2+} concentration. Geochimica et Cosmochimica Acta 71, 4704–4715.

Klein, R.T., Lohmann, K.C., Thayer, C.W., 1996. Sr/Ca and $^{13}C/^{12}C$ ratios in skeletal calcite of *Mytilus trossolus*: covariation with metabolic rate, salinity and carbon isotopic composition of seawater. Geochimica et Cosmochimica Acta 60, 4207–4221.

Kowalke, T., 2005. Mollusca in marginal marine and inland saline aquatic ecosystems—examples of Cretaceous to extant evolutionary dynamics. Zitteliana A45, 35–63.

Lécuyer, C., Grandjean, P., Paris, F., Robardet, M., Robineau, D., 1996. Deciphering 'temperature' and 'salinity' from biogenic phosphates: the $\delta^{18}O$ of coexisting fishes and mammals of the middle Miocene Sea of western France. Palaeogeography Palaeoclimatology Palaeoecology 126, 61–74.

Lécuyer, C., Reynard, B., Martineau, F., 2004. Stable isotope fractionation between mollusc shells and marine waters from Martinique Island. Chemical Geology 213, 293–305.

Lekkas, E., Danamos, G., Skourtsos, E., Sakellariou, D., 2001. Position of the middle Triassic tyros beds in the Gavrovo–Tripolis unit (Rhodes Island, Dodecanese, Greece). Geologica Carpathica 53, 37–44.

Levitus 94, 1994. World Ocean Atlas, An Atlas of Objectively Analyzed Fields of Major Ocean Parameters. http://ingrid.ldeo.columbia.edu/SOURCES/.LEVITUS94/.
Loeblich, A.R., Tappan, H., 1987. Foraminiferal Genera and Their Classification, vol. 2. Van Nostrand Reinhold, New York. 1182 pp.
Machiyama, H., Yamada, T., Kaneko, N., Iryu, Y., Odawara, K., Asami, R., Matsuda, H., Mawatari, S.F., Bone, Y., James, N.P., 2003. Carbon and oxygen isotopes of cool-water bryozoans from the Great Australian Bight, and their paleoenvironmental significance. In: Hine, A.C., Feary, D.C., Malone, M.J. (Eds.), Proceedings of the Ocean Drilling Program, Scientific Results 182 ((online) http://www-odp.tamu.edu/publications/182-SR/007/007.htm).
Maillet, M., 2003. Variations bathymétriques dans le Plio-Pléistocène de Rhodes d'après l'étude des assemblages de bryozoaires (Formation de Kritika, île de Rhodes, Grèce). Unpublished MSc Thesis, University of Lyon 1, 48 pp.
McConnaughey, T.A., 1989. ^{13}C and ^{18}O isotopic disequilibrium in biological carbonates: I. Patterns. Geochimica et Cosmochimica Acta 53, 151–162.
Meulenkamp, J.E., De Mulder, E.F.J., Van De Weerd, A., 1972. Sedimentary history and paleogeography of the late Cenozoic of the Island of Rhodos. Zeitschrift der Deutschen Geologischen Gesellschaft 123, 541–553.
Moissette, P., Spjeldnaes, N., 1995. Plio-Pliostecene deep-water bryozoans from Rhodes, Greece. Palaeontology 38, 771–799.
Mutti, E., Orombelli, G., Pozzi, R., 1970. Geological studies on the Dodecanese Islands (Aegean Sea). IX. Geological map of the island of Rhodes (Greece); explanatory notes. Annales Géologiques des Pays Helléniques 22, 79–226.
O'Neil, J.R., Clayton, R.N., Mayeda, T.K., 1969. Oxygen isotope fractionation in divalent metal carbonates. Journal of Chemical Physics 51, 5547–5558.
Pierre, C., 1999. The oxygen and carbon isotope distribution in the Mediterranean water masses. Marine Geology 153, 41–55.
Polyak, L., Stanovoy, V., Lubinski, D.J., 2003. Stable isotopes in benthic foraminiferal calcite from a river-influenced Arctic marine environment, Kara and Pechora Seas. Paleoceanography 18. http://dx.doi.org/10.1029/2001PA000752.
Regier, H.A., Holmes, J.A., 1990. Influence of temperature changes on aquatic ecosystems: an interpretation of empirical data. Transactions of the American Fisheries Society 119, 374–389.
Romanek, C.S., Jones, D.S., Williams, D.F., Krantz, D.E., Radtke, R., 1987. Stable isotopic investigation of physiological and environmental changes recorded in shell carbonate from the giant clam *Tridacna maxima*. Marine Biology 94, 385–393.
Scheurle, C., Hebbeln, D., 2003. Stable oxygen isotopes as recorders of salinity and river discharge in the German Bight, North Sea. Geo-Marine Letters 23, 130–136.
Smith, A.M., Key Jr., M.M., 2004. Controls, variation, and a record of climate change in detailed stable isotope record in a single bryozoan skeleton. Quaternary Research 61, 123–133.
Thomsen, E., Rasmussen, T.L., Hastrup, A., 2001. Calcareous nannofossil, ostracode and foraminifera biostratigraphy of Plio-Pleistocene deposits, Rhodes (Greece), with a correlation to the Vrica section (Italy). Journal of Micropalaeontology 20, 143–154.
Thunell, R.C., Williams, D.F., 1989. Glacial–Holocene salinity changes in the Mediterranean sea: hydrographic and depositional effects. Nature 338, 493–496.
Williams, D.F., Thunell, R.C., 1979. Faunal and oxygen isotopic evidence for surface water salinity changes during sapropel formation in the eastern Mediterranean. Sedimentary Geology 23, 81–93.
Zachos, J., Pagani, M., Sloan, L., Thomas, E., Billups, K., 2001. Trends, rhythms, and aberrations in global climate 65 Ma to present. Science 292, 686–693.

PUBLICATION 2.2

Freshwater fish $\delta^{18}O$ indicates a Messinian change of the precipitation regime in Central Africa

Olga Otero[1], Christophe Lécuyer[2], François Fourel[2], François Martineau[2], Hassane Taïsso Mackaye[3], Patrick Vignaud[1], and Michel Brunet[4]

[1]iPHEP (Institut de Paléoprimatologie, Paléontologie humaine: Evolution et Paléoenvironnements), UMR CRNS 6046, Université Poitiers, SFA, 40 Avenue du Recteur Pineau, 86 022 Poitiers cedex, France

[2]PEPS (PaléoEnvironnements et PaléobioSphère), UMR CRNS 5125, Université Lyon I, La Doua, 2 Rue Raphaël Dubois, 69 022 Villeurbanne cedex, France

[3]Département de Paléontologie, Université de N'Djaména, BP 1117, N'Djaména, Chad

[4]Collège de France, Chaire de Paléontologie Humaine, iPHEP, UMR CNRS 6046, 3 Rue d'Ulm, 75 231 Paris cedex 05, France

ABSTRACT

Tracking terrestrial environmental change throughout the Neogene is a challenge, notably in areas such as Central Africa where the few available data consist of a few vertebrate fossil assemblages. Here we aim to quantify the evolution of the $\delta^{18}O$ of the main water body between four Neogene wet episodes in the Chad basin, ranging from the Late Miocene to the early Pliocene. The $\delta^{18}O$ of the open water body was inferred from oxygen isotope measurements of phosphate in the apatite of open water fish tooth enamel. The more open the fish habitat, the lower the $\delta^{18}O$, as revealed by the teeth of the large tiger fish (*Hydrocynus*) sampled in the four available Chadian vertebrate fossiliferous areas, i.e., Toros-Menalla (anthracotherid unit), Kossom Bougoudi, Kolle, and Koro Toro, all located in the Djurab Desert (Chad) and dated at 7.04 ± 0.18 Ma, 5.26 ± 0.23 Ma, 3.96 ± 0.48 Ma, and 3.58 ± 0.27 Ma, respectively. The $\delta^{18}O$ values increased by ~2‰ between the two sites having ages that bracket the Messinian time period, and there was a slight increase of ~0.6‰ difference between the three Pliocene sites. These results reflect unambiguously change in the water cycle in Central Africa during the late Neogene, interpreted as a constant drying trend between the four successive wet episodes registered in the Djurab and a shift during the Messinian.

INTRODUCTION

The Neogene has long been recognized as the epoch during which the modern world emerged. However, the record of Neogene environments can be sporadic, depending on the quality of the fossil record and continuity in the sedimentary archives. In Africa, most of the data come from the eastern part of the continent, where nearly continuous rock series contain a rich and extensively studied fossil record, including fossil hominids. In this region the paleontological remains and geochemical proxies indicate an increase in aridity (e.g., Levin et al., 2004; Bobe, 2006) controlled by climate change and tectonic uplift (Bonnefille et al., 2004; deMenocal, 2004; Sépulchre et al., 2006). The comparative lack of records of the Neogene terrestrial environment elsewhere in Africa limits comparison of environmental change at a continental scale. This is notably the case with areas outside a rift context, including Central Africa, the other late Miocene–early Pliocene hominid-bearing region. We evaluated the environmental change recorded in Central Africa during the late Neogene by measuring the $\delta^{18}O$ of the tooth enamel phosphate of freshwater fossil fish associated with four wet Lake Chad phases (Fig. 1).

The oxygen isotope composition of fish bones and teeth depends on both the ambient temperature during skeletal mineralization and the composition of the water (Kolodny et al., 1983; Lécuyer et al., 1993; Vennemann et al., 2001). However, deciphering the role of the ambient temperature and the oxygen isotope composition of the water is a challenge when reconstructing aquatic environments. We first demonstrate our ability to select fossil fish representing a given aquatic environment, since the fish fossils chosen have different oxygen isotopic compositions congruent with their assumed habitat. We selected freshwater fossil fish with a known limited habitat with a small temperature range. Long-term variations in the $\delta^{18}O$ of such fish can therefore be interpreted as $\delta^{18}O$ changes in the continental water body in which they lived.

The habitat of the fossil fish is deduced from the ecology of their modern relatives combined with analysis of the fossil fish assemblage (Otero et al., 2010a). To test whether these criteria allow the sampling of a given aquatic environment, we compare the $\delta^{18}O_{fish}$ in contemporaneous fossil fish selected as inhabitants of three different water masses with distinct hydrological budgets recorded in their $\delta^{18}O$ values, i.e., open waters (minimum values), swamps (maximum ^{18}O enrichment), and marginal waters (intermediate values). Open waters can be sampled by selecting teeth of the large tiger fish (*Hydrocynus* teeth >10 mm high) and puffer beaks (*Tetraodon*) from assemblages with an overrepresentation of open water taxa (Otero et al., 2010a). Large tiger fish are exclusively pelagic, and big puffers live in open waters but frequently enter marginal waters (Bailey, 1994). The $\delta^{18}O_{fish}$ measured in puffers was expected to show the highest values of open water fish. We sampled a swamp in assemblages marked by the overabundance of clariid catfish and bichirs (both of which tolerate anoxic waters) and where fossils are preserved articulated (Otero et al., 2006). The $\delta^{18}O_{fish}$ was measured in the ganoid enamel that covers bichir scales (*Polypterus*). Finally, we sampled marginal waters in a fossil assemblage typical of lake and stream shores with abundant tetras (*Alestes* and *Brycinus*) and juveniles of pelagic fishes. We selected the teeth of young tiger fish (teeth of

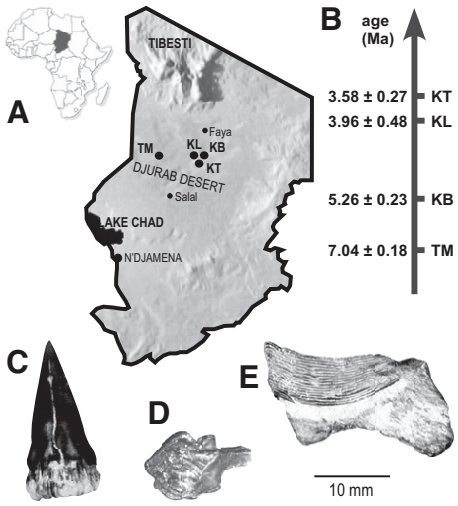

Figure 1. A: Neogene vertebrate evolution study areas in Central Africa, including Toros-Menalla (TM), Kossom Bougoudi (KB), Kolle (KL), and Koro Toro (KT), all located in Djurab Desert, northern Chad. B: Radiochronological ages (from Lebatard et al., 2008). C–E: Fish fossils from TM showing type of material sampled. C: *Hydrocynus* tooth in labial view. D: *Polypterus* scale with ganoin enamel cover in outer view. E: *Tetraodon* dentary showing pile of tooth plates.

Hydrocynus <5 mm high) because juveniles of this pelagic species stay in peripheral waters during their growth phase (Paugy, 1990). In parallel, we sampled and analyzed the $\delta^{18}O$ and δD of modern Chadian waters to document the possible range of values that may occur in different water bodies in the tropics.

To follow the $\delta^{18}O$ variation in open waters during wet episodes in the Chad basin over time, we chose large tiger fish teeth (*Hydrocynus*) within assemblages with an overrepresentation of pelagic taxa in each of the four areas of the Djurab (Fig. 1). The minimal motion of the African plate relative to the equator allowed us to suppose that insolation did not vary significantly in the Chadian region. Biological data support the suggestion that the mean temperature of the open water might have remained relatively constant over time. Fish, and particularly open water fish, tolerate a low range of variation in temperature, e.g., between 20 °C and 25 °C for modern *Hydrocynus* (Froese and Pauly, 2008). In fossils, Böhme (2004) demonstrated the stability of the temperature of the environment in the same fish family (Perciformes Channidae) during the Late Miocene and the Pliocene.

MATERIALS AND METHODS

We sampled different environments in Toros-Menalla because this area offers an exceptionally large number of semicontemporaneous sites of various aquatic environments (Otero et al., 2006, 2010a). Moreover, fish have been actively collected at certain sites at which a substantial amounts of fish teeth and ganoid scales were available (more than 100 scales and teeth at TM90, TM254 and TM377, and more than 400 at TM266). At the younger sites (Fig. 1), we were only able to sample open water environments. Available sedimentological information agrees with the aquatic environments based on ecological inferences about the fish fauna (Schuster, 2002; Vignaud et al., 2002).

We analyzed the oxygen isotope ratios of 39 fish samples (Table DR1 in the GSA Data Repository[1]). The samples consisted of enamel from several manually selected fossils in order to obtain an average of any potential interspecimen isotopic variability, which has often been documented when analyzing fish (Vennemann et al., 2001; Pucéat et al., 2003). To prepare the apatite before oxygen isotope ratio measurement (Appendix DR2), we followed a protocol derived from the original method of Crowson et al. (1991) with slight modifications (Lécuyer et al., 1993; O'Neil et al., 1994; Lécuyer et al., 1998).

[1]GSA Data Repository item 2011143, supplementary information for the fossil samples and geochemical analyses, is available online at www.geosociety.org/pubs/ft2011.htm, or on request from editing@geosociety.org or Documents Secretary, GSA, P.O. Box 9140, Boulder, CO 80301, USA.

We performed the analysis of $\delta^{18}O$ from fossil apatites (Appendix DR2) and in modern waters (Appendix DR3) at the Unité Mixte Recherche Centre National de la Recherche Scientifique 5125 'PEPS' laboratory (University Lyon 1). We assumed that the primary isotopic record in our samples was not significantly affected by diagenetic processes (Appendix DR4).

RESULTS

Oxygen Isotope Ratios of Phosphate from Fish Remains

The fish data set was characterized by a large range of $\delta^{18}O$ values (from 15.9‰ to 20.9‰). $\delta^{18}O$ values appear tightly controlled according to the aquatic environment; this is clearly emphasized by the distribution of data corresponding to the different sites of the anthracotherid unit at Toro-Menalla (Fig. 2). Fish that lived in open waters had a mean $\delta^{18}O$ value of 17.1‰ ± 0.8‰ (n = 13), which was significantly lower (permutation t-test, $p < 0.05$) than the mean value ($\delta^{18}O$ = 19.3‰ ± 0.9‰; n = 8) obtained for fish that lived in marginal waters or swamps (Fig. 2). Moreover, fish that lived in open waters displayed $\delta^{18}O$ that increased by ~2‰ between Toros-Menalla and Kossom Bougoudi (Fig. 3), the ages of which bracket the Messinian (7.25 to 5.33 Ma; Gradstein et al., 2004). Samples younger than 5 Ma had oxygen isotope ratios that resembled those analyzed in Kossom Bougoudi. However, there was a slight increase with time by ~0.6‰ of mean $\delta^{18}O$ values (Fig. 3), although this was associated with relatively large standard deviations in the range 0.4‰–0.8‰ (Table DR1).

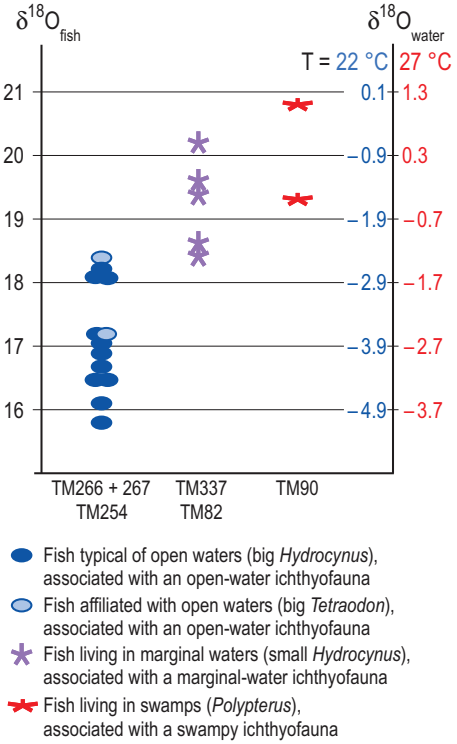

Figure 2. $\delta^{18}O_{fish}$ of teeth and scales of fish from contemporaneous sites of Toros-Menalla (TM, Djurab Desert, northern Chad) that correspond to different aquatic environments. Values of $\delta^{18}O_{water}$ of corresponding water are given for two mean temperatures, 22 °C and 27 °C; fractionation equation used is $\delta^{18}O_{water} = \delta^{18}O_{fish} - 25.9 + T/4.38$ (from Kolodny et al, 1983). To obtain given $\delta^{18}O_{fish}$, increase of ~4.4 °C implies increase in $\delta^{18}O_{water}$ of 1‰.

Oxygen and Hydrogen Isotope Ratios of Modern Chadian Waters

The present-day waters collected at 13°N on the Sahelian border and at 16°N in the Toros-Menalla area displayed oxygen and hydrogen isotope ratios that respectively ranged from −7.7‰ to 26.1‰ and from −54.4‰ to 100.6‰. These data define a straight line ($r^2 = 0.98$) with a slope of 4.7 that crosscuts the meteoric water line at isotopic coordinates corresponding to the sample made in a well at 13°N, which had the lowest $\delta^{18}O$ and δD values (Appendix DR3).

DISCUSSION

$\delta^{18}O$ of Fish and the Record of their Living Environment

In the Toros-Menalla area, fish from open waters, marginal waters, and swamps coexisted (Fig. 2). *Polypterus* from the swamp at TM90 had $\delta^{18}O_{fish}$ values as much as 5‰ higher than those recorded for *Hydrocynus* from the open waters of sites TM266 and TM267 (Fig. 2). If temperature was the only operating variable, then fish from swamps would have lived in waters with a mean temperature of ~20 °C lower than those of the lake, according to the slope of the fractionation equation determined by Kolodny et al. (1983). This interpretation underlines the great importance of the oxygen isotope composition of the water in the results obtained from fish apatite. Swamps and ponds are shallow reservoirs that are restricted in size and are relatively isolated from the open waters. By exposing a greater surface area relative to volume, they undergo more intense evaporation and are ^{18}O enriched compared to open waters. Moreover, their temperature is more variable than in large reservoirs but the mean temperature is similar or slightly higher. In agreement with this, fish living in swamps tolerate a wider range of temperatures than those from open waters, between ~20 °C and 30 °C instead of 20 °C and 25 °C (Froese and Pauly, 2008). Thus, if temperature played a role, it would be opposite to the ^{18}O enrichment of waters in closed environments and ~1‰ by 5 °C according to the equation of Kolodny et al. (1983) (Fig. 2). This leads to a probable underestimate of the ^{18}O enrichment in swamps if the values in the

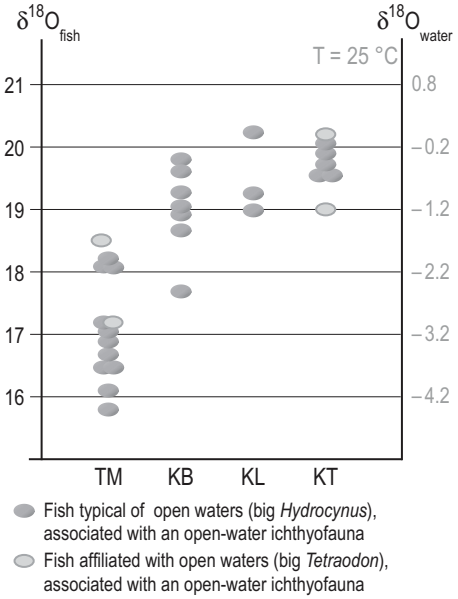

Figure 3. $\delta^{18}O_{fish}$ of open water fish teeth from Toros-Menalla (TM), Kossom Bougoudi (KB), Kolle (KL), and Koro Toro (KT), all located in Djurab Desert, northern Chad. Values of $\delta^{18}O_{water}$ of corresponding water are given for 25 °C according to fractionation equation $\delta^{18}O_{water} = \delta^{18}O_{fish} - 25.9 + T/4.38$ (from Kolodny et al., 1983).

fish apatite are interpreted as depending on the $\delta^{18}O_{water}$ only. Therefore, the high $\delta^{18}O_{fish}$ values of fish that lived in small aqueous reservoirs are interpreted to reflect more extensive evaporation when compared to the larger reservoir of open waters. A 5‰ variation in the $\delta^{18}O_{water}$ between the different reservoirs is not surprising given the isotopic composition of modern waters at tropical latitudes. For example, ^{18}O enrichment of waters by several parts per mil as a result of evaporation processes has been documented at similar latitudes in the Niger inland delta (Gourcy et al., 2001). Moreover, the δD and $\delta^{18}O$ values of Chad waters collected in this study are along a line with a slope of 4.7 that is typical of residual waters that undergo evaporation (Gat and Gonfiantini, 1981) (Appendix DR3). Extreme evaporation in ponds can result in exceptional deuterium and ^{18}O enrichment of these residual waters (Appendix DR3). The observed 5‰ variation in the $\delta^{18}O$ of fossil fish that lived in different environments can therefore be explained by the varying evaporation rates of the related water bodies. This demonstrates that we are able to sample fish fossils that record the $\delta^{18}O$ of a given water body by applying paleoecological and paleoenvironmental criteria.

$\delta^{18}O$ of Fish and the Onset of Aridity in the Pliocene in Central Africa

In Central Africa, only the four Chadian fossiliferous areas sampled (Fig. 1) provide windows onto the diversity and environments of the Neogene, ranging from the Late Miocene to the early Pliocene. The paleoenvironmental reconstructions indicate that mosaic landscapes associated with grassland, wooded savannah, and gallery forest bordered diverse aquatic environments (Brunet et al., 1995, 1997, 1998, 2000; Vignaud et al., 2002; Otero et al., 2009, 2010a, 2010b). The fossiliferous layers in the four Chadian areas correspond to lacustrine, perilacustrine, and fluvial deposits associated with wet episodes in Central Africa (Sépulchre et al., 2008). The persistent occurrence over time of a fish such as *Hydrocynus* indicates that the open waters of the wet episodes recorded in the Djurab Desert outcrops most likely kept their mean water temperature fairly constant. In this stable intracratonic basin, the increasing $\delta^{18}O$ measured in apatite from open water fish of wet episodes in the Lake Chad basin might be reasonably attributed to an aridification trend that affected Central Africa during the late Neogene with a marked shift around the Messinian period. The fact that some mammal species from the youngest areas (Koro Toro and Kolle) present stronger affinities with open environments, e.g., *Ceratotherium* cf. *praecox* of Koro Toro (Brunet et al., 1995), than any other taxon known from the oldest areas (Toros-Menalla) might result from such an environmental change.

However, these first data sets from Central Africa on the late Neogene environmental transition on continents (e.g., Van Zinderen and Mercer, 1986; Cerling et al., 1997) remain difficult to interpret. As exemplified in eastern Africa (e.g., Bonnefille et al., 2004; deMenocal, 2004; Sépulchre et al., 2006), interdependent climatic and geodynamic modification processes might be invoked to explain such an evolution of the $\delta^{18}O$ of the surface water recorded in Chad over time, including aridification. In the tropics, the $\delta^{18}O$ is controlled by the rainout of atmospheric moisture locally and during transport. Wet episodes to which those in Chad may be related are generally explained by a northward shift of the Intertropical Convergence Zone that reinforces the summer monsoon over tropical Africa (Braconnot et al., 2000). According to Sépulchre et al. (2008), the massive uplift in eastern Africa during the Neogene was responsible for the reorganization of atmospheric circulation. With a low topographic barrier, zonal circulation was associated with east-west moisture transport and strong precipitation. However, high topography would have favored aridity and local recycling of the water, as modeled for the last mega–Lake Chad phase (Sépulchre et al., 2006). At least part of the increase in $\delta^{18}O$ values (by ~2‰ between 7 Ma and 5 Ma) in Chad might be related to the eastern African uplift and suggests that the relief reached a critical height in terms of climatic impact during the Messinian. Other factors may have also played a role, notably the Late Miocene shift recorded in the South Atlantic thermohaline circulations that may have provided the initial conditions for early Pliocene climatic warmth between 6.6 Ma and 6 Ma (Billups, 2002). An amplifying effect of the Messinian salinity crisis may also be invoked, as it is known to have provoked aridity in the terrestrial environment in the eastern Mediterranean Sea (Zazzo et al., 2002, Fauquette et al., 2006).

ACKNOWLEDGMENTS

We thank the Chadian authorities (University N'Djamena, the Ministère de l'Education Nationale et de la Recherche [MENR]; and the National Centre for Support to Research [CNAR]) and French authorities (Ministère de l'Enseignement Supérieur et de la Recherche [MESR] Centre National de la Recherche Scientifique [CNRS]; Université Poitiers; Ministère des Affaires Ètrangères et Européennes [MAEE]) for field work support, and the Agence Nationale de la Recherche (Projet ANR 05-BLAN-0235) and the U.S. National Science Foundation (Revealing the Hominid Origin Initiative) programs for study support. We extend our gratitude to all members of the Mission Paléoanthropologique Franco-Tchadienne and particularly to Franck Guy for his comments.

REFERENCES CITED

Bailey, R.G., 1994, Guide to the fishes of the River Nile in the Republic of the Sudan: Journal of Natural History, v. 28, p. 937–970, doi: 10.1080/00222939400770501.

Billups, K., 2002, Late Miocene through early Pliocene deep water circulation and climate change viewed from sub-Antarctic South Atlantic: Palaeogeography, Palaeoclimatology, Palaeoecology, v. 185, p. 287–307, doi: 10.1016/S0031-0182(02)00340-1.

Bobe, R., 2006, The evolution of arid ecosystems in eastern Africa: Journal of Arid Environments, v. 66, p. 564–584, doi: 10.1016/j.jaridenv.2006.01.010.

Böhme, M., 2004, Migration history of air-breathing fishes reveals Neogene atmospheric circulation patterns: Geology, v. 32, p. 393–396, doi: 10.1130/G20316.1.

Bonnefille, R., Potts, R., Chalié, F., Jolly, D., and Peyron, O., 2004, High-resolution vegetation and climate change associated with Pliocene *Australopithecus afarensis*: National Academy of Sciences Proceedings, v. 101, p. 12125–12129, doi: 10.1073/pnas.0401709101.

Braconnot, P., Joussaume, S., de Noblet, N., and Ramstein, G., 2000, Mid-Holocene and last glacial maximum African monsoon changes as simulated within the Paleoclimate Modeling Intercomparison Project: Global and Planetary Change, v. 26, p. 51–66, doi: 10.1016/S0921-8181(00)00033-3.

Brunet, M., Beauvilain, A., Coppens, Y., Heintz, E., Moutaye, A.H.E., and Pilbeam, D., 1995, The first australopithecine 2500 kilometers west of the Rift Valley (Chad): Nature, v. 378, p. 273–275, doi: 10.1038/378273a0.

Brunet, M., Beauvilain, A., Geraards, D., Guy, F., Kasser, M., Mackaye, H.T., MacLatchy, L., Mouchelin, G., Sudre, J., and Vignaud, P., 1997, Tchad: un nouveau site à Hominidés Pliocène: Comptes Rendus de l'Académie des Sciences, sér. 2, Sciences de la Terre et des Planètes, v. 324, p. 341–345.

Brunet, M., Beauvilain, A., Geraards, D., Guy, F., Kasser, M., Mackaye, H.T., MacLatchy, L.,

Mouchelin, G., Sudre, J., and Vignaud, P., 1998, Tchad: découverte d'une faune de mammifères du Pliocène inférieur: Comptes Rendus de l'Académie des Sciences, sér. 2, Sciences de la Terre et des Planètes, v. 326, p. 153–158.

Brunet, M., and 40 others, 2000, Chad: Discovery of a vertebrate fauna close to the Mio-Pliocene boundary: Journal of Vertebrate Paleontology, v. 20, p. 205–209, doi: 10.1671/0272-4634(2000)020[0205:CDOAVF]2.0.CO;2.

Cerling, T.E., Harris, J.M., MacFadden, B.J., Leakey, M.G., Quade, J., Eisenmann, V., and Ehleringer, J.R., 1997, Global vegetation change through the Miocene/Pliocene boundary: Nature, v. 389, p. 153–158, doi: 10.1038/38229.

Crowson, R.A., Showers, W.J., Wright, E.K., and Hoering, T.C., 1991, A method for preparation of phosphate samples for oxygen analysis: Analytical Chemistry, v. 63, p. 2397–2400, doi: 10.1021/ac00020a038.

deMenocal, P.B., 2004, African climate change and faunal evolution during the Plio-Pleistocene Ethiopia: Earth and Planetary Science Letters, v. 220, p. 3–24, doi: 10.1016/S0012-821X(04)00003-2.

Fauquette, S., and 12 others, 2006, How much did climate force the Messinian salinity crisis? Quantified climatic conditions from pollen records in the Mediterranean region: Palaeogeography, Palaeoclimatology, Palaeoecology, v. 238, p. 281–301, doi: 10.1016/j.palaeo.2006.03.029.

Froese, R., and Pauly, D., eds., 2008, FishBase: A global information system on fishes: www.fishbase.org/home.htm.

Gat, J.R., and Gonfiantini, R., eds., 1981, Stable isotope hydrology: Deuterium and oxygen-18 in the water cycle: IAEA Technical Report Series 210: Vienna, Austria, International Atomic Energy Agency, 339 p.

Gourcy, L., Aranyossy, J.F., Olivry, J.C., and Zuppi, G.M., 2001, Evolution spatio-temporelle des teneurs isotopiques (δ^2H-δ^{18}O) des eaux de la cuvette lacustre du fleuve Niger (Mali): Comptes Rendus de l'Académie des Sciences, sér. 2, Sciences de la Terre et des Planètes, v. 331, p. 701–707.

Gradstein, F.M., and 38 others, 2004, A geologic time scale 2004: Cambridge University Press, 589 p.

Kolodny, Y., Luz, B., and Navon, O., 1983, Oxygen isotope variations in phosphate of biogenic apatites: I. Fish bone apatite, rechecking the rules of the game, Ethiopia: Earth and Planetary Science Letters, v. 64, p. 398–404, doi: 10.1016/0012-821X(83)90100-0.

Lebatard, A.-E., and 13 others, 2008, Cosmogenic nuclide dating of *Sahelanthropus tchadensis* and *Australopithecus bahrelghazali*: Mio-Pliocene hominids from Chad: National Academy of Sciences Proceedings, v. 105, p. 3226–3231, doi: 10.1073/pnas.0708015105.

Lécuyer, C., Grandjean, P., O'Neil, J.R., Capetta, H., and Martineau, F., 1993, Thermal excursions in the ocean at Cretaceous–Tertiary boundary (northern Morocco): δ^{18}O record of phosphatic fish debris: Palaeogeography, Palaeoclimatology, Palaeoecology, v. 105, p. 235–243, doi: 10.1016/0031-0182(93)90085-W.

Lécuyer, C., Grandjean, P., Barrat, J.A., Nolvak, J., Emig, C., Paris, F., and Robardet, M., 1998, δ^{18}O and REE contents of phosphatic brachiopods: A comparison between modern and lower Paleozoic populations: Geochimica et Cosmochimica Acta, v. 62, p. 2429–2436, doi: 10.1016/S0016-7037(98)00170-7.

Levin, N.E., Quade, J., Simpson, S.W., Semaw, S., and Rogers, M., 2004, Isotopic evidence from Plio-Pleistocene environmental change at Gona, Ethiopia: Earth and Planetary Science Letters, v. 219, p. 93–110, doi: 10.1016/S0012-821X(03)00707-6.

O'Neil, J.R., Roe, L.J., Reinhard, E., and Blake, R.E., 1994, A rapid and precise method of oxygen isotope analysis of biogenic phosphate: Israel Journal of Earth Sciences, v. 43, p. 203–212.

Otero, O., Likius, A., Vignaud, P., and Brunet, M., 2006, A new polypterid fish: *Polypterus faraou* sp. nov. (Cladistia, Polypteriformes) from the Late Miocene, Toros Menalla, Chad: Linnean Society Zoological Journal, v. 146, p. 227–237, doi: 10.1111/j.1096-3642.2006.00201.x.

Otero, O., Pinton, A., Mackaye, H.T., Likius, A., Vignaud, P., and Brunet, M., 2009, First description of a Pliocene ichthyofauna from Central Africa (site KL2, Kolle area, Eastern Djurab, Chad): What do we learn?: African Journal of Earth Science, v. 54, p. 62–74, doi: 10.1016/j.jafrearsci.2009.03.004.

Otero, O., Pinton, A., Mackaye, H.T., Likius, A., Vignaud, P., and Brunet, M., 2010a, The fish assemblage associated with the Late Miocene Chadian hominid (Toros–Menalla, western Djurab), and its palaeoenvironmental significance: Palaeontographica Abteilung A, v. 292, p. 21–51.

Otero, O., Pinton, A., Mackaye, H.T., Likius, A., Vignaud, P., and Brunet, M., 2010b, The Late Pliocene ichthyofauna from Koro-Toro, eastern Djurab, Chad: Geobios, v. 43, p. 241–251, doi: 10.1016/j.geobios.2009.10.003.

Paugy, D., 1990, Characidae, *in* Lévêque, C., et al., eds., Brackish and fresh water fish faunas from western Africa (in French): MRAC-Orstom, Collection Faune Tropicale, p. 195–236.

Pucéat, E., Lécuyer, C., Sheppard, S.M.F., Dromart, G., Reboulet, S., and Grandjean, P., 2003, Thermal evolution of Cretaceous Tethyan marine waters inferred from oxygen isotope composition of fish tooth enamels: Paleoceanography, v. 18, p. 7–12, doi: 10.1029/2002PA000823.

Schuster, M., 2002, Sédimentologie et paléoécologie des séries à vertébrés du paléolac Tchad depuis le Miocène supérieur [Ph.D. thesis]: Strasbourg, France, Université Strasbourg.

Sépulchre, P., Ramstein, G., Fluteau, F., Schuster, M., Tiercelin, J.J., and Brunet, M., 2006, Tectonic uplift and eastern Africa aridification: Science, v. 313, p. 1419–1423, doi: 10.1126/science.1129158.

Sépulchre, P., Schuster, M., Krinnezr, J., Girard, P., Vignaud, P., and Brunet, M., 2008, Evolution of Lake Chad Basin hydrology during the mid-Holocene: A preliminary approach from lake to climate modelling: Global and Planetary Change, v. 61, p. 41–48, doi: 10.1016/j.gloplacha.2007.08.010.

Van Zinderen, E.M., and Mercer, J.H., 1986, Major late Cainozoic climatic events and palaeoenvironmental changes in Africa viewed in a world wide context: Palaeogeography, Palaeoclimatology, Palaeoecology, v. 56, p. 217–235, doi: 10.1016/0031-0182(86)90095-7.

Vennemann, T.W., Hegner, E., Cliff, G., and Benz, G.W., 2001, Isotopic composition of recent shark teeth as a proxy for environmental conditions: Geochimica et Cosmochimica Acta, v. 65, p. 1583–1599, doi: 10.1016/S0016-7037(00)00629-3.

Vignaud, P., and 19 others, 2002, Geology and palaeontology of the upper Miocene Toros–Menalla fossiliferous area, Djurab Desert, northern Chad: Nature, v. 418, p. 152–155, doi: 10.1038/nature00880.

Zazzo, A., Mariotti, A., Lécuyer, C., and Heintz, E., 2002, Intra-tooth isotope variations in Late Miocene bovid enamel from Afghanistan: Paleobiological, taphonomical, and climatic implications: Palaeogeography, Palaeoclimatology, Palaeoecology, v. 186, p. 145–161, doi: 10.1016/S0031-0182(02)00449-2.

Manuscript received 12 March 2010
Revised manuscript received 7 December 2010
Manuscript accepted 8 December 2010

Printed in USA

Quaternary Research 75 (2011) 605–613

Contents lists available at ScienceDirect

Quaternary Research

journal homepage: www.elsevier.com/locate/yqres

Late Pleistocene climatic change in the French Jura (Gigny) recorded in the $\delta^{18}O$ of phosphate from ungulate tooth enamel

Magali Fabre [a], Christophe Lécuyer [b,*], Jean-Philip Brugal [a], Romain Amiot [b], François Fourel [b], François Martineau [b]

[a] UMR CNRS 6636, Maison Méditerranéenne des Sciences de l'Homme, 5 rue du Château de l'Horloge, BP 647, 13094, Aix-en-Provence cedex 2, France
[b] UMR CNRS 5125 "PaléoEnvironnements & PaléobioSphère", Université Lyon 1, Lyon, Campus de la Doua, F-69622 Villeurbanne, France

ARTICLE INFO

Article history:
Received 7 June 2010
Available online 5 April 2011

Keywords:
Oxygen isotope
Phosphate
Ungulate
Pleistocene
Climate

ABSTRACT

Oxygen isotope compositions of phosphate in tooth enamel from large mammals (i.e. horse and red deer) were measured to quantify past mean annual air temperatures and seasonal variations between 145 ka and 33 ka in eastern France. The method is based on interdependent relationships between the $\delta^{18}O$ of apatite phosphate, environmental waters and air temperatures. Horse (*Equus caballus germanicus*) and red deer (*Cervus elaphus*) remains have $\delta^{18}O$ values that range from 14.2‰ to 17.2‰, indicating mean air temperatures between 7°C and 13°C. Oxygen isotope time series obtained from two of the six horse teeth show a sinusoidal-like signal that could have been forced by temperature variations of seasonal origin. Intra-tooth oxygen isotope variations reveal that at 145 ka, winters were colder (-7 ± 2°C) than at present (3 ± 1°C) while summer temperatures were similar. Winter temperatures mark a well-developed West–East thermal gradient in France of about −9°C, much stronger than the −4°C difference recorded presently. Negative winter temperatures were likely responsible for the extent and duration of the snow cover, thus limiting the food resources available for large ungulates with repercussions for Neanderthal predators.

Introduction

The Late Pleistocene is characterized by marked and regular climatic cycles. Five Heinrich events (H6, H5, H4, H3 and H2) have been identified during marine oxygen isotope stages OIS4 and OIS3 (Heinrich, 1988). These abrupt cooling phenomena are thought to have resulted from the melting of ice in the Atlantic Ocean, thus reducing water density. As a result, thermohaline circulation changed to lower latitudes, leading to cooling in more northern latitudes. On the other hand, interstades have also been recognized such as the Moershoofd, Hengelo or Denekamp warmer periods. This succession from cold to warmer climate periods played an important role on species evolution and distribution. As a special case, it is largely debated whether climate and environment could have exerted a significant control on the replacement of Neanderthal by *Homo sapiens* in Europe during the Late Pleistocene (Gamble, 1995, 1999; D'Errico and Sanchez-Goni, 2003; Finlayson, 2004). Indeed, human behavior is closely related to food resources, which are themselves dependent on the climate mode (D'Errico and Sanchez-Goni, 2003; Finlayson, 2004). Methods for palaeoclimate reconstructions generally depend on proxies such as pollen spectra (De Beaulieu and Reille, 1984; Guiot et al., 1989) or mammal associations (Chaline, 1972; Andrews et al., 1979; Delpech et al., 1983; Legendre, 1986). The geochemical methods of air temperature determination most commonly used in continental environments involve the stable isotope analysis of speleothems, tree rings and mammals bones and teeth (e.g. Ayliffe et al., 1992; Bar-Matthews et al., 1997; Feng et al., 1999). The $\delta^{18}O$ value of tooth enamel phosphate from mammal is a function of the $\delta^{18}O$ value of the animal's body water as well as of its body temperature (Kolodny et al., 1983; Longinelli, 1984; Luz et al., 1984). The $\delta^{18}O$ value of body water is related to the $\delta^{18}O$ value of ingested water and to the animals' ecology and physiology. The main source of ingested oxygen is drinking or plant water, which is meteoric water or derived from it (D'Angela and Longinelli, 1990; Kohn et al., 1996). As the $\delta^{18}O$ value of meteoric water depends on climatic parameters such as air temperature, hygrometry and amount of precipitation (Dansgaard, 1964; Grafenstein et al., 1996), mammals thus indirectly record in their phosphatic tissues the climatic conditions of their living environment. Several paleoclimate studies have been successful in analyzing the oxygen isotope composition of large mammals such as mammoths, horses, deer and bison (Bryant et al., 1994; Sanchez Chillon et al., 1994; Delgado Huertas et al., 1997; Genoni et al., 1998; Koch et al., 1998; Sponheimer and Lee-Thorp, 2001; Higgings and MacFadden, 2004; Sharma et al., 2004; Bernard et al., 2009). Paleoclimatic interpretations of oxygen isotope data obtained from rodents teeth have been proposed even though they remain the subjects of debate and controversy (Longinelli et al., 2003; Navarro et al., 2004; Héran et al., 2010). Rodent

* Corresponding author.
E-mail address: clecuyer@univ-lyon1.fr (C. Lécuyer).

0033-5894/$ – see front matter © 2011 University of Washington. Published by Elsevier Inc. All rights reserved.
doi:10.1016/j.yqres.2011.03.001

remains are abundant and provide a high temporal resolution. However, the use of oxygen isotope compositions as a proxy of the composition of ingested water is limited by 1) a deposit location that can be different from the living area because of the large hunting domain of their predatory birds, 2) a short mineralization time at the seasonal scale, 3) a systematic use of the M1 tooth as the only diagnosis of species determination, and 4) the existence of two oxygen isotope fractionation equations that lead to significant differences in the quantification of the isotopic compositions of waters (Longinelli et al., 2003; Navarro et al., 2004). Large ungulate grazers such as horses present sizable advantages for reconstructing the $\delta^{18}O$ of past waters which are their regular presence throughout the Pleistocene, a source of drinking waters that is mainly meteoric waters reflecting mean air temperatures at mid-latitudes (Sanchez Chillon et al., 1994; Sharp and Cerling, 1998; Higgings and MacFadden, 2004), a high-crown tooth (i.e. hypsodonty) characterized by a multi-annual mineralization time (Bryant et al., 1996; Higgings and MacFadden, 2004), and a tight prey–predator relationship providing the climatic context of human occupations (Stiner, 1994; Gamble, 1999).

Meaning and validity of the oxygen isotope composition of rodent teeth in terms of climatic records (paleotemperatures, paleohydrology) can be assessed by comparing their isotopic compositions to those of large mammals co-occurring in the same sedimentary level. Therefore, we propose to study herbivore species from La Baume de Gigny Cave (BGC), French Jura, where sediments have been deposited from −145 ka to −33 ka (Campy et al., 1989). Age of the lower level of the cave is contemporaneous to level 4 of the Coudoulous I deposit in the southwestern part of France (Lot) where mean air temperatures and seasonal variations have been already inferred from the $\delta^{18}O$ of tooth enamel phosphate from *Bison priscus* (Bernard et al., 2009). At BGC, Navarro et al. (2004) have calculated air temperatures by using the $\delta^{18}O$ values of rodent teeth, however the large isotopic variations observed within sedimentary levels have not received satisfactory explanations so far. In this study, we performed oxygen isotope measurements of phosphate from 20 horse tooth enamels and four red deer tooth enamels to establish:

– a mean air temperature curve over about 100 ka within the middle Palaeolithic based on large mammals, which is then compared to temperatures inferred from the $\delta^{18}O$ values of rodent teeth. The validity of both isotopic records is discussed in terms of the most appropriate use of available oxygen isotope fractionation equations.

– an east–west climatic gradient in France at ca. 145 ka by comparing the calculated mean air temperatures and seasonality between the Coudoulous I (Lot) and BGC (Jura) sites.

Geological setting

The BGC, located in the French Jura, is a karstic cave (Fig. 1) with a 12 m thick stratigraphic sequence (Campy et al., 1989). The sediments are subdivided into 31 layers organized in three complexes according to Campy et al. (1989). Horse and red deer teeth come from the Middle Complex with the top (level VIII) dated by radiocarbon isotopes providing ages of 33.4 ± 1.4 cal ka BP and 32.2 ± 1.4 cal ka BP (Evin, 1989). Migration of the steppe lemming *Lagurus lagurus* was also used to estimate an age of about 60 ka (Campy and Chaline, 1993) for the bottom sequence (level XX). A speleothem located at the limit between the Middle Complex and the Lower Complex was dated at 145 ± 15 ka using the $^{234}U/^{230}Th$ method and at 145^{+66}_{-45} ka using the Electron Spin Resonance (ESR) method (Evin, 1989). Levels thickness range from 0.15 m to 0.50 m, which most likely correspond to a maximum time span of 3.5 ka per level. Flint tools and bone remains

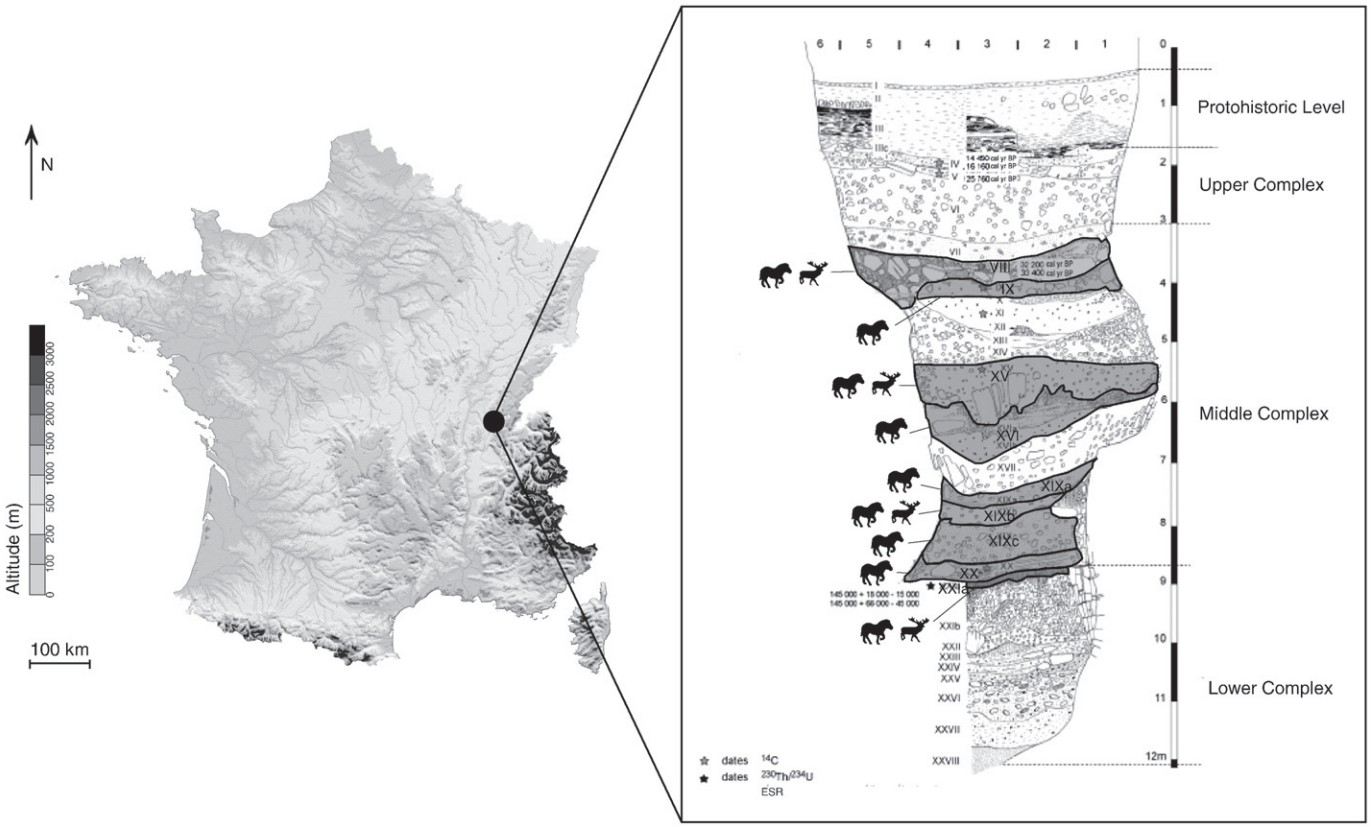

Fig. 1. Geographic location of the Late Pleistocene cave of "La Baume de Gigny" and the stratigraphic sequence of its sedimentary deposits with sampled levels (from Campy et al., 1989). Roman number: level number; Grey star: radiocarbon date; Black star: Electron Spin Resonance date or U^{234}/Th^{230} date. Map from Geoatlas France vectorielle 2, 1997.

occur together within every level suggesting recurrent human occupations of the cave. Zooarchaeological analyses suggest that the studied layers correspond to anthropogenic deposits. Indeed, horses and red deer were hunted by Neanderthals whose presence in the site decreased throughout levels XX to XV (Fabre, 2010).

Sample collection and sampling strategy

Twenty horse (*Equus caballus germanicus*) and four red deer (*Cervus elaphus*) teeth have been sampled from nine levels in BGC, selected as a function of their maximum crown conservation, which means molars of low wear from young individuals. All the teeth are isolated teeth, which do not belong to the same individual. Sample nomenclature corresponds to the tooth position in the dental sequence (Smith and Dodson, 2003) followed by the excavation number of the specimen (Table 1). Enamel powder samples were collected using a micro-drill equipped with a diamond-studded drill bit. Examination of samples was done to check that enamel samples were not contaminated by dentine. Two sampling strategies have been performed; the first consists in making grooves drilled perpendicularly to the tooth growth axis from the cervix to the apex of the tooth crown on the highest and best preserved cuspid. This sampling method is similar to the conventional method of enamel extraction (Bryant et al., 1996; Fricke and O'Neil, 1996) used for the reconstruction of seasonal temperature variations (Bernard et al., 2009). The second one consists in continuous sampling of enamel from the base to the apex of each tooth for obtaining average $\delta^{18}O_p$ values. Such kind of whole-tooth analysis may integrate, and mask, patterns of short-term (e.g. seasonal) changes because tooth formation may span from several months to a few years.

Table 1
Oxygen isotope compositions of red deer and horse tooth phosphates form the Late Pleistocene site "La Baume de Gigny" reported along with the corresponding sample number, tooth nature and the sedimentary level from which they were recovered. $\delta^{18}O_w$ values of ingested water were calculated using the phosphate–water oxygen isotope fractionation equations of Sanchez Chillon et al. (1994) for horses and D'Angela and Longinelli (1990) for red deer.

Level	Species	Tooth	Excavation number	$\delta^{18}O_p$ (‰ V-SMOW)	$\delta^{18}O_w$ (‰ V-SMOW)
VIII	*Equus caballus*	LR M2	28 F2	17.2	−6.5
VIII	*Cervus elaphus*	UP M2	82	16.0	−8.5
IX	*Equus caballus*	LR P4	812 GH	16.4*	−7.6
XV	*Equus caballus*	LR M3	255 G3	14.2	−10.6
XV	*Equus caballus*	UP P4	71 F2	14.2*	−10.6
XV	*Cervus elaphus*	LR M3	572	14.2	−10.0
XVI	*Equus caballus*	LR P3	157 F3	14.7	−9.9
XIXa	*Equus caballus*	LR M3	88 G3	15.2	−9.2
XIXa	*Equus caballus*	LR M2	120 G4	14.1	−10.7
XIXb	*Equus caballus*	UP M2	264 F3	15.1	−9.4
XIXb	*Equus caballus*	LR M3	267 F3	14.7	−9.9
XIXb	*Equus caballus*	LR P4	357 G3	14.8	−9.8
XIXb	*Cervus elaphus*	LR M1	128 G4	15.5	−8.9
XIX-c	*Equus caballus*	LR M1-2	623 GH	15.2	−9.2
XIX-c	*Equus caballus*	UP M3	317 G3	14.2	−10.6
XIX-c	*Equus caballus*	UP P4	307 E2	15.5*	−8.8
XIX-c	*Equus caballus*	UP P4	376 G3	14.5	−10.2
XIX-c	*Equus caballus*	LR M1	295 F3	15.5	−8.8
XIX-c	*Equus caballus*	UP M1	385 G3	14.9*	−9.7
XX	*Equus caballus*	UP P4	672 GH	15.0	−9.5
XX	*Equus caballus*	UP P4	245 H4	14.8	−9.8
XXIa	*Equus caballus*	LR M2	183 H3	15.6*	−8.7
XXIa	*Equus caballus*	UP P4	396 F3	15.8*	−8.4
XXIa	*Cervus elaphus*	LR M1	728 GH	15.7	−8.7

LR: lower; UP: upper; P: premolar tooth; M: molar tooth.
* Average $\delta^{18}O_p$ values calculated from intra-tooth ones given in Table 2.

Analytical techniques

Enamel samples have been treated following the wet chemistry protocol described by Crowson et al. (1991) and slightly modified by Lécuyer et al. (1993). This protocol consists of the isolation of phosphate from apatite as Ag_3PO_4 (Silver Phosphate) crystals using acid dissolution and anion-exchange resin. As it was already presented in several publications (e.g. Lécuyer et al., 1998, 2007; Daux et al., 2008), the wet chemical procedure used for the bulk tooth enamel samples (about 20 mg of powder) is not described here in detail. In the case of intra-tooth sampling, 2 to 3 mg of enamel powder were dissolved in 1 mL of 2 M HF (Fluohydric Acid) overnight. The CaF_2 (Calcium Fluoride) residue was separated by centrifugation and the solution was neutralized by adding 1 mL of 2 M KOH (Potassium Hydroxide). One and a half mL of Amberlite™ anion exchange resin was added to the solution to separate the PO_4^{3-} (Phosphate) ions. After 24 h, the solution was removed and the resin was eluted with 6 mL of 0.1 M NH_4NO_3 (Ammonium Nitrate). After 4 h, 0.1 mL of NH_4OH (Ammonium Hydroxyde) and 3 mL of an ammoniacal solution of $AgNO_3$ (Silver Nitrate) were added and the samples were placed in a warmed bath at 70°C for 6 h allowing for the precipitation of Ag_3PO_4 crystals.

For the macro-samples, the oxygen isotope data were obtained according to a "conventional off-line" method. Aliquots of 8 mg of silver phosphate along with 0.5 mg of pure graphite were weighed into tin reaction capsules and transferred to quartz tubes and degassed for 30 min at 80°C in vacuum. Silver phosphate was reduced to carbon dioxide at a temperature of 1100°C following the protocol of Lécuyer et al. (1998) adapted from O'Neil et al. (1994). The oxygen isotope ratio of the gas was measured with a PRISM II™ mass spectrometer in dual inlet mode. Isotopic compositions are quoted in the standard delta notation relative to V-SMOW. The reproducibility of measurements carried out on tooth enamel samples is better than 0.2‰ (1σ). Silver phosphate precipitated from standard SRM 120c (Miocene phosphorite from Florida) was repeatedly analyzed ($\delta^{18}O = 21.68 \pm 0.18$‰; $n = 24$) along with the silver phosphate samples. This mean $\delta^{18}O$ value for NBS120c is close to that obtained by Lécuyer (2004) using a BrF_5 method ($\delta^{18}O = 21.64 \pm 0.18$; $n = 20$). It is also consistent with other statistics published by O'Neil et al. (1994) and Fricke et al. (1998) who recommended a $\delta^{18}O$ value of 21.8 ± 0.25‰ as well as the value of 21.5 ± 0.2‰ given by Vennemann and Hegner (1998).

For the micro-samples, aliquots of 400–500 μg of silver phosphate samples were mixed with 500 μg of nickelized carbon in silver foil capsules. Pyrolysis was performed at 1270°C using a EuroVector EA3028-HT™ elemental analyzer. A ceramic reaction tube was packed with glassy carbon in the presence of nickelized graphite to generate CO that was then transferred to a GV IsoPrime™ mass spectrometer in continuous flow mode with helium (He) as the carrier gas (Lécuyer et al., 2007). The $\delta^{18}O$ value of SRM 120c was fixed at 21.7‰ for correction of instrumental mass fractionation during the CO isotopic analysis. The average standard deviation equals 0.27 ± 0.11‰. Aliquots of silver phosphate from SRM 120c were analyzed several times a day in order to account for possible instrumental drift.

Principles and limits of air temperature calculation

Oxygen isotope compositions of tooth enamel phosphate ($\delta^{18}O_p$) from mammals reflect the composition of body water, which in turn, depends on that of ingested water by drinking and eating (Longinelli, 1984; Luz et al., 1984; Luz and Kolodny, 1985). The water contained in food has a complicated relationship with meteoric water and can be significantly ^{18}O-enriched compared to it. The relative contribution of water entering the body as liquid and as food water varies from one species to another. For the vast majority of terrestrial vertebrates,

water turnover scales to body mass (Eberhardt, 1969). Therefore, the $\delta^{18}O$ of the tissue of large animals should be less affected by the solid food consumption than the $\delta^{18}O$ of smaller ones (Kohn et al., 1996). As a result, animals such as horses that are water-dependent display average $\delta^{18}O$ values closely correlated to the average $\delta^{18}O$ of local precipitation (Longinelli, 1984; D'Angela and Longinelli, 1990; Ayliffe et al., 1992; Bryant et al., 1994).

Oxygen isotope fractionation equations between apatite phosphate and water have been empirically determined for horses (1; Sanchez Chillon et al., 1994) and red deer (2; D'Angela and Longinelli, 1990):

$$\delta^{18}O_w = \left(\delta^{18}O_p - 22.04\right) / 0.74 \quad (1)$$

$$\delta^{18}O_w = \left(\delta^{18}O_p - 25.55\right) / 1.13 \quad (2)$$

For rodents, the two following equations have been published:

- Longinelli et al. (2003)'s equation determined on wild voles and mice:

$$\delta^{18}O_w = \left(\delta^{18}O_p - 23.07\right) / 1.14 \quad (3)$$

- Navarro et al. (2004)'s equation determined on wild voles:

$$\delta^{18}O_w = \left(\delta^{18}O_p - 20.980\right) / 0.572 \quad (4)$$

Incremental $\delta^{18}O$ analysis from apex to cervix of hypsodont teeth allows the reconstitution of seasonal variations in air temperatures (Fricke and O'Neil, 1996; Sharp and Cerling, 1998; Wiedemann et al., 1999; Higgings and MacFadden, 2004; Bernard et al., 2009). In that case, the process of tooth mineralization does not alter the mean $\delta^{18}O_p$, which is a proxy for the mean composition of environmental water ($\delta^{18}O_w$). However, enamel increments of most large mammals are fully mineralized in 6 months. Their $\delta^{18}O$ values average time, with the consequence of dampening the sinusoidal signal, a process that was defined by Kohn (2004) as the difference in amplitude of the environmental and of the recorded signals divided by the amplitude of the environmental signal. Averaging over 6 months leads to about 50% dampening in the case of bisons, horses and red deer (Hoppe et al., 2002; Passey and Cerling, 2002; Bernard et al., 2009). Corrections are then applied to minimum and maximum $\delta^{18}O_p$ values before converting them into water $\delta^{18}O_w$ values. According to Hoppe et al. (2004a; Fig. 3), the first adult horse tooth to appear in the jaw is the M1 which starts to mineralize around two weeks of age, and enamel continues to mineralize for approximately 1 year. The M2 is the second tooth to mineralize followed by the P2, P3, P4, and then finally the M3.

Water $\delta^{18}O_w$ values, calculated according to Eqs. (1) and (2), range from −10.7‰ to −6.5‰ (Table 1). Several equations were determined between the weighted oxygen isotope compositions of precipitations and the mean annual surface temperatures at mid- to high-latitude regions that can be applied to the global scale or to a restricted latitude range (Dansgaard, 1964; Yurtsever, 1975; Rozanski et al., 1992; Grafenstein et al., 1996; Amiot et al., 2004). The Eq. (5) established by Grafenstein et al. (1996) provides reliable estimates of mean air temperatures at mid-latitudes in Europe as shown by Daux et al. (2005). The 'precipitation composition-mean air temperature' relationship is also considered as conservative through time, at least throughout the Quaternary (Rozanski, 1985).

$$\delta^{18}O_{\text{meteoric waters}} = 0.58(\pm 0.11) \times T - 14.48 \quad (5)$$

Winter and summer temperatures are calculated according to Bernard et al. (2009) who used seasonal $\delta^{18}O_{mw}/T_{air}$ regressions using a sub-dataset restricted to the circum North-Atlantic stations of the IAEA-GNIP/ISOHIS dataset (2006).

$$\text{Summer (Jun.}-\text{Aug.)}: T_{air} = 1.06\,(\pm 0.07) \times \delta^{18}O_{mw} + 24.1(\pm 0.7)\ \left(n = 71, r^2 = 0.75, p < 0.001\right) \quad (6)$$

$$\text{Winter (Dec.}-\text{Feb.)}: T_{air} = 1.40(\pm 0.05) \times \delta^{18}O_{mw} + 15.3(\pm 0.8)\ \left(n = 72, r^2 = 0.92, p < 0.001\right) \quad (7)$$

Results

Mean oxygen isotope compositions of horse teeth ranges from 14.2‰ to 17.2‰ over the analyzed sedimentary sequence, i.e. from levels XXIa to VIII. Red deer teeth have been analyzed in five levels and their $\delta^{18}O_p$ values range from 14.2‰ to 16.0‰. From the base to the top of the sequence, $\delta^{18}O_p$ values decrease from 15.7‰ to 14.2‰ from levels XXIa to XV, while the highest $\delta^{18}O_p$ values (16.4 and 17.2‰) are observed in the most recent layers VIII and IX which overlay a sampling gap resulting from the absence of recovery of large mammal remains (Fig. 2). Mean $\delta^{18}O_p$ values of horse and deer teeth are close to each other within a sedimentary level, except for level VIII (Table 1). Except for levels XVI and VIII that contain only one sample, other levels display variability less than 2‰. This value is less than the variability within a single population of deer or horses (Bryant et al., 1996; Clementz and Koch, 2001; Hoppe et al., 2004b).

Incremental sampling from apex to cervix of six horse teeth has provided $\delta^{18}O_p$ temporal series (Table 2; Fig. 3). One M2 horse tooth from level XXIa displays a sinusoidal-like signal that could correspond to less than 1 year, thus allowing the estimation of a mean tooth growth rate of about 55 mm yr^{-1} (Fig. 3e). This value is in agreement with other growth rates between 40 and 55 mm yr^{-1} that were estimated for both modern and fossil large herbivorous mammals (Fricke and O'Neil, 1996; Sharp and Cerling, 1998; Gadbury et al., 2000; Feranec and MacFadden, 2000; Hoppe et al., 2002) but slightly

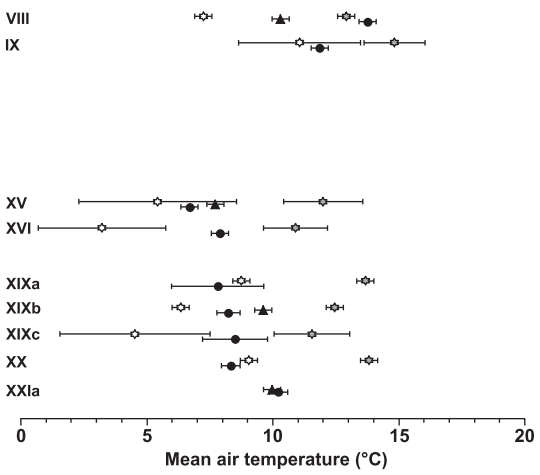

Fig. 2. Mean air paleotemperatures calculated from $\delta^{18}O_p$ values of mammals from "La Baume de Gigny" using the phosphate-water oxygen isotope fractionation equations of horses (Eq. (1); black circles), red deer (Eq. (2); black triangles), rodents (Eq. (3); grey stars and 4; white stars) and the MAAT − $\delta^{18}O_{mw}$ relationship of Grafenstein et al. (1996). Air temperature values are reported against their corresponding stratigraphic level. Error bars correspond to the standard deviation (2σ).

Table 2
Oxygen isotope compositions of enamels serially sampled along a selection of horse tooth crowns.

		Distance from apex (mm)	$\delta^{18}O_p$ (‰)
Level	IX	6	15.9
Sample	812 GH	14	15.7
Tooth	LR P4	20	15.5
		26	15.9
		33	17.0
		45	17.9
		51	17.0
		57	16.5
		63	16.5
		69	16.5
		75	16.2
Level	XV	7	14.5
Sample	71 F2	13	13.1
Tooth	UP P4	19	13.5
		25	13.7
		31	14.0
		36	13.9
		43	14.1
		49	14.9
		55	15.0
		61	14.6
		67	14.9
		72	14.6
Level	XIXc	5	16.7
Sample	307 E2	10	16.8
Tooth	UP P4	15	15.7
		20	15.9
		26	14.7
		31	15.1
		36	15.6
		42	14.8
		47	15.5
		52	15.8
		58	14.5
		63	15.3
		68	15.3
Level	XIXc	6	14.7
Sample	385 G3	12	14.8
Tooth	UP M1	18	14.6
		24	14.5
		30	14.8
		36	15.3
		41	15.5
		47	15.1
		53	14.8
Level	XXIa	7	18.1
Sample	183 H3	13	18.4
Tooth	LR M2	19	17.4
		25	15.6
		31	14.0
		37	13.0
		43	12.9
		49	14.6
		55	15.9
Level	XXIa	3	14.8
Sample	396 F3	9	15.8
Tooth	UP P4	15	14.7
		21	15.6
		27	15.8
		32	16.5
		37	16.5
		43	16.4
		48	16.3

higher than the estimates (from 35 to 40 mm yr^{-1}) of Hoppe et al. (2004a). It is noteworthy that this tooth recorded the maximal $\delta^{18}O_p$ amplitude of ≈5.5‰ among the studied teeth. By contrast, the isotopic signal from a P4 tooth sampled in the same level does not show any cyclicity and has an amplitude of only 1.8‰, however its mean $\delta^{18}O_p$ value of 15.8‰ compares well with the M2 tooth from the same level (Fig. 3f). A second horse tooth sampled in level IX exhibits a pattern of isotopic variations that could be compatible with a sinusoidal signal of seasonal origin, where at least minimal and maximal values are well marked and define an isotopic amplitude of 2.4‰ (Fig. 3a). Other horse teeth show a restricted range in isotopic amplitude values (1‰ to 2.3‰) and temporal variations which show either no periodicity (XXIa-P4; XIX-M1 and XV-P4) or are not in phase (XIXc-P4) with seasonal rhythms compatible with the tooth growth rate deduced from M2 horse tooth from level XXIa (Figs. 3b, c, d and f). Winter, summer and mean air temperatures were calculated using Eqs. (5)–(7) and are reported in Table 3.

Discussion

Oxygen isotope composition of phosphate and diagenetic alteration

Oxygen isotope composition of tooth enamel phosphate ($\delta^{18}O_P$) can be preserved over geological periods because the dense and well-crystallized hydroxyapatite is resistant to diagenetic alteration under inorganic conditions (Kolodny et al., 1983; Lécuyer et al., 1999). However, diagenetic alteration of biogenic apatites cannot be excluded since it has been shown that microbial activity has the potential to modify the oxygen isotope composition of tooth enamel phosphate after the animal's death (Blake et al., 1997; Zazzo et al., 2004). Some arguments plead in favour of a preservation of the pristine oxygen isotope compositions. We selected carefully teeth with a clean pale-yellowish enamel devoid of cracks and caries. For these samples, chemical yields of phosphate recovery during the wet chemistry procedure were characterized by clustered P_2O_5 contents of about 33%. These chemical data show that the original stoechiometry of the studied ungulate tooth apatite was preserved (Lécuyer, 2004; Navarro et al., 2004; Billon-Bruyat et al., 2005). This result supports the hypothesis that the studied sample collection did not suffer major diagenetic alteration such as recrystallization that commonly modifies the chemical composition of biogenic apatite, even though this does not constitute a definitive argument.

Meaning of the intra-tooth oxygen isotope record

The M2 tooth records the pre-weaning signal through a ^{18}O-enrichment of the body water due to breast-feeding (Wright and Schwarcz, 1998; Hoppe et al., 2004a, 2004b). However, Zazzo et al. (2002) indicate that the annual range of $\delta^{18}O$ values of ingested water or season of birth can mask this pre-weaning signal. For the M2 tooth, this ^{18}O-enrichment is probably not recorded because this tooth belongs to a middle age individual and the first sample comes from the middle of the crown, the most apical part having been worn out. Furthermore the mean M2 $\delta^{18}O$ values compare well with P4 ones from the same level (XIXb, XIXc and XXIa; Table 1). These observations lead to conclude that the M2 tooth does not record the pre-weaning signal.

Most horse teeth show a restricted range in isotopic amplitude values (1‰ to 2.3‰) and temporal variations which show either no periodicity (XXIa-P4; XIX-M1 and XV-P4) or are not in phase (XIXc-P4) with seasonal rhythms compatible with the tooth growth rate deduced from M2 horse tooth from level XXIa (Figs. 3b, c, d and f). Ruling out diagenetic processes and sampling contamination by dentine, the lack of seasonal variation can be explained in two ways. Firstly, smoothed isotopic patterns could from migratory behaviors, indeed, Britton et al. (2009) have shown that migratory movements can dampen the isotopic signal. However, it is noteworthy that horses and red deer are not migratory species according to Hainard (1971), and it should also be noted that there is little evidence for migrations in Epi-Palaeolithic equids or red deer (Pellegrini et al., 2008). Secondly, a plausible explanation concerns the water strategy; horses could have drunk water from a large reservoir such as a lake which residence time of water is long enough to erase any seasonal oxygen isotope variation of precipitations (Hoppe et al., 2004b).

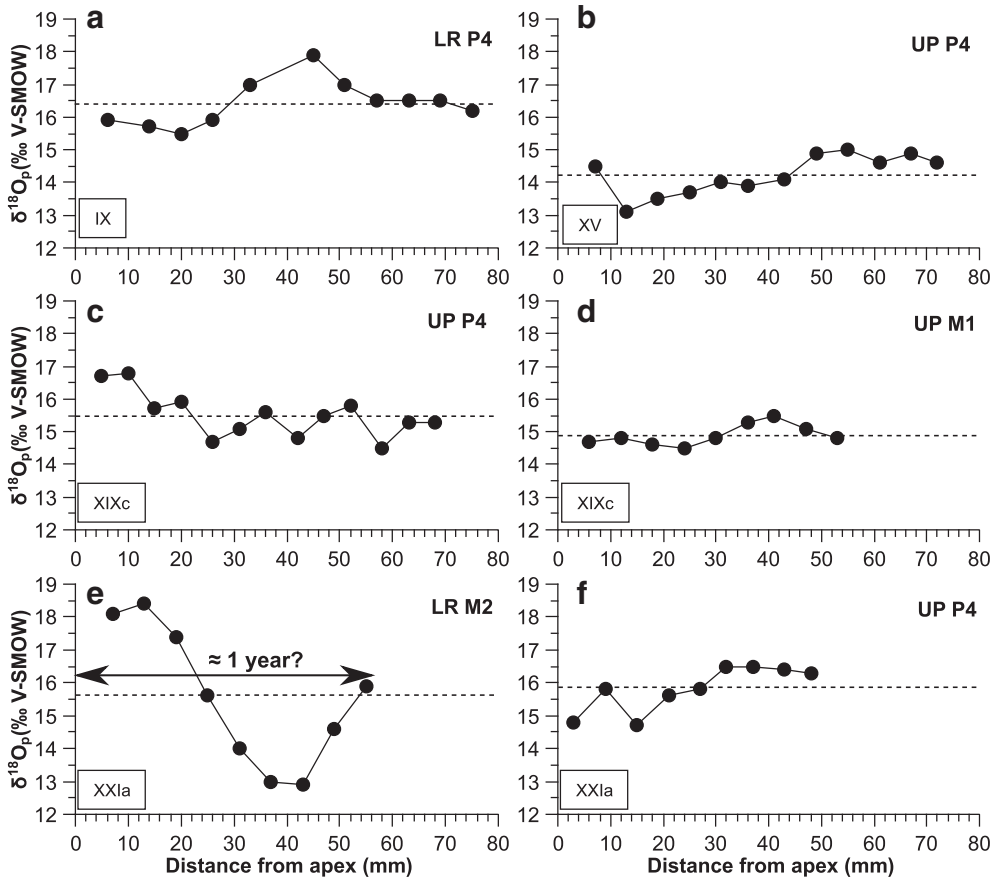

Fig. 3. Horse intra-tooth $\delta^{18}O_p$ values variations reported against their distance from crown apex. For graphs (a, b, c, d, e and f), tooth nature and stratigraphic level are marked. The dashed lines correspond to the average $\delta^{18}O_p$ values of each tooth crown. Symbol width includes analytical error associated with $\delta^{18}O_p$ values.

Mean air temperatures during the Middle Palaeolithic

Combining Eq. (5) with Eqs. (1) or (2) allows for calculation of past mean air temperatures, which were roughly 10°C ± 2°C during the deposition of level XXIa (ca. 145 kyr ago), a value comparable to present-day in Besançon, France (Table 3). On the basis of pollen spectra, rodent assemblages and sedimentary patterns, this level was linked to the last Rissian interstadial or to the Eemian (Campy et al., 1989). Results from our study are in agreement with those inferred from pollen data from Les Echets, eastern France (T = 8°C to 12°C), La Grande Pile, eastern France (9°C to 12°C), and Lac du Bouchet, central France (10 to 13°C) (Guiot, 1990; Fauquette et al., 1999). Oxygen isotope compositions of horses and red deer from BGC are also similar to those obtained from steppe bison teeth in Coudoulous I (Table 3), with a mean air temperature estimated at 9 ± 3°C (Bernard et al., 2009).

Table 3
Calculated mean annual, summer and winter air paleotemperatures as well as seasonal amplitudes at Coudoulous 1 and Gigny sites during the Late Pleistocene. Present day temperature values at neighboring climatic stations of Besançon and Villars are given for comparison.

	Present day	Level 4	Present day	Level XXIa
	Villars	Coudoulous I	Besançon	Gigny
	T (°C)	T (°C)	T (°C)	T (°C)
Mean annual air temperature	12 ± 1	9 ± 3	11 ± 1	10 ± 2
Winter temperature	6 ± 1	−1 ± 3	3 ± 1	−7 ± 2
Summer temperature	18 ± 1	19 ± 3	19 ± 1	22 ± 1
Amplitude	12	20	16	29

The Middle Palaeolithic BGC sequence can be divided into two distinct phases. From level XX to XV, mean air temperatures regularly decrease from 9°C to 7°C for horse teeth and from 10°C to 7°C for red deer teeth, which then are in good agreement. Upper levels (IX and VIII) recorded a warmer climate with mean air temperatures of 12°C and 13°C, determined on the basis of oxygen isotope ratios of horse teeth. Red deer $\delta^{18}O$ values are only available for level VIII, indicating a temperature close to 10°C. Sizable differences (2‰) between horse and red deer $\delta^{18}O$ values could result either from a sedimentary rework, as it was suggested for this sedimentary level (Campy et al., 1989), or from diet and habitat differences.

Meaning of oxygen isotope records obtained from both ungulates and rodents

Mean air temperatures recorded in the $\delta^{18}O$ values of large mammal teeth are generally comparable to those obtained from rodent teeth using Eq. (4) (Navarro et al., 2004; Supplementary Table), except in levels XIXc and XVI where temperatures inferred from rodent $\delta^{18}O$ values are lower by about 5°C (Fig. 2). Several factors could explain the observed discrepancies between the large mammal and rodent $\delta^{18}O$ records:

1) Allochtony: rodent teeth are concentrated in pellets rejected by different bird predator species whose hunting areas can reach several tens of kilometers, including neighbouring mountains. Therefore, the site where rodent teeth are deposited integrate potential geographic variations in the oxygen composition of ingested food and water.
2) Dietary behaviour: rodents are less water-dependent than horses since their main source of oxygen derives from food water. Indeed,

oxygen isotope compositions of leaf water are generally ^{18}O-enriched relative to free liquid water because of evapo-transpiration processes (Flanagan et al., 1991).

3) Short mineralization time: about one season is recorded in the oxygen isotope composition of rodent teeth (Navarro et al., 2004) while at least one or two years are recorded when using teeth of large mammals. For these latter, the amount of time represented depends on the crown height, and on the amount of wear as well as on how long the tooth actually took to form and mineralize.
4) Choice between fractionation equations: Two levels (XIXc and XV) allow statistical comparisons between the $\delta^{18}O_w$ values estimated from ungulates and those estimated using Eqs. (3) and (4) available for rodents. In the case of level XIXc, the Kruskal–Wallis test (alpha = 0.1) indicates that the difference is significant ($p = 0.0455$) between $\delta^{18}O_w$ values calculated for ungulates and those for rodents using both Eqs. (3) and (4). For level XV, there is no significant difference ($p = 0.3545$) when using Eq. (4) while a significant one is observed ($p = 0.0664$) when using Eq. (3). These statistical results suggest that the oxygen isotope fractionation Eq. (4) established by Navarro et al. (2004) provides mean $\delta^{18}O_w$ values close to those inferred from Eqs. (1) and (2) published for ungulates (Fig. 2; Supplementary Table). On the contrary, the Eq. (3) proposed by Longinelli et al. (2003) leads to overestimate $\delta^{18}O_w$ values by 2‰ to 5‰, which corresponds to mean air temperatures overestimated by 3°C to 8°C (Fig. 2; Supplementary Table).

Seasonal temperature variations and W–E gradient in France

Among the six teeth that were analyzed by serial sampling, only two of them (LR M2 from level XXIa and LR P4 from level IX) present a sinusoidal-like pattern (Fig. 3). The four other horse teeth do not show any similar pattern, or perhaps a strongly smoothed pattern, that could reflect temperature variations of seasonal origin. Higgings and MacFadden (2004) have shown that *Bison* should be preferred to *Equus* for reconstituting seasonal climatic variations that are based on the oxygen isotope composition of tooth enamel. High-resolution temporal estimates of temperature seasonality have indeed been performed in Coudoulous I (ca. 140 ka) where bison remains are abundant (Bernard et al., 2009). However, in the absence of any bison tooth remains at BGC sinusoidal-like oxygen isotope records obtained from the two horse teeth have been used to estimate seasonal variations in mean air temperatures. For teeth LR M2 and LR P4, summer and winter temperatures have been calculated by combining Eq. (1) to Eqs. (6) and (7), taking into account a 'dampening' effect of 50% due to the process of tooth mineralization (Higgings and MacFadden, 2004; Bernard et al., 2009). For level IX, we obtained winter and summer temperatures of 0.5 ± 1°C and 20 ± 2°C, and of -7 ± 2°C and 22 ± 1°C, respectively, for level XXIa. In both cases, thermal seasonal amplitudes of 20°C (level IX) and 29°C (level XXIa) are much higher than those prevailing today in the French Jura (Besançon) with an amplitude of about 16°C. During the Middle Palaeolithic (ca. 145 kyr ago), climatic conditions in Gigny look like those existing today in the eastern part of Europe where continentality is well marked by the succession of very warm summer and very cold winter seasons. It is noteworthy that the calculated amplitudes of seasonal temperatures are most likely underestimated because either migratory behaviours or the use of large water reservoirs with buffered oxygen isotope compositions tend to generate smoothed oxygen isotope records in tooth enamel.

Mean annual air temperatures inferred from ungulate and rodent tooth $\delta^{18}O_p$ values from the sub-contemporaneous level XXIa at BGC and level 4 from Coudoulous I are close to present-day temperatures. However, significant differences in the climate mode are revealed at the seasonal scale, summer temperatures were slightly warmer whereas winter temperatures were about 7°C and 10°C lower than those recorded today in the southwest and eastern parts of France, respectively. Winter temperatures document the existence of a well-developed West–East thermal gradient at 145 ka ago of about −9°C, much stronger than the −4°C difference recorded today between Villars and Besançon (Table 3). Winter temperature is a key parameter of the climatic mode that prevailed during the Middle Palaeolithic, setting the extent and duration of the snow cover and consequently limiting the amount of available food resources for medium and large ungulates, as well as for their Neanderthal predators.

Conclusion

Oxygen isotope compositions of phosphate have been measured from ungulate (*Equus* and *Cervus*) tooth enamels sampled in the thick sedimentary sequence of "La Baume de Gigny" (BGC), Jura, eastern France, that cover a period of ca. 100 ka. Results from this study emphasize some key aspects of the climate mode during the Late Pleistocene:

- the oxygen isotope record in ungulate tooth enamel provides climatic trends similar to those already inferred from rodent teeth (Navarro et al., 2004). From levels XXIa to XV, a smooth cooling trend is recorded with temperatures decreasing from 9 to 10°C to 7°C while levels IX and VIII are characterized by milder temperatures of 12–13°C.
- two horse teeth among a collection of six show isotopic times series with shapes compatible with a sinusoidal-like signal that could be driven by temperature variations of seasonal origin. These isotopic signals reveal that during the Middle Palaeolithic winters were colder than during present, while summer temperatures were similar. Consequently, one of the striking features of the glacial age could be the existence of large amplitudes in seasonal temperature transitions between warm and cold seasons. Moreover, low winter temperatures most likely constituted a limiting factor upon species dispersal and distribution. Climate in France resembled those known today in some countries of eastern Europe.
- Winter temperatures document the existence of a well-developed West–East thermal gradient at 145 ka of about −9°C, much stronger than the −4°C difference recorded today between Lot and Jura, France. Negative winter temperatures were likely responsible for the extent and duration of the snow cover, thus limiting the food resources available for large mammals and their Neanderthal predators. Consequently, the occupation of the site by Neanderthals could have been temporary with a possible desertion during the very cold season.

Supplementary materials related to this article can be found online at doi:10.1016/j.yqres.2011.03.001.

Acknowledgments

This study was funded by Fondation des Treilles, the French CNRS 'ECLIPSE II' Program, and by the Institut Universitaire de France (C.L.). We warmly thank the Musée of Lons-Le-Saulnier where the BGC fossil material is stored, and especially their past-curator Marie-Jeanne Lambert.

References

Amiot, R., Lécuyer, C., Buffetaut, E., Fluteau, F., Legendre, S., Martineau, F., 2004. Latitudinal temperature gradient during the Cretaceous Upper Campanian-Middle Maastrichtian: $\delta^{18}O$ record of continental vertebrates. Earth and Planetary Science Letters 226, 255–272.

Andrews, P., Lord, J., Evans, E., 1979. Patterns of ecological diversity in fossil and modern mammalian faunas. Biological Journal of the Linnean Society 11, 177–205.

Ayliffe, L.K., Lister, A.M., Chivas, A.R., 1992. The preservation of glacial-interglacial climatic signatures in the oxygen isotopes of elephant skeletal phosphate. Palaeogeography, Palaeoclimatology, Palaeoecology 99, 179–191.
Bar-Matthews, M., Ayalon, A., Kaufman, A., 1997. Late Quaternary paleoclimate in the eastern mediteranean region from stable isotope analysis of speleothems at Soreq Cave, Israel. Quaternary Research 47, 155–168.
Bernard, A., Daux, V., Lécuyer, C., Brugal, J.-P., Genty, D., Wainer, K., Gardien, V., Fourel, F., Jaubert, J., 2009. Pleistocene seasonal temperature variations recorded in the $\delta^{18}O$ of *Bison priscus* teeth. Earth and Planetary Science Letters 283, 133–143.
Billon-Bruyat, J.-P., Lécuyer, C., Martineau, F., Mazin, J.-M., 2005. Oxygen isotope compositions of Late Jurassic vertebrate remains from lithographic limestones of western Europe: implications for the ecology of fish, turtles, and crocodilians. Palaeogeography, Palaeoclimatology, Palaeoecology 216, 359–375.
Blake, R.E., O'Neil, J.R., Garcia, G.A., 1997. Oxygen isotope systematics of biologically mediated reactions of phosphate: I. Microbial degradation of organophosphorus compounds. Geochimica et Cosmochimica Acta 61, 4411–4422.
Britton, K., Grimes, V., Dau, J., Richards, M.P., 2009. Reconstructing faunal migrations using intra-tooth sampling and strontium and oxygen isotope analyses: a case study of modern caribou (Rangifer tarandus granti). Journal of Archaeological Science 36, 1163–1172.
Bryant, J.D., Luz, B., Froelich, P.N., 1994. Oxygen isotopic composition of fossil horse tooth phosphate as a record of continental paleoclimate. Palaeogeography, Palaeoclimatology, Palaeoecology 107, 303–316.
Bryant, J.D., Froelich, P.N., Showers, W.J., Genna, B.J., 1996. Biologic and climatic signals in the oxygen isotope composition of Eocene–Oligocene equid enamel phosphate. Palaeogeography Palaeoclimatology Palaeoecology 126, 75–90.
Campy, M., Chaline, J., 1993. Missing records and depositional breaks in French Late Pleistocene cave sediments. Quaternary Research 40, 318–331.
Campy, M., Chaline, J., Vuillemey, M., 1989. La Baume de Gigny (Jura). In: CNRS (Ed.), Gallia Préhistoire Supplément, 27. Paris, 258 pp.
Chaline, J., 1972. Les rongeurs du Pleistocene moyen et supérieur de France. Cahiers de Paléontologie, CNRS, Paris. 410 pp.
Clementz, M.T., Koch, P.L., 2001. Differentiating aquatic mammal habitat and foraging ecology with stable isotopes in tooth enamel. Oecologia 129, 461–472.
Crowson, R.A., Showers, W.J., Wright, E.K., Hoering, T.C., 1991. Preparation of phosphate samples for oxygen isotope analysis. Analytical Chemistry 63, 2397–2400.
D'Angela, D., Longinelli, A., 1990. Oxygen isotopes in living mammal's bone phosphate: further results. Chemical Geology (Isotope Geoscience Section) 86, 75–82.
Dansgaard, W., 1964. Stable isotopes in precipitation. Tellus 16, 436–468.
Daux, V., Lécuyer, C., Adam, F., Martineau, F., Vimeux, F., 2005. Oxygen isotope composition of human teeth and the record of climate changes in France (Lorraine) during the last 1700 years. Climatic Change 70, 445–464.
Daux, V., Lécuyer, C., Héran, M.-A., Amiot, R., Simon, L., Fourel, F., Martineau, F., Lynnerup, N., Reychler, H., Escarguel, G., 2008. Oxygen isotope fractionation between human phosphate and water revisited. Journal of Human Evolution 55, 1138–1147.
de Beaulieu, J.-L., Reille, M., 1984. A long upper Pleistocene pollen record from Les Echets, near Lyon, France. Boreas 13, 111–132.
Delgado Huertas, A., Iacumin, P., Longinelli, A., 1997. A stable isotope study of fossil mammal remains from the Paglicci cave, southern Italy, 13 to 33 ka BP: palaeoclimatological considerations. Chemical Geology 141, 211–223.
Delpech, F., Donard, E., Gilbert, A., Guadelli, J.-L., Le Gall, O., Martini-Jacquin, A., Paquereau, M.-M., Prat, F., Tournepiche, J.-F., 1983. Contribution à la lecture des paléoclimats quaternaires d'après les données de la paléontologie en milieu continental. AGSO. Bull. Inst. Géol. Bassin d'Aquitaine et Cahier du Quaternaire, Bordeaux, pp. 165–177.
D'Errico, F., Sanchez-Goni, M.F., 2003. Neandertal extinction and the millenial scale climatic variability of OIS 3. Quaternary Science Reviews 22, 769–788.
Eberhardt, L.L., 1969. Similarity, allometry and food chains. Journal of Theoretical Biology 24, 43–45.
Evin, 1989. Les datations radiocarbone. In: Campy, M., Chaline, J., Vuillemey, M. (Eds.), La Baume de Gigny (Jura). XXVII^{e} supplément à Gallia Préhistoire. Editions du CNRS, Paris, pp. 53–56.
Fabre, M., 2010. Environnement et subsistance au Pleistocene supérieur dans l'Est de la France. Etudes ostéologiques de la Baume de Gigny (Jura), Vergisson II (Saône et Loire) et Oetrange (Luxembourg). Ph D dissertation, Université de Provence, Aix-en-Provence.
Fauquette, S., Guiot, J., Menut, M., de Beaulieu, J.-L., Reille, M., Guenet, P., 1999. Vegetation and climate since the last interglacial in the Vienne area (France). Global Planetary Change 20, 1–17.
Feng, X., Cui, H., Tang, K., Conkey, L., 1999. Tree-ring δD as an indicator of Asian monsoon intensity. Quaternary Research 51, 262–266.
Feranec, R.C., MacFadden, B., 2000. Evolution of the grazing niche in Pleistocene mammals from Florida: evidence from stable isotopes. Palaeogeography, Palaeoclimatology, Palaeoecology 162, 155–169.
Finlayson, J.C., 2004. Neanderthals and modern humans. An ecological and evolutionary perspective. Cambridge University Press, Cambridge. 255 pp.
Flanagan, L.B., Bain, J.F., Ehleringer, J.R., 1991. Stable oxygen and hydrogen isotope composition of leaf water in C_3 and C_4 plant species under field conditions. Oecologia 88, 394–400.
Fricke, H.C., O'Neil, J.R., 1996. Inter- and intra-tooth variation in the oxygen isotope composition of mammalian tooth enamel phosphate: implication for paleoclimatological and paleobiological research. Palaeogeography, Palaeoclimatology, Palaeoecology 126, 91–99.
Fricke, H.C., Clyde, W.C., O'Neil, J.R., Gingerich, P.D., 1998. Evidence for rapid climate change in North America during the latest Paleocene thermal maximum: oxygen isotope compositions of biogenic phosphate from the Bighorn Basin (Wyoming). Earth and Planetary Science Letters 160, 193–208.
Gadbury, C., Todd, L., Jahren, A.H., Amundson, R., 2000. Spatial and temporal variations in the isotopic composition of bison tooth enamel from the Early Holocene Hudson-Meng Bone Bed, Nebraska. Palaeogeography, Palaeoclimatology, Palaeoecology 157, 79–93.
Gamble, C., 1995. Large mammals, climate and resource richness in Upper Pleistocene Europe. Acta Zoologica Cracovensia 38, 155–175.
Gamble, C., 1999. The Palaeolithic societies of Europe. Cambridge University Press. 505 pp.
Genoni, L., Iacumin, P., Nikolaev, V., Gribchenko, Y., Longinelli, A., 1998. Oxygen isotope measurements of mammoth and reindeer skeletal remains: an archive of Late Pleistocene environmental conditions in Eurasian Arctic. Earth and Planetary Science Letters 160, 587–592.
Geoatlas France vectorielle 2, 1997. France physique. Digital map accessible at: http://www.geoatlas.fr/fr/maps/cartes-de-france-0/france-physique-3502.
Grafenstein, U.v., Erlenkeuser, H., Muller, J., Trimborn, P., Alefs, J., 1996. A 200 year mid-European air temperature record preserved in lake sediments: an extension of the δ18Op-air temperature relation into the past. Geochimica et Cosmochimica Acta 60, 4025–4036.
Guiot, J., 1990. Methodology of the last climatic cycle reconstruction in France from pollen data. Palaeogeography, Palaeoclimatology, Palaeoecology 80, 49–69.
Guiot, J., Pons, A., Beaulieu (de), J.-L., Reille, M., 1989. A 140,000 years continental climate reconstruction from two European pollen records. Nature 338, 309–313.
Hainard, R., 1971. Mammifères sauvages d'Europe. II: Pinnipèdes, Ongulés, Rongeurs, Cétacés. Delachaux et Niestlé, Neuchâtel. 352 pp.
Heinrich, H., 1988. Origin and consequences of cyclic ice-rafting in the Northeast Atlantic ocean during the past 130,000 years. Quaternary Research 29, 142–152.
Héran, M., Lécuyer, C., Legendre, S., 2010. Cenozoic long-term terrestrial climatic evolution in Germany tracked by $\delta^{18}O$ of rodent tooth phosphate. Palaeogeography, Palaeoclimatology, Palaeoecology 285, 331–342.
Higgings, P., MacFadden, B.J., 2004. "Amount effect" recorded in oxygen isotopes of Late Glacial horse (Equus) and bison (Bison) teeth from Sonoran and Chihuahuan deserts, Southwestern United States. Palaeogeography, Palaeoclimatology, Palaeoecology 206, 337–353.
Hoppe, K.A., Christensen, K., Swanson, J.A., 2002. Fluorescence resonance energy transfer-based stoichiometry in living cells. Biophysical Journal 83, 3652–3664.
Hoppe, K.A., Stover, S.M., Pascoe, J.R., Amundson, R., 2004a. Tooth enamel biomineralization in extant horses: implications for isotopic microsampling. Palaeogeography, Palaeoclimatology, Palaeoecology 206, 355–365.
Hoppe, K.A., Amundson, R., Vavra, M., McClaran, M.P., Anderson, D.L., 2004b. Isotopic analysis of tooth enamel carbonate from modern North American feral horses: implications for paleoenvironmental reconstructions. Palaeogeography, Palaeoclimatology, Palaeoecology 203, 299–311.
IAEA/WMO, 2006. Global Network of Isotopes in Precipitation. The GNIP Database. Accessible at: http://isohis.iaea.org.
Koch, P.L., Hoppe, K.A., Webb, S.D., 1998. The isotopic ecology of late Pleistocene mammals in North America. Part 1. Florida. Chemical Geology 152, 119–138.
Kohn, M.J., 2004. Comment: tooth enamel mineralization in ungulates: implications for recovering a primary isotopic time-series, by B.H. Passey and T.E. Cerling (2002). Geochimica et Cosmochimica Acta 68, 403–405.
Kohn, M.J., Schoeninger, M.J., Valley, J.W., 1996. Herbivore tooth oxygen isotope compositions: effects of diet and physiology. Geochimica et Cosmochimica Acta 60, 3889–3896.
Kolodny, Y., Luz, B., Navon, O., 1983. Oxygen isotope variations in phosphate of biogenic apatites, I. Fish bone apatite-rechecking the rules of the game. Earth and Planetary Science Letters 64, 398–404.
Lécuyer, C., 2004. Oxygen Isotope Analysis of Phosphate. In: de Groot, P.A. (Ed.), Handbook of Stable Isotope Analytical Techniques. Elsevier, Amsterdam, 482–496.
Lécuyer, C., Grandjean, P., O'Neil, J.R., Capetta, H., Martineau, F., 1993. Thermal excursions in the ocean at the Cretaceous–Tertiary boundary (northern Morocco): $\delta^{18}O$ record of phosphatic fish debris. Palaeogeography, Palaeoclimatology, Palaeoecology 105, 235–243.
Lécuyer, C., Grandjean, P., Barrat, J.-A., Nolvak, J., Emig, C.C., Paris, F., Robardet, M., 1998. $\delta^{18}O$ and REE contents of phosphatic brachiopods: a comparison between modern and lower Paleozoic populations. Geochimica et Cosmochimica Acta 62, 2429–2436.
Lécuyer, C., Grandjean, P., Sheppard, S.M.F., 1999. Oxygen isotope exchange between dissolved phosphate and water at temperatures $\leq$135°C: inorganic versus biological fractionations. Geochimica et Cosmochimica Acta 63, 855–862.
Lécuyer, C., Fourel, F., Martineau, F., Amiot, R., Bernard, A., Daux, V., Escarguel, G., Morrison, J., 2007. High-precision determination of $^{18}O/^{16}O$ ratios of silver phosphate by EA-pyrolysis-IRMS continuous flow technique. Journal of Mass Spectrometry 42, 36–41.
Legendre, S., 1986. Analysis of mammalian communities from the Late Eocene and Oligocene of southern France. Palaeovertebrata 16, 191–212.
Longinelli, A., 1984. Oxygen isotopes in mammal bone phosphate: a new tool for paleohydrological and paleoclimatological research? Geochimica et Cosmochimica Acta 48, 385–390.
Longinelli, A., Iacumin, P., Davanzo, S., Nikolaev, V., 2003. Modern reindeer and mice: revised phosphate–water isotope equations. Earth and Planetary Science Letters 214, 491–498.
Luz, B., Kolodny, Y., 1985. Oxygen variations in phosphate of biogenic apatites. Earth and Planetary Science Letters 75, 29–36.
Luz, B., Kolodny, Y., Horowitz, M., 1984. Fractionation of oxygen isotopes between mammalian bone-phosphate and environmental drinking water. Geochimica et Cosmochimica Acta 48, 1689–1693.
Navarro, N., Lécuyer, C., Montuire, S., Langlois, C., Martineau, F., 2004. Oxygen isotope composition of phosphate from Arvicoline teeth: a continental proxy for Quaternary climatic changes, Gigny, French Jura. Quaternary Research 62, 172–182.

O'Neil, J.R., Roe, L.J., Reinhard, E., Blacke, R.E., 1994. A rapid and precise method of oxygen isotope analysis of biogenic phosphates. Israelian Journal of Earth Sciences 43, 203–212.
Passey, B.H., Cerling, T.E., 2002. Tooth enamel mineralization in ungulates: implications for recovering a primary isotopic time-series. Geochimica et Cosmochimica Acta 66, 3225–3234.
Pellegrini, M., Donahue, R.E., Chenery, C., Evans, J., Lee-Thorp, J., Montgomery, J., Mussi, M., 2008. Faunal migration in late-glacial central Italy: implications for human resource exploitation. Rapid Communications in Mass Spectrometry 22, 1714–1726.
Rozanski, K., 1985. Deuterium and oxygen-18 in European groundwaters — links to atmospheric circulation in the past. Chemical Geology 52, 349–363.
Rozanski, K., Araguas-Araguas, L., Gonfiantini, R., 1992. Relation between long-term trends of oxygen-18 isotope composition of precipitation and climate. Science 258, 981–985.
Sanchez Chillon, B., Alberdi, M.T., Bonadonna, F.P., Leone, G., Stenni, B., Longinelli, A., 1994. Oxygen isotopic composition of fossil equid tooth and bone phosphate: an archive of difficult interpretation. Palaeogeography, Palaeoclimatology, Palaeoecology 107, 317–328.
Sharma, S., Joachimski, M.M., Tobschall, H.J., Singh, I.B., Tewari, D.P., Tewari, R., 2004. Oxygen isotopes of bovid teeth as archives of paleoclimatic variations in archaeological deposits of the Ganga plain, India. Quaternary Research 62, 19–28.
Sharp, Z.D., Cerling, T.E., 1998. Fossil isotope records of seasonal climate and ecology: straight from the horse's mouth. Geology 26, 219–222.
Smith, J.H., Dodson, P., 2003. A proposal for a standard terminology of anatomical notation and orientation in fossil vertebrate dentitions. Journal of Vertebrate Paleontology 23, 1–12.
Sponheimer, M., Lee-Thorp, J.A., 2001. The oxygen isotope composition of mammalian enamel carbonate from Morea Estate, South Africa. Oecologia 126, 153–157.
Stiner, M.C., 1994. Honor among thieves. A zooarchaeological study of neandertal ecology. Princeton University Press, Princeton. 447 pp.
Vennemann, T.W., Hegner, E., 1998. Oxygen, strontium, and neodymium isotope composition of fossil shark teeth as a proxy for the palaeoceanography and palaeoclimatology of the Miocene northern Alpine Paratethys. Palaeogeography, Palaeoclimatology, Palaeoecology 142, 107–121.
Wiedemann, F.B., Bocherens, H., Mariotti, A., Von den Driesch, A., 1999. Methodological and archaeological implications of intra-tooth isotopic variations ($\delta^{13}C$, $\delta^{18}O$) in herbivores from Ain Ghazal (Jordan, Neolithic). Journal of Archaeological Science 26, 697–704.
Wright, L.E., Schwarcz, H.P., 1998. Stable carbon and oxygen isotopes in human tooth enamel: identifying breastfeeding and weaning in prehistory. American Journal of physical anthropology 106, 1–18.
Yurtsever, Y., 1975. Worldwide survey of stable isotopes in precipitation. Report of the Isotope Hydrology Section. International Atomic Energy Agency, Vienna. 40 pp.
Zazzo, A., Mariotti, A., Lécuyer, C., Heintz, E., 2002. Intra-tooth isotopic variations in late Miocene bovid enamel from Afganistan: paleobiological, taphonomical and climatical implications. Palaeogeography, Palaeoclimatology, Palaeoecology 186, 145–161.
Zazzo, A., Lécuyer, C., Mariotti, A., 2004. Experimentally-controlled carbon and oxygen isotope exchange between bioapatites and water under inorganic and microbially-mediated conditions. Geochimica et Cosmochimica Acta 68, 1–12.

PUBLICATION 2.4

Oxygen isotope evidence for semi-aquatic habits among spinosaurid theropods

Romain Amiot[1,3*], Eric Buffetaut[2], Christophe Lécuyer[3†], Xu Wang[4], Larbi Boudad[5], Zhongli Ding[4], François Fourel[3], Steven Hutt[6], François Martineau[3], Manuel Alfredo Medeiros[7], Jinyou Mo[8§], Laurent Simon[9], Varavudh Suteethorn[10], Steven Sweetman[11], Haiyan Tong[2], Fusong Zhang[4], and Zhonghe Zhou[1]

[1]Institute of Vertebrate Paleontology and Paleoanthropology, Chinese Academy of Sciences, #142 XiZhiMenWai DaJie, Beijing 100044, China

[2]CNRS UMR 8538, Laboratoire de Géologie de l'Ecole Normale Supérieure, 24 rue Lhomond, 75231 Paris Cedex 05, France

[3]UMR CNRS 5125, Paléoenvironnements et Paléobiosphère, Université Lyon 1, 2 rue Raphaël Dubois, 69622 Villeurbanne Cedex, France

[4]Institute of Geology and Geophysics, Chinese Academy of Sciences, 19 Beitucheng Xilu, Chaoyang, Beijing 100029, China

[5]Université Moulay Ismail, Laboratoire des Formations Superficielles, BP 509 Boutalamine, 52000 Errachidia, Morocco

[6]Dinosaur Isle, Culver Parade, Sandown, Isle of Wight PO36 8QA, UK

[7]Departamento de Biologia, Universidade Federal do Maranhão (UFMA), Campus do Bacanga, Avenida dos Portugueses, s/n São Luis, MA, Brazil

[8]Faculty of Earth Sciences, China University of Geosciences, 388 Lumo Road, Wuhan 430074, China

[9]UMR CNRS 5023, Ecologie des Hydrosystèmes Fluviaux, Université Lyon 1, Bâtiment Forel, 69622 Villeurbanne Cedex, France

[10]Department of Mineral Resources, Rama VI Road, Bangkok 10400, Thailand

[11]School of Earth and Environmental Sciences, University of Portsmouth, Burnaby Building, Burnaby Road, Portsmouth PO1 3QL, UK

ABSTRACT

Spinosaurs were large theropod dinosaurs showing peculiar specializations, including somewhat crocodile-like elongate jaws and conical teeth. Their biology has been much discussed, and a piscivorous diet has been suggested on the basis of jaw as well as tooth morphology and stomach contents. Although fish eating has been considered plausible, an aquatic or semiaquatic lifestyle has seldom been suggested because of the apparent lack of corresponding adaptations in the postcranial skeleton of spinosaurs, which on the whole is reminiscent of that of other large terrestrial theropods. On the basis of the oxygen isotopic composition of their phosphatic remains compared with those of coexisting terrestrial theropod dinosaurs and semiaquatic crocodilians and turtles, we conclude that spinosaurs had semiaquatic lifestyles, i.e., they spent a large part of their daily time in water, like extant crocodilians or hippopotamuses. This result sheds light on niche partitioning between large predatory dinosaurs, since spinosaurs coexisted with other large theropods such as carcharodontosaurids or tyrannosaurids. The likely ichthyophagy and aquatic habits of spinosaurids may have allowed them to coexist with other large theropods by reducing competition for food and territory.

INTRODUCTION

The theropod family Spinosauridae was erected for *Spinosaurus aegyptiacus*, from the Cenomanian of Egypt, characterized by extremely tall neural spines on the dorsal vertebrae and peculiar, more or less conical and unserrated teeth (Stromer, 1915). Since then, spinosaurid remains have been reported from the Cretaceous of various parts of the world, including Africa (Bouaziz et al., 1988; Buffetaut, 1989; Sereno et al., 1998; Stromer, 1915; Taquet and Russell, 1998), Europe (Charig and Milner, 1986; Ruiz-Omeñaca et al., 2005), South America (Kellner and Campos, 1996; Medeiros, 2006; Sues et al., 2002), and Asia (Buffetaut and Ingavat, 1986; Buffetaut et al., 2008; Hasegawa et al., 2003); the oldest representatives are from the Late Jurassic of Africa (Buffetaut, 2008). That spinosaurids probably had dietary adaptations and lifestyles that were unusual for theropods was first suggested on the basis of fragmentary material from Africa (Taquet, 1984). The discovery of a fairly complete spinosaurid skeleton from the Wealden of southern England, described as *Baryonyx walkeri*, revealed a peculiarly constructed skull, with narrow and elongate jaws, somewhat reminiscent of longirostrine crocodilians (Rayfield et al., 2007); this suggested piscivorous habits, a hypothesis strengthened by stomach contents including partially digested fish scales (Charig and Milner, 1997). However, direct evidence concerning spinosaurid diet is inconclusive since it appears that they also fed on dinosaurs (Charig and Milner, 1997) and pterosaurs (Buffetaut et al., 2004). Nevertheless, because of the above-mentioned convergences in jaw and tooth shape, the hypothesis of spinosaurs as "crocodile mimics" (Holtz, 1998) has been widely accepted. However, their postcranial anatomy differs relatively little from that of usual large, bipedal theropods, and is not particularly suggestive of aquatic habits. As evidence based on morphology and stomach contents remains equivocal, we have applied stable isotope geochemistry to this question.

Oxygen isotope compositions of phosphate ($\delta^{18}O_p$) from biogenic apatites can be used to assess possible aquatic habits in spinosaurid dinosaurs. At the global scale, variations in the $\delta^{18}O$ values of homeothermic vertebrate (such as mammals or theropod dinosaurs; Amiot et al., 2006; Barrick and Showers, 1994; Fricke and Rogers, 2000) phosphate and body water are mainly controlled by variations in the compositions of drinking and food water, as well as by differences in physiology and ecology (Longinelli, 1984; Luz et al., 1984). For example, physiological adaptations to specific habitat use (aquatic, semiaquatic, or terrestrial) affect the $\delta^{18}O_{bw}$ value by controlling the magnitude of the oxygen fluxes involved in body input and output, some of them being associated with oxygen isotopic fractionations (Bryant and Froelich, 1995; Kohn, 1996; Luz and Kolodny, 1985). From living and fossil communities of mammals and reptiles, it has been observed that differences in mean $\delta^{18}O_p$ values between coexisting aquatic or semiaquatic vertebrates and terrestrial forms are related to their habitat use, aquatic or semiaquatic vertebrates having $\delta^{18}O_p$ values significantly lower than the values of coexisting terrestrial animals (Amiot et al., 2006; Bocherens et al., 1996; Cerling et al., 2008; Clementz et al., 2008; Fricke and Rogers, 2000) (Fig. 1).

*E-mail: romain.amiot@univ-lyon1.fr.

†Also affiliated with Institut Universitaire de France, 103 Boulevard Saint-Michel, 75005 Paris, France.

§Also affiliated with Natural History Museum of Guangxi, 1-1 East Renmin Road, Nanning 530012, China.

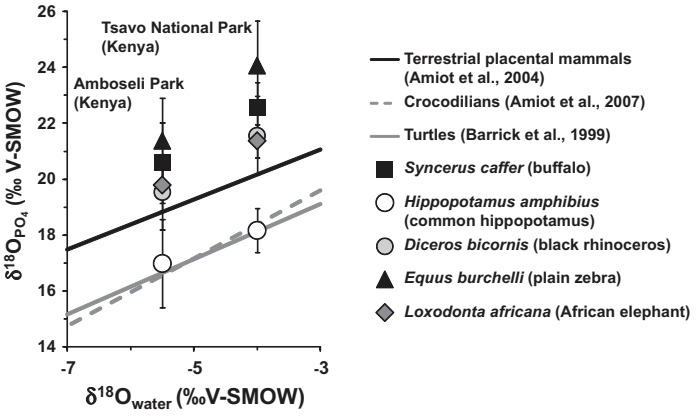

Figure 1. Mean oxygen isotope compositions of apatites versus drinking waters of mammals from two Kenyan parks showing difference in $\delta^{18}O_p$ values between semiaquatic hippopotamuses and terrestrial herbivorous mammals (error bars are ±1σ). V-SMOW—Vienna standard mean ocean water. Phosphate-water fractionation lines of terrestrial placental mammals, semiaquatic turtles, and crocodilians are displayed for comparison. Estimate of $\delta^{18}O$ value of water at Amboseli Park was arbitrarily chosen and explained in GSA Data Repository material (see footnote 1).

MATERIALS AND METHODS

We used 109 new and 24 published (Amiot et al., 2006) $\delta^{18}O_p$ values of tooth enamel from spinosaurs, other theropods, crocodilians, and turtle shell bones (for the complete data table, see the GSA Data Repository[1]). These fossil remains were recovered from 12 Cretaceous fluvial or fluvio-deltaic localities ranging from the Hauterivian–Barremian to the early Cenomanian, and are situated on all continents where spinosaurids have been identified so far (Asia—Buffetaut and Ingavat, 1986; Buffetaut et al., 2008; Europe—Charig and Milner, 1986; Africa—Bouaziz et al., 1988; Buffetaut, 1989; South America—Medeiros, 2006; Fig. 2). For consistency (e.g., to avoid body size differences that may lead to variations in $\delta^{18}O_p$ value differences between spinosaurs and coexisting terrestrial theropods), we selected spinosaur and coexisting other theropod teeth of similar sizes. Samples were prepared and measured for their oxygen isotope compositions using a standard procedure (Lécuyer, 2004; Lécuyer et al., 2007; see the Data Repository). Differences in oxygen isotope compositions of fossil remains were tested for significance using a nonparametric Wilcoxon signed-rank test and a two-way ANOVA (analysis of variance; see the Data Repository).

Figure 2. Location map of spinosaur samples. Inset is artist view of *Spinosaurus* (modified from Bogdanov's artwork). Locality numbers as in Table 1.

RESULTS

The $\delta^{18}O_p$ values obtained for spinosaurids were compared with those of associated terrestrial theropods and semiaquatic crocodilians and turtles (Fig. 3). The entire data set reveals that the $\delta^{18}O_p$ values of spinosaurid dinosaurs are 1.3‰ lower than $\delta^{18}O_p$ values of other coexisting theropods (Wilcoxon signed rank, n = 9, p = 0.02), but not significantly different from $\delta^{18}O_p$ values of coexisting crocodilians (Wilcoxon signed rank, n = 9, p = 0.515) and turtles (Wilcoxon signed rank, n = 6, p = 0.345). In some Moroccan and Tunisian localities, however, spinosaur values are either comparable to those of terrestrial theropods (location 12; Table 1) or extend from crocodilian and turtle values to terrestrial theropod values (locations 6, 8, and 11; Table 1).

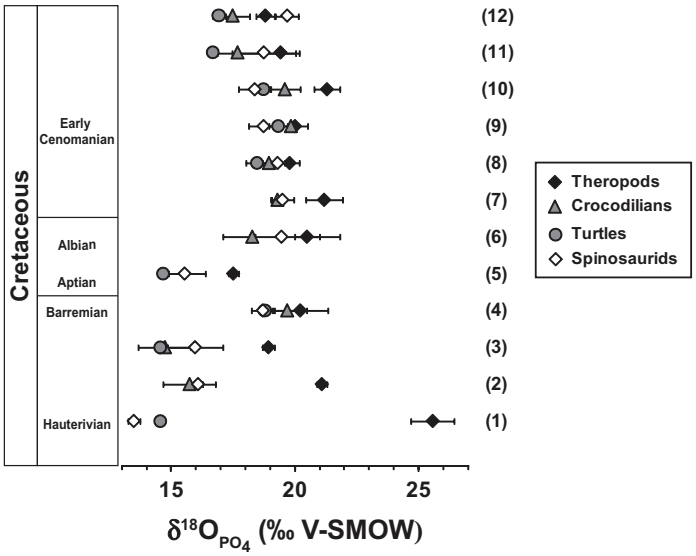

Figure 3. Mean phosphate $\delta^{18}O$ values of skeletal apatite from spinosaurs, theropods, freshwater turtles, and crocodilians sorted by geological age, from Hauterivian–Barremian to early Cenomanian (error bars are ±1σ). V-SMOW—Vienna standard mean ocean water. Locality numbers as in Table 1.

DISCUSSION

Secondary precipitation of apatite and isotopic exchange during microbially mediated reactions may alter the primary composition of biogenic apatites (Blake et al., 1997; Zazzo et al., 2004a). However, apatite crystals that make up tooth enamel are large and densely packed, and isotopic exchange under inorganic conditions has little effect on the oxygen isotope composition of phosphates, even at geological time scales (Kolodny et al., 1983; Lécuyer et al., 1999). Although no method is available to demonstrate definitely whether the oxygen isotope composition of fossil vertebrate phosphate was affected by diagenetic processes, several ways to assess the preservation state of the primary isotopic record have been proposed (Fricke and Rogers, 2000; Kolodny et al., 1996; Lécuyer et al., 2003; Pucéat et al., 2004; Zazzo et al., 2004b). Here, the main argument supporting the preservation of the original oxygen isotope

[1]GSA Data Repository item 2010038, oxygen isotope compositions of vertebrate phosphates, oxygen isotope analysis of phosphate procedure, statistical analyses, and estimation of Amboseli National Park water $\delta^{18}O$ value, is available online at www.geosociety.org/pubs/ft2010.htm, or on request from editing@geosociety.org or Documents Secretary, GSA, P.O. Box 9140, Boulder, CO 80301, USA.

TABLE 1. AVERAGE $\delta^{18}O_p$ AND STANDARD DEVIATION VALUES OF THEROPODS, SPINOSAURS, CROCODILIANS, AND TURTLES FOR EACH LOCALITY

	Spinosaurs			Theropods			Crocodilians			Turtles		
Loc.	N	Mean	St. dev.	N	Mean	St. dev.	N	Mean	St. dev.	N	Mean	St. dev.
12	6	19.7	0.5	4	18.8	0.4	3	17.5	0.7	2	17.0	0.3
11	7	18.8	1.3	6	19.4	0.8	3	17.7	0.9	1	16.7	–
10	5	18.4	0.7	4	21.3	0.5	2	19.6	0.6	2	18.8	0.1
9	4	18.7	0.6	2	20.0	0.1	2	19.9	0.7	2	19.3	0.4
8	3	19.3	0.3	3	19.8	0.4	3	19.0	0.3	3	18.5	0.4
7	8	19.5	0.5	3	21.2	0.8	3	19.3	0.2	–	–	–
6	3	19.5	2.4	3	20.5	0.5	2	18.3	0.1	–	–	–
5	2	15.6	0.8	3	17.5	0.2	–	–	–	1	14.7	-
4	4	18.7	0.5	5	20.2	1.1	9	19.7	0.8	2	18.8	0.2
3	3	16.0	1.1	2	18.9	0.2	2	14.8	1.1	–	–	–
2	1	16.1	–	1	21.1	–	2	15.8	1.1	–	–	–
1	2	13.5	0.2	3	25.6	0.9	–	–	–	2	14.6	0.1

Note: Dashes indicate no data, or not applicable. Loc.—locality numbers: 1—Phu Wiang1 (Thailand); 2—Khok Kong (Thailand); 3—Phu Phok (Thailand); 4—Isle of Wight (England); 5—Liu Bang Cun (China); 6—Bateun El Hmaima (Tunisia); 7—Laje do Coringa (Brazil); 8—Jebel al Qabla (Morocco); 9—Takemout (Morocco); 10—Chaaft (Morocco); 11—Khetitila Srhira (Morocco); 12—Bou Laalou (Morocco). N—number; St. dev.—standard deviation.

composition is the systematic offset observed between semiaquatic turtles and crocodilians and terrestrial theropods, the latter having significantly higher $\delta^{18}O_p$ values than coexisting crocodilians and turtles, whatever their age and geographical location (Wilcoxon signed rank, $n = 9$, $p < 0.01$). If early diagenetic processes had occurred, they would have homogenized $\delta^{18}O_p$ values of all vertebrate remains whatever the physiology and ecology of the corresponding taxa (Lécuyer et al., 2003). This observation is a strong argument supporting at least partial preservation of the original $\delta^{18}O_p$ values (Amiot et al., 2006; Fricke and Rogers, 2000). A diet-related difference as a possible explanation for $\delta^{18}O_p$ value offsets between spinosaurs and other coexisting theropods is highly unlikely, because there is direct fossil evidence indicating an opportunistic feeding behavior among spinosaurs, rather than strict ichthyophagy. Indeed, dinosaurs (Charig and Milner, 1997) and pterosaurs (Buffetaut et al., 2004) have been shown to be a part of the spinosaur diet either by scavenging (Buffetaut et al., 2004) or by predation (Kellner, 2004). Moreover, as opportunistic predators, coexisting crocodilians and spinosaurs most likely had similar diets, and the $\delta^{18}O_p$ values of crocodilians do not differ significantly from those of spinosaurs, despite their known semiaquatic lifestyle. Low $\delta^{18}O_p$ values of spinosaurs compared to other theropods can be interpreted as the result of differences between the oxygen isotope compositions of their body water. A semiaquatic behavior for spinosaurs would reduce daily aerial evapotranspiration, which is known to be one of the significant processes of ^{18}O enrichment of body water relative to surface water (Kohn, 1996). Moreover, low body fluids ^{18}O enrichment relative to drinking water in semiaquatic animals such as crocodilians or hippopotamuses is also the result of elevated water turnovers and water loss through urine or feces (Bentley and Schmidt-Nielsen, 1965; Clementz et al., 2008). From these considerations, a semiaquatic lifestyle is the most plausible explanation for the oxygen isotope difference observed between spinosaurs and other coexisting theropods, and the similar values shared by spinosaurs and semiaquatic crocodilians and turtles. This interpretation is also supported by similar offsets observed between the $\delta^{18}O_p$ values of present-day herbivorous mammals (zebras, buffalos, elephants, and rhinoceroses) and those of coexisting hippopotamuses from two Kenyan national parks (Bocherens et al., 1996; Cerling et al., 2008; Fig. 1). Considering that compared animals have similar diets (both hippopotamuses and other coexisting herbivorous mammals feed on land plants [Boisserie et al., 2005], and spinosaurs were predators like coexisting crocodilians and other theropods) and thermoregulations (mammals and theropod dinosaurs are both considered as homeotherms; Amiot et al., 2006; Fricke and Rogers, 2000; Luck and Wright, 1959), the similar isotopic offsets observed between spinosaurs versus theropods and hippopotamuses versus terrestrial mammals is most likely related to analogous aquatic lifestyles.

The amphibious habits of spinosaurs, given their apparent lack of anatomical adaptation to aquatic habits, may have been a thermoregulatory strategy. Modern crocodilians and hippopotamuses submerge to regulate their body temperature (Noirard et al., 2008; Seebacher et al., 2003). Such a behavior among spinosaurid theropods is therefore conceivable. Niche partitioning to avoid competition for resources with other vertebrates is another hypothesis that may explain the semiaquatic lifestyle of most spinosaurs. Indeed, at all localities where they occur, spinosaur remains are found associated with those of other theropods of comparable size. Fish eating and an aquatic habitat may have been a way for most spinosaurs to reduce competition for food and territory with other large theropods, which had an unequivocal terrestrial mode of life. This semiaquatic oxygen isotope signature is not clearly observed for *Spinosaurus* from Tunisia and Morocco, even though this genus possesses highly advanced specializations for fish catching in jaw elongation and tooth morphology. As shown by fossils from many African Cretaceous localities, spinosaurs apparently coexisted and competed for food resources with both other large theropods on land and large or giant crocodilians in rivers and lakes. These peculiar trophic conditions with multiple top predators may have forced some African spinosaurs to have a more opportunistic habitat use by alternating aquatic and terrestrial life.

Stable oxygen isotopes unambiguously show for the first time that some dinosaurs, i.e., the spinosaurid theropods, used freshwater environments more as a living habitat than just as temporary hunting (or fishing) grounds. Dinosaurs were thus a more ecologically diverse group than previously thought since at least some of them were not restricted to terrestrial habitats.

ACKNOWLEDGMENTS

We thank Thomas Tütken and two anonymous reviewers for constructive comments that helped to improve the manuscript. This study was supported by the French CNRS (Centre National de la Recherche Scientifique) ECLIPSE 2 program, the National Natural Science Foundation of China (grants 40730208, 40502019, and 40862001), the Chinese Academy of Sciences, the Major Basic Research Projects of the Ministry of Science and Technology of China (2006CB806400), the Jurassic Foundation, and a Thai-French joint project (PHC 16610UJ).

REFERENCES CITED

Amiot, R., Lécuyer, C., Buffetaut, E., Fluteau, F., Legendre, S., and Martineau, F., 2004, Latitudinal temperature gradient during the Cretaceous upper Campanian–middle Maastrichtian: $\delta^{18}O$ record of continental vertebrates: Earth and Planetary Science Letters, v. 226, p. 255–272, doi: 10.1016/j.epsl.2004.07.015.

Amiot, R., Lécuyer, C., Buffetaut, E., Escarguel, G., Fluteau, F., and Martineau, F., 2006, Oxygen isotopes from biogenic apatites suggest widespread endothermy in Cretaceous dinosaurs: Earth and Planetary Science Letters, v. 246, p. 41–54, doi: 10.1016/j.epsl.2006.04.018.

Amiot, R., Lécuyer, C., Escarguel, G., Billon-Bruyat, J., Buffetaut, E., Langlois, C., Martin, S., Martineau, F. and Mazin, J.M., 2007, Oxygen isotope fractionation between crocodilian phosphate and water: Palaeogeography, Palaeoclimatology, Palaeoecology, v. 243, p. 412–420, doi: 10.1016/j.palaeo.2006.08.013.

Barrick, R.E., and Showers, W.J., 1994, Thermophysiology of *Tyrannosaurus rex*: Evidence from oxygen isotopes: Science, v. 265, p. 222–224, doi: 10.1126/science.265.5169.222.

Barrick, R.E., Fischer, A.G., and Showers, W.J., 1999, Oxygen isotopes from turtle bone; applications for terrestrial paleoclimates?: Palaios, v. 14, p. 186–191.

Bentley, P.J., and Schmidt-Nielsen, K., 1965, Permeability to water and sodium of the crocodilian, *Caiman sclerops*: Journal of Cellular and Comparative Physiology, v. 66, p. 303–309, doi: 10.1002/jcp.1030660307.

Blake, R.E., O'Neil, J.R., and Garcia, G.A., 1997, Oxygen isotope systematics of biologically mediated reactions of phosphate; I, Microbial degradation of

organophosphorus compounds: Geochimica et Cosmochimica Acta, v. 61, p. 4411–4422, doi: 10.1016/S0016-7037(97)00272-X.
Bocherens, H., Koch, P.L., Mariotti, A., Geraads, D., and Jaeger, J.-J., 1996, Isotopic biogeochemistry (^{13}C, ^{18}O) of mammalian enamel from African Pleistocene hominid sites: Palaios, v. 11, p. 306–318, doi: 10.2307/3515241.
Boisserie, J.-R., Zazzo, A., Merceron, G., Blondel, C., Vignaud, P., Likius, A., and Mackaye, H.T., 2005, Diets of modern and late Miocene hippopotamids: Evidence from carbon isotope composition and micro-wear of tooth enamel: Palaeogeography, Palaeoclimatology, Palaeoecology, v. 221, p. 153–174, doi: 10.1016/j.palaeo.2005.02.010.
Bouaziz, S., Buffetaut, E., Ghanmi, M., Jaeger, J.-J., Martin, M., Mazin, J.-M., and Tong, H., 1988, New discoveries of fossil vertebrates from the Albian of south Tunisia: Bulletin de la Société Géologique de France, v. 4, p. 335–339.
Bryant, D.J., and Froelich, P.N., 1995, A model of oxygen isotope fractionation in body water of large mammals: Geochimica et Cosmochimica Acta, v. 59, p. 4523–4537, doi: 10.1016/0016-7037(95)00250-4.
Buffetaut, E., 1989, New remains of the enigmatic dinosaur *Spinosaurus* from the Cretaceous of Morocco and the affinities between *Spinosaurus* and *Baryonyx*: Neues Jahrbuch für Geologie und Palaontologie Abhandlungen, v. 1989, p. 79–87.
Buffetaut, E., 2008, Spinosaurid teeth from the Late Jurassic of Tendaguru, Tanzania, with remarks on the evolutionary and biogeographical history of the Spinosauridae: Documents des Laboratoires de Géologie de Lyon, v. 164, p. 26–28.
Buffetaut, E., and Ingavat, R., 1986, Unusual theropod dinosaur teeth from the Upper Jurassic of Phu Wiang, northeastern Thailand: Revue de Paléobiologie, v. 5, p. 217–220.
Buffetaut, E., Martill, D.M., and Escuillié, F., 2004, Pterosaurs as part of a spinosaur diet: Nature, v. 430, p. 33, doi: 10.1038/430033a.
Buffetaut, E., Suteethorn, V., Tong, H., and Amiot, R., 2008, An Early Cretaceous spinosaurid theropod from southern China: Geological Magazine, v. 145, p. 745–748, doi: 10.1017/S0016756808005360.
Cerling, T.E., Harris, J.M., Hart, J.A., Paleme, P., Klingel, H., Leakey, M.G., Levin, N.E., Lewison, R.L., and Passey, B.H., 2008, Stable isotope ecology of the common hippopotamus: Journal of Zoology, v. 276, p. 204–212, doi: 10.1111/j.1469-7998.2008.00450.x.
Charig, A.J., and Milner, A.C., 1986, *Baryonyx*, a remarkable new theropod dinosaur: Nature, v. 324, p. 359–361, doi: 10.1038/324359a0.
Charig, A.J., and Milner, A.C., 1997, *Baryonyx walkeri*, a fish-eating dinosaur from the Wealden of Surrey: Natural History Museum of London Bulletin, Geology Series, v. 53, p. 11–70.
Clementz, M.T., Holroyd, P.A., and Koch, P.L., 2008, Identifying aquatic habits of herbivorous mammals through stable isotope analysis: Palaios, v. 23, p. 574–585, doi: 10.2110/palo.2007.p07-054r.
Fricke, H.C., and Rogers, R.R., 2000, Multiple taxon-multiple locality approach to providing oxygen isotope evidence for warm-blooded theropod dinosaurs: Geology, v. 28, p. 799–802, doi: 10.1130/0091-7613(2000)28<799:MTLATP>2.0.CO;2.
Hasegawa, O., Buffetaut, E., Manabe, M., and Takakuwa, Y., 2003, A possible spinosaurid tooth from the Sebayashi Formation (Lower Cretaceous), Gunma, Japan: Gunma Museum of Natural History Bulletin, v. 7, p. 1–5.
Holtz, T.R., Jr., 1998, Spinosaurs as crocodile mimics: Science, v. 282, p. 1276–1277, doi: 10.1126/science.282.5392.1276.
Kellner, A.W.A., 2004, On a pterosaur neck with a dinosaur tooth: Scavenging or predation?: Natura Nascosta, v. 29, p. 41–43.
Kellner, A.W.A., and Campos, D., 1996, First Early Cretaceous theropod dinosaur from Brazil with comments on Spinosauridae: Neues Jahrbuch für Geologie und Palaeontologie Abhandlungen, v. 199, p. 151–166.
Kohn, M.J., 1996, Predicting animal $\delta^{18}O$: Accounting for diet and physiological adaptation: Geochimica et Cosmochimica Acta, v. 60, p. 4811–4829, doi: 10.1016/S0016-7037(96)00240-2.
Kolodny, Y., Luz, B., and Navon, O., 1983, Oxygen isotope variations in phosphate of biogenic apatites; I, Fish bone apatite; rechecking the rules of the game: Earth and Planetary Science Letters, v. 64, p. 398–404, doi: 10.1016/0012-821X(83)90100-0.
Kolodny, Y., Luz, B., Sander, M.P., and Clemens, W.A., 1996, Dinosaur bones: Fossils or pseudomorphs? The pitfalls of physiology reconstruction from apatitic fossils: Palaeogeography, Palaeoclimatology, Palaeoecology, v. 126, p. 161–171, doi: 10.1016/S0031-0182(96)00112-5.
Lécuyer, C., 2004, Oxygen isotope analysis of phosphates, *in* de Groot, P., ed., Handbook of stable isotope analytical techniques, Volume 1: Amsterdam, Elsevier B.V., p. 482–496.
Lécuyer, C., Grandjean, P., and Sheppard, S.M.F., 1999, Oxygen isotope exchange between dissolved phosphate and water at temperatures <135°C: Inorganic versus biological fractionations: Geochimica et Cosmochimica Acta, v. 63, p. 855–862, doi: 10.1016/S0016-7037(99)00096-4.
Lécuyer, C., Bogey, C., Garcia, J.-P., Grandjean, P., Barrat, J.-A., Floquet, M., Bardet, N., and Pereda-Superbiola, X., 2003, Stable isotope composition and rare earth element content of vertebrate remains from the Late Cretaceous of northern Spain (Lano); did the environmental record survive?: Palaeogeography, Palaeoclimatology, Palaeoecology, v. 193, p. 457–471, doi: 10.1016/S0031-0182(03)00261-X.
Lécuyer, C., Fourel, F., Martineau, F., Amiot, R., Bernard, A., Daux, V., Escarguel, G., and Morrison, J., 2007, High-precision determination of $^{18}O/^{16}O$ ratios of silver phosphate by EA-pyrolysis-IRMS continuous flow technique: Journal of Mass Spectrometry, v. 42, p. 36–41, doi: 10.1002/jms.1130.
Longinelli, A., 1984, Oxygen isotopes in mammal bone phosphate; a new tool for paleohydrological and paleoclimatological research?: Geochimica et Cosmochimica Acta, v. 48, p. 385–390, doi: 10.1016/0016-7037(84)90259-X.
Luck, C.P., and Wright, P.G., 1959, The body temperature of the hippopotamus: Journal of Physiology, v. 147, p. 53P–54P.
Luz, B., and Kolodny, Y., 1985, Oxygen isotope variations in phosphate of biogenic apatites; IV, Mammal teeth and bones: Earth and Planetary Science Letters, v. 75, p. 29–36, doi: 10.1016/0012-821X(85)90047-0.
Luz, B., Kolodny, Y., and Horowitz, M., 1984, Fractionation of oxygen isotopes between mammalian bone-phosphate and environmental drinking water: Geochimica et Cosmochimica Acta, v. 48, p. 1689–1693, doi: 10.1016/0016-7037(84)90338-7.
Medeiros, M.A., 2006, Large theropod teeth from the Eocenomanian of northeastern Brazil and the occurence of Spinosauridae: Revista Brasileira de Paleontologia, v. 9, p. 333–338, doi: 10.4072/rbp.2006.3.08.
Noirard, C., Le Berre, M., Ramousse, R., and Lena, J.P., 2008, Seasonal variation of thermoregulatory behaviour in the Hippopotamus (*Hippopotamus amphibius*): Journal of Ethology, v. 26, p. 191–193, doi: 10.1007/s10164-007-0052-1.
Pucéat, E., Reynard, B., and Lécuyer, C., 2004, Can crystallinity be used to determine the degree of chemical alteration of biogenic apatites?: Chemical Geology, v. 205, p. 83–97, doi: 10.1016/j.chemgeo.2003.12.014.
Rayfield, E.J., Milner, A.C., Xuan, V.B., and Young, P.G., 2007, Functional morphology of spinosaur 'crocodile-mimic' dinosaurs: Journal of Vertebrate Paleontology, v. 27, p. 892–901, doi: 10.1671/0272-4634(2007)27[892:FMOSCD]2.0.CO;2.
Ruiz-Omeñaca, J.I., Canudo, J.I., Cruzado-Caballero, P., Infante, P., and Moreno-Azanza, M., 2005, Baryonychine teeth (Theropoda: Spinosauridae) from the Lower Cretaceous of La Cantalera (Josa, NE Spain): Kaupia, v. 14, p. 59–63.
Seebacher, F., Elsey, R.M., and Trosclair, P.L.I., 2003, Body temperature null distributions in reptiles with nonzero heat capacity: Seasonal thermoregulation in the American Alligator (*Alligator mississippiensis*): Physiological and Biochemical Zoology, v. 76, p. 348–359, doi: 10.1086/375426.
Sereno, P.C., and 12 others, 1998, A long-snouted predatory dinosaur from Africa and the evolution of spinosaurids: Science, v. 282, p. 1298–1302, doi: 10.1126/science.282.5392.1298.
Stromer, E., 1915, Results of the research trip of Prof. E. Stromer in the deserts of Egypt; II, Vertebrate remains of the Baharije level (lower Cenomanian); 3, The original theropod *Spinosaurus aegyptiacus* nov. gen., nov. spec.: Abhandlungen der Bayerischen Akademie der Wissenschaften, Mathematisch-naturwissenschaftliche Abteilung, Neue Folge, v. 28, p. 1–32.
Sues, H.-D., Frey, E., Martill, D.M., and Scott, D.M., 2002, *Irritator challengeri*, a spinosaurid (Dinosauria; Theropoda) from the Lower Cretaceous of Brazil: Journal of Vertebrate Paleontology, v. 22, p. 535–547, doi: 10.1671/0272-4634(2002)022[0535:ICASDT]2.0.CO;2.
Taquet, P., 1984, A curious specialisation of the skull of some Cretaceous carnivorous dinosaurs: The long and narrow snout of spinosaurids: Académie des Sciences Comptes Rendus, ser. IIA, v. 299, p. 217–222.
Taquet, P., and Russell, D.A., 1998, New data on spinosaurid dinosaurs from the Early Cretaceous of the Sahara: Paris, Académie des Sciences Comptes Rendus, ser. IIA, v. 327, p. 347–353, doi: 10.1016/S1251-8050(98)80054-2.
Zazzo, A., Lécuyer, C., and Mariotti, A., 2004a, Experimentally-controlled carbon and oxygen isotope exchange between bioapatites and water under inorganic and microbially-mediated conditions: Geochimica et Cosmochimica Acta, v. 68, p. 1–12, doi: 10.1016/S0016-7037(03)00278-3.
Zazzo, A., Lécuyer, C., Sheppard, S.M.F., Grandjean, P., and Mariotti, A., 2004b, Diagenesis and the reconstruction of paleoenvironments: A method to restore original $\delta^{18}O$ values of carbonate and phosphate from fossil tooth enamel: Geochimica et Cosmochimica Acta, v. 68, p. 2245–2258, doi: 10.1016/j.gca.2003.11.009.

Manuscript received 20 May 2009
Revised manuscript received 25 August 2009
Manuscript accepted 28 August 2009

Printed in USA

PUBLICATION 2.5

Oxygen isotope composition of continental vertebrate apatites from Mesozoic formations of Thailand; environmental and ecological significance

ROMAIN AMIOT[1,2]*, ERIC BUFFETAUT[3], CHRISTOPHE LÉCUYER[2,4], VINCENT FERNANDEZ[5], FRANÇOIS FOUREL[2], FRANÇOIS MARTINEAU[2] & VARAVUDH SUTEETHORN[6]

[1]*Institute of Vertebrate Paleontology and Paleoanthropology, Chinese Academy of Sciences, #142 XiZhiMenWai DaJie, Beijing 100044, China*

[2]*UMR CNRS 5125, Paléoenvironnements et Paléobiosphère, Université Lyon1, 2 rue Raphaël Dubois, 69622 Villeurbanne Cedex, France*

[3]*CNRS (UMR 8538, Laboratoire de Géologie de l'Ecole Normale Supérieure), 24 rue Lhomond, 75231 Paris Cedex 05, France*

[4]*Institut Universitaire de France, 103 bld Saint-Michel, 75005 Paris, France*

[5]*European Synchrotron Radiation Facility, BP220, 6 rue Jules Horowitz, 38043 Grenoble Cedex, France*

[6]*Department of Mineral Resources, Rama VI Road, Bangkok 10400, Thailand*

**Corresponding author (e-mail: romain.amiot@ivpp.ac.cn)*

Abstract: Phosphatic remains (tooth enamel, turtle shell fragments and fish scales) of continental vertebrates (freshwater fish, crocodilians, turtles, and theropod and sauropod dinosaurs) recovered from eight localities of NE Thailand ranging in age from the Late Jurassic to the late Early Cretaceous have been analysed for their oxygen isotopic compositions ($\delta^{18}O_p$). From these preliminary data, local meteoric water $\delta^{18}O_w$ values estimated using $\delta^{18}O_p$ values of crocodilians and turtles range from $-4.1 \pm 2‰$ at the end of the Jurassic to $-8.3 \pm 2‰$ during the Early Cretaceous, suggesting a transition from dry to wetter climates with increasing amount of seasonal precipitation from several hundred millimetres per year to several thousand millimetres. Measurable offsets in $\delta^{18}O_p$ values observed between dinosaur taxa (the spinosaurid theropod *Siamosaurus*, other theropods and nemegtosaurid sauropods) are interpreted in terms of differences in water strategies, and suggest that *Siamosaurus* had habits similar to those of semi-aquatic vertebrates such as crocodilians or freshwater turtles.

Mesozoic non-marine formations cropping out on the Khorat Plateau, in NE Thailand, constitute the Khorat Group, a 3200 m thick succession of clastic sediments ranging from the Late Jurassic (Phu Kradung Formation) to Albian–Aptian (Khok Kruat Formation). Detrital material probably originated from the erosion of the Qinling orogenic belt (north of the Sichuan basin, China) and was transported by large braided river systems before being deposited in low-energy, meandering fluvial channels and on extensive floodplains (Mouret *et al.* 1993; Heggemann 1994; Racey *et al.* 1996; Carter & Bristow 2003). During the deposition of the Khorat Group, the Khorat Plateau (situated on the Indochina block) was estimated to be 500–1300 km north of its present position, within South China relatively close to the Sichuan foreland basin (Fig. 1), and was displaced to its present position during the Tertiary extrusion of SE Asia caused by the collision of India with Asia (Leloup *et al.* 1995; Sato *et al.* 1999; Carter & Bristow 2003). Dry climates prevailed during the deposition of the Khorat Group according to sedimentological and paleobotanical studies, except for the upper formations, which were probably deposited under wetter conditions (Hahn 1982; Mouret *et al.* 1993; Heggemann 1994; Philippe *et al.* 2004). However, quantitative estimates of these climatic variations have not been provided so far.

The Late Jurassic and Early Cretaceous Phu Kradung, Sao Khua and Khok Kruat Formations of the Khorat Group have yielded rich vertebrate

From: BUFFETAUT, E., CUNY, G., LE LOEUFF, J. & SUTEETHORN, V. (eds) *Late Palaeozoic and Mesozoic Ecosystems in SE Asia*. The Geological Society, London, Special Publications, **315**, 271–283.
DOI: 10.1144/SP315.19 0305-8719/09/$15.00

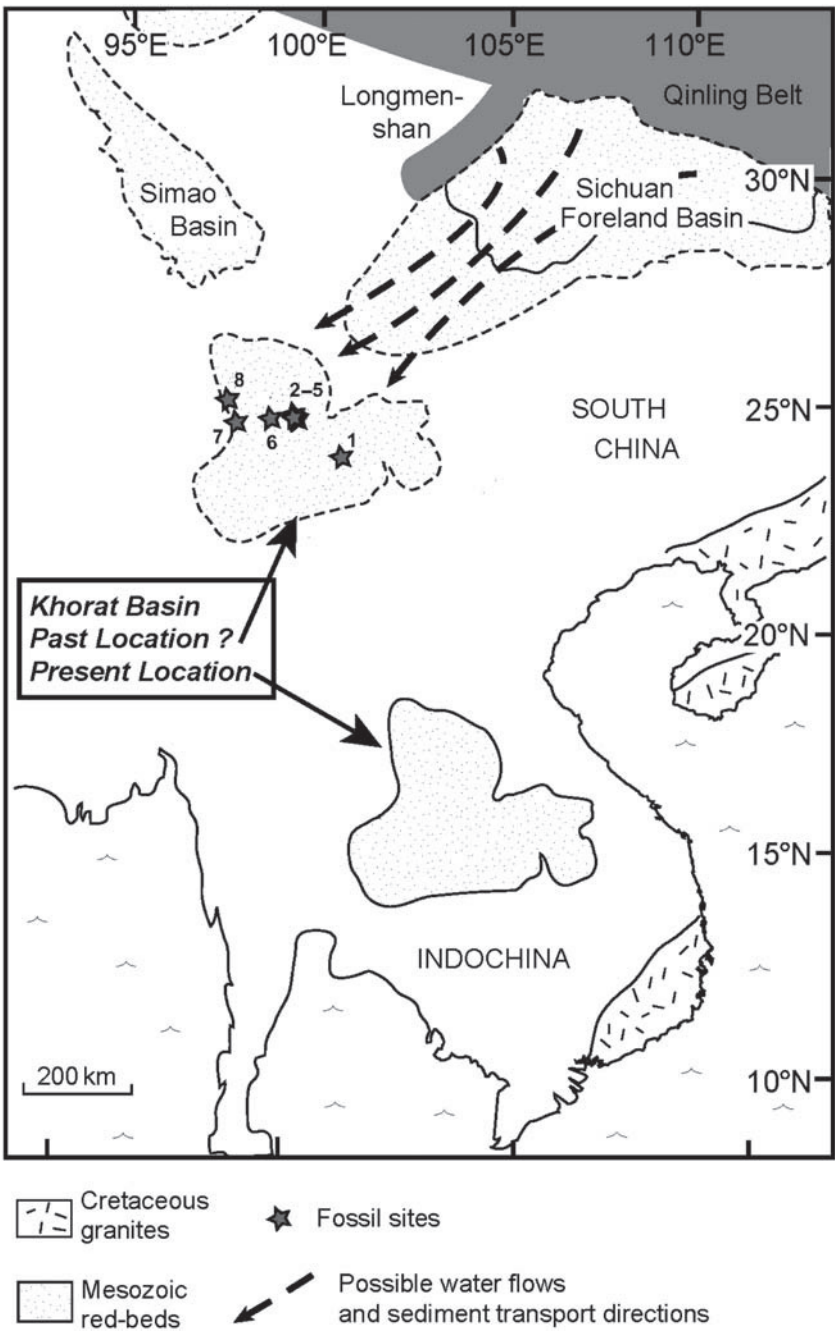

Fig. 1. General map of SE Asia showing the present (continuous lines) and restored Cretaceous (dashed lines) locations of the Khorat Basin. The pre-extrusion location places the Khorat Basin much closer to the Qinling orogenic belt and the Sichuan foreland basin, considered as the source of Khorat sediments. Fossil sites: 1, Khok Pha Suam; 2, Khok Kong; 3, Phu Phok; 4, Dan Luang; 5, Phu Nam Jun; 6, Ban Khok Sanam; 7, Phu Wiang 1; and 8, Chong Chad. Map modified from Carter & Bristow (2003).

faunas including lungfishes, elasmobranch and semionotid fishes, amphibians, crocodilians, turtles, pterosaurs, and theropod, sauropod, ornithopod, stegosaurid and psittacosaurid dinosaurs, as well as birds. The significance of these faunas in terms of vertebrate evolution and biogeographical history of SE Asia has been illustrated by numerous studies (e.g. Buffetaut & Suteethorn 1998, 1999; Buffetaut *et al.* 2000, 2006).

Oxygen isotopic compositions of vertebrate phosphate in bioapatite such as tooth enamel ($\delta^{18}O_p$) may allow a better knowledge of the palaeoclimatic or palaeoenvironmental conditions in which the Khorat Group was formed. The $\delta^{18}O_p$ value of vertebrate apatitic tissues (bones, teeth, fish scales) is a function of the $\delta^{18}O_{bw}$ value of the animal's body water as well as of its body temperature (Kolodny *et al.* 1983; Longinelli 1984; Luz *et al.* 1984). The $\delta^{18}O_{bw}$ value is related to the $\delta^{18}O_w$ value of ingested water and to the animal's ecology and physiology. For most continental vertebrates, the main source of ingested oxygen is drinking or plant water, which is meteoric water or derived from it (D'Angela & Longinelli 1990; Cormie *et al.* 1994; Kohn *et al.* 1996; Straight *et al.* 2004). As the $\delta^{18}O_w$ value of meteoric water depends on climatic parameters such as air temperature, hygrometry and amount of precipitation (Dansgaard 1964; von Grafenstein *et al.* 1996; Fricke & O'Neil 1999), vertebrates thus indirectly record in their phosphatic tissues the climatic conditions of their living environment. It is noteworthy that the $\delta^{18}O_w$ value of surface waters can differ from that of precipitation as a result of local processes such as evaporation or mixing with other water sources, thus complicating the interpretations in terms of climatic reconstructions. Physiological adaptations to specific habitat use (such as aquatic, semi-aquatic or terrestrial) affect the $\delta^{18}O_{bw}$ value by controlling the magnitude of body input and output oxygen fluxes, some of them being associated with oxygen isotopic fractionations (Luz & Kolodny 1985; Bryant & Froelich 1995; Kohn 1996). From living and fossil communities of mammals and reptiles, it has been observed that differences in the range of $\delta^{18}O_p$ values or in some cases differences in mean $\delta^{18}O_p$ values between coexisting aquatic or semi-aquatic vertebrates and terrestrial ones are related to their habitat use (Fricke & Rogers 2000; Clementz & Koch 2001; Clementz *et al.* 2003; Amiot *et al.* 2006). Ecological specificities such as plant-water use among herbivorous communities also affect the $\delta^{18}O_p$ value of vertebrates. Indeed, large differences in $\delta^{18}O_p$ value have been observed between coexisting herbivorous mammals that drink surface waters and those that only rely on water in plants, usually enriched by several per mil relative to surface waters (Kohn *et al.* 1996).

The $\delta^{18}O_w$ values of ingested water can be estimated from $\delta^{18}O_p$ values of fish, crocodilians, turtles and dinosaurs using PO_4–water fractionation equations established for extant species (e.g. Kolodny *et al.* 1983; Barrick *et al.* 1999; Amiot *et al.* 2007), the applicability of these equations having been tested with Mesozoic faunas (Barrick *et al.* 1999; Amiot *et al.* 2004, 2007; Billon-Bruyat *et al.* 2005). This study aims to interpret preliminary results obtained from the analysis of oxygen isotopic compositions of reptile and fish phosphatic tissues in terms of environmental conditions as well as to investigate physiological and ecological features of some dinosaurs from the Khorat Group.

Material and methods

Sample collection

Twenty-eight vertebrate samples were analysed for their oxygen isotope compositions. Samples include dinosaur (theropod and sauropod) and crocodilian tooth enamel, turtle bony plates and ganoine coating of fish scales. These fossil remains were collected as isolated specimens in eight localities belonging to the Khorat Group and ranging from the Late Jurassic to the late Early Cretaceous (Fig. 1; Table 1). The global palaeolatitude of the Khorat Plateau during the deposition of these Mesozoic formations was about 25°N (24.3°N for the Khok Pha Suam locality; Amiot *et al.* 2004), estimated using the method described by Besse & Courtillot (1988). The Dan Luang, Phu Nam Jun, Ban Khok Sanam and Chong Chad localities are in the Phu Kradung Formation, which is probably Late Jurassic or possibly earliest Cretaceous in age (Racey *et al.* 1996; Buffetaut & Suteethorn 1998). The Phu Phok, Khok Kong and Phu Wiang 1 localities belong to the Sao Khua Formation, the age of which is still uncertain, although it is clearly Early Cretaceous and ante-Aptian (see Buffetaut & Suteethorn 1999). The Khok Pha Suam locality is in the Khok Kruat Formation, considered as Aptian–Albian in age on the basis of the occurrence of the freshwater hybodont shark *Thaiodus* (Cappetta *et al.* 1990).

As reptile teeth are continuously replaced and take several months to grow (Erickson 1996*a*, *b*), they can record seasonal variations in ingested surface water $\delta^{18}O_w$ values. To retrieve mean annual values of local waters, enamel was sampled from the base to the apex of each tooth and several teeth from each locality were analysed. According to Clementz & Koch (2001), $\delta^{18}O$ values of at least 16 individuals per taxon may accurately reflect seasonal variability of their environment, but fossil reptile teeth from Thailand are too scarce to allow the gathering of such a

Table 1. *Oxygen isotope composition of phosphate from Late Jurassic–Early Cretaceous dinosaurs, fresh water crocodilians, turtles and fish*

Sample number	Nature	Taxon	Locality	Formation	Age	*n*	$\delta^{18}O$ (‰SMOW)
TH001*	Dinosaur tooth enamel	Theropoda	Khok Pha Suam	Khok Kruat	Aptian–Albian	1	15.5
TH005*	Dinosaur tooth enamel	Theropoda	Khok Pha Suam	Khok Kruat	Aptian–Albian	1	14.9
TH008*	Dinosaur tooth enamel	Theropoda	Khok Pha Suam	Khok Kruat	Aptian–Albian	1	17.3
TH006*	Dinosaur bulk tooth	Nemegtosauridae	Khok Pha Suam	Khok Kruat	Aptian–Albian	1	20.2
TH002*	Crocodilian tooth enamel	Crocodilia	Khok Pha Suam	Khok Kruat	Aptian–Albian	1	14.7
TH007*	Crocodilian tooth enamel	Crocodilia	Khok Pha Suam	Khok Kruat	Aptian–Albian	1	14.0
TH003*	Turtle osteoscute	Chelonia	Khok Pha Suam	Khok Kruat	Aptian–Albian	1	12.8
TH004	Fish scale	*Lepidotes*	Khok Pha Suam	Khok Kruat	Aptian–Albian	1	16.9
KPS-KKfm	Fish scale	*Lepidotes*	Khok Pha Suam	Khok Kruat	Aptian–Albian	16	17.7
PP-07	Dinosaur tooth enamel	Theropoda	Phu Phok	Sao Khua	Valanginian–Hauterivian	1	19.2
PP-08	Dinosaur tooth enamel	Theropoda	Phu Phok	Sao Khua	Valanginian–Hauterivian	1	18.7
PP-04	Dinosaur tooth enamel	*Siamosaurus*	Phu Phok	Sao Khua	Valanginian–Hauterivian	1	16.0
PP-05	Dinosaur tooth enamel	*Siamosaurus*	Phu Phok	Sao Khua	Valanginian–Hauterivian	1	14.6
PP-06	Dinosaur tooth enamel	*Siamosaurus*	Phu Phok	Sao Khua	Valanginian–Hauterivian	1	17.3
PP-02	Crocodilian tooth enamel	Crocodilia	Phu Phok	Sao Khua	Valanginian–Hauterivian	1	13.7
PP-03	Crocodilian tooth enamel	Crocodilia	Phu Phok	Sao Khua	Valanginian–Hauterivian	1	15.8
PP-SKfm	Fish scale	*Lepidotes*	Phu Phok	Sao Khua	Valanginian–Hauterivian	13	15.4
KK-04	Dinosaur tooth enamel	Theropoda	Khok Kong	Sao Khua	Valanginian–Hauterivian	1	21.1
KK-03	Dinosaur tooth enamel	*Siamosaurus*	Khok Kong	Sao Khua	Valanginian–Hauterivian	1	16.1
KK-01	Crocodilian tooth enamel	Crocodilia	Khok Kong	Sao Khua	Valanginian–Hauterivian	1	14.7
KK-02	Crocodilian tooth enamel	Crocodilia	Khok Kong	Sao Khua	Valanginian–Hauterivian	1	16.8
PW-03	Dinosaur tooth enamel	Theropoda	Phu Wiang 1	Sao Khua	Valanginian–Hauterivian	1	26.0
PW-04	Dinosaur tooth enamel	Theropoda	Phu Wiang 1	Sao Khua	Valanginian–Hauterivian	1	24.3
PW-05	Dinosaur tooth enamel	Theropoda	Phu Wiang 1	Sao Khua	Valanginian–Hauterivian	1	26.3
PW-06	Dinosaur tooth enamel	Nemegtosauridae	Phu Wiang 1	Sao Khua	Valanginian–Hauterivian	1	19.8
PW-01	Dinosaur tooth enamel	*Siamosaurus*	Phu Wiang 1	Sao Khua	Valanginian–Hauterivian	1	13.7
PW-02	Dinosaur tooth enamel	*Siamosaurus*	Phu Wiang 1	Sao Khua	Valanginian–Hauterivian	1	13.3
PW-07	Turtle osteoscute	Chelonia	Phu Wiang 1	Sao Khua	Valanginian–Hauterivian	1	14.5
PW-08	Turtle osteoscute	Chelonia	Phu Wiang 1	Sao Khua	Valanginian–Hauterivian	1	14.7
DL-01	Dinosaur tooth enamel	Theropoda	Dan Luang	Phu Kradung	Late Jurassic–earliest Cretaceous	1	19.7
DL-02	Crocodilian tooth enamel	Crocodilia	Dan Luang	Phu Kradung	Late Jurassic–earliest Cretaceous	1	17.0
DL-03	Crocodilian tooth enamel	Crocodilia	Dan Luang	Phu Kradung	Late Jurassic–earliest Cretaceous	1	19.5
PNJ-PKfm	Fish scale	*Lepidotes*	Phu Nam Jun	Phu Kradung	Late Jurassic–earliest Cretaceous	35	14.8
KS-PKfm	Fish scale	*Lepidotes*	Ban Khok Sanam	Phu Kradung	Late Jurassic–earliest Cretaceous	14	11.5
CC-PKfm	Fish scale	*Lepidotes*	Chong Chad	Phu Kradung	Late Jurassic–earliest Cretaceous	7	19.4

Sample identification, location and stratigraphic age are reported along with number of specimens per analysis (*n*). *, published values (Amiot *et al.* 2006).

sample collection for geochemical analysis. For each sample, the most mineralized apatitic part was used for geochemical analysis. Reptile tooth enamel was favoured against dentine, dense bone layers were selected from turtle shells, and ganoine (an enamel-like apatitic tissue) covering the surface of fish scales was sampled.

Analytical techniques

Measurements of oxygen isotope compositions of apatite consist in isolating PO_4^{3-} using acid dissolution and anion-exchange resin, according to a protocol derived from the original method published by Crowson *et al.* (1991) and slightly modified by Lécuyer *et al.* (1993). Silver phosphate was quantitatively precipitated in a thermostatic bath set at a temperature of 70 °C. After filtration, washing with double-deionized water, and drying at 50 °C, 15 mg of Ag_3PO_4 was mixed with 0.8 mg of pure powder graphite. $^{18}O/^{16}O$ ratios were measured by reducing silver phosphates to CO_2 using graphite reagent (O'Neil *et al.* 1994; Lecuyer *et al.* 1998). Samples were weighed into tin reaction capsules and loaded into quartz tubes and degassed for 30 min at 80 °C under vacuum. Each sample was heated at 1100 °C for 1 min to promote the redox reaction. The CO_2 produced was directly trapped in liquid nitrogen to avoid any kind of isotopic reaction with quartz at high temperature. CO_2 was then analysed with a GV Isoprime^{TM} mass spectrometer at the Laboratory UMR CNRS 5125 'PEPS', University Claude Bernard Lyon 1. Isotopic compositions are quoted in the standard δ notation relative to V-SMOW. Silver phosphate precipitated from standard NBS120c (natural Miocene phosphorite from Florida) was repeatedly analysed ($\delta^{18}O = 21.70 \pm 0.10‰$; $n = 12$) along with the silver phosphate samples derived from the fossil vertebrate remains.

Results

Oxygen isotope compositions of vertebrate phosphates are given in Table 1. The whole dataset including seven published $\delta^{18}O_p$ values (Amiot *et al.* 2004) ranges from 11.5 to 26.3‰ V-SMOW. Mean $\delta^{18}O_p$ values for each taxonomic group (theropod and sauropod dinosaurs, *Siamosaurus*, crocodilians, turtles and fish) are shown in Figure 2a. Estimates of the mean values of ingested surface waters, calculated using the oxygen isotope fractionation equations established between crocodilian phosphate and water (Amiot *et al.* 2007), turtle phosphate and water (Barrick *et al.* 1999), and fish phosphate and water (Kolodny *et al.* 1983), are given in Table 2 and displayed in Figure 2b. $\delta^{18}O_w$ values estimated using $\delta^{18}O_p$ values from crocodilians and turtles decrease from $-4.1 \pm 2.0‰$ in the upper part of the Phu Kradung Formation (Dan Luang locality) to values ranging from $-6.2 \pm 2.0‰$ to $-7 \pm 2.0‰$ in the Sao Khua Formation and from $-7.3 \pm 2.0‰$ to $-9.4 \pm 2.0‰$ in the Khok Kruat Formation. Assuming that typical subtropical temperatures of

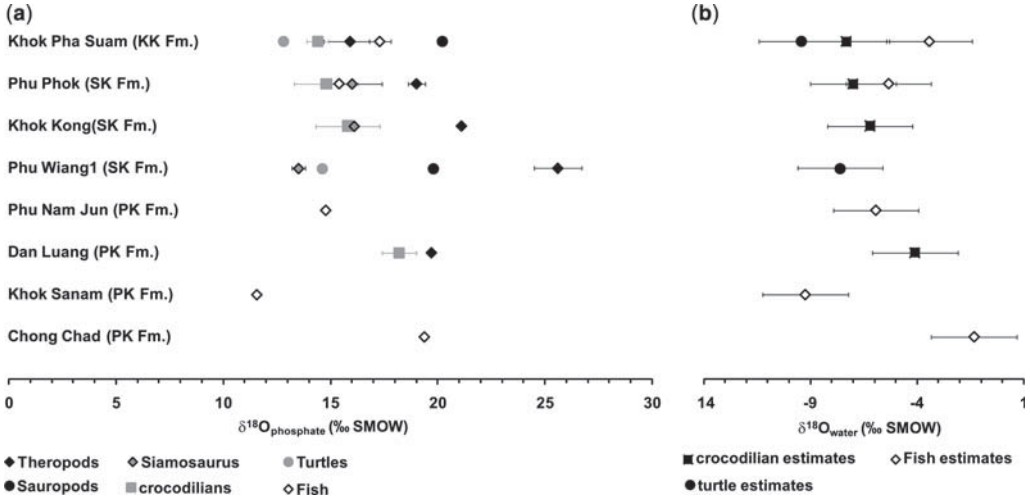

Fig. 2. (**a**) Mean $\delta^{18}O_p$ values of vertebrate faunas from the eight localities of the Khorat Group. Measurable offsets can be observed between coexisting dinosaurs (theropods, sauropods and the spinosaurid *Siamosaurus*), freshwater crocodilians, turtles and fish as a consequence of ecological and physiological differences. (**b**) $\delta^{18}O_w$ values of ingested waters estimated using crocodilian, turtle and fish $\delta^{18}O_p$ values and related fractionations equations. An uncertainty of $\pm 2‰$ is used for all estimated water $\delta^{18}O_w$ values although it only corresponds to the largest calculated uncertainty.

Table 2. *Mean oxygen isotopic composition of crocodilians, turtles and fish along with oxygen isotopic composition of environmental waters estimated for the Khorat Group localities*

Locality	Formation	$\delta^{18}O_p$ (‰SMOW) (crocodilians)			$\delta^{18}O_p$ (‰SMOW) (turtles)			$\delta^{18}O_p$ (‰SMOW) (fish at 20–25 °C)			$\delta^{18}O_w$ (‰SMOW) (from crocodilians)	$\delta^{18}O_w$ (‰SMOW) (from turtles)	$\delta^{18}O_w$ (‰SMOW) (from fish)	
		n	Mean	SD	*n*	Mean	SD	*n*	Mean	SD			20 °C	25 °C
Khok Pha Suam	Khok Kruat	2	14.4	0.5	1	12.8	–	2	17.3	0.5	−7.3	−9.4	−4.0	−2.9
Phu Phok	Sao Khua	2	14.8	1.5				1	15.4	–	−7		−5.9	−4.8
Khok Kong	Sao Khua	2	15.8	1.5							−6.2			
Phu Wiang 1	Sao Khua				2	14.6	0.2					−7.6		
Phu Nam Jun	Phu Kradung							1	14.8	–			−6.5	−5.4
Dan Luang	Phu Kradung	2	18.2	0.8							−4.1			
Ban Khok Sanam	Phu Kradung							1	11.5	–			−9.8	−8.7
Chong Chad	Phu Kradung							1	19.4	–			−1.9	−0.8

The following fractionation equations were used: crocodilians: $\delta^{18}O_w = 0.82 \times \delta^{18}O_p - 19.13$ (Amiot *et al.* 2007); turtles: $\delta^{18}O_w = 1.01 \times \delta^{18}O_p - 22.3$ (Barrick *et al.* 1999); fish: $T(°C) = 113.3 - 4.38 (\delta^{18}O_p - \delta^{18}O_w)$ (Kolodny *et al.* 1983).

about 20–25 °C occurred during the deposition of the Khorat Group (see discussion below), $\delta^{18}O_w$ values estimated using fish $\delta^{18}O_p$ values show significant fluctuations within the Phu Kradung Formation (-1.3 ± 2.0‰ at Chong Chad, -9.2 ± 2.0‰ at Khok Sanam and -5.9 ± 2.0‰ at Phu Nam Jun).

Discussion

Preservation of the original oxygen isotope compositions of vertebrate apatites?

Secondary precipitation of apatite and isotopic exchange during microbially mediated reactions may scramble the primary isotopic signal (Blake *et al.* 1997; Zazzo *et al.* 2004*a*). However, apatite crystals that make up tooth enamel or fish scale ganoine are large and densely packed, and isotopic exchange under inorganic conditions has little effect on the oxygen isotope composition of phosphates even at geological time scales (Kolodny *et al.* 1983; Lécuyer *et al.* 1999). Turtle shell bone should be more susceptible to diagenesis because hydroxylapatite crystals of bones are smaller and less densely intergrown than enamel (Kolodny *et al.* 1996), although several case studies have shown that the original oxygen isotope composition is preserved in Mesozoic turtle remains (Barrick *et al.* 1999; Amiot *et al.* 2004, 2006; Billon-Bruyat *et al.* 2005). Although no method is available to demonstrate definitely whether the oxygen isotope composition of fossil vertebrate phosphate was affected by diagenetic processes, several ways to assess the preservation state of the primary isotopic record have been proposed (e.g. Kolodny *et al.* 1996; Fricke & Rogers 2000; Lécuyer *et al.* 2003*a*; Pucéat *et al.* 2004; Zazzo *et al.* 2004*b*). Here, the main argument supporting the preservation of the original oxygen isotope composition is the systematic offset observed between dinosaurs and ectothermic reptiles (turtles and crocodilians), which probably resulted from differences in ecology and physiology. The present dataset illustrates systematic offsets between semi-aquatic animals (turtles and crocodilians) and terrestrial ones (dinosaurs, except *Siamosaurus*), the latter having $\delta^{18}O_p$ values 1.5–10‰ more positive than the values of crocodilians and turtles. If early diagenetic processes had occurred, they would have homogenized $\delta^{18}O_p$ values of all vertebrate remains whatever the physiology and ecology of the corresponding taxa (Lécuyer *et al.* 2003*a*). However, as only $\delta^{18}O_p$ values of scale ganoine from fish were measured for the localities of Chong Chad, Khok Sanam and Phu Nam Jun, the isotopic preservation state of these fossil scales remains uncertain, and the obtained values must be considered with caution.

Ecological implications

In low-latitude environments, ectothermic (here crocodilians and turtles) and endothermic (dinosaurs) animals should tend to have closely similar body temperatures, leading to very small differences in oxygen isotopic fractionation between their phosphate and body water. However, variable differences in $\delta^{18}O_p$ values are observed between crocodilians, turtles and the various groups of dinosaurs, and such offsets may be related to differences in physiology, ecology and origin of water intake. The most obvious difference is between semi-aquatic reptiles (crocodilians and turtles) and terrestrial dinosaurs, the latter having more positive $\delta^{18}O_p$ values, as a result of more important transcutaneous water evaporation, than crocodilians and turtles (which spend most of their life in water). Indeed, differences ranging from 1.6 to 3.1‰ between coexisting dinosaurs and both crocodilians and turtles have been predicted using model equations and measured on Cretaceous reptile faunas from low palaeolatitudes, assuming they had a common source of water intake (Amiot *et al.* 2006). However, such differences are observed here only between theropod dinosaurs (excluding *Siamosaurus*) and semi-aquatic reptiles from the Dan Luang and Khok Pha Suam localities. In all other localities, and between the sauropods and semi-aquatic reptiles from Khok Pha Suam, differences are larger, ranging from 4.2 to 11.0‰. Such differences suggest that these dinosaurs used different water sources from those used by crocodilians and turtles.

Assuming that these large isotopic offsets reflect different sources of ingested water, the following preliminary interpretations can be made.

(1) Water ingested by sauropod dinosaurs was water from plant leaves, generally enriched by several per mil relative to local water as a consequence of leaf evapotranspiration and inner physiological processes (e.g. Yakir *et al.* 1990; Flanagan & Ehleringer 1991). This may at least partly explain the 5.2–6.6‰ differences observed between sauropods and semi-aquatic reptiles.

(2) The main source of water used by theropod dinosaurs and more generally carnivorous animals is assumed to be surface waters such as streams, rivers and ponds. Some theropod dinosaurs from Thailand may have preferentially drunk from small temporary and evaporating ponds, rather than from main river streams, leading to the highly positive $\delta^{18}O_p$ values observed in the localities of Phu Phok, Khok Kong and Phu Wiang 1.

Siamosaurus suteethorni is a dinosaur having anomalous isotopic values compared with other dinosaurs (Table 1; Fig. 2a). It is a large spinosaurid theropod originally identified from isolated teeth (Buffetaut & Ingavat 1986), the systematic position of which was later confirmed by the discovery of a partial skeleton (Buffetaut *et al.* 2005). Some anatomical features of spinosaurid dinosaurs, such as their elongate snout bearing rather conical teeth, suggest that these dinosaurs ate preferentially, but not exclusively, fish (Taquet 1984; Charig & Milner 1986). This hypothesis has been supported by the discovery of partially digested fish scales in the stomach region of a nearly complete skeleton of *Baryonyx walkeri*, a spinosaurid dinosaur recovered from the Early Cretaceous of the Isle of Wight (Charig & Milner 1997). Also, some workers have emphasized that the massive forelimbs of *Baryonyx* certainly possessed sufficient strength and adequate musculature for the quadrupedal posture required when fishing either on the edge of the water or in it (Charig & Milner 1997).

On the other hand, despite the close resemblance between the jaws and teeth of spinosaurs and those of some crocodilians, and the likely ichthyophagy (fish diet) of spinosaurids, no evidence clearly supporting aquatic or semi-aquatic habits for these dinosaurs has been put forward. In fact, some anatomical features indicate that spinosaurs were terrestrial, largely bipedal, dinosaurs, like other theropods.

$\delta^{18}O_p$ values of *Siamosaurus* from the three localities of Phu Phok, Khok Kong and Phu Wiang1 are 3–12‰ lower than $\delta^{18}O_p$ values of other dinosaurs and, given the uncertainties attached to the values, are indistinguishable from those obtained for crocodilians or turtles. Two hypotheses may explain such low values. The first is that these spinosaurid dinosaurs were almost exclusively ingesting water that was ^{18}O-depleted relative to the water where coexisting crocodilians and turtles were drinking; however, the existence of ^{18}O-depleted sources different from the rivers where crocodilians and turtles were living is highly unlikely.

The second, and more likely, possibility is that *Siamosaurus* had somewhat semi-aquatic living habits similar to those of crocodilians and turtles. Because they spend much time in water, semi-aquatic animals have a higher body water turnover and less transcutaneous water evaporation than terrestrial forms. The body water (from which oxygen is used for apatite synthesis) of semi-aquatic animals is thus less ^{18}O-enriched than that of terrestrial animals, resulting in lower $\delta^{18}O_p$ values (Kohn 1996; Amiot *et al.* 2007). Although it has not yet been demonstrated that some dinosaurs had adapted to the ecological niche of a semi-aquatic predator, ichnological evidence of swimming theropods (Ezquerra *et al.* 2007) and evidence of fish as the preferential diet of spinosaurid dinosaurs (Charig & Milner 1997) suggest that such a hypothesis is not inconceivable. The hypothesis of physical adaptations to the semi-aquatic life of this group has to be tested with systematic oxygen isotope measurements of spinosaurid dinosaurs sampled from Africa, Europe and South America.

Climatic implications

It is now widely accepted that global climates during the Mesozoic, although being globally warmer than today, underwent important thermal fluctuations with significant cooling episodes, notably during the early Cretaceous, when 'icehouse' intervals have been recognized (Frakes & Francis 1988; Frakes 1999; Price 1999). During the deposition of the Khorat Group (from the late Jurassic–earliest Cretaceous to the Aptian–Albian), global palaeotemperatures estimated for latitudes of about 25°N roughly varied within a 20–25 °C range (Frakes *et al.* 1994; Frakes 1999; Lécuyer *et al.* 2003*b*; Pucéat *et al.* 2003; Steuber *et al.* 2005). It is also noteworthy that such mean palaeotemperatures are similar to those experienced today at subtropical latitudes (Table 3; IAEA–WMO 2004). We therefore hypothesize that this temperature range occurred in NE Thailand during the Early Cretaceous. As $\delta^{18}O_{mw}$ values of meteoric waters at tropical and subtropical latitudes are influenced more by precipitation amounts than by air temperatures (Dansgaard 1964), the mean air temperature–mean $\delta^{18}O_{mw}$ relationships are not applicable in this case, and $\delta^{18}O_w$ values of surface waters estimated from $\delta^{18}O_p$ values of vertebrates may be interpreted in terms of humidity (amount of precipitations) or aridity. For example, in subtropical climates with high amounts of seasonal precipitation (several thousands of millimetres per year), such as the monsoon climates of SE Asia, rain waters are characterized by negative mean $\delta^{18}O_w$ values of −8‰ to −6‰, whereas dry climates, experienced for example in the Middle East, are characterized by a very small amount of precipitation (less than 100 mm a^{-1}) having mean $\delta^{18}O_w$ values of −2‰ to −1‰ (Table 3). Intermediate situations, such as in Karachi (Pakistan), are characterized by intermediate $\delta^{18}O_w$ values and amounts of precipitation (i.e. −3.9‰ and 200 mm a^{-1}).

In NE Thailand, palaeoclimate markers for the time span of the deposition of the Khorat Group are very scarce and are mostly aridity indicators. Sedimentological and palaeobotanical data such as silicified wood or leaf cuticles showing xerophytic features suggest that rather dry climates prevailed during the deposition of the Phu Kradung Formation, and that climate became wetter during the

Table 3. *Climatic data (mean annual air temperatures (MAAT) and total annual precipitation) and mean annual $\delta^{18}O_w$ values of meteoric water for selected climatic stations of the IAEA–WMO (IAEA–WMO 2004)*

Station number	Name	Country	Latitude (N)	Mean $\delta^{18}O_w$ (‰ SMOW)	Mean precipitation (mm)	MAAT (°C)
4500400	Hong Kong (King's Park)	China	22°19′00″	−6.0	2252.4	23.0
5884700	Fuzhou	China	26°03′00″	−7.1	1340.8	20.2
5975800	Haikou	China	20°01′12″	−5.8	1654.5	25.0
4893000	Luang-Prabang	Lao PDR	19°52′48″	−8.1	1228.6	25.7
4178000	Karachi	Pakistan	24°54′0″	−3.9	199.8	25.8
4115001	Bahrain	Bahrain	26°16′12″	−1.1	76.2	26.3
4047700	Jeddah	Saudi Arabia	21°30′00″	−2.2	71.6	28.0

deposition of the overlying formations of the Khorat Group (Mouret *et al.* 1993; Racey *et al.* 1996; Philippe *et al.* 2004).

Low $\delta^{18}O_w$ values estimated for the Sao Khua (between -7 ± 2‰ and -6.2 ± 2‰) and Khok Kruat (between -9.4 ± 2‰ and -7.3 ± 2‰) Formations match those at similar latitudes today (between 20 and 25°N) in SE Asia (Table 3). This suggests that similar wet–dry climates with high amounts of seasonal precipitations of a few thousands of millimetres occurred during this period in the region of the present Khorat Plateau. Assuming mean air palaeotemperatures in the typical range of 20–25 °C occurring today in subtropical areas, $\delta^{18}O_w$ values estimated from fish match those estimated from crocodilians at the Phu Phok locality (Sao Khua Formation), but at the Khok Pha Suam site (Khok Kruat Formation), they are 4–6‰ higher (Fig. 2b). This difference may reflect peculiar conditions experienced by fish during apatite mineralization such as a temporary isolation of their living water followed by its intense evaporation. During periods of isolation of water bodies, tetrapods can move to other water bodies, whereas fish are trapped and record environmental changes in their phosphatic tissues. Higher $\delta^{18}O_w$ values are estimated for the uppermost part of the Phu Kradung Formation (-4.1 ± 2‰ at the Dan Luang locality). Such values are found today at similar latitudes in drier environments characterized by smaller amounts of precipitation (several hundred millimetres per year, as in Karachi; Table 3) and might reflect similar conditions during the deposition of the uppermost part of the Phu Kradung Formation. Oxygen isotope ratios of waters estimated using fish $\delta^{18}O_p$ values vary from high values (−1.9‰ to −0.8‰) at the Chong Chad locality to low values (−6.5‰ to −5.4‰) at Phu Nam Jun and even lower values at Ban Khok Sanam (−9.8‰ to −8.7‰). These values are difficult to interpret, as only fish remains were analysed from these localities. Keeping in mind that a diagenetic origin for these values cannot be excluded, the high $\delta^{18}O_w$ value obtained from Chong Chad fish may reflect extensive water evaporation of an isolated body of water. In contrast, the low $\delta^{18}O_w$ values documented at Ban Khok Sanam could result from wetter conditions with high amounts of precipitation.

However, the contribution of ^{18}O-depleted water inputs originating from high-altitude rainfall is another hypothesis that may explain the observed low $\delta^{18}O_w$ values. Numerous studies have shown that orography affects the $\delta^{18}O_w$ values of rainwater, the latter becoming more negative with increasing altitude (e.g. Fontes & Olivry 1976; Bortolami *et al.* 1978; Siegenthaler & Oeschger 1980; Gonfiantini *et al.* 2001). As the sediments of

the Khorat Group probably originated from the erosion of the Qinling belt, which underwent active orogenies during the Palaeozoic and Early Mesozoic (Triassic) (e.g. Mattauer *et al.* 1985; Ratschbacher *et al.* 2006, and references therein), it is possible that surface waters ingested by Cretaceous reptiles and fishes were ^{18}O-depleted waters coming from the Qinling area or partly mixed with local meteoric waters. However, the palaeoelevations of the Qinling Mountains during the deposition of Khorat sediments have not yet been estimated. Moreover, the Khorat basin was about 1000 km SW of the Qinling belt during the late Jurassic–early Cretaceous, and the waters flowing from the Qinling area to the Khorat basin may have been mixed on many occasions with local meteoric waters along their path, thus losing their original values. Therefore, the possible high-altitude origin of the low values obtained for Khorat waters remains purely hypothetical. Further investigations may clarify whether these values have a diagenetic or environmental origin, and the possible high-altitude origin of estimated waters could be tested by isotopic studies of contemporaneous faunas that lived closer to the Qinling belt, such as the vertebrate faunas from the Late Jurassic of Zigong (China), located in the Sichuan basin.

Conclusion

Oxygen isotope compositions of continental vertebrate remains from eight localities of the Khorat Group have been used to investigate environmental conditions that prevailed in NE Thailand during the Late Jurassic–Early Cretaceous. Ecological aspects of dinosaur faunas have also been inferred. When compared with various present-day tropical and subtropical climates, estimated $\delta^{18}O_w$ values of past meteoric water for the Khorat Group suggest a transition from dry tropical climates with low amounts of precipitation (of a few hundreds of millimetres per year) for the Phu Kradung Formation to wet–dry tropical climates for the Sao Khua and Khok Kruat Formations, characterized by high amounts of seasonal precipitation of several thousand millimetres per year, similar to present-day monsoon climates. However, a possible high-altitude origin of the low $\delta^{18}O_w$ values observed in some localities cannot be excluded. Significant offsets in $\delta^{18}O_p$ values observed between theropods, sauropods and the spinosaurid *Siamosaurus* are interpreted in terms of differences in ingested water sources (river, pond or plant water), and also suggest that *Siamosaurus* had semi-aquatic living habits similar to those of crocodilians or turtles. As new fossil remains are regularly found during the continuing excavation campaigns on the Khorat Plateau, a more extensive isotopic study of these faunas will allow a refinement of these preliminary interpretations.

The authors would like to thank G. Cuny and L. Cavin for their constructive comments, and are also grateful to the two reviewers H. Fricke and A. Zazzo, whose comments helped to greatly improve the manuscript. This study was supported by the ECLIPSE and ECLIPSE2 programmes of the Centre National de la Recherche Scientifique, by the Department of Mineral Resources (Bangkok) and by a joint project of CNRS and Thailand Research Fund.

References

AMIOT, R., LÉCUYER, C., BUFFETAUT, E., FLUTEAU, F., LEGENDRE, S. & MARTINEAU, F. 2004. Latitudinal temperature gradient during the Cretaceous Upper Campanian–Middle Maastrichtian: $\delta^{18}O$ record of continental vertebrates. *Earth and Planetary Science Letters*, **226**, 255–272.

AMIOT, R., LÉCUYER, C., BUFFETAUT, E., ESCARGUEL, G., FLUTEAU, F. & MARTINEAU, F. 2006. Oxygen isotopes from biogenic apatites suggest widespread endothermy in Cretaceous dinosaurs. *Earth and Planetary Science Letters*, **246**, 41–54.

AMIOT, R., LÉCUYER, C. *ET AL.* 2007. Oxygen isotope fractionation between crocodilian phosphate and water. *Palaeogeography, Palaeoclimatology, Palaeoecology*, **243**, 412–420.

BARRICK, R. E., FISCHER, A. G. & SHOWERS, W. J. 1999. Oxygen isotopes from turtle bone: Application for terrestrial paleoclimates? *Palaios*, **14**, 186–191.

BESSE, J. & COURTILLOT, V. 1988. Paleogeographic maps of the continents bordering the Indian Ocean since the Early Jurassic. *Journal of Geophysical Research, B, Solid Earth and Planets*, **93**, 791–808.

BILLON-BRUYAT, J.-P., LÉCUYER, C., MARTINEAU, F. & MAZIN, J.-M. 2005. Oxygen isotope compositions of Late Jurassic vertebrate remains from lithographic limestones of western Europe: Implications for the ecology of fish, turtles and crocodilians. *Palaeogeography, Palaeoclimatology, Palaeoecology*, **216**, 359–375.

BLAKE, R. E., O'NEIL, J. R. & GARCIA, G. A. 1997. Oxygen isotope systematics of biologically mediated reactions of phosphate; I, Microbial degradation of organophosphorus compounds. *Geochimica et Cosmochimica Acta*, **61**, 4411–4422.

BORTOLAMI, G. C., RICCI, B., SUSELLA, G. F. & ZUPPI, G. M. 1978. Isotope hydrology of the Corsaglia Maritime Alps, Piedmont, Italy. *Isotope Hydrology*, **1**, 327–350.

BRYANT, D. J. & FROELICH, P. N. 1995. A model of oxygen isotope fractionation in body water of large mammals. *Geochimica et Cosmochimica Acta*, **59**, 4523–4537.

BUFFETAUT, E. & INGAVAT, R. 1986. Unusual theropod dinosaur teeth from the Upper Jurassic of Phu Wiang, Northeastern Thailand. *Revue de Paléobiologie*, **5**, 217–220.

BUFFETAUT, E. & SUTEETHORN, V. 1998. The biogeographical significance of the Mesozoic vertebrates from Thailand. *In*: HALL, R. & HOLLOWAY, J. D.

(eds) *Biogeography and Geological Evolution of SE Asia*. Backhuys, Leiden, 83–90.

BUFFETAUT, E. & SUTEETHORN, V. 1999. The dinosaur fauna of the Sao Khua Formation of Thailand and the beginning of the Cretaceous radiation of dinosaurs in Asia. *Palaeogeography, Palaeoclimatology, Palaeoecology*, **150**, 13–23.

BUFFETAUT, E., SUTEETHORN, V., CUNY, G., TONG, H., LE LOEUFF, J., KHANSUBHA, S. & JONGAUTCHARIYAKUL, S. 2000. The earliest known sauropod dinosaur. *Nature*, **407**, 72–74.

BUFFETAUT, E., SUTEETHORN, V., LE LOEUFF, J., KHANSUBHA, S., TONG, H. & WONGKO, K. 2005. The dinosaur fauna from the Khok Kruat Formation (Early Cretaceous) of Thailand. *In*: WANNAKAO, L., SRISUK, K., YOUNGME, W. & LERTSIRIVORAKUL, R. (eds) *Proceedings of the International Conference on Geology, Geotechnology and Mineral Resources of Indochina (GEOINDO 2005)*. Khon Kaen University, Khon Kaen, 575–581.

BUFFETAUT, E., SUTEETHORN, V. & TONG, H. 2006. Dinosaur assemblages from Thailand: A comparison with Chinese faunas. *In*: LÜ, J., KOBAYASHI, Y., HUANG, D. & LEE, Y. N. (eds) *Papers from the 2005 Heyuan International Dinosaur Symposium*. Geological Publishing House, Beijing, 19–37.

CAPPETTA, H., BUFFETAUT, E. & SUTEETHORN, V. 1990. A new hybodont shark from the Lower Cretaceous of Thailand. *Neues Jahrbuch für Geologie und Palaeontologie, Abhandlungen*, **1990**, 659–666.

CARTER, A. & BRISTOW, C. S. 2003. Linking hinterland evolution and continental basin sedimentation by using detrital zircon thermochronology: A study of the Khorat Plateau Basin, eastern Thailand. *Basin Research*, **15**, 271–285.

CHARIG, A. J. & MILNER, A. C. 1986. *Baryonyx*, a remarkable new theropod dinosaur. *Nature*, **324**, 359–361.

CHARIG, A. J. & MILNER, A. C. 1997. *Baryonyx walkeri*, a fish-eating dinosaur from the Wealden of Surrey. *Bulletin of the Natural History Museum, Geology Series*, **53**, 11–70.

CLEMENTZ, M. T. & KOCH, P. L. 2001. Differentiating aquatic mammal habitat and foraging ecology with stable isotope in tooth enamel. *Oecologia*, **129**, 461–472.

CLEMENTZ, M. T., HOPPE, K. A. & KOCH, P. L. 2003. A paleoecological paradox: The habitat and dietary preferences of the extinct tethythere *Desmostylus*, inferred from stable isotope analysis. *Paleobiology*, **29**, 506–519.

CORMIE, A. B., LUZ, B. & SCHWARCZ, H. P. 1994. Relationship between the hydrogen and oxygen isotopes of deer bone and their use in the estimation of relative humidity. *Geochimica et Cosmochimica Acta*, **58**, 3439–3449.

CROWSON, R. A., SHOWERS, W. J., WRIGHT, E. K. & HOERING, T. C. 1991. A method for preparation of phosphate samples for oxygen isotope analysis. *Analytical Chemistry*, **63**, 2397–2400.

D'ANGELA, D. & LONGINELLI, A. 1990. Oxygen isotopes in living mammal's bone phosphate: Further results. *Chemical Geology*, **86**, 75–82.

DANSGAARD, W. 1964. Stable isotopes in precipitation. *Tellus*, **16**, 436–468.

ERICKSON, G. M. 1996*a*. Daily deposition of dentine in juvenile alligator and assessment of tooth replacement rates using incremental line counts. *Journal of Morphology*, **228**, 189–194.

ERICKSON, G. M. 1996*b*. Incremental lines of von Ebner in dinosaurs and the assessment of tooth replacement rates using growth line counts. *Evolution*, **93**, 14623–14627.

EZQUERRA, R., DOUBLET, S., COSTEUR, L., GALTON, P. M. & PÉREZ-LORENTE, F. 2007. Were non-avian theropod dinosaurs able to swim? Supportive evidence from an Early Cretaceous trackway, Cameros Basin (La Rioja, Spain). *Geology*, **35**, 507–510.

FLANAGAN, L. B. & EHLERINGER, J. R. 1991. Stable isotopic composition of stem and leaf water: Applications to the study of plant water use. *Functional Ecology*, **5**, 270–277.

FONTES, J.-C. & OLIVRY, J.-C. 1976. Gradient isotopique entre 0 et 4000 m dans les précipitations du Mont Cameroun. *Réunion Annuelle des Sciences de la Terre*, **4**, 171.

FRAKES, L. A. 1999. Estimating the global thermal state from Cretaceous sea surface and continental temperature data. *In*: BARRERA, E. & JOHNSON, C. C. (eds) *Evolution of the Cretaceous ocean-climate system*. Geological Society of America, Special Papers, **332**, 49–57.

FRAKES, L. A. & FRANCIS, J. E. 1988. A guide to Phanerozoic cold polar climates from high-latitude ice-rafting in the Cretaceous. *Nature*, **333**, 547–549.

FRAKES, L. A., PROBST, J.-L. & LUDWIG, W. 1994. Latitudinal distribution of paleotemperature on land and sea from early Cretaceous to middle Miocene. *Comptes Rendus de l'Académie des Sciences, Série IIA*, **318**, 1209–1218.

FRICKE, H. C. & O'NEIL, J. R. 1999. The correlation between $^{18}O/^{16}O$ ratios of meteoric water and surface temperature; its use in investigating terrestrial climate change over geologic time. *Earth and Planetary Science Letters*, **170**, 181–196.

FRICKE, H. C. & ROGERS, R. R. 2000. Multiple taxon–multiple locality approch to providing oxygen isotope evidence for warm-blooded theropod dinosaurs. *Geology*, **28**, 799–802.

GONFIANTINI, R., ROCHE, M.-A., OLIVRY, J.-C., FONTES, J.-C. & ZUPPI, G. M. 2001. The altitude effect on the isotopic composition of tropical rains. *Chemical Geology*, **181**, 147–167.

HAHN, L. 1982. Stratigraphy and marine ingressions of the Mesozoic Khorat group in northeastern Thailand. *Geologisches Jahrbuch*, **43**, 7–35.

HEGGEMANN, H. 1994. Sedimentäre Entwicklung de Khorat-Gruppe (Ober Trias bis Paläogen) in NE- und N-Thailand. *Göttinger Arbeiten zur Geologie und Paläontologie*, **63**, 1–146.

IAEA–WMO 2004. Global Network of Isotopes in Precipitation. The GNIP Database. World Wide Web Address: http://isohis.iaea.org

KOHN, M. J. 1996. Predicting animal $\delta^{18}O$: Accounting for diet and physiological adaptation. *Geochimica et Cosmochimica Acta*, **60**, 4811–4829.

KOHN, M. J., SCHOENINGER, M. J. & VALLEY, J. W. 1996. Herbivore tooth oxygen isotope compositions; effects of diet and physiology. *Geochimica et Cosmochimica Acta*, **60**, 3889–3896.

KOLODNY, Y., LUZ, B. & NAVON, O. 1983. Oxygen isotope variations in phosphate of biogenic apatites; I, Fish bone apatite; rechecking the rules of the game. *Earth and Planetary Science Letters*, **64**, 398–404.

KOLODNY, Y., LUZ, B., SANDER, M. & CLEMENS, W. A. 1996. Dinosaur bones: Fossils or pseudomorphs? The pitfalls of physiology reconstruction from apatitic fossils. *Palaeogeography, Palaeoclimatology, Palaeoecology*, **126**, 161–171.

LÉCUYER, C., GRANDJEAN, P., O'NEIL, J. R., CAPPETTA, H. & MARTINEAU, F. 1993. Thermal excursions in the ocean at Cretaceous–Tertiary boundary (northern Morocco): $\delta^{18}O$ record of phosphatic fish debris. *Palaeogeography, Palaeoclimatology, Palaeoecology*, **105**, 235–243.

LÉCUYER, C., GRANDJEAN, P., BARRAT, J.-A., NOLVAK, J., EMIG, C., PARIS, F. & ROBARDET, M. 1998. $\delta^{18}O$ and REE contents of phosphatic brachiopods; a comparison between modern and lower Paleozoic populations. *Geochimica et Cosmochimica Acta*, **62**, 2429–2436.

LÉCUYER, C., GRANDJEAN, P. & SHEPPARD, S. M. F. 1999. Oxygen isotope exchange between dissolved phosphate and water at temperatures $<135°C$: Inorganic versus biological fractionations. *Geochimica et Cosmochimica Acta*, **63**, 855–862.

LÉCUYER, C., BOGEY, C. *ET AL.* 2003*a*. Stable isotope composition and rare earth element content of vertebrate remains from the Late Cretaceous of northern Spain (Lano); did the environmental record survive? *Palaeogeography, Palaeoclimatology, Palaeoecology*, **193**, 457–471.

LÉCUYER, C., PICARD, S., GARCIA, J. P., SHEPPARD, S. M. F., GRANDJEAN, P. & DROMART, G. 2003*b*. Thermal evolution of Tethyan surface waters during the Middle–Late Jurassic: Evidence from $\delta^{18}O$ values of marine fish teeth. *Paleoceanography*, **18**, 1076–1091.

LELOUP, P. H., LACASSIN, R. *ET AL.* 1995. The Ailao Shan–Red River shear zone (Yunnan, China), Tertiary transform boundary of Indochina. *Tectonophysics*, **251**, 3–10.

LONGINELLI, A. 1984. Oxygen isotopes in mammal bone phosphate; a new tool for paleohydrological and paleoclimatological research? *Geochimica et Cosmochimica Acta*, **48**, 385–390.

LUZ, B. & KOLODNY, Y. 1985. Oxygen isotope variations in phosphate of biogenic apatites; IV, Mammal teeth and bones. *Earth and Planetary Science Letters*, **75**, 29–26.

LUZ, B., KOLODNY, Y. & HOROWITZ, M. 1984. Fractionation of oxygen isotopes between mammalian bone-phosphate and environmental drinking water. *Geochimica et Cosmochimica Acta*, **48**, 1689–1693.

MATTAUER, M., MATTE, P. *ET AL.* 1985. Tectonics of the Qinling Belt: Build-up and evolution of eastern Asia. *Nature*, **317**, 496–500.

MOURET, C., HEGGEMANN, H., GOUADAIN, J. & KRASIDASIMA, S. 1993. Geological history of the siliciclastic Mesozoic strata of the Khorat Group in the Phu Phan range area, northeastern Thailand. *In*: THANASUTHIPITAK, T. (ed.) *Proceedings of the International Symposium on Biostratigraphy of Mainland Southeast Asia:* Facies and Paleontology. Chiang Mai University, Chiang Mai, 23–49.

O'NEIL, J. R., ROE, L. J., REINHARD, E. & BLAKE, R. E. 1994. A rapid and precise method of oxygen isotope analysis of biogenic phosphate. *Israel Journal of Earth-Sciences*, **43**, 203–212.

PHILIPPE, M., SUTEETHORN, V., LUTAT, P., BUFFETAUT, E., CAVIN, L., CUNY, G. & BARALE, G. 2004. Stratigraphical and palaeobiogeographical significance of fossil wood from the Mesozoic Khorat Group of Thailand. *Geological Magazine*, **141**, 319–328.

PRICE, G. D. 1999. The evidence and implications of polar ice during the Mesozoic. *Earth-Science Reviews*, **48**, 183–210.

PUCÉAT, E., LÉCUYER, C., SHEPPARD, S. M. F., DROMART, g., REBOULET, S. & GRANDJEAN, P. 2003. Thermal evolution of Cretaceous Tethyan marine waters inferred from oxygen isotope composition of fish tooth enamels. *Paleoceanography*, **18**, 7–12.

PUCÉAT, E., REYNARD, B. & LÉCUYER, C. 2004. Can crystallinity be used to determine the degree of chemical alteration of biogenic apatites? *Chemical Geology*, **205**, 83–97.

RACEY, A., LOVE, M. A., CANHAM, A. C., GOODALL, J. G. S., POLACHAN, S. & JONES, P. D. 1996. Stratigraphy and reservoir poential of the Mesozoic Khorat Group, NE Thailand. Part 1: Stratigraphy and sedimentary evolution. *Journal of Petroleum Geology*, **19**, 5–40.

RATSCHBACHER, L., FRANZ, L. *ET AL.* 2006. The Sino-Korean–Yangtze suture, the Huwan detachment, and the Paleozoic–Tertiary exhumation of (ultra)high-pressure rocks along the Tongbai–Xinxian–Dabie Mountains. *In*: HACKER, B. R., MCCLELLAND, W. C. & LIOU, J. G. (eds) *Ultrahigh-pressure Metamorphism: Deep Continental Subduction*. Geological Society of America, Special Papers, **403**, 45–75.

SATO, K., LIU, Y., ZHU, Z., YANG, Z. & OTOFUJII, Y. 1999. Palaeomagnetic study of middle Cretaceous rocks from Yunlong, western Yunnan, China: Evidence of southward displacement of Indochina. *Earth and Planetary Science Letters*, **165**, 1–15.

SIEGENTHALER, U. & OESCHGER, H. 1980. Correlation of $\delta^{18}O$ in precipitation with temperature and altitude. *Nature*, **285**, 314–317.

STEUBER, T., RAUCH, M., MASSE, J. P., GRAAF, J. & MALKOČ, M. 2005. Low-latitude seasonality of Cretaceous temperatures in warm and cold episodes. *Nature*, **437**, 1341–1344.

STRAIGHT, W. H., BARRICK, R. E. & EBERTH, D. A. 2004. Reflections of surface water, seasonality and climate in stable oxygen isotopes from tyrannosaurid tooth enamel. *Palaeogeography, Palaeoclimatology, Palaeoecology*, **206**, 239–256.

TAQUET, P. 1984. Une curieuse spécialisation du crâne de certains dinosaures carnivores du Crétacé: Le museau long et étroit des Spinosauridés. *Comptes Rendus de l'Académie des Sciences, Série IIA*, **299**, 217–222.

VON GRAFENSTEIN, U., ERLENKEUSER, H., MUELLER, J., TRIMBORN, P. & ALEFS, J. 1996. A 200 year mid-European air temperature record preserved in lake sediments; an extension of the $\delta^{18}O_P$–air temperature relation into the past. *Geochimica et Cosmochimica Acta*, **60**, 4025–4036.

YAKIR, D., DENIRO, M. J. & GAT, J. R. 1990. Natural deuterium and oxygen-18 enrichment in leaf water of cotton plants grown under wet and dry conditions: Evidence for water compartmentation and its dynamics. *Plant, Cell and Environment*, **13**, 49–56.

ZAZZO, A., LÉCUYER, C. & MARIOTTI, A. 2004*a*. Experimentally-controlled carbon and oxygen isotope exchange between bioapatites and water under inorganic and microbially-mediated conditions. *Geochimica et Cosmochimica Acta*, **68**, 1–12.

ZAZZO, A., LÉCUYER, C., SHEPPARD, S. M. F., GRANDJEAN, P. & MARIOTTI, A. 2004*b*. Diagenesis and the reconstruction of paleoenvironments: A method to restore original $\delta^{18}O$ values of carbonate and phosphate from fossil tooth enamel. *Geochimica et Cosmochimica Acta*, **68**, 2245–2258.

PUBLICATION 2.6

Earth and Planetary Science Letters 283 (2009) 133–143

Contents lists available at ScienceDirect

Earth and Planetary Science Letters

journal homepage: www.elsevier.com/locate/epsl

Pleistocene seasonal temperature variations recorded in the $\delta^{18}O$ of *Bison priscus* teeth

Aurélien Bernard [a], Valérie Daux [b,c], Christophe Lécuyer [a,*,1], Jean-Philip Brugal [d], Dominique Genty [b,c], Karine Wainer [b,c], Véronique Gardien [a], François Fourel [a], Jacques Jaubert [e]

[a] Laboratoire CNRS UMR 5125 "PaléoEnvironnements & PaléobioSphère", Université Claude Bernard Lyon 1, Campus de la Doua, F-69622 Villeurbanne, France
[b] Laboratoire des Sciences du Climat et de l'Environnement, UMR CEA/CNRS 1572, L'Orme des Merisiers, Bât. 701, CEA Saclay, 91191 Gif/Yvette Cedex, France
[c] Université Paris 6, Jussieu, France
[d] UMR CNRS 6636, Maison Méditerranéenne des Sciences de l'Homme, 5 rue du Château de l'Horloge, BP 647, 13094, Aix-en-Provence cedex 2, France
[e] Université Bordeaux 1, PACEA-UMR 5199 CNRS, Institut de Préhistoire et de Géologie du Quaternaire, Avenue des Facultés, 33405 Talence, France

ARTICLE INFO

Article history:
Received 2 October 2008
Received in revised form 6 April 2009
Accepted 7 April 2009
Available online 9 May 2009

Editor: M.L. Delaney

Keywords:
Pleistocene
climate
steppe bison
seasonality
oxygen isotope
apatite

ABSTRACT

Oxygen isotope analysis of phosphate in tooth enamel of mammals ($\delta^{18}O_p$) constitutes a valuable method to reconstruct past air temperatures in continental environments. The method is based on interdependent relationships between the $\delta^{18}O$ of apatite phosphate, body fluids, environmental waters and air temperatures. Continuous tooth growth and absence of enamel remodelling in bovid teeth ensures a reliable record of the intra-annual variability of air temperature through an incremental $\delta^{18}O$ analysis from apex to cervix. This method has been applied to *Bison priscus* dental remains of the late Middle Pleistocene from the fossiliferous layer of a cave at Coudoulous I in South-Western France (Layer 4). The stacked oxygen isotope signal obtained by combining 9 bison teeth shows sinusoidal variations (15.0‰ to 19.1‰ V-SMOW) of seasonal origin over 2.5 yr. The corresponding computed MAT of 9 ± 3 °C is about 4 °C lower than at present. Seasons appear more contrasted in Coudoulous I during Layer 4 deposition with summers as warm as present ones (19 ± 3 °C) and significantly colder winters about 0 ± 3 °C compared to 6 ± 1 °C at present.

1. Introduction

The Quaternary period is marked by drastic climatic events with the onset of glacial–interglacial cycles of different dominant periodicity (41 kyr at ca. 2.6 Ma then 100 kyr at ca. 1 Ma). Glacial stages are characterized by increased seasonality and decreased precipitations (deMenocal, 2004; Mosbrugger et al., 2005). Colder and drier climatic conditions caused decisive changes in the structure of herbivore community in Western Europe, as seen by very high turnover peaks during the Middle Pleistocene and the predominance of large bodied and cold-adapted species (e.g., bison, reindeer) as well as peculiar microfauna associations (Chaline, 1972). Multiple migrations follow the East–West climate gradient from strong continental and seasonal conditions in the Asian heartland to a mild humid climate that prevailed in Western Europe for a longer time (Brugal and Croitor, 2007; Croitor and Brugal, 2007).

In continental environments, the most widespread geochemical method of air temperature determination is derived from measurements of the oxygen isotope composition of speleothems, ostracods, and vertebrate bones and teeth. The method is based on the dependence of the $\delta^{18}O$ of the mineral on the isotopic composition of environmental water ($\delta^{18}O_{ew}$) via percolating fluids, streams or body fluids, and on the dependence of $\delta^{18}O_{ew}$ on the air temperature.

In some cases, the conversion of the isotopic composition of the mineral into $\delta^{18}O_{ew}$ is not straightforward as the relation of the former to the latter depends on the temperature at which the precipitation of the mineral takes place (Longinelli and Nuti, 1973; Kolodny et al., 1983). When the precipitation temperature is a known and constant parameter (e.g. apatite precipitation from body fluids in homeotherms), the oxygen isotope composition of the mineral only depends on the corresponding $\delta^{18}O_{ew}$. The ratio of oxygen isotopes in mammal body fluids and tissues (flesh, bones and teeth) reflects the origin of water not only from imbibed liquid but also from ingested food. The water contained in food has a complicated relationship with meteoric water and can be significantly ^{18}O-enriched compared to it. The relative contribution of water entering the body as liquid and as food water varies from one species to another. Animals with low water turnover are expected to derive more water from isotopically-

* Corresponding author.
E-mail address: Christophe.Lecuyer@univ-lyon1.fr (C. Lécuyer).
[1] Institut Universitaire de France, France.

0012-821X/$ – see front matter © 2009 Elsevier B.V. All rights reserved.
doi:10.1016/j.epsl.2009.04.005

enriched food sources and less from drinking water than those with high water turnover (Luz et al., 1984; Kohn et al., 1996). For the vast majority of terrestrial vertebrates, water turnover scales to body mass (Eberhardt, 1969). Therefore, the $\delta^{18}O$ of the tissue of big animals should be less affected by the solid food consumption than the $\delta^{18}O$ of smaller ones (Kohn et al., 1996). As a result, animals that are water-dependent display average $\delta^{18}O$ values closely correlated with the average $\delta^{18}O$ of local precipitation (Longinelli, 1984; D'Angela and Longinelli, 1990; Ayliffe et al., 1992; Bryant et al., 1994). For bisons, which fall into the category of water-dependent animals, Hoppe (2006) demonstrated, indeed, that the mean value of $\delta^{18}O$ of the carbonate component ($\delta^{18}O_c$) of the hydroxyapatite is related to the values of environmental waters.

Several equations were determined between $\delta^{18}O_{ew}$ and the mean annual air temperatures that can be applied to the global scale or to a restricted latitude range (Dansgaard, 1964; Yurtsever, 1975; Rozanski et al., 1992; Von Grafenstein et al., 1996; Amiot et al., 2004). However, high-resolution data are needed to assess the inter-annual variability of air temperature in continental environments. The oxygen isotopic composition of tooth enamel or tusk of individual large mammal fossils was shown to reflect accurately the seasonal $\delta^{18}O$ variations of environmental waters (Koch et al., 1989; Bryant et al., 1996; Fricke and O'Neil, 1996; Fricke et al., 1996; Stuart-Williams and Schwarcz, 1997; Sharp and Cerling, 1998; Gadbury et al., 2000; Zazzo et al., 2002; Sharma et al., 2004).

Knowledge of the climate mode that prevailed during the late Middle Pleistocene is fundamental to understand its impact on the evolution of mammal biodiversity, including hominids. More than the mean annual temperature, seasonal amplitude and the temperatures of the warmest and coldest months are critical parameters contributing to control the biomass and its diversity. Therefore, the purpose of this study is to measure the magnitude of the $\delta^{18}O$ variations within bison teeth to reconstruct the climate seasonality during the late Middle Pleistocene in South-Western France. To achieve this aim, we analyzed the phosphate oxygen isotopic composition of enamel ($\delta^{18}O_p$) sampled along profiles in bison teeth collected at the Coudoulous I site (Lot, France, Fig. 1). These compositions are converted into the isotopic composition of the environmental waters and then to air temperatures. The results are compared to present-day data and to other estimates of air temperatures in France at the end of the Middle Pleistocene.

2. Sampling site and stratigraphy

The Coudoulous I site is located in a limestone plateau (Causse de Gréalou) in South-Western France (44°28′N, 1°39E; elevation = 280 m; Fig. 1). It is a 7 m thick karstic infilling composed of detrital material, containing many fossil and archaeological remains. Bison teeth belong to the 40 cm thick Layer 4 which was defined among ten sedimentological layers (Jaubert et al., 2005). Layer 4 is made up of calcareous stones or rocks and bone fragments preserved in a silto-sand matrix. Microfauna is scarce and consistent with a continental to intermediate steppe climate. The dominant species of the macrofauna is the steppe bison (*Bison priscus*) that represents almost 98% of the identifiable large mammal remains, with the occurrence of 232 individuals spread on 25 m^2 (Jaubert et al., 2005). The metrical features of bones and mortality curve inferred from bison remains is consistent with the structure of a natural population (herd), mainly constituted of juvenile and female individuals. Such a nearly monospecific fossil assemblage with this age distribution generally corresponds to 'catastrophic' events interpreted

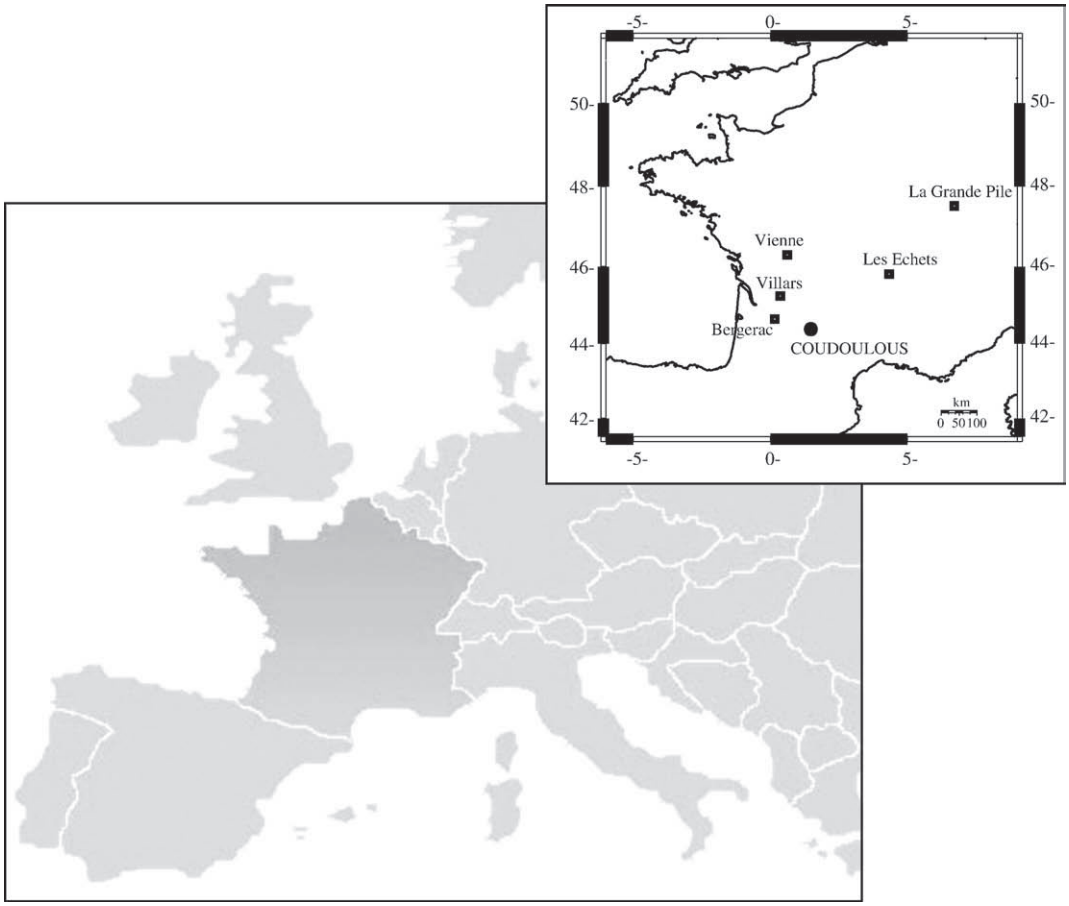

Fig. 1. Geographic map with the location of the French sites mentioned in this study.

as repeated hunting episodes by Neanderthals (Brugal, 1999). Moreover, remains of lithic industry of the early Middle Paleolithic (mostly quartz and flints) were found along with many butchery grooves on bones produced during the cutting up of carcasses. The dentary of the young trapped individuals reveals that the hunting episodes took place in late spring–early summer.

According to biochronological data, the sedimentary sequence of Coudoulous I is from late Middle Pleistocene to Late Pleistocene (Jaubert et al., 2005). The sedimentary series of Layer 4 was deposited between two stalagmitic floors that provided U/Th ages of 240 ± 80 ka and 126 ± 17 ka. Bison bones ($n=5$) and teeth ($n=3$) collected in Layer 4 were dated by U/Th and ESR combined methods. The results obtained by the two methods are in agreement and indicate a closed system or weak leaching. The ages range from 137 to 151 ka for bones, and from 140 to 209 ka for teeth (Jaubert et al., 2005; Table 1). Considering an accepted uncertainty of 15% for the dating (Jaubert et al., 2005), a median value of 149 ± 6 ka can be calculated by a Monte Carlo method (e.g. Metropolis and Ulam, 1949; Willink, 2006). This age corresponds to Marine Isotope Stage 6 (MIS 6). It is consistent with the ages of the stalagmitic floors.

3. Bison ecology

The steppe bison (*B. priscus*) is an extinct large mammal (700–800 kg, ca. 2 m at the withers), well-adapted to cool steppe-like grasslands, that lived during the glacial times (Kurten, 1968; Brugal, 1985). During the Pleistocene, it was widely distributed throughout Europe, Central Asia and North America. Both morphological (Groves, 1981; Geraads, 1992) and molecular (Pitra et al., 1997; Buntjer et al., 2002) phylogenies show that the North American bison, *Bison bison*, and the European bison, *Bison bonasus*, are very close relatives among the Bovidae. Paleontological studies (McDonald, 1981; Brugal, 1985) set the position of *B. priscus* among the evolutionary history of the Bovidae as the direct ancestor of the wisent, *B. bonasus*. More recently, new genetic data on mitochondrial and Y-chromosomal DNA (Verkaar et al., 2004) suggested that the origin of *B. bonasus* could be more complicated than a direct lineage from *B. priscus*. However *B. priscus* remains phylogenetically closer to the modern bison than any of the other bovids.

The diet of *B. priscus* was mainly composed of grass as confirmed by the microwear pattern of molars collected in South-Western France (Merceron and Madelaine, 2006) or by plant cuticle fragments trapped between the cusps of steppe bison molars (Guthrie, 1990). There is a poor knowledge about *B. priscus* migratory habits so far. *B. bison* is a rotational grazer which migrates through the Great Plains travelling over hundreds of kilometres to find fresh grass (Nowak, 1999). *B. bonasus* is restricted presently in the deciduous forest of Bialowiesza, Poland, and in the Western Caucasus. It is more sedentary, with limited movements between higher locations in summer to more open spaces during winters, as it was probably the case for the steppe bison. *B. bonasus* eats grass, tree leaves, bark, lichens and mosses and drinks up to 45 L water per day (Ricciutu, 1973). Birth season of *B. bonasus* is May–June (Krasinski and Raczynski, 1967). The calf is weaned between 8 and 12 months (Gadbury et al., 2000) but it is able to eat grass and leaves as soon as it is three weeks old.

Bovids have high crowned teeth ('hypsodont') which grow from the dentine–enamel junction towards the surface as well as from the

Table 1
Bones and teeth dating by combined U/Th and ESR methods.

Sample	Bone 1	Bone 2	Bone 3	Bone 4	Bone 5	Tooth 1	Tooth 2	Tooth 3	Median
U/Th-ESR	149	137	138	151	145	209	167	140	149 ± 6

From Jaubert et al. (2005).

Table 2
Late Middle Pleistocene bison teeth collected at Coudoulous I, South-Western France.

	d (mm)	d_c (mm)	$\delta^{18}O_p$ (‰)
P3-351	1.0	109.5	18.9
	3.5	107.0	17.7
$h=25$	5.5	105.0	17.3
sf = 1	7.5	103.0	18.0
$R=53$	9.5	101.0	19.1
	11.0	99.5	18.8
	13.0	97.5	18.8
	15.5	95.0	17.9
	17.0	93.5	18.6
	19.0	94.5	18.6
P4-350	4.0	124.0	16.1
	7.0	121.0	16.6
$h=34$	9.5	118.5	16.7
sf = 1	12.0	116.0	17.2
$R=53$	14.5	113.5	17.6
	17.0	111.0	17.9
	19.0	109.0	18.2
	21.5	106.5	17.7
	24.0	104.0	17.5
	26.0	102.0	18.4
	28.5	99.5	18.3
M1-371	7.0	33.0	16.0
	15.5	24.5	15.4
$h=40$	24.0	16.0	15.6
sf = 1	31.5	8.5	17.0
$R=53$	40.0	0.0	17.9
M2-371	6.0	79.5	16.3
	13.5	72.0	15.7
$h=55$	19.5	66.0	16.9
sf = 1	25.5	60.0	17.6
$R=53$	33.5	52.0	18.0
	41.0	44.5	17.2
	47.0	38.5	16.7
	53.5	32.0	15.9
M2-190	5.0	85.0	15.6
	8.0	82.6	15.5
$h=68$	10.5	80.6	15.8
sf = 0.81	13.0	78.6	16.0
$R=65$	15.5	76.5	15.9
	18.0	74.5	15.8
	20.5	72.5	15.8
	23.0	70.5	16.4
	26.0	68.0	15.6
	28.5	66.0	16.1
	31.5	63.6	16.9
	34.0	61.5	17.6
	36.5	59.5	17.4
	39.0	57.5	17.1
	42.0	55.1	17.3
	44.0	53.4	17.5
	46.5	51.4	18.4
	48.5	49.8	18.0
	51.5	47.4	18.2
	54.0	45.3	18.1
	56.5	43.3	18.2
M2-328b	8.0	78.3	15.3
	10.0	76.5	15.2
$h=60$	12.5	74.2	15.0
sf = 0.92	15.0	71.9	15.6
$R=58$	17.0	70.1	15.7
	21.0	66.4	16.8
	23.5	64.1	16.5
	26.0	61.8	17.7
	28.0	59.9	18.4
	30.0	58.1	17.3
	32.5	55.8	17.5
	35.0	53.5	18.1
	40.0	48.9	18.5
	42.0	47.1	17.7
	44.0	45.2	18.4
	46.5	42.9	17.8
	49.0	40.6	17.6
	51.0	38.8	17.4
	53.5	36.5	17.4

(continued on next page)

Table 2 (*continued*)

	d (mm)	d_c (mm)	$\delta^{18}O_p$ (‰)
M3-371	1.0	133.5	15.7
	4.5	130.0	16.1
$h=60$	15.0	119.5	16.4
sf = 1	20.0	114.5	17.1
$R=53$	25.0	109.5	17.9
	30.0	104.5	18.0
	35.0	99.5	17.6
	40.0	94.5	17.0
	45.0	89.5	16.8
	51.0	83.5	16.4
	57.0	77.5	16.6
M3-291	15.0	120.1	16.5
	22.5	113.0	17.9
$h=64$	31.0	105.0	18.2
sf = 0.94	40.0	96.6	17.5
$R=56$	48.0	89.0	16.6
	55.0	82.5	16.5
M3-331	5.0	115.8	16.4
	10.5	110.5	16.6
$h=62$	25.5	95.9	17.5
sf = 0.97	31.0	90.6	17.1
$R=55$	36.5	85.2	16.2
	42.0	79.9	15.9
	53.0	69.2	16.6
	60.0	62.4	17.1

d: distance (mm) of the sampling grooves from the root; d_c: composite distance for the stacked oxygen isotope record (mm); $\delta^{18}O_p$: oxygen isotope composition of phosphate from bison tooth enamel (‰ V-SMOW); h: crown height (mm); sf: scaling factor; R: tooth growth rate (mm yr^{-1}).

cervix to the apex (Hillson, 1992). The oldest part of the crown therefore occurs at the tip and the youngest one at the root. Tooth growth lasts around one year so that young animals may exhibit teeth not completely grown. When the tooth is grown, the abrasion of the apex during masticatory processes is not compensated anymore and the size of the tooth decreases. Haynes (1984) estimated a tooth wear rate of 1.7 mm yr^{-1} for the first molar of modern bison, and Reher and Frison (1980) proposed a 3.5–3.8 mm yr^{-1} rate for bison from the Prehistoric Vore site. The tooth formation sequence of *B. priscus* is assumed to be similar to those known for the modern bison (Gadbury et al., 2000) and bos (Fricke and O'Neil, 1996) that are very close to each other. This sequence starts with the growth of M1 *in utero* at the end of winter, followed by the mineralization of M2 during the first year of animal's life (summer to summer), then by M3, P2, P3 and P4 during the next year. It is noteworthy that when M1 growth is finishing, M2 growth begins and is followed by M3 growth with a small overlap (Wegrzyn and Serwatkas, 1984; Gadbury et al., 2000).

4. Materials and methods

4.1. Sampling

Nine well preserved teeth from prime adult bison with complete erupted tooth sequences have been selected from Layer 4 in Coudoulous I. Sample nomenclature (Table 2) corresponds to the tooth position in the dental sequence (Smith and Dodson, 2003) followed by the excavation number of the specimen. All the teeth are from lower jaws with three molars corresponding to one individual (M1-371, M2-371 and M3-371), the others (one P3, one P4, two M2, two M3) possibly belonging to different bison (Table 2).

Enamel powder samples were collected using a micro-driller equipped with a diamond-studded drill bit. Grooves were drilled perpendicularly to the tooth growth axis from the cervix to the apex of the tooth crown on the highest and best preserved cuspid (Fig. 2). This sampling method is similar to the conventional method of enamel extraction (Bryant et al., 1996; Fricke and O'Neil, 1996).

Two sampling strategies have been adopted chronologically. We have first collected macro-samples (40 mg, 5–10 samples/tooth, 3 mm wide grooves) on five teeth (M1-371, M2-371, M3-371, M3-291 and M3-331). In a second step, the analytical procedure has been adapted to smaller samples. To take advantage of this improvement, we collected micro-samples (3 mg, 10–21 samples per tooth, 1–1.5 mm wide grooves) on four teeth (P3-351, P4-350, M2-190 and M2-328b), resulting in a better time resolution (Table 2; Figs. 2 and 3).

The oxygen isotopic composition and temperature respectively collected and recorded at Villars (~130 km North-West from Coudoulous, elevation = 180 m; Fig. 1) are used in this paper for comparison to reconstructed Pleistocene data (Section 6.3). Both data were collected monthly from 1996 to 2006. The temperature data were collected and homogenised by Meteo-France.

4.2. Oxygen isotope analysis

Enamel samples have been treated following the wet chemistry protocol described by Crowson et al. (1991) and slightly modified by Lécuyer et al. (1993). This protocol consists in the isolation of phosphate from apatite as Ag_3PO_4 crystals using acid dissolution and anion-exchange resin. As it was already presented in several publications (e.g. Lécuyer et al., 1998, 2007; Daux et al., 2008), the wet chemical procedure used for the 5 macro-samples (about 20 mg of powder) is not described here in detail. For the 4 micro-samples, 2 to 3 mg of enamel powder was dissolved in 1 mL of 2 M HF overnight. The CaF_2 residue was separated by centrifugation and the solution was neutralized by adding 1 mL of 2 M KOH. One and a half mL of Amberlite™ anion-exchange resin was added to the solution to

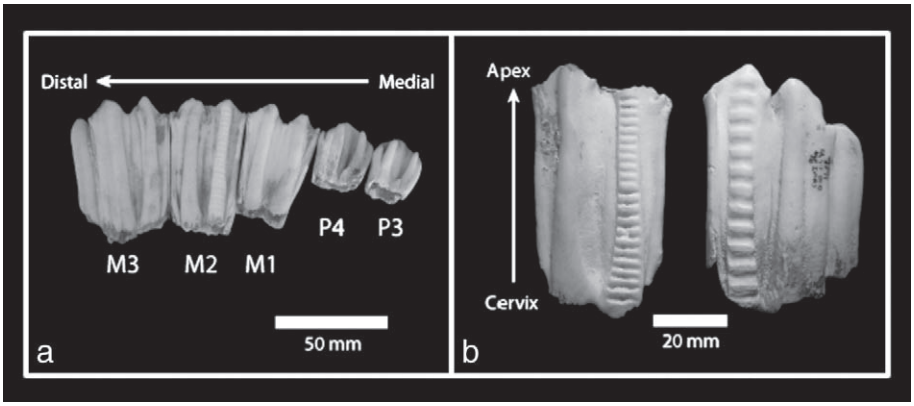

Fig. 2. Example of bison teeth from Coudoulous I, France, which have been sampled for oxygen isotope analysis of enamel phosphate. (a) *Bison priscus* teeth from lower left rows in lingual view; (b) micro-sampled right M2 in lingual view (left) and macro-sampled right M3 in lingual view (right).

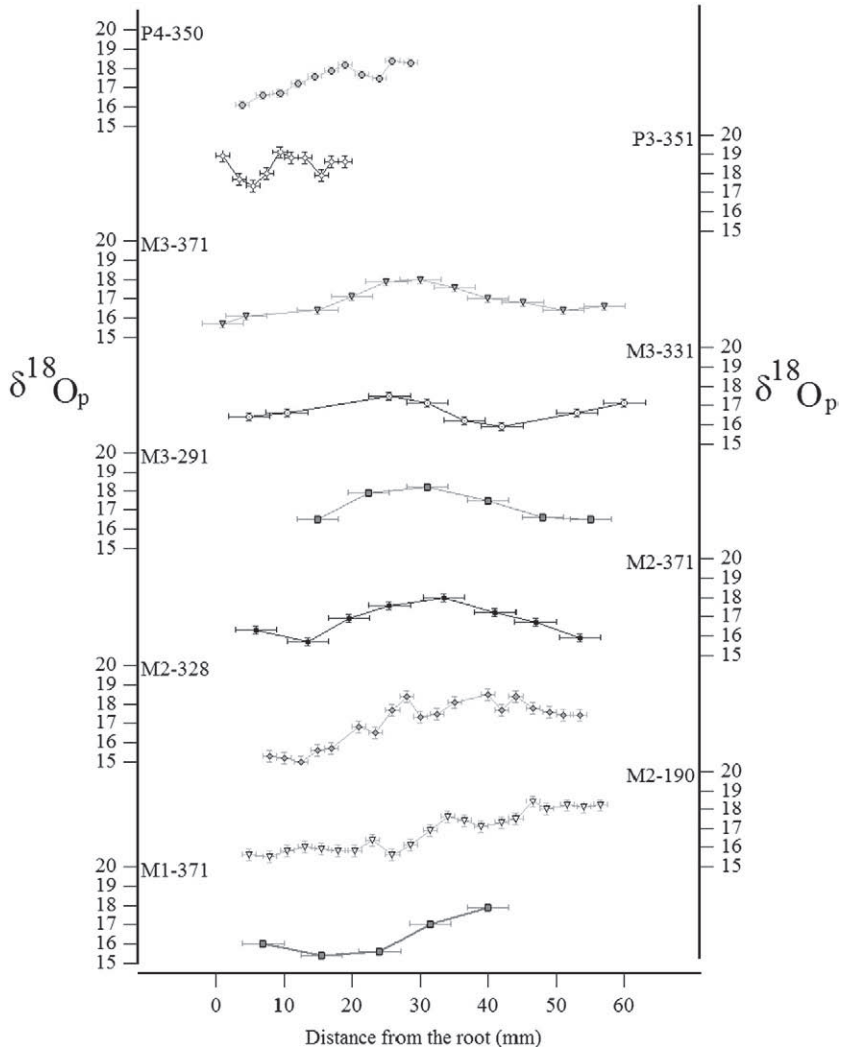

Fig. 3. Oxygen isotope compositions of the nine sampled bison teeth ($\delta^{18}O_p$ in ‰ V-SMOW) reported against the distance (in mm) from the cervix. Teeth list — M1-371: grey-filled square; M2-190: open triangle; M2-328: filled diamond; M2-371: black-filled circle; M3-291: grey-filled square; M3-331: dotted circle; M3-371: filled triangle; P3-351: open diamond; P4-350: grey-filled circle.

separate the PO_4^{3-} ions. After 24 h, the solution was removed and the resin was eluted with 6 mL of 0.1 M NH_4NO_3. After 4 h, 0.1 mL of NH_4OH and 3 mL of an ammoniacal solution of $AgNO_3$ were added and the samples were placed in a thermostated bath at 70 °C during 6 h allowing the precipitation of Ag_3PO_4 crystals.

For the macro-samples, the oxygen isotope data were obtained according to a 'conventional off-line method'. Aliquots of 8 mg of silver phosphate along with 0.5 mg of pure graphite were weighed into tin reaction capsules and loaded into quartz tubes and degassed for 30 min at 80 °C in vacuum. Silver phosphate was reduced to carbon dioxide at a temperature of 1100 °C following the protocol of Lécuyer et al. (1998) adapted from O'Neil et al. (1994). The oxygen isotope ratio of the gas was measured with a PRISM II™ mass spectrometer in dual inlet mode. Isotopic compositions are quoted in the standard delta notation relative to V-SMOW. The reproducibility of measurements carried out on tooth enamel samples is better than 0.2‰ (1σ). Silver phosphate precipitated from standard SRM 120c (formerly NBS 120c; natural Miocene phosphorite from Florida) was repeatedly analyzed ($\delta^{18}O = 21.7 \pm 0.1$‰; $n = 10$) along with the silver phosphate samples.

For the micro-samples, aliquots of 400–500 µg of silver phosphate samples were mixed with 500 µg of nickelized carbon in silver foil capsules. Pyrolysis was performed at 1270 °C using a EuroVector EA3028-HT™ elemental analyzer. Ceramic reaction tube was packed with glassy carbon in the presence of nickelized graphite to generate CO which was transferred to a GV IsoPrime™ mass spectrometer in continuous flow mode with He as the carrier gas (Lécuyer et al., 2007). The $\delta^{18}O$ value of SRM 120c was fixed at 21.7‰ for correction of instrumental mass fractionation during the CO isotopic analysis. The average standard deviation equals 0.27 ± 0.11‰. Aliquots of silver phosphate from SRM 120c were analyzed several times a day in order to account for possible instrumental drift.

The oxygen isotope compositions of the precipitation samples collected at Villars were determined using water–carbon dioxide equilibration methods (Horita et al., 1989). Equilibrated CO_2 was analyzed with a THERMO Finnigan MAT 252 stable isotope ratio mass spectrometer at LSCE, Gif/Yvette. External reproducibility of oxygen isotope measurements is close to 0.05‰.

5. Results

Oxygen isotope compositions of enamel from the nine Bison teeth range from 15.0‰ to 19.1‰ (Table 2 and Fig. 3) with intra-tooth $\delta^{18}O$ variation ranging from 1.6‰ to 3.5‰. The 3 sets of samples collected in the molars coming from the same individual (# 371) are assembled according to the tooth formation sequence. At the M1–M2 junction

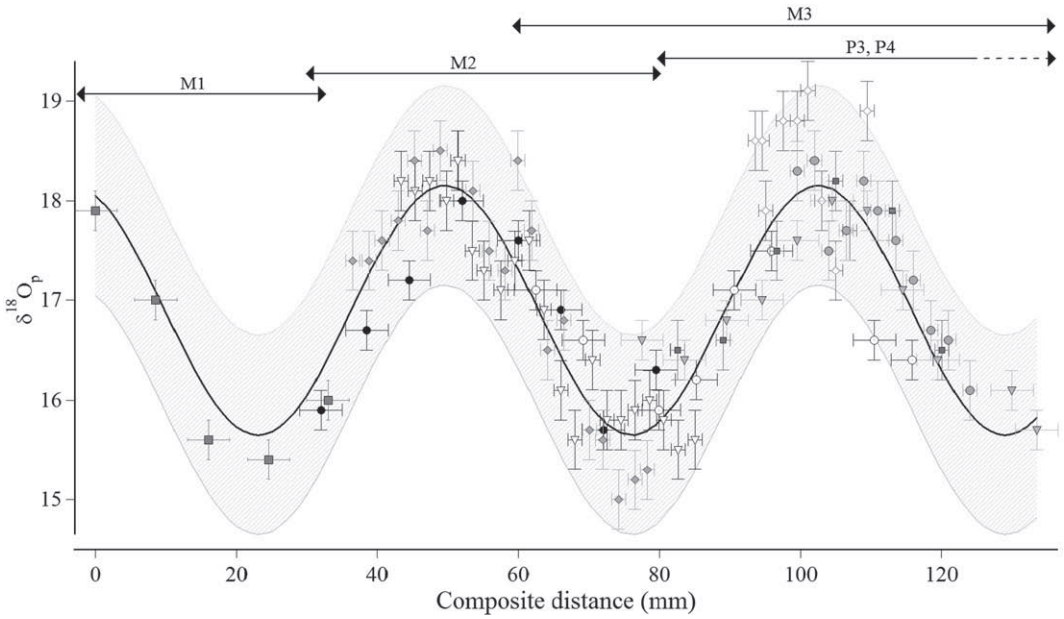

Fig. 4. Stacked temporal series of $\delta^{18}O_p$ (‰ V-SMOW) obtained from nine *Bison priscus* teeth from the late Middle Pleistocene of Coudoulous I, France. Solid line is the best sinusoidal fit and dashed line is the 95% confidence interval. Arrows indicate the period of enamel formation for each tooth. Teeth list — M1-371: grey-filled square; M2-190: open triangle; M2-328: filled diamond; M2-371: black-filled circle; M3-291: grey-filled square; M3-331: dotted circle; M3-371: filled triangle; P3-351: open diamond; P4-350: grey-filled circle.

points, the $\delta^{18}O$ values are close to each other and the isotopic records of the two teeth can be easily connected. At the M2–M3 junction, no overlap between the two datasets is observed, which may be ascribed to an incomplete preservation of the cervical margin of the M3 or to wear at the M2 apex. The M2 and M3 curves were connected end to end according to similar $\delta^{18}O$ and the known small growth overlap as mentioned above (16‰ at 7 mm of M1-371 root and 15.9‰ at 53.3 mm of M2-371 root; Fig. 4). The $\delta^{18}O$ *versus* the composite distance for the 9 bison teeth yields a sinusoidal-like signal with period and amplitude that are consistent throughout the whole combined record (Fig. 4).

As tooth length varies from one individual to another, M2 and M3 lengths (crown height) were normalized to the M2 and M3 belonging to bison 371 (coefficients listed in Table 2). A stacked isotopic curve was then constructed by using the highest and lowest values of the sinusoidal pattern of bison 371 as anchor points (Fig. 4). Non-linear regressions were performed with the best fit of isotopic data obtained with the following sinusoidal function:

$$\delta^{18}O_p = -(A/2)\cdot \sin[(2\pi/T)\times d_c - \varphi] + k \quad (1)$$

where: d_c is the composite distance. The amplitude of the sinusoid A is 2.5 ± 0.5‰ (1σ), the period T is ~53 mm, the phase φ equals 1.16 rad, and the constant k is 16.9‰. The determination coefficient is $r^2 = 0.78$ ($n = 99$, $p \ll 0.001$).

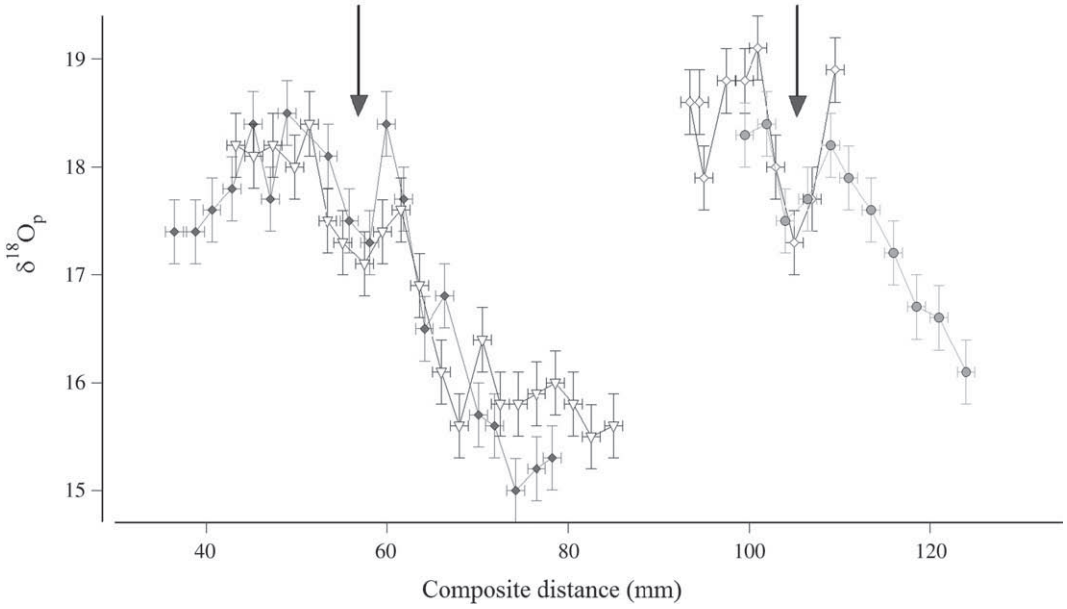

Fig. 5. High-resolution temporal $\delta^{18}O_p$ (‰ V-SMOW) records reveal the existence of cusp shape in the four micro-sampled teeth (M2-190, M2-328, P3-351, and P4-350, same symbols as in Figs. 3 and 4) of *Bison priscus* from the late Middle Pleistocene of Coudoulous I, France. Drops in oxygen isotope compositions occur during the two recorded summer seasons (arrows). Composite distance values are from Table 2.

In the micro-sampled teeth (M2-190, M2-328b, P3-351, and P4-350), the top of the isotopic signal shows a cusp disturbing the sinusoidal curve. Isotopic values drop by ~1‰ over less than 5–10 mm along the tooth growth axis (Fig. 5).

6. Discussion

6.1. Meaning of the oxygen isotope compositions of bison tooth enamel phosphate

The quality of the sinusoidal curve fit is a strong argument in favour of the preservation of the original isotopic signal. Assuming that the bison tooth enamel records the sinusoidal input signal of $\delta^{18}O$ in precipitation which is expected under mid-latitudes for a non-arid climate, low and high $\delta^{18}O$ values may be interpreted as winter and summer seasons, respectively. The stacked isotopic record therefore corresponds approximately to a 2 yr and a half record allowing the calculation of a mean tooth growth rate of about 55 mm yr^{-1}. This value is in good agreement with other growth rates between 40 and 55 mm yr^{-1} that were estimated for both modern and fossil bison (Fricke and O'Neil, 1996; Gadbury et al., 2000; Feranec and MacFadden, 2000). Ninety percent of the data are included in a 1.5‰ range around the best sinusoidal fit. This variability corresponds essentially to inter-individual differences. The analyzed teeth indeed correspond to different individuals, which had different ages at the time of their death, and to several hunting episodes but within a same short climatic frame. The range of variation of 1–2‰, observed by Fricke et al. (1996) for modern groups of cattle, sheep or elks from different localities across North America and Europe brackets the 1.5‰ value found for the *B. priscus* population of Coudoulous I.

The mineralization process does not alter the mean $\delta^{18}O_p$ which is a proxy for the mean composition of environmental water ($\delta^{18}O_{ew}$). However, it is known to modify more or less both the phase and amplitude of the sinusoidal input signal (Passey and Cerling, 2002; Higgins and MacFadden, 2004; Kohn, 2004). Corrections of these two parameters are theoretically required to estimate the amplitude of seasonal temperature variations. Passey and Cerling (2002) studied the growth and enamel maturation of the first molar of a modern bison. They showed that the percentage of mineralization ranges from 25% at the root to 100% at the apex (at 26–30 mm). This means that the enamel increments in Coudoulous I bison are fully mineralized in 6 months according to the computed growth rate of 55 mm yr^{-1}. This is in agreement with the estimates of 6–7 months for the completion of enamel maturation in steers (Balasse, 2002).

As a second consequence of the mineralization process, the sinusoidal signal is dampened. Dampening is defined here as in Kohn (2004) as the difference in amplitude of the environmental and of the recorded signals divided by the amplitude of the environmental signal. Averaging over 6 months leads to a 40–45% dampening to which ~10% must be added due to the residence time of the oxygen in the animal (Kohn and Cerling, 2002; Kohn et al., 2002). The resulting dampening factor (d_f) of 50–55% is in agreement with the value of 50–70% proposed by Kohn (2004).

The dampened $\delta^{18}O_p$ signal measured in Bison teeth has an amplitude of 2.5 ± 0.5‰ and a mean value of 16.9‰ (Eq. (1), Fig. 4). Determining the input, not dampened, signal is an ill-posed inverse problem. As it cannot be solved, the amplitude of the input isotope signal was estimated using a Monte Carlo approach. A set of amplitudes (A) of the input signal was generated so that: $A \times (1 - d_f)$ is in the range $[2.5 - \sigma;\ 2.5 + \sigma]$ that is [2‰; 3‰] with d_f in the range [0.50–0.55]. The estimation obtained by averaging 1000 independent replications is: 5.3 ± 0.7‰. Neglecting such a dampening effect would lead to largely underestimate both variations in environmental water $\delta^{18}O$ and air temperature.

The validity of such an approach was tested by using the following model:

- The input signal, that is the annual variation of the $\delta^{18}O$ of the environmental water, was modelled as $x(t)$, a sinusoidal function of time: $x(t) = (A/2).\sin(\omega t)$, where ω is $\pi/6$ if the periodicity of the signal is annual.
- The effect of the residence of the water in the body over a τ-long time period was modelled by integrating function $x(t)$ over a time length τ. The resulting function $y(t)$, as an integer of a sinusoidal function, is also a sinusoidal function:

$$y(t) = \frac{1}{\tau} \times \int_{t}^{t+\tau} x(t). \tag{2}$$

- To model the effect of mineralization the two steps character of the process must be taken into account. The mineralization is known to be 'instantaneous' for 25%, the 75% left corresponding to a 6 months long maturation. It was modelled as follows:

$$\begin{aligned} z(t) &= 0.25 \times y(t-6) + \frac{1}{6} \times \int_{t-6}^{t} y(t) \\ &= -0.25 \times \frac{A}{2}[\sin(\omega t) + (1/\omega) \times \cos(\varpi t)] \end{aligned} \tag{3}$$

$z(t)$ is also a sinusoidal function.

The unknown parameters here are the amplitude of the input signal, A, and the residence time of the water in the bison body, τ. We adjusted these values in order to obtain an amplitude of the output signal $z(t)$ of about 2.5‰ (amplitude of the dampened signal $\delta^{18}O_p$ in bison teeth). The results of this modelling are presented in Fig. 6. The best fit is obtained with $t = 3$ months and $A = 5.3$‰. The dampening subsequent to the residence of body water is ca. 10% and the one due to mineralization is ca. 45% which is in agreement with the data presented above.

6.2. Estimates of $\delta^{18}O$ of environmental waters ($\delta^{18}O_{ew}$)

Hoppe (2006) demonstrated that the mean $\delta^{18}O$ value of the carbonate component ($\delta^{18}O_c$) of bison hydroxyapatite is related to the value of environmental waters. Since carbonate and phosphate in mammalian enamel are in isotopic equilibrium, $\delta^{18}O_c$ can be converted in $\delta^{18}O_p$ using the fractionation equation determined by Zazzo et al. (2004):

$$\delta^{18}O_p = 0.973 \times \delta^{18}O_c - 8.12. \tag{4}$$

The ordinary least squares analysis of the calculated $\delta^{18}O_p$ *versus* the $\delta^{18}O_{ew}$ listed in Hoppe (2006) produces the following equation:

$$\begin{aligned} \delta^{18}O_{ew} = 1.18(\pm 0.07) \times \delta^{18}O_p - 27.2(\pm 1.1) \\ \times \left(n = 62;\ r^2 = 0.8;\ p < 0.0001\right). \end{aligned} \tag{5}$$

In order to take into account the uncertainties associated with the regression coefficient, the intercept, and the mean value and amplitude of variation of $\delta^{18}O_p$, the values of $\delta^{18}O_{ew}$ (amplitude and yearly mean) were calculated using a Monte Carlo approach. To do so, we generated 1000 sets of inputs randomly in their domain (e.g. the regression coefficient was sampled in [1.11‰; 1.25‰]), we performed the computation of $\delta^{18}O_{ew}$ using the inputs and we aggregated the results of the 1000 individual computations into the final result (mean ± standard deviation at 1σ). According to Eq. (5), the conversion of the corrected amplitude of 5.3 ± 0.7‰ and the mean value

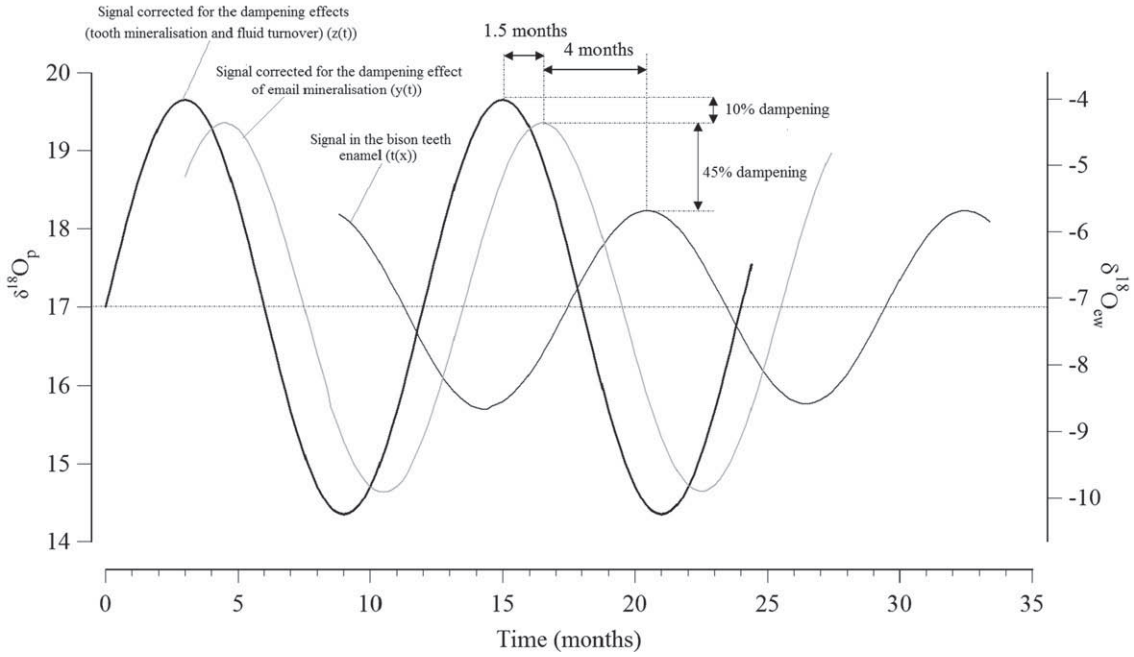

Fig. 6. The $\delta^{18}O_p$ values measured in Bison teeth constitute the output oxygen isotope signal that was dampened by the combination of mineralization process and residence time of water in the animal's body. The restoration of the original amplitude of the sinusoidal signal has been used to calculate the $\delta^{18}O$ of waters (‰ V-SMOW). See Section '6.1' for the calculation method. $\delta^{18}O_p$ (‰ V-SMOW; left axis) are converted into $\delta^{18}O_{ew}$ (‰ V-SMOW; right axis) using Eq. (5).

of 16.9‰ of the $\delta^{18}O_p$ signal yields an amplitude of 6.3 ± 0.5‰ and a mean value of -7.2 ± 0.9‰ for $\delta^{18}O_{ew}$. Still using a Monte Carlo method, we computed a $\delta^{18}O_{ew}$ range from about -10.3 ± 0.5‰ to -4.1 ± 0.5‰. This isotopic range slightly differs from the oxygen isotopic compositions of present-day meteoric waters sampled at Villars (close to Coudoulous, Fig. 1) which vary between −8‰ and −4.6‰ (Table 3). Note that the mean $\delta^{18}O_{ew}$ calculated above can differ from the value of the amount-weighted $\delta^{18}O_{ew}$ of precipitation if precipitation is strongly season-dependent.

Drops in $\delta^{18}O_p$ during the two recorded summer seasons of some bison teeth (Fig. 5) may be ascribed to various processes. According to the ~55 mm yr^{-1} tooth growth rate calculated for bison teeth from Coudoulous I, the relatively low isotopic values span over a distance along the tooth corresponding to about 1 month. In summer, at mid-latitudes, the variation of precipitation $\delta^{18}O$ may result from various effects: intra-season temperature variations, different precipitation sources and amount effect. The amount effect corresponds to a relative ^{18}O-depletion of the precipitation and occurs when the temperature is above a threshold of ~20 °C, and the precipitation amount is large (Dansgaard, 1964; Rozanski et al., 1993; Fricke and O'Neil, 1999; Bowen and Wilkinson, 2002; Straight et al., 2004). It was advocated by Higgins and MacFadden (2004) for being responsible of ~2‰ drops in the pattern of the intra-tooth $\delta^{18}O$ values collected in late glacial bison and horse teeth from South-Western United States. At Coudoulous I the summer depletion is minor compared to the yearly variation, however none of the three mentioned effects can be discarded.

Table 3
Oxygen isotope composition of environmental water (‰ V-SMOW) and air temperature (°C) measured at Villars and Bergerac (Fig. 1) in summer (June–August) and winter (December–February).

	Present day (1996–2006)			Level 4		
	Villars	Villars	Bergerac	Coudoulous		
	$\delta^{18}O_{ew}$	T (°C)	T (°C)	$\delta^{18}O_{ew}$	T (1)	T (2)
Summer	−4.7	18 ± 1	20 ± 1	−4.4 ± 0.9	19 ± 1	19 ± 3
Winter	−7.9	5 ± 1	6 ± 1	−10.6 ± 0.9	1 ± 1	−1 ± 3
Annual		12 ± 1	13 ± 1			9 ± 3

$\delta^{18}O_{ew}$ (‰ V-SMOW) at Coudoulous deduced from Eq. (5) and converted in temperature using (1) T–$\delta^{18}O_{ew}$ summer and winter relationships according to Eqs. (6) and (7) and (2) T–$\delta^{18}O_{ew}$ relationship according to Eq. (8).

6.3. Air temperature during the late Middle Pleistocene

According to the frequency of the sinusoidal pattern of the $\delta^{18}O_p$ signal in *B. priscus* teeth, it appears clearly that each enamel sample corresponds to a period of several weeks only. Therefore, seasonality of air temperatures (T_{air}) at Coudoulous I during Layer 4 deposition needs to be estimated by using linear regression equations '$\delta^{18}O_{ew} - T_{air}$' either based on mean summer and winter values or monthly data close to the study area instead of those based on annual average values inferred from global datasets. Using the same approach as Fricke and O'Neil (1999), we calculated seasonal $\delta^{18}O_{ew}/T_{air}$ regressions using a sub-dataset restricted to the circum North-Atlantic stations of the IAEA-GNIP/ISOHIS dataset (2006).

$$\text{Summer (Jun.–Aug.)}: \quad T_{air} = 1.06(\pm 0.07) \times \delta^{18}O_{ew} + 24.1(\pm 0.7) \times \left(n = 71,\ r^2 = 0.75,\ p < 0.001\right) \tag{6}$$

$$\text{Winter (Dec.–Feb.)}: \quad T_{air} = 1.40(\pm 0.05) \times \delta^{18}O_{ew} + 15.3(\pm 0.8) \times \left(n = 72,\ r^2 = 0.92,\ p < 0.001\right). \tag{7}$$

We also calculated a local regression based on 10 yr monthly averaged series of precipitation $\delta^{18}O$ and mean temperature recorded at Villars over 1996–2006.

$$T_{air} = 3.66(\pm 0.40) \times \delta^{18}O_{ew} + 35.1(\pm 2.6) \quad (\text{Spearman's rank correlation}: \rho = 0.98,\ p < 0.01). \tag{8}$$

The robustness of this present-day $\delta^{18}O_{ew}$–T_{air} relationship has been shown by Rozanski (1985) who documented, on the basis of modern groundwater compositions, a systematic depletion in deuterium of mean annual precipitation as air masses move eastward over Europe. A parallel trend in groundwater dated from the last glacial maximum (10,000–35,000 yr), and shifted toward lower δD values by about 10‰ due to air cooling, reveals that the paleo-atmospheric circulation was similar to present-days. Therefore, it is assumed that such a relationship was also valid for the late Middle Pleistocene; the calculated summer (June to August) mean temperature at Coudoulous I during the time of deposition of Layer 4 is ca 19 °C according to both methods expressed by Eqs. (6) and (8) (Table 3). The winter (December to February) temperature is around +1 °C according to Eq. (7) and −1 °C according to Eq. (8). Present-day air temperatures in South-West of France (e.g. Villars and Bergerac; Fig. 1) are close to 18–20 °C in summer and 5–6 °C in winter (Table 3). According to the two kinds of linear regression equations used to relate air temperature to $\delta^{18}O_{ew}$, seasons may have been more contrasted in Coudoulous I during Layer 4 deposition with summers as warm as the present ones and winters significantly colder. Combination of mean $\delta^{18}O_{ew}$ and the local 'Villars' $\delta^{18}O_{ew}/T_{air}$ relationship leads to estimate a MAT of 9±3 °C which is ca. 4 °C less than the present-day annual mean value (Table 3).

Various studies based on pollen data have reconstructed cold climates in France at the end of the Rissian period (Saalian; MIS 6; Fig. 7): winter and summer temperatures at La Grande Pile (North-Eastern France, Fig. 1) were estimated to be respectively 21±3 °C and 4±8 °C lower than today resulting in a higher seasonality (Rousseau et al., 2006). The MAT was estimated to be 8 to 12 °C lower by Guiot (1990) and 14 to 19 °C by Fauquette et al. (1999) at the same site. It was calculated to be lower by 8 to 12 °C at Les Echets (Eastern France) and 15 °C lower at Vienne (Centre of France) (Fauquette et al., 1999). At the very beginning of the Eemian (MIS 5e), the temperatures have risen. For instance, at La Grande Pile, at about 125 ka, the warming has been ca. 20 °C in summer and winter resulting in summer temperature higher than today (Guiot, 1990), winter temperature similar to present-day temperature and still marked seasonality. The calculated mean annual temperature (MAT) were 9 to 12 °C at La Grande Pile (9.5 °C today), 8 to 12 °C at Les Echets (10.5 °C today), and 10 to 13 °C at Lac du Bouchet (7 °C today), which is about the same as or higher than today (Fauquette et al., 1999).

The age of Layer 4 (149±6 ka) corresponds to the end of the Rissian, European equivalent to MIS 6, that is a glacial period. The MAT reconstructed at Coudoulous I is higher than those estimated in previous studies for this period (Fig. 7). Apparent discrepancies between the geochemical and palynological approaches could result from two kind of origins. The first one could be linked for both methods to the use of 'transfer functions' (floral associations and $\delta^{18}O$–T relationship) that were established in present-days and that could be not valid when transposed to the late Middle Pleistocene of Europe. The second one could be the age of Layer 4 in Coudoulous that could mark the end of the Rissian glacial stage with the onset of a milder climate resembling that estimated for the Eemian. However, it is noteworthy that the estimated mean temperature and seasonality in Coudoulous by using the $\delta^{18}O_p$ of bison teeth are comparable to the well quantified glacial conditions of the last glacial (e.g. Davis et al., 2003).

7. Concluding remarks

Fossil bison intra-tooth oxygen isotopic compositions show variations consistent with the annual cycle of the isotopic composition of precipitation. Taking into account a 50–55% dampening, the annual range of variation of the $\delta^{18}O_{ew}$ can be reconstructed. This last parameter can be translated to temperature seasonality using local or monthly T–$\delta^{18}O_{ew}$ relationships. Summers were as warm as today whereas winters were about 6 °C colder and the MAT is estimated to be about 4 °C lower than today. This result challenges previous studies providing much colder climatic conditions for the late Middle Pleistocene. The incremental oxygen isotope analysis of phosphate in bison enamel apatite offers interesting perspectives to quantify temperature seasonality that is a key parameter in assessing glacial *versus* interglacial climatic modes.

Acknowledgments

The authors thank F. Martineau, M.-A. Héran, R. Amiot, K. Poure, M. Fabre, and S. Chelouah for assistance in sample preparation and isotopic analysis. Thanks are also due to O. Mestre from Meteo-France for providing homogenised temperature data from Villars-Nontron, to F. Veinante for mathematical assistance and to S. Belmecheri and G. Escarguel for early comments on the manuscript. This work was

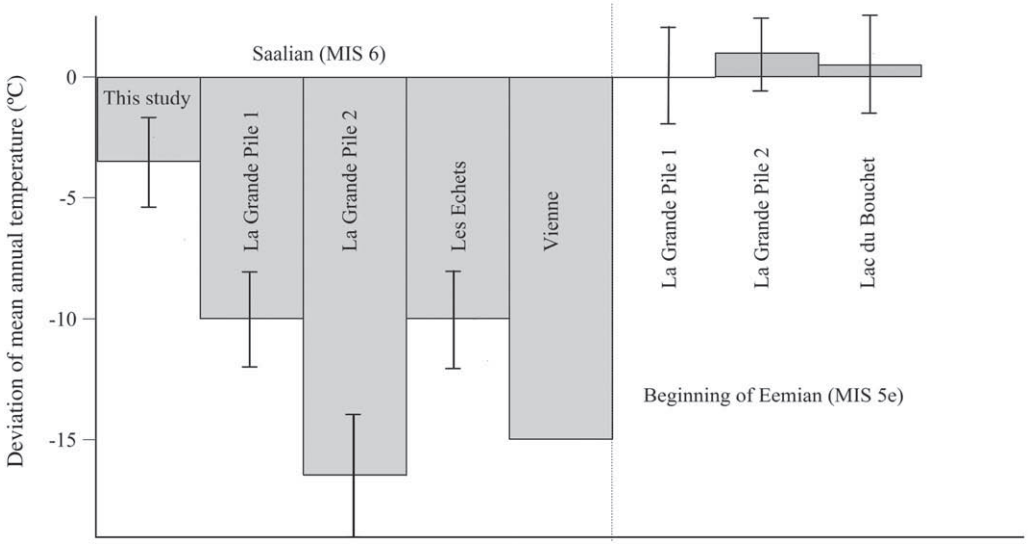

Fig. 7. Diagram summarizing the published mean air temperature estimates for the Saalian (MIS 6) and Eemian (MIS 5e) periods deduced from the floral associations and the oxygen isotope compositions of phosphate from Bison tooth enamel (this study) in France. The data are from: Guiot (1990) for La Grande Pile 1, Fauquette et al. (1999) for La Grande Pile 2, Les Echets, Vienne and lac du Bouchet.

supported by CNRS 'ECLIPSE' program and IUF. The authors thank P. Delaney and two anonymous reviewers for their constructive comments which help in improving the scientific content of this study.

References

Amiot, R., Lécuyer, C., Buffetaut, E., Fluteau, F., Legendre, S., Martineau, F., 2004. Latitudinal temperature gradient during the Cretaceous Upper Campanian–Middle Maastrichtian: $\delta^{18}O$ record of continental vertebrates. Earth Planet. Sci. Lett. 226, 255–272.

Ayliffe, L.K., Lister, A.M., Chivas, A.R., 1992. The preservation of glacial–interglacial climatic signatures in the oxygen isotopes of elephant skeletal phosphate. Palaeogeogr. Palaeoclimatol. Palaeoecol. 99, 179–191.

Balasse, M., 2002. Reconstructing dietary and environmental history from enamel isotopic analysis: time resolution of intra-tooth sequential sampling. Int. J. Osteoarchaeol. 12, 155–165.

Bowen, G.J., Wilkinson, B., 2002. Spatial distribution of $\delta^{18}O$ in meteoric precipitation. Geology 30, 315–318.

Brugal, J.-P., 1985. Le Bos primigenius Boj., 1827 du Pléistocène moyen des grottes de Lunel-Viel (Hérault). Bull. Mus. Anthr. Préh.Monaco, vol. 28, pp. 7–62 (In French).

Brugal, J.-P., 1999. Middle palaeolithic subsistence on large bovids: La Borde and Coudoulous I (Lot, France). In: Gaudzinski, S., Turner, E. (Eds.), The Role of Early Humans in the Accumulation of European Lower and Middle Palaeolithic Bone Assemblages. Monographien des Römisch-Germanischen Zentralmuseums Mainz, vol. 42, pp. 263–266 (In French).

Brugal, J.P., Croitor, R., 2007. Evolution, ecology and biochronology of herbivore associations in Europe during the last 3 millions years. Quaternaire 18, 129–151.

Bryant, J.D., Luz, B., Froelich, P.N., 1994. Oxygen isotopic composition of fossil horse tooth phosphate as a record of continental paleoclimate. Palaeogeogr. Palaeoclimatol. Palaeoecol. 107, 303–316.

Bryant, J.D., Froelich, P.N., Showers, W.J., Genna, B.J., 1996. Biologic and climatic signals in the oxygen isotope composition of Eocene–Oligocene equid enamel phosphate. Palaeogeogr. Palaeoclimatol. Palaeoecol. 126, 75–90.

Buntjer, J.B., Otsen, M., Nijman, I.J., Kuiper, M.T.R., Lenstra, J.A., 2002. Phylogeny of bovine species based on AFLP fingerprinting. Heredity 88, 46–51.

Chaline, J., 1972. Middle and late Pleistocene rodent in France. Cahiers de Paléontologie (eds CNRS, Paris), pp 411. In French.

Croitor, R., Brugal, J.P., 2007. News insights concerning Early Pleistocene cervids and bovids in Europe: dispersal and correlation. Cour. Forsch.inst. Senckenb. 259, 47–59.

Crowson, R.A., Showers, W.J., Wright, E.K., Hoering, T.C., 1991. Preparation of phosphate samples for oxygen isotope analysis. Anal. Chem. 63, 2397–2400.

D'Angela, D., Longinelli, A., 1990. Oxygen isotopes in living mammal's bone phosphate: further results. Chem. Geol. 86, 75–82.

Dansgaard, W., 1964. Stable isotopes in precipitation. Tellus 16, 436–468.

Daux, V., Lécuyer, C., Héran, M.-A., Amiot, R., Simon, L., Fourel, F., Martineau, F., Lynnerup, N., Reychler, H., Escarguel, G., 2008. Oxygen isotope fractionation between human phosphate and water revisited. J. Hum. Evol. 55, 1138–1147.

Davis, B.A.S., Brewer, S., Stevenson, A.C., Guiot, J., Data Contributors, 2003. The temperature of Europe during the Holocene reconstructed from pollen data. Quat. Sci. Rev. 22, 1701–1716.

deMenocal, P.B., 2004. African climate change and faunal evolution during the Pliocene–Pleistocene. Earth Planet. Sci. Lett. 220, 3–24.

Eberhardt, L.L., 1969. Similarity, allometry and food chains. J. Theor. Biol. 24, 43–55.

Fauquette, S., Guio, J., Menut, M., de Beaulieu, J.-L., Reille, M., Guenet, P., 1999. Vegetation and climate since the last interglacial in the Vienne area (France). Glob. Planet. Change 20, 1–17.

Feranec, R.C., MacFadden, B., 2000. Evolution of the grazing niche in Pleistocene mammals from Florida: evidence from stable isotopes. Palaeogeogr. Palaeoclimatol. Palaeoecol. 162, 155–169.

Fricke, H.C., O'Neil, J.R., 1996. Inter- and intra-tooth variation in the oxygen isotope composition of mammalian tooth enamel phosphate: implications for palaeoclimatological and palaeobiological research. Palaeogeogr. Palaeoclimatol. Palaeoecol. 126, 91–99.

Fricke, H.C., O'Neil, J.R., 1999. The correlation between $^{18}O/^{16}O$ ratio of meteoric water and surface temperature: its use in investigating terrestrial climate change over geologic time. Earth Planet. Sci. Lett. 170, 181–196.

Fricke, H.C., Clyde, W.C., O'Neil, J.R., 1996. Intra-tooth variations in $\delta^{18}O$ (PO_4) of mammalian tooth enamel as a record of seasonal variations in continental climate variables. Earth Planet. Sci. Lett. 62, 1839–1850.

Gadbury, C., Todd, L., Jahren, A.H., Amundson, R., 2000. Spatial and temporal variations in the isotopic composition of bison tooth enamel from the Early Holocene Hudson-Meng Bone Bed, Nebraska. Palaeogeogr. Palaeoclimatol. Palaeoecol. 157, 79–93.

Geraads, D., 1992. Phylogenetic analysis of the tribe Bovini (Mammalia: Artiodactyla). Zool. J. Linn. Soc. 104, 193–207.

Groves, C.P., 1981. Systematic relationships in the Bovini (Artiodactyla, Bovidae). Z. Zoolog. Syst. Evol.forsch. 19, 264–278.

Guiot, J., 1990. Methodology of the last climatic cycle reconstruction in France from pollen data. Palaeogeogr. Palaeoclimatol. Palaeoecol. 80, 49–69.

Guthrie, R.D., 1990. Frozen Fauna of the Mammoth Steppe: The Story of Blue Babe. University of Chicago Press, Chicago, p. 338.

Haynes, G., 1984. Tooth wear rate in northern bison. J. Mammal. 65, 87–491.

Higgins, P., MacFadden, B.J., 2004. "Amount Effect" recorded in oxygen isotopes of Late Glacial horse (*Equus*) and bison (*Bison*) teeth from the Sonoran and Chihuahuan deserts, Southwestern United States. Palaeogeogr. Palaeoclimatol. Palaeoecol. 206, 337–353.

Hillson, S., 1992. Mammal Bones and Teeth: an Introductory Guide to Methods of Identification. Institute of Archaeology, London. 76 pp.

Hoppe, K.A., 2006. Correlation between the oxygen isotope ratio of North American bison teeth and local waters, implication for paleoclimatic reconstructions. Earth Planet. Sci. Lett. 244, 408–417.

Horita, J., Veda, A., Mizukami, K., Takatori, I., 1989. Automatic δD and $\delta^{18}O$ analyses of multi-water samples using H_2- and CO_2- water equilibration methods with a common equilibration set-up. Appl. Radiat. Isotopes 40, 801–805.

IAEA/WMO, 2006. Global Network of Isotopes in Precipitation. The GNIP Database. Retrieved August 2008 at: http://isohis.iaea.org.

Jaubert, J., Kervazo, B., Bahain, J.-J., Brugal, J.-P.h., Chalard, P., et al., 2005. Coudoulous I (Tour-de-Faure, Lot), Middle Pleistocene site in Quercy: pluridisciplinary approach. In: Molines, N., Moncel, M.-H., Monnier, J.-L. (Eds.), Données récentes sur les modalités de peuplement et sur le cadre chronostratigraphique, géologique et paléogéographique des industries du Paléolithique ancien et moyen en Europe. Brit. Archaeol. Rep., International Series / S1364. Hedges Ltd, Oxford, pp. 227–251 (In French).

Koch, P.L., Fisher, D.C., Dettman, D., 1989. Oxygen isotope variation in the tusks of extinct proboscideans: A measure of season of death and seasonality. Geology 17, 515–519.

Kohn, M.J., 2004. Comment: Tooth enamel mineralization in ungulates: implications for recovering a primary isotopic time-series, by B. H. Passey and T. E. Cerling (2002). Geochim. Cosmochim. Acta 68, 403–405.

Kohn, M.J., Cerling, T.E., 2002. Stable isotope compositions of biological apatite. In: Kohn, M.J., Rakovan, J., Hughes, J.M. (Eds.), Phosphates. Geochemical, Geobiological and Materials Importance. Review in Mineralogy and Geochemistry, vol. 48. Mineralogical Society of America, Wahington, D.C., pp. 455–488.

Kohn, M.J., Schoeninger, M.J., Valley, J.W., 1996. Herbivore tooth oxygen isotope compositions: effects of diet and physiology. Geochim. Cosmochim. Acta 60, 3889–3896.

Kohn, M.J., Miselis, J.L., Fremd, T.J., 2002. Oxygen isotope evidence for progressive uplift of the Cascade Range, Oregon. Earth Planet. Sci. Lett. 204, 151–165.

Kolodny, Y., Luz, B., Navon, O., 1983. Oxygen isotope variations in phosphate of biogenic apatites, I. Fish bone apatite — rechecking the rules of the game. Earth Planet. Sci. Lett. 64, 398–404.

Krasinski, Z., Raczynski, J., 1967. The reproduction biology of European bison living in reserves and freedom. Acta Theriol. 12, 407–444.

Kurten, B., 1968. Pleistocene Mammals of Europe. Weidenfeld and Nicolson, London. 317 pp.

Lécuyer, C., Grandjean, P., O'Neil, J.R., Capetta, H., Martineau, F., 1993. Thermal excursions in the ocean at the Cretaceous–Tertiary boundary (northern Morocco): $\delta^{18}O$ record of phosphatic fish debris. Palaeogeogr. Palaeoclimatol. Palaeoecol. 105, 235–243.

Lécuyer, C., Grandjean, P., Barrat, J.-A., Nolvak, J., Emig, C., Paris, F., Robardet, M., 1998. $\delta^{18}O$ and REE contents of phosphatic brachiopods: a comparison between modern and lower Paleozoic populations. Geochim. Cosmochim. Acta 62, 2429–2436.

Lécuyer, C., Fourel, F., Martineau, F., Amiot, R., Daux, V., 2007. High-precision determination of $^{18}O/^{16}O$ ratios of silver phosphate by EA-pyrolysis-IRMS continuous flow technique. J. Mass Spectrom. 42, 36–41.

Longinelli, A., 1984. Oxygen isotopes in mammal bone phosphate: a new tool for paleohydrological and paleoclimatological research? Geochim. Cosmochim. Acta 48, 385–390.

Longinelli, A., Nuti, S., 1973. Oxygen isotope measurements of phosphate from fish teeth and bones. Earth Planet. Sci. Lett. 19, 373–376.

Luz, B., Kolodny, Y., Horowitz, M., 1984. Fractionation of oxygen isotopes between mammalian bone-phosphate and environmental drinking water. Geochim. Cosmochim. Acta 48, 1689–1693.

McDonald, J.N., 1981. North American Bison: Their Classification and Evolution. University of California Press, Berkeley, p. 316.

Merceron, G., Madelaine, S., 2006. Molar microwear pattern and palaeoecology of ungulates from La Berbie (Dordogne, France): environment of Neanderthals and modern human populations of the Middle/Upper Palaeolithic. Boreas 35, 272–278.

Metropolis, N., Ulam, S., 1949. The Monte Carlo method. J. Am. Stat. Assoc. 44 (247), 335–341.

Mosbrugger, V., Uteschert, T., Dilcher, D.L., 2005. Cenozoic continental climatic evolution of Central Europe. Proc. Natl. Acad. Sci. 102, 14964–14969.

Nowak, R.M., 1999. Bison, Walker's Mammals of the World, 6th Ed. J. Hopkins Univ. Press, Baltimore, pp. 1161–1163.

O'Neil, J.R., Roe, L.J., Reinhard, E., Blake, R.E., 1994. A rapid and precise method of oxygen isotope analysis of biogenic phosphates. Isr. J. Earth-Sci. 43, 203–212.

Passey, B.H., Cerling, T.E., 2002. Tooth enamel mineralization in ungulates: implications for recovering a primary isotopic time-series. Geochim. Cosmochim. Acta 66, 3225–3234.

Pitra, C., Fürbass, R., Seyfert, H.-M., 1997. Molecular phylogeny of the tribe Bovini (Mammalia: Artiodactyla): alternative placement of the Anoa. J. Evol. Biol. 10, 589–600.

Reher, C., Frison, G., 1980. The Vore site, a stratified buffalo jump in the Wyoming Black Hills Plains. Anthropol. Mem. 16, 1–190.

Ricciutu, E.R., 1973. To the Brink of Extinction. Holt, Rinehart and Winston? New York, Chicago, San Francisco.

Rousseau, D.-D., Hatté, C., Guiot, J., Duzer, D., Schevin, P., Kukla, G., 2006. Reconstruction of the Grande Pile Eemian using inverse modeling of biomes and $\delta^{13}C$. Quat. Sci. Rev. 25, 2806–2809.

Rozanski, K., 1985. Deuterium and oxygen-18 in European groundwaters — links to atmospheric circulation in the past. Chem. Geol. 52, 349.

Rozanski, K., Araguás-Araguás, L., Gonfiantini, R., 1992. Relation between long-term trends of oxygen-18 isotope composition of precipitation and climate. Science 258, 981–985.

Rozanski, K., Araguás-Araguás, L., Gonfiantini, R., 1993. Isotope pattern in modern global precipitation. In: Swart, P.K., Longmann, K.C., Mckenzie, J., Savin, S. (Eds.),

Continental Isotope Indicators of Climate, AGU Geophysical Monograph. American Geophysical Union, Washington DC, pp. 1–36.
Sharma, S., Joachimski, M.M., Tobschall, H.J., Singh, I.B., Tewari, D.P., Tewari, R., 2004. Oxygen isotopes of bovid teeth as archives of paleoclimatic variations in archaeological deposits of the Ganga plain, India. Quat. Res. 62, 19–28.
Sharp, Z.D., Cerling, T.E., 1998. Fossil isotope records of seasonal climate and ecology: straight from the horse's mouth. Geology 26, 19–22.
Smith, J.B., Dodson, P., 2003. A proposal for a standard terminology of anatomical notation and orientation in fossil vertebrate dentitions. J. Vertebr. Paleontol. 23, 1–12.
Straight, W.H., Barrick, R.E., Eberth, D.A., 2004. Reflections of surface water, seasonality and climate in stable oxygen isotopes from tyrannosaurid tooth enamel. Palaeogeogr. Palaeoclimatol. Palaeoecol. 206, 239–256.
Stuart-Williams, H.L.Q., Schwarcz, H.P., 1997. Oxygen isotopic determination of climatic variation using phosphate from beaver bone, tooth enamel, and dentine. Geochim. Cosmochim. Acta 61, 2539–2550.
Verkaar, E.L.C., Nijman, I.J., Beeke, M., Hanekamp, E., Lenstra, J.A., 2004. Maternal and paternal lineages in cross-breeding bovine species. Has wisent a hybrid origin? Mol. Biol. Evol. 21, 1165–1170.
Von Grafenstein, U., Erlenkeuser, H., Müller, J., Trimborn, P., Alefs, J., 1996. A 200 year mid-European air temperature record preserved in lake sediments, an extension of the $\delta^{18}O_p$–air temperature relation into the past. Geochim. Cosmochim. Acta 60, 4025–4036.
Wegrzyn, M., Serwatkas, S., 1984. Teeth eruption in the European bison. Acta Theriol. 29, 111–121.
Willink, R., 2006. On using the Monte Carlo method to calculate uncertainty intervals. Metrologia 43, 39–42.
Yurtsever, Y., 1975. Worldwide Survey of Stable Isotopes in Precipitation. Intern. Rep. IAEA (Vienna), p. 40.
Zazzo, A., Mariotti, A., Lécuyer, C., Heintz, E., 2002. Intra-tooth isotope variations in late Miocene bovid enamel from Afghanistan paleobiological, taphonomic, and climatic implications. Palaeogeogr. Palaeoclimatol. Palaeoecol. 186, 145–161.
Zazzo, A., Lécuyer, C., Sheppard, S.M.F., Grandjean, P., Mariotti, A., 2004. Diagenesis, and the reconstruction of paleoenvironments: a method to restore original $\delta^{18}O$ values of carbonate and phosphate from fossil tooth enamel. Geochim. Cosmochim. Acta 68, 2245–2258.

Palaeogeography, Palaeoclimatology, Palaeoecology 264 (2008) 85–92

Contents lists available at ScienceDirect

Palaeogeography, Palaeoclimatology, Palaeoecology

journal homepage: www.elsevier.com/locate/palaeo

Oxygen isotope compositions of phosphate from Middle Miocene–Early Pliocene marine vertebrates of Peru

Romain Amiot [a,*,1], Ursula B. Göhlich [b,2], Christophe Lécuyer [a,3], Christian de Muizon [c], Henri Cappetta [d], François Fourel [a], Marie-Anne Héran [a], François Martineau [a]

[a] Laboratoire Paléoenvironnements & Paléobiosphère, CNRS UMR 5125, Université Lyon I, 2 rue Raphaël Dubois, 69622 Villeurbanne, France
[b] Humboldt Fellow (Feodor-Lynen-Program) at the Laboratoire Paléoenvironnements & Paléobiosphère, CNRS UMR 5125, Université Claude Bernard Lyon I, 2 rue Raphaël Dubois, 69622 Villeurbanne, France
[c] Muséum National d'Histoire Naturelle de Paris, UMR 5143 (CNRS, MNHN, UPMC), Département Histoire de la Terre CP 38, 8, rue Buffon, F-75005 Paris, France
[d] Institut des Sciences de l'Evolution, CNRS UMR 5554, Université Montpellier II, Place Eugène Bataillon, 34095 Montpellier, France

ARTICLE INFO

Article history:
Received 25 September 2007
Received in revised form 29 February 2008
Accepted 4 April 2008

Keywords:
Miocene
Pliocene
Peru
Pisco Formation
Oxygen isotopes
Vertebrates

ABSTRACT

Phosphatic remains of marine vertebrates recovered from five fossil sites of the Pisco Formation ranging from the latest Middle/earliest Late Miocene (Ca 11–13 Ma) to the Early Pliocene (Ca 3.5 Ma) have been analysed for their oxygen isotope compositions ($\delta^{18}O_p$). Coexisting seals, dolphins, whales, penguins and sharks from each locality have distinct $\delta^{18}O_p$ values reflecting ecology and physiology differences, ranging from 18.2‰ to 21.4‰ for marine mammals, from 19.5‰ to 21.5‰ for marine birds and from 20.9‰ to 23.1‰ for sharks. Systematic offsets observed between dolphin teeth and bones as well as between dolphin and whale bones indicate that the fractionation equation established by using data from extant cetaceans may not be directly applicable to Miocene cetaceans in order to estimate water $\delta^{18}O_w$ values. Assuming that polar ice-caps were not totally developed during this time interval, marine palaeotemperatures ranging from 13.0 ± 1.3 °C to 17.2 ± 1.3 °C were estimated. Comparison of our results with those obtained in other World's areas suggests that the oxygen isotope ratios of Pisco vertebrates reflect the influence of both global and local events, such as the setting of the Atacama Desert, the cold Humboldt Current or the global phases of ice-cap growth and decay.

1. Introduction

Quantitative reconstitutions of temperatures and oxygen isotope compositions of past seawater ($\delta^{18}O_{sw}$) mainly rely on the oxygen isotope analysis of skeletal phosphate ($\delta^{18}O_p$) and carbonate ($\delta^{18}O_c$) secreted by marine organisms. As the oxygen isotope fractionation between these biominerals and water is temperature-dependent, the $\delta^{18}O_p$ or $\delta^{18}O_c$ value of aquatic ectothermic organisms (such as marine invertebrates and most fish) both reflect environmental temperature and water composition whereas endothermic organisms (marine mammals) provide $\delta^{18}O_w$ estimates. Temporal variations in both temperature and $\delta^{18}O_w$ value of sea or fresh waters can be tracked by analysing the phosphatic tissues of both coexisting marine mammals and fish or reptiles and fish (Barrick et al., 1993; Lécuyer et al., 1996; Barrick et al., 1999) using the fractionation equations established between phosphate and water for cetaceans ($\delta^{18}O_p = 0.773\ \delta^{18}O_w + 17.8$; Yoshida and Miyazaki, 1991), fish (T °C = 113.3 − 4.38 ($\delta^{18}O_p - \delta^{18}O_w$); Kolodny et al., 1983), turtles ($\delta^{18}O_w = 1.01\ \delta^{18}O_p - 22.3$; Barrick et al., 1999) or crocodilians ($\delta^{18}O_w = 0.82\ \delta^{18}O_p - 19.13$; Amiot et al., 2007). It is noteworthy that using cetaceans is not possible for periods older than the Eocene when these marine mammals appeared (Fordyce, 1994).

The Miocene and Pliocene were periods of great changes in the Earth's global climatic regime marked by the development of polar ice-caps and by the progressive global cooling that followed the Middle Miocene Climatic Optimum (see Zachos et al., 2001 for a review). Oxygen isotope compositions of phosphatic remains from coexisting cetaceans and fish have been used as proxies of thermal changes and ice volume fluctuations (Barrick et al., 1992, 1993). Surprising conclusions were drawn from their study of fossil samples recovered from Miocene deposits of the Chesapeake Bay (North America, Atlantic coast). Assuming that the studied samples were not diagenetically altered, Barrick et al. (1992) applied the oxygen isotope fractionation equation established for modern cetaceans (Yoshida and Miyazaki, 1991) to Miocene porpoises and whales. They obtained unrealistically high $\delta^{18}O_w$ values ranging from +2 to +4.7‰. They also observed a positive correlation between estimated marine temperatures and $\delta^{18}O_w$ values, meaning that warmer marine conditions prevailed during polar glaciations and conversely cooler temperatures during ice-cap melting. Moreover, the inferred variations in $\delta^{18}O_w$ values suggest larger volumes of polar ice involved during the Miocene growth

* Corresponding author.
E-mail address: romain.amiot@ivpp.ac.cn (R. Amiot).
[1] Now at the Institute of Vertebrate Paleontology and Paleoanthropology, Chinese Academy of Sciences, #142 XiZhiMenWai DaJie, Beijing 100044, China.
[2] Now at the Natural History Museum Vienna, Geological–Paleontological Department, Burgring 7, A-1010 Vienna, Austria.
[3] Also at Institut Universitaire de France.

0031-0182/$ – see front matter © 2008 Elsevier B.V. All rights reserved.
doi:10.1016/j.palaeo.2008.04.001

and decay stage than previously suspected (Haq et al., 1987; Miller et al., 1991). These results raised several questions concerning the meaning of the oxygen isotope compositions recorded in Miocene cetacean bones from Chesapeake Bay. Do they reflect global palaeoenvironmental conditions or local ones (Barrick et al., 1992, 1993)? To which extent is the equation established by Yoshida and Miyazaki (1991) applicable to any fossil cetacean given the excessively high $\delta^{18}O_w$ values estimated from the $\delta^{18}O_p$ values of their Miocene counterparts?

The fossil sites of the Pisco Formation (Peru, Pacific coast) have yielded rich and well-preserved marine vertebrate fauna of Miocene and Pliocene ages that include cetaceans (porpoises, whales), pinnipeds (seals), birds (among others, penguins), turtles, crocodiles and sharks. Fossil remains of these animals having various ecologies and physiologies have been analysed for their oxygen isotope contents in order to estimate the variations in marine temperatures and ice volume changes as well as to search for answers to questions raised by the results provided by Barrick et al. (1993)'s study.

2. Geological settings

The Pisco Formation consists of marine Neogene deposits located along the southern coast of Peru, and is known for its abundant marine vertebrate fauna. The Pisco Formation extends about 300 km from the city of Pisco south to Yauca (Fig. 1) and is about 640 m thick (Brand et al., 2003). Its geology and palaeoecology in the Sacaco area were studied by Muizon and DeVries (1985). The age of the sediments is constrained by vertebrate and molluscan biostratigraphies and radioisotopic dating. Samples come from different localities within the Pisco Formation representing different age levels: El Jahuay (ELJ, ca. 9–10 Ma), Late Miocene; Aguada de Lomas (AGL, ca. 7–8 Ma; Muizon and Bellon, 1986; Muizon et al., 2003), Late Miocene; Sacaco Sud (SAS, ca. 5 Ma), Early Pliocene; Sacaco (SAO, ca. 3.5 Ma; Muizon and Bellon, 1981), Early Pliocene. All these localities are in the Sacaco area, Arequipa Department. Northwards, the latest Middle/earliest Late Miocene locality of Cerro la Bruja, belongs to the Ica Department (ca. 11–13 Ma; Muizon, 1988). Deposits from the Pisco Formation range in age from the Middle Miocene (ca. 14 Ma) to the Late Pliocene (ca. 2 Ma) with a time span of about 12 Ma (Muizon and DeVries, 1985).

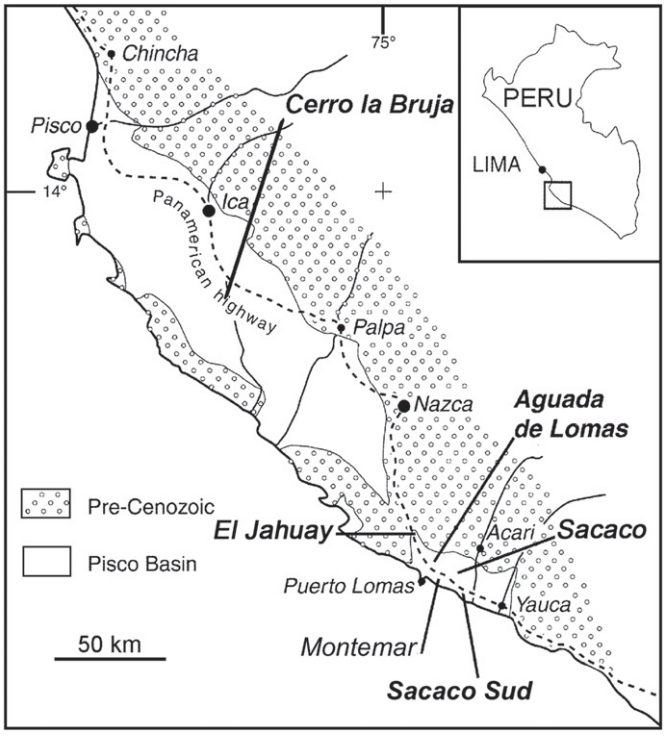

Fig. 1. Map showing the Miocene and Pliocene localities of the Pisco formation, Peru. Localities where samples have been analysed are printed in bold. Modified after McDonald & Muizon (2002: fig.1).

3. Sample collection

Phosphatic remains of marine vertebrates (whales, dolphins, seals, penguins, marine sloths, turtles, crocodilians and sharks) recovered from five fossil sites of the Pisco Formation were collected, cleaned and analysed for their oxygen isotope compositions. Except for small teeth for which bulk analyses were performed as well as two aquatic sloth teeth covered with durodentine, enamel was preferentially selected and sampled with a microdrill. Cortical regions of various bones which are the most compact bone parts were selected from penguins, whales, seals and marine sloth skeletal remains. Dense periotic and tympanic bones of dolphins and whales were also sampled. Number of samples, location and age, the phosphatic tissues analysed and taxonomic identification are reported in Table 1.

4. Analytical techniques

Measurements of oxygen isotope ratios of apatite consist of isolating phosphate ions using acid dissolution and anion-exchange resin, according to a protocol derived from the original method published by Crowson et al. (1991) and slightly modified by Lécuyer et al. (1993). Silver phosphate is quantitatively precipitated in a thermostatic bath set at a temperature of 70 °C. After filtration, washing with double deionised water, and drying at 50 °C, 8 mg of Ag_3PO_4 are mixed with 0.5 mg of pure powder graphite. $^{18}O/^{16}O$ ratios are measured by reducing silver phosphates to CO_2 using graphite reagent (O'Neil et al., 1994; Lecuyer et al., 1998). Samples are weighed into tin reaction capsules and loaded into quartz tubes and degassed for 30 min at 80 °C under vacuum. Each sample was heated at 1100 °C for 1 min to promote the redox reaction. The CO_2 produced was directly trapped in liquid nitrogen to avoid any kind of isotopic reaction with quartz at high temperature. CO_2 was then analyzed with a GV Isoprime™ and a GV Prism™ mass spectrometer at the Laboratory UMR CNRS 5125 'PEPS', University Claude Bernard Lyon 1. Isotopic compositions are quoted in the standard δ notation relative to V-SMOW. Silver phosphate precipitated from standard NBS120c (natural Miocene phosphorite from Florida) was repeatedly analyzed ($\delta^{18}O = 21.70 \pm 0.13‰$; $n = 37$) along with the silver phosphate samples derived from the Miocene and Pliocene vertebrate remains.

5. Results

Oxygen isotope measurements of tooth and bone phosphate are reported in Table 1. The whole $\delta^{18}O$ dataset ranges from 17.5‰ to 23.1‰. For each of the five localities sampled, mean $\delta^{18}O_p$ values of teeth and bones for each taxonomic group are plotted against their relative age in Fig. 2. Significant isotopic differences are observed at any given locality between the various groups of vertebrates, with ranges from 18.2‰ to 21.4‰ for marine mammals, 19.5‰ to 21.5‰ for marine birds and 20.9‰ to 23.1‰ for sharks. Relationship between the oxygen isotope composition of teeth and bones is not the same for any taxon. Indeed, teeth have $\delta^{18}O$ values higher than bones in the case of dolphins and one crocodile and conversely in the case of seals and one whale, and there is no significant isotopic difference between the tooth and bone for the specimen of marine sloth from "Sacaco Sud". Oxygen isotope compositions define distinct trends with time as a function of the considered taxon; only shark and seal teeth have $\delta^{18}O$ values that clearly increase by about 1‰ from the Miocene to the Pliocene. Oxygen isotope compositions of penguin bones show two maxima during the Late Miocene and the Pliocene. All taxa, including tooth and bone data, show $\delta^{18}O$ values for the latest Middle/earliest

Table 1
Taxon, location, phosphatic tissue, and oxygen isotope composition of Miocene and Pliocene Pisco vertebrate samples, Peru

Sample	Tissue	Taxon	Common name	Locality	Age (My)	$\delta^{18}O$ (‰ V-SMOW)
AL	Tooth enamel	*Hexanchus* sp.	Shark	Sacaco	3.5	23.1
AO	Tooth enamel	*Carcharhinus* sp.	Shark	Sacaco	3.5	21.5
SAO 69-AW	Femur	*Spheniscus urbinai*	Penguin	Sacaco	3.5	20.7
SAO 70-AX	Femur	*Spheniscus urbinai*	Penguin	Sacaco	3.5	20.9
BE	Periotic	*Kojia* sp.	Sperm whale	Sacaco	3.5	19.7
SAO 32-BF	Periotic	Delphinidae	Dolphin	Sacaco	3.5	18.2
SAO 82-BG	Periotic	Delphinidae	Dolphin	Sacaco	3.5	19.3
BH	Periotic	Delphinidae	Dolphin	Sacaco	3.5	18.6
SAO 13-BI	Humerus	*Thalassocnus carolomartini*	Aquatic sloth	Sacaco	3.5	21.2
SAO 201-BJ	Metatarse MTV	*Thalassocnus carolomartini*	Aquatic sloth	Sacaco	3.5	20.7
SAO 136-BL	Tooth bulk	Phocidae	Seal	Sacaco	3.5	19.7
BM	Humerus	Phocidae	Seal	Sacaco	3.5	20.4
SAO 11-BN	Periotic	Mysticete	Whale	Sacaco	3.5	20.3
SAO 11-BN	Periotic	Mysticete	Whale	Sacaco	3.5	19.4
BP	Periotic	Mysticete	Whale	Sacaco	3.5	20.1
SAS 1380w-A	Tibiotarsus	*Spheniscus urbinai*	Penguin	Sacaco Sud	5	20.4
SAS 1036-B	Tibiotarsus	*Spheniscus urbinai*	Penguin	Sacaco Sud	5	19.8
SAS 1380u-C	Femur	*Spheniscus urbinai*	Penguin	Sacaco Sud	5	20.5
SAS 305-D	Coracoid	*Spheniscus urbinai*	Penguin	Sacaco Sud	5	20.2
SAS 126-E	Tibiotarsus	*Spheniscus* sp.	Penguin	Sacaco Sud	5	20.3
SAS 501-F	Tooth enamel	*Piscophoca pacifica*	Seal	Sacaco Sud	5	18.7
SAS-G	Tooth enamel	*Piscophoca pacifica*	Seal	Sacaco Sud	5	18.9
SAS 1610-H	Tooth dentine	*Thalassocnus littoralis*	Semi-aquatic sloth	Sacaco Sud	5	21.3
SAS-I	Tooth dentine	*Thalassocnus littoralis*	Semi-aquatic sloth	Sacaco Sud	5	21.6
SAS-J	Tooth enamel	*Piscolithax longirostris*	Dolphin	Sacaco Sud	5	19.8
SAS-K	Tooth bulk	*Piscolithax longirostris*	Dolphin	Sacaco Sud	5	19.6
SAS-L	Tympanic	*Piscobalaena nana*	Whale	Sacaco Sud	5	19.9
SAS-M	Radius	*Piscobalaena nana*	Whale	Sacaco Sud	5	20.1
SAS-N	Tooth enamel	-	Sperm whale	Sacaco Sud	5	19.6
SAS-O	Tooth enamel	*Carcharodon carcharias*	Shark	Sacaco Sud	5	21.3
AR	Tooth enamel	*Cosmopolitodus* sp.	Shark	Sacaco Sud	5	21.6
AS	Tooth enamel	*Cosmopolitodus* sp.	Shark	Sacaco Sud	5	21.6
SAS-P	Tooth bulk	*Indet.*	Longirostrine crocodilian	Sacaco Sud	5	21.6
SAS-Q	Osteoderm	*Indet.*	Longirostrine crocodilian	Sacaco Sud	5	20.2
SAS 50-BQ	Rib	*Thalassocnus littoralis*	Semi-aquatic sloth	Sacaco Sud	5	21.4
SAS 53-BR	Rib	*Thalassocnus littoralis*	Semi-aquatic sloth	Sacaco Sud	5	21.7
AGL 145F-AE	Carpometacarpe	*Spheniscus urbinai*	Penguin	Aguada de Lomas	7–8	21.2
AGL PPI 145G-AY	Distal femur	*Spheniscus urbinai*	Penguin	Aguada de Lomas	7–8	20.4
AGL PPI 145C-AZ	Humerus	*Spheniscus urbinai*	Penguin	Aguada de Lomas	7–8	21.0
SMNK-AGL-AF	Tooth enamel	*Tursiops oligodon*	Dolphin	Aguada de Lomas	7–8	19.5
AT	Tooth enamel	*Cosmopolitodus hastalis*	Shark	Aguada de Lomas	7–8	21.8
AV	Tooth enamel	*Cosmopolitodus hastalis*	Shark	Aguada de Lomas	7–8	21.7
BS	Tooth enamel	Phocidae	Seal	Aguada de Lomas	7–8	18.9
BT	Tooth enamel	Phocidae	Seal	Aguada de Lomas	7–8	17.5
BU	Tooth enamel	Phocidae	Seal	Aguada de Lomas	7–8	18.9
BV	Periotic	–	Dolphin	Aguada de Lomas	7–8	18.1
BW	Periotic	–	Dolphin	Aguada de Lomas	7–8	18.8
BX	Tympanic	–	Whale	Aguada de Lomas	7–8	19.3
BY	Radius	*Piscolithax* sp.	Dolphin	Aguada de Lomas	7–8	19.0
AJ	Tooth enamel	*Cosmopolitodus hastalis*	Shark	El Jahuay	9–10	21.5
AK	Tooth enamel	*Cosmopolitodus hastalis*	Shark	El Jahuay	9–10	21.6
ELJ PPI 141B-BA	Prox. radius	*Spheniscus urbinai*	Penguin	El Jahuay	9–10	21.5
ELJ PPI 141C-BB	Carpometacarpe	*Spheniscus urbinai*	Penguin	El Jahuay	9–10	21.4
ELJ PPI 141D-BC	Dist. Femur	*Spheniscus urbinai*	Penguin	El Jahuay	9–10	20.8
ELJ PPI 142-BD	Tibiotarsus	*Spheniscus urbinai*	Penguin	El Jahuay	9–10	21.1
BZ	Tooth bulk	–	Dolphin	El Jahuay	9–10	20.4
CA	Periotic	–	Dolphin	El Jahuay	9–10	18.9
CB	Periotic	–	Dolphin	El Jahuay	9–10	18.6
CC	Mandible	–	Whale	El Jahuay	9–10	21.4
CD	Long bone	*Piscobalena* sp.	Whale	El Jahuay	9–10	20.6
PPI2-CE	Humerus	Phocidae	Seal	El Jahuay	9–10	20.3
PPI3-CF	Humerus	Phocidae	Seal	El Jahuay	9–10	20.5
CLB PPI-T	Osteoscute	–	Marine turtle	Cerro la Bruja	11–13	21.3
CLB PPI-U	Osteoscute	–	Marine turtle	Cerro la Bruja	11–13	20.7
CLB PPI-V	Tooth bulk	*Atocetus iquensis*	Dolphin	Cerro la Bruja	11–13	19.5
CLB PPI-W	Tympanic	*Atocetus iquensis*	Dolphin	Cerro la Bruja	11–13	18.6
CLB PPI-X	Tooth enamel	*Megaselachus megalodon*	Shark	Cerro la Bruja	11–13	20.9
AG	Tooth enamel	*Cosmopolitodus hastalis*	Shark	Cerro la Bruja	11–13	21.3
AH	Tooth enamel	*Cosmopolitodus hastalis*	Shark	Cerro la Bruja	11–13	21.2
AI	Tooth enamel	*Cosmopolitodus hastalis*	Shark	Cerro la Bruja	11–13	21.0
CLB PPI-Y	Tooth enamel	*Monachine n.* sp.	Seal	Cerro la Bruja	11–13	18.8
CLB PPI-Z	Tooth enamel	*Monachine n.* sp.	Seal	Cerro la Bruja	11–13	18.2
CLB PPI 151-AA	Femur	*Spheniscus muizoni*	Penguin	Cerro la Bruja	11–13	19.5
CLB PPI 147f-AB	Tibiotarsus	*Spheniscus muizoni*	Penguin	Cerro la Bruja	11–13	20.1
CLB PPI 147e-AC	Femur	*Spheniscus muizoni*	Penguin	Cerro la Bruja	11–13	19.5

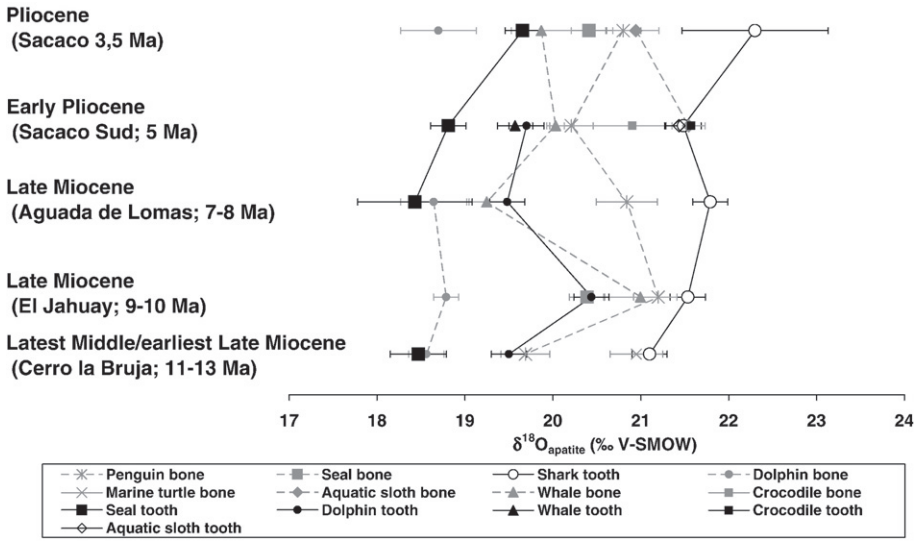

Fig. 2. Mean oxygen isotope compositions of teeth and bones from the various studied vertebrate taxa from Pisco, Peru. Fossil sites are ordered by their relative geological age.

Late Miocene that are lower than for the Late Miocene recorded in "El Jahuay" (time span = 9–10 Ma).

6. Discussion

6.1. Pristine oxygen isotope conservation of fossil apatite

Secondary precipitation of apatite and isotopic exchange during microbially-mediated reactions may scramble the primary isotopic signal (Blake et al., 1997; Zazzo et al., 2004). However, apatite crystals that make up tooth enamel are large and densely packed, and isotopic exchange under inorganic conditions has little effect on the oxygen isotope composition of phosphates even at geological time scales (Kolodny et al., 1983; Lécuyer et al., 1999). Although no method is available to demonstrate definitely whether diagenetic processes may have affected oxygen isotope compositions of bulk tooth or bone phosphate, several indicators of preservation of the pristine oxygen isotope compositions of phosphates are given by the present dataset.

Body temperature differences between ectotherms and endotherms as well as differences in ecology between coexisting animals result in different $\delta^{18}O$ values of apatite phosphate (e.g. Kohn, 1996; Fricke et al., 1998; Amiot et al., 2006). Diagenetic processes are expected to modify and homogenise $\delta^{18}O_p$ values of all vertebrate phosphatic remains during isotopic exchange between apatite and local groundwaters through processes of dissolution–recrystallization (see Lécuyer et al. 2003). Mio-Pliocene vertebrates from the Pisco Formation have $\delta^{18}O_p$ values ordered by their physiology (body temperature, metabolism rates) and ecology (diet, living environment) at any sampling locality. Indeed, sharks and aquatic reptiles (turtles and crocodilians) have the highest $\delta^{18}O_p$ values due to their body temperature which depends on that prevailing in the water mass where they live whereas marine mammals maintain a constant body temperature around 37 °C, having therefore lower $\delta^{18}O_p$ values. Penguins have higher $\delta^{18}O_p$ values than marine mammals most likely because of avian metabolism known to be somewhat higher than the mammal one. It is also noteworthy that oxygen isotope differences between cetacean bones and shark teeth are similar to those obtained from Miocene cetacean and shark remains from the Chesapeake Bay (Barrick et al., 1992). A slight difference pointed out by Barrick and colleagues between the $\delta^{18}O_p$ values of whales and porpoises is also observed in the present dataset with $\delta^{18}O_p$ values of whales that are more positive than dolphins. From these observations, primary physiological or ecological oxygen isotopic record of vertebrate phosphate is assumed to be preserved in marine vertebrate teeth and most likely in bones for which, however, care is required for further interpretations because bones have been shown to be potentially highly sensitive to diagenetic processes (see Kolodny et al. (1996) and references herein).

6.2. Meaning of the oxygen isotope composition of phosphate from Pisco vertebrates

6.2.1. Dolphins

Based on previous works (Yoshida and Miyazaki, 1991; Barrick et al., 1992, 1993; Lécuyer et al., 1996), $\delta^{18}O_p$ values of aquatic endotherms are expected to track water $\delta^{18}O_w$ values. Thus offsets in $\delta^{18}O_p$ values between seals, cetaceans and penguins should remain constant at any locality, but significant differences are observed. A first source of variations might be due to differences between bone and tooth isotopic records. Dolphin teeth have a $\delta^{18}O_p$ value systematically more positive (about 1.1 to 1.7‰) than bones (Fig. 2). As mammals, young dolphins breast-feed during the first 12 to 18 months of their life and have ingested mother milk that is ^{18}O-enriched compared to environmental water (Wright and Schwarcz, 1998). Dolphins have only one generation of teeth that grow a little bit each year until they reach their adult size. It is thus expected that the oxygen isotope compositions of teeth mineralized during this period could be influenced by the mother milk unlike bones which are constantly remodeled during the animal's life using newly ingested oxygen. However, only slight differences of about 0.1‰ or 0.2‰ between $\delta^{18}O_p$ values of teeth and bones of present-day dolphins (*Stenella* and *Delphinus*) were observed by Barrick et al. (1992), indicating that a 'milk signature' cannot explain the observed isotopic offsets. Another possible source of variations proposed by Barrick et al. (1992) is local heterothermy that dolphins may experience between their body core and their thin rostral region. In cold waters, dolphin rostrum and teeth may have a lower temperature than the main body thus leading to higher $\delta^{18}O_p$ values. Keeping in mind that bone diagenesis can be responsible for these differences, further investigations should be performed on modern dolphins to allow a better understanding of the origin of these offsets.

6.2.2. Seals vs. dolphins

It is noteworthy that in the sites of Cerro la Bruja, Aguada de Lomas and Sacaco Sud, seal and dolphin teeth have a constant $\delta^{18}O_p$ value offset of 1.0 ± 0.1‰ (Fig. 2). This suggests that both of them have most

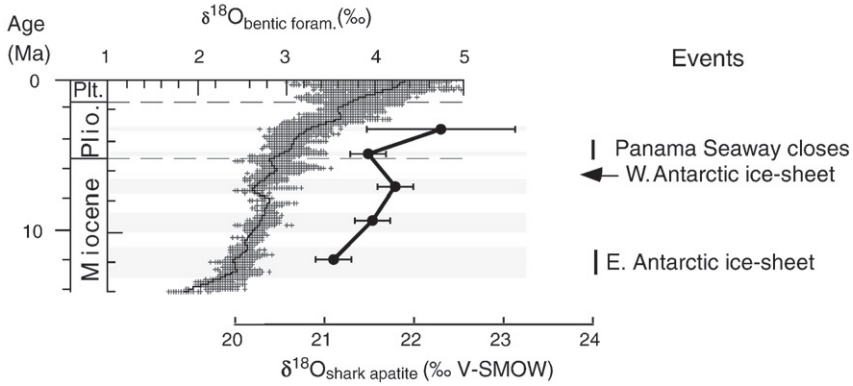

Fig. 3. Comparison between the $\delta^{18}O_p$ curve of sharks (bold black) and the synthetic curve of $\delta^{18}O_c$ values of benthic foraminifera (Zachos et al., 2001). Shaded horizontal areas represent the uncertainties associated with the geological ages of the Pisco localities.

likely recorded the same environmental signal, the offset being caused by differences in physiology. Indeed, contrary to dolphins, seals have a daily sun-basking activity on land, which allow them spending less metabolic energy for keeping their body at 37 °C. From a study carried out on modern cetaceans and seals, it has been observed that the metabolic rates of marine mammals resting on the water surface are higher than those of mammals resting in air (Williams et al., 2001). If seals of the Pisco Formation shared a similar basking behaviour, this may contribute to explain their lower $\delta^{18}O_p$ values.

6.2.3. Whales vs. dolphins

Large cetacean (whales and sperm whales) from Pisco localities have $\delta^{18}O_p$ values higher than dolphins and porpoises. Such differences have already been observed for Miocene cetaceans (Barrick et al., 1992) but not for modern species (Yoshida and Miyazaki, 1991). Several hypotheses have been proposed to account for these isotopic offsets such as differences in body temperatures between fossil whales and porpoises or differences in $\delta^{18}O$ values of body fluids (Barrick et al., 1992). The systematic isotopic offset between whales and dolphins points out a major problem concerning the applicability of the oxygen isotope fractionation equation between any cetacean phosphate and water (Yoshida and Miyazaki, 1991) to fossil cetaceans. Yoshida and Miyazaki (1991) did not find any relationship between body size and oxygen isotope fractionation, a goal difficult to reach when taking into account the uncertainty associated with the $\delta^{18}O_{sw}$ value of seawater where cetaceans live. Moreover, in the computed equation of Yoshida and Miyazaki, whales are only represented by one species *Balaenoptera acutorostrata* with four $\delta^{18}O_p$ values ranging from 17.5‰ to 18.4‰, all having the same $\delta^{18}O_w$ value. If recalculated without using whale values, the new regression does not significantly differ from the original one ($\delta^{18}O_p = 0.763\ \delta^{18}O_w + 17.7$ instead of $\delta^{18}O_p = 0.773\ \delta^{18}O_w + 17.8$). From these considerations, the direct applicability of the fractionation equation of Yoshida and Miyazaki (1991) seems to be restricted to dolphins. For further use of the $\delta^{18}O_p$ value of cetaceans to estimate past seawaters' $\delta^{18}O_w$ values, separate calibrations are needed for whales, and more modern dolphin teeth have to be measured for comparison with bone values.

6.2.4. Aquatic sloths

A few $\delta^{18}O_p$ values of bones and teeth from two species of the sloths *Thalassocnus* were obtained. These vertebrates were unusual xenarthran mammals having phylogenetic affinities with other Nothrothere ground sloths (Muizon and Mc Donald, 1995; Mc Donald and Muizon, 2002; Muizon et al., 2004b). The most striking feature is their progressive anatomical adaptations to semi-aquatic or aquatic habits (Muizon and Mc Donald, 1995) and to feed on marine plants (Muizon et al., 2004a). Interestingly, these sloths have high $\delta^{18}O_p$ values about 1‰ to 3‰ more positive than other coexisting aquatic mammals. Despite their marine foraging environments, these high values can suggest that marine sloth kept some physiological characteristics of land mammals with ^{18}O-enriched body fluids due to elevated metabolic activity, evaporation and sweat. However, given that no terrestrial vertebrates have been discovered so far in these localities, it is also likely that differences in $\delta^{18}O_p$ values between these sloths and other marine mammals reflect differences in physiology. Indeed, at least two species of modern ground sloth (*Choelophus didactylus* and *Choelophus hoffmanni*) have incomplete homeothermy with body temperatures lower than 34.4 °C for *C. didactylus* (Bush and Gilroy, 1979) and varying within a day between 33.4 °C and 36.2 °C for *C. hoffmanni* (Goffart, 1971). According to the phosphate-water temperature scale (Longinelli and Nuti, 1973), a 4 °C difference in temperature (between a sloth at 33 °C and another mammal at 37 °C) should result in a 1‰ offset in the $\delta^{18}O_p$ value. If Pisco marine sloths also possessed low and fluctuating body temperatures, then the differences in $\delta^{18}O_p$ values observed between *Thalassocnus* and other marine mammals may at least partly reflect differences in body temperatures.

6.2.5. Sharks

Stable isotope and trace element contents of shark teeth are commonly used for palaeoenvironmental studies (e. g. Kolodny and Raab, 1988; Lécuyer et al., 1993, 1996; Pucéat et al., 2003; Scher and Martin, 2006). However, significant variations in $\delta^{18}O_p$ values have been observed between various species of present-day sharks living in the same region, most likely as a consequence of different living habitats, and also between teeth from the same individual (Vennemann et al., 2001). Most of the shark teeth available for this study were sampled from species belonging to the great white shark lineage (*Carcharodon carcharias*, *Megaselachus megalodon* (Cappetta, 2006) and *Cosmopolitodus hastalis*). These sharks are ubiquist large predators that can forage over long distances and large ranges of water depths, i.e. their teeth $\delta^{18}O_p$ values may reflect marine environments well distinct from those where Pisco vertebrates lived. Mean $\delta^{18}O_p$ values of shark teeth from the five Pisco localities are at variance with the global trend (Fig. 3) provided by the temporal synthetic curve of benthic foraminifera $\delta^{18}O$ values which are considered to reflect global temperatures and continental ice volume (Zachos et al., 2001).

6.2.6. Crocodilians and turtles

Reptile remains are very scarce in the Pisco formation, and only two scute fragments of marine turtles from the locality of Cerro la Bruja, one tooth and one osteoderm fragment of a longirostrine crocodilian from the locality of Sacaco Sud were available for oxygen isotope analysis. Although being ectotherm animals, thus having fluctuating body temperatures as a function of environmental ones, they synthesise bone or tooth phosphate under relatively narrow temperature ranges (Barrick et al., 1999; Amiot et al., 2007). Using

empirical linear fractionation equations established between their phosphate and environmental waters, a mean living water $\delta^{18}O_w$ value of −1.1 ± 0.3‰ is inferred from the $\delta^{18}O_p$ values of marine turtles from Cerro la Bruja, and −1.4 ± 1‰ from the crocodilian tooth from Sacaco Sud. Whereas the value of −1.1‰ for Middle Miocene seawaters at Cerro la Bruja recorded by marine turtles is expected considering the absence of polar ice-caps, the origin (brackish or pure marine) of the water value estimated from the crocodilian tooth is questionable. Indeed, very little is known about Pisco crocodilians. One crocodilian species *Piscogavialis jugaliperforatus* (Kraus, 1998) recovered from the locality of Montemar (Pisco Formation; ca. 6 Ma to 4.5 Ma) has been described and attributed to the family Gavialidae. The living environment of these gharials is still unclear. Their occurrence in marine deposits of Peru, Chile and Venezuela (Kraus, 1998; Sánchez-Villagra et al., 2001; Brochu and Rincon, 2004; Walsh and Suárez, 2005) suggests that they were marine animals but it cannot be excluded that they lived in brackish waters or estuarine environments.

6.2.7. Penguins

Bone remains of Miocene and Pliocene penguins *Spheniscus urbinai* (Stucchi, 2002) and *Spheniscus muizoni* (Göhlich, 2007) have higher $\delta^{18}O_p$ values than bones or teeth of coexisting marine endotherms (cetaceans and seals) probably reflecting differences in metabolic activities. Indeed, birds and especially marine birds tend to have activity metabolic rates greater than mammals, leading to higher $\delta^{18}O_p$ values (see Kohn, 1996; Nagy et al., 1999 and references therein). Interestingly, penguin $\delta^{18}O_p$ values roughly vary the same way than shark teeth values. Although diets and drinking behaviours of these two penguin species are not known, most of the oxygen constituting their phosphatic tissues likely comes from seawater, directly from drinking water, or indirectly from eaten marine ectothermic organisms (krill, fish or cephalopods), themselves reflecting seawater conditions ($\delta^{18}O_{sw}$ value and temperature variations).

6.3. Reconstruction of seawater temperatures and $\delta^{18}O_{sw}$ values

Given the significant differences in $\delta^{18}O_p$ values observed between whales and dolphins and between dolphin teeth and bones, it is not possible to calculate ocean $\delta^{18}O_w$ values by simply applying the phosphate-water fractionation equation established for cetaceans (Yoshida and Miyazaki, 1991) to any Pisco whale or dolphin remains. Only relative variations in sea $\delta^{18}O_w$ values through time may be calculated using dolphin values from the Pisco Formation, considering that the above isotopic calibration almost exclusively relies on dolphin bone $\delta^{18}O_p$ values. For this purpose, $\delta^{18}O_p$ values of dolphin teeth (Fig. 2) have been selected because tooth enamel is the most resistant biomineral in terms of isotopic preservation. Given the near constant offset of 1.0 ± 0.1‰ measured between seals and dolphins, suggesting that they have both recorded similar variations in sea $\delta^{18}O_w$ values, a hypothetical dolphin tooth $\delta^{18}O_p$ value of 20.7‰ has been estimated using seal tooth $\delta^{18}O_p$ value from the Sacaco site (as no dolphin tooth was available). The difference in oxygen isotope compositions calculated between two sites is multiplied by the slope (0.773) of the fractionation equation of Yoshida and Miyazaki (1991) (Table 2). By using −1.1 ± 0.3‰ (calculated from the $\delta^{18}O_p$ values of marine turtles) as the seawater $\delta^{18}O_w$ value at Cerro la Bruja, then absolute values are tentatively estimated for each site (Table 2). These computed isotopic values as well as shark tooth $\delta^{18}O_p$ values of the same sites are inserted into the oxygen isotope fractionation equation established between fish phosphate and water (Kolodny et al., 1983) to retrieve Sea Surface Temperature (SST) (Table 2; Fig. 4). The overall range is about 1‰ in ocean $\delta^{18}O_w$ values and about 5 °C in SST.

Table 2
Variations in seawater $\delta^{18}O_w$ values and marine temperatures calculated using $\delta^{18}O_p$ values of dolphins, seals, and shark tooth enamels and marine turtle scutes

	$\delta^{18}O_w$ (‰ V-SMOW)	$D\delta^{18}O_w$ (‰ V-SMOW)	SD	T °C	SD
Sacaco – Sacaco Sud	+0.7	−0.2	0.3	14.8	1.3
Sacaco Sud – Aguada de Lomas	+0.2	−0.9	0.3	15.2	1.3
Aguada de Lomas – El Jahuay	−0.7	−1.1	0.3	13.0	1.3
El Jahuay – Cerro la Bruja	+0.7	−0.4	0.3	17.2	1.3
Cerro la Bruja		−1.1[a]	0.3[a]	16.1	1.3

Variations in $\delta^{18}O_w$ values were estimated using the slope of the Yoshida and Miyazaki (1991) equation, and palaeotemperatures were calculated using the equation of Kolodny et al. (1983).
[a] Value calculated using $\delta^{18}O_p$ values of marine turtles.

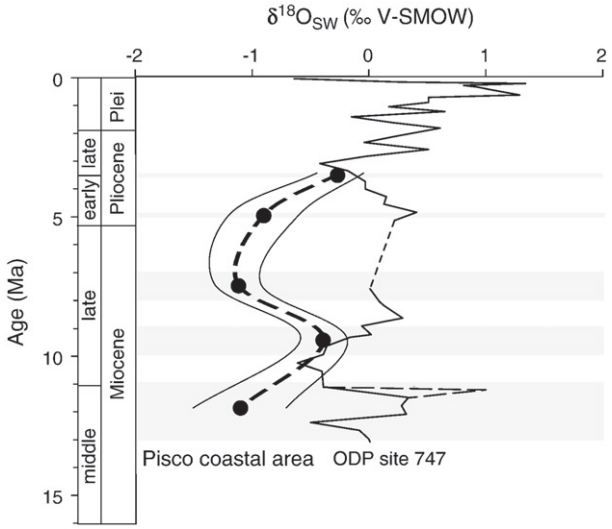

Fig. 4. Comparison between two seawater $\delta^{18}O_w$ curves obtained from the $\delta^{18}O_p$ values (bold black) of dolphins, seals and marine turtles (this study) and by using paired Mg/Ca and $\delta^{18}O_c$ values (black) of benthic foraminifera (Billups and Schrag, 2002). The $\delta^{18}O_{sw}$ value of −1.1‰ was estimated for the oldest site (Cerro la Bruja) using $\delta^{18}O_p$ values of marine turtles. Shaded areas represent the uncertainties associated with the geological ages of the Pisco localities.

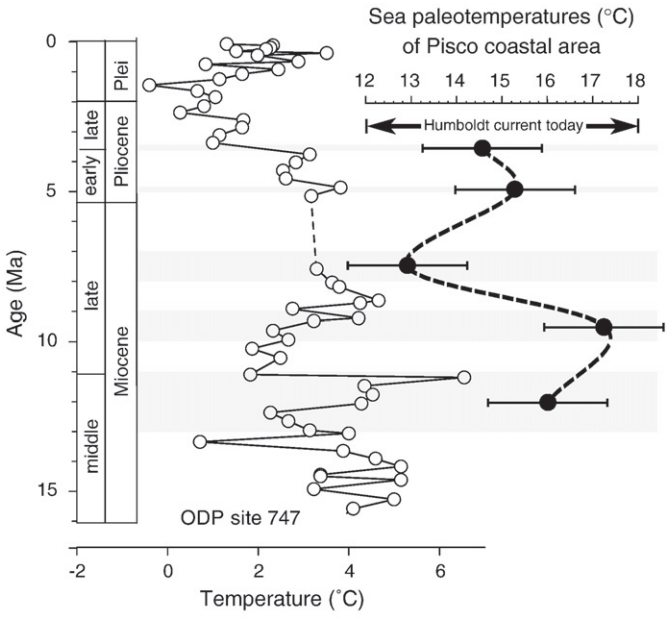

Fig. 5. Comparison between two seawater temperature curves, the first one obtained from the $\delta^{18}O_p$ values (bold black) of dolphins, seals, turtles and sharks (this study), and the second one by using paired Mg/Ca and $\delta^{18}O_c$ values (black) of benthic foraminifera (Billups and Schrag, 2002). Shaded areas represent the uncertainties associated with the geological ages of the Pisco localities.

Marine palaeotemperatures estimated from shark tooth $\delta^{18}O_p$ values ranged from 13.0 ± 1.3 °C to 17.2 ± 1.3 °C (Table 2; Fig. 5). These temperatures match those observed today off the coasts of Peru. The Humboldt Current brings deep, cold (between 12 °C and 18 °C) and nutrient-rich Antarctic waters to the surface. This current originates from the Antarctic Circumpolar Current (ACC) and moves northwards along the Peruvian coasts. According to a Late Eocene age for the complete establishment of the circum-Antarctic pathway allowed by the opening of the Drake Passage and Tasmanian Gateway (see Scher and Martin, 2006), the Humboldt Current might have been already active during the Miocene, a hypothesis supported by the relatively low palaeotemperatures estimated from shark teeth $\delta^{18}O_p$ values.

The $\delta^{18}O_{sw}$ curve obtained from Pisco vertebrates is compared to the one calculated on the basis of Mg/Ca and $\delta^{18}O_c$ values of benthic foraminifera recovered from the Ocean Drilling Program (ODP) Leg 120 Site 747 (Billups and Schrag, 2002). This Core was drilled in the Kerguelen Plateau in the Indian Ocean sector of the Southern Ocean at a water depth of 1695 m. Combined measurements of Mg/Ca and $\delta^{18}O_c$ of benthic foraminifera allow the calculation of both marine $\delta^{18}O_{sw}$ values and palaeotemperatures. The estimated evolution of $\delta^{18}O_{sw}$ values in the Pisco area roughly follows the isotopic record at site 747 except between 5 Ma and 3.5 Ma when the $\delta^{18}O_{sw}$ value of seawater off Peru increased, a pattern in contradiction with the global isotopic decreasing trend (Fig. 4). This period is marked by the closure of the Panama isthmus as well as by the main stage of aridification of the Atacama Desert (Hartley and Chong, 2002). Consequently, high evaporation rates of sea surface waters may have been recorded by the relative high $\delta^{18}O_p$ values of Pisco aquatic mammal phosphatic remains.

A counterintuitive relationship is observed between estimated temperatures and $\delta^{18}O_{sw}$ values of marine waters, as warmer temperatures correspond to episodes of glaciations and cooler temperatures to ice-cap decay. This correlation has also been observed in the Miocene (Barrick et al., 1992, 1993) and Pleistocene (Ruddiman and Mc Intyre, 1979; Ruddiman and Mc Intyre, 1984) sediments of the Atlantic Ocean. Warmer temperatures may have increased seawater evaporation at low latitudes and created a poleward transport of moisture as well as extensive precipitations and storage of ice at the poles, the so called “snow gun” effect (Johnson and Mc Clure, 1976; Sergin, 1980; Ruddiman and Mc Intyre, 1984).

Therefore, estimated variations in palaeotemperature and $\delta^{18}O_{sw}$ values of seawater for the Miocene and Pliocene Pacific coastal sea of Peru suggest that both local and global environmental factors have been recorded in the $\delta^{18}O_p$ values of coexisting aquatic vertebrates recovered from the Pisco Formation.

7. Conclusion

The study of the oxygen isotope compositions of marine vertebrates from Miocene and Pliocene localities of the Pisco formation leads to the following conclusions:

- Coexisting marine mammals, reptiles, birds and fish have different $\delta^{18}O_p$ values as a result of different ecologies and physiologies. Fish and reptiles tend to have higher $\delta^{18}O_p$ values than mammals and birds due to their lower body temperature, and birds have higher $\delta^{18}O_p$ values than marine mammals due to their higher metabolic rates. Body mass may also lead to differences in oxygen isotope compositions between coexisting mammals. In this study, seals tend to have lower $\delta^{18}O_p$ values than dolphins, themselves lower than those of whales.
- Significant oxygen isotope offsets are observed between dolphin teeth and bones and between dolphin and whale bones, indicating that the phosphate-water fractionation equation established for living cetaceans is not directly applicable to their fossil counterparts in order to retrieve the oxygen isotope composition of seawater.
- Relatively low marine temperatures (between 13.0 ± 1.3 °C and 17.2 ± 1.3 °C) were inferred from shark teeth $\delta^{18}O_p$ values which are in agreement with the existence of a cold, nutrient-rich Humboldt Current already active during the Miocene and Pliocene.
- Variations in $\delta^{18}O_w$ values and marine palaeotemperatures recorded by Pisco vertebrates are influenced by both global and local climatic and oceanographic factors.
- Warmer temperatures recorded in both Calvert (Barrick et al., 1992, 1993) and Pisco formations correspond to periods of glacial episodes in polar areas. This relationship suggests that a global rising of marine temperatures at low and mid latitudes may increase moisture transport toward the poles, thus contributing to the development of ice-caps during the Miocene.

Acknowledgements

The authors would like to thank E. Frey from the Staatliches Museum für Naturkunde Karlsruhe, Germany (SMNK) for providing samples of the Miocene dolphin *Tursiops oligodon*. Thomas Tütken and an anonymous reviewer provided critical reviews that greatly helped us to improve the manuscript. U. G. was supported by a fellowship in the Feodor-Lynen-Program by the Alexander von Humboldt Foundation.

References

Amiot, R., et al., 2006. Oxygen isotopes from biogenic apatites suggest widespread endothermy in Cretaceous dinosaurs. Earth and Planetary Science Letters 246 (1–2), 41–54.
Amiot, R., et al., 2007. Oxygen isotope fractionation between crocodilian phosphate and water. Palaeogeography, Palaeoclimatology, Palaeoecology 243, 412–420.
Barrick, R.E., Fischer, A.G., Bohaska, D.J., 1993. Paleotemperatures versus sea-level — oxygen isotope signal from fish bone phosphate of the Miocene Calvert Cliffs, Maryland. Paleoceanography 8 (6), 845–858.
Barrick, R.E., Fischer, A.G., Kolodny, Y., Luz, B., Bohaska, D., 1992. Cetacean bone oxygen isotopes as proxies for Miocene ocean composition and glaciation. Palaios 7 (5), 521–531.
Barrick, R.E., Fischer, A.G., Showers, W.J., 1999. Oxygen isotopes from turtle bone: application for terrestrial paleoclimates? Palaios 14, 186–191.
Billups, K., Schrag, D.P., 2002. Paleotemperatures and ice volume of the past 27 Myr revisited with paired Mg/Ca and $^{18}O/^{16}O$ measurements on benthic foraminifera. Paleoceanography 17 (1), 3–1–3-11.
Blake, R.E., O' Neil, J.R., Garcia, G.A., 1997. Oxygen isotope systematics of biologically mediated reactions of phosphate; I, Microbial degradation of organophosphorus compounds. Geochimica et Cosmochimica Acta 61 (20), 4411–4422.
Brand, L.R., Urbina, M., Carvajal, C.R., DeVries, T.J., 2003. Stratigraphy of the Miocene/Pliocene Pisco Formation in the Pisco Basin, Peru. Geological Society of America, 2003 annual meeting. Geological Society of America, Seattle, p. 160.
Brochu, C.A., Rincon, A.D., 2004. A gavialoid crocodylian from the Lower Miocene of Venezuela. In: Sánchez-Villagra, M.R., Clack, J.A. (Eds.), Fossils of the Miocene Castillo Formation, Venezuela: Contributions on Neotropical Palaeontology. Special Papers in Palaeontology, pp. 61–80.
Bush, M., Gilroy, B.A., 1979. A bleeding technique for nonpalpable vessels in anesthetized two-toed sloths (*Choloepus didactylus*)-plus hematological data. Journal of Zoo Animal Medicine 10, 26–27.
Cappetta, H., 2006. Elasmobranchii post-Triadici (index specierum et generum). Fossilium Catalogus, vol. 142. Backhuys Publish, Leiden. 472 pp.
Crowson, R.A., Showers, W.J., Wright, E.K., Hoering, T.C., 1991. A method for preparation of phosphate samples for oxygen isotope analysis. Analytical Chemistry 63, 2397–2400.
Fordyce, R.E., 1994. The evolutionary history of whales and dolphins. Annual Review of Earth and Planetary Sciences 22, 419–455.
Fricke, H.C., Clyde, W.C., O'Neil, J.R., Gingerich, P.D., 1998. Evidence for rapid climate change in North America during the latest Paleocene thermal maximum; oxygen isotope compositions of biogenic phosphate from the Bighorn Basin (Wyoming). Earth and Planetary Science Letters 160 (1–2), 193–208.
Goffart, M., 1971. Function and Form in the Sloth. Pergammont Press Ltd, Oxford. 225pp.
Göhlich, U.B., 2007. The oldest fossil record of the extant penguin genus *Spheniscus*—a new species from the Miocene of Peru. Acta Palaeontologica Polonica 52 (2), 285–298.
Haq, B.U., Hardenbol, J., Vail, P.R., 1987. Chronology of fluctuating sea levels since the Triassic. Science 235 (4793), 1156–1167.
Hartley, A.J., Chong, G., 2002. Late Pliocene age for the Atacama Desert: implications for the desertification of Western America. Geology 30 (1), 43–46.
Johnson, R.G., Mc Clure, B.T., 1976. A model for Northern Hemisphere continental ice sheet variation. Quaternary Research 6, 325–353.
Kohn, M.J., 1996. Predicting animal $\delta^{18}O$: accounting for diet and physiological adaptation. Geochimica et Cosmochimica Acta 60 (23), 4811–4829.
Kolodny, Y., Raab, M., 1988. Oxygen isotopes in phosphatic fish remains from Israel; paleothermometry of tropical Cretaceous and Tertiary shelf waters. Palaeogeography, Palaeoclimatology, Palaeoecology 64 (1–2), 59–67.

Kolodny, Y., Luz, B., Navon, O., 1983. Oxygen isotope variations in phosphate of biogenic apatites; I, Fish bone apatite; rechecking the rules of the game. Earth and Planetary Science Letters 64 (3), 398–404.
Kolodny, Y., Luz, B., Sander, M., Clemens, W.A., 1996. Dinosaur bones: fossils or pseudomorphs? The pitfalls of physiology reconstruction from apatitic fossils. Palaeogeography, Palaeoclimatology, Palaeoecology 126, 161–171.
Kraus, R., 1998. The cranium of *Piscogavialis jugaliperforatus* n. gen., n. sp. (Gavialidae, Crocodylia) from the Miocene of Peru. Paläontologische Zeitschrift 72 (3–4), 389–406.
Lecuyer, C., et al., 1998. $\delta^{18}O$ and REE contents of phosphatic brachiopods; a comparison between modern and lower Paleozoic populations. Geochimica et Cosmochimica Acta 62 (14), 2429–2436.
Lécuyer, C., Grandjean, P., O' Neil, J.R., Cappetta, H., Martineau, F., 1993. Thermal excursions in the ocean at Cretaceous–Tertiary boundary (northern Morocco): $\delta^{18}O$ record of phosphatic fish debris. Palaeogeography, Palaeoclimatology, Palaeoecology 105, 235–243.
Lécuyer, C., Grandjean, P., Paris, F., Robardet, M., Robineau, D., 1996. Deciphering "temperature" and "salinity" from biogenic phosphates: the $\delta^{18}O$ of coexisting fishes and mammals of the Middle Miocene sea of western France. Palaeogeography, Palaeoclimatology, Palaeoecology 126 (1–2), 61–74.
Lécuyer, C., Grandjean, P., Sheppard, S.M.F., 1999. Oxygen isotope exchange between dissolved phosphate and water at temperatures <135 °C: inorganic versus biological fractionations. Geochimica et Cosmochimica Acta 63 (6), 855–862.
Lécuyer, C., et al., 2003. Stable isotope composition and rare earth element content of vertebrate remains from the Late Cretaceous of northern Spain (Lano); did the environmental record survive? Palaeogeography, Palaeoclimatology, Palaeoecology 193 (3–4), 457–471.
Longinelli, A., Nuti, S., 1973. Revised phosphate-water isotopic temperature scale. Earth and Planetary Science Letters 19 (3), 373–376.
Mc Donald, G., Muizon, C.d., 2002. The cranial anatomy of *Thalassocnus* (Xenarthra, Mammalia), a derived Nothrothere from the Neogene of the Pisco Formation (Peru). Journal of Vertebrate Paleontology 22 (2), 349–365.
Miller, K.G., Wright, J.D., Fairbanks, R.G., 1991. Unlocking the ice house: Oligocene–Miocene oxygen isotopes, eustasy, and margin erosion. Journal of Geophysical Research 96 (C2), 6829–6848.
Muizon, C.d., 1988. Les vertébrés fossiles de la formation Pisco (Pérou). III - Les odontocètes (Cetacea, Mammalia) du Miocène. Travaux de l'Institut Français d'Études Andines 42 Paris, 244 pp.
Muizon, C.d., Bellon, H., 1981. L'âge mio-pliocène de la Formation Pisco (Pérou). Comptes rendus hebdomadaires des séances de l'Académie des Sciences. Paris, série D 290, 1063–1066.
Muizon, C.d., DeVries, T.J., 1985. Geology and paleontology of late Cenozoic marine deposits in the Sacaco area (Peru). Geologische Rundschau 74 (3), 547–563.
Muizon, C.d., Bellon, H., 1986. Nouvelles données sur l'âge de la Formation Pisco (Pérou). Comptes Rendus hebdomadaires des séances de L'Académie des Sciences. Paris, série II 303 (5), 1401–1404.
Muizon, C.d., Mc Donald, G., 1995. An aquatic sloth from the Pliocene of Peru. Nature 375, 224–227.
Muizon, C.d., Mc Donald, G., Salas, R., Urbina, M., 2003. A new early species of the aquatic sloth *Thalassocnus* (Mammalia, Xenarthra) from the Late Miocene of Peru. Journal of Vertebrate Paleontology 23 (4), 886–894.
Muizon, C.d., Mc Donald, G., Salas, R., Urbina, M., 2004a. The evolution of feeding adaptation of the aquatic sloth *Thalassocnus*. Journal of Vertebrate Paleontology 24 (2), 398–410.
Muizon, C.d., Mc Donald, G., Salas, R., Urbina, M., 2004b. The youngest species of the aquatic sloth *Thalassocnus* and a reassessment of the relationships of the Nothrothere sloths (Mammalia, Xenarthra). Journal of Vertebrate Paleontology 24 (2), 387–397.
Nagy, K.A., Girard, I.A., Brown, T.K., 1999. Energetics of free-ranging mammals, reptiles, and birds. Annual Review of Nutrition 19, 247–277.
O'Neil, J.R., Roe, L.J., Reinhard, E., Blake, R.E., 1994. A rapid and precise method of oxygen isotope analysis of biogenic phosphate. Israel Journal of Earth-Sciences 43 (3–4), 203–212.
Pucéat, E., et al., 2003. Thermal evolution of Cretaceous Tethyan marine waters inferred from oxygen isotope composition of fish tooth enamels. Paleoceanography 18 (2), 7–12.
Ruddiman, W.F., Mc Intyre, A., 1979. Warmth of the subpolar North Atlantic Ocean during northern hemisphere ice-sheet growth. Science 204, 173–175.
Ruddiman, W.F., Mc Intyre, A., 1984. Ice-age thermal response and climatic role of the surface Atlantic Ocean, 40°N to 63°N. Geological Society of America Bulletin 95, 381–396.
Sánchez-Villagra, M.R., Lozsán, R., Moody, J.M., Uhen, M.D., 2001. New discoveries of vertebrates from a near-shore marine fauna from the Early Miocene of northwestern Venezuela. Paläontologische Zeitschrift 75, 227–231.
Scher, H.D., Martin, E.E., 2006. Timing and climatic consequences of the opening of drake passage. Science 312, 428–430.
Sergin, V.Y., 1980. Origin and mechanism of large-scale climatic oscillations. Science 209, 1477–1482.
Stucchi, M., 2002. Una nueva especie de Spheniscus (Aves: Spheniscidae) de la Formación Pisco, Perú. Boletín de la Sociedad Geológica del Perú 94, 17–24.
Vennemann, T.W., Hegner, E., Cliff, G., Benz, G.W., 2001. Isotopic composition of recent shark teeth as a proxy for environmental conditions. Geochimica et Cosmochimica Acta 65 (10), 1583–1599.
Walsh, S.A., Suárez, M., 2005. First post-Mesozoic record of Crocodyliformes from Chile. Acta Palaeontologica Polonica 50 (3), 595–600.
Williams, T.M., Haun, J., Davis, R.W., Fuiman, L.A., Kohin, S., 2001. A killer appetite: metabolic consequences of carnivory in marine mammals. Comparative Biochemistry and Physiology; Part A 129, 785–796.
Wright, L.E., Schwarcz, H.P., 1998. Stable carbon and oxygen isotopes in human tooth enamel: identifying breastfeeding and weaning in prehistory. American Journal of Physical Anthropology 106, 1–18.
Yoshida, N. and Miyazaki, N., 1991. Oxygen isotope correlation of cetacean bone phosphate with environmental water.Journal of Geophysical Research. 96(C1): 815–820.
Zachos, J., Pagani, M., Sloan, L., Thomas, E., Billups, K., 2001. Trends, rhythms, and aberrations in global climate 65 Ma to Present. Science 292, 686–693.
Zazzo, A., Lécuyer, C., Mariotti, A., 2004. Experimentally-controlled carbon and oxygen isotope exchange between bioapatites and water under inorganic and microbially-mediated conditions. Geochimica et Cosmochimica Acta 68 (1), 1–12.

« L'homme de l'avenir est celui qui aura la mémoire la plus longue »

Friedrich Nietzsche

CHAPITRE 3 : Utilisation des isotopes pour comprendre certains mécanismes physiologiques actuels et fossiles

Au-delà des études paléoenvironnementales, les isotopes stables ont été utilisés dans ce travail comme traceurs de certaines réactions métaboliques sur du matériel fossile, comme dans les publications 3.1 et 3.2, mais également sur du matériel actuel, comme dans les publications 3.3, 3.4 et 3.5. Les isotopes stables ont en effet cette propriété unique de permettre de retracer l'origine de la molécule à laquelle ils appartiennent et donc de ses conditions de formation [1]. Pour du matériel fossile, les isotopes du carbone et de l'oxygène sont bien évidemment des outils précieux et uniques pour essayer de retracer la physiologie d'organismes vivants qui se sont éteints il y a des millions d'années et dont nous n'avons pas toujours d'organismes actuels équivalents [2]. De la même manière, pour des organismes actuels, les variations des rapports isotopiques peuvent être utilisés afin de tracer la physiologie ou bien le mode de vie de certains êtres vivants, soit en mesurant les variations isotopiques naturelles, soit également en utilisant des molécules marquées en un des isotopes stables afin de suivre ce marquage au cours des différentes réactions physico-chimiques qui constituent la physiologie des organismes vivants étudiés [3,4,5].

En ce qui concerne le matériel fossile, tout d'abord, dans la publication 3.1 nous avons analysé les $\delta^{18}O_p$ sur des dents d'humains actuels prélevées sur 12 sites de latitudes variant de 4°N à 72°N (voir figure 3.1). En parallèle nous avons analysé les $\delta^{18}O_w$ sur les eaux de boissons des régions considérées.

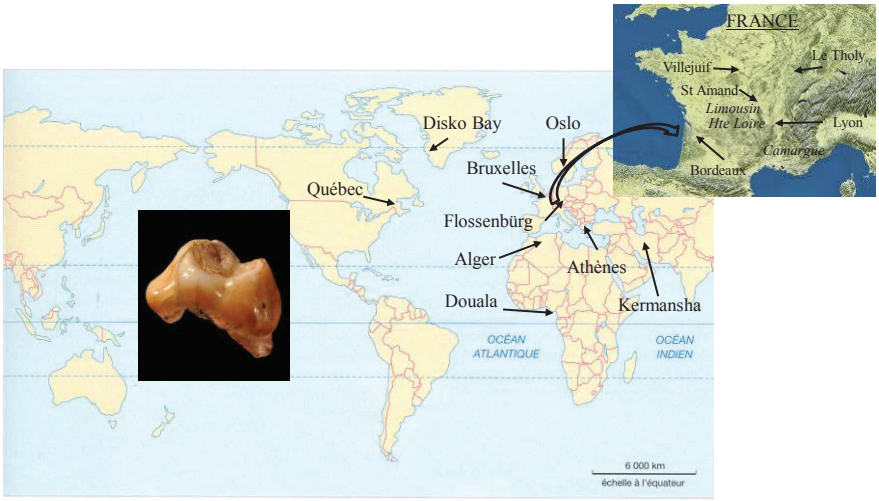

Figure 3.1 : Répartition des sites de prélèvements des échantillons de dents analysés.

En plus de ces analyses, nous nous sommes intéressés aux analyses $\delta^{18}O$ d'aliments crus et bouillis afin d'en déduire l'impact de la consommation d'aliments solides sur la composition isotopique de l'oxygène de l'eau totale ingérée c'est-à-dire l'eau de boisson cumulée avec l'eau des aliments. Ces résultats, associés à d'autres résultats antérieurs nous permettent d'établir une relation linéaire entre $\delta^{18}O_w$ et $\delta^{18}O_p$:

$$\delta^{18}O_w = 1{,}54(\pm 0{,}09) \times \delta^{18}O_p - 33{,}72\ (\pm 1{,}51)$$

Une des différences fondamentales de l'homme par rapport aux autres êtres vivants est qu'il lui arrive de cuisiner ses aliments. Or il arrive souvent que l'influence de cette cuisson alimentaire soit négligée lors de l'interprétation des données isotopiques. Or, une conséquence intéressante de cette étude est que, d'après nos résultats, le $\delta^{18}O$ des eaux ingérées par les humains actuels est enrichi de +1,05 à 1,2 ‰ par rapport aux valeurs des eaux de boissons de

la région considérée. De plus, si l'on considère que le régime alimentaire de nos lointains ancêtres était vraisemblablement plutôt à dominante carnée [6-9] et pauvre en céréales, alors dans ce cas-là la différence pourrait même être légèrement supérieure et donc l'équation proposée pourrait légèrement surestimer les $\delta^{18}O_w$ dans ce cas.

Sur du matériel beaucoup plus ancien cette fois, nous avons utilisé là aussi les analyses $^{18}O/^{16}O$ sur des phosphates extraits de l'émail dentaire ou de l'os fossilisé pour étudier le mode de régulation de la température corporelle de reptiles marins du Mésozoïque (publication 3.2). Cette démarche avait déjà été utilisée par Amiot et al. [2] en ce qui concerne les dinosaures du Crétacé. Retracer la thermo physiologie de ces animaux aujourd'hui disparus nous aide à mieux comprendre leurs stratégies nutritionnelles qui sont des paramètres fondamentaux si l'on considère la quantité d'énergie journalière nécessaire à leur métabolisme. Au-delà de ces paramètres métaboliques, comprendre la thermo physiologie de ces animaux nous aide également à mieux appréhender leur capacité à conquérir des environnements présentant des températures plus basses. L'endothermie représente la capacité d'emmagasiner suffisamment d'énergie pour amener et maintenir la température corporelle d'un individu à un niveau élevé et stable alors que l'homéothermie consiste à maintenir la température à un niveau stable dans différents environnements thermiques [10,11]. Contrairement aux idées reçues, l'endothermie n'est pas réservée aux seuls mammifères et oiseaux. Paladino et al. [12] ont ainsi proposé que certaines tortues qui sont des reptiles marins puissent présenter des caractères endothermes. De la même manière des caractères endothermes sont également reconnus chez certaines espèces de requins, de thons et même de fleurs et d'insectes [13,14,15]. Actuellement l'origine et l'évolution du caractère endotherme constituent un sujet de controverses scientifiques [16,17,18]. Son origine pourrait même remonter aussi loin que le

Permien (295-250 Ma). Nous nous sommes intéressés dans notre étude aux ichtyosaures, plésiosaures et mosasaures qui ont peuplés les océans entre le Trias et le Crétacé (250-65 Ma).

Figure 3.2: Reconstitution de mosasaure. *(Tylosaurus. DAMNFX © 2005 National Geographic)*

Ces espèces représentent trois lignées qui se sont adaptées secondairement à la vie marine ce qui rend d'autant plus intéressant la connaissance de leur mode de thermo régulation d'autant plus que cela permet de mieux comprendre pourquoi elles ont eu un développement très important au cours du Mésozoïque pour devenir même les principaux prédateurs des océans de l'ère secondaire à leur apogée. Le principe de notre étude a été de comparer les $\delta^{18}O$ des phosphates des dents de reptiles aux $\delta^{18}O$ de poissons contemporains. En utilisant les modèles existants [19-24] et en reportant la différence $\delta^{18}O_{reptile}$- $\delta^{18}O_{poisson}$ en fonction de $\delta^{18}O_{poisson}$ on peut mettre en évidence que ces énormes reptiles marins étaient capables de maintenir une température corporelle constante et élevée dans des environnements marins allant des zones tropicales aux zones tempérées froides. De plus, en estimant leurs températures corporelles entre 35(±2) °C et 39(±2)°C on peut en déduire des taux de métabolisme élevés chez ces animaux nécessaires pour rechercher les proies devant combler leurs besoins alimentaires et des vitesses de nage rapides sur des distances très importantes.

Mais dans le même domaine de l'étude physiologique nous avons également travaillé sur du matériel actuel avec d'autres traceurs isotopiques puisque nous nous sommes cette-fois intéressés aux rapports $^{13}C/^{12}C$ et $^{15}N/^{14}N$ de la matière organique ainsi qu'à d'autres techniques d'analyses isotopiques en utilisant un couplage analyseur élémentaire-spectromètre de masse de rapports isotopiques (EA-IRMS).

Les articles 3.3 et 3.4 sont le résultat d'une collaboration avec l'UMR CNRS 5023 « Ecologie des systèmes fluviaux » de l'Université Claude Bernard Lyon 1 avec qui nous sommes partenaires au sein de l'IFR41.

Les écosystèmes aquifères souterrains sont considérés comme hétérotrophiques et leur fonctionnement dépend de l'apport de matière organique externe provenant des écosystèmes de surface. Ces milieux particuliers sont considérés comme fonctionnant du bas vers le haut « bottom-up » du fait de la qualité et de la quantité des apports en matière organique [32-35]. Dans la publication 3.3 nous nous sommes intéressés au rôle de l'amphipode *Niphargus rhenorhodanensis* (Figure 3.3) qui est un invertébré cavernicole vivant dans la zone hyporhéique des eaux souterraines hyporhéique (zone bordant un cours d'eau où l'on a mélange entre l'eau interstitielle du sol et l'eau de surface). Le but de cette étude est d'abord d'essayer de quantifier l'influence relative de l'activité de *Niphargus rhenorhodanensis* et du flux de DOC sur l'évolution de la matière organique du sol, l'activité microbienne et l'évolution de la biomasse, et ensuite de déterminer les taux de nutrition de *Niphargus rhenorhodanensis* sur les microbes vivant dans les sédiments en traçant le flux d'une source de DOC enrichie en ^{13}C dans des colonnes expérimentales reproduisant les conditions d'un aquifère naturel.

Figure 3.3: Individus de Niphargus rhenorhodanensis.

Les résultats de notre étude sur nos colonnes expérimentales à filtration lente montrent que l'abondance et l'activité microbienne ainsi que la biomasse sont principalement régies par le flux de matière organique dans la colonne plutôt que par l'activité de *Niphargus rhenorhodanensis* La modélisation des flux de carbone dans les expériences faites avec de l'acétate enrichie en ^{13}C indique que l'activité nutritionnelle de *Niphargus rhenorhodanensis* est trop faible pour avoir une influence sur l'activité microbienne. Nos résultats confirment ainsi l'hypothèse que les écosystèmes fluviatiles souterrains sont contrôlés du bas vers le haut. La faible influence de *Niphargus rhenorhodanensis* sur le compartiment microbien du sol est probablement liée à son métabolisme réduit. Ceci souligne la nécessité de développer d'autres expériences afin d'examiner les relations entre le taux de métabolisme des organismes vivant dans les sols et leur rôle dans le fonctionnement de leur écosystème.

Dans la publication 3.4 nous nous sommes également intéressés au cycle de la matière organique dans les sols mais d'une façon quelque peu différente. D'une manière générale, la classification par mode de nutrition est largement utilisée pour décrire les communautés d'invertébrés benthiques en relation avec les ressources en matière organique. A l'intérieur de ce cadre général, des interactions entre les divers groupes nutritionnels ont été imaginés dans

ce que l'on a appelé le « River Continuum Concept » (RCC) et en particulier entre les « broyeurs » et les « ramasseurs collecteurs » [36-39]. Cependant les relations avec les flux de matière organique demeurent peu documentées pour les invertébrés vivant dans la zone hyporhéique. Nous avons de nouveau utilisé l'amphipode *Niphargus rhenorhodanensis* et nous avons fait l'hypothèse que *Niphargus rhenorhodanensis* se nourrirait préférentiellement de matière particulaire fine (« Fine Particulate Organic Matter » : FPOM) plutôt que de matière particulaire grossière (« Coarse Particulate Organic Matter » : CPOM) dans la zone hyporéique et devrait donc être favorisé par la présence d'individus de type « broyeurs » qui produisent de la FPOM à partir de CPOM. Nous avons développé des expériences de laboratoires sur des réservoirs reconstituant les conditions naturelles mais en contrôlant certains paramètres. Nous avons utilisé ces systèmes artificiels pour quantifier l'utilisation de litière provenant des feuilles par *Niphargus rhenorhodanensis* ainsi que par un autre amphipode appartenant au groupe des broyeurs : *Gammarus roeselii*. En utilisant les variations la signature isotopique en ^{15}N de ces deux espèces d'abord séparément, puis ensemble pour mettre en évidence des relations de type broyeurs-collecteurs entre eux. Les mesures de pertes de masse de litière nous ont montré que *Niphargus rhenorhodanensis* n'était pas un organisme broyeur contrairement à *Gammarus roeselii*. L'étude des rapports isotopiques $^{15}N/^{14}N$ des tissus de Niphargidés nous ont permis de voir que *Niphargus rhenorhodanensis* était plutôt un organisme de type ramasseurs - collecteur se nourrissant préférentiellement de FPOM. Au-delà de ces résultats, nous avons également pu mettre en évidence une influence des Gammaridés broyeurs sur le taux d'assimilation de *Niphargus rhenorhodanensis* qui semble se nourrir de la FPOM produite par les individus broyeurs. Ces résultats viennent renforcer l'hypothèse d'une interaction entre les individus broyeurs de surface et les individus ramasseurs – collecteurs de la zone hyporhéique.

Enfin, dans la publication 3.5 nous avons utilisé la double signature isotopique $^{13}C/^{12}C$ et $^{15}N/^{14}N$ en abondance naturelle pour étudier les relations entre l'environnement et les stratégies de reproduction d'insectes phytophages de la famille des curculionidés. Nous avons utilisé les isotopes stables ici pour tester l'hypothèse que quatre espèces de Curculio qui cohabitent sur une ressource alimentaire très fluctuante utilisée pour la ponte de leurs œufs seraient toutes de type synovigénique (commençant la maturation de leurs œufs avec un délai après savoir atteint le stade adulte) plutôt que de type proovigénique (ayant la plupart de leurs œufs déjà matures au début de leur vie d'adulte), cela en réponse aux conditions environnementales [40-42]. Nous avons choisi un site où les insectes se nourrissent de glands de chênes de type *Quercus spp*. Au cours de l'étude, nous avons essayé de contrôler au maximum les paramètres pouvant influencer nos mesures par exemple en allant étudier sur le terrain les dates d'émergences des individus adultes ou bien en caractérisant isotopiquement des individus dès qu'ils émergent puis après les phases de nutrition afin d'obtenir des informations sur leurs régimes alimentaires [43-45] .

En combinant les analyses $\delta^{13}C_{PDB}$ et $\delta^{15}N_{AIR}$ et contrairement aux hypothèses qui avaient été faites les quatre espèces étudiées qui ont toutes été exposées à des conditions environnementales variables ont montré des stratégies nutritionnelles différentes. Trois espèces se sont montrées clairement synovigéniques alors que la quatrième correspond plutôt au type proovigénique. Ceci signifie que des variations environnementales ne favorisent pas un seul type de stratégie énergétique pour la reproduction mais semble devoir favoriser leur diversification.

On voit bien au travers de ces différentes études, les immenses possibilités des analyses isotopiques des isotopes stables des éléments légers tels que C, N, O aussi bien pour obtenir des indices et des contraintes sur la physiologie d'organismes vivants ayant occupé notre planète à des époques très anciennes que pour mieux comprendre l'écologie, le mode de

nutrition, les stratégies de reproduction d'organismes actuels ainsi que pour étudier le mode de vie de nos ancêtres. Au travers de ces études nous avons également illustré le potentiel des analyses isotopiques à la fois en abondance naturelle ainsi que la technique du marquage en isotopes stables, beaucoup plus facile et moins contraignant à utiliser que le marquage radioactif par exemple au Tritium ou au ^{14}C. Un autre intérêt que nous avons essayé de mettre en évidence ici est la capacité d'utiliser une approche multi-isotopique en combinant l'analyse de plusieurs éléments comme N et C par exemple sur la même prise d'essai.

References Chapitre 3

(1) H.L. Schmidt (2003) *Naturwissenschaften.,* **90**: 537-552.

(2) R. Amiot, C. Lécuyer, E. Buffetaut, G. Escarguel, F. Fluteau & F. Martineau (2006) *Earth Planet. Sci. Let.,* **246**: 41-54.

(3) M.J. De Niro & S. Epstein (1978) *Geochim. Cosmochim. Acta*, **42** : 495-506.

(4) M.F. Estep & H. Dabrowski (1980) *Science*, **209**: 1537-1538.

(5) K.A. Hobson & L.I. Wassanaar (1997) *Oecologia*, **109**: 142-148.

(6) M. Fizet, A. Mariotti, H. Bocherens, B. Lange Badré, B. Vandermeersch, J.P. Borel & G. Bellon (1995) J. *Archaeol. Sci.,* **22**:67-79.

(7) M.P. Richards, P.B. Pettitt, E. Trinkaus, F.H. Smith, M. Paunovic & I. Karavanic (2000) *Proc. Nat. Acad. Sci. U.S.A.,* **97**: 7663-7666.

(8) H. Bocherens, D.G. Drucker, D. Billiou, M. Patou-Mathis & B. Vandermeersch (2005) *J. Hum. Evol.,* **49**: 71-87.

(9) V. Balter & L. Simon (2006) *J. Hum. Evol.,* **51**: 329-338.

(10) A.F. Bennett, J.W. Hicks & A.J. Cullum (2000) *Evolution*, **54**: 1768.

(11) C.P. Hickman, L.S. Roberts & A. Larson (2000) *Integrated principles of zoology McGraw-Hill Sciences New York Eds.*

(12) F.V. Paladino, M.P. O'Conner & J.R. Spotila (1990) *Nature*, **344**: 858.

(13) B. Heinrich (1989) *Integr. Comp. Biol.,* **29**: 1157.

(14) B.A. Block, J.R. Finnerty, A.F. Stewart & J. Kidd (1993) *Science*, **260**: 210.

(15) R.S. Seymour (2004) *Plant Cell. Environ.,* **27**: 1014.

(16) V; De Buffrenil & J.M. Mazin (1990) *Paleobiology*, **16**: 435.

(17) R.S. Seymour (1976) *Nature*, **262**: 207.

(18) R.S. Seymour, C.L. Bennett-Stamper, S.D. Johnston, D.R. Carrier & G.C. Grigg (2004) *Physiol. Biochem. Zool.,* **77**: 1051.

(19) A. Longinelli & S. Nuti (1973a) *Earth Planet. Sci. Lett.,* **19**: 373-376.

(20) Y. Kolodny, B. Luz & O. Navon (1983) *Earth Planet. Sci. Lett.,* **64**: 298-404.

(21) B. Luz, Y. Kolodny & J. Kovach (1984) *Earth Planet. Sci. Lett.,* **69**: 255-262.

(22) J. Kharu & S. Epstein (1986) *Geochim. Cosmochim. Acta*, **50**: 1745-1756.

(23) Y. Kolodny & M. Raab (1988) *Palaeogeogr., Palaeoclimatol., Palaeoecol.,* **64**: 59-67.

(24) D. D'Angela & A. Longinelli (1990) *Chem. Geol. (Isot. Geosci. Sect.),* **86** : 75-82.

(25) C. Lécuyer, P. Grandjean, J.R. O'Neil, H. Capette & F. Martineau (1993) *Palaeogeogr., Palaeoclimatol., Palaeoecol.,* **105**: 235-243.

(26) H.C. Fricke, J.R. O'Neil & N. Lynnerup (1995) *Geology*, **23**: 869.

(27) H.C. Fricke, W.C. Clyde, J.R. O'Neil & P. D. Gingerich (1998a) *Earth Planet. Sci. Let*., **160**: 193.

(28) H.C. Fricke, W.C. Clyde, J.R. O'Neil & P.D. Gingerich (1998b) *Geochim. Cosmochim. Acta*., **62**: 1839.

(29) L. Genoni, P. Iacumin, V. Nikolaev, Y. Gribchenko & A. Longinelli (1998) *Earth Planet. Sci. Let*., **160**: 587-592.

(30) S. Picard, J.P. Garcia, C. Lécuyer, S.M.F. Sheppard, H. Capetta & C.C. Emig (1998) *Geology*, **26(11)** : 975-978.

(31) T.W. Vennemann & E. Egner (1998) *Palaeogeogr., Palaeoclimatol., Palaeoecol.,* **142**: 107-121.

(32) J. Gibert & L. Deharveng (2002) *Bioscience*, **52** :473-481.

(33) F. malard, J.L. Reygrobellet, J. Mathieu & M. Lafont (1994) *Archiv für Hydrobiologie*, **131** : 93-110.

(34) J. Notenboom, S. Plénet & M.J. Turquin (1994) *In : Groundwater Ecology (Eds Gibert J. Danielopol D.L. & Stanford J.A.):* 477-504.

(35) T. Datry, F. Malard & J. Gibert (2005) *Journ. North Amer. Benthol. Soc.,* **24**: 461-477.

(36) K.W. Cummins (1973) *Ann. Rev. of Entomol.,* **18**: 183-206.

(37) L.G. Willoughby & D.W. Sutcliffe (1976) *Freshwater Biol*., **6**: 577-586.

(38) K.W. Cummins, M.J. Klug (1979) *Ann. Rev. of Ecol. and Systematics,* **10**: 147-172.

(39) R.L. Vannote, G.W. Minshall, K.W. Cummins, J.R. Sedell & C.E. Cushing (1980) *Can. Journ. of Fisheries and Aquat. Sci.,* **37**, 130-137.

(40) M.A. Jervis, G.E. Eimpel, P.N. Ferns, J.A. Harvey & N.A.C. Kidd (2001) *Journ. of Anim. Ecol*., **70**: 442-458.

(41) M.A. Jervis & P.N. Ferns (2004) *Oikos,* **107**: 449-461.

(42) M.A. Jervis, J. Ellers & J.A. Harvey (2008) *Ann. Rev. of Entomol.,* **53**: 361-385.

(43) M.J. De Niro & S. Epstein (1978) *Geochim. Cosmochim.* Acta, **42** : 495-506.

(44) R. Hood Novotny & B.G.J. Knols (2007) *Entomologia Experimentalis et Applicata*, **124** : 3-16.

(45) R. Inger & S. Bearhop (2008) *Ibis*, **150** :447-461.

Journal of Human Evolution 55 (2008) 1138–1147

Contents lists available at ScienceDirect

Journal of Human Evolution

journal homepage: www.elsevier.com/locate/jhevol

Oxygen isotope fractionation between human phosphate and water revisited

Valérie Daux [a,*], Christophe Lécuyer [b], Marie-Anne Héran [b], Romain Amiot [b], Laurent Simon [c], François Fourel [b], François Martineau [b], Niels Lynnerup [d], Hervé Reychler [e], Gilles Escarguel [b]

[a] Laboratoire des Sciences du Climat et de l'Environnement/IPSL, UMR CEA/CNRS 1572, L'Orme des Merisiers, Bât. 701, CEA Saclay, 91191 Gif/Yvette Cedex, France
[b] Laboratoire CNRS UMR 5125 "Paléoenvironnements & Paléobiosphère," Université Claude Bernard Lyon 1, Campus de la Doua, F-69622 Villeurbanne, France
[c] Laboratoire CNRS UMR 5023 "Ecologie des hydrosystèmes fluviaux," Université Claude Bernard Lyon 1, Campus de la Doua, F-69622 Villeurbanne, France
[d] Laboratory of Biological Anthropology, The Panum Institute, Blegdamsvej 3, DK–2200 Copenhagen, Denmark
[e] Service de Stomatologie et Chirurgie maxillo-faciale, Université Catholique de Louvain, Cliniques universitaires Saint-Luc, av. Hippocrate 10, 1200 Bruxelles, Belgium

ARTICLE INFO

Article history:
Received 28 January 2008
Accepted 26 June 2008

Keywords:
Fractionation equation
Homo sapiens
Tooth enamel
Climate

ABSTRACT

The oxygen isotope composition of human phosphatic tissues ($\delta^{18}O_P$) has great potential for reconstructing climate and population migration, but this technique has not been applied to early human evolution. To facilitate this application we analyzed $\delta^{18}O_P$ values of modern human teeth collected at 12 sites located at latitudes ranging from 4°N to 70°N together with the corresponding oxygen composition of tap waters ($\delta^{18}O_W$) from these areas. In addition, the $\delta^{18}O$ of some raw and boiled foods were determined and simple mass balance calculations were performed to investigate the impact of solid food consumption on the oxygen isotope composition of the total ingested water (drinking water + solid food water). The results, along with those from three, smaller published data sets, can be considered as random estimates of a unique $\delta^{18}O_W/\delta^{18}O_P$ linear relationship: $\delta^{18}O_W = 1.54(\pm0.09) \times \delta^{18}O_P - 33.72(\pm1.51)$ ($R^2 = 0.87$: $p[H_0:R^2 = 0] = 2 \times 10^{-19}$). The $\delta^{18}O$ of cooked food is higher than that of the drinking water. As a consequence, in a modern diet the $\delta^{18}O$ of ingested water is +1.05 to 1.2‰ higher than that of drinking water in the area. In meat-dominated and cereal-free diets, which may have been the diets of some of our early ancestors, the shift is a little higher and the application of the regression equation would slightly overestimate $\delta^{18}O_W$ in these cases.

Introduction

In recent years, the study of prehistoric cultures has benefited from the use of stable isotope analyses. The majority of these studies have focused on the Holocene portion of human evolution, however, isotopic investigations may provide critical information about our earliest ancestors' diet and ecological setting (climate and environment). Such information plays a critical role in scenarios that seek to explain the evolution of early humans. For example, stable nitrogen and carbon isotope analyses of bone collagen (e.g., Ambrose and De Niro, 1986; Bocherens et al., 1991; Fizet et al., 1995; Richards et al., 2005) and carbon isotope analysis of bone and tooth carbonate (Lee-Thorp et al., 1994; Van der Merwe et al., 2003; Sponheimer et al., 2005) have been used to reconstruct the diet of some of our pre-Holocene ancestors. However, oxygen isotope compositions of human phosphatic tissues, which can be used to reconstruct climatic conditions (e.g., Fricke et al., 1995; Müller et al., 2003; Daux et al., 2005; Evans et al., 2006), identify foreigners in a population, assess the mobility of human groups (e.g., White et al., 2000; Dupras and Schwarcz, 2001; White et al., 2007), or reconstruct infant feeding behavior (e.g., Wright and Schwarcz, 1998), have not been applied, to our knowledge, to issues of early human evolution.

The ratio of oxygen isotopes in mammalian flesh, bones, and teeth reflects the origin of water imbibed as a liquid and ingested from food. The water contained in food has a complicated relationship with meteoric water and can be significantly enriched in ^{18}O compared to meteoric water. The relative contribution of water entering the body as a liquid and from food varies from one species to another. Animals with low water turnover are expected to derive more water from isotopically-enriched food sources and less from drinking water than are those with high water turnover (Kohn et al., 1996). For the vast majority of terrestrial vertebrates, water turnover scales to body mass (e.g., Altman and Dittmer, 1968; Eberhardt, 1969). Therefore, the $\delta^{18}O$ of the tissues of large animals should be less affected by their solid food consumption than is the $\delta^{18}O$ of smaller animals. However, the influence of diet on the isotopic composition of the tissues may not depend only on water turnover but also on the proportion of water taken up as water contained in food. By way of example, larger herbivores consume plants that are highly hydrated (80 to 95% water by weight) and may contribute up to 50% of the total ingested water (from statistics

* Corresponding author.
E-mail addresses: valerie.daux@lsce.ipsl.fr (V. Daux), clecuyer@univ-lyon1.fr (C. Lécuyer).

0047-2484/$ – see front matter © 2008 Elsevier Ltd. All rights reserved.
doi:10.1016/j.jhevol.2008.06.006

of *Agriculture and Agri-food Canada*). As a result, large herbivores obtain a large proportion (up to 50% for wild herbivores; Kohn et al., 1996) of their oxygen from plants that are isotopically enriched. In contrast, the influence of food on tissue $\delta^{18}O$ is insignificant in animals that are fed dry food (Luz et al., 1984).

Humans are medium size mammals with moderate water turnover. As we are mainly omnivores, we ingest less water from food sources than do herbivores. Therefore, the $\delta^{18}O$ ingested by humans is strongly imprinted by the composition of our drinking water, which is strongly linked to environmental water (Longinelli, 1984; Luz et al., 1984; Levinson et al., 1987). Although there is a linear relationship between the oxygen isotope composition of human phosphate and the composition of meteoric water, the three previously-published fractionation equations differ in both their slope and intercept values (Longinelli, 1984; Luz et al., 1984; Levinson et al., 1987). This variation may result from the use of different analytical techniques among studies, small datasets that sample a restricted range of variation, or differences in the timing and duration of crown mineralization from one individual to another. Additionally, although not thought to be a big influence, diet may influence the oxygen isotopic composition of human tissues and contribute to the variation among studies. Although thought to be small, the effect of specific diets on $\delta^{18}O_P$ is unknown. One can question the impact on $\delta^{18}O_P$ of a vegetarian or a meat-based diet, the effect of cereal consumption, or the consequence of cooking food. If specific diets prove to have a sizable influence on $\delta^{18}O_P$, they would need to be considered when reconstructing paleoclimate from the isotopic signature of phosphatic tissues. Conversely, the $\delta^{18}O_P$ of individuals of known isotopic context ($\delta^{18}O_W$) can provide information on their dietary practices.

In this study, we refine our knowledge of the oxygen isotope fractionation between water and phosphate in human tooth enamel. We provide a new set of oxygen isotope data for teeth of recent humans from 4°N to 70°N. We compare regressions between $\delta^{18}O_P$ and the $\delta^{18}O_W$ of their likely drinking water and of meteoric water. We test whether the differences among the previously published datasets (Longinelli, 1984; Luz et al., 1984; Levinson et al., 1987; this study) are statistically significant. We then investigate the effect of diet on $\delta^{18}O_P$ by measuring the oxygen isotope compositions of water from raw and cooked vegetables, fish, and meat by modeling the impact of variable proportions of these constituents on $\delta^{18}O_P$.

Materials and methods

Tooth enamel samples

We analyzed the oxygen isotopic ratios of 38 molars (36 M1 and M2; 2 M3) from modern or historical (18th century Inuit) individuals from 12 geographic areas that range from about 4°N (Cameroon) to 70°N (Greenland; Fig. 1). Only one tooth was sampled per individual. In the case of living individuals, informed consent was given by the patients whose teeth were analyzed. Both maxillary and mandibular molars were sampled. Teeth of living individuals were extracted because of periodontal disease or for prosthodontic reasons. Teeth were selected that met the following criteria: 1) the person, according to their own statement, had lived all their childhood in the same place and had drunk local water during this time; and 2) the molar exhibited no evidence of decay.

Once obtained, teeth were crushed and enamel was sorted by handpicking under a microscope. The fragments were cleaned with 15% hydrogen peroxide for half an hour in an ultrasonic bath and dried in an oven before being crushed to powder in an agate mortar.

Most studies dedicated to the oxygen isotope composition of apatite start by isolating PO_4^{3-} using acid dissolution and anion-exchange resin. The protocol used here is derived from the original method published by Crowson et al. (1991) and slightly modified by Lécuyer et al. (1993). After dissolution of 15 to 30 mg of powdered tooth enamel in 2 M HF at 25 °C for 24 hours, the CaF_2 that precipitates is separated from the solution that includes the phosphate by centrifugation. The CaF_2 precipitate is rinsed three times using double deionized water (DDW) and the rinse water is added to the solution that is neutralized with a 2 M KOH solution. Cleaned Amberjet™ resin (2 ml) is added to the neutralized solution in polypropylene tubes. The tubes are placed on a shaker table for 12 hours to promote the ion exchange process. Excess solution is discarded and the resin is washed five times with DDW to remove the traces of ionic contaminants. To elute the phosphate ions quantitatively from the resin, 25–30 ml of 0.5 M NH_4NO_3 is added to bring the pH of the solution to 7.5–8.5, and the tubes are gently shaken for about 5 hours. Silver phosphate is precipitated from the eluted solution following the method of Firshing (1961). The solution is placed in a 250 ml Erlenmeyer flask and about 1 ml of concentrated NH_4OH is added to raise the pH to 9–10. Fifteen ml of ammoniacal $AgNO_3$ solution is added to the flask. Upon heating this solution to 70 °C in a thermostatic bath, millimeter-size yellowish crystals of Ag_3PO_4 are quantitatively precipitated. The crystals of silver phosphate are collected on a Millipore filter, washed three times with DDW, and air dried at 50 °C.

The $^{18}O/^{16}O$ ratios are measured after reaction of silver phosphate with graphite to form CO_2 (O'Neil et al., 1994; Lécuyer et al., 1998). Ag_3PO_4 samples are mixed with pure graphite powder with precise proportions of 0.5 mg of C to 8 mg of Ag_3PO_4. They are weighed into tin reaction capsules, loaded into quartz tubes, and degassed for 30 minutes at 80 °C in vacuum. The samples are then heated at 1100 °C for 1 minute to promote the redox reaction. CO_2 samples are analyzed at the University of Lyon with a GV IsoPrime™ or a GV PRISM II stable isotope ratio mass spectrometer using dual inlet systems with automated cold fingers. Isotopic compositions are quoted in the standard δ notation relative to Standard Mean Ocean Water (SMOW). The reproducibility of measurements carried out on tooth enamel samples is better than 0.2‰ (1σ). Silver phosphate precipitated from standard NBS120c (natural Miocene phosphorite from Florida) was repeatedly analyzed ($\delta^{18}O = 21.73 \pm 0.20$; $n = 20$) along with the silver phosphate samples derived from the human tooth collection. Calibration of the "graphite method" has been made with oxygen isotope measurements using fluorination. As this technique ensures a total conversion of apatite oxygen to carbon dioxide, any bias resulting from the so called "scale compression factor" (Vennemann et al., 2002) has been corrected by using two standards of distinct oxygen isotope composition. For NBS120c, we obtained a comparable mean $\delta^{18}O$ value of 21.70 ± 0.14‰ ($n = 21$). To bracket the isotopic range documented in this study, we analyzed the "Durango apatite" which gives a mean $\delta^{18}O$ value of +9.45‰ ($n = 3$) by offline pyrolysis against a value of +9.6‰ obtained by fluorination using BrF_5 reagent (C. France-Lanord, pers. comm.). It must be taken into account, however, that former studies (Longinelli, 1984; Luz et al., 1984; Levinson et al., 1987) used both $BiPO_4$ chemistry and fluorination protocols for isolation of phosphate and extraction of its oxygen. The robustness of the oxygen isotope measurement by various methods has been reported by Lécuyer et al. (1996) who used the two kinds of data to generate an oxygen isotope fractionation equation for lingulids, with the fair and appreciated contribution of Dr. A. Longinelli.

Tap and meteoric waters

At 11 of the geographic locations from which enamel sampling was undertaken, samples of tap water were collected for oxygen isotope analysis. Oxygen isotope compositions were determined using water-carbon dioxide equilibration methods (Epstein and Mayeda, 1953; O'Neil et al., 1975). Aliquots of 3 ml of water were equilibrated with 30 μmoles of CO_2 at 25 °C for 48 hours (8 hours at LSCE in the Finnigan equilibration device). Equilibrated CO_2 was

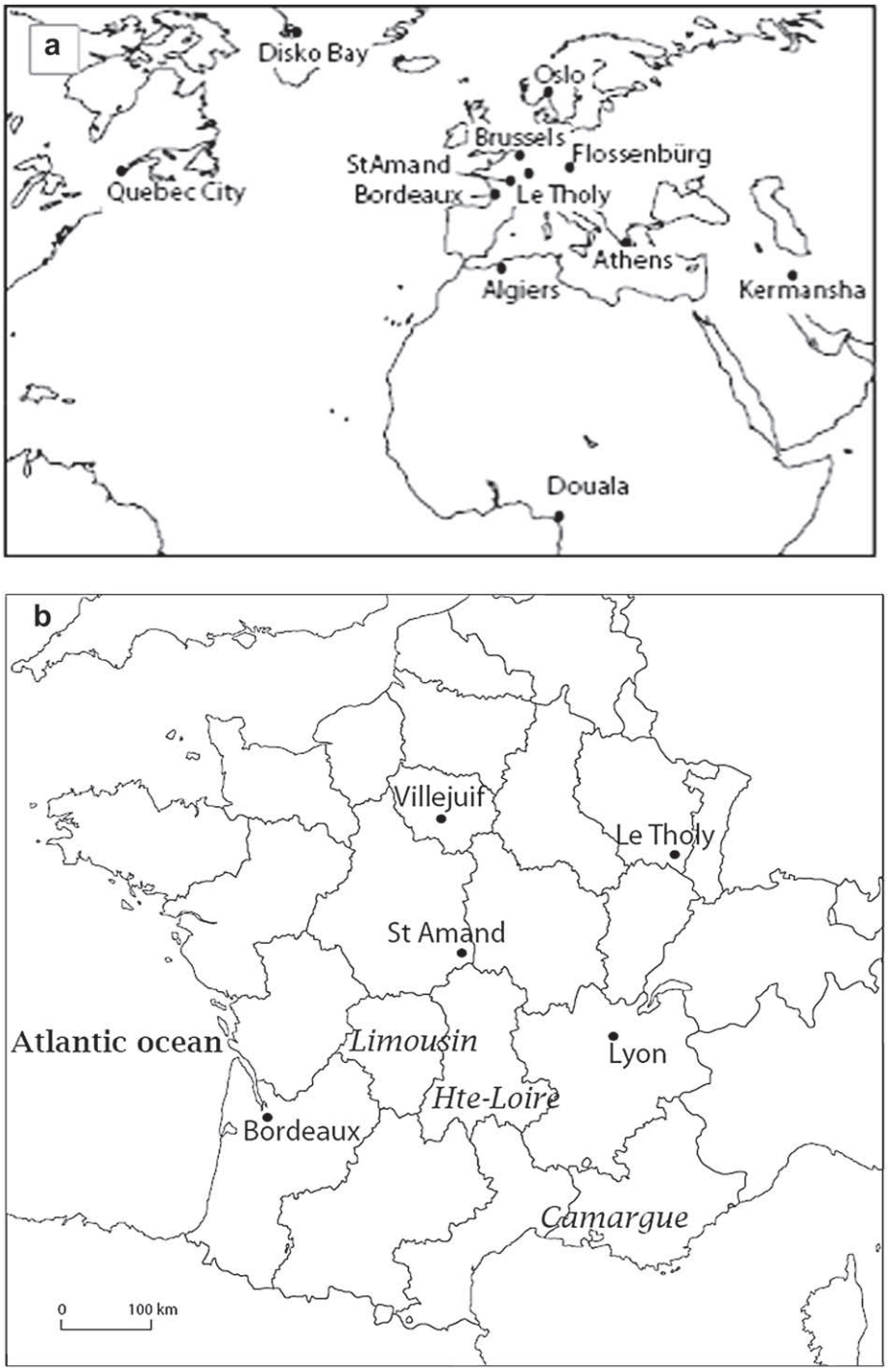

Fig. 1. Geographic locations of the sites mentioned in this study: a) teeth and tap water at Algiers (Algeria), Athens (Greece), Brussels (Belgium), Douala (Cameroon), Flossenbürg (Germany), Kermansha (Iran), Oslo (Norway), Québec (Canada), and Bordeaux, Le Tholy, and St. Amand (France), teeth at Disko Bay (Greenland); and b) focus on the French locations: teeth and tap water as mentioned above, carrots, zucchinis, and chicken at Lyon, rice, lentils, and beef in the Haute-Loire, Camargue, and Limousin areas, respectively.

then analyzed with a GV IsoPrime™, a GV PRISM II stable isotope ratio mass spectrometer at the University of Lyon, or a THERMO Finnigan MAT 252 stable isotope ratio mass spectrometer at LSCE, Gif/Yvette. External reproducibility of oxygen isotope measurements is close to 0.05‰. Tap water samples were not collected at Disko Bay (Greenland).

In addition, for each sampling site, the $\delta^{18}O$ value of precipitation was estimated from a global dataset according to an algorithm developed by Bowen and Wilkinson (2002) and refined by Bowen and Revenaugh (2003). The dataset is derived from the International Energy Association/World Meteorological Organization Global Network for Isotopes in Precipitation by using the Online Isotopes in Precipitation Calculator (OIPC; version updated in 2004).

We have chosen to use both tap water and OIPC estimates for $\delta^{18}O$ to consider how these two may differ and which may be the more appropriate proxy for modeling past $\delta^{18}O$ levels. We prefer tap water because we believe that in the past humans likely utilized surface water sources, and at present, the tap water of most human beings is pumped from shallow aquifers supplied by precipitation. The residence time of the water in these aquifers is on the order of several years (e.g., Jacques, 1996). As a result, most aquifers tend to

resemble the weighted mean rainfall of an area within relatively narrow limits (Clark and Fritz, 1997; Darling, 2004). In some of our studied areas, however, tap water is not derived from local shallow ground waters, but from distant lakes higher in altitude than the areas of water use. In Algiers (alt. 25 m), the tap water is supplied mainly by the Kaddara Dam reservoir that collects water at 350 m above sea level. In Athens, Greece (alt. 28 m), the Mornos Lake, at 435 m above sea level, serves as the main storage reservoir. In Bordeaux (France), the tap water is derived from deep ground water approximately 20,000 years old (water supplier "Lyonnaise des Eaux," pers. comm.). Thus, it should prove possible to test our predictions of the offset that should result from these different sources of tap water and the OIPC predictions.

Food water

To examine the contribution of water from food, various types of food were collected. With the exception of mackerel that was caught in the northern Atlantic, the food came from southeastern and southern Central France in an area relatively close to Lyon, which is also the source of the French tap water used in the experiment. The rice is from Camargue; the beef from Limousin; the chicken, zucchini, and carrots from Lyon city; and the lentils from Haute-Loire (Fig. 1).

Carrots, zucchini, mackerel, beef, and chicken were cut into 1 mm diameter pieces. Rice and lentil samples were ground and the resulting powders were sieved between 100 μm and 500 μm. Five grams of each food sample (called hereafter "raw food") were boiled in 200 ml distilled water ("initial water") in open beakers for 20 minutes. Cooking water ("final water") and food ("cooked food") were collected after filtration. Sodium azide was added to an aliquot of 1 g of food to prevent fermentation. Food water was directly equilibrated with 30 μmoles of CO_2 for 20 hours at 25 °C according to the protocol given by Koehler et al. (2000). Oxygen isotope compositions of distilled and cooking waters have been measured using the same equilibration method as for tap waters.

Methods for $\delta^{18}O_W/\delta^{18}O_P$ fractionation equations and modeling influence of food water on total water

Using a linear regression model, we generated a regression equation to describe the fractionation of $\delta^{18}O_W/\delta^{18}O_P$ for our samples. We then compared our equation with those published by Longinelli (1984), Luz et al. (1984; human bones), and Levinson et al. (1987; human teeth) using a single classification Analysis of Covariance (ANCOVA; Sokal and Rohlf, 1995). Statistics were calculated using the BIOMstat program.

Table 1
Oxygen isotope compositions (‰ versus SMOW) of 1) tooth enamel of M1 and M2 teeth of modern or historical (18th century Greenland) individuals, 2) tap water, and 3) atmospheric precipitation at 12 locations

Country	Site	Lat, Long, Alt[a]	$\delta^{18}O_P$	$\delta^{18}O_P$ mean value[b]	SD (1σ)	$\delta^{18}O_W$ measured[b]	$\delta^{18}O_W$ estimated[b]	Δ‰
Cameroon	Douala	4.0, 9.8, 10	18.8					
	" "		18.5					
	" "		18.2	18.5	0.3	−3.4	−3.2	−0.2
Algeria	Algiers	36.7, 3.3, 25	17.5					
	" "		16.7					
	" "		17.6	17.3	0.5	−6.1	−4.5	−1.6
Iran	Kermanshah	34.3, 47.2, 1320	18.2					
			18.4	18.3	0.2	−7.0	−7.3	0.3
			17.7[c]					
			17.6[c]					
Greece	Athens	37.9, 23.7, 28	16.9	16.9		−7.9	−6.2	−1.7
France	Le Tholy[d]	48.1, 6.7, 740	17.0					
	" "		17.3					
	" "		17.3					
	" "		16.3					
	" "		16.2					
	" "		16.4	16.7	0.5	−8.5	−8.9	0.4
France	Bordeaux	44.8, 0.7, 49	18.3	18.3		−8.1	−6.2	−1.9
France	St. Amand	46.7, 2.5, 162	17.3	17.3		−6.5	−7.3	0.8
Belgium	Brussels	50.9, 4.5, 55	17.0					
	" "		15.9					
	" "		16.6					
	" "		16.5					
	" "		16.5					
	" "		17.5					
	" "		16.9					
	" "		16.7					
	" "		16.5	16.7	0.4	−7.6	−8.0	0.4
Germany	Flossenbürg	49.5, 12.5, 650	16.4	16.4		−10.1	−9.4	−0.7
Canada	Québec City[d]	46.7, −71.4, 110	14.1					
	" "		15.0					
	" "		15.3					
	" "		14.4					
	" "		15.3	14.8	0.5	−11.0	−11.4	0.4
Norway	Oslo	59.9, 10.7, 10	15.1	15.1		−10.5	−10.8	0.3
Greenland	Disko Bay	70.0, −52.0, 1	12.3					
	" "		12.5					
	" "		11.0	11.9	0.8	n.d.	−17.3	

[a] Lat = degrees North latitude. Long = degrees East longitude. Alt = altitude in meters.
[b] $\delta^{18}O_P$ and $\delta^{18}O_W$ in ‰ versus SMOW.
[c] M3 teeth.
[d] published in Daux et al. (2005).

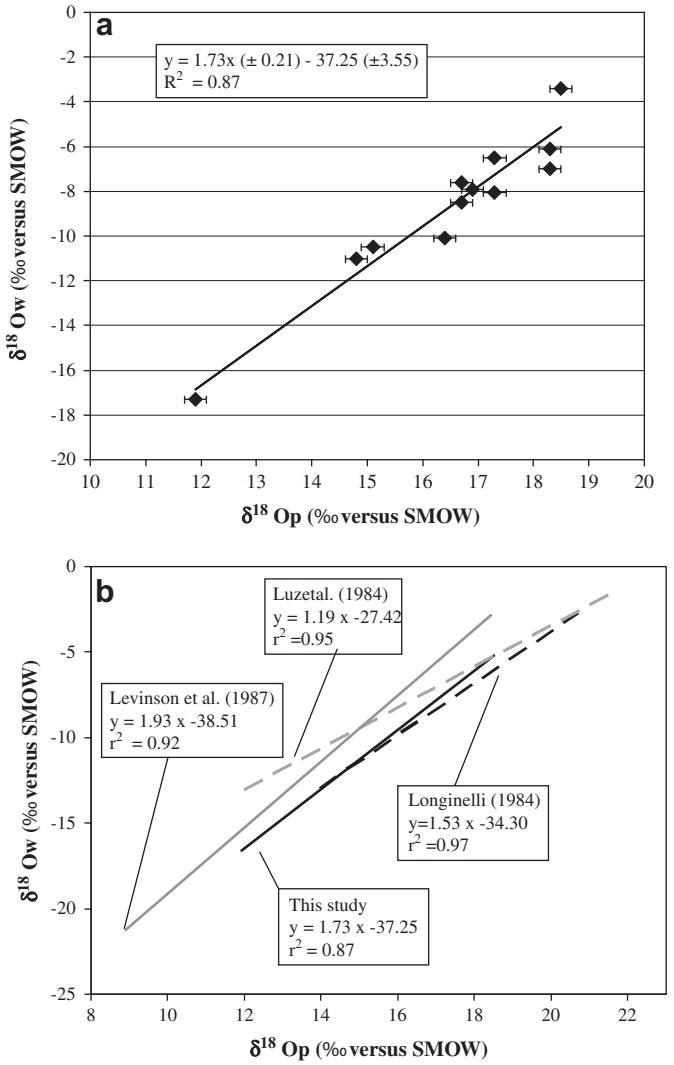

Fig. 2. a) Oxygen isotope fractionation equation computed by using modern human tooth enamel ($\delta^{18}O_P$) and tap water ($\delta^{18}O_W$) from Table 1 (IAEA precipitation data for Disko Bay, Greenland). The error bars correspond to the external reproducibility: ±0.2‰ for $\delta^{18}O_P$ and ± 0.05‰ for $\delta^{18}O_W$ (smaller than the symbols); and b) comparison of the equation shown in (a) with those previously published by Longinelli (1984), Luz et al. (1984), and Levinson et al. (1987).

Simple mass balance calculations were performed to quantify the effect of raw and cooked food consumption on the oxygen isotope composition of the total ingested water. We calculated $\Delta\delta^{18}O$, or the difference between the isotopic composition of the drinking water and of the total ingested water as follows:

$$\Delta\delta^{18}O = \delta^{18}O_{tot} - \delta^{18}O_W \quad (1)$$

where:

$$\delta^{18}O_{tot} = \delta^{18}O_W \times M_W + M_F \times (f_{veg} \cdot [H_2O]_{veg} \cdot \delta^{18}O_{veg} + f_{cl}[H_2O]_{cl}\delta^{18}O_{cl} + f_{mf}[H_2O]_{mf}\delta^{18}O_{mf})/M_{tot}, \quad (2)$$

and

$$M_{tot} = M_W + M_F \times f_{veg}[H_2O]_{veg} + f_{cl}[H_2O]_{cl} + f_{mf}[H_2O]_{mf}. \quad (3)$$

M_F and M_W are the masses of daily ingested drinking water and total food (assumed to be constant); M_{tot} is the mass of water ingested (as a liquid plus in solid food); f_{veg}, f_{cl}, f_{mf} are the fractions of vegetables, cereals and legumes, and of meat and fish in the diet ($f_{veg} + f_{cl} + f_{mf} = 1$); and $[H_2O]_{veg}$, $[H_2O]_{cl}$, and $[H_2O]_{mf}$ are the water contents of these food categories.

Results

Oxygen isotope compositions of tooth enamel ($\delta^{18}O_P$) and drinking water

The oxygen isotope ratios of tooth enamel from human beings measured in this study range from 11.9‰ (Greenland) to 18.5‰ (Cameroon) with a corresponding water isotopic range from −17.3‰ to −3.4‰ (Table 1). The 1σ standard deviations, calculated for the seven sites where at least three individuals have been sampled, range from 0.3‰ to 0.8‰, indicating an isotopic variability larger than the analytical uncertainty (1σ = 0.2‰).

As predicted, the relationship between tap water and OIPC $\delta^{18}O$ values is generally good (not exceeding 0.8‰), but diverges in areas where tap water does not sample shallow aquifers. Our samples from Algiers, Athens, and Bordeaux differ by 1.6 and 1.7‰ between the oxygen isotopic values of their tap waters and of OIPC estimates of present day rain in each region (Table 1). We discuss the causes of these differences below.

Fractionation equations: $\delta^{18}O_W$ versus $\delta^{18}O_P$

Because of the differences in tap water and OIPC values, the $\delta^{18}O_W$ versus $\delta^{18}O_P$ regressions yield slightly different isotopic fractionation equations when using tap water values (OIPC estimate is used for Disko Bay; equation 4; Fig. 2a; Table 2) or the OIPC precipitation database (equation 5; Table 2). The ordinary least squares analysis of the data produces the following equations:

$$\delta^{18}O_W = 1.73(\pm 0.21) \times \delta^{18}O_P - 37.25(\pm 3.55)$$

$$(n = 12; R^2 = 0.87; p[H_0 : R^2 = 0] = 1 \times 10^{-5}), \quad (4)$$

and

$$\delta^{18}O_W = 1.70(\pm 0.22) \times \delta^{18}O_P - 39.28(\pm 3.68)$$

$$(n = 12; R^2 = 0.88; p[H_0 : R^2 = 0] = 7 \times 10^{-6}) \quad (5)$$

The Greenlandic sample (Disko Bay) lies at the extreme of the correlation. Therefore, it exerts a large influence on the slope of the regression line and on the value of the correlation coefficient (see Table 2). The Greenland sample corresponds to Inuit people who lived during the 18th century. The value of the $\delta^{18}O_W$ at Disko Bay at this time may have been different from the present day. We therefore explore if this uncertainty regarding the $\delta^{18}O_W$ must be seen as a motive for excluding the sample.

The variation through time of the isotopic composition of oxygen in Greenland precipitation can be estimated from ice cores. The data reported by Andersen et al. (2006), which are calculated by stacking the record at Dye-3, GRIP, and GNIP drilling sites, represent an integrated North-South value of the isotopic composition of the precipitation (data available on http://icecores.dk). These data are expressed as anomalies, (i.e., differences to the mean calculated from the entire period; S.O. Rasmussen, pers. comm.). The mean values of the $\delta^{18}O_W$ during the 18th and 20th centuries ($m \pm 1\sigma$: $-0.089\% \pm 0.3805$ and -0.005 ± 0.2237, respectively) are not significantly different at a 95% level of confidence (unequal variance Welch test: $t = 1.56$, d.f. = 173, $p = 0.12$). Therefore, if differences exist between the $\delta^{18}O_P$ of the Inuits of the 18th and of the 20th centuries, they are not due to different oxygen compositions of the precipitation. In addition, this sample is clearly not an outlier when

Table 2
Regression and correlation parameter estimates for the linear models $\delta^{18}O_W = (a \times \delta^{18}O_P) + b$ associated to the available individual sets of $\delta^{18}O$-values[a]

	N	Slope			Intercept			Correlation	
		Mean	SE	SE/Mean %	Mean	SE	SE/Mean %	R	p-value[a]
Longinelli (1984)	10	1.53	0.10	6.5	−34.30	1.81	5.3	0.97	4×10^{-7}
Luz et al. (1984)	6	1.20	0.19	15.8	−27.42	3.05	11.1	0.95	3×10^{-3}
Levinson et al. (1987)	14	1.93	0.18	9.3	−38.51	2.53	6.6	0.92	1×10^{-7}
This study–tap water except for Disko Bay (OIPC estimate)	12	1.73	0.21	12.1	−37.25	3.55	9.5	0.88	1×10^{-5}
This study without the Disko Bay sample–tap water	11	1.49	0.35	23.5	−33.08	5.87	17.7	0.67	2×10^{-3}
This study–OIPC estimates[b]	12	1.87	0.22	11.8	−39.28	3.68	9.4	0.89	7×10^{-6}
This study without the Disko Bay sample–OIPC estimates[b]	11	1.75	0.37	21.1	−37.21	6.29	16.9	0.71	1×10^{-3}
Overall equation	42	1.54	0.09	5.8	−33.72	1.51	4.5	0.87	2×10^{-19}

[a] SE = Standard errors associated to the mean estimates of the slope and intercept. The p-value associated to the coefficient of determination (R^2) tests the null hypothesis H_0: $R^2 = 0$.
[b] Not used in the overall equation.

considering all published data simultaneously (see Discussion). So, we conclude that there is no obvious reason to exclude the Greenlandic samples from our dataset. However, we also provide all the parameters of the regression equations calculated without the Greenlandic sample in Table 2.

The regression equation (4) presented here differs slightly from those published by Longinelli (1984), Luz et al. (1984; human bones), and Levinson et al. (1987; human teeth) (Table 2, Fig. 2b). The application of these various equations to extreme conditions can generate differences of several ‰ in the estimates of $\delta^{18}O_W$ values. Nevertheless, a single classification Analysis of Covariance (ANCOVA; Sokal and Rohlf, 1995) indicates that these four models do not differ from each other at a $\alpha = 0.01$ significance level (Table 3), a more secure and preferable type-I error rate than the usual $\alpha = 0.05$ error rate. This stricter criterion was preferred because: 1) different analytical techniques have been used by authors, 2) there are measurement errors and between-measures variability for most points, and 3) the number of points available in each of the four samples is small.

Consequently, the linear models calculated for the four sets of $\delta^{18}O_W/\delta^{18}O_P$ values (Longinelli, 1984; Luz et al., 1984; Levinson et al., 1987; this study) can be considered as random estimates of a unique $\delta^{18}O_W/\delta^{18}O_P$ linear relation that can be more accurately estimated by compiling the four sets into a single super-sample ($n = 42$). The least squares analysis of the whole set leads to the following overall equation (see also Fig. 3):

$$\delta^{18}O_W = 1.54(\pm 0.09) \times \delta^{18}O_P - 33.72(\pm 1.51)$$

$$(R^2 = 0.87 : p[H_0 : R^2 = 0] = 2 \times 10^{-19}) \quad (6)$$

Oxygen isotope composition of food water

The oxygen isotope compositions of the waters used for the experiment are ^{18}O-depleted (−10. or −11.2‰; water a) or enriched (7.8‰; water b) relative to SMOW (Table 4). While cooking, two chemical reactions operate: first, the water evaporates and becomes ^{18}O enriched, and second, there are exchanges of H_2O molecules between cooking water and food water. As a result, the oxygen isotopic compositions of the water of the cooked food ($\delta^{18}O_{cf}$) and of the final water ($\delta^{18}O_{fw}$) are close to each other and higher than the $\delta^{18}O$ of the initial water. The $\delta^{18}O$ of the water of the cooked food is closer to the value of the water of the raw food for initially highly-hydrated food (zucchinis and carrots; see Table 4) than for drier food (mackerel, beef, chicken, rice, lentils). The apparent isotopic fractionation between the water of the cooked food and the initial water ($\delta^{18}O_{cf} - \delta^{18}O_{iw}$ in Table 4) ranges from 1.2‰ to 6.2‰. The highest values are observed for vegetables.

Modeling the impact of solid food on the oxygen isotopic composition of ingested water

The values of $\Delta\delta^{18}O$ calculated according to equation 1, using the isotopic compositions of the tap water at Lyon (−10.5‰) and the parameters reported in Table 5, are shown in Fig. 4a (raw food) and 4b (cooked food). The vegetables, legumes, cereals, meat, and fish analyzed in this study were grown at some distance from the place where the water was collected in Lyon (see *Food water*). Thus, their oxygen isotopic composition is not linked to that of the local water (carrots, zucchini, and chicken are excepted as they are grown and farmed in the Lyon area). However, all foods originate from southeastern and southern Central France and cannot differ much isotopically from those of the Lyon area.

Discussion

Variability in the oxygen isotopic composition of drinking water

In most cases, the oxygen isotope compositions of measured tap waters differ only slightly from the yearly mean oxygen isotope

Table 3
Results of the single classification ANCOVA[a]

	Among groups		Within groups		Statistics	
	Sum of squares	d.f.	Sum of squares	d.f.	Fisher F	p-value[b]
Slopes	23.678	3	100.338	37	2.91	0.048
Intercepts	23.166	3	100.338	40	3.08	0.042

[a] d.f. = degrees of freedom.
[b] Associated to the slope and intercept comparisons indicating that the four individual $\delta^{18}O_P - \delta^{18}O_W$ linear models do not differ significantly from each other at the $\alpha = 0.01$ significance level (see text for comment).

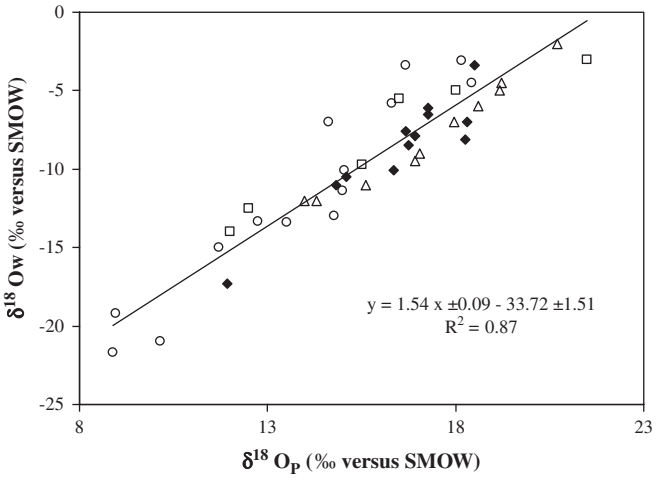

Fig. 3. Oxygen isotope fractionation equation resulting from the compilation of all the available data. Filled diamonds: this study; open triangles: Longinelli (1984); open circles: Levinson et al. (1987); open squares: Luz et al. (1984).

Table 4
H_2O content of the raw food in wt% (according to US Dept. Agriculture, Agricultural research Service, 2005), and oxygen isotope compositions ($\delta^{18}O_{‰}$ versus SMOW) of the water in the raw and in the cooked food initial and final waters. $\Delta_{c\text{-}iw} = \delta^{18}O_{cooked\ food} - \delta^{18}O_{initial\ water}$

	Zucchinis	Carrots	Mackerel	Beef	Chicken	Rice (a)	Rice (b)	Lentils (a)	Lentils (b)
H_2O wt%	95	88	63	65	75	10	10	10	10
$\delta^{18}O$									
Raw food	−4.0	−2.9	−2.1	−1.7	−3.7	−5.9	−5.9	0.8	0.8
Initial water	−10.5	−10.5	−11.2	−10.5	−10.5	−10.5	7.8	−10.5	7.8
Cooked food	−4.3	−4.3	−7.5	−7.7	−8.3	−7.9	9.7	−7.9	9.0
Final water	−6.4	−5.4	−9.5	−8.8	−9.9	−8.4	9.9	−8.4	9.3
$\delta^{18}O_{cf} - \delta^{18}O_{iw}$	6.2	6.2	3.7	2.8	2.2	2.6	1.9	2.6	1.2

compositions of precipitation calculated with the OIPC (Table 1). In Athens, Algiers, and Bordeaux there are larger discrepancies. The 1.6 and 1.7‰ differences between the oxygen isotopic values of tap waters and of OIPC estimates of present day rain at Algiers and Athens (Table 1) may be ascribed, at least partly, to an altitude influence. In the Mediterranean area, an altitude effect of −0.2 to −0.4‰/100 m has been measured (Bortolami et al., 1978; Leontiadis et al., 1996). A mean −0.3‰/100 m lapse rate would produce a $\delta^{18}O$ decrease of 1.0 to 1.3‰. The $\delta^{18}O$ value from Bordeaux (France) is 1.6‰ lower than the OIPC estimates for the area. If a $\delta^{18}O/T$ gradient of 0.6‰/°C (e.g., Von Grafenstein et al., 1996; Fricke and O'Neil, 1999) is considered, this difference corresponds to an atmospheric temperature 20,000 years ago that was 3 °C lower than today. During the Last Glacial Maximum, annual temperatures in this area are thought to have been ca. 12 °C lower (Jost et al., 2005; Kageyama et al., 2007), but the lack of precision of the dating and the likely mixing of waters of different ages preclude further comparison. In some areas, tap waters derive from tributaries or rivers that are not buffered by large reservoirs and are characterized by seasonal isotopic variations (e.g., Chao et al., 1996; Darling, 2004). In those cases, a one-off sampling is not representative of the yearly mean. The good correlation between our measured tap waters and the OIPC estimates ($R^2 = 0.89$) demonstrates that this effect, if any, is limited.

Even though the fractionation equations obtained with the tap waters and OIPC estimates of precipitations resemble each other, we argue, for the reasons stated above, that local measured waters (equation 4) should be preferred to estimated precipitations. Because drinking water represents from 0.6 to 0.75% of the total water ingested by a human, drinking water has a larger influence on $\delta^{18}O_P$. As tap water may differ from environmental water in modern countries, the isotope composition of the oxygen input flux is closer to the composition of the tap water. Therefore, the $\delta^{18}O_P/\delta^{18}O_W$ fractionation equation based on tap water is more appropriate. In historical and prehistorical times, human beings may have derived much of their water from surface water sources (lakes, rivers, streams), and hence, some of the limitations presented above may not be significant at these times (deep water catchments are less likely for instance). However, a range of factors (e.g., preservation of the "altitude signature" downstream for rivers, evaporative fractionation) may influence the isotopic composition of surface waters. Therefore, correcting back ancient teeth $\delta^{18}O_P$ signal to local rainfall isotopic composition may not be straightforward.

Table 5
Parameters of the mass balance calculation shown in Fig. 4

Parameter	Raw	Cooked	Reference
$[H_2O]_{veg}$ (weight %)	90	90	US Dept. Agriculture
$[H_2O]_{cl}$ (weight %)	10	72	US Dept. Agriculture
$[H_2O]_{mf}$ (weight %)	65	65	US Dept. Agriculture
$\delta^{18}O_{veg}$ (‰)	−3.5	−4.3	This work
$\delta^{18}O_{cl}$ (‰)	−2.6	−7.9	This work
$\delta^{18}O_{mf}$ (‰)	−2.5	−7.8	This work
M_W (Kg)	2.0		Howard and Bartram, 2003
M_F (Kg)	0.982		US Dept. Agriculture

Compatibility of the different $\delta^{18}O_W/\delta^{18}O_P$ fractionation equations

When compared to the four initial models (Table 2), the overall model (equation 6) shows markedly reduced uncertainties allowing more accurate predictions (lower associated standard error) of $\delta^{18}O_W$ values on the entire range of sampled $\delta^{18}O_P$ values (Table 6). For instance, for $\delta^{18}O_P$ values in the range of 12.5–19, where most of the individuals have been sampled, using the overall model allows the prediction of $\delta^{18}O_W$ values in the range from −4 to −14.5 with a 95% confidence interval <2 δ units (i.e., 1σ prediction error < 0.5 δ unit). Let us note that the 18th century Greenlandic sample, the representativeness of which was questioned earlier, is not an outlier in the overall scatter plot (Fig. 3).

Influence of the dietary behavior on the oxygen isotopic composition of enamel

Although oxygen isotopic signature of tooth enamel is related to drinking water, the inter-individual variability in the enamel composition is quite important (SD = 0.5‰ on average, up to 0.8‰ at Disko Bay). Food and cooking may play a part in this variation since the water absorbed by consumers ("total water") is the sum of drinking water and water ingested from solid food. Some food (cereals, legumes) contains only a few wt % water, whereas most vegetables are up to 95% water by weight (Table 4). Plants and meat are ^{18}O–enriched compared to meteoric water (e.g., Schmidt et al., 2001; Thiem et al., 2004). Therefore, the total water ingested by consumers may be ^{18}O–enriched compared to the meteoric water of their living place.

Kohn (1996) has shown the effect of diet on the oxygen isotopic composition of tooth enamel by studying some East African herbivores. The consumption of C_3 versus C_4 plants, in particular, accounts for at least a part of the isotopic interspecific variability. In humans, cooking complicates the relationship. In boiling, food becomes hydrated from the cooking water, which is ^{18}O–enriched through progressive evaporation. According to our data, the $\delta^{18}O$ of raw and cooked food are similar to each other if the food is initially hydrated (e.g., carrots, zucchinis). Therefore, the effect of such food consumption on the isotopic composition of the total water is more or less the same whether the food is raw or cooked. Cereals and legumes (rice, lentils) and meat and fish, which are seldom eaten raw, incorporate significant amounts of ^{18}O-enriched water during cooking (Tables 4 and 5). Therefore, their consumption is likely to increase the $\delta^{18}O$ of a person's total water.

According to our mass balance calculations, the maximum ^{18}O–enrichment of the total water compared to the drinking water is ca. 2‰ (corresponding to 1.1‰ in human enamel). This maximum enrichment occurs in a raw food diet with very high proportions of meat or vegetables, or in diets mainly based on cooked vegetables (Fig. 4). Therefore, at any given place, the water ingested by human beings via solid foods, whether it is raw or cooked, should not be richer in ^{18}O than is the total water ingested by herbivorous animals of the same place whose diet is composed of

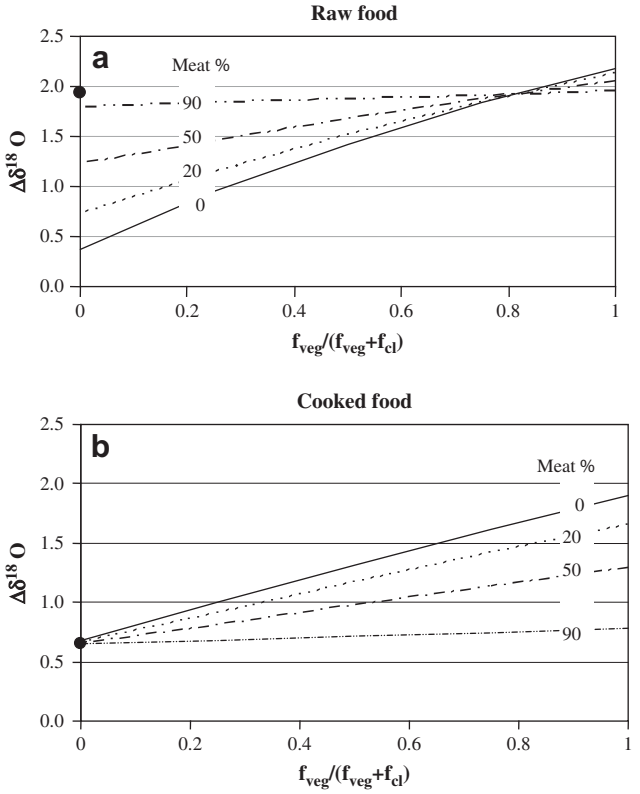

Fig. 4. Modeled isotopic enrichment of the total ingested water ($\Delta\delta^{18}0$ in ‰ versus SMOW). Three categories of food are considered: meat and fish (*mf*), vegetables and fruits (*veg*) and cereals and legumes (*cl*). The figures on the lines correspond to the fractions of meat + fish in the total food (f_{mf}). The figures of the x-axis represent the fractions of vegetables in the remaining part of the food ($f_{veg}/(f_{veg}+f_{cl})$).

raw plants (tree-leaves, fruits, and grass). Iacumin et al. (2004) have calculated the oxygen isotopic composition of precipitation ($\delta^{18}O_W$) 5,000 to 500 years ago in European Russia from humans and herbivorous animals (sheep, horse, deer). They observed that the $\delta^{18}O_W$ calculated from the herbivores was higher than that calculated from the human samples. They attributed this discrepancy to different drinking water sources or to diets. However, according to our calculations the effects of herbivorous versus omnivorous diets on the isotopic composition of the ingested water may be responsible for the observed difference.

Current human diet relies mainly on cooked food. Although the percentages of meat-fish, cereals-legumes, and vegetables-fruits consumed vary from individual to individual, mean values of 20–30% for the meat-fish component, 30–40% for the vegetables-fruits component, and 30–50% for the cereals-legumes components ($f_{veg}/(f_{veg}+f_{cl})$ of 0.4 to 0.6) are in general agreement with the statistics produced by the Food and Agriculture Organization (http://www.fao.org/). Such a diet induces a difference between the drinking water and the total ingested water of +1.05 to +1.20‰ (Fig. 4b). This difference corresponds to a shift in the $\delta^{18}O_P$ ranging from +0.6 to +0.7‰. Although there is the variability in the origin, amount, and proportion of the various types of food consumed, these figures show that the $\delta^{18}O_P$ recorded in tooth enamel of contemporaneous people is likely shifted towards values slightly higher than the values that would result from their drinking water alone. It is not possible to correct the measured $\delta^{18}O_P$ data for the effect of solid food consumption because the diets of the individuals are not known and may differ from one another. According to the estimation presented above, the interindividual variability of the $\delta^{18}O_P$ values (SD ca. ± 0.5‰ in this study; Table 1) may be ascribed only partly to intraindividual dietary differences (0.7–0.6 = 0.1‰ from the calculation above).

The regression of $\delta^{18}O_W$ on $\delta^{18}O_P$ (as in equation 6) implicitly assimilates the $\Delta\delta^{18}O$ shift, which is controlled by the relative proportions of the food components, to a systematic bias. It follows that the reconstruction of $\delta^{18}O_W$ from $\delta^{18}O_P$ yields accurate results if the proportions of an individual's diet are similar to modern proportions. If the $\Delta\delta^{18}O$ is higher than the contemporaneous value (1.05–1.20‰), the application of the regression equation leads to an overestimation of $\delta^{18}O_W$. An underestimation would result if $\Delta\delta^{18}O$ is lower.

Archaeological and isotopic evidence suggests that Paleolithic diets varied considerably through time and space. It is far beyond our goal to retrace the history of human diet. However, we can explore the effect on $\Delta\delta^{18}O$ of some specific diets (meat-rich and cereal-poor) that may approximate the extremes during the Paleolithic.

The influence of carnivory and cereal free diets in Neandertals and modern humans

The Neandertal diet has been argued to be essentially carnivorous (Fizet et al., 1995; Richards et al., 2000; Bocherens et al., 2005; Balter and Simon, 2006). If we take an extreme value, a raw diet composed of more than 90% fish and meat would have a $\Delta\delta^{18}O$ that is +1.9‰, or slightly higher than the modern diet (Fig. 4a). For the boiled equivalent, the shift decreases to +0.6‰. Archaeological sites deliver few clues about cooking practices. As a result, little is known about Neandertal recipes, but boiling may not have been a widespread practice. Indeed, it is likely that some meat was cooked on broach or cured (Kozlowski and Kozlowski, 1996; Patou-Mathis, 2006; methods referred to hereafter as "dry"). Due to the fact that ^{18}O preferentially remains and is enriched during evaporation, the $\delta^{18}O$ of the meat water increases with drying (Franke et al., 2007). The consumption of dry cooked meat induces a $\Delta\delta^{18}O$ larger than the shift corresponding to raw meat or to boiled or braised meat (i.e., > 1.9‰). Therefore, if the Neandertal diet is assumed to rely mainly on dry-cooked meat, the isotopic enrichment would be larger than the modern shift. As a consequence, using $\delta^{18}O_P$ of Neandertal teeth to reconstruct the oxygen isotopic

Table 6
$\delta^{18}O_W$ predicted values for $\delta^{18}O_W = 10, 15$, and 20, illustrating the markedly-better prediction accuracy of the overall model over the four individual models on the full range of measured $\delta^{18}O_P$-values. Mean and 95% confidence intervals in brackets

	$\delta^{18}O_P$			
	n	10	15	20
Longinelli (1984)	10	N.A.	−11.4 [−12.4; −10.4]	−3.8 [−4.9; −2.7]
Luz et al. (1984)	6	N.A.	−9.5 [−11.8; −7.0]	−3.5 [−7.0; 0.1]
Levinson et al. (1987)	14	−19.2 [−21.7; −16.7]	−9.5 [−11.1; −8.0]	N.A.
Daux et al. (This Study)	12	N.A.	−11.3 [−12.7; −9.8]	N.A.
Total	42	−18.3 [−19.9; −16.8]	−10.6 [−11.3; −9.9]	−2.9 [−4.1; −1.7]

N.A. = not available.

composition of ancient precipitation may overestimate this last parameter. However, roasting meat and fish on hot stones may also have been a common practice among Neandertal humans. This cooking method may not influence the water content, and correlatively the $\Delta\delta^{18}O$, as much as the other drying methods. Clearly, more experiments are needed to measure the extent of the isotopic enrichment induced by different dry cooking methods. Additional information about Neandertal diet would also be very valuable to refine these conclusions.

In some areas, cereals were staple foods as early as 23,000 years BP (wild wheat and barley at Ohalo II site, Israel; Weiss et al., 2004). Cooking is necessary for the processing of cereal grains. A diet containing cooked cereals induces a lower $\Delta\delta^{18}O$ than a cereal-free diet (Fig. 4b). During most of the Paleolithic times, human diet was cereal free ($fveg/(fveg + fcl) = 1$). In these conditions, the isotopic shift ranges between 1.3 and 1.7‰ for 50 to 20% meat and fish; this is 0.10 to 0.65‰ higher than the modern shift. Therefore, it can be concluded that the $\delta^{18}O_W$, deduced from the $\delta^{18}O_P$ of humans whose diets were cereal free (using equation 6), would be slightly overestimated.

Conclusions

The oxygen isotope composition of tooth enamel phosphate ($\delta^{18}O_P$) is related to the composition of the water ingested during the time of tooth mineralization. In this study, we propose a fractionation equation ($\delta^{18}O_P/\delta^{18}O_W$) defined over a large range of isotopic compositions (equation 6). This new equation is characterized by markedly reduced uncertainties allowing lower associated standard error (1σ prediction error < 0.5 δ unit) of $\delta^{18}O_W$ values on the entire range (12.5–19) of sampled $\delta^{18}O_P$ values.

During historical and prehistorical times, humans probably derived much of their drinking water from surface sources. These waters, however, may be different from the mean $\delta^{18}O$ of rainfall. Therefore, the paleo-environmental significance of the $\delta^{18}O_W$ values reconstructed from $\delta^{18}O_P$ may be complicated to infer. Ideally, a full understanding of the hydrological factors at the local scale is necessary to be confident in the validity of the interpretation.

The consumption of solid food (particularly vegetables) tends to increase the $\delta^{18}O$ of the total water ingested (drink + water in solids) by more than 1‰. In meat-rich and cereal-free diets, the difference between the $\delta^{18}O$ of the total ingested water and the drinking water is slightly higher than a modern diet (containing meat, fish, vegetables, fruits, cereals, and legumes). As a consequence, the oxygen isotopic composition of precipitation deduced from the $\delta^{18}O_P$ using equation 6 is slightly overestimated when the teeth analyzed belonged to humans whose diets were meat-rich or cereal-free. In the case of a meat-rich diet, this conclusion, however, depends on the type of cooking employed. Only certain kinds of heating that significantly reduce the water content of the meat (curing, cooking on broach) would have a sizable effect on $\delta^{18}O_W$. More information is needed to refine the estimation of the influence of specific diets on $\delta^{18}O_P$.

In addition to other isotopic ($\delta^{15}N$, $\delta^{13}C$) or archaeological methods, the analysis of the oxygen isotopic composition of teeth enamel can be used, in an independent manner, to compare the diets of human groups that lived close to each other (drinking water of the same isotopic composition) or to analyze the evolution of culinary practices at some places over climatically stable periods (constant $\delta^{18}O$ in the drinking water).

Acknowledgements

We are grateful to Drs. C. Gillet, P. Gaudreault, B. Belmecheri, D. Fontan, T.-P. Brisker, O. Lewden, and N'Tamak; the surgeons of the "Service de Stomatologie et Chirurgie maxillo-faciale" of the University of Louvain (B); and to an anonymous Iranian surgeon, for assistance in teeth collection. We thank U. Von Grafenstein, S. Belmecheri, M.–J. N'Tamak-Nida, D. Lewden, G. Matias, A. Bergeron, and Shoukou for helping in teeth collection, and B. Daux, E. Mercier, C. Robin, F. Baudin, B. Malaizé, and J.L. Turon for water collection. We are also grateful to M.J. Kohn for providing a comprehensive review of an early version of the paper, and to anonymous reviewers and S. Antón for their constructive remarks. This work was financially supported by the CNRS through the ECLIPSE program.

References

Altman, P.L., Dittmer, D.S., 1968. Metabolism. Federation of the American Society of Experimental Biologists, Bethesda, MD.
Ambrose, S.H., De Niro, M.J., 1986. Reconstruction of African human diet using bone collagen carbon and nitrogen isotope. Nature 319, 321–324.
Andersen, K.K., Ditlevsen, P.D., Rasmussen, S.O., Clausen, H.B., Vinther, B.M., Johnsen, S.J., Steffensen, J.P., 2006. Retrieving a common accumulation record from Greenland ice cores for the past 1800 years. J. Geophys. Res. 111 (D15), 11.
Balter, V., Simon, L., 2006. Diet and behavior of the Saint-Cézaire Néanderthal inferred from biogeochemical data inversion. J. Hum. Evol. 51, 329–338.
Bocherens, H., Drucker, D.G., Billiou, D., Patou-Mathis, M., Vandermeersch, B., 2005. Isotopic evidence for diet and subsidence pattern of the Saint-Cézaire I Neanderthal: review and use of a multi-source mixing model. J. Hum. Evol. 49, 71–87.
Bocherens, H., Fizet, M., Mariotti, A., Lange-Badré, B., Vandermeersch, B., Borel, J.P., Bellon, G., 1991. Isotopic biogeochemistry (^{13}C, ^{15}N) of fossil vertebrate collagen: implications for the study of fossil food web including Neandertal Man. J. Hum. Evol. 20, 481–492.
Bortolami, G.C., Ricci, B., Zuppi, G.M., 1978. Isotope hydrology of Val Corsiglia, Maritime Alps, Piedmont Italy. Isotope Hydrol. 1, 327–350.
Bowen, G.J., Revenaugh, J., 2003. Interpolating the isotopic composition of modern meteoric precipitation. Water Resour. Res. 39, 1299.
Bowen, G.J., Wilkinson, B., 2002. Spatial distribution of $\delta^{18}O$ in meteoric precipitation. Geology 30, 315–318.
Chao, Y., Telmer, K., Veizer, J., 1996. Chemical dynamics of the St. Lawrence riverine system: δD_{H2O}, $\delta^{18}O_{H2O}$, $\delta^{13}C_{H2O}$, $\delta^{34}S_{sulfate}$, and dissolved $^{87}Sr/^{86}Sr$. Geochim. Cosmochim. Acta 60, 851–866.
Clark, I.D., Fritz, P., 1997. Environmental Isotopes in Hydrogeology. Lewis Publishers, Boca Raton, pp. 328.
Crowson, R.A., Showers, W.J., Wright, E.K., Hoering, T.C., 1991. A method for preparation of phosphate samples for oxygen isotope analysis. Anal. Chem. 63, 2397–2400.
Darling, W.G., 2004. Hydrological factors in the interpretation of stable isotopic proxy data present and past: a European perspective. Quatern. Sci. Rev. 23, 743–770.
Daux, V., Lécuyer, C., Adam, F., Martineau, F., Vimeux, F., 2005. Oxygen isotope composition of human teeth and the record of climate changes in France (Lorraine) during the last 1700 years. Clim. Change 70, 445–464.
Dupras, T.L., Schwarcz, H.P., 2001. Strangers in a strange land: stable isotope evidence for human migration in the Dakhleh Oasis, Egypt. J. Archaeol. Sci. 28, 1199–1208.
Eberhardt, L.L., 1969. Similarity, allometry and food chains. J. Theor. Biol. 24, 43–55.
Epstein, S., Mayeda, T., 1953. Variations of $\delta^{18}O$ content of water from natural sources. Geochim. Cosmochim. Acta 4, 213.
Evans, J., Stoodley, N., Chenery, C., 2006. A strontium and oxygen isotope assessment of a possible fourth century immigrant population in a Hampshire cemetery, southern England. J. Archaeol. Sci. 33 (2), 265–272.
Firshing, F.H., 1961. Precipitation of silver phosphate from homogeneous solution. Anal. Chem. 33, 873–874.
Fizet, M., Mariotti, A., Bocherens, H., Lange-Badré, B., Vandermeersch, B., Borel, J.P., Bellon, G., 1995. Effect of diet, physiology and climate on carbon and nitrogen stable isotopes of collagen in a Late Pleistocene anthropic palaeoecosystem: Marillac, Charente, France. J. Archaeol. Sci. 22, 67–79.
Franke, B., Koslitz, S., Micaux, F., Maury, V., Pfammatter, E., Wunderli, S., Gremaud, G., Bosset, J.-O., Hadorn, R., Kreuzer, M., 2007. Tracing the geographic origin of poultry meat and dried beef with oxygen and strontium isotope ratios. Eur. Food Res. Technol, 9. Online.
Fricke, H.C., O'Neil, J.R., 1999. The correlation between $^{18}O/^{16}O$ ratios of meteoric water and surface temperature: its use in investigating terrestrial climate change over geologic time. Earth Planet. Sci. Lett. 170, 181–196.
Fricke, H.C., O'Neil, J.R., Lynnerup, N., 1995. Oxygen isotope composition of human tooth enamel from medieval Greenland: linking climate and society. Geology 23, 869–872.
Howard, G., Bartram, J., 2003. Water Supply Surveillance: A Reference Manual. WEDC, Loughborough, UK.
Iacumin, P., Nikolaev, V., Ramigni, M., Longinelli, A., 2004. Oxygen isotopes analyses of mammal bone remains from Holocene sites in European Russia: palaeoclimatic implications. Glob. Planet. Change 40 (1–2), 169–176.
Jacques, G., 1996. Le Cycle de l'Eau. Hachette, Paris, pp. 157.

Jost, A., Lunt, D., Kageyama, M., Abe-Ouchi, A., Peyron, O., Valdes, P.J., Ramstein, G., 2005. High resolution simulations of the last glacial maximum climate over Europe: a solution to discrepancies with continental paleoclimatic reconstructions? Clim. Dyn. 24, 577–590.

Kageyama, M., Lainé, A., Abe-Ouchi, A., Braconnot, P., Cortijo, E., 2007. Last glacial maximum temperatures over the North Atlantic, Europe and Western Siberia: a comparison between PMIP models, MARGO sea-surface temperatures and pollen-based reconstructions. Quatern. Sci. Rev. 25, 2082–2102.

Koehler, G., Wassenaar, L.I., Hendry, M.J., 2000. An automated technique for measuring δD and $\delta^{18}O$ values of porewater by direct CO_2- and H_2- equilibration. Anal. Chem. 72, 5659–5664.

Kohn, M.J., 1996. Predicting animal δ18O: accounting for diet and physiological adaptation. Geochim. Cosmochim. Acta 60, 4811–4829.

Kohn, M.J., Schoeninger, M.J., Valley, J.W., 1996. Herbivore tooth oxygen isotope compositions: effects of diet and physiology. Geochim. Cosmochim. Acta 60, 3889–3896.

Kozlowski, J.K., Kozlowski, S.K., 1996. Le paléolitique en Pologne. Préhistoire de l'Europe 2. Milton, Grenoble, France, pp. 240.

Lécuyer, C., Grandjean, P., Barrat, J.-A., Nolvak, J., Emig, C., Paris, F., Robardet, M., 1998. $\delta^{18}O$ and REE contents of phosphatic brachiopods: a comparison between modern and lower Paleozoic populations. Geochim. Cosmochim. Acta 48, 385–390.

Lécuyer, C., Grandjean, P., Emig, C.C., 1996. Determination of oxygen isotope fractionation between water and phosphate from living lingulids: potential application to palaeo-environmental studies. Palaeogeogr. Palaeoclimatol. Palaeoecol. 126, 101–108.

Lécuyer, C., Grandjean, P., O'Neil, J.R., Cappetta, H., Martineau, F., 1993. Thermal excursions in the ocean at the Cretaceous-Tertiary boundary (northern Morocco): the $\delta^{18}O$ record of phosphatic fish debris. Palaeogeogr. Palaeoclimatol. Palaeoecol. 105, 235–243.

Lee-Thorp, J.A., van der Merwe, N.J., Brain, C.K., 1994. Diet of *Australopithecus robustus* at Swartkrans from stable carbon isotopic analysis. J. Hum. Evol. 27, 361–372.

Leontiadis, J.L., Vergis, S., Christodoulou, Th., 1996. Isotope hydrology of areas in Eastern Macedonia and Thrace, Northern Greece. J. Hydrol. 182, 1–17.

Levinson, A.A., Luz, B., Kolodny, Y., 1987. Variations in oxygen isotopic compositions of human teeth and urinary stones. Appl. Geochem. 2, 367–371.

Longinelli, A., 1984. Oxygen isotopes in mammal bone phosphate: a new tool for paleohydrological and paleoclimatological research? Geochim. Cosmochim. Acta 48, 385–390.

Luz, B., Kolodny, Y., Horowitz, M., 1984. Fractionation of oxygen isotopes between mammalian bone-phosphate and environmental drinking water. Geochim. Cosmochim. Acta 48, 1689–1693.

Müller, W., Fricke, H., Halliday, A.N., McCulloch, M.T., Wartho, J.-A., 2003. Origin and migration of the Alpin Iceman. Science 302, 862–866.

OIPC: The Online Isotopes in Precipitation Calculator. Available from: http://www.waterisotopes.org/, 2008.

O'Neil, J.R., Adami, L.H., Epstein, S., 1975. Revised value for the ^{18}O fractionation between CO_2 and H_2O at 25°C. J. Res. US Geol. Surv. 3, 623–624.

O'Neil, J.R., Roe, J.L., Reinhard, E., Blake, R.E., 1994. A rapid and precise method of oxygen isotope analysis of biogenic phosphate. Isr. J. Earth Sci. 43, 203–212.

Patou-Mathis, M., 2006. Neanderthal. Une autre humanité. Perrin, Paris, pp. 342.

Richards, M.P., Jacobi, R., Cook, J., Pettitt, P.B., Stringer, C.B., 2005. Isotope evidence for the intensive use of marine foods by Late Upper Paleolithic humans. J. Hum. Evol. 49, 390–394.

Richards, M.P., Pettitt, P.B., Trinkaus, E., Smith, F.H., Paunovic, M., Karavanic, I., 2000. Neanderthal diet at Vindija and Neanderthal predation: the evidence from stable isotopes. Proc. Nat. Acad. Sci. U.S.A. 97, 7663–7666.

Schmidt, H.-L., Werner, R.A., Roßmann, A., 2001. ^{18}O pattern and biosynthesis of natural plant products. Phytochemistry 58, 9–32.

Sokal, R.R., Rohlf, F.J., 1995. Biometry: The Principles and Practice of Statistics in Biological Research. W.H. Freeman and Co., New York, pp. 887.

Sponheimer, M., Lee-Thorp, J., de Ruitter, D., Codron, D., Codron, J., Baugh, A.T., Thackeray, F., 2005. Hominids, sedges and termites: new carbon isotope data from the Sterkfontein valley and Kruger National Park. J. Hum. Evol. 48, 301–312.

Thiem, I., Lüpke, M., Seifert, H., 2004. Factors influencing the $^{18}O/^{16}O$ ratio in meat juices. Isot. Environ. Health Stud. 40, 191–197.

U.S. Department of Agriculture, Agricultural Research Service, 2005. USDA Nutrient Database for Standard Reference, Release 18. Nutrient Data Laboratory Home Page. Available from: http://www.ars.usda.gov/ba/bhnrc/ndl.

Van der Merwe, N.J., Thackeray, J.F., Lee-Thorp, J.A., Luyt, J., 2003. The carbon isotope ecology and diet of *Australopithecus africanus* at Sterkfontein, South Africa. J. Hum. Evol. 44, 581–597.

Vennemann, T.W., Fricke, H.C., Blake, R.E., O'Neil, J.R., Colman, A., 2002. Oxygen isotope analysis of phosphates: a comparison of techniques for analysis of Ag_3PO_4. Chem. Geol. 185, 321–336.

Von Grafenstein, U., Erlenkeuser, H., Müller, J., Trimborn, P., Alefs, J., 1996. A 200 year mid-European air temperature record preserved in lake sediments: an extension of the $\delta^{18}Op$-air temperature relation in the past. Geochim. Cosmochim. Acta 60, 4025–4036.

Weiss, E., Kislev, M.E., Simchoni, O., Nadel, D., 2004. Small-grained wild grasses as staple food at the 23 000-year-old site of Ohalo II, Israel. Econ. Bot. 58, 125–134.

White, C.D., Longstaffe, F.J., Spence, M.W., Law, K.R., 2000. Teotihuacan state representation at Kaminaljuyú: evidence from oxygen isotopes. J. Anthropol. Res. 56, 535–558.

White, C.D., Price, T.D., Longstaffe, F.J., 2007. Residential histories of the human sacrifices at the moon pyramid, Teotihuacan. Ancient Mesoamerica 18, 159–172.

Wright, L.E., Schwarcz, H.P., 1998. Stable carbon and oxygen isotopes in human tooth enamel: identifying breastfeeding and weaning in prehistory. Am. J. Phys. Anthropol. 106, 1–18.

References and Notes

1. T. Wirth, Ed., *Hypervalent Iodine Chemistry (Topics in Current Chemistry)* (Springer, Berlin, 2003), vol. 224.
2. V. V. Zhdankin, P. J. Stang, *Chem. Rev.* **108**, 5299 (2008), and references therein.
3. M. Ochiai, K. Miyamoto, *Eur. J. Org. Chem.* **2008**, 4229 (2008), and references therein.
4. T. Dohi, Y. Kita, *Chem. Commun. (Cambridge)* **2009**, 2073 (2009), and references therein.
5. According to International Union of Pure and Applied Chemistry rules, compounds with nonstandard bonding numbers are named using λ notation; thus, tri- and penta-valent iodine compounds are designated λ^3- and λ^5-iodanes, indicating that the iodine atoms have 10 and 12 valence electrons, respectively.
6. S. Quideau *et al.*, *Angew. Chem. Int. Ed.* **48**, 4605 (2009).
7. S. M. Altermann *et al.*, *Eur. J. Org. Chem.* **2008**, 5315 (2008).
8. T. Dohi *et al.*, *Angew. Chem. Int. Ed.* **47**, 3787 (2008).
9. M. Uyanik, T. Yasui, K. Ishihara, *Angew. Chem. Int. Ed.* **49**, 2175 (2010).
10. For the oxidation of iodide or iodine with hydrogen peroxide, see (*11*).
11. I. Matsuzaki, T. Nakajima, H. A. Liebhafsky, *Chem. Lett.* **3**, 1463 (1974), and references therein.
12. D. M. Bowen, J. I. DeGraw Jr., V. R. Shah, W. A. Bonner, *J. Med. Chem.* **6**, 315 (1963).
13. A. H. Banskota *et al.*, *J. Nat. Prod.* **61**, 896 (1998).
14. C. L. Céspedes, A. Uchoa, J. R. Salazar, F. Perich, F. Pardo, *J. Agric. Food Chem.* **50**, 2283 (2002).
15. G. Q. Shi *et al.*, *J. Med. Chem.* **48**, 5589 (2005).
16. G.-H. Chu *et al.*, *Bioorg. Med. Chem. Lett.* **15**, 5114 (2005).
17. J. L. Cohen, A. Limon, R. Miledi, A. R. Chamberlin, *Bioorg. Med. Chem. Lett.* **16**, 2189 (2006).
18. C. Ito *et al.*, *J. Nat. Prod.* **69**, 138 (2006).
19. J. A. Duan, L. Wang, S. Qian, S. Su, Y. Tang, *Arch. Pharm. Res.* **31**, 965 (2008).
20. Y. Uozumi, K. Kato, T. Hayashi, *J. Am. Chem. Soc.* **119**, 5063 (1997).
21. R. M. Trend, Y. K. Ramtohul, E. M. Ferreira, B. M. Stoltz, *Angew. Chem. Int. Ed.* **42**, 2892 (2003).
22. S. C. Pelly, S. Govender, M. A. Fernandes, H.-G. Schmalz, C. B. de Koning, *J. Org. Chem.* **72**, 2857 (2007).
23. S. Tanaka, T. Seki, M. Kitamura, *Angew. Chem. Int. Ed.* **48**, 8948 (2009), and references therein.
24. Materials and methods are available as supporting material on *Science* Online.
25. T. Ooi, K. Maruoka, *Angew. Chem. Int. Ed.* **46**, 4222 (2007), and references therein.
26. D. A. Evans, K. R. Fandrick, H.-J. Song, K. A. Scheidt, R. Xu, *J. Am. Chem. Soc.* **129**, 10029 (2007).
27. W. A. Bonner *et al.*, *Tetrahedron* **20**, 1419 (1964).
28. Y. Kawase, S. Yamaguchi, O. Inoue, M. Sannomiya, K. Kawabe, *Chem. Lett.* **9**, 1581 (1980).
29. S. Yamaguchi, S. Muro, M. Kobayashi, M. Miyazawa, Y. Hirai, *J. Org. Chem.* **68**, 6274 (2003).
30. Potassium hypoiodite (IOK) is generated in situ from I_2 and two equivalents of KOH, see (*31*).
31. S. Yamada, D. Morizono, K. Yamamoto, *Tetrahedron Lett.* **33**, 4329 (1992)
32. Financial support for this project was partially provided by a Grant-in-Aid for Scientific Research (#20245022) from the Japan Society for the Promotion of Science, the New Energy and Industrial Technology Development Organization, the Shionogi Award in Synthetic Organic Chemistry, Japan, and the Global Centers of Excellence Program in Chemistry of Nagoya University from the Ministry of Education, Culture, Sports, Science and Technology.

Supporting Online Material

www.sciencemag.org/cgi/content/full/328/5984/1376/DC1
Materials and Methods
SOM Text
Scheme S1
Tables S1 to S4
References

11 February 2010; accepted 23 April 2010
10.1126/science.1188217

Regulation of Body Temperature by Some Mesozoic Marine Reptiles

Aurélien Bernard,[1] Christophe Lécuyer,[1,2]* Peggy Vincent,[3] Romain Amiot,[1] Nathalie Bardet,[3] Eric Buffetaut,[4] Gilles Cuny,[5] François Fourel,[1] François Martineau,[1] Jean-Michel Mazin,[1] Abel Prieur[1]

What the body temperature and thermoregulation processes of extinct vertebrates were are central questions for understanding their ecology and evolution. The thermophysiologic status of the great marine reptiles is still unknown, even though some studies have suggested that thermoregulation may have contributed to their exceptional evolutionary success as apex predators of Mesozoic aquatic ecosystems. We tested the thermal status of ichthyosaurs, plesiosaurs, and mosasaurs by comparing the oxygen isotope compositions of their tooth phosphate to those of coexisting fish. Data distribution reveals that these large marine reptiles were able to maintain a constant and high body temperature in oceanic environments ranging from tropical to cold temperate. Their estimated body temperatures, in the range from 35° ± 2°C to 39° ± 2°C, suggest high metabolic rates required for predation and fast swimming over large distances offshore.

The metabolic status of extinct vertebrates is a key to understand their feeding strategy, which was critical for satisfying their daily energy requirements, as well as their potential to exploit cold environments. Phylogeny and ecology most likely had a large influence on the thermophysiology of past vertebrates. High metabolic rates mean the need to access large amounts of high-quality food, which may be satisfied by adopting predatory behavior, as shared by many carnivorous mammals, except scavengers. Endothermy is the ability to generate and retain enough heat to elevate body temperature to a high but stable level, whereas homeothermy is the maintenance of a constant body temperature in different thermal environments (*1*, *2*). Such internal production of heat is not restricted to mammals and birds. Heat generation can have several origins: digestive organs in mammals and birds (*1*) or muscles in endothermic lamniform sharks (*3*). Paladino *et al.* (*4*) proposed that some marine reptiles such as leatherback turtles display endothermy instead of inertial homeothermy, thus helping them to feed in cold waters. However, Lutcavage *et al.* (*5*) showed that the studied gravid female specimens raised their metabolic rates because of egg laying, thus biasing the evaluation of their true metabolic status. Most biologists agree that full or incomplete endothermy arose several times during species evolution and developed independently in several lineages. For example, partial endothermy is known in sharks, tunas, and even in some insects and flowers (*6*–*8*). The origin and spreading of endothermy are still a matter of great debate (*9*–*11*); its oldest occurrence could be as early as the Permian, with the appearance and radiation of the Synapsida. Among archosaurs, mass homeothermy or even endothermy have been proposed for dinosaurs (*12*) and pterosaurs (*13*) and suggested for the ancestors of crocodilians, because of the existence of a four-chambered heart, which modern crocodiles share with mammals and birds (*11*).

Large marine reptiles, including ichthyosaurs, plesiosaurs, and mosasaurs, inhabited the oceans from the Triassic to the Cretaceous. They represent three different lineages that became secondarily adapted to a marine mode of life. Ichthyosaurs evolved from basal neodiapsid reptiles, with the most obvious aquatic adaptations: a dolphin-like streamlined body without a neck, paddles, and a fish-like tail. Plesiosaurs are derived diapsids, which belong to the Sauropterygia, the sister group of the Lepidosauria (lizards and snakes). They are highly adapted for submarine locomotion, with powerful paddle-like limbs and heavily reinforced limb girdles. Motani (*14*) already discussed the possibility that plesiosaurs could not have had a typical reptilian physiology, thus indicating high metabolic activity. Mosasaurs constitute a family of Late Cretaceous varanoid anguimorphs highly adapted to marine life; they are derived lepidosaurs with an elongate body, deep tail, and paddle-like limbs (*15*). Both tooth morphology and the stomach contents of these three groups of marine reptiles indicate predatory behavior. Their anatomy could afford high cruising speeds and a basal metabolic rate similar to that of modern tunas (*16*). Moreover, the bone structure of adult

[1]CNRS UMR 5125, Paléoenvironnements et Paléobiosphère, Université Lyon 1, Lyon, 2 Rue Raphaël Dubois, 69622 Villeurbanne Cedex, France. [2]Institut Universitaire de France, 103 Boulevard Saint-Michel, 75005 Paris, France. [3]CNRS UMR 5143, Département Histoire de la Terre, Muséum National d'Histoire Naturelle, 8 Rue Buffon 75231 Paris, France. [4]CNRS UMR 8538, Laboratoire de Géologie de l'École Normale Supérieure, 24 Rue Lhomond, 75231 Paris, France. [5]Natural History Museum of Denmark, University of Copenhagen, Øster Voldgade 5-7, 1350 Copenhagen, Denmark.

*To whom correspondence should be addressed. E-mail: clecuyer@univ-lyonl.fr

plesiosaurs and mosasaurs corresponds to that of large pelagic marine predators designed for long cruises in open waters (*17*). The stomach contents of these marine reptiles have revealed that they were predators feeding on highly diverse foods, including other marine reptiles, fish, cephalopods, and crinoids (*18*). The metabolic status of these aquatic reptiles was also investigated through histological bone studies. It has been shown that Jurassic ichthyosaurs had rapid postnatal growth, followed by intense bone remodelling that could be related to a sustained metabolic rate close to that of marine endotherms (*9*).

Adaptation to cold marine waters was also revealed by the fossil reptile assemblage discovered in the Aptian southern high-latitude deposits of the White Cliffs in southeast Australia (*19*). The specimens were attributed to at least three families of plesiosaurs and at least one of ichthyosaurs. Paleoclimatic proxies indicate cold to near-freezing conditions at the seasonal scale, a climate mode that is not tolerated by modern ectothermic reptiles such as turtles or crocodiles. This observation suggests that some Mesozoic marine reptile taxa were able to cope with low-temperature marine environments (*19*). In this study, we investigated the metabolic status of ichthyosaurs, plesiosaurs, and mosasaurs using the oxygen isotope compositions ($\delta^{18}O$) of their phosphatic tissues.

The $\delta^{18}O$ value of vertebrate phosphate depends on both body temperature and the composition of ingested water (*20*). In the case of the studied reptiles, the estimated body temperatures recorded in the $\delta^{18}O$ value reflect that of the blood during tooth development; this should be also the case for some plesiosaurs that had protruding teeth. Within each studied reptile group, the

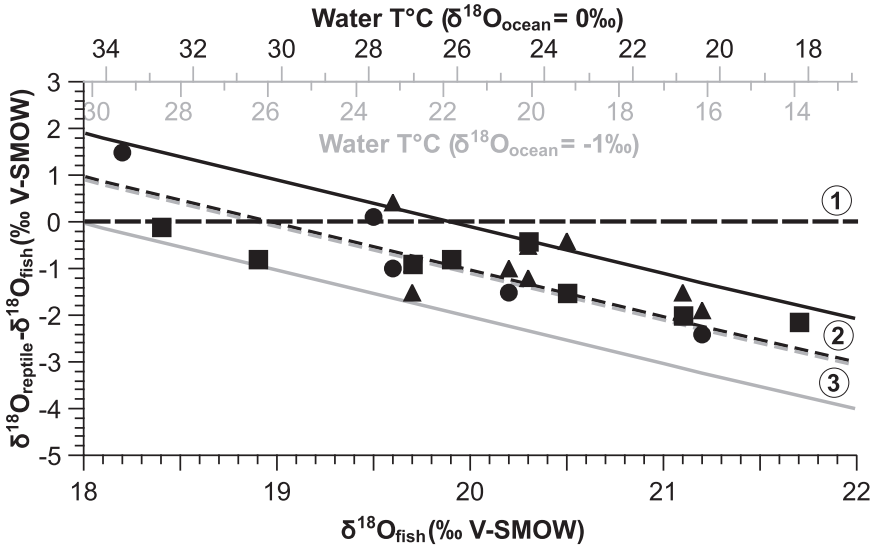

Fig. 1. Model variation of the differences in the $\delta^{18}O$ of tooth phosphate between marine reptiles and fish against the variation of the $\delta^{18}O$ of fish teeth, assuming (1) an ectothermic and poikilothermic reptile [body water $\delta^{18}O$ and body temperature (*T*) equal seawater $\delta^{18}O$ and seawater temperature]; (2) an endothermic reptile with body temperature ranging from 35°C (solid black line) to 39°C (dashed black line) and body water 2‰ enriched relative to a seawater value of 0‰; and (3) an endothermic reptile with body temperature ranging from 35°C (dashed gray line) to 39°C (solid gray line) and body water 2‰ enriched relative to a seawater value of −1‰. For comparison, ichthyosaur (circles), plesiosaur (triangles), and mosasaur (squares) values are reported. V-SMOW, Vienna SMOW values.

Table 1. Mean $\delta^{18}O$ values of tooth phosphate from worldwide Mesozoic ichthyosaurs, mosasaurs, and plesiosaurs, as well as coexisting marine fish.

Locality number	Locality	Age	Fish $\delta^{18}O$			Ichthyosaur $\delta^{18}O$			Plesiosaur $\delta^{18}O$			Mosasaur $\delta^{18}O$			Reference
			n	$\delta^{18}O$	SD	*n*	$\delta^{18}O$	SD	*n*	$\delta^{18}O$	SD	*n*	$\delta^{18}O$	SD	
1	South Dakota, USA	Early Campanian	2	19.8	0.1							1	18.5		(*24*)
2	Kansas, USA	Late Coniacian	3	18.9	0.8							1	18.1		(*24*)
3	Oulad Abdoun, Morocco	Maastrichtian	5	20.3	0.9				3	19.8	0.6	1	19.9		This study
4	Cambridge, UK	Late Albian	2	20.2	0.1	3	18.7	0.2	2	19.2	0.6				This study
5	Kimmeridge Clay, Westbury, UK	Kimmeridgian	4	19.5	0.1	2	19.6	0.6							This study
6	Oxford Clay, Peterborough, UK	Early Callovian	5	19.6	0.3	4	18.6	1.4	2	20.0	0.4				(*23*)
7	Sorel, France	Sinemurian	1	19.7					1	18.8					This study
8	Crussol, France	Middle Oxfordian	2	20.3	1.0				1	19.1					This study; (*26*)
9	Bourgogne, France	Early Oxfordian	1	21.2		1	18.8		1	19.3					This study
10	Maastricht, Netherlands	Maastrichtian	1	21.7					2	19.6					This study
11	Monte San Giorgio, Switzerland	Anisian	1	18.2		2	19.7	0.4							(*27*)
12	Asen, Sweden	Campanian	4	21.1	0.9				2	19.6	0.4	2	19.1	0.1	This study
13	Ullstorp, Sweden	Campanian	4	20.5	0.6				2	20.1	0.5	3	19.0	0.1	This study
14	Zefa, Israel	Late Campanian	3	19.7	0.4							1	18.8		(*25*)
15	Ruseifa, Jordan	Late Campanian	1	18.4								1	18.3		(*25*)
16	Toolebuc Formation, Australia	Albian	1	19.7					2	18.2	0.1				This study

taxonomic resolution is at the family level. Assuming that both reptiles and fish lived in the same water mass, differences in their $\delta^{18}O$ values would reflect differences in body temperature. To estimate the dependence of reptile body temperature on that of ambient water, we reported the difference in $\delta^{18}O$ value between coexisting marine reptiles and fish (belonging to the same sedimentary bed) as a function of the fish $\delta^{18}O$ value, which has been proven to be a valuable proxy of seawater temperature (*21*). A compilation was performed by combining 53 new (*22*) and 27 published (*23*–*27*) (table S1) $\delta^{18}O$ values of coexisting marine fish and reptile tooth remains recovered from worldwide sedimentary deposits of Triassic to Cretaceous ages. Figure 1 illustrates the principles of the relationship between coexisting reptile and fish temperature differences and seawater temperature. If reptile body temperatures mimic those of fish, $\delta^{18}O$ pairs are expected to plot along the horizontal null line. In the hypothetical scenario where reptile body temperature is constant and nearly independent of ambient water temperature, the isotopic pairs should lie on or close to a line with a slope of –1. Paired $\delta^{18}O$ data (Table 1) are compatible with linear distributions whose slopes for ichthyosaurs, plesiosaurs, and mosasaurs are –1.38 ± 0.20 [coefficient of determination (R^2) = 0.937], –1.08 ± 0.27 (R^2 = 0.480), and –0.70 ± 0.20 (R^2 = 0.588), respectively. Significant scattering in paired data is observed in Fig. 2, and it exceeds uncertainties associated with analytical measurements. Diagenetic alteration cannot be excluded for some samples, even though tooth enamel was favored because of its remarkable resistance to postdepositional alteration and recrystallization (*28*). Reptiles and fish collected from the same sedimentary bed may not be strictly contemporaneous, depending on how much time was condensed in the sedimentary layer. Contemporaneous reptiles and fish could have recorded distinct sea surface temperatures or water $\delta^{18}O$, because they lived at various depths or migrated seasonally for hunting or reproduction. However, the observed linear correlations are robust enough to indicate that reptile body temperature does not vary significantly with seawater temperature, except for mosasaurs, whose slope could suggest that body temperature could slightly decrease with decreasing ambient water temperature. Indeed, the range in $\delta^{18}O$ of fish close to 3 per mil (‰) means a temperature variation of 13°C, according to the slope of the oxygen isotope fractionation equation between fish phosphate and water [temperature (°C) = 113.3 – 4.38 ($\delta^{18}O_{phosphate}$ – $\delta^{18}O_{water}$)] that was determined by Kolodny *et al.* (*21*). This temperature range is valid only if the $\delta^{18}O$ value of surface marine waters was constant at various latitudes and for distinct water masses.

It is known that budgets of evaporation and precipitation over the oceans are responsible for various trends between $\delta^{18}O$ values of seawater and salinity (*29*). These relationships are difficult to apply to the past, especially for geological periods as old as the Mesozoic. At first order, we can consider that there is an ^{18}O enrichment of water by at least 1‰ relative to the mean ocean composition under low latitudes. Seawater tends to be ^{18}O-depleted by at least 1‰ when reaching latitudes above 50° as a consequence of precipitation dominating over evaporation; the $\delta^{18}O$ value can be even lower in the presence of continental masses with fluvial discharge, as observed in the present-day North Atlantic ocean off Canada, Greenland, and Norway. Consequently, the range in Mesozoic fish $\delta^{18}O$ values must be corrected by at least 2‰ because of the $\delta^{18}O$-salinity latitudinal gradient. In other words, the observed

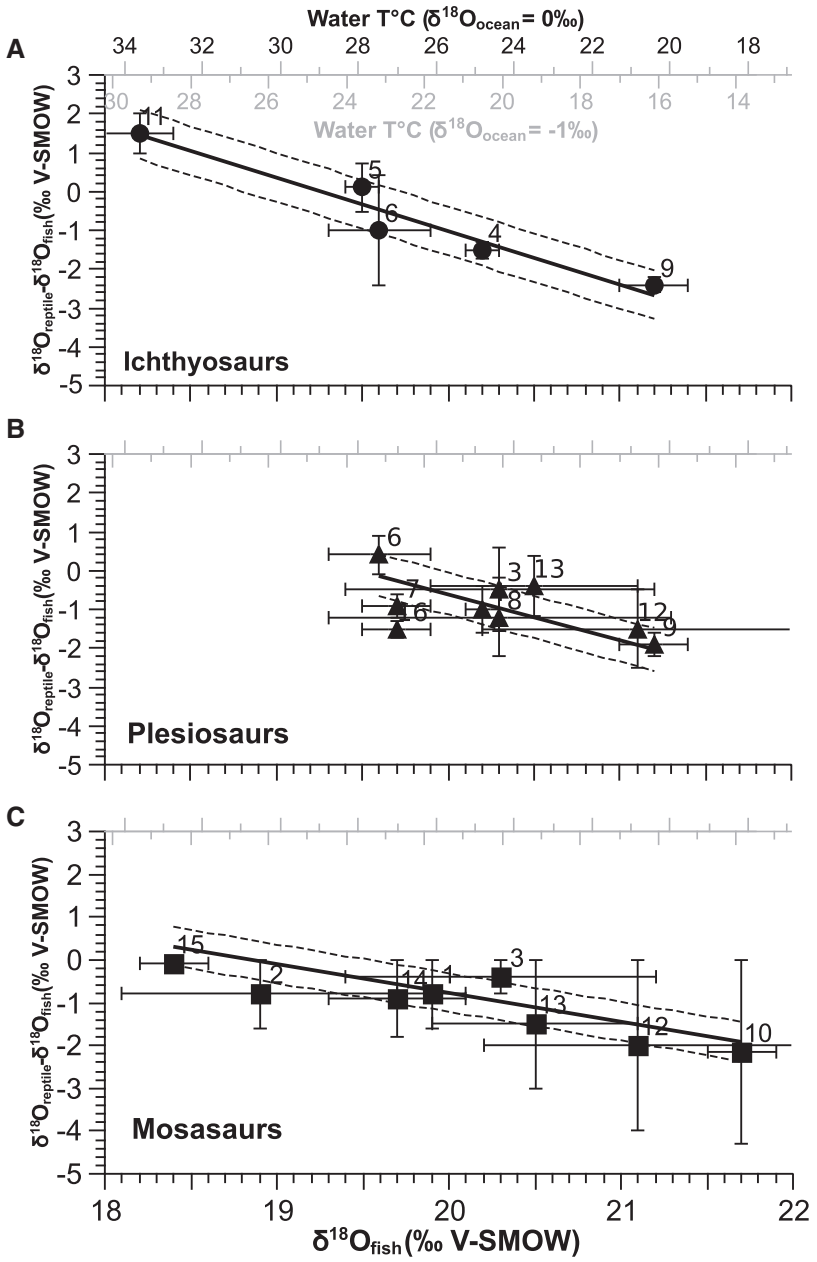

Fig. 2. Differences in the $\delta^{18}O$ of tooth phosphate between the three marine reptiles [(**A**) ichthyosaurs, (**B**) plesiosaurs, and (**C**) mosasaurs] and fish are reported against the $\delta^{18}O$ of fish teeth, approximating the body temperature differences between coexisting reptiles and fish and the seawater temperature where they lived (upper axis). The following reduced major axis regression lines with their 95% confidence limits are drawn: $y = -1.38\ (\pm 0.20) \times +26.53\ (\pm 3.07)$, $R^2 = 0.94$ (ichthyosaurs); $y = -1.08\ (\pm 0.27) \times +20.92\ (\pm 5.02)$, $R^2 = 0.48$ (plesiosaurs); and $y = -0.70\ (\pm\ 0.20) \times +12.89\ (\pm 3.37)$, $R^2 = 0.59$ (mosasaurs). Numbers refer to localities given in Table 1. Ichthyosaur and fish samples 11 from Monte San Giorgio should be considered cautiously for the following reasons: (i) a poor knowledge of the water salinity and consequently of the $\delta^{18}O$ value of ambient water. (ii) Triassic ichthyosaurs were not tuna-shaped yet, so their thermoregulation was most likely not well developed and difficult to compare with that of other Jurassic specimens. However, removing these data does not significantly change the slope value of the regression line (–1.336 instead of –1.377).

range of fish $\delta^{18}O$ values is translated into a temperature range of at least 25°C. Lécuyer *et al.* (*26*) have shown that the $\delta^{18}O$ of the global ocean most likely ranged from –1 to 0‰ [standard mean ocean water (SMOW) values] throughout the Jurassic and Cretaceous. Accordingly, the lowest temperatures of 12° ± 2°C correspond to the highest fish $\delta^{18}O$ values approaching 22‰, and the highest temperatures of 36° ± 2°C correspond to the lowest fish $\delta^{18}O$ values close to 18‰ (Fig. 2). Ichthyosaurs and plesiosaurs have $\delta^{18}O$ values similar to those of fish at a corresponding temperature range of 26° ± 2°C estimated from fish and seawater $\delta^{18}O$ values of 19.5‰ and –1 to 0‰, respectively (Fig. 2). The regression line for mosasaurs intercepts the horizontal null line at a lower $\delta^{18}O$ value of 18.5‰, thus indicating a possible higher body temperature of 30° ± 2°C. These temperature ranges are the minimal values that can be considered for ichthyosaur, plesiosaur, and mosasaur body temperatures if the $\delta^{18}O$ of their body equaled that of ambient seawater.

However, aquatic breathing vertebrates have body waters that are slightly ^{18}O-enriched relative to ambient water in the absence of transcutaneous evapotranspiration, and published data for modern aquatic reptiles reveal that this isotopic enrichment does not exceed 2‰ (*30*, *31*). Consequently, the body temperatures of studied ichthyosaurs and plesiosaurs could have been as high as 35° ± 2°C and even close to 39° ± 2°C for mosasaurs, according to Kolodny *et al.*'s equation (*21*). Both slope values of linear regressions and estimates of body temperatures are in good agreement with the swimming performances that were modeled for these three groups of marine reptiles. Massare (*32*, *33*) and Motani (*14*) suggested that ichthyosaurs were pursuit predators, whereas most mosasaurs were ambush predators, not requiring high metabolic rates all the time. Plesiosaurs were considered to have been cruisers, although slower than ichthyosaurs in sustained speed.

The $\delta^{18}O$ values of Mesozoic ichthyosaurs and plesiosaurs support the hypothesis that these large predators were able to regulate their body temperature independently of the surrounding water temperature even when it was as low as about 12° ± 2°C. In the case of mosasaurs, we cannot exclude the possibility that their body temperature was partly influenced by the temperature of ambient water. In any case, estimated body temperatures in the range from 35° ± 2°C to 39° ± 2°C encompass those of modern cetaceans (*34*) and suggest a high metabolic rate required for predation and fast swimming over large distances, especially in cold waters. $\delta^{18}O$ data from tooth phosphate reveal the existence of homeothermy for ichthyosaurs and plesiosaurs, and of at least partial homeothermy for mosasaurs, with in all cases a taxonomic resolution that does not exceed the family or infraclass. These three distinct phylogenetic groups of large marine reptiles were able to maintain a body temperature substantially higher than that of ambient marine waters, indicating that some kind of endothermy operated as an internal source of heat.

References and Notes

1. A. F. Bennett, J. W. Hicks, A. J. Cullum, *Evolution* **54**, 1768 (2000).
2. C. P. Hickman, L. S. Roberts, A. Larson, *Integrated Principles of Zoology* (McGraw-Hill Science, New York, 2000).
3. J. K. Carlson, K. J. Goldman, C. G. Lowe, in *Biology of Sharks and Their Relatives*, J. C. Carrier, J. A. Musick, M. R. Heithaus, Eds. (CRC Press, Boca Raton, FL, 2004), pp. 203–224.
4. F. V. Paladino, M. P. O'Connor, J. R. Spotila, *Nature* **344**, 858 (1990).
5. M. E. Lutcavage, P. G. Bushnell, D. R. Jones, *Can. J. Zool.* **70**, 348 (1992).
6. B. Heinrich, *Integr. Comp. Biol.* **29**, 1157 (1989).
7. B. A. Block, J. R. Finnerty, A. F. Stewart, J. Kidd, *Science* **260**, 210 (1993).
8. R. S. Seymour, *Plant Cell Environ.* **27**, 1014 (2004).
9. V. De Buffrénil, J. Mazin, *Paleobiology* **16**, 435 (1990).
10. R. S. Seymour, *Nature* **262**, 207 (1976).
11. R. S. Seymour, C. L. Bennett-Stamper, S. D. Johnston, D. R. Carrier, G. C. Grigg, *Physiol. Biochem. Zool.* **77**, 1051 (2004).
12. R. T. Bakker, *Nature* **238**, 81 (1972).
13. P. Wellnhofer, *The Illustrated Encyclopedia of Pterosaurs* (Crescent Books, New York, 1991).
14. R. Motani, *Paleobiology* **28**, 251 (2002).
15. M. J. Benton, *Vertebrate Palaeontology* (Wiley-Blackwell, Oxford, 2005).
16. R. Motani, *Nature* **415**, 309 (2002).
17. J. Wiffen, V. De Buffrénil, A. De Ricqlès, J.-M. Mazin, *Geobios* **28**, 625 (1995).
18. J. A. Massare, *J. Vertebr. Paleontol.* **7**, 121 (1987).
19. B. P. Kear, *Cretac. Res.* **26**, 769 (2005).
20. A. Longinelli, *Geochim. Cosmochim. Acta* **48**, 385 (1984).
21. Y. Kolodny, B. Luz, O. Navon, *Earth Planet. Sci. Lett.* **64**, 398 (1983).
22. Materials and methods are available as supporting material on *Science* Online.
23. T. F. Anderson, B. N. Popp, A. C. Williams, L. Ho, J. D. Hudson, *J. Geol. Soc. London* **151**, 125 (1994).
24. Y. Kolodny, B. Luz, in *Stable Isotope Geochemistry: A Tribute to Samuel Epstein*, H. P. Taylor, J. R. O'Neil, I. R. Kaplan, Eds. (Geochemical Society, University Park, St. Louis, MO, 1991), vol. 3, pp. 105–119.
25. Y. Kolodny, M. Raab, *Palaeogeogr. Palaeoclimatol. Palaeoecol.* **64**, 59 (1988).
26. C. Lécuyer *et al.*, *Paleoceanography* **18**, 1076 (2003).
27. Z. D. Sharp, V. Atudorei, H. Furrer, *Am. J. Sci.* **300**, 222 (2000).
28. A. Zazzo, C. Lécuyer, A. Mariotti, *Geochim. Cosmochim. Acta* **68**, 1 (2004).
29. M. R. Wadley, G. R. De Oliveira, E. J. Rohling, A. J. Payne, *Global Planet. Change* **32**, 89 (2002).
30. R. Amiot *et al.*, *Palaeogeogr. Palaeoclimatol. Palaeoecol.* **243**, 412 (2007).
31. R. E. Barrick, A. G. Fischer, W. J. Showers, *Palaios* **14**, 186 (1999).
32. J. A. Massare, *Paleobiology* **14**, 187 (1988).
33. J. A. Massare, in *Mechanics and Physiology of Animal Swimming*, L. Maddock, Q. Bone, J. M. V. Rayner, Eds. (Cambridge Univ. Press, Cambridge, 1994), pp. 133–149.
34. P. Morrison, *Biol. Bull.* **123**, 154 (1962).

35. The authors thank M. Sander, B. McNab, and R. Seymour for preliminary discussions of these data during the workshop dedicated to "Sauropod gigantism" that was held in Bonn, Germany, in November 2008. We are also grateful to D. Brinkman and J. Gardner (Royal Tyrrell Museum), S. Etches and J. Clarke, G. Suan, J. Lindgren (Lund University), B. Kear (La Trobe University), and A. Schulp (Maastricht University) for providing samples. L. Simon and G. Escarguel helped us in the statistical treatment of data. This study was funded by both CNRS and the Institut Universitaire de France.

Supporting Online Material

www.sciencemag.org/cgi/content/full/328/5984/1379/DC1
Materials and Methods
Table S1

25 January 2010; accepted 28 April 2010
10.1126/science.1187443

Climate Change Will Affect the Asian Water Towers

Walter W. Immerzeel,[1,2]* Ludovicus P. H. van Beek,[2] Marc F. P. Bierkens[2,3]

More than 1.4 billion people depend on water from the Indus, Ganges, Brahmaputra, Yangtze, and Yellow rivers. Upstream snow and ice reserves of these basins, important in sustaining seasonal water availability, are likely to be affected substantially by climate change, but to what extent is yet unclear. Here, we show that meltwater is extremely important in the Indus basin and important for the Brahmaputra basin, but plays only a modest role for the Ganges, Yangtze, and Yellow rivers. A huge difference also exists between basins in the extent to which climate change is predicted to affect water availability and food security. The Brahmaputra and Indus basins are most susceptible to reductions of flow, threatening the food security of an estimated 60 million people.

Mountains are the water towers of the world (*1*), including for Asia, whose rivers all are fed from the Tibetan plateau and adjacent mountain ranges. Snow and glacial melt are important hydrologic processes in these areas (*2*, *3*), and changes in temperature and precipitation are expected to seriously affect the melt characteristics (*4*). Earlier studies have addressed the importance of glacial and snow melt and the potential effects of climate change on downstream hydrology, but these are mostly qualitative (*4*–*6*) or local in nature (*7*, *8*). The relevance of snow and glacial melt for Asian river basin hydrology therefore remains largely unknown, as does how climate change could affect the downstream water supply and food security.

We examined the role of hydrological processes in the upstream areas, which we defined as

[1]FutureWater, Costerweg 1G, 6702 AA Wageningen, Netherlands. [2]Department of Physical Geography, Utrecht University, Post Office Box 80115, Utrecht, Netherlands. [3]Deltares, Post Office Box 80015, 3508 TC Utrecht, Netherlands.

*To whom correspondence should be addressed. E-mail: w.immerzeel@futurewater.nl

Freshwater Biology

Freshwater Biology (2010) **55,** 1560–1576 doi:10.1111/j.1365-2427.2010.02385.x

Relative influences of DOC flux and subterranean fauna on microbial abundance and activity in aquifer sediments: new insights from ^{13}C-tracer experiments

ARNAUD FOULQUIER*, LAURENT SIMON*, FRANCK GILBERT†,‡, FRANCOIS FOUREL§, FLORIAN MALARD* AND FLORIAN MERMILLOD-BLONDIN*

*UMR CNRS 5023, Ecologie des Hydrosystèmes Fluviaux, Université Claude Bernard Lyon 1, Villeurbanne Cedex, France

†Université de Toulouse, UPS, INP, EcoLab (Laboratoire d'écologie Fonctionnelle), Toulouse, France

‡CNRS, EcoLab, Toulouse, France

§UMR CNRS 5125, PaléoEnvironnements & PaléobioSphère, Université Claude Bernard Lyon 1, Villeurbanne Cedex, France

SUMMARY

1. Aquifers are considered to be controlled bottom-up because of their dependence on organic matter supply from surface ecosystems. Microorganisms are generally assumed to form the base of the food web and to respond strongly to organic matter supply. Although the bottom-up control of microorganisms by carbon sources has been well documented, the potential top-down control of obligate groundwater invertebrates on microorganisms has never been addressed in alluvial aquifers.

2. The main aims of the present study were (i) to quantify the relative influences of the activity of a subterranean amphipod (*Niphargus rhenorhodanensis*) and the flux of dissolved organic carbon (DOC) on organic matter processing and microbial activity, biomass and abundance in slow filtration columns mimicking an alluvial aquifer, and (ii) to determine the feeding rate of *N. rhenorhodanensis* on sedimentary microbes by tracing the flux of a ^{13}C-labelled source of DOC in batches (closed systems).

3. Slow filtration column experiments showed that microbial abundance, biomass and activity were primarily controlled by DOC flux, whereas the activity of *N. rhenorhodanensis* had only a slight effect on the microbial compartment. Modelling of carbon fluxes in the ^{13}C-tracer experiments indicated that the feeding activity of the amphipod was too low to significantly modify microbial growth and activity.

4. Our experiments supported the hypothesis that groundwater ecosystems are controlled bottom-up. The small influence of *N. rhenorhodanensis* on the microbial compartment was probably linked to its slow metabolism. Our results highlight the need for further experiments to examine the relationship between metabolic rates of subterranean organisms and their role in ecosystem functioning.

Keywords: animal–microbe interactions, bottom-up control, carbon cycle, *Niphargus rhenorhodanensis*, top-down control

Introduction

Aquatic subterranean ecosystems are heterotrophic, their functioning depending on the supply of allochthonous organic matter originating from surface ecosystems. The lack of photosynthesis (and primary production) in ground water implies that the food

Correspondence: Florian Mermillod-Blondin, UMR CNRS 5023, Ecologie des Hydrosystèmes Fluviaux, Université Claude Bernard Lyon 1, Bât Forel, 43 Bd 11 Novembre 1918, F-69622 Villeurbanne Cedex, France.
E-mail: mermillo@univ-lyon1.fr

webs are truncated (Gibert & Deharveng, 2002). Theory predicts that heterotrophic and organic matter-limited environments such as groundwater ecosystems are controlled bottom-up because the quantity and quality of organic matter entering the system determine food web structure (Malard *et al*., 1994; Notenboom, Plénet & Turquin, 1994; Datry, Malard & Gibert, 2005). The soil and vadose zone (between the ground surface and the water table) act as strong physical, chemical and biological filters that dramatically reduce the transfer of organic detritus (particulate organic matter – POM) from surface to ground water. Consequently, dissolved organic carbon (DOC) is the main source of food for life in aquifers (e.g. Starr & Gillham, 1993). Accordingly, Simon, Benfield & Macko (2003) showed that microorganisms which process DOC represented the main food resource for higher trophic levels in a karstic system. In the hyporheic zone, several studies (e.g. Findlay *et al*., 1993; Claret & Fontvieille, 1997; Craft, Stanford & Pusch, 2002) have demonstrated the significance of DOC availability for microbial growth, with microorganisms being a potential food source for invertebrates (Bärlocher & Murdoch, 1989). In a phreatic aquifer, Datry *et al*. (2005) reported increased densities of groundwater invertebrates in zones enriched with DOC and suggested that a DOC-induced enrichment of microbial biomass stimulated the abundances of groundwater invertebrates.

Although this 'bottom-up view' of groundwater ecosystems is largely accepted, there have been no attempts to quantify the influence of the obligate groundwater fauna on the microbial compartment and DOC consumption and assimilation in alluvial groundwater ecosystems (Gibert *et al*., 2009). In a recent review, Boulton *et al*. (2008) pointed out that obligate groundwater invertebrates should affect many of the microbial processes involved in the C and N cycles in a similar way to that observed for surface-dwelling aquatic invertebrates. In sediments, grazing activities of invertebrates may enhance biofilm productivity (e.g. Traunspurger, Bergtold & Goedkoop, 1997), whereas bioturbation activities (burrowing, gallery building, and faecal pellet production) may indirectly influence microbial communities through modifications of physicochemical conditions (Danielopol, 1989; Mermillod-Blondin & Rosenberg, 2006). However, clear evidence of the role of invertebrates in microbial processes in sediment has essentially been limited to surface-dwelling species that lack many of the behavioural and physiological adaptations to food limitation shared by most obligate groundwater invertebrates (Hervant, Mathieu & Barré, 1999a). Thus, the main aim of the present study was to test whether a model obligate groundwater species, the amphipod *Niphargus rhenorhodanensis* Schellenberg had a significant influence on the microbial compartment and organic matter processing in aquifer sediments. This species was selected because it is the most abundant and widely distributed subterranean macroinvertebrate in the alluvial aquifer of the Rhône River (Dole-Olivier & Marmonier, 1992). Two laboratory experiments were developed (i) to quantify the relative influences of amphipod activities (top-down control) and the flux of DOC (bottom-up control) on the microbial compartment and DOC processing in slow filtration columns mimicking an alluvial aquifer habitat and (ii) to determine the feeding rate of *N. rhenorhodanensis* on attached bacteria by tracing the flux of a ^{13}C-labelled source of DOC in batches.

Methods

Collection of sediments

Gravel collected from the Rhône River was sieved manually to select particle sizes ranging from 5 to 8 mm and then was cleaned with deionised water before being dried at 60 °C. For the two experiments, 10 kg of fresh sand was collected at a depth of 1 m below the bed of a gravel pit intersecting the water table of a glaciofluvial aquifer using the Bou–Rouch method (Bou & Rouch, 1967). DOC concentrations in ground water collected from this glaciofluvial aquifer ranged from 0.4 to 0.9 mg L^{-1}. Groundwater temperature was 14.5 ± 0.3 °C, and dissolved oxygen (DO) concentrations ranged from 5.8 to 6.7 mg L^{-1}. Particulate organic carbon contained in the collected sand was 0.42 ± 0.03 mg g^{-1} of sediment dry mass, and the abundance of bacteria associated with sand was 2.1 10^8 bacteria g^{-1} of sediment dry mass. After collection, the sand was manually sieved to select particle sizes ranging from 100–1000 μm and then kept in an oxygenated water bath in the laboratory two days before experiments started.

Collection of subterranean organisms

The obligate groundwater amphipod *Niphargus rhenorhodanensis* (dry weight = 1.0–1.3 mg), which inhabits both karstic and alluvial aquifers, is an opportunistic species showing a generalist feeding strategy (Ginet, 1960; Danielopol, 1989). Individuals of *N. rhenorhodanensis* were collected using traps buried at a depth of 5 cm in the sediment of a ditch draining the alluvial aquifer of the Dombes Forest, France (45°58′28′N, 5°24′25′E, clade I in Lefébure *et al*., 2007). To acclimatise animals to experimental conditions (temperature, granulometry and food), they were maintained in the laboratory for more than 15 days before the experiment started.

Experiment I: relative influences of N. rhenorhodanensis and DOC flux on microbial compartment in slow filtration microcosms

Slow filtration column experiments were conducted to test for the influences of amphipod activity (top-down control) and the flux of DOC (bottom-up control) on microbial compartment and DOC processing in sediments. Columns had an inside diameter of 10 cm and consisted of two experimental modules (10 cm high) topped by a third module of 5 cm in height (Fig. 1a). They were filled with inert gravel and fresh sand to a height of 15 cm. About 10 cm of water was left above the sediment surface. Masses of gravel (500, 500 and 400 g) and sand (150, 150 and 120 g) were alternately introduced into the columns to obtain a heterogeneous porous media. During sediment introduction, particle tracers (luminophores) were deposited at depths of 2.5–3.5 cm (1 g of yellow luminophores) and 6–7 cm (1 g of pink luminophores) below the sediment surface to estimate sediment reworking induced by amphipods (method described below).

Experiments were performed at constant temperature (15 ± 0.5 °C) in the dark. The columns were supplied from the top with reconstituted ground water (96 mg L^{-1} $NaHCO_3$, 39.4 mg L^{-1} $CaSO_4$ $2H_2O$, 60 mg L^{-1} $MgSO_4$ $7H_2O$ and 4 mg L^{-1} KCl, 19 mg L^{-1} $Ca(NO_3)_2$ $4H_2O$) using a peristaltic pump controlling a constant infiltration flow rate of 2 mL min^{-1}. Supplied water was aerated to maintain concentrations of DO between 8.5 and 9.5 mg L^{-1} at the inlet of the columns. The experiment was designed to couple three modalities of DOC flux (i.e. 60, 180 and 300 μg h^{-1} of C by modifying the concentration of easily degradable DOC sodium acetate supplied to columns) with two modalities of fauna (absence or

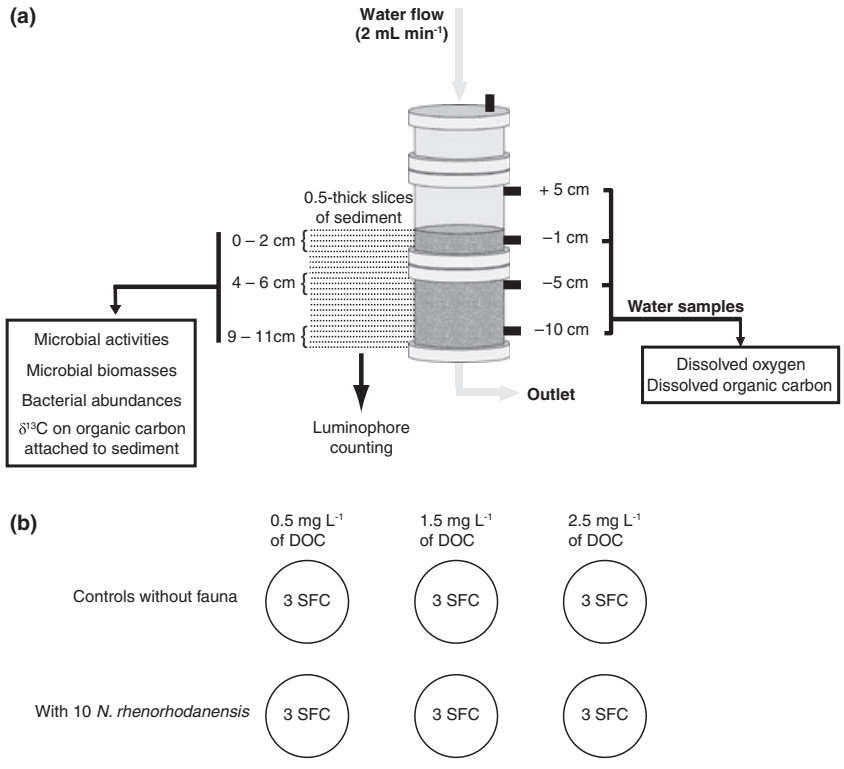

Fig. 1 Schematic representation of slow filtration columns indicating the positions of sampling (a) and experimental design of the experiment I in slow filtration columns (b). SFC = slow filtration column.

presence of 10 individuals of *N. rhenorhodanensis*) to test for the interaction between DOC supply and the activity of *N. rhenorhodanensis* on organic matter processing and microbial parameters (Fig. 1b). A total of six experimental treatments were tested with three replicate columns per treatment. Dissolved acetate supplied to all columns was enriched with 0.2% of ^{13}C-marked acetate ($^{13}C_2H_4O_2$, 99 atom% ^{13}C; Sigma–Aldrich, Saint-Quentin Fallavier, France) to determine the assimilation of DOC in attached bacteria and amphipods. The δ^{13}C of the DOC solution supplied to columns was 135 ‰.

After 1 week of column stabilisation, 10 individuals of *N. rhenorhodanensis* were introduced in half of the columns (n = 3 columns per DOC treatment). Amphipod density in slow filtration columns (i.e. 8.4 individuals L^{-1} of sediment) was similar to that measured in artificial substrata inserted in the bed sediment of streams (7.2 ± 2.6 individuals L^{-1} of sediment, Mathieu & Essafi-Chergui, 1990). Measurements of DOC and DO were made at four depths (5 cm above the sediment surface, and 1, 5 and 10 cm below the sediment surface) on days 0 (before addition of amphipods in the system), 6, 10, 14, 18, 22 and 26 after the addition of *N. rhenorhodanensis* to determine the removal rates of DOC and DO (aerobic respiration) in slow filtration columns (Fig. 1a). After the last measurements (day 26), columns were dismantled, the water layer was removed and columns were opened to sample sediment (Fig. 1a). The top 11 cm of fresh sediment were sampled in 0.5 cm thick slices. Each layer was sieved to remove gravel and invertebrates, homogenised, and a 1 g sub-sample was used for sediment reworking analyses (see below). Remaining fresh sediments corresponding to three layers (0–2, 4–6 and 9–11 cm below the sediment surface) were used to analyse the $^{13}C/^{12}C$ ratio of bacteria (incorporation of acetate in bacteria, see model in Data analysis section), bacterial abundance (numbers of bacteria and active eubacteria), microbial activities (hydrolytic activity, dehydrogenase activity) and biochemical markers of biofilm biomass (carbohydrates and proteins). Carbohydrates and proteins were used to estimate biomasses of extracellular polymeric substances and bacterial cells, respectively (Foulquier A., Mermillod-Blondin F., Malard F. & Gibert J., *submitted*). Individuals of *N. rhenorhodanensis* were recovered from columns to analyse their $^{13}C/^{12}C$ ratio and calculate the incorporation rate of ^{13}C-enriched microbial biomass in animals (see model in Data analysis section). After collection, *N. rhenorhodensis* were kept 48 h in glass bowls with tap water to clear their gut contents before stable isotope analyses.

Experiment II: incorporation of DOC in the food web

We designed a second experiment with simplified experimental units to quantify the assimilation of DOC in attached bacteria and subterranean amphipods. A total of 36 erlenmeyer flasks were used to measure bacterial growth and the temporal dynamics of $^{13}C/^{12}C$ ratio in bacteria and amphipods. Flasks (250 mL) were filled with 30 g dry mass of fresh sand (collected and treated as in Experiment I) and 160 mL of reconstituted ground water (ionic composition as in Experiment I). Reconstituted ground water was enriched with ^{13}C-labelled acetate ($^{13}C_2H_4O_2$, 99 atom% ^{13}C) to fit an initial concentration of 25 mg L^{-1} of DOC and a $^{13}C/^{12}C$ ratio of 47 atom%. The concentration of DOC (25 mg L^{-1}) used in this experiment was higher than the DOC concentrations used in slow filtration columns (<3 mg L^{-1}). However, the application of a high concentration of ^{13}C-labelled DOC was necessary to obtain significant ^{13}C enrichments in bacteria and amphipods for the calculation of carbon assimilation rates. Four individuals of *N. rhenorhodanensis* were introduced in half of the flasks (n = 18) to measure their capacity to modify DOC incorporation in attached bacteria and to feed and incorporate bacterial carbon in their tissues. At six dates during the experiment (0, 12, 24, 48, 72 and 96 h), three flasks of each treatment (absence or presence of *N. rhenorhodanensis*) were killed to determine DOC concentrations in the overlying water, number of bacteria and active eubacteria on the sediment, and the $^{13}C/^{12}C$ ratios of the bacteria and amphipods (used for calculation of assimilation rates, see model in Data analysis section). As indicated for experiment I, collected amphipods were kept 48 h in glass bowls with tap water to clear their gut contents.

Physical, chemical and microbial analyses

Sediment reworking analyses. Sediment reworking by amphipods was assessed using luminophores (natural sediment particles of 350–500 μm in size, dyed with a fluorescent paint) as particle tracers (Gerino *et al.*, 1998). Each sub-sample of fresh sediment

collected at the end of the experiment from 0.5 cm thick slices was lyophilised for luminophore counting. Detection of luminophores was performed under UV light (digital camera Olympus C-2500L; Olympus France, Rungis, France) for automatised counting on acquired images (image analysis software Image-Pro Plus). Luminophore quantities were reported in terms of quantity of dry sand collected in each slice.

Dissolved oxygen and DOC analyses. Dissolved oxygen measurements in slow filtration columns were made with an oxygen microsensor probe (Unisense, Aarhus, Denmark) directly connected to the four lateral water outlets, thereby preventing any contact with atmospheric oxygen. Water samples for DOC analyses were filtered through HAWP filters (porosity: 0.45 μm; Millipore, Billerica, MA, U.S.A.) and analysed with a total carbon analyser (multi N/C® 3100; Analytik Jena, Jena, Germany) based on thermocatalytic oxidation and MC-NDIR detection after removing inorganic carbon with hydrochloric acid (5 μL mL^{-1}) and CO_2 stripping under 15 min oxygen flow.

Stable isotope analysis. Sediment samples (with attached bacteria) and amphipods were oven dried at 50 °C for at least 48 h and then crushed using a mortar and pestle. About 500 mg of dry sediments were placed in pre-cleaned Oakridge centrifugation tubes and 2 M HCl was added for 12 h at room temperature to remove calcite. After centrifugation at 2500 *g* during 5 min, the supernatant was discarded; sediments were rinsed three times with ultrapure water and oven dried at 50 °C. An amount of 2.5 mg of dry sediments were weighted in tin capsules for stable isotope analysis. Dry amphipods were placed in glass vials and acidified with 400 μL of 2 M HCl to remove calcium carbonate. Samples were oven dried at 50 °C without subsequent rinse. A total of 250 μg of dry amphipod were weighted in tin capsules for stable isotope analysis.

Stable isotope ratios of carbon ($^{13}C/^{12}C$) were measured by continuous flow stable isotope ratio mass spectrometer (CF-IRMS) using a GVI Isoprime mass spectrometer interfaced with a Eurovector Euro-EA3028-HT elemental analyser. $^{13}C/^{12}C$ ratios were expressed as δ in part per thousand (‰) and referenced to V-PDB standard. The analytical precision achieved for tyrosine standards analysed along with the samples was better than 0.1‰ (± standard deviation).

Microbial analyses. The DNA intercalating dye (DAPI) and a Cy3 probe (EUB 338, eubacteria) were used on sediment samples to determine the total number of bacteria and the percentages of active eubacteria. Sediment samples (1 g) were fixed, homogenised, spotted on slides and hybridised according to Mermillod-Blondin *et al.* (2005). Slides were mounted with Citifluor solution (Citifluor Ltd, London, U.K.), and the preparations were examined at 1000× magnification with a BH2-RFCA Olympus microscope fitted for epifluorescence with a high-pressure mercury bulb (50 W) and filter sets BP 405 (for DAPI) and BP 545 (for Cy3). Bacteria from the samples were analysed in 20 fields per sample with up to 30 cells per field. Numbers of DAPI and Cy3 bacteria were counted separately from the same field to determine the percentages of active eubacteria (% Cy3 bacteria/DAPI bacteria). Total numbers of bacteria were expressed as number of cells g^{-1} dry weight (DW) of sediment.

The 2-(p-iodophenyl)-3-(p-nitrophenyl)-5-phenyl tetrazolium chloride (INT) was used to measure dehydrogenase activity as modified from Houri-Davignon, Relexans and Etcheher (1989). Sediment samples (1 g fresh weight) were incubated into a 0.02% INT solution (final solution) for 2 h at 15 °C and then filtered on a nylon membrane (0.22 μm, MSI). Controls were prepared by adding formaldehyde (2% final) in INT solution. Extraction of INT formazan was made in vials containing 5 mL of methanol. Each vial was sonicated at 100 W during two periods of 60 s using a sonicator fitted with a 2-mm-diameter probe (Sonicator XL 2020; Misonix Inc., Farmingale, NY, U.S.A.) to increase solvent extraction yield (Maurines-Carboneill *et al.*, 1998). The INT formazan extract was measured by a spectrophotometer adjusted at 480 nm against control blank. The quantity of INT formazan was computed by using the molar extinction coefficient of 18 000 M^{-1} cm^{-1} at 480 nm and was expressed as μmol of INT h^{-1} g^{-1} DW of sediment.

Hydrolytic activity was estimated using the fluorescein diacetate (FDA) hydrolysis method (Jørgensen, Eriksen & Jensen, 1992). Sediment samples (1 g fresh weight) were placed into 3 mL of a pH 7.6 phosphate buffer solution with 0.15 mL of 4.8 mM FDA solution. The incubation was maintained for 1 to 3 h until a green colouration of fluorescein appeared. The reaction was stopped by freezing the sample after the addition of 4.5 mL of a solution of $HgCl_2$

(400 mg L^{-1}). Fluorescein concentration was estimated from the absorbance of the filtered supernatant (0.45 μm, Millipore) measured at 490 nm and was expressed as μmol of FDA h^{-1} g^{-1} DW of sediment.

Total proteins on sediment were measured according to the Lowry method modified by Peterson (1977), using the Sigma Protein Assay Kit (P 5656 Sigma Diagnostics, St Louis, MO, USA). Concentration was expressed as mg of protein g^{-1} DW of sediment.

Carbohydrates were quantified on dry sediment (24 h at 60 °C in an oven) using the Dubois method (Dubois *et al.*, 1956). A homogenised sample of dry sediment (0.25 g) was mixed with 1 mL of a phenol solution (10%) and 5 mL of sulphuric acid (95%). Incubation was performed at room temperature in the dark for 1 h. Absorbance of the supernatant was measured at 495 nm, and carbohydrate content was expressed as mg of carbohydrates g^{-1} DW of sediment.

Data analysis

Experiment I. The quantification of luminophore redistribution following sediment reworking by *N. rhenorhodanensis* was realised using a model inspired by the gallery-diffusion model of François *et al.* (2002). This model describes both the diffusive-like mixing of particles in the region of intense burrowing activity (D_b) and the non-local mixing pattern (r) associated with a biologically induced transfer of particles from one layer to another in a discontinuous pattern (i.e. a non-continuous transport; Boudreau, 1986; Meysman, Boudreau & Middelburg, 2003). Detailed information about this model can be found in Gilbert *et al.* (2007). Biodiffusion-like coefficients of particles obtained for yellow and rose luminophores were compared among DOC and fauna treatments using a two-way analysis of variance (ANOVA). Tukey's *post hoc* tests were performed to identify significant pairwise differences between treatments.

Concentrations of DO and DOC measured on day 26 at 4 depths in slow filtration columns were used to calculate the removal rate of DOC and DO in three sediment layers (i.e. 0–2, 2–5 and 5–10 cm below the sediment surface) as follows:

$$RR = (\Delta_C \times Q)/(V \times P) \quad (1)$$

Where:

RR: Removal rate of DOC and DO in mg h^{-1} L^{-1} sediment

Δ_C: Difference in DOC or DO concentration (mg L^{-1}) between two consecutive layers

Q: water discharge (L h^{-1}) through the sediment layer

V: volume of the sediment layer (L)

P: porosity

A three-way ANOVA was used to test for the effects of depth, DOC flux and amphipods on the removal rates of DO and DOC, microbial parameters (abundance, activities and biochemical markers) and $^{13}C/^{12}C$ ratio of attached bacteria. A one-way ANOVA was used to compare the $^{13}C/^{12}C$ ratio of amphipod tissues collected at the end of the experiment between DOC treatments. Tukey's *post hoc* tests were performed to identify significant pairwise differences between treatments.

Experiment II. Student's *t*-tests were performed on measurements made at 0 h to verify that there were no differences in DOC concentrations, bacterial counts and $^{13}C/^{12}C$ ratios of attached bacteria between the 2 series of flasks (n = 3) attributed to each fauna treatment before addition of *N. rhenorhodanensis*. After 0 h, a two-way ANOVA with fauna (presence or absence of *N. rhenorhodanensis*) and time (12, 24, 48, 72 and 96 h) was used to test for differences in the temporal dynamics of DOC, bacterial counts and $^{13}C/^{12}C$ ratios of attached bacteria between fauna treatments. A one-way ANOVA was used to compare the $^{13}C/^{12}C$ ratios of amphipod tissues among dates.

Modelling of carbon fluxes. The modelling of carbon fluxes between DOC, attached bacteria and *N. rhenorhodanensis* was performed using a similar approach as in Mauclaire *et al.* (2003). Bacteria growth was assumed to follow Monod kinetics (Monod, 1942). The bacterial uptake of DOC (C_{DOC}) over time t in the experimental system was described by the following differential equation:

$$\frac{dC_{DOC}}{dt} = -\frac{1}{Y_1}\mu_1 \frac{C_{DOC}}{K_s + C_{DOC}} B \quad (2)$$

where B was the carbon biomass of bacteria (g C bacteria), K_S was the Monod constant (mg C), μ_1 was the maximum growth rate of bacteria (day^{-1}) and Y_1 was the carbon conversion efficiency between acetate and bacterial biomass (g C bacteria g^{-1} C_{DOC}). The

feeding rate of amphipods on bacteria was assumed to depend on the bacterial biomass and we neglected biomass changes because of natural decay, which yielded the equation:

$$\frac{dN}{dt} = \mu_2 BN \quad (3)$$

with N as amphipod biomass (g C amphipods) and μ_2 as growth rate (g^{-1} C bacteria day^{-1}).

Total change of bacteria biomass was then calculated as follows:

$$\frac{dB}{dt} = \left(\mu_1 \frac{C_{DOC}}{K_s + C_{DOC}} B\right) - \mu_3 B - \frac{1}{Y_2}\mu_2 BN \quad (4)$$

where μ_3 was the bacteria natural decay rate (day^{-1}) and Y_2 was the carbon conversion efficiency between bacteria and amphipod biomasses (g C amphipods g^{-1} C bacteria).

^{13}C fluxes were modelled to describe changes in the $^{13}C/^{12}C$ ratio of attached bacteria and amphipod tissues. We assumed that there was no isotopic fractionation between DOC and attached bacteria, and between bacteria and amphipods during C assimilation. This assumption was a reasonable simplification because C isotope fractionations during aerobic metabolism are generally low (0 to few ‰), thus negligible relatively to the high ^{13}C enrichment of this study. The change of ^{13}C mass in DOC was given by:

$$\frac{d^{13}C_{DOC}}{dt} = -\frac{1}{Y_1}\mu_1 \frac{^{13}C_{DOC}}{K_s + C_{DOC}} B \quad (5)$$

while the evolution through time of ^{13}C in bacteria ($^{13}C_B$) and amphipods ($^{13}C_N$) was expressed as:

$$\frac{d^{13}C_B}{dt} = \left(\mu_1 \frac{^{13}C_{DOC}}{K_s + C_{DOC}} B\right) - \mu_3\, ^{13}C_B - \frac{1}{Y_2}\mu_2\, ^{13}C_B N \quad (6)$$

$$\frac{d^{13}C_N}{dt} = \mu_2\, ^{13}C_B N \quad (7)$$

The carbon mass and the isotopic compositions of the DOC, bacteria and amphipods were computed at each time step by solving the system of differential equations (2–7) that described the carbon and ^{13}C mass balances using a fourth-order Runge-Kutta numerical integration procedure (Press *et al.*, 1992). To compare the result of the model to the experimental data, the carbon isotope composition of total organic carbon attached to sediment (comprising the organic carbon contained in bacterial cells and bacterial exopolymeric substances) was calculated using a simple mass-balance equation:

$$\delta^{13}C_{TOC} = \frac{B\delta^{13}C_B + C^i_{TOC}\delta^{13}C^i_{TOC}}{B + C^i_{TOC}} \quad (8)$$

where C^i_{TOC} was the total organic carbon attached to sediments at the start of the experiment.

Cell bacterial biomass at the start of the experiment was estimated from DAPI counts using a conversion factor of 30 fg of C $cell^{-1}$ (Fukuda *et al.*, 1998; Troussellier *et al.*, 1997). Invertebrates contained about 500 μg of C per individual at $t = 0$.

Unknown parameters of the model (μ_1, μ_2, μ_3, K_S, Y_1 and Y_2, Table 1) were calculated by adjusting the simulation results to measured DOC concentrations, $\delta^{13}C$ values of total organic carbon and $\delta^{13}C$ of amphipod tissues. The quality of the fit between modelled and measured data was evaluated by calculating the sum of the squared differences between observed and calculated values.

For all parametric tests, homoscedasticity and data normality were checked using Levene's tests and Shapiro's tests, respectively. Whenever necessary, data were ln or square-root transformed to homogenise variances and fit data normality. For variables

Table 1 Biodiffusion-like coefficients (Db) calculated for luminophores deposited in two depth layers of the columns for the six experimental treatments. DOC1 = 60 μg C h^{-1}, DOC2 = 180 μg C h^{-1}, and DOC3 = 300 μg C h^{-1}. Values are means (SD). n = 3 columns per treatment

Depth of luminophore deposition (cm)	Treatment	Db (cm^2 $year^{-1}$)
2.5–3.5	DOC1 * control	0.76 (0.39)
	DOC1 * *N. renorhodanensis*	0.52 (0.32)
	DOC2 * control	0.36 (0.17)
	DOC2 * *N. renorhodanensis*	0.47 (0.40)
	DOC3 * control	0.15 (0.02)
	DOC3 * *N. renorhodanensis*	0.17 (0.05)
6.0–7.0	DOC1 * control	0.85 (0.19)
	DOC1 * *N. renorhodanensis*	1.07 (0.46)
	DOC2 * control	1.29 (0.66)
	DOC2 * *N. renorhodanensis*	0.84 (0.28)
	DOC3 * control	1.09 (0.76)
	DOC3 * *N. renorhodanensis*	0.84 (0.14)

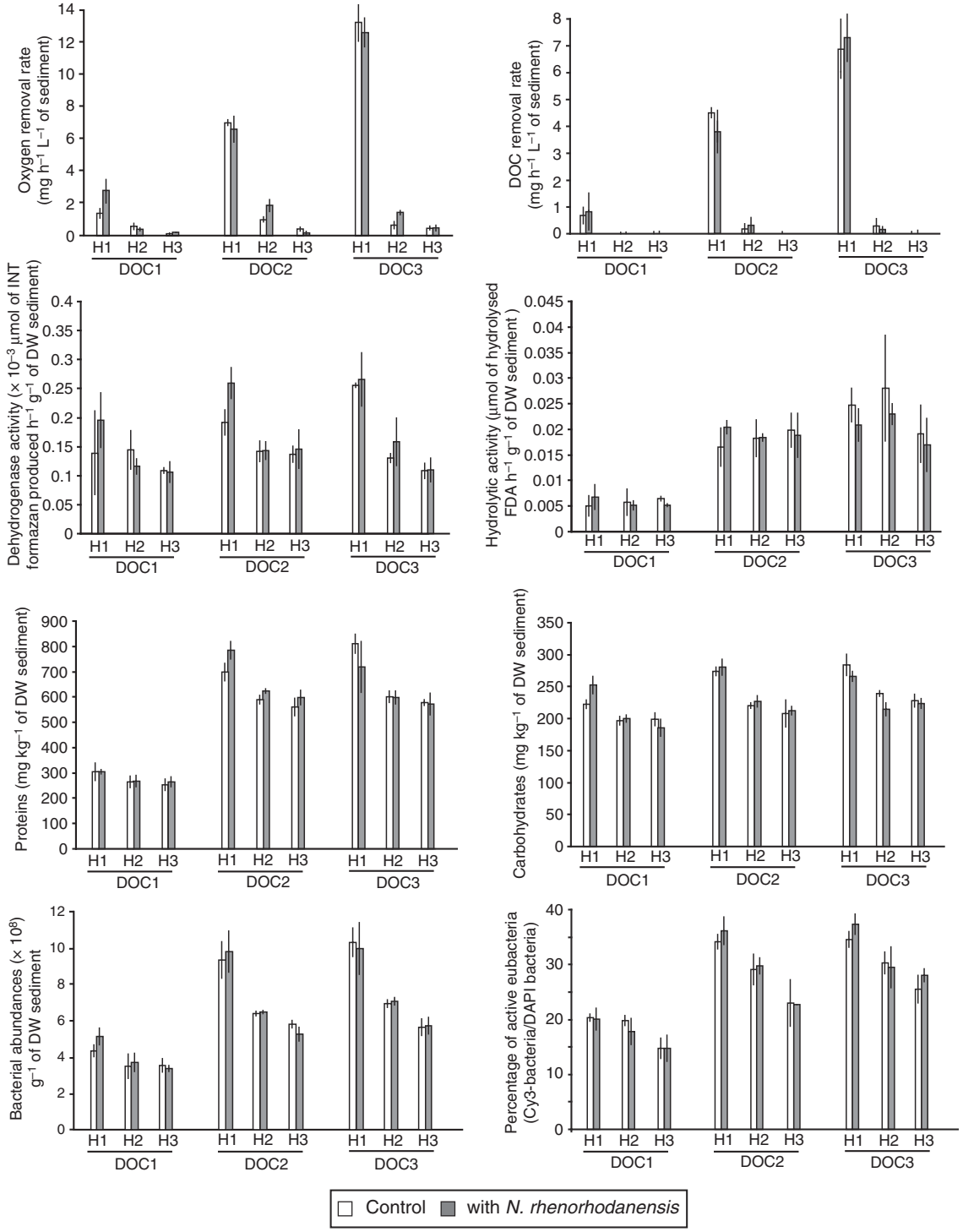

Fig. 2 DO and DOC removal rates, and microbial activities, biomasses and abundances measured at three layers in columns for the six tested treatments (3 DOC flux treatment × 2 animal treatments) in experiment I. Symbols for DOC supply: DOC1 = 60 μg C h^{-1}, DOC2 = 180 μg C h^{-1} and DOC3 = 300 μg C h^{-1}. Symbols for depth layers: H1 = 0–2 cm, H2 = 4–6 cm and H3 = 9–11 cm below the sediment surface. Values are means ± SD (n = 3 columns per treatment).

expressed as percentages (% of active eubacteria), data were arcsine transformed. All statistical analyses were performed using Statistica 5™ (Statsoft, Tulsa, OK, U.S.A.).

Results

Experiment I: relative influences of N. rhenorhodanensis and DOC flux on microbial compartment in slow filtration microcosms

The luminophore vertical profiles were diffusive-like shapes, indicating a preferential occurrence of random mixing events over short distances in the columns. This induced the production of diffusion-like coefficients (D_b) and the absence of non-local coefficients (r) by the gallery-diffusor model. The diffusion-like coefficients (Db) were not significantly affected by the presence and activity of the amphipods (Table 1, two-way ANOVA, fauna effect, $F_{(1.12)} < 0.4$, $P > 0.5$ for the two investigated sediment layers).

Most variables showed no significant influence of *N. rhenorhodanensis* on the microbial compartment (Fig. 2, Table 2). Amphipods had only significant positive effects on DO removal rate and dehydrogenase activity in slow filtration columns, but these effects depended on depth as well as on 'depth × DOC flux' interactions for DO removal rate (Table 2). For instance, *Niphargus rhenorhodanensis* increased DO removal rate by 97% in the top 2 cm of sediment columns receiving a DOC flux of 60 μg C h^{-1}, whereas it had no significant effect (−5.4%) at the same depth in the treatment with a DOC flux of 180 μg h^{-1} (Fig. 2).

On the contrary, the increase in DOC flux had a significant positive effect (Table 2, Fig. 2) on microbial processes (DO removal, DOC removal, and dehydrogenase and hydrolytic activities), microbial biomass (proteins and carbohydrates) and bacterial counts (total number of cells and percentage of active eubacteria). In the top 2 cm of sediments, the DOC removal rate, DO consumption, protein concentration and bacterial abundance increased by 552, 389, 129 and 102%, respectively, as the DOC flux increased from 60 to 180 μg C h^{-1}. The influence of DOC supply on microbial parameters decreased with increasing depth in slow filtration columns except for hydrolytic activity (Table 2). As a consequence of the influence of vertical DOC fluxes on microorganisms, all microbial variables were positively correlated with the DOC removal rates measured in slow filtration columns (Table 3).

The δ^{13}C value of total organic carbon attached to sediment also increased significantly with increasing DOC flux and decreased with depth (Fig. 3a, Table 2). This δ^{13}C signature was highly correlated with the DOC removal rate and the microbial variables (Table 3) indicating that carbon from acetate was incorporated into bacterial biomass. *N. rhenorhodanensis* did not have a significant influence on δ^{13}C of total organic carbon attached to sediment (Table 2) but δ^{13}C values of amphipods showed a higher incorporation of organic carbon in their tissues for the highest DOC treatment (Fig. 3b, one-way ANOVA, $F_{(3,9)} = 7.4$, $P < 0.01$).

Experiment II: incorporation of DOC in the food web

DOC decreased rapidly with time (Fig. 4a, Table 4) owing to consumption by the microbial compartment, the abundance of which concomitantly increased over time (Fig. 4b, Table 4). The percentage of active eubacteria also evolved significantly during the experiment but to a lesser extent than the total number of bacteria (Fig. 4c). The occurrence of *N. rhenorhodanensis* did not significantly affect the microbial compartment although amphipods significantly delayed the DOC decrease during the experiment (Fig. 4a, Table 4).

A significant increase in δ^{13}C was measured in bacteria attached to sediment (Fig. 5b, two-way ANOVA, time effect, $F_{(4,18)} = 67.3$, $P < 0.001$) and tissues of amphipods (Fig. 5c, one-way ANOVA, $F_{(5,12)} = 39.9$, $P < 0.001$). The best model fit of DOC concentration (Fig. 5a) and $^{13}C/^{12}C$ ratio of total organic carbon associated with sediments (Fig. 5b) and amphipods (Fig. 5c) was obtained with parameter values reported in Table 5. According to differences in DOC decrease with time between control and fauna treatments ('time × fauna' effect in Table 4), a lower half velocity constant (K_S) and a higher maximum growth rate of bacteria (μ_1) were estimated in the control treatment in comparison with the fauna treatment (Table 5). Although amphipods delayed DOC decrease and reduced bacterial growth rate, the conversion coefficient of DOC into bacterial carbon (Y_1) was increased by 18% with *N. rhenorhodanensis*

Table 2 ANOVA results for the effects of DOC fluxes, occurrence of *N. rhenorhodanensis* and depth on removal rates of dissolved oxygen and dissolved organic carbon, microbial activities, proteins, carbohydrates and bacterial abundances in slow filtration columns (d.f.: degrees of freedom; DOC RR: dissolved organic carbon removal rate; DO RR: dissolved oxygen removal rate; INT: deshydrogenase activity; FDA: hydrolytic activity, BA: bacterial abundance; % AE: percentage of active eubacteria)

		DOC RR		DO RR		INT		FDA		Proteins		Carbohydrates		BA		% AE		Sedimentary $\delta^{13}C$	
Effect	d.f.	*F*	*P*	*F*	*P*	*F*	*P*	*F*	*P*	*F*	*P*	*F*	*P*	*F*	*P*	*F*	*P*	*F*	*P*
DOC flux	2	13.20	<0.001	313.1	<0.001	11.76	<0.001	128.3	<0.001	950.3	<0.001	49.59	<0.001	226.69	<0.001	179.0	<0.001	64.69	<0.001
Fauna	1	0.25	0.62	13.12	<0.001	5.23	<0.05	0.10	0.75	0.76	0.39	0.12	0.73	0.41	0.52	0.23	0.63	0.35	0.56
Depth	2	109.5	<0.001	1884	<0.001	67.75	<0.001	0.93	0.40	84.09	<0.001	133.2	<0.001	120.54	<0.001	62.17	<0.001	185.7	<0.001
DOC flux * Fauna	2	0.28	0.75	1.08	0.35	0.53	0.59	0.85	0.43	7.08	<0.01	6.16	<0.01	0.52	0.60	0.99	0.38	0.79	0.46
DOC flux * Depth	4	11.84	<0.001	226.5	<0.001	5.68	<0.01	1.90	0.13	6.92	<0.001	1.83	0.15	2.54	0.06	1.9	0.13	32.8	<0.001
Fauna * Depth	2	0.47	0.63	5.02	<0.05	4.165	<0.05	0.56	0.58	0.32	0.73	1.63	0.21	1.54	0.23	0.9	0.41	0.43	0.65
DOC flux * Fauna * Depth	4	0.95	0.44	12.93	<0.001	1.56	0.21	0.80	0.54	1.77	0.16	3.21	<0.05	1.02	0.40	0.29	0.88	2.11	0.10
Error	36																		

(Table 5). The growth rate of amphipods reported as bacterial biomass (μ_2) was 0.35 μg C bacteria day^{-1}. The carbon conversion efficiency of bacteria biomass to amphipods (Y_2) was 0.06, indicating that *N. rhenorhodanensis* incorporated 6% of the bacterial carbon it consumed into biomass.

Discussion

In recent years, there has been increased interest in the role potentially played by fauna in ground water (Boulton, 2000; Boulton *et al*., 2008). Several studies were performed on animal communities living in the hyporheic zone (Danielopol, 1989; Marshall & Hall, 2004; Mermillod-Blondin *et al*., 2004) or in karstic systems (Edler & Dodds, 1996; Kinsey, Cooney & Simon, 2007; Cooney & Simon, 2009), but very few attempts were made to specifically assess the role of obligate groundwater invertebrates inhabiting alluvial aquifers. In conformance with the bottom-up hypothesis, our results clearly showed that microbial biomass and activity in our experimental columns were predominantly driven by DOC fluxes. As observed along subsurface flowpaths (Findlay *et al*., 1993; Marmonier *et al*., 1995; Sobczac & Findlay, 2002), sediment respiration (DO removal rate), bacterial activity and abundance were controlled by the availability of DOC flowing through the slow filtration columns. The occurrence of the subterranean amphipod *N. rhenorhodanensis* had a slight influence on microbial activities and DOC processing. For instance, even if *N. rhenorhodanensis* could increase by 97% the oxygen respiration in the uppermost 2 cm of sediments (but only with a DOC flux of 60 μg h^{-1}), an increase in DOC flux from 60 to 180 μg h^{-1} enhanced by 389% the oxygen respiration in the same sediment layer. The overriding effect of DOC supply on microbial activities (respiration rate, organic carbon consumption, dehydrogenase and hydrolytic activities), biomass (protein and carbohydrate contents) and abundances (total number of bacteria and number of active eubacteria) indicated a predominance of bottom-up control over top-down control on groundwater microbial communities in our experiments. This finding is in accordance with the generally held view that microbial growth and activities are essentially dependent on dissolved organic matter entering ground water (Ghiorse & Wilson, 1988; Goldscheider, Hunkeler & Rossi, 2006).

Table 3 Correlations between biogeochemical processes, microbial variables and sedimentary $\delta^{13}C$ obtained in slow filtration columns (DOC RR: dissolved organic carbon removal rate; DO RR: dissolved oxygen removal rate; INT: dehydrogenase activity; FDA: hydrolytic activity, BA: bacterial abundance; % AE: percentage of active eubacteria)

Variables	DOC RR	DO RR	INT	FDA	Proteins	Carbohydrates	BA	% AE
DO RR	$R = 0.912$							
	$P < 0.001$							
INT	$R = 0.786$	$R = 0.805$						
	$P < 0.001$	$P < 0.001$						
FDA	$R = 0.368$	$R = 0.425$	$R = 0.420$					
	$P < 0.05$	$P < 0.01$	$P < 0.01$					
Proteins	$R = 0.529$	$R = 0.609$	$R = 0.580$	$R = 0.873$				
	$P < 0.001$	$P < 0.001$	$P < 0.001$	$P < 0.001$				
Carbohydrates	$R = 0.801$	$R = 0.824$	$R = 0.816$	$R = 0.463$	$R = 0.694$			
	$P < 0.001$	$P < 0.001$	$P < 0.001$	$P < 0.01$	$P < 0.001$			
BA	$R = 0.646$	$R = 0.738$	$R = 0.717$	$R = 0.760$	$R = 0.901$	$R = 0.835$		
	$P < 0.001$	$P < 0.001$	$P < 0.001$	$P < 0.001$	$P < 0.001$	$P < 0.001$		
% AE	$R = 0.565$	$R = 0.652$	$R = 0.624$	$R = 0.747$	$R = 0.897$	$R = 0.757$	$R = 0.908$	
	$P < 0.001$	$P < 0.001$	$P < 0.001$	$P < 0.001$	$P < 0.001$	$P < 0.001$	$P < 0.001$	
Sedimentary $\delta^{13}C$	$R = 0.866$	$R = 0.957$	$R = 0.779$	$R = 0.485$	$R = 0.630$	$R = 0.772$	$R = 0.740$	$R = 0.661$
	$P < 0.001$	$P < 0.001$	$P < 0.001$	$P < 0.01$	$P < 0.001$	$P < 0.001$	$P < 0.001$	$P < 0.001$

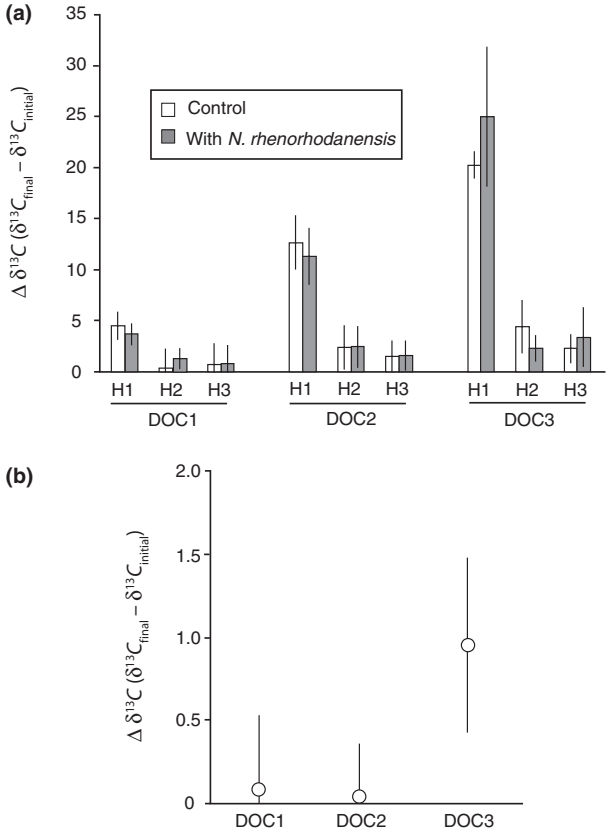

Fig. 3 Changes in $\delta^{13}C$ of total organic carbon attached to sediment (a) and tissues of *N. rhenorhodanensis* (b) during the course of the experiment I. Values are means ± SD ($n = 3$ columns per treatment).

In slow filtration columns, we detected significant increases in oxygen consumption and dehydrogenase activity of bacteria with *N. rhenorhodanensis*. With a DOC flux of 60 μg h^{-1}, amphipods produced an increase in oxygen consumption of 1.3 mg of O_2 h^{-1} L^{-1} of sediment in the uppermost 2 cm of sediments that could not be attributed to the sole respiration of 10 individuals of *N. rhenorhodanensis* (0.04 mg of O_2 h^{-1} L^{-1} of sediment calculated with respiration data of Hervant *et al.*, 1997). Such results indicate that feeding and/or bioturbation activity of *N. rhenorhodanensis* apparently had a positive influence on respiratory activity of bacteria. In batches, the occurrence of amphipods also delayed the DOC decrease (increase in *Ks* and decrease in μ_1) and increased the efficiency of DOC incorporation into bacteria (Y_1). The amphipod-induced modifications of carbon conversion efficiency Y_1 in batches and dehydrogenase activity in slow filtration columns suggested that amphipods could have slightly influenced the physiology of the microbial communities. However, this effect of *N. rhenorhodanensis* on microbial function was not associated with a significant change in the biomass (proteins and carbohydrates) and abundances of bacteria (total number and number of active bacteria). Modelling of carbon fluxes in batches clearly indicated that the feeding rate of *N. rhenorhodanensis* on sedimentary biomass was too low to influence significantly the bacterial biomass (top-down effect). The fast and efficient assimilation of DOC by

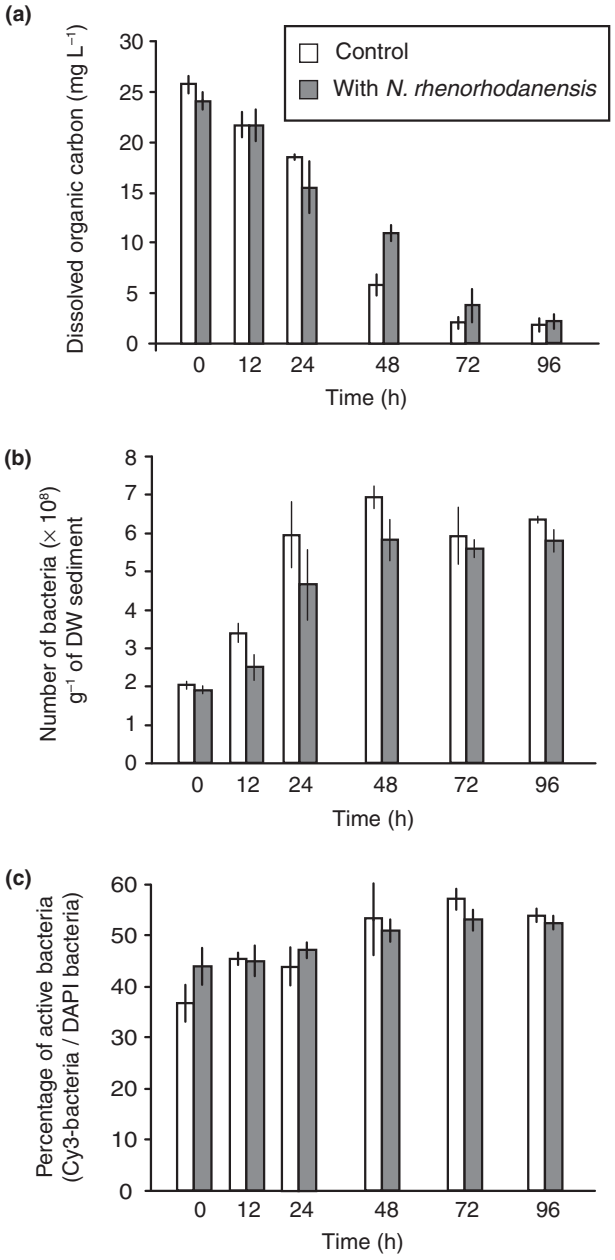

Fig. 4 Changes in the concentration of dissolved organic carbon (a), bacterial abundance (b) and percentage of active eubacteria (c) during experiment II in treatments with or without individuals of *N. rhenorhodanensis*. Values are means ± SD (n = 3 flasks per treatment).

microorganisms probably compensated for the microbial loss induced by the feeding rate of *N. rhenorhodanensis*. Indeed, we computed from our model that a total of 890 μg of DOC was incorporated into bacterial carbon in each batch during the 4 days of the experiment, whereas only 41 μg of bacterial carbon

Table 4 ANOVA results for the effects of time and occurrence of *N. rhenorhodanensis* on concentrations of dissolved organic carbon, bacterial abundances, percentages of active eubacteria and sedimentary δ^{13}C during the experiment II (d.f.: degrees of freedom for each tested effect; DOC: dissolved organic carbon; BA: bacterial abundance; % AE: percentage of active eubacteria)

		DOC concentration		BA		% AE		Sedimentary δ^{13}C	
Effect	d.f.	*F*	*P*	*F*	*P*	*F*	*P*	*F*	*P*
Fauna	1	4.13	0.18	0.36	0.58	0.49	0.53	0.09	0.78
Time	4	163	<0.001	32.9	<0.001	16.1	<0.001	67.3	<0.001
Fauna * Time	4	7.12	<0.01	2.02	0.14	1.46	0.26	0.42	0.79
Error	18								

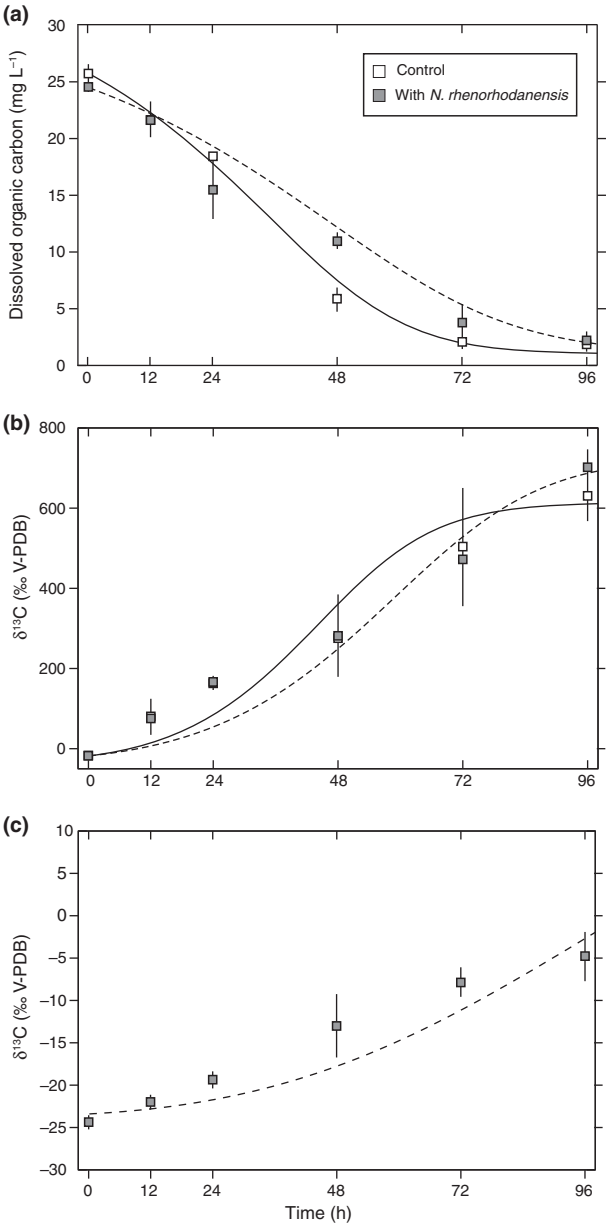

Fig. 5 Changes in DOC concentrations (a) and $\delta^{13}C$ values of total organic carbon attached to sediment (b) and *N. rhenorhodanensis* (c) during experiment II. Values are means ± SD (n = 3 flasks per treatment). Curves represent modelling results with (dashed lines) and without *N. rhenorhodanensis* (plain lines).

were fed (only 2.5 μg being incorporated in animal tissues) by amphipods during the same time period.

We did not detect any significant effect of *N. rhenorhodanensis* on the physical structure of sandy sediment. Amphipods did not influence the sediment transport coefficients (calculated with luminophore tracers), although they were observed to move in large interstices of the sediment column (visual observations on inner wall of the columns) and were collected in the whole sediment columns at the end of the experiment. The lack of sediment reworking implied that the bioturbation by amphipods did not significantly modify the living conditions for microorganisms growing on sand particles. Thus, our experiments clearly indicated that the feeding and bioturbation activities of *N. rhenorhodanensis* were much too low to significantly affect microbial processes in sediments.

Our findings differ markedly from those obtained by Edler & Dodds (1996) and Cooney & Simon (2009) with cave animals. Edler & Dodds (1996) reported a stimulation by 300–400% of attached bacteria (both abundance and activity) by the subterranean isopod *Caecidotea tridentata*, whereas organic carbon addition (D-glucose) had no effect on bacteria. They suggested that microbial activity was limited by N, rather than C, in their experiments. In such conditions, the excretion of nitrogen by isopods could have stimulated microbial abundances and activities (Edler & Dodds, 1996). In our experiments, N was not limiting because $N\text{–}NO_3^-$ concentration in water (10 mg of $N\text{–}NO_3^-$ L^{-1}) was more than tenfold higher than those used by Edler & Dodds (1996). Such comparison suggests that the influence of invertebrates on microbial processes may vary as a function of nutrient limitation. Significance of invertebrates on ecosystem processes may also depend on the functional traits of the species (Mermillod-Blondin & Rosenberg, 2006). If the amphipod *N. rhenorhodanensis* had slight effect in our experiments, Cooney & Simon (2009) reported that the cave amphipod *Gammarus minus* could reduce the bacterial production on rocks, offsetting the stimulatory effect as a result of glucose amendment. The contrasting influences of *G. minus* and *N. rhenorhodanensis* on bacterial activity were probably related to differences in metabolic activities between these two species. The ecophysiology of *N. rhenorhodanensis* and *G. minus* were studied by Hervant *et al.* (1997) and Hervant, Mathieu & Culver (1999b), respectively. At a temperature of 11 °C, the obligate groundwater amphipod *N. rhenorhodanensis* had a respiration rate of 12.9 μmol O_2 g^{-1} of dry mass h^{-1} (Hervant *et al.*, 1997). Comparatively, the amphipod *Gammarus minus* studied by Cooney & Simon (2009) exhibited a threefold higher respiration rate in normoxia at the

Table 5 Parameters used in the model and best estimated values from the fitting procedure in control and amphipod treatments

Parameters	Definition	Estimated value	
		Control	With amphipods
K_S	Monod constant (half velocity constant) (mg C)	2.55	2.66
μ_1	Maximum growth rate for bacteria (day^{-1})	1.17	1.11
μ_2	Growth rate parameter for amphipods (μg C bacteria $day)^{-1}$	–	0.35
μ_3	Rate of natural decay (day^{-1})	<0.05	<0.05
Y_1	Carbon conversion efficiency between DOC and bacteria [g C (g C bacteria)$^{-1}$]	0.22	0.26
Y_2	Carbon conversion efficiency between bacteria and *N. rhenorhodanensis* [g C bacteria (g C amphipods)$^{-1}$]	–	0.06

same temperature (between 40 and 45 μmol O_2 g^{-1} of dry mass h^{-1}, Hervant *et al.*, 1999b). Consequently, *G. minus* probably needs a threefold higher grazing activity than *N. rhenorhodanensis* to acquire its energy from microorganisms. Differences in metabolic demands could thus explain why *G. minus* can exert a higher control on microbial communities than *N. rhenorhodanensis*. In the same way, Kinsey *et al.* (2007) reported that *G. minus* produced a mean leaf litter breakdown of 0.14 g^{-1} of leaf g^{-1} of dry animal day^{-1}, whereas recent laboratory experiments showed that *Niphargus rhenorhodanensis* had a 20-fold lower effect on leaf litter breakdown (0.007 g^{-1} of leaf g^{-1} of dry animal day^{-1}, Simon Navel, unpubl. data).

The low metabolism of *N. rhenorhodanensis* is a characteristic shared by most subterranean species (Hüppop, 1985; Hervant *et al.*, 1997). Indeed, most subterranean invertebrates have developed efficient energy-saving strategies (low metabolism, storage of energy reserves) for fitting their physiological function to food-limited conditions prevailing in most aquifers (e.g. Hüppop, 1985; Danielopol *et al.*, 1994; Hervant & Renault, 2002). Hervant *et al.* (1997) also demonstrated that *N. rhenorhodanensis*, by depressing its metabolism, could survive without feeding for periods largely exceeding 200 days. We can therefore presume that the low influence of *N. rhenorhodanensis* on microorganisms in our experiments was linked to its low metabolic demand. However, we cannot exclude that the low influence of this omnivorous amphipod on microorganisms might have resulted from a low feeding preference for sedimentary bacteria. Although experiments showed that *N. rhenorhodanensis* could be maintained several years in laboratory under a large variety of foods (leaves, sediment, meat) (Ginet, 1960; Mathieu, 1967), knowledge about the feeding preferences of this species are lacking and we only detected small quantities of faecal pellets with fine sediment in boils used for gut content clearing (personal observation). Further experiments in the laboratory and in the field (using $\delta^{13}C$ and $\delta^{15}N$ to reconstitute food webs) are therefore greatly needed to determine the feeding preferences of *N. rhenorhodanensis* in the alluvial ecosystems. Nevertheless, the present study highlighted that, in sand-gravel sediments characteristics of the alluvial aquifer of the Rhône River, *N. rhenorhodanensis* was not able to influence significantly dissolved organic matter processing (DOC removal rate). This result was linked to the lack of significant activity of the amphipods in sandy zones where microbial processes predominantly occurred in our experimental systems (Mermillod-Blondin *et al.*, 2001). Although *N. rhenorhodanensis* is a dominant hypogean species of the alluvial aquifer of the Rhône River, other less abundant subterranean organisms that are strict microbivores and effective sediment bioturbators would have more influence on microbial processes than amphipods. In surface environments, tubificid worms such as *Tubifex tubifex* or *Limnodrilus hoffmeisteri* are known to strongly affect organic matter processing in freshwater sediments (Pelegri & Blackburn, 1995; Mermillod-Blondin *et al.*, 2001). Therefore, experiments with strict subterranean tubificid worms of the genus *Trichodrilus* (Creuzé des Châtelliers *et al.*, 2009) will be needed to more widely explore the potential influence of subterranean fauna on microbial processes in alluvial sediments. Moreover, comparisons of physiological traits and roles of tubificid worms living in both surface and subterranean habitats would allow us to determine whether it exits a

relationship between the ecological status of the animals, their metabolic rates and their roles in ecosystem functioning.

Finally, our laboratory experiments did not confirm the assumption of Boulton *et al.* (2008) according to which subterranean amphipods could have a significant influence on organic matter processing in interstitial systems. Microbial activity was tightly linked to the flux of dissolved organic matter in slow filtration columns, but the feeding and burrowing activities of *N. rhenorhodanensis* were far too low for influencing microbial processes. We suggest that the feeding preferences and the low metabolism of *N. rhenorhodanensis* probably induced by a natural adaptation to low-food conditions might have severely reduce its ability to influence its environment. Testing our hypothesis of a relationship between metabolism and functional role of subterranean fauna needs to extend our experiments to a wide range of strict microbivore organisms, including species with multiple populations living in habitats with contrasted food supply.

Acknowledgments

This study was funded by the French programme EC2CO-Cytrix from INSU/CNRS (project 'NAPCOD'), the Institut Fédératif de Recherche No. 41 (Bio-Environnement et Santé), the urban community of Lyon (project OTHU, http://www.graie.org/othu/) and the Rhône-Alpes Region. We thank two anonymous referees for helpful comments on the manuscript.

References

Bärlocher F. & Murdoch J. (1989) Hyporheic biofilm – a potential food source for interstitial animals. *Hydrobiologia*, **184**, 61–67.

Bou C. & Rouch R. (1967) Un nouveau champ de recherches sur la faune aquatique souterraine. *Comptes-Rendus de l'Académie des Sciences, Paris*, **265**, 369–370.

Boudreau B.P. (1986) Mathematics of tracer mixing in sediments: I. Spatially-dependent, diffusive mixing. *American Journal of Science*, **286**, 161–198.

Boulton A.J. (2000) The functional role of the hyporheos. *Verhandlungen International Vereinigung Limnologie*, **27**, 51–63.

Boulton A.J., Fenwick G.D., Hancock P.J. & Harvey M.S. (2008) Biodiversity, functional roles and ecosystem services of groundwater invertebrates. *Invertebrate Systematics*, **22**, 103–116.

Claret C. & Fontvieille D. (1997) Characteristics of biofilm assemblages in two contrasted hydrodynamic and trophic contexts. *Microbial Ecology*, **34**, 49–57.

Cooney T.J. & Simon K.S. (2009) Influence of dissolved organic matter and invertebrates on the function of microbial films in groundwater. *Microbial Ecology*, **58**, 599–610.

Craft J.A., Stanford J.A. & Pusch M. (2002) Microbial respiration within a floodplain aquifer of a large gravel-bed river. *Freshwater Biology*, **47**, 251–261.

Creuzé des Châtelliers M., Juget J., Lafont M. & Martin P. (2009) Subterranean aquatic oligochaeta. *Freshwater Biology*, **54**, 678–690.

Danielopol D.L. (1989) Groundwater fauna associated with riverine aquifers. *Journal of the North American Benthological Society*, **8**, 18–35.

Danielopol D.L., Creuzé Des Châtelliers M., Moeszlacher F., Pospisil P. & Popa R. (1994) Groundwater contamination and its impact on groundwater animals and ecosystems. In: *Groundwater Ecology* (Eds Gibert J., Danielopol D.L. & Stanford J.A.), pp. 217–243. Academic Press, UK.

Datry T., Malard F. & Gibert J. (2005) Response of invertebrate assemblages to increased groundwater recharge rates in a phreatic aquifer. *Journal of the North American Benthological Society*, **24**, 461–477.

Dole-Olivier M.-J. & Marmonier P. (1992) Patch distribution of interstitial communities: prevailing factors. *Freshwater Biology*, **27**, 177–191.

Dubois M., Gilles K.A., Hamilton J.K., Rebers P.A. & Smith F. (1956) Colorimetric method for determination of sugars and related substances. *Analytical Chemistry*, **28**, 350–356.

Edler C.C. & Dodds W.K. (1996) The ecology of a subterranean isopod, *Caecidotea tridentata*. *Freshwater Biology*, **35**, 249–259.

Findlay S.E.G., Strayer D., Goumbala C. & Gould K. (1993) Metabolism of stream water dissolved organic carbon in the shallow hyporheic zone. *Limnology and Oceanography*, **38**, 1493–1499.

François F., Gerino M., Stora G., Durbec J.-P. & Poggiale J.-C. (2002) A functional approach to sediment reworking by gallery-forming macrobenthic organisms: modelling and application with the polychaete *Nereis diversicolor*. *Marine Ecology Progress Series*, **229**, 127–136.

Fukuda R., Ogawa H., Nagata T. & Koike I. (1998) Direct determination of carbon and nitrogen contents of natural bacterial assemblages in marine environments. *Applied and Environmental Microbiology*, **64**, 3352–3358.

Gerino M., Aller R.C., Lee C., Cochran J.K., Aller J.Y., Green M.A. & Hirschberg D. (1998) Comparison of different tracers and methods used to quantify bioturbation during a spring bloom: 234-Thorium, luminophores and chorophyll a. *Estuarine, Coastal and Shelf Science*, **46**, 531–547.

Ghiorse W.C. & Wilson J.T. (1988) Microbial ecology of the terrestrial subsurface. *Advances in Applied Microbiology*, **33**, 107–172.

Gibert J. & Deharveng L. (2002) Subterranean ecosystems: a truncated functional biodiversity. *BioScience*, **52**, 473–481.

Gibert J., Culver D.C., Dole-Olivier M.J., Malard F., Christman M.C. & Deharveng L. (2009) Assessing and conserving groundwater biodiversity: synthesis and perspectives. *Freshwater Biology*, **54**, 930–941.

Gilbert F., Hulth S., Grossi V., Poggiale J.-C., Desrosiers G., Rosenberg R., Gerino M., François-Carcaillet F., Michaud E. & Stora G. (2007) Sediment reworking by marine benthic species from the Gullmar Fjord (Western Sweden): importance of faunal biovolume. *Journal of Experimental Marine Biology and Ecology*, **348**, 133–144.

Ginet R. (1960) Écologie, éthologie et biologie de *Niphargus*. *Annales de Spéléologie*, **15**, 127–237.

Goldscheider N., Hunkeler D. & Rossi P. (2006) Review: microbial biocenoses in pristine aquifers and an assessment of investigative methods. *Hydrogeology Journal*, **14**, 926–941.

Hervant F. & Renault D. (2002) Long-term fasting and realimentation in hypogean and epigean isopods: a proposed adaptive strategy for groundwater organisms. *The Journal of Experimental Biology*, **205**, 2079–2087.

Hervant F., Mathieu J., Barré H., Simon K. & Pinon C. (1997) Comparative study on the behavioral, ventilatory, and respiratory responses of hypogean and epigean crustaceans to long-term starvation and subsequent feeding. *Comparative Biochemistry and Physiology, Part A*, **118**, 1277–1283.

Hervant F., Mathieu J. & Barré H. (1999a) Comparative study on the metabolic responses of subterranean and surface-dwelling amphipods to long-term starvation and subsequent refeeding. *The Journal of Experimental Biology*, **202**, 3587–3595.

Hervant F., Mathieu J. & Culver D.C. (1999b) Comparative response to severe hypoxia and subsequent recovery in closely related amphipod populations (*Gammarus minus*) from cave and surface habitats. *Hydrobiologia*, **392**, 197–204.

Houri-Davignon C., Relexans J.C. & Etcheher H. (1989) Measurements of actual electron transport system (ETS) activity in marine sediments by incubation with INT. *Environmental Technology*, **10**, 91–100.

Hüppop K. (1985) The role of metabolism in the evolution of cave animals. *Bulletin of the National Speleological Society*, **47**, 136–146.

Jørgensen P.E., Eriksen T. & Jensen B.K. (1992) Estimation of viable biomass in wastewater and activated sludge by determination of ATP, oxygen utilisation rate and FDA hydrolysis. *Water Research*, **26**, 1495–1501.

Kinsey J., Cooney T.J. & Simon K.S. (2007) A comparison of the leaf shredding ability and influence on microbial films of surface and cave forms of *Gammarus minus* Say. *Hydrobiologia*, **589**, 199–205.

Lefébure T., Douady C.J., Malard F. & Gibert J. (2007) Testing dispersal and cryptic diversity in a widely distributed groundwater amphipod (*Niphargus rhenorhodanensis*). *Molecular Phylogenetics and Evolution*, **42**, 676–686.

Malard F., Reygrobellet J.L., Mathieu J. & Lafont M. (1994) The use of invertebrate communities to describe groundwater flow and contaminant transport in a fractured rock aquifer. *Archiv für Hydrobiologie*, **131**, 93–110.

Marmonier P., Fontvieille D., Gibert J. & Vanek V. (1995) Distribution of dissolved organic carbon and bacteria at the interface between the Rhône river and its alluvial aquifer. *Journal of the North American Benthological Society*, **14**, 382–392.

Marshall M.C. & Hall R.O.J. (2004) Hyporheic invertebrates affect N cycling and respiration in stream sediment microcosms. *Journal of the North American Benthological Society*, **23**, 416–428.

Mathieu J. (1967) Recherches sur les températures létales et les températures d'acclimatation de *Niphargus longicaudatus* (Crustacés, Amphipodes) épigés et hypogés. Doctoral Thesis, University of Lyon, 76 pp.

Mathieu J. & Essafi-Chergui K. (1990) Le peuplement aquatique interstitiel à l'interface karst/plaine alluviale. 1. Cas d'une alimentation en eau essentiellement karstique. *Mémoires de Biospéologie*, **17**, 113–122.

Mauclaire L., Pelz O., Thullner M., Abraham W.-R. & Zeyer J. (2003) Assimilation of toluene carbon along a bacteria-protist food chain determined by ^{13}C-enrichment of biomarker fatty acids. *Journal of Microbiological Methods*, **55**, 635–649.

Maurines-Carboneill C., Pernelle J.J., Morin L., Sachon G. & Leblon G. (1998) Relevance of the INT test response as an indicator of the ETS activity in monitoring heterotrophic aerobic bacterial populations in activated sludges. *Water Research*, **32**, 1213–1221.

Mermillod-Blondin F. & Rosenberg R. (2006) Ecosystem engineering: the impact of bioturbation on biogeochemical processes in marine and freshwater benthic habitats. *Aquatic Sciences*, **68**, 434–442.

Mermillod-Blondin F., Gerino M., Degrange V., Lensi R., Chassé J.-L., Rard M. & Creuzé des Châtelliers M. (2001) Testing the functional redundancy of Limnodrilus and Tubifex in hyporheic sediments: an experimental study in microcosms. *Canadian Journal of Fisheries and Aquatic Sciences*, **58**, 1747–1759.

Mermillod-Blondin F., Gerino M., Sauvage S. & Creuzé des Châtelliers M. (2004) Influence of nontrophic interactions between benthic invertebrates on river sediment processes: a microcosm study. *Canadian Journal of Fisheries and Aquatic Sciences*, **61**, 1817–1831.

Mermillod-Blondin F., Nogaro G., Datry T., Malard F. & Gibert J. (2005) Do tubificid worms influence the fate of organic matter and pollutants in stormwater sediments? *Environmental Pollution*, **134**, 57–69.

Meysman F.J.R., Boudreau B.P. & Middelburg J.J. (2003) Relations between local, nonlocal, discrete and continuous models of bioturbation. *Journal of Marine Research*, **61**, 391–410.

Monod J. (1942) *Recherches sur la Croissance des Cultures Bactériennes*. Hermann & Co, Paris.

Notenboom J., Plénet S. & Turquin M.-J. (1994) Groundwater contamination and its impact on groundwater animals and ecosystems. In: *Groundwater Ecology* (Eds Gibert J., Danielopol D.L. & Stanford J.A.), pp. 477–504. Academic Press, UK.

Pelegri S.P. & Blackburn T.H. (1995) Effects of *Tubifex tubifex* (Oligochaeta: tubificidae) on N-mineralization in freshwater sediments, measured with ^{15}N isotopes. *Aquatic Microbial Ecology*, **9**, 289–294.

Peterson G.L. (1977) A simplification of the protein assay method of Lowry *et al*. which is more generally applicable. *Analytical Biochemistry*, **83**, 346–356.

Press W.H., Teukolsky S.A., Vetterling W.T. & Flannery B.P. (1992) *Numerical recipes in Fortran 77*, 2nd edn. Cambridge University Press, UK.

Simon K.S., Benfield E.F. & Macko S.A. (2003) Food web structure and the role of epilithic biofilms in cave streams. *Ecology*, **84**, 2395–2406.

Sobczac W.V. & Findlay S. (2002) Variation in bioavailability of dissolved organic carbon among stream hyporheic flowpaths. *Ecology*, **83**, 3194–3209.

Starr R.C. & Gillham R.W. (1993) Denitrification and organic carbon availability in two aquifers. *Ground Water*, **31**, 934–947.

Traunspurger W., Bergtold M. & Goedkoop W. (1997) The effects of nematodes on bacterial activity and abundance in a freshwater sediment. *Oecologia*, **112**, 118–122.

Troussellier M., Bouvy M., Courties C. & Dupuy C. (1997) Variation of carbon content among bacterial species under starvation condition. *Aquatic Microbial Ecology*, **13**, 113–119.

(Manuscript accepted 25 November 2009)

Freshwater Biology

Freshwater Biology (2011) **56,** 481–490 doi:10.1111/j.1365-2427.2010.02513.x

The shredding activity of gammarids facilitates the processing of organic matter by the subterranean amphipod *Niphargus rhenorhodanensis*

SIMON NAVEL*,†,‡, LAURENT SIMON*,†,‡, CHRISTOPHE LECUYER*,†,§, FRANÇOIS FOUREL*,†,§ AND FLORIAN MERMILLOD-BLONDIN*,†,‡

*Université de Lyon, Lyon, France

†Université Lyon 1, Villeurbanne Cedex, France

‡CNRS, UMR5023, Laboratoire d'Écologie des Hydrosystèmes Fluviaux

§CNRS, UMR5125, PaleoEnvironnements et PaleobioSphère

SUMMARY

1. The functional feeding group approach has been widely used to describe the community structure of benthic invertebrates in relation to organic matter resources. Based on this functional framework, positive interactions between feeding groups (especially shredders and collector-gatherers) were postulated in the River Continuum Concept. However, relationships with organic matter have been poorly documented for invertebrates living in the hyporheic zone.

2. We hypothesised that the common subterranean amphipod *Niphargus rhenorhodanensis* would feed on fine particulate organic matter (FPOM), which is more abundant than coarse particulate organic matter (CPOM) in hyporheic habitats, and should be favoured by the occurrence of shredders that produce FPOM from CPOM.

3. We used laboratory experiments to quantify leaf litter processing by *N. rhenorhodanensis* and a common shredder, the surface amphipod *Gammarus roeselii*. We estimated rates of feeding and assimilation (using nitrogen stable isotopes) of the two species separately and together to reveal any potential shredder–collector facilitation between them.

4. Measured leaf litter mass loss showed that *N. rhenorhodanensis* did not act as a shredder, unlike *G. roeselii*. Organic matter dynamics and $^{15}N/^{14}N$ ratios in tissues of niphargids indicated that *N. rhenorhodanensis* was a collector-gatherer feeding preferentially on FPOM. We also found a positive influence of the gammarid shredders on the assimilation rate of *N. rhenorhodanensis*, which fed on FPOM produced by the shredders, supporting the hypothesis of a positive interaction between surface shredders and hyporheic collector-gatherers.

Keywords: coarse particulate organic matter, fine particulate organic matter, leaf litter breakdown, nitrogen isotopes, river continuum concept, subterranean amphipod

Introduction

The functional feeding group approach was developed to evaluate the influence of invertebrate communities on organic matter processing in aquatic ecosystems (Cummins, 1973; Willoughby & Sutcliffe, 1976; Cummins & Klug, 1979). Based on this approach and on the physical structure of lotic habitats, the River Continuum Concept (RCC) proposed a strong link between downstream changes in organic matter resources and in the structure of invertebrate communities along the length of a river (Vannote *et al.*, 1980). The hypothesis that fine particulate organic matter (FPOM) produced

Correspondence: Simon Navel, UMR – CNRS 5023 Laboratoire d'Ecologie des Hydrosystèmes Fluviaux – Université Claude Bernard Lyon1, 6 rue Dubois, Campus de la Doua; 69622 Villeurbanne Cedex, France. E-mail: simon.navel@univ-lyon1.fr

by shredders serves as food for collectors-gatherer downstream has frequently been tested in benthic ecological studies (Short & Maslin, 1977; Dieterich, Anderson & Anderson, 1997; Usio, Konishi & Nakano, 2001). However, studies are lacking for invertebrates living in the hyporheic zone (the transition zone between the river and the subterranean aquifer).

Recently, Boulton *et al.* (2008) hypothesised that most hyporheic invertebrates mainly affect ecosystem functioning through their feeding and bioturbation activities. From studies performed in gravel bars, these authors presented a functional inventory of hyporheic invertebrates that are potentially important drivers of particulate organic matter decomposition (Table 1 in Boulton *et al.*, 2008), pointing out that groundwater amphipods should be active shredders involved in the breakdown of coarse particulate organic matter (CPOM) as observed for surface amphipods (such as gammarids). However, the functional classification of hyporheic amphipods as shredders has not been experimentally demonstrated. Moreover, the classification appears to contradict the RCC prediction that the functional characteristics of invertebrate communities should be in equilibrium with the quantity and quality of organic matter resources. Because hyporheic sediments act as a mechanical filter that greatly reduces CPOM transport from surface to hyporheic habitats (Vervier *et al.*, 1992), dissolved organic matter (DOM) and FPOM are the main sources of organic matter for subterranean fauna in hyporheic habitats. Therefore, we expect subterranean amphipods to be better adapted to feed on FPOM than CPOM, which would not penetrate far into sediments (except during spates). Moreover, the growth and densities of subterranean amphipods should be strongly dependent on the quantity of organic matter entering the hyporheic zone. Joyce & Wotton (2008) showed that shredding activity of surface shredders (gammarids) produced large amounts of FPOM (mainly faecal pellets) that penetrated into the hyporheic zone and suggested that FPOM produced by gammarids could serve as food for hyporheic invertebrates. We thus hypothesize a positive shredder–collector interaction between surface shredders and hyporheic invertebrates feeding preferentially on FPOM (collector-gatherers). Our aims were (i) to determine the role of hyporheic amphipods on organic matter (OM) processing and (ii) to quantify the potential shredder–collector interactions between surface and hyporheic invertebrates. The obligate-groundwater species *Niphargus rhenorhodanensis* Schellenberg was selected as the most abundant and widely distributed amphipod in the hyporheic zone of the Rhône River (Dole-Olivier & Marmonier, 1992). *Gammarus roeselii* Gervais was chosen as a common surface shredder that feeds on leaf litter (V. Médoc *et al.*, submitted). In laboratory experiments, we compared leaf litter processing by the two amphipods both separately and together. Assimilation rates were measured using nitrogen stable isotopes ($^{15}N/^{14}N$ ratio) and we also analysed the influence of amphipods on ammonium and dissolved organic carbon (DOC), which are mineralisation products of OM processing (France *et al.*, 1997; McTiernan, Ineson & Coward, 1997).

Methods

Collection of sediments, leaves and amphipods

Gravel particles ranging from 2 to 4 mm were collected from the Rhône River, cleaned with deionised water, dried at 60 °C and kept for 2 weeks in the laboratory before use. We used senescent leaves of alder [*Alnus glutinosa* (L.)] collected in the riparian zone of the Rhône River during abscission (October, 2008), air-dried and stored at the laboratory. Before insertion into the experimental systems, leaves were conditioned in small-mesh bags immersed in river (artificial river located on the campus of the University Claude Bernard Lyon 1, Lyon, France) for 10 days and cut into 21.8-mm-diameter fresh discs. *Gammarus roeselii* (dry weight = 6.68 ± 2.00 mg; n = 10) were collected from the Rhône River using a Surber sampler. *Niphargus rhenorhodanensis* (dry weight = 1.47 ± 0.49 mg; n = 10) were collected using traps buried at a 5 cm depth in the sediment of a ditch draining the surface aquifer of the Dombes Forest, France (45°58′28″N, 5°24′25″E, clade I in Lefébure *et al.*, 2007). *Gammarus roeselii* and *N. rhenorhodanensis* were acclimated to experimental conditions (temperature, sediment characteristics and food) for 14 days and at least 15 days, respectively, before experiments started.

Microcosms and experimental design

Experiments were carried out in cylindric microcosms at a constant temperature (15 ± 0.5 °C) under a 12 h light/12 h dark cycle for 60 days. Each microcosm

consisted of a 12 cm-diameter, 1000 mL-capacity jar (Nalgene Labware; Thermo Fisher Scientific Inc., Waltham, MA, U.S.A.) containing a 4 cm-deep layer of 2–4 mm gravels (400 g) kept in the dark (by addition of three layers of black adhesive tape covering the sedimentary part of the microcosm) to provide a sedimentary habitat for *N. rhenorhodanensis*. After installation of sediment, microcosms were provided with 700 mL of aerated river reconstituted water (96 mg L^{-1} $NaHCO_3$, 39.4 mg L^{-1} $CaSO_4{\cdot}2H_2O$, 60 mg L^{-1} $MgSO_4{\cdot}7H_2O$, 4 mg L^{-1} KCl, 19 mg L^{-1} $Ca(NO_3)_2{\cdot}4H_2O$ and 1.6 mg L^{-1} $(CH_3CO_2)_2CaH_2O$; pH = 7.5; US EPA, 1991). During the experiment, a constant volume of water (700 mL) was maintained by adding demineralised water every 2 days to correct losses to evaporation.

Six treatments (n = 4 microcosms per treatment) were tested: (i) three *G. roeselii* per microcosm, (ii) six *G. roeselii*, (iii) three *N. rhenorhodanensis*, (iv) six *N. rhenorhodanensis*, (v) an assemblage of three each of *G. roeselii* and *N. rhenorhodanensis* and (vi) one animal-free treatment acting as control. Total densities of *Gammarus* (265 ind m^{-2} and 530 ind m^{-2}) were in the range reported by Fruget (1989) for the Rhône river. The densities of *N. rhenorhodanensis*, per unit volume of hyporheic habitat, were 6.6 and 13.2 ind L^{-1} sediment and correspond to median and highest densities measured in artificial substrata inserted in the bed of a stream (mean density = 7.2 ± 2.6 ind L^{-1} sediment; Mathieu & Essafi-Chergui, 1990).

A set of 30 alder discs was deposited on the surface of the sediment in each microcosm as a source of CPOM. In addition, two treatments were performed to determine the change in $^{15}N/^{14}N$ ratio of amphipod tissues when starved (four microcosms without CPOM per treatment, n = 3 *G. roeseli* or 3 *N. rhenorhodanensis* per microcosm). Assessment of this ratio allowed us to determine whether *N. rhenorhodanensis*, a species that can survive without feeding for periods exceeding 200 days (Hervant *et al.*, 1997), starved during the course of the experiment.

Analyses

At the end of the experiment (60 days), water samples were taken from each microcosm and filtered through Whatman GF/F filters (pore size: 0.7 μm; Millipore, Billerica, MA, U.S.A.) before measuring $N\text{-}NH_4^+$ and $N\text{-}NO_3^-$ concentrations using an automatic analyzer (Easychem Plus; Systea, Anagni, Italy) based on standard colorimetric methods (Grashoff, Ehrhardt & Kremling, 1983). DOC concentration was measured in water samples filtered through Whatman GSWP filters (pore size: 0.22 μm) and acidified with three drops of HCl (35%), using a total carbon analyzer (multi N/C 3100; Analytik Jena, Jena, Germany) based on high temperature combustion at 850 °C after removing dissolved inorganic C with hydrochloric acid and CO_2 stripping under O_2 flow.

For each microcosm, all invertebrates, leaves and organic detritus (leaf degradation products not retained on a sieve with a pore size of 1 mm) were retrieved, stored at −80 °C, freeze-dried (at least 48 h) and weighed. Leaf mass loss was then calculated from the initial dry mass estimated for five sets of 30 alder discs (607.72 ± 6.25 mg, mean ± SD). Dry mass loss of leaf litter, production/consumption of FPOM and total OM consumption (mass loss of leaf litter + consumption of FPOM) were calculated for each treatment, by comparison with the mass of OM introduced into microcosms at the start of the experiment.

Freeze-dried leaves were ground in a ball mill (Mixer Mill MM 200; Retsch, Haan, Germany) to obtain a homogenised leaf litter powder. Total organic carbon (TOC) and total nitrogen (TN) were analysed for leaf litter powder and FPOM (mainly faecal pellets) using an elemental analyser (FlashEA; Thermo Fisher Scientific) set up for C and N analysis. TOC and TN were also used to calculate C : N molecular ratio for litter from each microcosm. For stable isotope analyses, 1 mg dry leaf litter powder, 1.5 mg FPOM and 0.5 mg dry amphipod were weighed in tin capsules (Thermo Electron S.p.A., Milan, Italy). Stable isotope ratios of nitrogen ($^{15}N/^{14}N$) were measured by continuous flow stable isotope ratio mass spectrometry (CF-IRMS) using an Isoprime mass spectrometer (Isoprime Ltd, Cheadle, U.K.) interfaced with a Eurovector EuroEA3028-HT elemental analyser (EuroVector, Milan, Italy). $^{15}N/^{14}N$ ratios were expressed as δ in part per thousand (‰) and referenced to atmospheric air. The analytical precision achieved for tyrosine, triphenylamine and ascorbic acid standards analysed along with the samples was better than 0.3‰.

Data treatment

Regression analyses were performed to determine the influence of density of *G. roeselii* or *N. rhenorho-*

danensis on leaf litter mass loss, FPOM production/consumption and net OM consumption. We used the coefficients of the significant linear regressions to determine OM processing rates of the two amphipod species. Comparison of TOC and TN between leaves and faecal pellets (FPOM) was performed using a Student *t*-test. Differences in $N\text{-}NH_4^+$, $N\text{-}NO_3^-$ and DOC concentrations measured at the end of the experiment were tested using one-way ANOVA with animal treatments (i.e. 'Controls', 'three *G. roeselii*', 'six *G. roeselii*', 'three *N. rhenorhodanensis*' and 'six *N. rhenorhodanensis*') as main effects. The $\delta^{15}N$ values of *G. roeselii* or *N. rhenorhodanensis* collected during the experiment in the different treatments were compared using one-way ANOVA. When significant differences were detected among treatments for $N\text{-}NH_4^+$, $N\text{-}NO_3^-$ and DOC concentrations or $\delta^{15}N$ values, we used Tukey's HSD *post hoc* tests to determine which treatments differed. When necessary, data were log-transformed before statistical analysis to fit the assumptions of homoscedasticity and normality. All statistical analyses were performed using STATISTICA 5™ (Statsoft, Tulsa, OK, U.S.A.).

Gammarus–Niphargus interactions. We tested the effects of the interaction between *G. roeselii* and *N. rhenorhodanensis* on OM processing and nutrient concentrations using an additive model (Raffaelli *et al.*, 2003) based on single-species effects against which we compared observed multi-species effects. To determine the significance of interactions among species on processes, we compared measurements from the assemblage with three of each species [E (three *G. roeselii* + three *N. rhenorhodanensis*)$_{n\,=\,4}$] to predicted values calculated using the additive model (n = 16, four microcosms × four microcosms) = E (three *G. roeselii*)$_{n\,=\,4}$ + E (three *N. rhenorhodanensis*)$_{n\,=\,4}$ where E (three *G. roeselii*) and E (three *N. rhenorhodanensis*) are the individual effects of three *G. roeselii* and three *N. rhenorhodanensis* in one species treatments.

We expected that, in the absence of interactions, the effects of *G. roeselii* and of *N. rhenorhodanensis* would simply be additive in the assemblage. For OM processing and nutrient concentrations, measured and predicted values were compared using Student *t*-tests. A significant (negative or positive) difference indicates that interactions between *G. roeselii* and *N. rhenorhodanensis* modified organic matter processing or concentrations of DOC or $N\text{-}NH_4^+$ in the microcosms. In the figures, we represent the expected and measured effects of the treatments (three *G. roeselii*, three *N. rhenorhodanensis* and the assemblage) on OM processing and nutrient concentrations by subtracting the average values measured in the control without amphipods.

Calculation of N assimilation from leaf litter. Organic matter assimilation by amphipods was calculated from the $^{15}N/^{14}N$ ratio of *G. roeselii* and *N. rhenorhodanensis* at the end of the experiments. Nitrogen stable isotopes are preferred to quantify food assimilation against carbon isotopes because the natural $^{13}C/^{12}C$ ratio of *G. roeselii* at the beginning of the experiment ($\delta^{13}C = -29.5‰ \pm 0.7$) did not differ significantly from the $^{13}C/^{12}C$ ratio of leaf litter ($\delta^{13}C = -29.0‰ \pm 0.5$), precluding the determination of assimilation. On the other hand, the $^{15}N/^{14}N$ ratios measured for amphipods (both *G. roeselii* and *N. rhenorhodanensis*) and leaf litter at the start of the experiment were sufficiently different to estimate assimilation rates.

The fraction F of N assimilated by amphipods was calculated using a simple mass balance equation (e.g. Cerling *et al.*, 2007):

$$F = (\delta^{15}N_t - \delta^{15}N_{eq})/(\delta^{15}N_{eq} - \delta^{15}N_i) - 1 \quad (1)$$

where $\delta^{15}N_i$ and $\delta^{15}N_t$ are the N isotope compositions of amphipods at the beginning and at the end of the experiment, respectively, and $\delta^{15}N_{eq}$ is the isotope composition of amphipods at complete isotope equilibrium with the food source. $\delta^{15}N_{eq}$ is equal to $\delta^{15}N_F + \Delta^{15}N$, where $\delta^{15}N_F$ is the N isotope composition of leaf litter and $\Delta^{15}N$ is the trophic fractionation between amphipods and their food source. We have chosen the commonly accepted value of +3.4‰ for $\Delta^{15}N$ (Post, 2002). Assuming a comparable assimilation of N and other OM constituents by amphipods, leaf litter assimilation (A_F), expressed in mass of leaf litter per mass of dry amphipod (obtained for each treatment after freeze-drying), was then calculated as following:

$$A_F = F \times N_t/N_F \quad (2)$$

where N_t and N_F are the N concentration in amphipods and leaf litter, respectively.

Results

Organic matter processing by Gammarus and Niphargus

Loss of leaf litter dry mass was positively correlated with the density of *G. roeselii* (Fig. 1a; $R^2 = 0.94$, $P < 10^{-4}$) as was the mass of FPOM originating from leaf litter (Fig. 1c; $R^2 = 0.93$, $P < 10^{-4}$). Each individual *G. roeselii* contributed an average loss of 28.2 mg leaf litter and production of 16.1 mg FPOM. The net OM consumption (leaf litter mass loss–FPOM production) per *G. roeselii* was thus 12.1 mg during the course of the experiment (Fig. 1e), corresponding to OM consumption of 35.4 mg day^{-1} g^{-1} gammarid.

We detected no significant influence of *N. rhenorhodanensis* density on loss of leaf litter dry mass or net OM consumption (Fig. 1b,f; $R^2 < 0.1$, $P > 0.3$ for both). Leaf litter consumption by amphipods was therefore negligible and could not be quantified using this approach. However, the quantity of FPOM decreased significantly and linearly with the density of *N. rhenorhodanensis* (Fig. 1d; $R^2 = 0.27$, $P < 0.05$).

Influence of Gammarus and Niphargus on water chemistry

The concentration of $N\text{-}NH_4^+$ in water differed significantly among treatments (Fig. 2a; ANOVA; $F_{4,15} = 18.3$, $P < 10^{-3}$). *Niphargus rhenorhodanensis* did not significantly modify $N\text{-}NH_4^+$ concentrations in comparison with the animal-free control whereas the presence of six *G. roeselii* was associated with a 10-fold increase in $N\text{-}NH_4^+$ concentrations. Concentrations of DOC increased from the beginning (1 mg DOC L^{-1}) to the end of the experiment for all treatments (mean values ranging from 7.46 to 10.04 mg DOC L^{-1}). Although *N. rhenorhodanensis* had no effect on DOC concentrations, a significant reduction (ANOVA; $F_{4,15} = 13.6$, $P < 0.001$) was associated with the presence of *G. roeselii* (Fig. 2b). The measured concentrations of $N\text{-}NO_3^-$ ranged between 0.65 and 0.99 mg L^{-1}

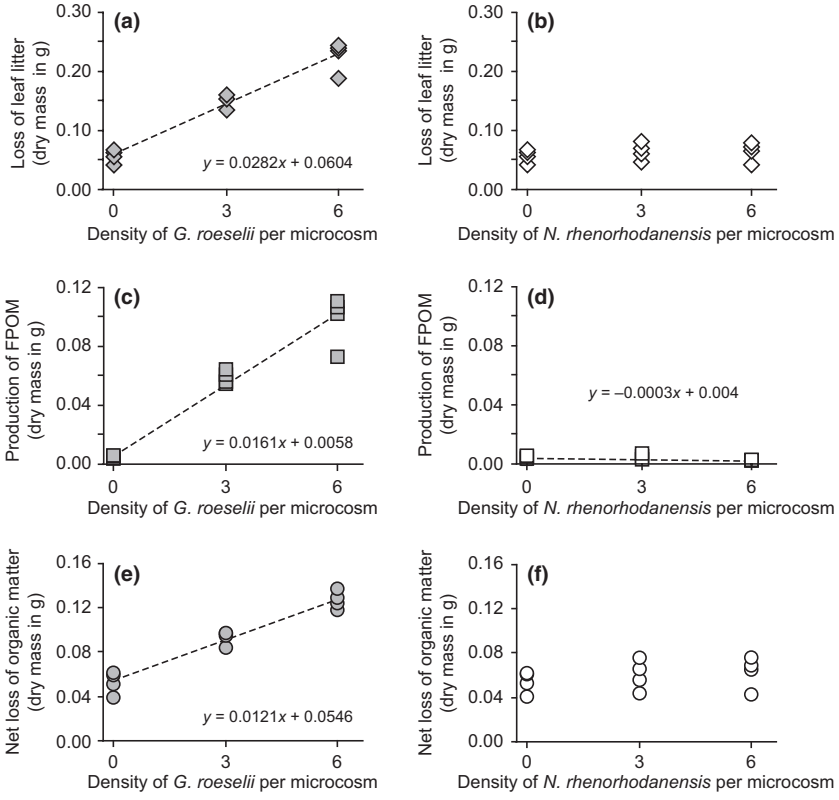

Fig. 1 Linear relationships between amphipod densities and (a and b) leaf litter mass loss, (c and d) fine particulate organic matter production and (e and f) net mass loss of organic matter. Graphs with densities of *Gammarus roeselii* are on the left (a,c and e) and *Niphargus rhenorhodanensis* on the right (b,d and f). Equations are indicated on the graphs when linear relationships are significant.

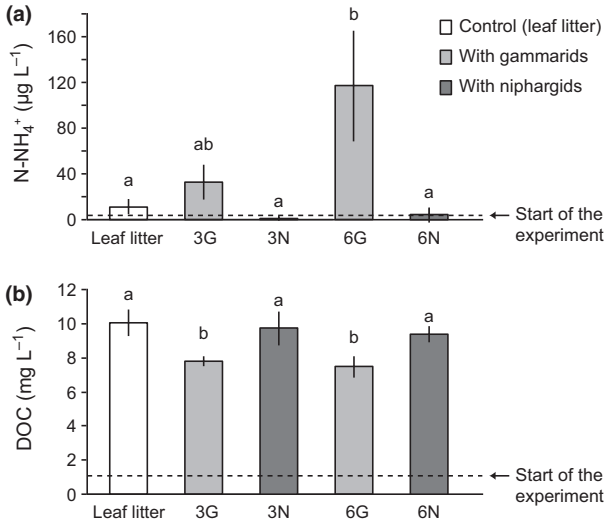

Fig. 2 Concentrations of (a) N-NH_4^+ and (b) dissolved organic carbon measured at the end of the experiment in five treatments (means ± SD, $n = 4$): control without amphipods (leaf litter), three *Gammarus roeselii* (3G), three *Niphargus rhenorhodanensis* (3N), six *G. roeselii* (6G) and six *N. rhenorhodanensis* (6N). Measurements performed at the start of the experiment are indicated by dashed lines.

without any clear trend among experimental treatments (data not shown).

Interactions between Gammarus and Niphargus

Dry mass loss of leaf litter was not significantly affected by the interaction between *G. roeselii* and *N. rhenorhodanensis* (Student *t*-test; $P = 0.53$) as this process was mainly affected by *G. roeselii* (Fig. 3a). In contrast, FPOM dry mass measured at the end of the experiment was significantly lower (Student *t*-test, $P < 10^{-3}$) in the treatment containing three *G. roeselii* and three *N. rhenorhodanensis* than expected from the additive model (Fig. 3b). This interaction between *G. roeselii* and *N. rhenorhodanensis* on FPOM accumulation led to a higher net OM consumption in the species mixture than expected from the additive model (Fig. 3c; Student *t*-test; $P < 0.05$). The interaction between *G. roeselii* and *N. rhenorhodanensis* did not influence DOC concentration (Fig. 3d; Student *t*-test; $P = 0.91$), but stimulated N-NH_4^+ production in the water (Fig. 3e; Student *t*-test; $P < 10^{-3}$).

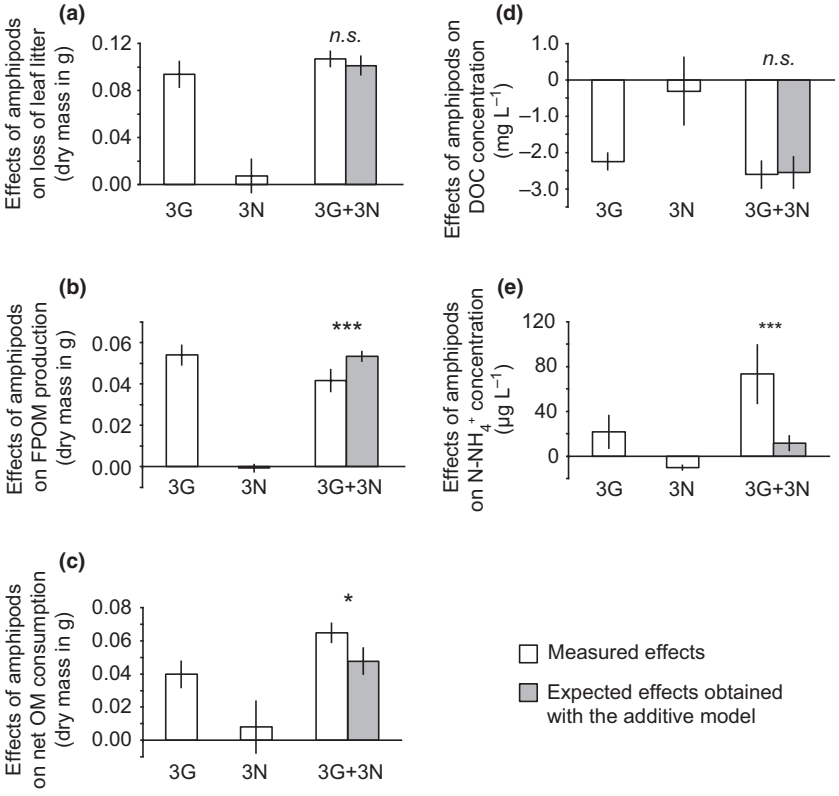

Fig. 3 Effects of three *Gammarus roeselii* (3G), three *Niphargus rhenorhodanensis* (3N) and three *G. roeselii* + three *N. rhenorhodanensis* (3G + 3N) on (a) leaf litter mass loss, (b) fine particulate organic matter production, (c) net mass loss of organic matter, (d) dissolved organic carbon and (e) N-NH_4^+ concentrations (means ± SD, $n = 4$). Expected effects are indicated for the treatment containing both three *G. roeselii* and three *N. rhenorhodanensis*. The results of the statistical comparison between observed and expected effects are indicated on the graphs for $P > 0.05$ (n.s.), $P < 0.05$ (*) and $P < 0.001$ (***).

TOC and TN of leaves and faecal pellets (FPOM)

Similar concentrations of TN (3.15–3.39%) were measured in FPOM and leaves (Student *t*-test, $P = 0.403$). In contrast, TOC concentrations were significantly lower in FPOM than in leaves (43.3 ± 0.9 and 48.2 ± 0.3%, respectively; Student *t*-test, $P = 10^{-3}$). The molecular C : N ratio of FPOM was therefore lower than that of leaves (15.5 ± 0.5 and 16.9 ± 0.3, respectively; Student *t*-test, $P = 10^{-3}$).

Assimilation rates ($^{15}N/^{14}N$ ratios)

The $^{15}N/^{14}N$ ratios of leaf litter and FPOM measured at the start and end of the experiment were comparable ($\delta^{15}N$: −0.94 ± 0.38 versus −1.19 ± 0.22‰) and significantly lower than $^{15}N/^{14}N$ ratios of *G. roeselii* ($\delta^{15}N$: 8.43 ± 0.18‰) and *N. rhenorhodanensis* ($\delta^{15}N$: 7.13 ± 0.43‰) measured at the start of the experiment (Student *t*-test, $P < 10^{-4}$ for both). While the $^{15}N/^{14}N$ ratios of starved amphipods measured at the end of experiment were comparable to the ratio measured at the start, assimilation of leaf litter or FPOM during the experiment decreased the $^{15}N/^{14}N$ ratios of *G. roeselii* and *N. rhenorhodanensis* (Fig. 4a,b). Significant differences in $\delta^{15}N$ values were measured among treatments for *G. roeselii* (ANOVA; $F_{4,16} = 3.6$, $P < 0.05$) and *N. rhenorhodanensis* (ANOVA; $F_{4,16} = 10.1$, $P < 10^{-3}$). The decrease in $^{15}N/^{14}N$ ratios of *G. roeselii* between the start and the end of the experiment was significant in treatment with six *G. roeselii* and when together with *N. rhenorhodanensis* (Fig. 4a). The $^{15}N/^{14}N$ ratios of *N. rhenorhodanensis* tended to decrease from the start to the end of the experiment but the difference was significant only when together with *G. roeselii* (Fig. 4b).

Using the changes in $^{15}N/^{14}N$ ratio of *G. roeselii* obtained from the treatment with six *G. roeselii* or a mixture of *G. roeselii* and *N. rhenorhodanensis*, we calculated (eqn 2) a mean (±SD) assimilation of 14.8 ± 5.8 mg OM day^{-1} g^{-1} dry gammarid. For the treatments with three or six *N. rhenorhodanensis*, we calculated a mean assimilation of 7.5 ± 5.9 mg OM day^{-1} g^{-1} dry niphargid. In comparison, a mean assimilation of 12.3 ± 3.1 mg OM day^{-1} g^{-1} dry *N. rhenorhodanensis* was estimated for the treatment with an assemblage of three *G. roeselii* and three *N. rhenorhodanensis*.

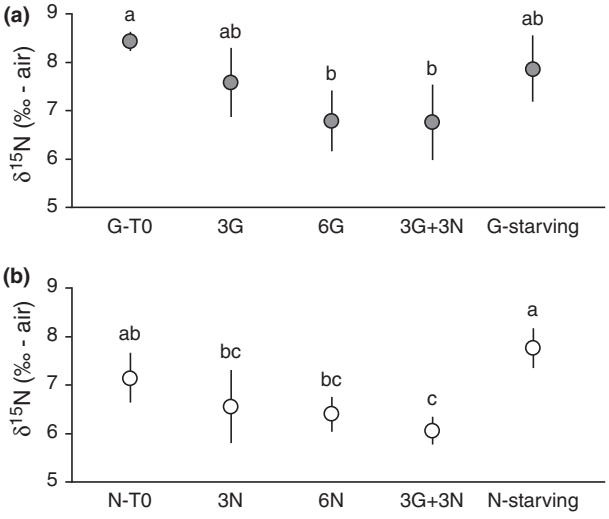

Fig. 4 $\delta^{15}N$ values on tissues of (a) *Gammarus roeselii* and (b) *Niphargus rhenorhodanensis* at the start of the experiment (G-T0 and N-T0), at the end of the experiment in treatments with three amphipods (3G and 3N), with six amphipods (6G and 6N), with the assemblage of three *G. roeselii* and three *N. rhenorhodanensis* (3G + 3N), and for specimens which were without food for the duration of the experiment (G-starving for *G. roeselii* and N-starving for *N. rhenorhodanensis*). Significant differences in $\delta^{15}N$ values between treatments (Tukey's HSD *post hoc* tests following one-way ANOVAs) are indicated by different letters.

Discussion

Our laboratory experiment did not confirm the assumption of Boulton *et al.* (2008) that groundwater amphipods act as shredders similarly to surface amphipods. Our results showed that the surface amphipod *G. roeselii* and the subterranean amphipod *N. rhenorhodanensis* exhibited distinct modes of OM processing and thus could not be classified in the same functional feeding group. *Gammarus roeselii* shredded 0.07 g dry leaf litter day^{-1} g^{-1} dry gammarid and transformed around 60% of this dry mass into FPOM (mainly faecal pellets). Assessments of leaf litter breakdown by *G. roeselii* were comparable to those reported in the literature for animals feeding on conditioned alder leaves [around 0.1 (±0.04) g dry leaf litter day^{-1} g^{-1} dry gammarid, estimated from Figure 2 in Gergs & Rothhaupt, 2008]. The considerable quantity of FPOM produced by *G. roeselii* was also in accordance with the assimilation efficiency calculated from the N stable isotope ratio (40%), a value in agreement with the low assimilation efficiency (10–40%) previously reported for *Gammarus*

feeding on leaves (Wotton, 1994). The active mechanical working of leaf litter by *G. roeselii* increased the production of NH_4^+ as a mineralisation product of leaf litter breakdown (Gessner, Chauvet & Dobson, 1999). Moreover, we observed a reduction in DOC concentration that was probably linked to shredding activities of the gammarids which (i) reduced the mass of leaf litter producing DOC and (ii) produced faecal pellets that may stimulate both attached and free-living DOC-consuming microorganisms (Thor, Dam & Rogers, 2003). In comparison with the CPOM processing induced by *G. roeselii*, the subterranean amphipod *N. rhenorhodanensis* did not significantly shred leaf litter and transform it into FPOM nor did it affect NH_4^+ and DOC concentrations. The linear decrease of FPOM originating from leaf litter (small leaf fragments) with density of *N. rhenorhodanensis* most likely indicates that this species feeds on FPOM rather than CPOM. The lack of shredding activity by *N. rhenorhodanensis* in our experiment could be linked to its low metabolic demand, a characteristic shared by most subterranean species (Hüppop, 1985; Hervant *et al*., 1997). Measurements of $^{15}N/^{14}N$ ratios in tissues of *N. rhenorhodanensis* showed that they did not starve during the experiment and assimilated around 7.5 mg OM day^{-1} g^{-1} dry niphargid. Such results suggest that *N. rhenorhodanensis* assimilated N by consuming small debris originating from leaf litter.

The idea that *N. rhenorhodanensis* does not act as a shredder like *G. roeselii* and can be classified as a collector-gatherer is confirmed by the measures of OM dynamics in the treatment containing both species. The lower accumulation of FPOM in this treatment in comparison with the expected value obtained from treatments with the two species separately suggested that FPOM produced by *G. roeselii* constituted a preferential food for *N. rhenorhodanensis*. The mean assimilation rates of leaf litter N by *N. rhenorhodanensis* confirmed this assumption, because this efficiency increased by 60% in the presence of FPOM produced by *G. roeselii*. By feeding on FPOM produced by gammarids, we estimated that *N. rhenorhodanensis* increased by 35% the total OM consumption in the system (Fig. 3c). This shredder–collector interaction also influenced the quantity of ammonium released into the system. For a comparable CPOM breakdown rate, the fact that the NH_4^+ concentration in the treatment containing both gammarids and niphargids was sevenfold higher than those calculated with the additive model is most likely linked to the consumption of faecal pellets of gammarids by niphargids. By feeding on faecal pellets with a higher N : C than leaves, *N. rhenorhodanensis* probably contributes to OM mineralisation and nutrient recycling in stream ecosystems. However, more experiments are needed to clearly quantify the links between nutrient dynamics and FPOM processing by the subterranean amphipod.

The classification of *N. rhenorhodanensis* into the feeding group of collector-gatherers can be linked to the OM sources available in the hyporheic zone. The sedimentary habitat of rivers acts as a strong physical filter that dramatically reduces the transfer of CPOM from the surface to the hyporheic zone (Vervier *et al*., 1992). Consequently, dissolved and fine particulate forms of OM may be the main sources of energy for hyporheic microorganisms and invertebrates (Leichtfried, 2007). These constraints carry the implication that hyporheic fauna is better adapted to feed on FPOM and microorganisms that consume DOM than on CPOM. The importance of microorganisms in the diet of *N. rhenorhodanensis* has been recently quantified by Foulquier *et al*. (2010). By tracing the flux of a ^{13}C-labelled source of DOC in bacteria and amphipods, these authors reported that *N. rhenorhodanensis* assimilated only 0.625 mg bacterial C day^{-1} g^{-1} dry niphargid. They suggested that the low functional significance of *N. rhenorhodanensis* on DOC processing and bacteria developed on sediment may be linked to either (i) the low metabolic rate of this subterranean species or (ii) its low feeding preference for sedimentary bacteria. The results of our study support the second explanation, the influence of *N. rhenorhodanensis* being more significant in a system with FPOM. In fact, by using a measured C concentration of leaf litter of 48.2% and assuming a comparable assimilation rate of C and N in *N. rhenorhodanensis*, we obtain a mean assimilation rate of C (5.9 mg C of FPOM day^{-1} g^{-1} dry amphipod) which is one order of magnitude higher than the assimilation rate measured by Foulquier *et al*. (2010) on bacterial carbon. Despite the strong assumption that *N. rhenorhodanensis* feeding on FPOM displays similar assimilation efficiencies for C and N, these rough estimates are different enough to conclude that *N. rhenorhodanensis* preferentially feeds on FPOM rather than sedimentary bacteria.

Finally, our results indicate that the subterranean amphipod *N. rhenorhodanensis* acts as a collector-gatherer and can significantly influence OM

processing by feeding on the fine fraction. We also demonstrated that FPOM production by surface shredders facilitated the feeding activity of hyporheic invertebrates. As expected by Wotton (2007) and Joyce, Warren & Wotton (2007), faecal pellets may be a key energy resource for invertebrates and microorganisms in the hyporheic zone. The RCC predicts that downstream collector-gatherers take advantage of upstream shredding that converts leaves (CPOM) into FPOM (Cummins, 1974; Vannote *et al*., 1980). The shredder–collector interactions observed in the present study suggest that this prediction, which was proposed for the longitudinal dimension of streams, can be extended to their vertical dimension.

Acknowledgments

We thank Félix Vallier (UMR-CNRS 5023, Villeurbanne) for his assistance with chemical analyses. We also appreciate the help of Guillaume Meiffren with sample freeze-drying. This study was funded by the ANR Biodiversity programme (ANR-06-BDIV-007) InBioProcess 2007–2010. We also thank C. Townsend and two anonymous reviewers for advice and constructive comments of the manuscript.

References

Boulton A.J., Fenwick G.D., Hancock P.J. & Harvey M.S. (2008) Biodiversity, functional roles and ecosystem services of groundwater invertebrates. *Invertebrate Systematics*, **22**, 103–116.

Cerling T.E., Ayliffe L.K., Dearing M.D., Ehleringer J.R., Passey B.H., Podlesak D.W., Torregrossa A.M. & West A.G. (2007) Determining biological tissue turnover using stable isotopes: the reaction progress variable. *Oecologia*, **151**, 175–189.

Cummins K.W. (1973) Trophic relation of aquatic insects. *Annual review of entomology*, **18**, 183–206.

Cummins K.W. (1974) Structure and function of stream ecosystems. *BioScience*, **24**, 631–641.

Cummins K.W. & Klug M.J. (1979) Feeding ecology of stream invertebrates. *Annual Review of Ecology and Systematics*, **10**, 147–172.

Dieterich M., Anderson N.H. & Anderson T.M. (1997) Shredder–collector interactions in temporary streams of western Oregon. *Freshwater Biology*, **38**, 387–393.

Dole-Olivier M.-J. & Marmonier P. (1992) Patch distribution of interstitial communities: prevailing factors. *Freshwater Biology*, **27**, 177–191.

Foulquier A., Simon L., Gilbert F., Fourel F., Malard F. & Mermillod-Blondin F. (2010) Relative influences of DOC flux and subterranean fauna on microbial abundance and activity in aquifer sediments: new insights from 13C-tracer experiments. *Freshwater Biology*, **55**, 1560–1576.

France R., Culbert H., Freeborough C. & Peters R. (1997) Leaching and early mass loss of boreal leaves and wood in oligotrophic water. *Hydrobiologia*, **345**, 209–214.

Fruget J.-F. (1989) *L'aménagement du bas-Rhône. Evolution du fleuve et influence sur les peuplements de macro-invertébrés benthiques*. PhD Thesis, Université Claude Bernard Lyon1, Lyon.

Gergs R. & Rothhaupt K.O. (2008) Feeding rates, assimilation efficiencies and growth of two amphipod species on biodeposited material from zebra mussels. *Freshwater Biology*, **53**, 2494–2503.

Gessner M.O., Chauvet E. & Dobson M. (1999) A perspective on leaf litter breakdown in streams. *Oikos*, **85**, 377–384.

Grashoff K., Ehrhardt M. & Kremling K. (1983) *Methods of Seawater Analysis*, 2nd edn. Verlag Chemie, Berlin.

Hervant F., Mathieu J., Barré H., Simon K. & Pinon C. (1997) Comparative study on the behavioral, ventilatory, and respiratory responses of hypogean and epigean crustaceans to long-term starvation and subsequent feeding. *Comparative Biochemistry and Physiology, Part A*, **118**, 1277–1283.

Hüppop K. (1985) The role of metabolism in the evolution of cave animals. *Bulletin of the National Speleological Society*, **47**, 136–146.

Joyce P. & Wotton R.S. (2008) Shredder fecal pellets as stores of allochtonous organic matter in streams. *Journal of the North American Benthological Society*, **27**, 521–528.

Joyce P., Warren L.L. & Wotton R.S. (2007) Faecal pellets in streams: their binding, breakdown and utilization. *Freshwater Biology*, **52**, 1868–1880.

Lefébure T., Douady C.J., Malard F. & Gibert J. (2007) Testing dispersal and cryptic diversity in a widely distributed groundwater amphipod (*Niphargus rhenorhodanensis*). *Molecular Phylogenetics and Evolution*, **42**, 676–686.

Leichtfried M. (2007) The energy basis of the consumer community in streams yesterday, today and tomorrow. *International Review of Hydrobiology*, **92**, 363–377.

Mathieu J. & Essafi-Chergui K. (1990) Le peuplement aquatique interstitiel à l'interface karst/plaine alluviale. Cas d'une alimentation en eau essentiellement karstique. *Mémoire de Biospéologie*, **17**, 113–122.

McTiernan K.B., Ineson P. & Coward P.A. (1997) Respiration and nutrient release from tree leaf litter mixtures. *Oikos*, **78**, 527–538.

Post D.M. (2002) Using stable isotopes to estimate trophic position: models, methods, and assumptions. *Ecology*, **83**, 703–718.

Raffaelli D.G., Emmerson M.C., Solan M., Biles C. & Paterson D. (2003) Biodiversity and ecosystem processes in shallow coastal waters: an experimental approach. *Journal of Sea Research*, **49**, 133–141.

Short R.A. & Maslin P.E. (1977) Processing of leaf litter by a stream detritivore – Effect on nutrient availability for collectors. *Ecology*, **58**, 935–938.

Thor P., Dam H.G. & Rogers D.R. (2003) Fate of organic carbon released from decomposing copepod fecal pellets in relation to bacterial production and ectoenzymatic activity. *Aquatic Microbial Ecology*, **33**, 279–288.

US EPA (1991) *Methods for Measuring the Acute Toxicity of Effluents and Receiving Waters to Freshwater and Marine Organisms*, 4th edn. US Environmental Protection Agency, Washington. EPA/600/4-90/027, pp. 34–35.

Usio N., Konishi M. & Nakano S. (2001) Is invertebrate shredding critical for collector invertebrates? A test of the shredder-collector facilitation hypothesis *Ecological Research*, **16**, 319–326.

Vannote R.L., Minshall G.W., Cummins K.W., Sedell J.R. & Cushing C.E. (1980) The river continuum concept. *Canadian Journal of Fisheries and Aquatic Sciences*, **37**, 130–137.

Vervier P., Gibert J., Marmonier P. & Dole-Olivier M.-J. (1992) A perspective on the permeability of the surface freshwater-groundwater ecotone. *Journal of the North American Benthological Society*, **11**, 93–102.

Willoughby L.G. & Sutcliffe D.W. (1976) Experiments on feeding and growth of amphipod *Gammarus pulex* (L.) related to its distribution in the river Duddon. *Freshwater Biology*, **6**, 577–586.

Wotton R.S. (1994) Particulate and dissolved organic matter as food. In: *The Biology of Particles in Aquatic Systems*, 2nd edn (Ed. R.S. Wotton), pp. 235–288. CRC Press, Boca Raton, FL.

Wotton R.S. (2007) Do benthic biologists pay enough attention to aggregates formed in the water column of streams and rivers? *Journal of the North American Benthological Society*, **26**, 1–11.

(Manuscript accepted 12 September 2010)

Functional Ecology

British Ecological Society

Functional Ecology 2012, **26**, 198–206 doi: 10.1111/j.1365-2435.2011.01925.x

Contrasted breeding strategies in four sympatric sibling insect species: when a proovigenic and capital breeder copes with a stochastic environment

Pierre-François Pélisson*[1], Marie-Claude Bel-Venner[1], Benjamin Rey[1], Lorraine Burgevin[1], François Martineau[2,3], François Fourel[2,3], Christophe Lecuyer[2,3], Frédéric Menu[1] and Samuel Venner*[,1]

[1]*Université de Lyon, F-69000, Lyon; Université Lyon 1; CNRS, UMR5558, Laboratoire de Biométrie et Biologie Evolutive, F-69622, Villeurbanne, France;* [2]*Université de Lyon, F-69000, Lyon; Université Lyon 1; CNRS, UMR5125, PaléoEnvironnements et Paléobiosphère, F-69622, Villeurbanne, France; and* [3]*Université de Lyon, F-69000, Lyon; Université de Lyon 1; CNRS-UMR 5276, Laboratoire de Géologie de Lyon: Terre, Planètes, Environnement, F-69622, Villeurbanne, France*

Summary

1. The evolution of strategies of resource acquisition and allocation is often considered to be closely dependent on the degree of environmental variability. Within this framework, female insects that experience stochastic fluctuations in the availability of their egg-laying sites in time or space can be expected to be fully synovigenic (i.e. they start maturing eggs after a delay once reaching adulthood), which allows them to tailor their reproductive investment to variations in the resource. Proovigenic females (that have most of their eggs already mature at the onset of their adult life, which corresponds to a capital breeding strategy), on the contrary, should have an advantage when the availability of the egg-laying sites is predictable. There is, however, a dearth of empirical studies testing these predictions.

2. Here, we tested the hypothesis that four phytophagous insect species of the genus *Curculio*, which coexist on a strongly fluctuating resource that they exploit for egg-laying purposes, would all be synovigenic as strict proovigeny should be counterselected. The resource consisted of the acorns of oak trees *Quercus* spp. We conducted field surveys to determine the date of adult emergence in each weevil species and the ability of newly emerged females to produce eggs. We also analysed the stable isotope profile of wild-caught females as a proxy for their feeding activity. Finally, we tested females under laboratory conditions for their ability to produce mature eggs when not fed and investigated whether dietary intake influenced their longevity.

3. Taken together, our results show that, contrary to the usual predictions, the four weevil species that were all exposed to a markedly fluctuating environment exhibited sharply contrasting strategies of resource acquisition and allocation: three species were synovigenic, while the fourth was proovigenic. Unexpectedly, therefore, our findings show that a strict capital breeding species might not always be counterselected in a temporally stochastic environment. They further suggest that fluctuations in the environment should not promote a sole, optimal strategy of energy acquisition and allocation to reproduction but instead should favour their diversification.

Key-words: *Curculio* spp., Curculionidae, energy allocation, fecundity, income breeding, stable isotopes, synovigeny

Introduction

Current theories in evolutionary ecology predict that a single optimal pattern of resource acquisition and allocation to reproduction should be favoured in a given environment, as an evolutionary response to environmental productivity, seasonality or unpredictability (Perrin & Sibly 1993; Ellers, Sevenster & Driessen 2000; Ellers & Jervis 2004; Houston *et al*. 2006; Fischer, Taborsky & Dieckmann 2009; Stephens *et al*. 2009; Fischer, Dieckmann & Taborsky 2010). These strategies have been finely investigated among insects from

*Correspondence authors. E-mails: pierre-francois.pelisson@univ-lyon1.fr; samuel.venner@univ-lyon1.fr

physiological processes to population dynamics through field surveys, laboratory experiments and theoretical modelling (Boggs 1997; Ellers & van Alphen 1997; Rivero-Lynch & Godfray 1997; Casas *et al*. 2000, 2009; Papaj 2000; Rosenheim, Heimpel & Mangel 2000; Jervis, Ellers & Harvey 2008; Richard & Casas 2009; Rosenheim 2011).

In insect populations exposed to stochastic fluctuations of their egg-laying sites (which constitute a limiting and fluctuating resource for population growth), proovigeny should be precluded (i.e. the females have all of their eggs mature at the onset of their adult life; Jervis *et al*. 2001; Jervis, Ellers & Harvey 2008; Jervis & Ferns 2004). Instead, the strategy of more synovigenic females, starting adult life with some immature eggs, can be expected to be optimal owing to the flexibility of the laying behaviour induced: such a strategy enables females to adjust the amount of energy allocated to reproduction to the perceived availability of the oviposition sites encountered (Heimpel 1998; Jervis & Ferns 2004; Richard & Casas 2009). There is evidence of a high egg maturation rate induced by such encounters (Casas *et al*. 2009), which might lower the cost for these females of being transiently egg-limited (Rosenheim, Heimpel & Mangel 2000). Such flexibility can be even increased by egg resorption that confers to synovigenic females the capacity of reallocating the energy from reproduction towards maintenance whenever current conditions are unfavourable because of either poor egg-laying sites or lack of food availability (Rivero-Lynch & Godfray 1997; Rosenheim, Heimpel & Mangel 2000; Jervis *et al*. 2001; Jervis, Boggs & Ferns 2005; Richard & Casas 2009). The flexible allocation of nutrients towards lifetime reproduction might be linked to the capacity for synovigenic females to fuel their gametes with energy gained concurrently through adult feeding, which corresponds to an income breeding strategy. Adult feeding has been reported in many synovigenic species among Hymenoptera and Lepidoptera (Jervis *et al*. 2001), and there is evidence of a negative relationship between the dependency on nutrients acquired at the adult stage and the ovigeny index that is the proportion of eggs produced throughout life that are mature at adult emergence (Jervis, Boggs & Ferns 2005; Jervis, Ellers & Harvey 2008). Yet the link between synovigeny and income breeding is complex because females synovigenic insect species have been shown to incorporate nutrients of both larval and adult origin into their eggs, thereby possibly using a mixed strategy, depending on the nutrient category, the feeding history or even ageing (Rivero & Casas 1999; Rivero, Giron & Casas 2001; O'Brien, Fogel & Boggs 2002; Casas *et al*. 2005; Jervis, Ellers & Harvey 2008).

In contrast, strict proovigeny corresponds to a capital breeding strategy as all nutrients incorporated into the eggs have been acquired at the larval stage. Females emerging with significant egg loads have a limited ability to disperse before ovipositing owing to their weak thoracic musculature and to the limited amount of energy available for flight (Dixon, Horth & Kindlmann 1993; Tammaru & Haukioja 1996; Jervis, Boggs & Ferns 2005). Proovigeny and capital breeding strategies are thus expected to be optimal when the local availability of laying sites is both stable and predictable (Ellers & Jervis 2004).

While the proportion of eggs mature at emergence is well documented in holometabolous insects and shows empirical evidence of a continuum between strict proovigeny and synovigeny (Jervis, Ellers & Harvey 2008), the key role of the environmental fluctuations or of their steadiness in the evolution towards either extremes remains largely unexplored. This study aims to start filling this gap by investigating natural communities composed of four insect sibling species, all of which belong to the same genus and are exposed to the same, natural environment characterized by strong between-year fluctuations in the number of available egg-laying sites. Under this temporally stochastic environment, these species should all exhibit a synovigenic and income-like strategy, while none is expected to be strictly proovigenic and capital breeder.

We focused on insect communities composed of four weevil species – *Curculio glandium* (Marsham), *Curculio elephas* (Gyllenhal), *Curculio pellitus* (Boheman) and *Curculio venosus* (Gravenhorst) (Coleoptera, Curculionidae) – that are specialized on oak trees (*Quercus* spp.) in southern Europe, coexist on the same individual host plants (Hoffmann 1954; Coutin 1992; Hughes & Vogler 2004) and use oak acorns as their egg-laying sites (Venner *et al*. 2011). Females deposit eggs into oak acorns from early June to the end of the summer following their emergence as adults. Each larva fully develops into a unique, mature acorn before self-extracting from that fruit and burrowing into the soil in the fall (Venner *et al*. 2011). The fully mature larvae then enter diapause for variable periods of time (from 1 to 4 years), depending on the species and even on individuals within the same species (Coutin 1992; Menu & Debouzie 1993; Venner *et al*. 2011). Following that period, larvae experience full metamorphosis before emerging above-ground and breeding the same year. Because oaks are known to be 'masting' species, i.e. ones that produce seeds massively but intermittently, the availability of the resource suitable for larval development (i.e. mature oak acorns) varies considerably and partly randomly from 1 year to the next (Kelly & Sork 2002; See Appendix S1, Fig. S1, in Supporting Information). The spatial distribution of acorn availability is also heterogeneous, because trees located near each other are only partly synchronized (Liebhold *et al*. 2004). Each year, the population growth of the four weevil species might be severely limited whenever mature acorns are lacking locally, that is, in the spatial range that can be explored during the breeding season by adult weevils from the same population (Venner *et al*. 2011). The four weevil sibling species that exploit the same egg-laying sites and experience the same, unpredictable environment are thus expected to be synovigenic, which might allow them to cope optimally with the marked spatio-temporal fluctuations of the acorns.

Adults of the four weevil species under study do exclusively breed the year they emerge, even if the resource is locally depleted (which can occur in years when there are almost no oak acorns, neither on the tree on which an individual has matured nor on neighbouring trees). They must therefore be

able to escape from poor environmental conditions by moving to trees producing more acorns. Accordingly, adults need to emerge well before the laying period, so that they have enough time to prospect for suitable laying sites. As the energy required for this early dispersal is likely to be unavailable for oogenesis (according to the oogenesis-flight syndrome theory), very limited amounts of teneral reserves might be allocated towards reproduction (Jervis, Boggs & Ferns 2005; Zera 2005; Lorenz 2007). Accordingly, adult females should be synovigenous and could require additional energy to mature their eggs that they would obtain through feeding.

We conducted both field surveys and several experiments under controlled laboratory conditions for each species to examine these predictions following four steps: (i) we checked whether adults do emerge much before ovipositing by determining the emergence date of adults in the field and comparing it with the laying period, (ii) we determined whether the four species are synovigenic by estimating the ability of newly emerged females to produce eggs, (iii) to test whether they do feed as adults, first we analysed the stable isotope profile of wild-caught females and second we conducted a laboratory experiment to compare the longevity of adult females that were either unfed or fed a standard diet and finally, (iv) we checked under laboratory conditions the inability of unfed females to allocate energy towards reproduction, i.e. their inability to mature eggs.

Materials and methods

DETERMINATION OF THE EMERGENCE DATE OF ADULTS FROM THE FOUR WEEVIL SPECIES, SURVEYED YEARLY BETWEEN 2008 AND 2010

Following larval diapause and metamorphosis, adults emerge from the soil to take part in a single breeding season. In these species, females lay eggs in acorns from June to September. Each year between 2008 and 2010, we consistently surveyed the emergence date of adults of the four species in two natural communities located 30 km apart near Lyon in France, each community being found on isolated oak trees [site A (*Quercus robur*): N45°35′; E5°01′; site B (*Quercus petraea*): N45°45′; E5°16′]. Dormancy strategies vary greatly from one species to another (ranging in duration from 1 to 3 years): while *C. elephas* adults mostly emerge over the first 2 years following larval development, the number of years spent diapausing underground is fixed for the three other species (i.e. almost 2 years for *C. glandium* and almost 3 years for *C. pellitus* and *C. venosus*), irrespective of annual field conditions (Venner *et al.* 2011).

Here, we were surveying the emergence of adults from five consecutive larval cohorts (2005–2009). To do this, during each of these 5 years, we harvested all mature acorns that had dropped off the two oak trees studied onto a net laid on the soil over half the surface covered by the tree. These acorns were placed in wire-netting boxes in an outdoor arena that allowed us to collect and count daily all mature weevil larvae that emerged spontaneously from the acorns during the emergence season, i.e. from mid-August to the end of December. The larvae were then randomly assigned to several covered, water-permeable plastic receptacles that had previously been filled with sifted soil and buried under each host tree. The five cohorts were assigned to separate devices, which allowed larvae from a known cohort and tree to develop in confined, semi-natural conditions until the adults emerge. Yearly from 2008 to 2010, the devices were surveyed on a weekly basis from early March. As soon as an adult was detected in one of the receptacles, we started a daily survey of all of them that continued until no further adults had emerged in either device during at least eight consecutive days. After identifying the species and the sex, each newly emerging adult weevil was weighed (to the nearest 0·1 mg, balance: Scaltec SBA 32): no significant difference was detected for any species in the weight of adults belonging to the different annual larval cohorts (see Appendix S2; Fig. S2).

CHARACTERIZATION OF FEEDING ACTIVITY IN THE FIELD

Isotope analysis of biological samples is an appropriate method for obtaining information about the diet of animals (Hood-Nowotny & Knols 2007), notably in natural populations (Markow, Anwar & Pfeiler 2000). The stable isotope ratios of nitrogen and of carbon, in particular, are influenced by the diet of animals to a large extent (DeNiro & Epstein 1978, 1981; Inger & Bearhop 2008). Capital and income resources can be identified with the use of naturally stable isotope profiles (Fischer, O'Brien & Boggs 2004; Warner *et al.* 2008; Wessels, Jordan & Hahn 2010). In this study, we used this property to explore the feeding activity of adults of the four weevil species in the field. In holometabolous insects, the larval and adult stages present very contrasting morphological and physiological traits and are mostly exposed to distinct environments. Throughout their underground life, none of the four weevil species does feed, which means that the tissues of a newly emerging adult are entirely derived from nutrients acquired from the oak acorn at the larval stage. The isotope signature of an emerging adult therefore only reflects the isotope composition of the oak acorn in which it developed. Moreover, because after becoming adult, no further moulting occurs, metabolically inactive tissues, such as the keratinized exoskeleton (integument), retain this larval isotope signature throughout the insect's life. Field and laboratory observations justified our assumption that adults do not feed on acorns. Thus, any change detected in the isotope profile of metabolically active tissues such as muscles, genital organs or fat body is likely to be due to adult feeding. By analysing the isotope profile of both the exoskeleton and internal tissues of wild-caught females, we attributed any absolute difference between these pairs of measures to adult feeding. This allowed us to use each adult female as her own control and thus to circumvent any possible variability in the isotope profiles of individual oak acorns, i.e. the larval food resource. We focused on the weevil community at the site A, where we sampled oak acorns as well as adults of the four weevil species both at emergence and later in the breeding season.

Sampling

For each insect species, we compared the isotope signature of newly emerged individuals captured before they had displayed any feeding activity with that of adults trapped on the oak tree between June and September 2009. Newly emerged individuals were obtained using the same experimental design as for determining the emergence date and were collected individually and freeze-dried at −20 °C. The other adult weevils were captured on the oak trees by beating branches with a wooden stick within the first hour after sunrise (Schauff 1986). Insects were collected on a white sheet laid under the

tree and were individually frozen at −20 °C after their sex and species were identified on the basis of morphological criteria (Hoffmann 1954). We examined the isotope profile of individual oak acorns and its variability across trees and years: eight acorns per tree were harvested from three different trees at site A, which was repeated in 2007 and 2009. Acorns were sampled at the time of the larval development of the insects, and they too were stored at −20 °C prior to analysis.

Sample preparation

Adult females were dissected under a binocular microscope (Zeiss STEMI-C, Illkirch, France) to collect separately the keratinized tissues (elytra) and the soft tissues (ovaries and the fat body, avoiding the gut). The acorns were dissected to retrieve the kernel, which constitutes the sole food source of weevil larvae. The insect and plant samples were then dried in the oven (Memmert Celsius 2005) at 60 °C for 48 h, after which the acorns were crushed using Stainless Steel Beads and shaken for 30 s at 25 Hz (Tissue Lyser; Qiagen, Courtaboeuf, France). We took four 2 mg (±0·2 mg) samples from each acorn and placed each of them in a tin capsule. The elytra and internal tissues of each adult insect were sampled separately the same way (four repeats per tissue per insect, each weighing 250 ± 50 μg). Overall, 44 newly emerged females (11 *C. elephas*, 15 *C. glandium*, 10 *C. pellitus* and eight *C. venosus*) and 49 live-trapped females (nine *C. elephas*, 10 *C. glandium*, 15 *C. pellitus* and 15 *C. venosus*) were analysed. As a larva depends on a single acorn for its entire development, and because the isotope signature of oak acorns was found to be very variable (see Appendix S3; Fig. S3), we computed for each insect the difference between its keratinized tissue – resulting from its larval diet – and its internal tissue that was assumed to reflect its adult diet.

Stable isotope analysis

Stable isotope ratios of carbon ($^{13}C/^{12}C$) and nitrogen ($^{15}N/^{14}N$) were measured by continuous flow stable isotope ratio mass spectrometry using an Isoprime mass spectrometer (Isoprime Ltd, Cheadle, UK) interfaced with a Eurovector EuroEA3028-HT elemental analyser (EuroVector, Milan, Italy). Carbon and nitrogen isotope ratios were expressed as δ in parts per thousand (‰) and referenced to Pee Dee Belemnite and atmospheric air, respectively. The analytical precision achieved for tyrosine, triphenylamine and ascorbic acid standards analysed along with the samples was better than 0·1‰ for $\delta^{13}C$ values and better than 0·3‰ for $\delta^{15}N$ values.

INFLUENCE OF FOOD INTAKE ON THE LONGEVITY OF THE FEMALES

We tested in the four weevil species the extent to which dietary intake by adult females influences their survival. Females were collected the day they emerged and were placed individually in Plexiglas rearing boxes (5·8 × 4·4 × 5 cm). These boxes were kept in a room at constant temperature (22 ± 1 °C), hygrometry (60 ± 5% relative humidity) and under artificial light simulating the natural photoperiod (±15 min). Adults were randomly assigned to one of three dietary groups as follows: distilled water alone (diet 1: D1); sugar solution (sucrose 10%, diet 2: D2); and sugar (10%) plus fresh chestnut pollen (ca. 5 mg, 'Percie du sert' Penne d'Agenais, France; diet 3: D3). The number of individuals provided with the various diets was as follows: *C. elephas* (D1: $n = 31$, D2: $n = 34$ and D3: $n = 26$), *C. glandium* (D1: $n = 11$, D2: $n = 10$ and D3: $n = 10$), *C. venosus* (D1: $n = 7$, D2: $n = 8$ and D3: $n = 8$) and *C. pellitus* (D1: $n = 5$, D2: $n = 8$ and D3: $n = 6$). Adults were supplied *ad libitum* with their respective diet: water and the sugar solution were both provided using a piece of cotton wool soaked in 2 mL of the dietary solution that was renewed every 3 days. Pollen was compressed in a fine gauze bag hung at the top of the rearing box and was renewed weekly. We checked daily whether adult females were still alive until all of them naturally died.

OOGENESIS IN FOOD-DEPRIVED FEMALES

To test whether females required feeding before maturing eggs, we first dissected newly emerged females of the four species (*C. elephas*: $n = 17$, *C. glandium*: $n = 20$, *C. pellitus*: $n = 13$ and *C. venosus*: $n = 12$) under a binocular microscope to count the number of chorioned eggs in their ovaries. Second, to test the ability of unfed females to produce mature eggs, 10 *C. glandium* and 11 *C. elephas* females were provided with distilled water (D1) *ad libitum* for 8 days and were then sacrificed and dissected. *C. venosus* and *C. pellitus* were not included in this experiment, because of the too small sample size available.

STATISTICAL ANALYSIS

To find out whether adults from the four species differed with regard to the time of year they emerged, we used a generalized linear mixed model with a Poisson distribution of error (lme4 package). We tested the effect of the interaction between the species and the week in the year when an adult emerged. In this analysis, we considered the site (i.e. the oak trees A and B) and the year of adult emergence as random effects.

To assess the effects of the tree or of the year on the relationship between $\delta^{15}N$ and $\delta^{13}C$, we used the multivariate analysis of variance (MANOVA), which allows the response variable to be multidimensional (Tomassone *et al.* 1988). We used MANOVA to test whether the isotope enrichment differed between the four insect species. To do this, we computed for each individual the absolute difference between the keratinized tissue and the internal tissue in the $\delta^{15}N$ and in the $\delta^{13}C$ isotope profiles ($|\Delta\delta^{15}N|$ and $|\Delta\delta^{13}C|$).

We analysed the effect of the diet on the longevity of adult females with a generalized linear model assuming a Gamma distribution of the residuals (inverse link). All analyses were performed with the R free software environment (Ihaka & Gentleman 1996; http://cran.at.r-project.org).

Results

EMERGENCE DATE OF ADULTS WITHIN THE YEAR

As shown in Fig. 1, the comparative kinetics of the emergence dates clearly reveals two distinct patterns (interaction between the species and the week in the year when an adult emerged $\chi^2_{d.f.=66} = 2725$; $P < 0{\cdot}0001$) that showed consistency across years and for the two communities: three

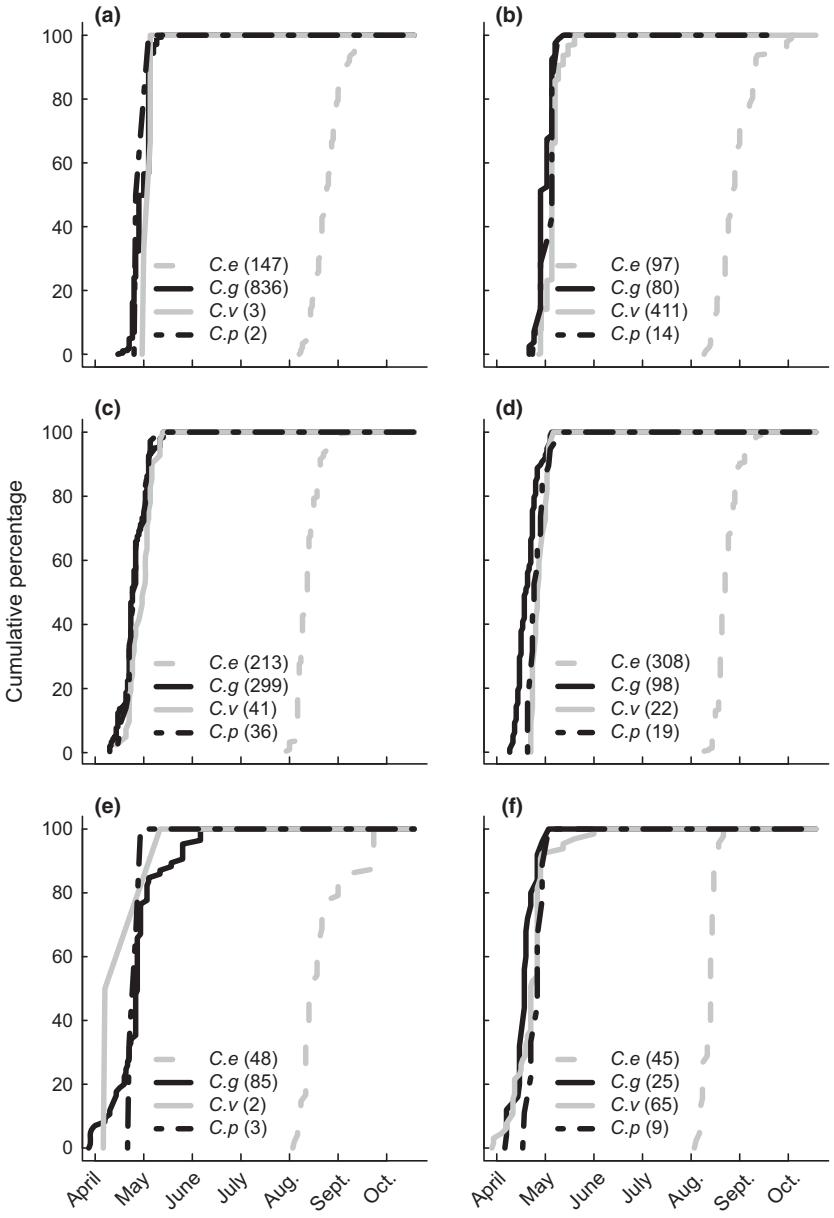

Fig. 1. Timing of the adult emergence in the four weevil species investigated. The cumulative abundance of emerging adults of each species is shown at the site A in 2008 (a), 2009 (c) and 2010 (e) and at the site B in 2008 (b), 2009 (d) and 2010 (f). Three of these species, *Curculio venosus*, *Curculio pellitus* and *Curculio glandium,* emerged synchronously and early in the season, while the emergence date of the fourth (*Curculio elephas*) differed markedly.

species (*C. glandium*, *C. pellitus* and *C. venosus*) emerged simultaneously in April, at a time when oak pollen was being produced (Bonnet Masimbert 1984), that is 2 months before egg laying, whereas the *C. elephas* females emerged much later in the year, in August during their laying period.

FEEDING ACTIVITY IN THE FIELD

The isotope signature of oak acorns varies considerably from year to year and between oak trees, as is shown by the $\delta^{15}N$ and $\delta^{13}C$ isotope ratios (MANOVA, years: $F_{2,\ 41} = 19{\cdot}0$; $P < 0{\cdot}001$; trees: $F_{6,\ 84} = 20{\cdot}6$; $P < 0{\cdot}001$; interaction: $F_{2,\ 41} = 3{\cdot}82$; $P = 0{\cdot}03$; see Appendix S3; Fig. S3). The $|\Delta\delta^{13}C|$ and $|\Delta\delta^{15}N|$ values differed significantly between the newly emerged adults (emerging) and adults captured later in the field (trapped) in three of the four weevil species (*C. venosus, C. pellitus* and *C. glandium*), indicating that individuals from these three species had fed at the adult stage. In contrast, no such difference was found in *C. elephas*, suggesting that adult females belonging to this species had not fed in the field until the time of egg laying (Fig. 2; Table 1; see Appendix S4; Fig. S4).

INFLUENCE OF FOOD INTAKE ON THE LONGEVITY OF THE FEMALES

We found that the longevity of adult weevil females varies from one species to another depending on diet (diet: $\chi^2_{d.f.=2} = 26$; $P < 0{\cdot}0001$; species: $\chi^2_{d.f.=3} = 40$; $P < 0{\cdot}0001$; diet × species interaction: $\chi^2_{d.f.=6} = 23$; $P < 0{\cdot}0001$; Fig. 3). These results were consistently observed at the two sites studied ($\chi^2_{d.f.=1} = 0.016$; $P = 0{\cdot}842$). Under controlled laboratory conditions, the longevity of *C. elephas* females was not

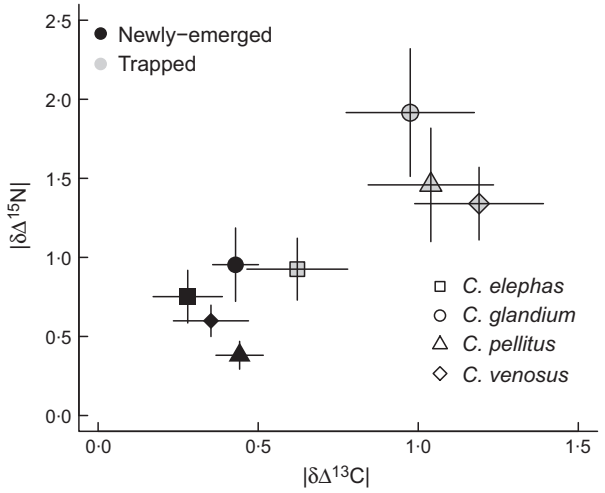

Fig. 2. Isotope signature displayed by females of the four weevil species when they emerge and at the time of breeding. $|\Delta\delta^{15}N|$ and $|\Delta\delta^{13}C|$ are the absolute differences, computed for each individual, between the isotope ratio of its keratinized tissue – of larval origin – and that of its internal, soft tissues (mean ± SE; newly emerged adults: *Curculio elephas* $n = 11$; *Curculio glandium* $n = 15$; *Curculio pellitus* $n = 10$; *Curculio venosus* $n = 8$; adults caught later in the breeding season: *C. elephas* $n = 9$; *C. glandium* $n = 10$; *C. pellitus* $n = 15$; *C. venosus* $n = 15$).

influenced by their diet ($\chi^2_{d.f.=2} = 1.182$; $P = 0{\cdot}264$) and averaged 20·46 ± 13·27 days (mean ± SD; $n = 91$). *C. glandium* females lived the longest when fed a mixed diet: 123·40 ± 57·53 days (mean ± SD; $n = 10$) vs. only 12·45 ± 4·8 days (mean ± SD; $n = 11$) when unfed. Feeding also improved the longevity of *C. venosus* and *C. pellitus* females, similar for the two species (diet: $\chi^2_{d.f.=2} = 17$; $P < 0{\cdot}0001$; species: $\chi^2_{d.f.=1} = 0.0001$; $P = 0{\cdot}98$; diet × species interaction: $\chi^2_{d.f.=2} = 0.13$; $P = 0{\cdot}83$) and lived 43·3 ± 33·74 (mean ± SD; $n = 30$), vs. only 10·75 ± 3·4 days when unfed.

OOGENESIS IN FOOD-DEPRIVED FEMALES

Dissection of ovaries of newly emerged females showed that except *C. elephas*, none of them had mature eggs at the day of their emergence (*C. glandium*: $n = 20$, *C. pellitus*: $n = 13$ and *C. venosus*: $n = 12$). *Curculio elephas* females had 3·82 mature eggs at emergence, on average (±0·3 SD; $n = 17$ females). In the same way, only *C. elephas* females were able to produce mature eggs after 8 days without any nutrient intake (6·3 ± 3·9 mature eggs, mean ± SD; $n = 10$ females). By contrast, none of the 11 *C. glandium* 8-day-old adult females started maturing eggs when unfed.

Discussion

Theoretical evolutionary ecology studies usually predict that when the reproductive success of insects is limited by unpredictable variations in their laying sites, synovigenic ovarian development can be expected, because this should give them considerable flexibility in the way they acquire energy and allocate it to survival or reproduction (Ellers & Jervis 2003; Jervis, Ellers & Harvey 2008). Despite this prediction, we show that four weevil species that occur together in the same communities and exploit the same egg-laying sites (oak acorns) – the availability of which fluctuates markedly over time – display radically different strategies of resource acquisition and allocation. Three of these species (*C. glandium*, *C. venosus* and *C. pellitus*) are strictly synovigenic and possess characteristics consistent with an income breeding strategy, while the fourth (*C. elephas*) is proovigenic and a capital breeder.

No significant between-year variation was detected over the 3-year survey and at the two sites, neither in the timing of adult emergence of each species across the breeding season nor in the fresh weight of adults at emergence (Fig. 1; see Appendix S2; Fig. S2). These findings suggest that the strategies followed by the four weevil species are robust to variations in the environmental conditions met each year by the different larval cohorts, and corroborate the consistency found previously in the patterns of dormancy and in the period of egg laying during the year found in these species (Venner *et al.* 2011). Three of the four species studied (*C. glandium*, *C. venosus* and *C. pellitus*) emerge in April, which is well before the breeding period begins in June (Venner *et al.* 2011): this 2-month interval may be long enough for them to escape from the original tree and to find a more suitable breeding site. Suitable trees can probably be identified from early April, when oak trees flower (Bonnet Masimbert 1984). Our results show that these three early-emerging species all are synovigenic (i.e. their ovigeny index equals 0), and they further suggest that these ones might be income breeders. Indeed, females of these three species all have empty ovaries at emergence, and in the field they feed as adults, as demonstrated by the isotopic signature of wild-caught females (more specifically, by the difference between isotope ratios in the

Table 1. Variability in the relationship between $|\Delta\delta^{15}N|$ and $|\Delta\delta^{13}C|$ across the four weevil species

	Mean$|\Delta\delta^{13}C|$ ± (SE)		Mean$|\Delta\delta^{15}N|$ ± (SE)			
Species	Newly emerged	Trapped	Newly emerged	Trapped	$F_{(d.f.,d.f.)}$	P
Curculio venosus	0·352 ± (0·11)	1·190 ± (0·20)	0·598 ± (0·09)	1·340 ± (0·22)	$F_{(2,20)}$5·1972	0·015*
Curculio pellitus	0·442 ± (0·07)	1·039 ± (0·19)	0·381 ± (0·08)	1·458 ± (0·35)	$F_{(2,22)}$4·2018	0·028*
Curculio glandium	0·429 ± (0·07)	0·975 ± (0·20)	0·954 ± (0·23)	1·916 ± (0·40)	$F_{(2,22)}$7·3868	0·003**
Curculio elephas	0·280 ± (0·10)	0·622 ± (0·15)	0·751 ± (0·16)	0·925 ± (0·19)	$F_{(2,17)}$1·7565	0·202^{NS}

NS, not significant, *P < 0·05; **P < 0·01; ***P < 0·001.

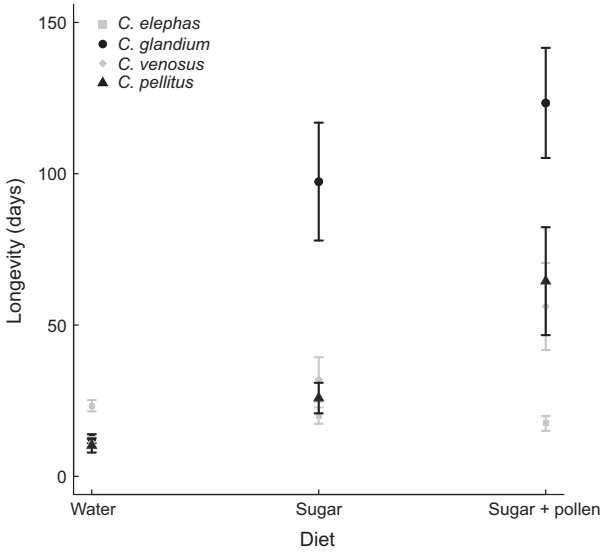

Fig. 3. Influence of diet on the longevity of females (mean ± SE). While the longevity of *Curculio elephas* females (water: $n = 31$, sugar: $n = 34$ and sugar + pollen: $n = 26$) seems to be unaffected by their diet, the life span of *Curculio glandium* females markedly increases with an enriched diet (water: $n = 11$, sugar: $n = 10$ and sugar + pollen: $n = 10$). Feeding also improves, albeit to a lesser extent than *C. glandium*, the survival of *Curculio venosus* (water: $n = 7$, sugar: $n = 8$ and sugar + pollen: $n = 8$) and *Curculio pellitus* (water: $n = 5$, sugar: $n = 8$ and sugar + pollen: $n = 6$), with no difference being detected between these two species.

keratinized and soft tissues). Moreover, when females belonging to each of these three species are deprived of food in the laboratory, they have a very short life span (around 10 days), which is incompatible with the 2-month interval they have to survive in the field before egg laying starts (Venner *et al.* 2011). Furthermore, we also show that unfed *C. glandium* females approaching death were unable to produce mature eggs in the laboratory. Taken together, these observations suggest that when the females of these three species emerge, they do not have enough energy stored to enable them even to survive until the breeding season, let alone have energy available for allocation to ovarian development. Yet some specific nutrients stored from larval reserves could be incorporated into eggs, and the three synovigenic weevil species could act as both capital and income breeders, as it has been shown experimentally in other insects (Rivero, Giron & Casas 2001; Casas *et al.* 2005). This question deserves further investigations into the isotope signature of eggs or into the fecundity of females reared with various diets.

In contrast, if females of these three species are given a rich diet based on sugar plus pollen, their life span is comparable to that observed in the field (Venner *et al.* 2011). The life span of adults of two species (*C. venosus* and *C. pellitus)* fed a rich diet was extended by about 2 months. This would give them the advantage of prior access to the egg-laying sites and allow them to breed within a short time interval early in the season (Venner *et al.* 2011). *Curculio glandium* females fed on a rich diet increased their adult life span by up to 4 months, which allowed them to lay eggs over a longer interval, in accordance with field observations [from June to September; (Venner *et al.* 2011)]. The major differences observed in the way energy is allocated to adult survival obviously explain the disparate longevities among oak weevil species and largely contribute to the strong temporal partitioning of their use of the communal resource. Such partitioning seems to constitute one of the major mechanisms underlying the coexistence of species that compete with each other in a fluctuating environment. Hence, under the general niche theory, stable coexistence is predicted among competing species whenever their ecological traits are sufficiently distinct from each other to lower the competition between them relative to that occurring within species, which enables any species within a community to grow whenever it becomes rare (Chesson 2000; Chesson *et al.* 2004). The intra-annual partitioning mechanism actually seems to be involved in the coexistence of these four weevil species (Venner *et al.* 2011).

Although the fourth species, *C. elephas*, exploits the same unpredictable environment as the other three species, it is clearly a capital breeder. The between-year fluctuations in the availability of oviposition sites could even be increased for this species: while years of high resource abundance could provide all weevil species with unlimited egg-laying sites, *C. elephas* would suffer more than the other species on years of low acorn production as the resource is likely to be already used by early species at the time of their emergence. In spite of this environment highly variable between years, we found that *C. elephas* adults emerge in August when females readily start laying eggs (Venner *et al.* 2011): females have mature oocytes as soon as they emerge, when oak acorns are already mature and ready for exploitation by weevil larvae. *Curculio elephas* adult females do not seem to need to feed, because the stable isotope profile of wild-caught females remained unchanged from their larval stage. Moreover, when these females were given a rich diet, their life span was not longer than that of unfed individuals. Nor did they require feeding during adulthood to produce mature oocytes. To summarize, these proovigenic females can breed successfully drawing solely on energy of larval origin, which corresponds to a capital breeding strategy (Jervis, Ellers & Harvey 2008).

Curculio elephas mature larvae are much heavier than those of the three other species when they leave the acorn (Pélisson *et al.* 2011), and similarly, *C. elephas* newly emerging adults are heavier than the other species (see Appendix S2, Fig. S2): besides their greater body size, they may therefore have greater energy reserves acquired during the larval stage than the other three species. This interspecific difference between adults composing the community a given year is unlikely to be due to heterogeneous conditions experienced by the distinct larval cohorts, which might occur owing to their distinct life cycles (Venner *et al.* 2011). Indeed, we did not detect any variation in the weight of emerging adults across years, for any species (see Appendix S2). This suggests that the quality of acorns, possibly varying between years, does not impact the energetic status of adults at emergence. Thus, ecophysiological characteristics of the breeding strategy should also be consistent across years for a given species. This energy seems

to be rapidly and entirely allocated to reproduction as soon as the adult emerges, which should make this species very efficient in exploiting acorns when local resources are abundant. However, when the local resource is scarce, the adults that emerge might fail to breed owing to their poor ability to move towards more favourable, but distant sites (because they are carrying excess body reserves destined for ovarian development that prevent them from dispersing spatially (Jervis, Boggs & Ferns 2005) and/or because they do not have enough time to prospect). We suggest that such a capital breeder strategy can only be efficient in a fluctuating environment if it is combined with other life-history traits that buffer unpredictable temporal environmental fluctuations. Thus, *C. elephas* is the only weevil species in this system that spreads significantly the emergence of adults belonging to the same larval cohort over several years, which has been interpreted as a form of bet-hedging (Menu, Roebuck & Viala 2000; Menu & Desouhant 2002; Gourbière & Menu 2009; Venner *et al.* 2011). This strategy ensures that at least some of the individuals that share the same genotype will encounter favourable local conditions and go on to breed successfully. Adults emerging when the resource is locally abundant should be able to maximize their lifetime reproductive success, while individuals emerging in a year when the resource is depleted would be sacrificed. In *C. elephas*, capital breeding might have evolved alongside with this bet-hedging strategy. In contrast, the other three species do not spread significantly their adult emergence over several years (Venner *et al.* 2011), and they can be expected to exploit the oviposition sites less efficiently than *C. elephas* when these are locally abundant: hence, adults from these early-emerging species face a significant risk of mortality during the prolonged interval between emergence and breeding, and they have to find food before they can breed. In contrast, these three species may be more efficient than *C. elephas* in taking advantage of the spatial variability of resource availability when resources are locally absent. The co-occurrence of both pro- and synovigenic species sharing the same fluctuating environment provides evidence that the different species cope in various ways with the spatial and temporal heterogeneity in the egg-laying site availability. This may be a key aspect of niche partitioning and of the coexistence of species that compete for the same fluctuating resource.

Insects display multiple strategies of acquiring energy and allocating it to different activities, and these have been studied in great detail (see Strand & Casas 2008 for a review among parasitoids). These strategies show great plasticity in response to numerous factors, including environmental stress (Wessels, Jordan & Hahn 2010), the quality of energy resources (Fischer, O'Brien & Boggs 2004) and diet or metabolism (O'Brien, Boggs & Fogel 2004; Min *et al.* 2006). At the individual level, there may be several strategies ranging from income to capital breeding, depending on the nutrient considered (Casas *et al.* 2005). Our work was not designed to reveal differences at such a fine scale, but it still provides the first report of the simultaneous occurrence of synovigeny and proovigeny breeding strategies in a community of sibling species that are competing with each other for the same fluctuating resource. Unlike previously proposed hypotheses, our result show an exception to the conventional wisdom that environmental stochasticity necessarily selects for synovigenic and income breeding insects and selects against proovigeny and capital breeding. Our findings suggest that environmental stochasticity does not favour the evolution of a single optimal breeding strategy, but may instead favour the diversification of these strategies. Our work should encourage future studies designed at testing this hypothesis.

Acknowledgements

This work was funded by the French National Research Agency (ANR: CoCoReCo project JC09_470585) and by the CNRS. We thank F. Debias for his technical help in field surveys and two anonymous reviewers for their comments on an earlier draft of the manuscript.

References

Boggs, C.L. (1997) Reproductive allocation from reserves and income in butterfly species with differing adult diets. *Ecology*, **78**, 181–191.

Bonnet Masimbert, M. (1984) Biologie florale et cycle de reproduction de quelques arbres forestiers. *Douglas, pin sylvestre, chêne. Pollinisation et productions végétales* (eds P. Pesson & J. Louveaux), pp. 219–242. INRA, Paris.

Casas, J., Nisbet, R.M., Swarbrick, S. & Murdoch, W.W. (2000) Eggload dynamics and oviposition rate in a wild population of a parasitic wasp. *Journal of Animal Ecology*, **69**, 185–193.

Casas, J., Pincebourde, S., Mandon, N., Vannier, F., Poujol, R. & Giron, D. (2005) Lifetime nutrient dynamics reveal simultaneous capital and income breeding in a parasitoid. *Ecology*, **86**, 545–554.

Casas, J., Vannier, F., Mandon, N., Delbecque, J.P., Giron, D. & Monge, J.P. (2009) Mitigation of egg limitation in parasitoids: immediate hormonal response and enhanced oogenesis after host use. *Ecology*, **90**, 537–545.

Chesson, P. (2000) Mechanisms of maintenance of species diversity. *Annual Review of Ecology and Systematics*, **31**, 343–366.

Chesson, P., Gebauer, R.L.E., Schwinning, S., Huntly, N., Wiegand, K., Ernest, M.S.K., Sher, A., Novoplansky, A. & Weltzin, J.F. (2004) Resource pulses, species interactions, and diversity maintenance in arid and semi-arid environments. *Oecologia*, **141**, 236–253.

Coutin, R. (1992) Original characteristics of the evolving cycles of some European weevil species: *Curculio elephas* Gyll., *C. nucum* L., *C. glandium* Marsh., *C. venosus* Grav. and *C. villosus* F. *Memoires de la Societe Royale Belge d'Entomologie*, **35**, 259–266.

DeNiro, M.J. & Epstein, S. (1978) Influence of diet on the distribution of carbon isotopes in animals. *Geochimica et Cosmochimica Acta*, **42**, 495–506.

DeNiro, M.J. & Epstein, S. (1981) Influence of diet on the distribution of nitrogen isotopes in animals. *Geochimica et Cosmochimica Acta*, **45**, 341–351.

Dixon, A.F.G., Horth, S. & Kindlmann, P. (1993) Migration in insects: cost and strategies. *Journal of Animal Ecology*, **62**, 182–190.

Ellers, J. & Jervis, M.A. (2003) Body size and the timing of egg production in parasitoid wasps. *Oikos*, **102**, 164–172.

Ellers, J. & Jervis, M.A. (2004) Why are so few parasitoid wasp species proovigenic? *Evolutionary Ecology Research*, **6**, 993–1002.

Ellers, J., Sevenster, J.G. & Driessen, G. (2000) Egg load evolution in parasitoids. *The American Naturalist*, **156**, 650–665.

Ellers, J. & van Alphen, J.J.M. (1997) Life history evolution in *Asobara tabida*: plasticity in allocation of fat reserves to survival and reproduction. *Journal of Evolutionary Biology*, **10**, 771–785.

Fischer, B., Dieckmann, U. & Taborsky, B. (2010) When to store energy in a stochastic environment. *Evolution*, **65**, 1221–1232.

Fischer, K., O'Brien, D.M. & Boggs, C.L. (2004) Allocation of larval and adult resources to reproduction in a fruit-feeding butterfly. *Functional Ecology*, **18**, 656–663.

Fischer, B., Taborsky, B. & Dieckmann, U. (2009) Unexpected patterns of plastic energy allocation in stochastic environments. *The American Naturalist*, **173**, E108–E120.

Gourbière, S. & Menu, F. (2009) Adaptive dynamics of dormancy duration variability: evolutionary trade-off and priority effect lead to suboptimal adaptation. *Evolution*, **63**, 1879–1892.

Heimpel, G. (1998) Egg limitation in parasitoids: a review of the evidence and a case study. *Biological Control*, **11**, 160–168.
Hoffmann, A. (1954) *Faune de France. Coleopteres Curculionides, (Deuxième partie)*. Fédération Française des Sociétés de Sciences Naturelles, Paris, France.
Hood-Nowotny, R. & Knols, B.G.J. (2007) Stable isotope methods in biological and ecological studies of arthropods. *Entomologia Experimentalis et Applicata*, **124**, 3–16.
Houston, A.I., Stephens, P.A., Boyd, I.L., Harding, K.C. & McNamara, J.M. (2006) Capital or income breeding? A theoretical model of female reproductive strategies. *Behavioral Ecology*, **18**, 241–250.
Hughes, J. & Vogler, A.P. (2004) The phylogeny of acorn weevils (genus *Curculio*) from mitochondrial and nuclear DNA sequences: the problem of incomplete data. *Molecular Phylogenetics and Evolution*, **32**, 601–615.
Ihaka, R. & Gentleman, R. (1996) R: a language for data analysis and graphics. *Journal of Computational and Graphical Statistics*, **5**, 299–314.
Inger, R. & Bearhop, S. (2008) Applications of stable isotope analyses to avian ecology. *Ibis*, **150**, 447–461.
Jervis, M.A., Boggs, C.L. & Ferns, P.N. (2005) Egg maturation strategy and its associated trade-offs: a synthesis focusing on Lepidoptera. *Ecological Entomology*, **30**, 359–375.
Jervis, M.A., Ellers, J. & Harvey, J.A. (2008) Resource acquisition, allocation, and utilization in parasitoid reproductive strategies. *Annual Review of Entomology*, **53**, 361–385.
Jervis, M.A. & Ferns, P.N. (2004) The timing of egg maturation in insects: oviegeny index and initial egg load as measures of fitness and of resource allocation. *Oikos*, **107**, 449–461.
Jervis, M.A., Heimpel, G.E., Ferns, P.N., Harvey, J.A. & Kidd, N.A.C. (2001) Life-history strategies in parasitoid wasps: a comparative analysis of 'ovigeny'. *Journal of Animal Ecology*, **70**, 442–458.
Kelly, D. & Sork, V.L. (2002) Mast seeding in perennial plants: why, how, where? *Annual Review of Ecology and Systematics*, **33**, 427–447.
Liebhold, A., Sork, V.L., Peltonen, M., Bjørnstad, O.N., Westfall, R., Elkinton, J. & Knops, M.H.J. (2004) Within-population spatial synchrony in mast seeding of North American oaks. *Oikos*, **104**, 156–164.
Lorenz, M.W. (2007) Oogenesis-flight syndrome in crickets: age-dependent egg production, flight performance, and biochemical composition of the flight muscles in adult female *Gryllus bimaculatus*. *Journal of Insect Physiology*, **53**, 819–832.
Markow, T.A., Anwar, S. & Pfeiler, E. (2000) Stable isotope ratios of carbon and nitrogen in natural populations of *Drosophila* species and their hosts. *Functional Ecology*, **14**, 261–266.
Menu, F. & Debouzie, D. (1993) Coin-flipping plasticity and prolonged diapause in insects: example of the chestnut weevil *Curculio elephas* (Coleoptera: Curculionidae). *Oecologia*, **93**, 367–373.
Menu, F. & Desouhant, E. (2002) Bet-hedging for variability in life cycle duration: bigger and later-emerging chestnut weevils have increased probability of a prolonged diapause. *Oecologia*, **132**, 167–174.
Menu, F., Roebuck, J.P. & Viala, M. (2000) Bet-hedging diapause strategies in stochastic environments. *The American Naturalist*, **155**, 724–734.
Min, K.J., Hogan, M.F., Tatar, M. & O'Brien, D.M. (2006) Resource allocation to reproduction and soma in Drosophila: a stable isotope analysis of carbon from dietary sugar. *Journal of Insect Physiology*, **52**, 763–770.
O'Brien, D.M., Boggs, C.L. & Fogel, M.L. (2004) Making eggs from nectar: the role of life history and dietary carbon turnover in butterfly reproductive resource allocation. *Oikos*, **105**, 279–291.
O'Brien, D.M., Fogel, M.L. & Boggs, C.L. (2002) Renewable and nonrenewable resources: amino acid turnover and allocation to reproduction in Lepidoptera. *Proceedings of the National Academy of Sciences of the United States of America*, **99**, 4413–4418.
Papaj, D.R. (2000) Ovarian dynamics and host use. *Annual Review of Entomology*, **45**, 423–448.
Pélisson, P.F., Henri, H., Bel-Venner, M.C., Allemand, R., Merville, A., Menu, F. & Venner, S. (2011) Identification at the larval stage of four Curculio species coexisting on oak trees using PCR-RFLP. *Entomologia Experimentalis et Applicata*, **138**, 77–82.
Perrin, N. & Sibly, R.M. (1993) Dynamic models of energy allocation and investment. *Annual Review of Ecology and Systematics*, **24**, 379–410.
Richard, R. & Casas, J. (2009) Stochasticity and controllability of nutrient sources in foraging: host-feeding and egg resorption in parasitoids. *Ecological Monographs*, **79**, 465–483.
Rivero, A. & Casas, J. (1999) Incorporating physiology into parasitoid behavioral ecology: the allocation of nutritional resources. *Researches on Population Ecology*, **41**, 39–45.
Rivero, A., Giron, D. & Casas, J. (2001) Lifetime allocation of juvenile and adult nutritional resources to egg production in a holometabolous insect. *Proceedings of the Royal Society of London Series B, Biological Sciences*, **268**, 1231–1237.
Rivero-Lynch, A.P. & Godfray, H.C.J. (1997) The dynamics of egg production, oviposition and resorption in a parasitoid wasp. *Functional Ecology*, **11**, 184–188.
Rosenheim, J.A. (2011) Stochasticity in reproductive opportunity and the evolution of egg limitation in insects. *Evolution*, **65**, 2300–2312.
Rosenheim, J.A., Heimpel, G.E. & Mangel, M. (2000) Egg maturation, egg resorption and the costliness of transient egg limitation in insects. *Proceedings of the Royal Society of London Series B, Biological Sciences*, **267**, 1565–1573.
Schauff, M.E. (1986) *Collecting and preserving insects and mites: techniques & tools*. Museum of Washington, USA, Washington DC.
Stephens, P., Boyd, I., McNamara, J.M. & Houston, A.I. (2009) Capital breeding and income breeding: their meaning, measurement, and worth. *Ecology*, **90**, 2057–2067.
Strand, M.R. & Casas, J. (2008) Parasitoid and host nutritional physiology in behavioral ecology. *Behavioral ecology of insect parasitoids* (eds E. Wajnberg, C. Bernstein & J. van Alphen), pp. 113–128. Blackwell, Oxford, UK.
Tammaru, T. & Haukioja, E. (1996) Capital breeders and income breeders among Lepidoptera – consequences to population dynamics. *Oikos*, **77**, 561–564.
Tomassone, R., Danzard, M., Daudin, J.J. & Masson, J.P. (1988) *Discrimination et classement*. Masson, Paris.
Venner, S., Pélisson, P.F., Bel-Venner, M.C., Débias, F., Rajon, E. & Menu, F. (2011) Coexistence of insect species competing for a pulsed resource: toward a unified theory of biodiversity in fluctuating environments. *PLoS ONE*, **6**, 18039.
Warner, D.A., Bonnet, X., Hobson, K.A. & Shine, R. (2008) Lizards combine stored energy and recently acquired nutrients flexibly to fuel reproduction. *Journal of Animal Ecology*, **77**, 1242–1249.
Wessels, F.J., Jordan, D.C. & Hahn, D.A. (2010) Allocation from capital and income sources to reproduction shift from first to second clutch in the flesh fly, *Sarcophaga crassipalpis*. *Journal of insect physiology*, **56**, 1269–1274.
Zera, A.J. (2005) Intermediary metabolism and life history trade-offs: lipid metabolism in lines of the wing-polymorphic cricket, *Gryllus firmu*s, selected for flight capability *vs.* early age reproduction. *Integrative and Comparative Biology*, **45**, 511–524.

Received 4 May 2011; accepted 16 September 2011
Handling Editor: Alison Brody

Supporting Information

Additional supporting information may be found in the online version of this article.

Figure S1. Between-year fluctuations of the acorn crop at the two sites.

Figure S2. Between-year comparison of fresh adult weight.

Figure S3. Representation of isotope signature of oak acorns.

Figure S4. Representation of relative differences between keratinized tissues and internal tissues of females.

Appendix S1. Between-year fluctuations of the acorn crop.

Appendix S2. Between-year comparison of the fresh weight of adult weevils.

Appendix S3. Isotope signature of oak acorns.

Appendix S4. Relative differences between keratinized tissues and internal tissues of females.

As a service to our authors and readers, this journal provides supporting information supplied by the authors. Such materials may be reorganized for online delivery, but are not copy-edited or typeset. Technical support issues arising from supporting information (other than missing files) should be addressed to the authors.

« La théorie, c'est quand on sait tout et que rien ne fonctionne. - La pratique, c'est quand tout fonctionne et que personne ne sait pourquoi. - Si la pratique et la théorie sont réunies, rien ne fonctionne et on ne sait pas pourquoi. »

Albert Einstein

CHAPITRE 4 : Développements méthodologiques pour améliorer l'outil isotopique

Une grande partie de ce travail de thèse a consisté à essayer d'améliorer les outils isotopiques à notre disposition afin de pousser plus loin les investigations scientifiques. Bien évidemment les domaines dans lesquels nous avons travaillé sont ceux qui concernent la majorité des analyses que nous utilisons et qui viennent d'être décrits dans les chapitres précédents.

Le premier domaine auquel nous nous sommes intéressés est celui des analyses isotopiques des eaux, et plus particulièrement des analyses par la technique dite « d'équilibration » que nous avons essayé de mieux contraindre. Puis nous avons essayé d'améliorer l'outil isotopique concernant les analyses isotopiques des carbonates à la fois pour le rapport $^{13}C/^{12}C$ et le rapport $^{18}O/^{16}O$.

En ce qui concerne les analyses isotopiques des carbonates nous avons travaillé sur des questions techniques fondamentales variées comme le fractionnement isotopique de l'oxygène entre les carbonates d'apatites et l'eau, les fractionnements isotopiques du carbone et de l'oxygène entre aragonite et calcite sur des organismes vivants actuels, la possibilité d'accéder de manière semi-automatique aux signatures isotopiques en carbone et en oxygène de la calcite et de la dolomite dans des mélanges de proportions variables ainsi que la comparaison entre la variabilité naturelle et la variabilité instrumentale des analyses isotopiques du carbone et de l'oxygène sur des microfossiles.

Puis, nous nous sommes intéressés à un domaine qui constitue une part importante de notre travail analytique, à savoir les analyses isotopiques $^{18}O/^{16}O$ des phosphates biogéniques afin d'améliorer la qualité des analyses, de les automatiser le plus possible et de réduire la taille de la prise d'essai afin d'accéder à des échantillons de taille plus réduite.

Enfin nous avons abordé les analyses isotopiques du soufre au moyen d'un nouveau système de préparation permettant à la fois de réduire la prise d'essai en conservant le même qualité d'analyse mais permettant également de réaliser des analyses multi-isotopiques simultanées sur les éléments N, C et S.

Le but de tous ces travaux étant toujours de fournir à l'analyste des outils de plus en plus performants afin de pouvoir répondre à de nouvelles interrogations scientifiques.

4.1/ Analyse des eaux

Depuis les débuts des analyses isotopiques des isotopes stables, l'eau a toujours été une cible de choix pour de nombreuses études. Les premières analyses isotopiques $^{18}O/^{16}O$ des eaux utilisant la technique d'équilibration eau-dioxyde de carbone remontent à 1953 par Epstein et Mayeda [1]. Puis au cours de la deuxième moitié du vingtième siècle cette technique d'équilibration a été également utilisée pour déterminer les rapports isotopiques D/H des eaux en utilisant l'équilibration entre l'eau et l'hydrogène [2-5]. L'apparition de systèmes automatisés et l'amélioration des instruments de mesures ont permis d'améliorer considérablement les précisons des analyses aussi bien $\delta^{18}O_{SMOW}$ (± 0,05 ‰) que δD_{SMOW} (± 0,5 ‰), ainsi que de réduire les prises d'essai jusqu'à des aliquotes de 200 µL. Ceci permet d'augmenter la résolution des interprétations concernant par exemple l'origine des masses d'eaux ainsi que les phénomènes de mélange, d'évaporation-condensation qu'elles peuvent subir dans l'hydrosphère ou lors de leurs interactions avec l'atmosphère ou la croute terrestre. En particulier ces phénomènes peuvent changer la composition ionique de ces eaux entre des

dilutions faibles et des eaux sursaturées. Par exemple certaines eaux de pluies continentales ont des salinités proches de $0gL^{-1}$ alors que les eaux de la Mer Morte présentent des salinités de 250-300 gL^{-1} eq. NaCl. Il est connu depuis les premières études de ces réactions d'équilibration que les coefficients d'équilibration dépendent à la fois de la composition chimique et de la force ionique des solutions salées [6-9]. Ainsi, il a été montré que des décalages systématiques supérieurs aux incertitudes de mesures pouvaient apparaître lors des mesures isotopiques de solutions salées si l'on utilisait les facteurs de fractionnement établis pour de l'eau pure [10-14]. Devant le manque de données de la littérature sur ce sujet il nous est donc apparu important d'envisager une approche systématique afin d'essayer de déterminer les facteurs de fractionnements et les cinétiques d'échange pour les réactions d'équilibration $CO_2 – H_2O$ et $H_2 – H_2O$. C'est ce que nous avons fait respectivement dans les publications 4.1 et 4.2 en reconstituant des solutions de KCl et NaCl ayant des salinités de 0 à 250 gL^{-1}. Cette étude systématique a été rendue possible par l'utilisation d'un système d'équilibration automatisée de type MultiPrep (voir figure 4.1) en mode AquaPrep en ligne avec un IRMS équipé d'un dual inlet de type IsoPrime dont le principe de fonctionnement est illustré dans la figure 4.2.

Figure 4.1 : Système IsoPrime-MultiPrep installé dans le laboratoire d'isotopes stables de LGL-TPE.

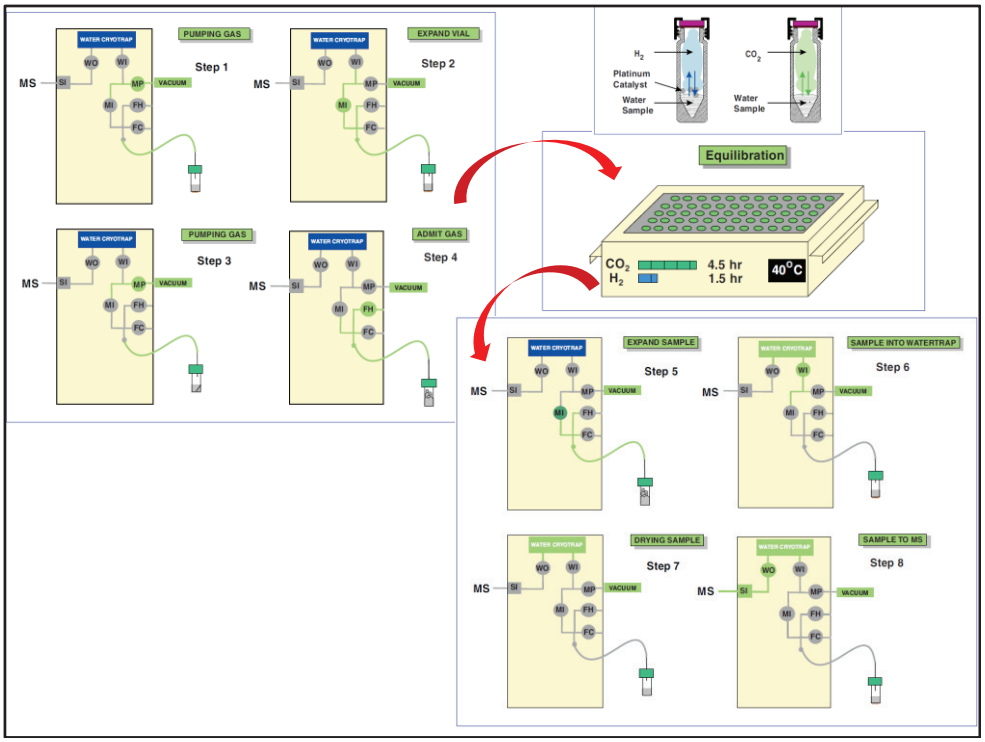

Figure 4.2 : Principe de fonctionnement du de l'AquaPrep : Etapes 1 à 4 introduction du gaz de référence en contact avec l'eau à analyser. Ensuite équilibration H_2-H_2O ou CO_2-H_2O ; Etapes 5 à 8 : séchage du gaz équilibré et introduction dans le dual inlet du spectromètre de masse.

Les premiers résultats que nous avons obtenus concernent le temps pour atteindre l'équilibre. Pour des eaux pures, dans les conditions standards d'utilisation du système MultiPrep qui effectue l'équilibration à 40°C les temps d'équilibrations recommandés par le constructeur sont de 5h pour CO_2 – H_2O et de 2h pour H_2-H_2O moyennant l'utilisation d'un catalyseur à base de platine. Nous avons mis en évidence que pour les gammes de salinités que nous avons utilisées les temps nécessaires pour atteindre l'équilibre varient de 5 à 12h pour CO_2 – H_2O et doit être porté à 3h pour H_2-H_2O. Ces résultats sont similaires pour KCl et NaCl. De plus, nous avons mis en évidence que si les analyses isotopiques de l'eau de mer ayant des salinités proche de 35 gL^{-1} nécessitent des corrections mineures dues à leur concentrations en sel (-0,15 ‰ pour le $\delta^{18}O_{SMOW}$ et -2 ± 0,5 ‰ pour le δD_{SMOW}, il n'en est pas de même pour les

concentrations plus élevées en sel. En effet nous avons calculé que les analyses $\delta^{18}O_{SMOW}$ étaient surévaluées de 0,4 ‰ à 0,6 ‰ dans le cas de salinité entre 100 et 250 gL^{-1} et que les analyses δD_{SMOW} étaient surévaluées de 5 ± 0,5 ‰ à 10 ± 0.5‰ dans le cas de salinité entre 100 et 265 gL^{-1}. Ainsi au vu de nos travaux, nous recommandons que les deux signatures isotopiques $\delta^{18}O_{SMOW}$ et δD_{SMOW} mesurées par équilibration soient corrigées de l'effet de la salinité sur le coefficient de fractionnement dans le cas d'échantillons d'eaux riches en sel comme des lagunes, lacs salés ou des eaux hydrothermales hypersalines.

Chemical Geology 264 (2009) 122–126

Contents lists available at ScienceDirect

Chemical Geology

journal homepage: www.elsevier.com/locate/chemgeo

Oxygen isotope fractionation and equilibration kinetics between CO_2 and H_2O as a function of salinity of aqueous solutions

Christophe Lécuyer [a,b,*], Véronique Gardien [a], Thomas Rigaudier [a], François Fourel [a], François Martineau [a], Alexandre Cros [a]

[a] Laboratoire UMR CNRS 5125, 'Paléoenvironnements et Paléobiosphère', Université Lyon 1, Lyon 69003, France
[b] Institut Universitaire de France, 103, bd Saint-Michel, 75005 Paris, France

ARTICLE INFO

Article history:
Received 26 November 2008
Received in revised form 24 February 2009
Accepted 25 February 2009

Editor: D. Rickard

Keywords:
Oxygen isotope
Fractionation
Kinetics
Salinity
Equilibration technique
Aqueous solutions

ABSTRACT

Oxygen isotope fractionation and equilibration kinetics between CO_2 and H_2O have been investigated at 313 K for salinities (S) ranging from 0 to 250 g L^{-1}. In this range of salinity, times needed to reach oxygen isotope equilibrium between CO_2 and H_2O increase from 4 h to 12 h. Isotopic exchanges are comparable for KCl and NaCl-like (sea salt) solutions and are described by first-order kinetic reactions with $\ln(k) = -8.1485(\pm 0.0057) - 0.00474(\pm 3.87\times10^{-5})S$. The oxygen isotope fractionation factor between CO_2 and H_2O increases with salinity for both sea salt and KCl solutions with concentrations ranging from 0 to 250 g L^{-1} according to the following equation: $1000\ln(\alpha_{CO2-H2O})\text{sea salt} = 37.02(\pm5\times10^{-3}) + 3.96\times10^{-3}(\pm1.1\times10^{-4})S - 6.38\times10^{-6}(\pm4.5\times10^{-7})S^2$ ($R^2 = 0.998$). The oxygen isotope analysis of seawater samples with a salinity of 35 g L^{-1} requires minor corrections of −0.15‰ (V–SMOW). However, oxygen isotope ratios are overestimated by 0.4‰ to 0.6‰ in the case of highly saline natural waters ($100 < S < 250$ g L^{-1}). Corrections of the oxygen isotope ratios due to changes in the salinity-dependent fractionation factors between CO_2 and H_2O must be taken into account during the study of waters sampled from salt marshes, hypersaline lakes and lagoons, or hydrothermal brines.

1. Introduction

Determination of oxygen isotope ratios of natural waters is commonly obtained by equilibration with carbon dioxide according to Epstein and Mayeda's (1953) fundamental study. Since the recent development of automated preparation systems for the measurement of stable oxygen and hydrogen isotope ratios of waters, analytical precisions of ±0.05‰ and ±0.5‰ can be reached routinely with samples of about 200 µL by using isotopic equilibration techniques between CO_2 and H_2O (e.g. Horita et al., 1989; McCarthy et al., 2005). These high-precision isotopic measurements allow an increase in resolution of source water identification, and mixing or evaporation–condensation processes that can affect them in the hydrosphere or during interactions with the atmosphere or the Earth's crust. These physical and chemical processes are able to change the ionic concentration of aqueous solutions from highly diluted to over-saturated solutions. For example, rainfall located in the central parts of continents have a salinity (S) ≈ 0 g L^{-1} whereas highly evaporated waters of the Dead Sea or hydrothermal brines of the Red Sea have S = 250–300 g L^{-1} eq. NaCl.

It is known since the studies pioneered by Taube (1954), Craig and Gordon (1965), O'Neil and Adami (1969) and Truesdell (1974) that oxygen isotope fractionation between CO_2–H_2O depends on both the chemical composition and the ionic strength of aqueous salt solutions. Other studies have confirmed that the resulting oxygen isotopic offsets relative to the fractionation factor determined for pure water are much higher than analytical precisions (Sofer and Gat, 1972; Kazahaya, 1986; O'Neil and Truesdell, 1991; Fortier, 1994) even though

Table 1
X-ray-fluorescence chemical analysis of a natural sea salt from the salt marsh of Guérande, France.

Element wt.%	Sea salt "Guérande"
SiO_2	0.06
MgO	0.32
CaO	0.2
Na_2O	88
K_2O	0.06
H_2O^+	4.04
H_2O^-	7.29
Sum	99.97
Ppm	
Sr	62
Rb	7
S	21200

* Corresponding author. Laboratoire UMR CNRS 5125, 'Paléoenvironnements et Paléobiosphère', Université Lyon 1, Lyon 69003, France.
E-mail address: clecuyer@univ-lyon1.fr (C. Lécuyer).

0009-2541/$ – see front matter © 2009 Elsevier B.V. All rights reserved.
doi:10.1016/j.chemgeo.2009.02.017

Table 2
Comparison of the $\delta^{18}O$ of an aqueous solution of $S = 150$ g L^{-1} obtained by dissolution of the non-dried sea salt (TES150-1 and TES150-2 samples) with double-deionized water ($\delta^{18}O = -10.38$‰ V–SMOW) with a third one (TES150-D) obtained with the same salt dried at 110 °C overnight before being dissolved.

Aqueous solution	Salinity (g L^{-1})	H_2O in salt wt.%	$\delta^{18}O$ (‰ V–SMOW)
TES150-1	150	7	−10.35
TES150-2	150	7	−10.38
TES150-D	150	0	−10.37

Horita et al. (1995) concluded that NaCl has little effect (within analytical uncertainties) on the oxygen isotope fractionation factor at temperatures below 200 °C. Precise knowledge of the relationship that linked fractionation factors to the salt content is a prerequisite to the oxygen isotope analysis of waters from salt marshes, hypersaline lagoons, and hydrothermal brines (e.g. Chiodini et al., 2001; Pierret et al., 2001; Kloppmann et al., 2002; Risacher et al., 2003; Ladouche and Weng, 2005; Alexeev et al., 2007). Mixing of water end-members is also commonly performed by using both D/H and $^{18}O/^{16}O$ as natural tracers. This quantification can be weakened without applying the adequate salinity-dependent fractionation factors during the case study of water reservoirs with highly contrasted salinities. Approximations on the knowledge of these isotopic fractionation factors would also generate errors on the determination of the source of rainfall that are based on the slopes and intercepts of evaporation trajectories relative to the meteoric water line.

However, a systematic approach to calculate oxygen isotope fractionation factors and exchange kinetics for the CO_2–H_2O system as a function of salinity is still lacking. Therefore we have determined oxygen isotope fractionation factors and exchange kinetics between CO_2 and H_2O in NaCl (sea salt) and KCl aqueous solutions with salinities ranging from 0 to 250 g L^{-1}.

2. Analytical techniques

Two hundred and ninety-nine oxygen isotope measurements of water have been performed to determine kinetics and oxygen isotope fractionation between CO_2 and H_2O at 313 K for salinities ranging from 0 to 250 g L^{-1}. Two salts have been used for the experiments, a synthetic sylvite (99.9% KCl) and a natural sea salt mainly made of NaCl (Table 1) that was sampled in the Guérande salt marsh along the Northern Atlantic seaside in North-western France. Aqueous solutions of salinity ranging from 15 to 250 g L^{-1} have been prepared by dissolving from 1.9 to 31.5 g of KCl and a natural sea salt from the salt marsh of Guérande, France, in 125 mL of double-distilled water (DDW) which has a $\delta^{18}O$ value of -10.38 ± 0.05‰ (V–SMOW). A 3 L aliquot of this doubly distilled water was stored in a glass bottle. The natural sea salt is mainly NaCl with a minor sulfate content and 7 wt.% of adsorbed H_2O (Table 1) according to XRF analysis performed at the University Claude Bernard Lyon 1 (LST UMR 5570). This salt was therefore dried at 110 °C overnight before to be dissolved in double-distilled water (DDW). It is however noteworthy that the $\delta^{18}O$ of DDW and of the same water of $S = 150$ g L^{-1} obtained by dissolution of the non-dried sea salt are similar within analytical uncertainties (Table 2).

It was calibrated versus SMOW GISP and SLAP to determine its $\delta^{18}O$ value and it was used for all the salt solutions. Prior to equilibration analyses of salty solutions, we investigated the variations of the equilibration time as a function of the salinities of the solutions. For $S = 0$; 35; 150 and 250 g L^{-1}, the rate of oxygen isotope exchange with time between CO_2 and H_2O is reported as '$\delta^{18}O$ offset' where $\delta^{18}O\ \text{offset} = (({}^{18}O/{}^{16}O_{SAM} - {}^{18}O/{}^{16}O_{DDW})/{}^{18}O/{}^{16}O_{DDW} - 1) \times 10^3$ (SAM = sample; DDW = doubly distilled water).

Aliquots of 200 µL of water were automatically reacted at 313 K with CO_2 and analyzed using a MultiPrep™ system on line with an Elementar IsoPrime™ dual inlet IRMS. Internal and external $\delta^{18}O$ reproducibilities were ±0.03‰ and ±0.1‰, respectively. Oxygen isotope ratios are reported relative to V–SMOW in the ‰ δ unit after scaling the raw data to the "true" isotopic ratios of SMOW, SLAP and GISP international standards. Kinetics experiments were performed analyzing water samples immediately after the autofill sequence was completed. The autofilling time was taken into account to determine the total equilibration time. All the experiments have been performed at 313 K, a temperature routinely used by some of the automated preparation systems dealing with the stable isotope analysis of large series of water samples.

3. Results

The Doubly Distilled Water (DDW) has a $\delta^{18}O$ value of −10.38‰ (V–SMOW). For each sea salt solution, steady-state isotopic

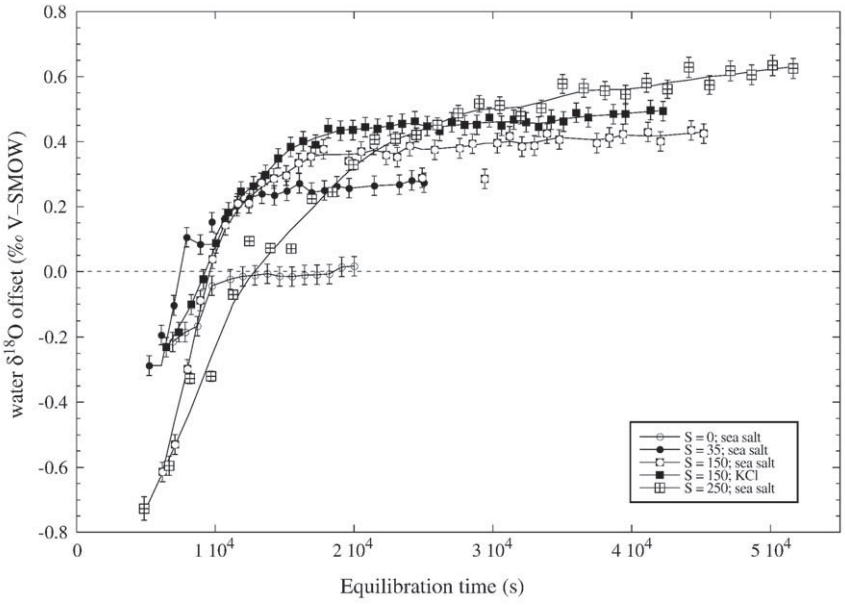

Fig. 1. Variations with equilibration time of the oxygen isotope offset (defined as the difference between measured water $\delta^{18}O$ at any time t and the composition of pure water with a $\delta^{18}O$ of −10.38‰ V–SMOW) of sea salt (NaCl-like) and KCl aqueous solutions at 313 K. Note that for the five experiments, oxygen isotope compositions of waters reach steady-state values for equilibration times depending on salinities and not on salt composition.

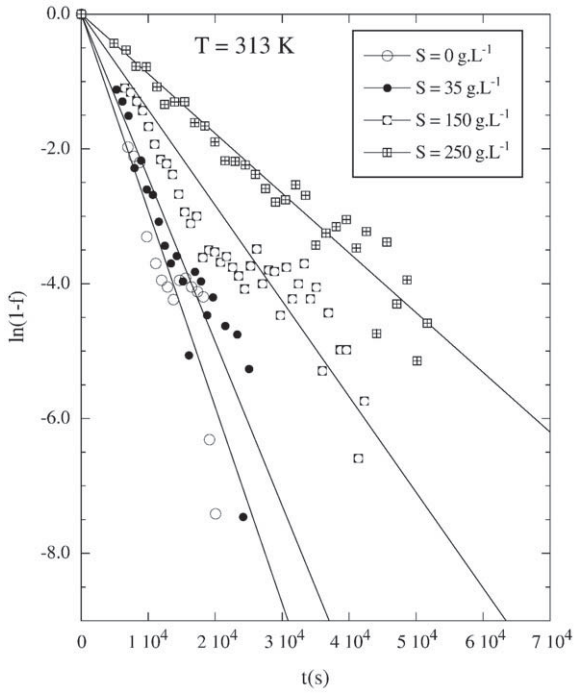

Fig. 2. Progress with time of the fraction of oxygen isotopes exchanged between carbon dioxide and water at 313 K. The absolute values of the slopes of the straight lines are the rate constants k of the reaction for salinities of 0, 35, 150, and 250 g L^{-1}, respectively. For $S=0$: $\ln(1-f)=-2.91\times10^{-4}(\pm1.29\times10^{-5})$ with $R^2=0.835$; for $S=35$: $\ln(1-f)=-2.43\times10^{-4}(\pm8.27\times10^{-6})$ with $R^2=0.877$; for $S=150$: $\ln(1-f)=-1.42\times10^{-4}(\pm3.49\times10^{-6})$ with $R^2=0.831$ and for $S=250$: $\ln(1-f)=-8.85\times10^{-5}(\pm1.72\times10^{-6})$ with $R^2=0.946$.

compositions are observed and are considered to represent isotopic equilibrium values between CO_2 and H_2O (Fig. 1; data are available as electronic supplement).

The order of the reaction was tested by a best fit of the data with a first-order law:

$$f = 1 - exp(-kt) = \frac{\delta^{18}O_i - \delta^{18}O_t}{\delta^{18}O_i - \delta^{18}O_e} \text{ with } k = Ae^{-\frac{E_a}{RT}} \quad (1)$$

where f is the fraction of isotopic exchange between carbon dioxide and water, $\delta^{18}O_i$ is the initial oxygen isotope composition of CO_2 (at

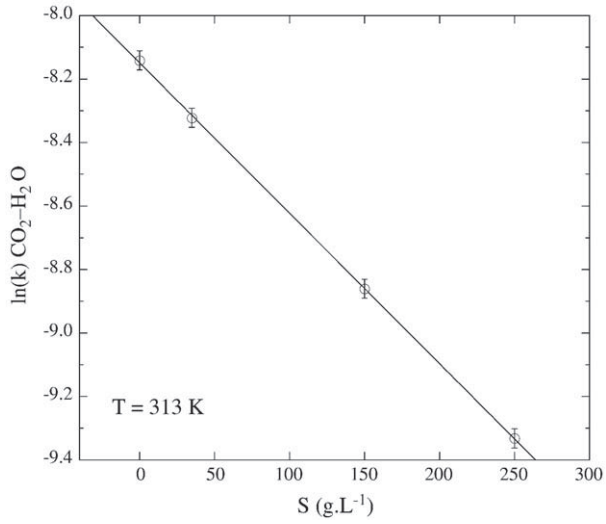

Fig. 3. Linear variations of $\ln(k)$ with the salinity of a sea salt solution at 313 K. k is the rate constant (s^{-1}) of the reaction of oxygen isotope exchange between CO_2 and H_2O. $\ln(k)$ sea salt $=-8.1485(\pm0.0057)-0.00474(\pm3.87\times10^{-5})S$ with $R^2=0.999$.

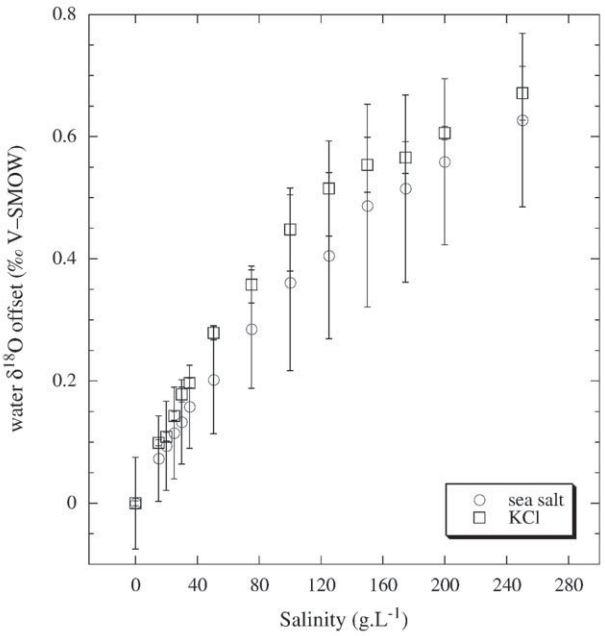

Fig. 4. Variations of water $\delta^{18}O$ offsets (defined as the difference between measured water $\delta^{18}O$ at equilibrium and the composition of pure water with a $\delta^{18}O$ of −10.38‰ V–SMOW) as a function of salinity for a sea salt and a KCl solution at 313 K. Note that both curves are similar to each other taking into account analytical uncertainties.

$t=0$; $\delta^{18}O=25.23\pm0.02$‰; $n=5$), $\delta^{18}O_t$ is the composition of CO_2 measured at any time t, $\delta^{18}O_e$ is its composition at equilibrium (deduced from observed steady-state values), and k (s^{-1}) is the rate constant of the reaction. Using Eq. (1), for each set of $\delta^{18}O_t$ obtained for a given salinity, the linear regression of data yield the rate constant k (Fig. 2) which is related to the salinity (Fig. 3) according to the following equation:

$$\ln(k)\text{ sea salt} = -8.1485(\pm0.0057) - 0.00474\left(\pm3.87.10^{-5}\right)S \quad (2)$$
$$\left(R^2 = 0.999\right).$$

In this range of salinity, times needed to reach oxygen isotope equilibrium between CO_2 and H_2O increase from 4 h to 12 h. These values are considered to be minimal reaction times required to accurately determine the oxygen isotope ratios of aqueous salt solutions by fluid equilibration techniques. It is noteworthy that "equilibration curves" for sea salt and KCl solutions of $S=150$ g L^{-1} are close each other (Fig. 4), showing that the nature of the cation does not influence the kinetics of isotopic exchange between CO_2 and H_2O.

Steady-state values of isotopic offsets have also been obtained for 14 sea salt and KCl solutions of salinity ranging from 0 to 250 g L^{-1} (Tables 3 and 4). The oxygen isotope offsets increase similarly with increasing salinity for both KCl and sea salt solutions (Fig. 4). Assuming that they represent equilibrium isotopic values between CO_2 and H_2O, oxygen isotope fractionation factors α are fitted as a function of salinity at a constant temperature of 313 K for sea salt (NaCl-like) and KCl solutions (Tables 3 and 4). These fractionation factors are linearly correlated to the salt content when $S\leq35$ g L^{-1}, above this value the experimental data deviate from the straight line (Fig. 5). The whole data set can be empirically described by the following equation:

$$1000\ln\left(\alpha_{CO_2-H_2O}\right)\text{sea salt} = 37.02\left(\pm5.10^{-3}\right) + 3.96.10^{-3} \quad (3)$$
$$\left(\pm1.05.10^{-4}\right)S - 6.38.10^{-6}$$
$$\left(\pm4.5.10^{-7}\right)S^2\ \left(R^2 = 0.998\right).$$

Table 3
Variations of the oxygen isotope offset (defined as the difference between measured water $\delta^{18}O$ at equilibrium between CO_2 and H_2O and the composition of pure water with a $\delta^{18}O$ of −10.38‰ V–SMOW) with the salinity of sea salt (NaCl-like) aqueous solutions.

Salinity	$\delta^{18}O$ offset	$\delta^{18}O$ offset	$\delta^{18}O$ offset	$\delta^{18}O$ offset	$\delta^{18}O$ offset	$\delta^{18}O$ offset	$\delta^{18}O$ offset	$\delta^{18}O$ offset	$\delta^{18}O$ offset	$\delta^{18}O$ offset	SD	$\alpha(CO_2–H_2O)$
g L^{-1} Sea salt	Exp. 1	Exp. 2	Exp. 3	Exp. 4	Exp. 5	Exp. 6	Exp. 7	Exp. 8	Exp. 9	Mean		
0	0.00	0.00	0.00	0.00	0.00	0.00	0.00	0.00	0.00	0.00	0.075	1.037700
15.02	0.00	−0.02	0.15	0.08	0.05	0.09	0.20	0.05	0.04	0.07	0.070	1.037774
20.06	0.01	−0.03	0.16	0.09	0.14	0.14	0.19	0.07	0.07	0.09	0.073	1.037794
25.00	0.02	0.02	0.19	0.12	0.12	0.21	0.21	0.06	0.09	0.11	0.075	1.037816
29.92	0.03	0.03	0.19	0.15	0.15	0.20	0.23	0.11	0.11	0.13	0.069	1.037834
35.04	0.09	0.03	0.20	0.13	0.20	0.21	0.25	0.16	0.14	0.16	0.068	1.037859
50.54	0.12	0.04	0.22	0.15	0.23	0.32	0.31	0.19	0.22	0.20	0.088	1.037904
75.02	0.20	0.10	0.29	0.22	0.35	0.41	0.40	0.30	0.29	0.28	0.097	1.037988
100.09	0.20	0.14	0.32	0.28	0.47	0.53	0.56	0.36	0.40	0.36	0.144	1.038064
125.12	0.25	0.18	0.38	0.34	0.50	0.58	0.57	0.42	0.43	0.40	0.136	1.038109
150.00	0.29	0.24	0.46	0.40	0.69	0.71	0.63	0.46	0.49	0.49	0.166	1.038192
174.65	0.35	0.29	0.44	0.43	0.68	0.70	0.70	0.52	0.53	0.51	0.153	1.038220
199.81	0.41	0.37	0.50	0.48	0.75	0.69	0.72	0.56	0.56	0.56	0.136	1.038264
250.12	0.46	0.42	n.d.	0.56	0.78	0.80	0.74	0.63	0.63	0.63	0.142	1.038333

Mean values and standard deviations (SD) have been obtained with nine experiments (exp.).

Eq. (3) provides solutions to correct isotopic biases resulting from the "salt effect" when measuring oxygen isotope compositions of natural saline waters. In the case of seawater-like samples with a salinity of 35 g L^{-1}, the $\delta^{18}O$ offset of 0.15‰ is rather small but significant relative to analytical uncertainties. For hypersaline solutions with $S \geq 200$ g L^{-1}, the large $\delta^{18}O$ offsets of 0.6–0.7‰ can induce large analytical errors and misinterpretations if not corrected from raw data.

4. Discussion

Quality of the data fit computed and illustrated in Fig. 2 suggests that oxygen isotope exchange between CO_2 and H_2O obeys a first-order reaction, a conclusion previously reached by Fortier (1994) for calcium chloride solutions from 0 to 4.0 M between 25 °C and 50 °C. However, at 313 K and 2.5 M, the rate constant for a $CaCl_2$ solution ($\ln(k) = -7.83$) is about one order higher than the one inferred from this study for a NaCl solution ($\ln(k) = -8.86$). Time needed to reach oxygen isotope equilibrium between CO_2 and H_2O increases with the increasing salinity of aqueous solutions. Our recommended values ranging from 4 h to 12 h for salinities ranging from 0 to 250 g L^{-1} need to be compared to those recommended for the use of automated preparation systems: "typical equilibration times are 4.5 h for CO_2" (System Description, p.12, in MultiPrep™ User's Guide, Micromass UK).

Table 4
Variations of the oxygen isotope offset (defined as the difference between measured water $\delta^{18}O$ at equilibrium between CO_2 and H_2O and the composition of pure water with a $\delta^{18}O$ of −10.38‰ V–SMOW) with the salinity of KCl aqueous solutions.

Salinity	$\delta^{18}O$ offset	$\delta^{18}O$ offset	$\delta^{18}O$ offset	SD	$\alpha(CO_2–H_2O)$
g L^{-1} KCl	Exp. 1	Exp. 2	Mean		
0	0.00	0.00	0.00	0.004	1.037700
15.02	0.10	0.10	0.10	0.005	1.037800
20.04	0.10	0.11	0.11	0.007	1.037810
24.96	0.14	0.15	0.14	0.007	1.037845
30.05	0.17	0.19	0.18	0.012	1.037880
35.04	0.19	0.20	0.20	0.008	1.037899
50.54	0.29	0.27	0.28	0.012	1.037982
75.06	0.38	0.34	0.36	0.030	1.038062
99.87	0.50	0.40	0.45	0.068	1.038153
124.98	0.57	0.46	0.51	0.078	1.038220
150.05	0.59	0.52	0.55	0.045	1.038260
174.93	0.58	0.55	0.57	0.026	1.038272
200.32	0.61	0.60	0.61	0.011	1.038311
250.14	0.64	0.70	0.67	0.044	1.038377

Mean values and standard deviations (SD) have been obtained with two experiments (exp.).

For salinities higher than 35 g L^{-1}, values of $1000\ln\alpha$ deviate from a straight line when reported against solution salinities. This result differs from what was described by Bourg et al. (2001) who concluded that there is no significant oxygen-18 salt effect in a range of concentrations from 0.5 to 2 times that of seawater. The observed complex relationship between these two parameters could result from changes in carbon speciation with increasing solute concentration. Indeed, Millero et al. (2007) have studied the dependence of dissociation constants of carbonic acid on both molality (0–6 M) and temperature (0–50 °C) of NaCl solutions. One of the main conclusions of their study is that both activity coefficients of HCO_3^- and CO_3^{2-} are very sensitive to molality at a given temperature and that this dependence must be taken into account during studies of the carbonate system in hydrothermal brines. From our data, a simple second-order polynomial equation allows to calculate values of $1000\ln\alpha(CO_2–H_2O)$ for NaCl or KCl solutions with any salinity lower or equal to 250 g L^{-1}.

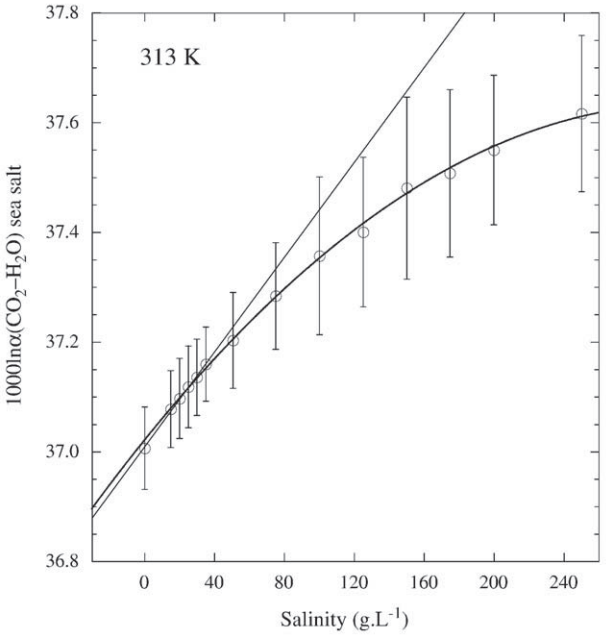

Fig. 5. Variations of $1000\ln\alpha(CO_2–H_2O)$ as function of salinity for a sea salt solution at 313 K. Experimental data follow empirically a second-order polynomial law, they deviate from a straight line which relates $1000\ln\alpha(CO_2–H_2O)$ to salinity for sea salt solutions of $S \leq 35$ g L^{-1}. Equation of the straight line is: $1000\ln\alpha(CO_2–H_2O) = 4.32 \times 10^{-3}(\pm 1.02 \times 10^{-4})S + 37.009(\pm 2.41 \times 10^{-3})$ with $R^2 = 0.998$.

Fitted fractionation factors for oxygen isotopes increase with increasing solute concentrations (Fig. 5). These results mean that values of $1000\ln\alpha$ between pure water and water bound to ions are negative (O'Neil and Truesdell, 1991), and more and more negative with the increasing solute concentration. O'Neil and Truesdell (1991) proposed that these salts act as breakers of the water structure. The solute alters the water structure with cation–H_2O bonds that are weaker than the co-existing H_2O–H_2O bonds, resulting in modified vibrational frequencies of the water molecules (Feder and Taube, 1952; O'Neil and Adami, 1969). For example, fractionations of both hydrogen and oxygen isotopes have been documented between hydrated and free water molecules in aqueous urea solution (Kakiuchi and Matsuo, 1985). Oxygen isotope fractionation factors between CO_2–H_2O are then strongly correlated to the concentration of the solute.

O'Neil and Truesdell (1991) made oxygen isotope equilibrations with alkali chloride solutions and their results revealed that K^+ is a stronger water structure breaker than Na^+. Moreover, these authors consider that NaCl constitutes a unique salt that fails to produce a sizable oxygen isotope fractionation between carbon dioxide and water as previously observed by Taube (1954) and Sofer and Gat (1972). Cole and Wesolowski (1989) have shown the influence of NaCl aqueous solutions on both equilibrium constants and rates of isotopic exchange in mineral–fluid systems. Results obtained from this study are at variance with the conclusions inferred from these pioneering studies. Direction and amplitude of oxygen isotope fractionation between CO_2–H_2O as a function of salinity are similar when using either KCl or NaCl solutions taking into account analytical uncertainties (Fig. 4). In addition, for salinities equal or above those of seawater-like solutions, changes in the fractionation factor values are large enough (Fig. 5) to cause errors much larger than those resulting from the chemical procedures and isotopic ratio mass spectrometer measurements.

5. Conclusions

Direction and relative amplitudes of the measured $^{18}O/^{16}O$ fractionations at 313 K between CO_2 and H_2O are well correlated to the water structure-breaking capacity of the NaCl and KCl solutes. Kinetics of reaction lead to propose minimal times needed to reach equilibrium depending on the solute content of analyzed waters. Oxygen isotope fractionations between CO_2 and H_2O increase with salinity for both NaCl and KCl solutions, therefore allowing the correction of fractionation factors for any salinity comprised between 0 and 250 g L^{-1}. Isotopic fractionations known between CO_2 and pure H_2O must be corrected from such a "salinity" effect for aqueous solutions whose salinity is equal or higher to that of marine waters.

Acknowledgements

This study has been supported by funds provided by French CNRS and IUF. The authors thank the two anonymous reviewers who contributed to improve the quality of this work.

Appendix A. Supplementary data

Supplementary data associated with this article can be found, in the online version, at doi:10.1016/j.chemgeo.2009.02.017.

References

Alexeev, S.V., Alexeeva, L.P., Borisov, V.N., Shouakar-Stash, O., Frape, S.K., Chabaux, F., Kononov, A.M., 2007. Isotopic composition (H, O, Cl, Sr) of ground brines of the Siberian Platform. Russ. Geol. Geophys. 48, 225–236.
Bourg, C., Stievenard, M., Jouzel, J., 2001. Hydrogen and oxygen isotopic composition of aqueous salt solutions by gas–water equilibration method. Chem. Geol. 173, 331–337.
Chiodini, G., Marini, L., Russo, M., 2001. Geochemical evidence for the existence of high-temperature hydrothermal brines at Vesuvio volcano, Italy. Geochim. Cosmochim. Acta 65, 2129–2147.
Cole, D.R., Wesolowski, D.J., 1989. Influence of NaCl aqueous solutions on isotopic equilibria and rates of exchange in mineral–fluid systems. Trans. Geotherm. Res. Council 13, 227–234.
Craig, H., Gordon, L.I., 1965. Deuterium and oxygen-18 variations in the ocean and the marine atmosphere. In: Tongiorgi, E. (Ed.), Stable Isotopes in Oceanographic Studies and Paleotemperatures. Lab. Geol. Nucl., pp. 9–130.
Epstein, S., Mayeda, T.K., 1953. Variation in O^{18} content of waters from natural sources. Geochim. Cosmochim. Acta 4, 213–224.
Feder, H.M., Taube, H., 1952. Ionic hydration: an isotopic fractionation technique. J. Chem. Phys. 20, 1335–1336.
Fortier, S.M., 1994. An on-line experimental/analytical method for measuring the kinetics of oxygen isotope exchange between CO_2 and saline/hypersaline salt solutions at low (25–50 °C) temperatures. Chem. Geol. 116, 155–162.
Horita, J., Ueda, A., Mizukami, K., Takatori, I., 1989. Automatic δD and $\delta^{18}O$ analyses of multi-water samples using H_2– and CO_2–water equilibration methods with a common equilibration set-up. Appl. Radiat. Isotopes 40, 801–805.
Horita, J., Cole, D.R., Wesolowski, D.J., 1995. The activity–composition relationship of oxygen and hydrogen isotopes in aqueous salt solutions: III. Vapor–liquid water equilibration of NaCl solutions to 350 °C. Geochim. Cosmochim. Acta 59, 1139–1151.
Kakiuchi, M., Matsuo, S., 1985. Fractionation of hydrogen and oxygen isotopes between hydrated and free water molecules in aqueous urea solution. J. Phys. Chem. 89, 4627–4632.
Kazahaya, K. (1986) Chemical and isotopic studies on hydrothermal solutions. Ph. D. dissertation, Tokyo Inst. Techn., pp. 185.
Kloppmann, W., Girard, J.-P., Négrel, Ph., 2002. Exotic stable isotope compositions of saline waters and brines from the crystalline basement. Chem. Geol. 184, 49–70.
Ladouche, B., Weng, Ph., 2005. Hydrochemical assessment of the Rochefort marsh: role of surface and groundwater in the hydrological functioning of the wetland. J. Hydrol. 314, 22–42.
McCarthy, K.T., Pichler, T., Price, R.E., 2005. Geochemistry of Champagne Hot Springs shallow hydrothermal vent field and associated sediments, Dominica, Lesser Antilles. Chem. Geol. 224, 55–68.
Millero, F., Huang, F., Graham, T., Pierrot, D., 2007. The dissociation of carbonic acid in NaCl solutions as a function of concentration and temperature. Geochim. Cosmochim. Acta 71, 46–55.
O'Neil, J.R., Adami, L.H., 1969. The oxygen isotope partition function ratio of water and the structure of liquid water. J. Phys. Chem. 73, 1553–1558.
O'Neil, J.R., Truesdell, A.H., 1991. Oxygen isotope fractionation studies of solute–water interactions. In: Taylor, H.P., O'Neil, J.R., Kaplan, I.R. (Eds.), Stable Isotope Geochemistry: A Tribute to Samuel Epstein. The Geochemical Society, Special Publication n°, vol. 3, pp. 17–25.
Pierret, M.C., Clauer, N., Bosch, D., Blanc, G., France-Lanord, C., 2001. Chemical and isotopic ($^{87}Sr/^{86}Sr$, $\delta^{18}O$, δD) constraints to the formation processes of Red-Sea brines. Geochim. Cosmochim. Acta 65, 1259–1275.
Risacher, F., Alonso, H., Salazar, C., 2003. The origin of brines and salts in Chilean salars: a hydrochemical review. Earth Sci. Rev. 63, 249–293.
Sofer, Z., Gat, J.R., 1972. Activities and concentrations of oxygen-18 in concentrated aqueous salt solutions: analytical and geophysical implications. Earth Planet. Sci. Lett. 15, 232–238.
Taube, H., 1954. Use of oxygen isotope effects in the study of hydrated ions. J. Chem. Phys. 58, 523–528.
Truesdell, A.H., 1974. Oxygen isotope activities and concentrations in aqueous salt solutions at elevated temperatures: consequences for isotope geochemistry. Earth Planet. Sci. Lett. 23, 387–396.

Chemical Geology 291 (2012) 236–240

Contents lists available at SciVerse ScienceDirect

Chemical Geology

journal homepage: www.elsevier.com/locate/chemgeo

Research paper

D/H equilibrium fractionation between H_2O and H_2 as a function of the salinity of aqueous solutions

François Martineau, François Fourel, Anne-Marie Bodergat, Christophe Lécuyer *,[1]

Laboratoire CNRS UMR 5125 'Paléoenvironnements &Paléobiosphère', Université Lyon 1, Lyon, 69003, France

ARTICLE INFO

Article history:
Received 15 February 2011
Received in revised form 14 October 2011
Accepted 26 October 2011
Available online 4 November 2011

Editor: U. Brand

Keywords:
Hydrogen isotope
Isotope activity
Fractionation
Kinetics
Salinity
Water

ABSTRACT

Hydrogen isotope fractionation between H_2O and H_2 has been investigated at 313 K for sodium chloride solutions with salinities (S) ranging from 0 to 265 $g.L^{-1}$. In the presence of a Pt catalyst, time needed to reach hydrogen isotope equilibrium between H_2O and H_2 is close to 3 h ($t_{1/2} \approx 30$ min), independently on the salinity of the aqueous solution. Hydrogen isotope fractionation between H_2O and H_2 increases with increasing molality (m) for a NaCl-like (sea salt) solution according to the following linear function: $\alpha_{H_2O\text{-}H_2}(\text{sea salt}) = 3.387(\pm 8.4\times10^{-5}) + 3.4\times10^{-3}(\pm 5\times10^{-5})m$ ($R^2 = 0.997$). The hydrogen isotope analysis of seawater samples with a salinity of 35 $g.L^{-1}$ requires minor corrections of -2 ± 0.5‰ (V-SMOW) whilst δD values are overestimated by 5 ± 0.5‰ to 10 ± 0.5‰ in the case of highly saline natural waters ($100 < S < 265$ $g.L^{-1}$). In combination to previously published salinity-dependent fractionation factors between CO_2 and H_2O (Lécuyer et al., 2009), corrections of both hydrogen and oxygen isotope ratios must be taken into account during the analysis by equilibration techniques of waters sampled from salt marshes, hypersaline lakes and lagoons, or hydrothermal brines.

1. Introduction

Waters with salinities higher than that of seawater define the field of brines that contain sodium chloride as the most abundant and widespread electrolyte in natural aqueous fluids. Most common brines occurring on Earth come from saline lakes in arid areas or are associated with sedimentary basins, crystalline rocks and hydrothermal vents. Fractionation of stable hydrogen and oxygen isotopes within the hydrological cycle is of prime importance in stable isotope geochemistry as measurements of isotope compositions can help to identify water sources, to estimate the importance of phase changes, and to quantify mixing, unmixing and distillation processes. However, the activity of water in brines decreases with increasing salinity. Indeed, Taube (1954), Craig and Gordon (1965), O'Neil and Adami (1969) and Truesdell (1974) have shown that the isotope activity ratio of water in brines differs from the isotope concentration ratio; this difference being the so-called "salt-effect". During the second half of the twentieth century, the stable hydrogen and oxygen isotope ratios of natural waters were determined by equilibration with hydrogen gas (Horita, 1988; Horita et al., 1989; Coplen et al., 1991) and carbon dioxide (Cohn and Urey, 1938). The liquid–gas equilibration techniques yield hydrogen and oxygen isotope activity ratios of water in the case of brines whereas water reduction methods (Coleman et al., 1982; Dugan et al., 1985; Kendall and Coplen, 1985; Gehre et al., 1996; Yang et al., 1996; Morrison et al., 2001) provide hydrogen and oxygen isotope concentration ratios. Numerous studies confirmed that hydrogen and oxygen isotopic offsets relative to the fractionation factor determined between pure liquid water and vapour are much higher than analytical precisions in most cases (Sofer and Gat, 1972; Kazahaya, 1986; Horita, 1988; O'Neil and Truesdell, 1991; Fortier, 1994; Horita et al., 1995; Bourg et al., 2001), even though no consensus was reached so far on the amplitude of these isotopic offsets. Therefore, depending on the method used for the isotopic analysis of brines, uncorrected data could be responsible for misleading interpretations of the source and evolution of these salted waters (Horita, 1989). Since the recent development of automated preparation systems for the measurement of stable oxygen and hydrogen isotope ratios of waters, analytical precisions of ±0.05‰ and ±0.5‰, respectively, can be reached routinely with samples of about 200–400 μL by using isotopic equilibration techniques between CO_2 and H_2O, and H_2O and H_2 (e.g. Horita et al., 1989; McCarthy et al., 2005). These high-precision isotopic measurements allow an increase in resolution of the identification of the sources of water and mixing or evaporation–condensation processes that can affect them in the hydrosphere or during interactions with the lithosphere, biosphere or atmosphere of the Earth. This quantification can be weakened without applying the adequate salinity-dependent fractionation factors during the case study of water reservoirs with highly contrasted salinities. An approximate knowledge of these isotopic fractionation factors would also generate errors

* Corresponding author.
E-mail address: Christophe.Lecuyer@univ-lyon1.fr (C. Lécuyer).
[1] Also at Institut Universitaire de France.

0009-2541/$ – see front matter © 2011 Elsevier B.V. All rights reserved.
doi:10.1016/j.chemgeo.2011.10.017

associated with the determination of the source of precipitations. The same problem also applies to the hydrogen and oxygen isotope analysis of aqueous inclusions trapped in evaporitic minerals. Protocols of gas extraction that are based on crushing or thermal decrepitation involve distillation processes under vacuum which produce both hydrogen and oxygen isotope fractionations, if not all of the hydrogen or the oxygen of the fluid phase is extracted.

Recently, Lécuyer et al. (2009) investigated the oxygen isotope fractionation and equilibration kinetics between CO_2 and H_2O at 313 K for salinities (S) ranging from 0 to 250 g.L^{-1} using an automated multi-sample analyser (MultiPrep™ coupled to Elementar Isoprime™). These authors found that the oxygen isotope fractionation factor between CO_2 and H_2O increases with salinity to such an extent that oxygen isotope ratios of a natural sea-salt solution measured by isotope-activity methods differ from isotope-concentration methods by 0.4‰ to 0.6‰ in the case of highly saline natural waters (100<S<250 g.L^{-1}). In this study based on the automated D/H measurements of waters by equilibration, we propose to determine the D/H fractionation factors in the system H_2O–H_2 at 313 K for sodium chloride solutions with salinities (S) ranging from 0 to 265 g.L^{-1}.

2. Analytical techniques

Hydrogen isotope measurements of water have been performed to determine kinetics and hydrogen isotope fractionation between H_2O and H_2 at 313 K for salinities ranging from 0 to 265 g.L^{-1}. Aqueous solutions of salinity ranging from 15 to 265 g.L^{-1} (0.25 to 3.5 m) have been prepared by dissolving a natural sea salt from the salt marsh of Guérande, France, and a pure grade (≥99.9‰ wt.%) NaCl salt, each of them in 125 mL of double distilled water (DDW). A 3 L aliquot of this doubly distilled water was stored in a glass bottle. The natural sea salt is mainly NaCl with a minor sulphate content and 7 wt.% of adsorbed H_2O according to XRF analysis performed at the University Claude Bernard Lyon 1 (Lécuyer et al., 2009). This salt was therefore dried at 110 °C overnight before dissolution in double-distilled water (DDW).

The double distilled water was calibrated versus SMOW, GISP and SLAP to determine its δD value of −79.5 ± 0.8‰ (V-SMOW) and it was used for all the analysed salt solutions. Prior to equilibration analyses of the salt solutions, the variations of the equilibration time were investigated as a function of the salinities of the natural sea salt aqueous solutions. For S = 0; 36; 107; 145 and 265 g.L^{-1}, the rate of hydrogen isotope exchange with time between H_2O and H_2 is reported as 'δD offset' where δD offset = $((D/H_{SAM} - D/H_{DDW})/D/H_{DDW} - 1) * 10^3$ (SAM = sample; DDW = doubly distilled water).

Aliquots of 400 μL of water were automatically reacted at 313 K with H_2 and analysed using a MultiPrep™ system on line with an Elementar IsoPrime™ dual inlet IRMS. For hydrogen isotopic analyses the sample vials are loaded into the temperature controlled rack and the autosampler is used to evacuate the headspace of the vials and then fill them automatically with hydrogen equilibration gas coming from a gas cylinder. Then equilibration vials are left to equilibrate for a user-definable period. A platinum-based hydrophobic catalyst made of platinum coated polymer beads trapped inside a stainless steel coil was used to reach isotopic equilibrium between liquid water and gaseous hydrogen. It consists of approximately 10 "Hokko-beads" (Shoko Co Ltd-Japan). At the end of the equilibration time, the valve system of the MultiPrep transfers the equilibrated gas from the headspace of each vial to an on-line cryogenic water trap where the water vapour is removed. Finally the dried gas is passed to the dual inlet system of the mass spectrometer to be analysed. Internal and external reproducibilities of δD values were ± 0.4‰ and ± 1‰, respectively. Hydrogen isotope ratios are reported relative to V-SMOW in the ‰ δ unit after scaling the raw data to the "true" isotopic ratios of SMOW, SLAP and GISP international standards. Experiments on the rates of exchange were made by analysing the hydrogen isotope composition of molecular hydrogen immediately after the autofill sequence was completed and at various times thereafter. The autofilling time was taken into account to determine the total equilibration time. All the experiments have been performed at 313 K, a temperature routinely used by some of the automated preparation systems dealing with the stable isotope analysis of large series of water samples.

3. Results

For each natural sea salt solution, steady-state isotopic compositions are observed and are considered to represent isotopic equilibrium values between H_2O and H_2 (Fig. 1; Table 1).

The order of the reaction was tested by a best fit of the data with a first order law:

$$f = 1 - \exp(-kt) = \frac{\delta D_i - \delta D_t}{\delta D_i - \delta D_e} \quad \text{with} \quad k = Ae - \frac{E_a}{RT} \tag{1}$$

where f is the fraction of isotopic exchange between H_2O and H_2, δD_i is the initial hydrogen isotope composition of H_2 (at t = 0; δD = −742.2 ± 0.8‰; n = 3), δD_t is the composition of H_2 measured at any time t, δD_e is its composition at equilibrium (deduced from observed steady-state values), and k (s^{-1}) is the rate constant of the reaction.

Using Eq. (1), for each set of δD_t obtained for a given salinity, the linear regression of data yields a mean rate constant ln(k) of −7.93 ± 0.03 that is independent of the salt content (Fig. 2). In this range of salinity, the period required to reach hydrogen isotope equilibrium between H_2O and H_2 is close to 3 h. This value is considered to be the minimal reaction time required to accurately determine the hydrogen isotope ratios of aqueous salt solutions by fluid equilibration techniques.

Steady-state values of isotopic offsets have also been obtained for 14 natural sea salt solutions and NaCl solutions of salinity ranging from 0 to 265 g.L^{-1} (Tables 2 and 3). Similar isotopic results for both salts suggest that the natural sea salt–water system can be approximated by the NaCl–water system. It also means that any potential contamination by water from hydrated magnesium chloride can be neglected throughout the course of these experiments. The hydrogen isotope offsets increase with increasing salinity for these sea salt solutions. Assuming that they represent equilibrium isotopic values between H_2O and H_2, hydrogen isotope fractionation factors α are fitted as a function of salinity at a constant temperature of 313 K according to the following quadratic equation:

$$\begin{aligned}\alpha_{H_2O-H_2}(\text{sea salt}) = {} & 3.387\left(\pm 1.1 \times 10^{-4}\right) + 5.9 \\ & \times 10^{-5}\left(\pm 2.3 \times 10^{-6}\right)\text{S} - 4.8 \\ & \times 10^{-8}\left(\pm 9.1 \times 10^{-9}\right)\text{S}^2 \left(R^2 = 0.998\right)\end{aligned} \tag{2a}$$

$$\begin{aligned}\alpha_{H_2O-H_2}(\text{NaCl}) = {} & 3.388\left(\pm 4.5 \times 10^{-4}\right) + 6.7 \\ & \times 10^{-5}\left(\pm 1.5 \times 10^{-5}\right)\text{S} - 9.6 \\ & \times 10^{-8}\left(\pm 4.4 \times 10^{-8}\right)\text{S}^2 \left(R^2 = 0.958\right)\end{aligned} \tag{2b}$$

that can be reduced to a simple linear equation when considering the molality of solutions:

$$\alpha_{H_2O-H_2}(\text{sea salt}) = 3.387\left(\pm 8.4 \times 10^{-5}\right) + 3.4 \times 10^{-3}\left(\pm 5 \times 10^{-5}\right)\text{m} \quad \left(R^2 = 0.997\right) \tag{3a}$$

$$\alpha_{H_2O-H_2}(\text{NaCl}) = 3.388\left(\pm 3.6 \times 10^{-4}\right) + 3.3 \times 10^{-3}\left(\pm 2 \times 10^{-4}\right)\text{m} \quad \left(R^2 = 0.952\right). \tag{3b}$$

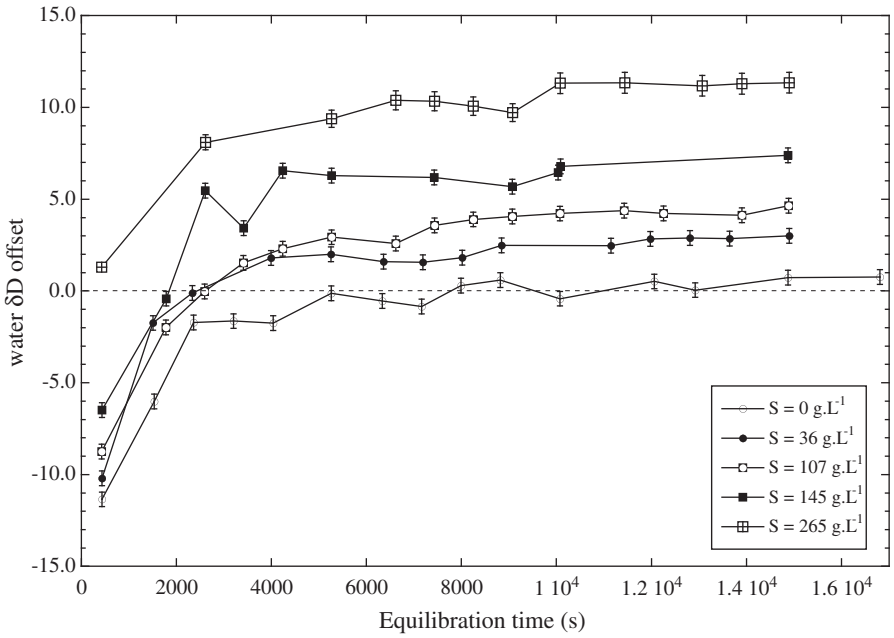

Fig. 1. Variations with equilibration time of the hydrogen isotope offset (defined as the difference between measured water δD at any time t and the composition of pure water with a δD of −79.5‰ V-SMOW) of natural sea salt (NaCl-like) aqueous solutions at 313 K. Note that for the five experiments, hydrogen isotope compositions have reached steady-state values for equilibration times of at least 3 h.

The measured fractionation factor of ≈3.39 between water and hydrogen gas at 313 K is bracketed by several previous determinations. Low α values of 3.20 and 3.27 were determined by Cerrai et al. (1954) and Suess (1949), respectively, a higher value of 3.48 was proposed by Rolston et al. (1976) whilst Richet et al. (1977) computed a value of 3.40. Therefore we consider that our determination of the D/H fractionation factor between water and hydrogen gas should be close to the equilibrium value at 313 K.

Eq. (3a) and (3b) provide solutions to correct isotopic biases resulting from the "salt effect" when measuring hydrogen isotope compositions of natural saline waters. In the case of seawater-like samples with a salinity of 35 g.L^{-1}, the δD offset of 2 ± 0.5‰ is rather small but significant relative to analytical uncertainties. For hypersaline solutions with S ≥ 200 g.L^{-1}, sizable δD offsets from 5‰ to 10‰ can induce large analytical errors and misinterpretations if not corrected from raw data.

4. Discussion

Quality of the data fit computed and illustrated in Fig. 2 shows that hydrogen isotope exchange between H_2O and H_2 obeys a first-order reaction as already observed by Horita (1988). In the studied salinity range 0–265 g.L^{-1}, we estimate half-time reactions $t_{1/2}$ close to 30 min along with times needed to reach isotopic equilibration (t_{eq}) of ≈3 h; those values being significantly higher than those proposed by Horita (1988) who calculated $t_{1/2}$ less than 10 min and t_{eq} of ≈1 h for pure water and a Dead Sea brine. Our recommended value of 3 h is also twice than that recommended for the use of automated preparation systems: "typical equilibration times are 1 h 30 min for H_2 at 40 °C" (MultiPrep™ User's Guide, IsoPrime UK Ltd). In contrast with the CO_2–H_2O system, for which kinetics of oxygen isotope exchange increase with salinity (Lécuyer et al., 2009), exchange rate between H_2O and H_2 is not sensitive to the salt content of the aqueous solution,

Table 1
Variations of the hydrogen isotope offset (defined as the difference between measured δD values of water at equilibrium between H_2O and H_2 and the composition of pure water with a δD of −79.5‰ V-SMOW) as a function of time (s) for (NaCl-like) natural sea salt aqueous solutions with salinities ranging from 0 to 265 g.L^{-1}.

Eq. time (s)	δD offset	Eq. time (s)	δD offset	Eq. time (s)	δD offset	Eq. time (s)	δD offset	Eq. time (s)	δD offset
S = 0 g.L^{-1}; sea salt		S = 36 g.L^{-1}; sea salt		S = 107 g.L^{-1}; sea salt		S = 145 g.L^{-1}; sea salt		S = 265 g.L^{-1}; sea salt	
434	−11.35	438	−10.20	428	−8.75	437	−6.49	433	1.29
1538	−6.02	1509	−1.74	1785	−1.99	1787	−0.42	2614	8.10
2365	−1.72	2338	−0.11	2594	−0.03	2610	5.46	5270	9.39
3205	−1.64	3994	1.80	3412	1.53	3419	3.43	6624	10.38
4042	−1.75	5254	2.00	4238	2.30	4238	6.55	7436	10.34
5265	−0.12	6363	1.60	5271	2.93	5271	6.28	8249	10.07
6335	−0.55	7190	1.57	6621	2.59	7427	6.18	9080	9.72
7167	−0.84	8018	1.81	7436	3.57	9070	5.69	10080	11.32
7991	0.29	8848	2.48	8253	3.90	10038	6.46	11437	11.34
8823	0.59	11146	2.47	9073	4.06	10086	6.79	13073	11.18
10077	−0.42	11976	2.84	10073	4.22	14877	7.39	13902	11.29
12059	0.52	12812	2.89	11429	4.38			14901	11.35
12921	0.05	13647	2.85	12252	4.23				
14875	0.73	14900	3.01	13906	4.13				
16809	0.76			14888	4.64				

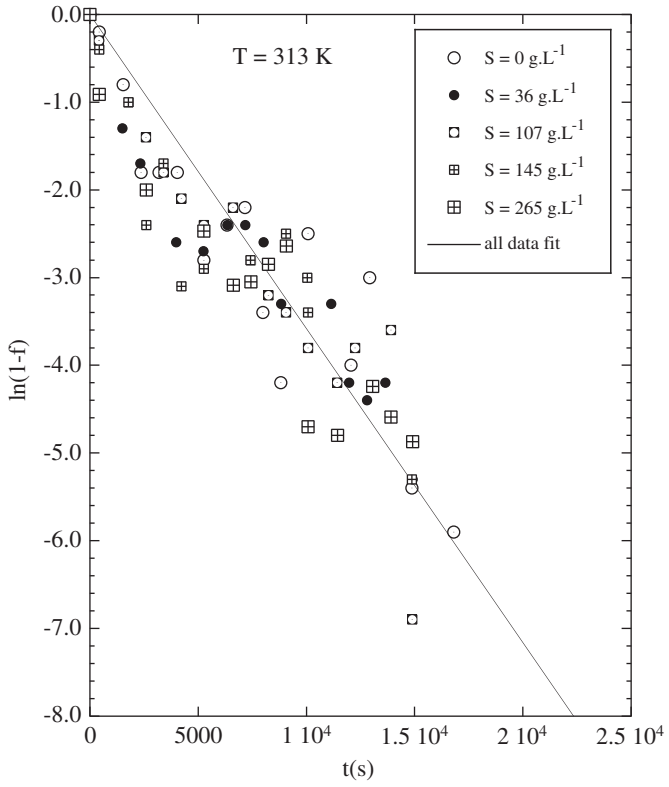

Fig. 2. Progress with time of the fraction of hydrogen isotopes exchanged between water and hydrogen gas at 313 K. The absolute value of the slope of the straight line is the rate constant k of the exchange reaction, which is independent on salinity in the studied range 0–265 $g.L^{-1}$, respectively. $Ln(1\text{-}f) = -3.58.10^{-4}(\pm 1.43.10^{-5})$ with $R^2 = 0.863$.

an observation that could be the result of the prime role played by the Pt catalyst in the hydrogen isotope exchange between water and hydrogen gas.

From our data, a simple linear equation allows the fitting of $\alpha(H_2O\text{–}H_2)$ values for NaCl-like solution with molalities ranging from 0 to 3.5 $mol.kg^{-1}$ (Fig. 3). These results mean that values of $1000ln\alpha$ between water bound to ions and pure water are positive

Table 2
Variations of the hydrogen isotope offset (defined as the difference between measured δD values of water at equilibrium between H_2O and H_2 and the composition of pure water with a δD of −79.5‰ V-SMOW) with the salinity of (NaCl-like) natural sea salt aqueous solutions. Mean values and standard deviations (SD) have been obtained with four experiments (exp.).

Salinity	δD offset	δD offset	δD offset	δD offset	δD offset	SD	$\alpha(H_2O\text{–}H_2)$
$g.L^{-1}$ sea salt	Exp. 1	Exp. 2	Exp. 3	Exp. 4	Mean value		
0.00	0.00	0.00	0.00	0.00	0.00	–	3.38686
14.60	0.72	0.77	0.79	0.70	0.75	0.043	3.38767
19.57	1.01	0.97	1.77	1.10	1.21	0.375	3.38818
26.02	1.31	1.10	1.78	0.78	1.24	0.419	3.38821
30.14	1.43	1.11	1.92	1.03	1.38	0.405	3.38836
35.94	1.90	1.79	1.98	1.58	1.81	0.176	3.38883
49.58	2.62	2.34	2.59	2.72	2.57	0.161	3.38965
76.95	3.82	3.45	3.42	2.90	3.40	0.377	3.39055
107.53	5.41	5.65	4.93	5.16	5.29	0.312	3.39259
124.78	6.18	7.12	6.22	5.54	6.26	0.650	3.39364
145.72	7.32	7.13	7.02	6.18	6.91	0.506	3.39434
172.67	7.96	8.29	7.95	7.91	8.03	0.176	3.39553
192.84	8.53	8.74	8.60	8.99	8.72	0.204	3.39627
264.41	11.49	11.19	10.95	11.00	11.16	0.244	3.39887

Table 3
Variations of the hydrogen isotope offset (defined as the difference between measured δD values of water at equilibrium between H_2O and H_2 and the composition of pure water with a δD of −79.5‰ V-SMOW) with the salinity of NaCl aqueous solutions. Mean values and standard deviations (SD) have been obtained with two experiments (exp.).

Salinity	δD offset	δD offset	δD offset	SD	$\alpha(H_2O\text{-}H_2)$
$g.L^{-1}$ NaCl	Exp. 1	Exp. 2	Mean values		
0.00	0.00	0.00	0.00	–	3.38686
15.02	2.96	1.38	2.17	1.118	3.38922
20.06	0.72	4.11	2.42	2.394	3.38949
25.00	3.66	2.52	3.09	0.807	3.39022
29.92	3.11	3.50	3.30	0.275	3.39044
35.00	5.05	3.83	4.44	0.862	3.39167
50.15	3.07	3.87	3.47	0.561	3.39063
75.02	4.57	5.80	5.19	0.875	3.39248
100.09	7.37	8.02	7.70	0.463	3.39518
125.12	6.42	7.70	7.06	0.907	3.39450
149.99	6.74	10.15	8.44	2.410	3.39598
174.65	7.58	9.22	8.40	1.158	3.39593
199.81	9.79	10.76	10.28	0.688	3.39793
250.12	10.69	12.71	11.70	1.429	3.39945

(O'Neil and Truesdell, 1991), and more and more positive with the increasing solute concentration. O'Neil and Truesdell (1991) proposed that these salts act as breakers of the water structure. The solute alters the water structure with cation–H_2O bonds that are stronger than the co-existing H_2O–H_2O bonds, resulting in modified vibrational frequencies of the water molecules (Feder and Taube, 1952; O'Neil and Adami, 1969). O'Neil and Truesdell (1991) also showed that this effect was not as important as probable changes in the structure of water that develop as solutions become more concentrated. In other words, D/H activity ratios of water in NaCl solutions are higher than their D/H compositions ratios. The difference between activity and composition ratios is the so-called "isotope salt effect", which is defined as following in the case of the system liquid

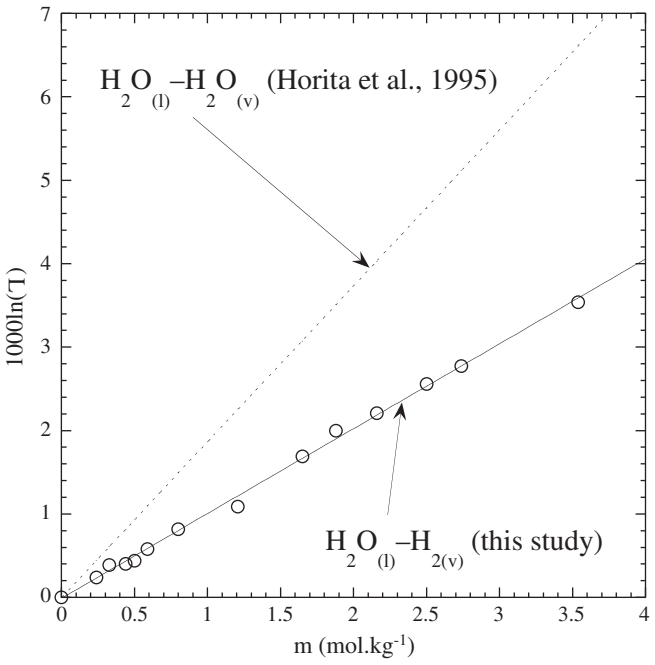

Fig. 3. D/H exchange in the systems $H_2O_{(l)}$–$H_{2(g)}$ (this study) and $H_2O_{(l)}$–$H_2O_{(v)}$ (Horita et al., 1995). Variations of the "isotope salt effect" $1000ln\Gamma$ (defined after Horita et al., 1993; see also Eq. (4) in the text) as a function of the molality (m) of the studied (NaCl-like) natural sea salt solution at 313 K. The fitted linear equation for the studied system $H_2O_{(l)}$–$H_{2(g)}$ is: $1000ln\Gamma = 1.0173(\pm 0.0147)m - 0.0122(\pm 0.0249)$ with $R^2 = 0.997$, and is compared to that obtained by Horita et al. (1995) for the system $H_2O_{(l)}$–$H_2O_{(v)}$.

water–hydrogen gas after the formalism developed by Horita et al. (1993):

$$\Gamma = \frac{\alpha_{l-v}(\text{solution})}{\alpha_{l-v}(\text{water})} \quad (4)$$

where $\alpha_{l\text{-}v}$ is the fractionation factor between liquid water and hydrogen gas, 'solution' is the saline aqueous solution of molality m, and 'water' represents the pure water end-member. The "isotope salt effect" Γ has been documented in other liquid gas-systems such as between $H_2O_{(l)}$ and $H_2O_{(v)}$ (Horita et al., 1995) for which its direction and amplitude are comparable to those measured in our study, following in both cases a simple linear relationship with the molality of NaCl solutions (Fig. 3).

Combining the results obtained for the salinity-dependent oxygen isotope fractionation during CO_2–H_2O equilibration to those obtained for hydrogen isotopes during H_2O–H_2 equilibration, sizable corrections must be applied to both H and O isotope measurements of waters with $S \geq 35$ g.L^{-1} if D/H composition ratios need to be considered instead of D/H activity ratios.

5. Conclusions

Direction and relative amplitudes of the measured D/H fractionations at 313 K between H_2O and H_2 are well correlated to the NaCl content of aqueous solutions. Kinetics of reaction lead to propose a minimal time of 3 h needed to reach equilibrium independently on the solute content of analysed waters. Hydrogen isotope fractionation between H_2O and H_2 increases with salinity for NaCl solutions in a similar way as observed for the fractionation of oxygen isotopes during equilibration between CO_2 and H_2O. Corrections must be applied to both H and O isotope measurements of waters with $S \geq 35$ g.L^{-1} if D/H composition ratios need to be considered instead of D/H activity ratios.

Acknowledgements

The authors thank J. O'Neil and T. Vennemann for their reviews that helped the authors to improve the scientific content of this study. This work has been supported by funds provided by French CNRS and IUF (C.L.).

References

Bourg, C., Stievenard, M., Jouzel, J., 2001. Hydrogen and oxygen isotopic composition of aqueous salt solutions by gas–water equilibration method. Chemical Geology 173, 331–337.
Cerrai, E., Marchetti, R., Renzoni, R., Roseo, L., Silvestri, M., Villani, S., 1954. A thermal method for concentrating heavy water. Chemical Engineering Progress Symposium 50, 271–280.
Cohn, M., Urey, H.C., 1938. Oxygen exchange reactions of organic compounds and water. Journal of the American Chemical Society 60, 679–682.
Coleman, M.L., Shepherd, T.J., Durham, J.J., Rouse, J.E., Moore, G.R., 1982. Reduction of water with zinc for hydrogen isotope analysis. Analytical Chemistry 54, 993–995.
Coplen, T.B., Wildman, J.D., Chen, J., 1991. Improvements in the gaseous hydrogen–water equilibration technique for hydrogen isotope ratio analysis. Analytical Chemistry 63, 910–912.
Craig, H., Gordon, L.I., 1965. Deuterium and oxygen-18 variations in the ocean and the marine atmosphere. In: Tongiorgi, E. (Ed.), Stable Isotopes in Oceanographic Studies and Paleotemperatures. Lab, Geol. Nucl., pp. 9–130.
Dugan Jr., J.P., Borthwick, J., Harmon, R.S., Gagnier, M.A., Glahn, J.E., Kinsel, E.P., MacLeod, S., Viglino, J.A., 1985. Guanidine hydrochloride method for determination of water isotope ratios and the oxygen-18 fractionation between carbon dioxide and water at 25 °C. Analytical Chemistry 57, 1734–1736.
Feder, H.M., Taube, H., 1952. Ionic hydration: an isotopic fractionation technique. Journal of Chemical Physics 20, 1335–1336.
Fortier, S.M., 1994. An on-line experimental/analytical method for measuring the kinetics of oxygen isotope exchange between CO_2 and saline/hypersaline salt solutions at low (25–50 °C) temperatures. Chemical Geology 116, 155–162.
Gehre, M., Hoefling, R., Kowski, P., Strauch, G., 1996. Sample preparation device for quantitative hydrogen isotope analysis using chromium metal. Analytical Chemistry 68, 4414–4417.
Horita, J., 1988. Hydrogen isotope analysis of natural waters using an H_2–water equilibration method: a special implication to brines. Chemical Geology 72, 89–94.
Horita, J., 1989. Analytical aspects of stable isotopes in brines. Chemical Geology 79, 107–112.
Horita, J., Ueda, A., Mizukami, K., Takatori, I., 1989. Automatic δD and $\delta^{18}O$ analyses of multi-water samples using H_2– and CO_2–water equilibration methods with a common equilibration set-up. Applied Radiation and Isotopes 40, 801–805.
Horita, J., Cole, D.R., Wesolowski, D.J., 1993. The activity composition relationship of oxygen and hydrogen isotopes in aqueous salt solutions, II. Vapor–liquid water equilibration of mixed salt solutions from 50 to 100 °C and geochemical implications. Geochimica et Cosmochimica Acta 57, 4703–4711.
Horita, J., Cole, D.R., Wesolowski, D.J., 1995. The activity-composition relationship of oxygen and hydrogen isotopes in aqueous salt solutions: III. Vapor–liquid water equilibration of NaCl solutions to 350 °C. Geochimica et Cosmochimica Acta 59, 1139–1151.
Kazahaya, K., 1986. Chemical and isotopic studies on hydrothermal solutions. Ph. D. dissertation, Tokyo Inst. Techn., pp. 185.
Kendall, C., Coplen, T.B., 1985. Multisample conversion of water to hydrogen by zinc for stable isotope determination. Analytical Chemistry 57, 1437–1440.
Lécuyer, C., Gardien, V., Rigaudier, T., Fourel, F., Martineau, F., Cros, A., 2009. Oxygen isotope fractionation and equilibration kinetics between CO_2 and H_2O as a function of salinity of aqueous solutions. Chemical Geology 264, 122–126.
McCarthy, K.T., Pichler, T., Price, R.E., 2005. Geochemistry of Champagne Hot Springs shallow hydrothermal vent field and associated sediments, Dominica, Lesser Antilles. Chemical Geology 224, 55–68.
Morrison, J., Brockwell, T., Merren, T., Fourel, F., Philipps, A., 2001. On-line high-precision stable hydrogen isotopic analyses on nanolitre water samples. Analytical Chemistry 73, 3570–3575.
O'Neil, J.R., Adami, L.H., 1969. The oxygen isotope partition function ratio of water and the structure of liquid water. Journal of Physical Chemistry 73, 1553–1558.
O'Neil, J.R., Truesdell, A.H., 1991. Oxygen isotope fractionation studies of solute–water interactions. In stable isotope geochemistry: a tribute to Samuel Epstein. In: Taylor, H.P., O'Neil, J.R., Kaplan, I.R. (Eds.), The Geochemical Society, Special Publication No. 3, pp. 17–25.
Richet, P., Bottinga, Y., Javoy, M., 1977. A review of H, C, N, S and Cl stable isotope fractionation among gaseous molecules. Annual Review of Earth and Planetary Sciences 5, 65–110.
Rolston, J.H., den Hartog, J., Butler, J.P., 1976. The deuterium isotope separation factor between hydrogen and liquid water. Journal of Physical Chemistry 80, 1064–1067.
Sofer, Z., Gat, J.R., 1972. Activities and concentrations of oxygen-18 in concentrated aqueous salt solutions: analytical and geophysical implications. Earth and Planetary Science Letters 15, 232–238.
Suess, H.E., 1949. Das Gleichgewicht $H_2 + HDO = HD + H_2O$ und die weiteren Austauschgleichgewichte im System H_2, D_2 und H_2O. Zeitschrift fur Naturforschung 4a, 328–332.
Taube, H., 1954. Use of oxygen isotope effects in the study of hydrated ions. Journal of Chemical Physics 58, 523–528.
Truesdell, A.H., 1974. Oxygen isotope activities and concentrations in aqueous salt solutions at elevated temperatures: consequences for isotope geochemistry. Earth and Planetary Science Letters 23, 387–396.
Yang, W., Krouse, H.R., Spencer, R.J., 1996. Improved techniques for stable isotope analyses of microlitre quantities of water from fluid inclusions in halite and concentrated brines. Chemical Geology 130, 139–145.

4.2/ Analyse des carbonates

Comme nous l'avons déjà exprimé, les isotopes stables ayant été développés à leurs débuts par des géochimistes après les analyses isotopiques des eaux, les carbonates ont été très tôt un matériel de prédilection pour ce type de mesures [15-17].

Comme nous l'avons évoqué au chapitre 2 les compositions isotopiques des apatites biogéniques sont maintenant très utilisées pour les reconstructions environnementales à la fois marines et terrestres. Or il se trouve que de faibles quantités de carbonates (3-6 %poids) apparaissent naturellement en substitution des phosphates dans le réseau cristallin des apatites [18-21]. Au sein de l'apatite des vertébrés, l'oxygène des phosphates et des carbonates échange isotopiquement avec l'oxygène de l'eau corporelle de l'individu et les valeurs $\delta^{18}O_p$ et $\delta^{18}O_c$ sont généralement corrélées linéairement [22,23]. Ainsi des modèles ont été proposés afin d'utiliser ces données comme enregistrements de variations saisonnières de paléo températures [24-29]. De plus en plus souvent les signatures isotopiques $\delta^{18}O_c$ sont mesurées de manière simultanée aux signatures $\delta^{18}O_p$ des phosphates sur les mêmes échantillons de dents ou d'os [28,30-32]. L'obtention d'une équation de fractionnement représente donc un apport fondamental pour l'interprétation de ces données $\delta^{18}O_c$ des carbonates d'apatite. Nous avons donc recréé en laboratoire les conditions de co-précipitation d'ions carbonates et d'HAP dans des solutions aqueuses dont la température a été contrôlée entre 10 °C et 37 °C représentant les températures de la surface de la terre et les températures corporelles des vertébrés. Ensuite les analyses isotopiques $\delta^{18}O_w$ des eaux ont été effectuées selon la technique d'équilibration utilisant un système MultiPrep-IsoPrime comme décrit dans le paragraphe 4.1. Les analyses de carbonates d'apatite ont également été analysées avec un système MultiPrep-IsoPrime cette fois en configuration MultiCarb dont le fonctionnement est illustré dans la figure 4.3.

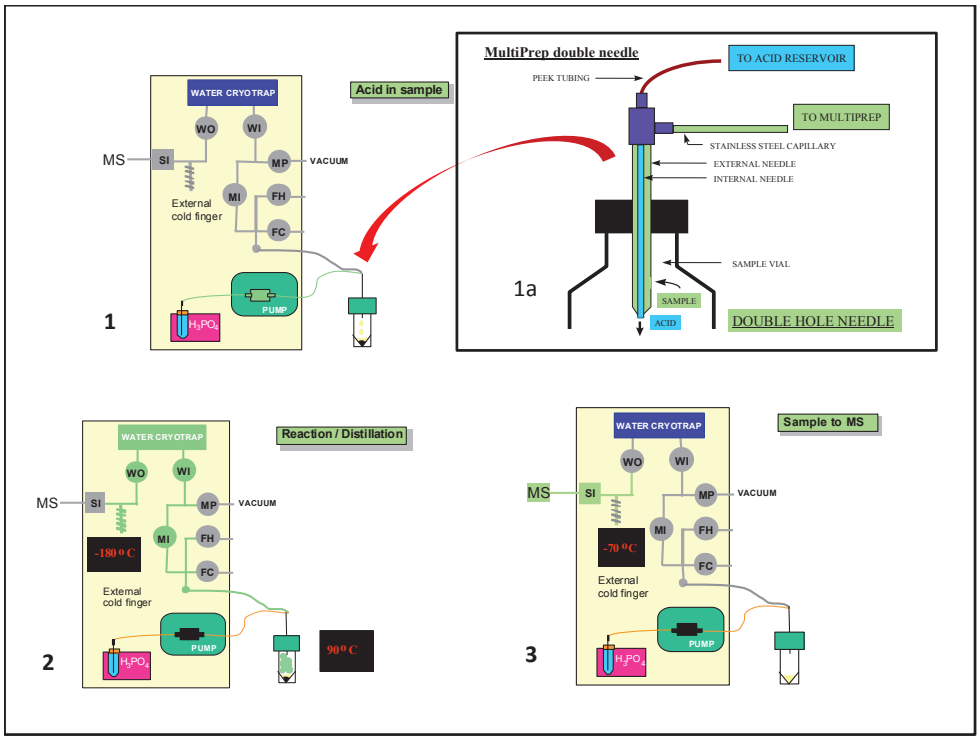

Figure 4.3 : Principe de fonctionnement du MultiCarb : 1) dégazage de l'échantillon et introduction de l'acide phosphorique au moyen d'une aiguille double – insert 1-a ; 2) réaction du carbonate avec l'acide phosphorique et distillation du CO_2 ; 3) Transfert du CO_2 issu de la réaction vers le spectromètre de masse.

Pour ce faire nous avons dû quelque peu modifier les protocoles analytiques du MultiCarb établis pour des échantillons de calcite pure puisqu'ici nous avons analysé des échantillons présentant moins de 5 %poids ce calcite dans une matrice phosphatée. Une fois ce développement méthodologique effectué nous avons pu analyser des aliquotes aux alentours de 1200µg d'HAP contenant des carbonates en les faisant réagir avec de l'acide phosphorique anhydre dans des réacteurs maintenus à 90°C. Dans ces conditions, les résultats de cette étude nous ont permis de proposer l'équation de fractionnement suivante :

$$1000\ln\alpha(CO_3^{2-} - H_2O) = 25{,}19 \cdot T^{-1} - 56{,}47\ (\pm 1{,}81)\ \ (R^2 = 0{,}998)$$

Reliant le coefficient de fractionnement $\alpha\, CO_3^{2-}$ - eau à la température T. Cette équation fournit une pente légèrement plus importante que celle établie auparavant pour le couple calcite-eau [33,34]. Ainsi l'on observe un fractionnement isotopique de l'oxygène entre la calcite et l'eau variant de 4,5 ‰ à 9,1 ‰ pour des températures allant de 37°C à 10°C.

Ensuite, toujours dans le but d'améliorer l'outil isotopique appliqué aux carbonates, nous nous sommes intéressés au fractionnement isotopique du carbone et de l'oxygène entre aragonite et calcite qui sont les deux formes principales de carbonates de calcium secrétées par les organismes vivants. En effet, une proportion importante d'invertébrés marins (mollusques, céphalopodes, foraminifères, brachiopodes) présente des exosquelettes constitués d'aragonite ou de calcite [35]. Les compositions isotopiques de ces deux polymorphes de carbonates de calcium représentent des outils importants pour caractériser certains paramètres des océans comme la température, la salinité ou l'activité biologique. Ainsi les analyses $\delta^{13}C$ et $\delta^{18}O$ de coquilles fossiles ont été largement utilisées pour effectuer des reconstructions paléoenvironnementales [36,37]. Mais l'estimation des paléo températures et la composition isotopique en carbone des eaux anciennes nécessite une connaissance précise du fractionnement isotopique entre les deux espèces de polymorphes de carbonate de calcium. Dans la publication 4.4 nous nous sommes intéressés au fractionnement isotopique aragonite-calcite en carbone et en oxygène en analysant des spécimens de gastéropodes marins, et de bivalves vivant dans des milieux tempérés à tropicaux. Certaines espèces sécrétant à la fois de l'aragonite et de la calcite ont été utilisées comme témoins des variations extérieures du milieu autres que la température comme la composition isotopique de l'eau, le régime alimentaire… Les coquilles analysées ont été caractérisées et cartographiées par spectroscopie RAMAN. Ensuite les échantillons ont été obtenus par micro forage dans les coquilles des différents spécimens et ainsi 36 paires d'échantillons d'aragonite-calcite ont été obtenues à partir de dix espèces de gastéropodes et cinq espèces de bivalves. Ces échantillons ont ensuite

été analysés avec notre système MultiPrep en configuration MultiCarb (voir description ci-dessus) pour les signatures isotopiques $\delta^{13}C_{VPDB}$ et $\delta^{18}O_{VPDB}$. Les échantillons d'eaux prélevées en même temps que les coquilles ont également été analysés avec notre MultiPrep en configuration AquaPrep afin de mesurer leurs $\delta^{18}O_{SMOW}$. Une nouvelle fois ici c'est l'automatisation et la rapidité d'analyses du système de préparation des échantillons qui nous a permis de mener à bien cette étude qui n'aurait pas pour être envisagée sur des systèmes conventionnels utilisant des lignes sous vide compte tenu de la quantité d'analyses nécessaire pour obtenir des résultats significatifs.

Les résultats de nos travaux montrent que l'aragonite biogénique est enrichie par rapport à la calcite biogénique associée :

- en $\delta^{13}C_{VPDB}$ d'une valeur de 0,95 ± 1,81 ‰
- en $\delta^{18}O_{VPDB}$ d'une valeur de 0,37 ± 0,65 ‰

Nos résultats indiquent que les deux variétés polymorphes de calcite précipitent dans des conditions proches de l'équilibre isotopique avec l'eau de mer mais pas tout à fait en équilibre. D'où la recommandation d'utiliser les équations empiriques de fractionnement isotopique de l'oxygène établies sur la bases d'analyses de mollusques actuels et des eaux ambiantes afin de déterminer des paleotemperatures.

Puis nous nous sommes attelés à un développement analytique répondant à une question posée depuis longtemps par la communauté des géochimistes : « Comment analyser la signature isotopique d'espèces carbonatées présentes ensemble dans un échantillon ; en particulier les mélanges Calcite-Dolomie ? ». La plupart des roches sédimentaires carbonatées ont des histoires diagénétiques complexes. Cela se traduit par des assemblages minéraux variables [38]. Une des façons de décrypter les mécanismes de formation de ces assemblages minéraux est d'analyser leur composition isotopique en carbone et en oxygène [39,40]. Mais les analyses isotopiques sur les différentes phases carbonatées présentes (aragonite, calcite,

dolomite) n'est pas chose facile car dans la plupart des cas ces différentes phases ne sont pas séparables physiquement. On utilise donc généralement les réactivités différentes lors de l'attaque acide pour mesurer les $\delta^{13}C_{VPDB}$ et $\delta^{18}O_{VPDB}$ respectifs des différentes phases présentes afin de retracer leurs processus de formation [41-43]. Dans ce travail nous avons une nouvelle fois exploité les performances de notre système MultiPrep en mode MultiCarb (voir description ci-dessus). Cependant le système a été développé pour réaliser l'analyse d'échantillons de carbonates purs et l'analyse de carbonates complexes a nécessité une partie de développement analytique impliquant également la comparaison des analyses automatisées avec des analyses effectuées manuellement sur les lignes à vide de notre laboratoire. Cette mise au point a été possible grâce à le réalisation de mélanges artificiels de calcite et de dolomite caractérisées isotopiquement sous formes de pôles purs. Nous avons utilisé des temps de réaction et des températures de réaction différents pour les deux phases, ainsi pour la calcite nous avons programmé le système pour opérer une réaction à l'acide phosphorique pendant 20 minutes à 40°C et pour la dolomite une réaction pendant 45 minutes à 90 °C. L'utilisation de ce protocole nous a permis d'obtenir des valeurs fiables de $\delta^{13}C_{VPDB}$ et $\delta^{18}O_{VPDB}$ sur nos phases de calcite et de dolomite. Il est à noter que l'utilisation de cette méthode sur des échantillons naturels requiert la connaissance précise des abondances relatives en calcite et dolomite.

Enfin, toujours dans le domaine de l'analyse isotopique des carbonates nous nous sommes intéressés à la variabilité naturelle des compositions isotopiques en $\delta^{13}C_{VPDB}$ et $\delta^{18}O_{VPDB}$ sur des individus sélectionnés de populations de foraminifères et d'ostracodes.

Comme nous l'avons déjà souligné dans les chapitres précédents, les pionniers de l'analyse des isotopes stables comme Urey, Epstein ou McRea ont très tôt utilisé les compositions isotopiques des carbonates biogéniques afin d'accéder aux paleotemperatures des eaux océaniques [1,15,16]. Des organismes unicellulaires tels que les foraminifères ont par exemple été

souvent utilisés au travers de leurs signatures isotopiques afin d'estimer des paléo températures aussi bien que les paléo productivités des océans [44-47]. Depuis une vingtaine d'année, l'évolution technologique des systèmes d'analyse des isotopes stables à la fois en ce qui concerne les spectromètres de masse eux-mêmes et les systèmes de préparation automatisés, ont permis d'accéder à des résultats précis et reproductibles sur des prises d'essais de plus en plus petites jusqu'à arriver à des masses d'échantillons de 5-10 µg. Dans le cas d'animaux unicellulaires comme les foraminifères cela a conduit à établir des interprétations de données isotopiques de carbone ou d'oxygène basées sur des analyses d'un seul individu [48-50]. Cependant, des variabilités naturelles des rapports isotopiques en carbone et en oxygène entre individus ont déjà été mentionnées dans la littérature qui ne peuvent pas être uniquement attribuées à des biais instrumentaux [51-53]. Ainsi dans l'étude qui est détaillée dans la publication 4.6 nous avons essayé d'évaluer les importances relatives des variabilités naturelles et des biais instrumentaux. Pour ce faire nous avons d'abord évalué les performances de notre système MultiCarb (décrit ci-dessus) pour des prises d'essais de plus en plus faibles sur un matériel carbonaté homogène : le marbre de Carrare. Nous avons ainsi pu démontrer la fiabilité du système en mesurant des aliquotes de marbre de carrare entre 5 et 400 mg avec des répétabilités de 0,057 ‰ en $\delta^{13}C_{PDB}$ et 0,133 ‰ en $\delta^{18}O_{PDB}$. Ensuite nous nous sommes intéressés à une série d'analyses isotopiques en carbone et oxygène sur des populations de foraminifères (*Elphidium* et *Ammonia*) et d'ostracodes (*Aurila*) où nous avons mis en évidence une augmentation sytématique de la déviation standard des analyses avec la réduction du nombre d'individus analysés.

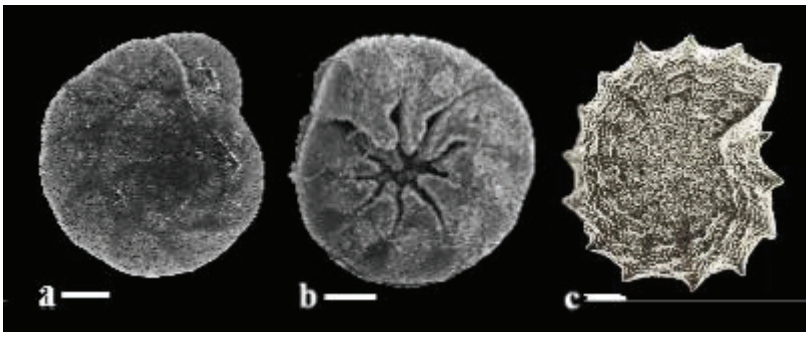

Figure 4.4 Photographie de foraminifères étudiés (Elphidium aculeatum)

Partant de là nous avons mis en place une série d'analyses systématiques à partir d'une population supposée homogène de foraminifères Elphidium en faisant varier le nombre d'individus analysés dans des gammes de masse où nous savons que notre système est instrumentalement fiable. Nous avons ainsi mis en évidence que sur cette population, nous avons 95% de chances d'obtenir des déviations standards analytiques entre individus supérieures à 1,02 ‰ en $\delta^{18}O_{PDB}$ et supérieures à 1,45 ‰ en $\delta^{13}C_{PDB}$ en analysant un seul individu. Ces valeurs sont donc bien supérieures aux biais instrumentaux. De la même manière nous avons pu recommander que pour cette population, un nombre d'individu nécessaire de 35 pour le $\delta^{18}O_{PDB}$ et 44 pour le $\delta^{13}C_{PDB}$ afin d'avoir une probabilité de 95% d'obtenir une déviation standard inférieure ou égale à 0,25 ‰. Ces résultats permettent donc de prévenir des risques qu'il peut y avoir à réduire la prise d'essai et alertent la communauté sur les dangers de la course au « toujours plus petit ».

Nous avons vu sur ces exemples d'applications plus fondamentales des analyses isotopiques sur les carbonates comment l'apport analytique d'in système automatisé performant tel que le MultiCarb, parfois utilisé au-delà de ses capacités initiales, permettait d'une part d'apporter de nouvelles données sur des coefficients de fractionnement isotopique, aussi bien que de mesurer plusieurs types d'espèces carbonatées simultanément, mais également de placer des limites et d'alerter sur la réduction de la taille de l'échantillon à

analyser. Ceci illustre bien l'apport des évolutions technologiques pour aider à répondre à des questions scientifiques.

Available online at www.sciencedirect.com
ScienceDirect
Geochimica et Cosmochimica Acta 74 (2010) 2072–2081
Geochimica et Cosmochimica Acta
www.elsevier.com/locate/gca

Oxygen isotope fractionation between apatite-bound carbonate and water determined from controlled experiments with synthetic apatites precipitated at 10–37 °C

Christophe Lécuyer [a,*], Vincent Balter [b], François Martineau [a], François Fourel [a], Aurélien Bernard [a], Romain Amiot [a], Véronique Gardien [a], Olga Otero [c], Serge Legendre [a], Gérard Panczer [d], Laurent Simon [e], Rossana Martini [f]

[a] *Laboratoire Paléoenvironnements & Paléobiosphère, CNRS UMR 5125, Université Lyon 1, Lyon 69622, France*
[b] *Laboratoire de Sciences de la Terre, CNRS UMR 5570, Université Lyon 1 et Ecole Normale Supérieure de Lyon, Lyon 69007, France*
[c] *iPHEP (Institut international de Paléoprimatologie, Paléontologie humaine: Evolution et Paléoenvironnements), UMR CNRS 6046, Université Poitiers, SFA, 40 avenue du recteur Pineau, F-86022 Poitiers Cedex, France*
[d] *Laboratoire de Physico-Chimie des Matériaux Luminescents, CNRS UMR 5620, Université Lyon 1, Lyon 69300, France*
[e] *Laboratoire d'Ecologie des Hydrosystèmes Fluviaux, UMR CNRS 5023, Université Lyon 1, Lyon, Bât. Forel, 69622 Villeurbanne Cedex, France*
[f] *Département de Géologie et Paléontologie, 13 rue des Maraîchers, CH-1205 Genève, Switzerland*

Received 5 June 2009; accepted in revised form 18 December 2009; available online 4 January 2010

Abstract

The oxygen isotope fractionation between the structural carbonate of inorganically precipitated hydroxyapatite (HAP) and water was determined in the range 10–37 °C. Values of 1000 ln $\alpha(CO_3^{2-}$–$H_2O)$ are linearly correlated with inverse temperature (K) according to the following equation: 1000 ln $\alpha(CO_3^{2-}$–$H_2O) = 25.19\ (\pm 0.53)\cdot T^{-1} - 56.47\ (\pm 1.81)$ ($R^2 = 0.998$). This fractionation equation has a slightly steeper slope than those already established between calcite and water (O'Neil et al., 1969; Kim and O'Neil, 1997) even though measured fractionations are of comparable amplitude in the temperature range of these experimental studies. It is consequently observed that the oxygen isotope fractionation between apatite carbonate and phosphate increases from about 7.5‰ up to 9.1‰ with decreasing temperature from 37 °C to 10 °C. A compilation of $\delta^{18}O$ values of both phosphate and carbonate from modern mammal teeth and bones confirms that both variables are linearly correlated, despite a significant scattering up to 3.5‰, with a slope close to 1 and an intercept corresponding to a 1000 ln $\alpha(CO_3^{2-}$–$PO_4^{3-})$ value of 8.1‰. This apparent fractionation factor is slightly higher or close to the fractionation factor expected to be in the range 7–8‰ at the body temperature of mammals.

1. INTRODUCTION

Stable isotope compositions of biogenic apatites are now widely used to reconstruct terrestrial and marine environments. Since the pioneering studies of Longinelli (1965, 1966), Longinelli and Nuti (1968, 1973) and Kolodny et al. (1983), several oxygen isotope fractionation equations between apatite phosphate and water have been established (e.g. Longinelli, 1984; Luz and Kolodny, 1985; Kohn, 1996; Lécuyer et al., 1996; Amiot et al., 2007) to quantify marine and air temperatures over the Phanerozoic (Kolodny and Luz, 1991; Fricke et al., 1998; Vennemann and Hegner, 1998; Joachimski and Buggisch, 2002; Pucéat et al., 2003; Daux et al., 2005; Kocsis et al., 2007; Trotter et al., 2008). Minor amounts of carbonate (3–6 wt%) occur natu-

* Corresponding author. Tel.: +33 4 72 44 83 76; fax: +33 4 72 43 16 88.
E-mail address: clecuyer@univ-lyon1.fr (C. Lécuyer).

0016-7037/$ - see front matter © 2009 Elsevier Ltd. All rights reserved.
doi:10.1016/j.gca.2009.12.024

rally in substitution of phosphate in the crystal lattice of apatites (LeGeros, 1981; Okazaki et al., 1982; Schuffert et al., 1990; LeGeros et al., 1996). Decreasing amounts of structural carbonate are correlated with increasing apatite crystallinity, thus improving the stability of apatite crystals by reducing its solubility (Shemesh, 1990; Kohn et al., 1999). These carbonate contents have been used as indicators of bone or enamel diagenesis (Shemesh, 1990; Bryant et al., 1994). In the apatite of living vertebrates, oxygen from phosphate and carbonate exchanges isotopes with body water, and co-existing $\delta^{18}O_c$ and $\delta^{18}O_p$ values are linearly correlated (Bryant et al., 1996; Iacumin et al., 1996). This property was used as a test for identifying diagenetic alteration in fossil teeth and bones (Iacumin et al., 1996; Tütken et al., 2006). Because different rates of oxygen isotope exchange in the phosphate–water and carbonate–water systems are expected in the case of inorganic or microbially mediated interactions, the $\delta^{18}O$ values of altered fossils should deviate from equilibrium values (Zazzo et al., 2004). For samples which escaped diagenetic alteration, both carbon and oxygen isotope ratios of carbonate from apatites constitute valuable proxies of the diet, ecology and environments of many terrestrial vertebrates since the Mesozoic (e.g. Wright and Schwarcz, 1998; Kohn and Cerling, 2002; Smith et al., 2002; Zazzo et al., 2002; Jim et al., 2004; Hoppe, 2006). The record of seasonal temperature variations has been proposed on the basis of measured sinusoidal-like isotopic time series obtained from the intra-tooth sampling of hypsodont vertebrates (e.g. Feranec and MacFadden, 2000; Gadbury et al., 2000; Bocherens et al., 2001; Balasse, 2002; Stanton Thomas and Carlson, 2004; Arppe and Karhu, 2006). However, the quantification of temperatures is still lacking in the absence of any experimental determination of the oxygen isotope fractionation between hydroxyapatite (HAP) carbonate and water. Such an isotopic fractionation equation would be very useful for understanding the meaning of $\delta^{18}O$ values of apatite carbonate that are now commonly measured along those of apatite phosphate in the same tooth or bone samples (Zazzo et al., 2002; Lécuyer et al., 2003; Stanton Thomas and Carlson, 2004; Tütken et al., 2004). Oxygen isotope ratios of phosphate and carbonate are roughly linearly correlated (Bryant et al., 1996; Iacumin et al., 1996; Zazzo et al., 2004). However, the isotopic difference between carbonate and phosphate recorded in terrestrial mammals samples is not a constant ($\Delta^{18}O_{(CO_3^{2-}-PO_4^{3-})}$ differences range from about 8‰ to 11‰) despite near constant body temperatures ($T = 37 \pm 2$ °C). Therefore, we propose to determine the oxygen isotope fractionation between the carbonate ions of inorganically precipitated HAP and water in the range (10 °C < T < 37 °C) of Earth's surface and terrestrial vertebrate body temperatures.

2. EXPERIMENTAL PROTOCOL AND ANALYTICAL TECHNIQUES

2.1. Precipitation of inorganic hydroxyapatites

In this study, carbonate-bearing hydroxyapatite was synthesized by adapting the protocol given by Balter and Lécuyer (2004). A first aqueous solution ("PC") was prepared by adding 0.5 ml of $KNaCO_3$ (10^{-1} M) to 500 ml of $Na_2HPO_4{\cdot}2H_2O$ (10^{-2} M), pH was then adjusted to 7.4 by adding 0.3% HNO_3. A second solution was made by adding NaOH (10^{-1} M) to 500 ml of $CaCl_2{\cdot}2H_2O$ (10^{-2} M) until a pH of 7.4 was reached (solution "CA"). Aqueous solutions were held at constant temperatures of 10 °C, 15 °C, 20 °C, 25 °C, 30 °C and 37 °C, respectively, for 48 h to ensure oxygen isotope equilibrium in the carbonate–water system for the "PC" solutions according to kinetic data determined by Zeebe and Wolf-Gladrow (2001). Equal volumes of "PC" and "CA" solutions were mixed at a given temperature. Concentrations of Ca^{2+} and PO_4^{3-} in the resulting solution are the same order of magnitude as in blood plasma ($[Ca^{2+}] = 2.5$ mM and $[PO_4^{3-}] = 1$ mM) and seawater ($[Ca^{2+}] = 10$ mM), but P in seawater typically has a concentration of 1 μM (Broecker and Peng, 1982; Kaim and Schewderski, 1994) compared to our solutions having a $[PO_4^{3-}]$ of 5.3×10^{-3} M. According to Balter and Lécuyer (2004), at least 96 h of maturation of the solid phase is required to obtain well-crystallized HAP crystals in the temperature range of this study. During the maturation of the solid phase, the Erlenmeyer flasks, covered with watch glasses to prevent evaporation of the solution, were gently shaken at regular intervals in order to avoid extensive sedimentation as well as the development of a concentration gradient in the solution. At the end of the experiment, the solid phase was separated from the supernatant by centrifugation, washed with distilled water and dried at room temperature whereas the aqueous solutions were filtered through a 0.22 μm filter and sealed in a glass tube.

2.2. Scanning Electron Microscopy and Infrared Spectroscopy

HAP samples were mounted on the conductive support (i.e., aluminium stub) with double-sided conductive carbon tape. An ultra-thin coating (ca 20 nm) of gold was then deposited on the samples by low vacuum sputter coating prior to imaging with a Jeol JSM 6400 SEM (University of Geneva, Geneva, Switzerland). Transmission IR spectra were recorded using a Perkin-Elmer GX II FTIR spectrometer. Disks containing 1 mg of sample in 150 mg of KBr were employed. The spectra were collected after 40 accumulations with a spectral resolution of 0.4 cm^{-1} in the 400–4000 cm^{-1} range.

2.3. Oxygen isotope analysis of HAP-bound carbonate

Oxygen isotope ratios were determined by using a MultiPrep™ automated preparation system coupled to a dual-inlet Elementar™ Isoprime™ isotope ratio mass spectrometer (IRMS). For each sample, an aliquot of about 1200 μg of carbonate-bearing HAP was reacted with anhydrous supersaturated phosphoric acid at 90 °C for 90 min. An acid fractionation factor value of 1.0080 was used to calculate the oxygen isotope composition of carbonate, the same as that used for calcite reacted with anhydrous phosphoric acid at 90 °C (Swart et al., 1991), which is also the value

recommended by Passey et al. (2007) for F-poor apatite (modern tooth enamel). Isotopic compositions are reported in the delta notation in ‰ relative to V-SMOW. All sample measurements were adjusted to the international reference NIST NBS19 according to the method developed by Werner and Brand (2001). Reproducibility of oxygen isotope measurement was ±0.1‰ (1σ).

2.4. Oxygen isotope analysis of water

Oxygen isotope measurements of water from HAP synthesis experiments were also performed by using a MultiPrep™ automated preparation system coupled to a dual-inlet Elementar™ Isoprime™ isotope ratio mass spectrometer. The method used was the water–carbon dioxide equilibration technique (Cohn and Urey, 1938). Aliquots of 200 µl of water were automatically reacted at 40 °C with CO_2. Reproducibility of oxygen isotope measurements was ±0.05‰. Oxygen isotope ratios are reported relative to V-SMOW in ‰ δ units after scaling the raw data to the "true" isotopic ratios of SMOW, SLAP and GISP international standards.

3. RESULTS

3.1. Mineralogy of the chemical precipitates

IR-spectroscopy (Fig. 1) spectra show that the mineral phases that were precipitated in the temperature range 10–37 °C are well-crystallized HAP. According to previous IR-spectroscopy studies of apatite (e.g. Pucéat et al., 2004), the three intense absorbance peaks of the phosphate group occur at 1035, 603 and 565 cm^{-1} (Fig. 1A) whereas the three peaks representing the B-type carbonate substitution

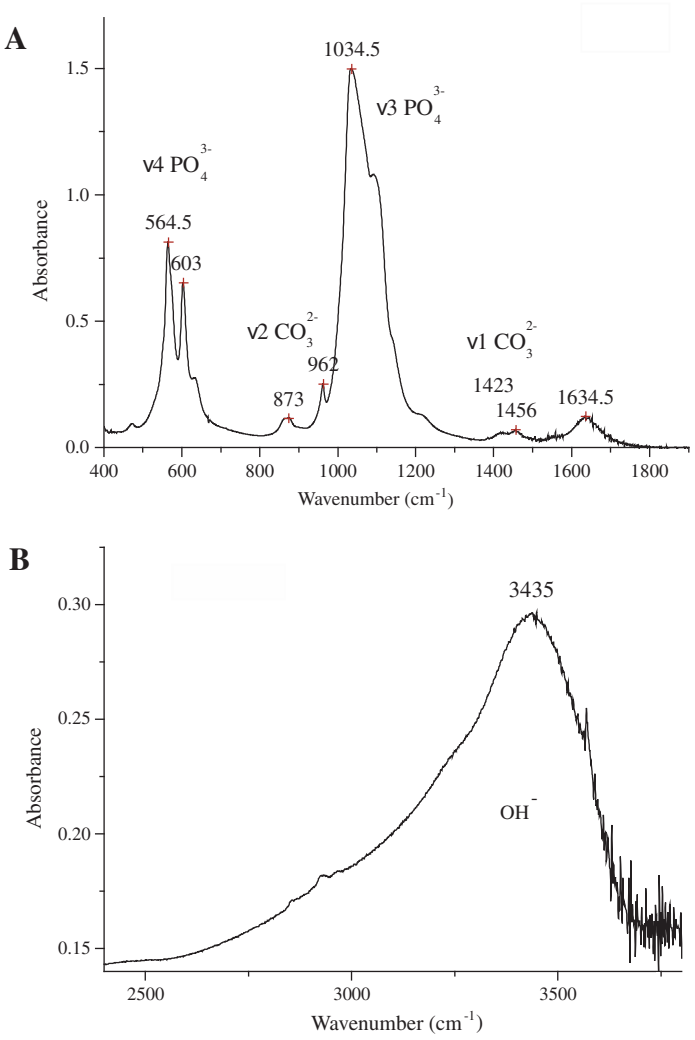

Fig. 1. Infrared spectrum of a carbonate-bearing hydroxyapatite precipitated at a temperature of 37 °C. (A) Three intense peaks of the phosphate group occur at 1035, 603 and 565 cm^{-1}. Three small peaks are observed at 1456, 1423 (stretching modes) and 873 cm^{-1} (deformational modes) and correspond to the B-type carbonate substitution with the replacement of PO_4^{3-} by CO_3^{2-} along with the substitution of Ca^{2+} by Na^+ and K^+ to preserve the crystal electroneutrality. (B) The large peaks observed at 3435 cm^{-1} are attributed to the OH^- goups.

are observed at 1456, 1423 (stretching modes) and 873 cm^{-1} (deformational modes). The peaks observed at 3435 cm^{-1} can be attributed to the OH^- groups (Fig. 1B). Scanning Electron Microscope (SEM) photomicrographs show that HAP precipitates form subhedral to euhedral hexagonal crystals with a tabular habit (5–10 μm in size) co-existing with smaller (<1 μm) poorly crystallized HAP (Fig. 2). Carbonate-bearing HAP is the only solid phase that was identified during these experiments. It is noteworthy that below 10 °C, brushite was precipitated instead of HAP as was previously observed by Balter and Lécuyer (2004). The amount of structural carbonate has been roughly estimated by measuring the CO_2 pressure generated from the carbonate reactions with phosphoric acid using the calibrated transducer readings from the dual inlet of the IRMS. Carbonate content ranges from 0.05 to 0.23 ± 0.05 wt% (Table 1).

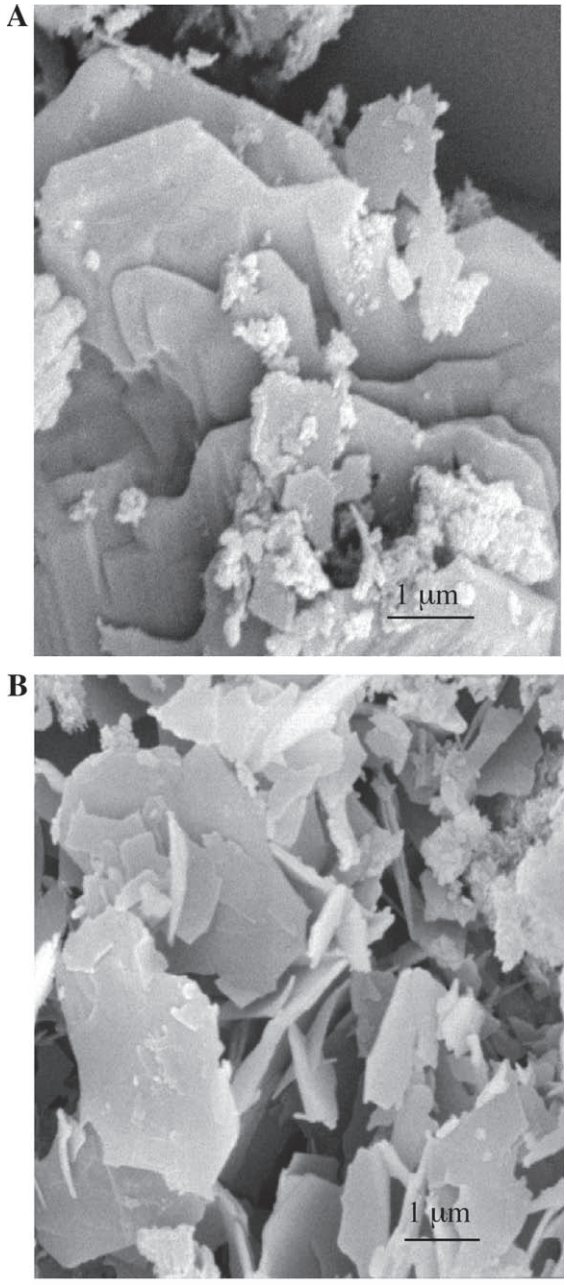

Fig. 2. Photomicrograph by Scanning Electron Microscopy of inorganically precipitated crystals of carbonate-bearing hydroxyapatite. (A) HAP crystals precipitated at 10 °C (magnification of 9000×). (B) HAP crystals precipitated at 37 °C (magnification of 5000×).

3.2. Oxygen isotope fractionation between HAP-bound carbonate and water

Carbonate-bearing HAP was precipitated in waters with $\delta^{18}O$ ranging from −10.46‰ to −6.89‰ V-SMOW (Table 1). Experiments were performed in a restricted range of low temperatures from 10 °C to 37 °C, therefore resulting values of $1000 \ln \alpha(CO_3^{2-}\text{–}H_2O)$ were reported as a function of the inverse of the temperature (K) according to the recommendation given by O'Neil (1986). Both variables are linearly correlated according to the following equation (Fig. 3):

$$1000 \ln \alpha(CO_3^{2-}\text{–}H_2O) = 25.19\ (\pm 0.53) \cdot T^{-1} - 56.47\ (\pm 1.81)\ (R^2 = 0.998) \quad (1)$$

This fractionation equation has a slightly steeper slope than those already established between calcite and water (O'Neil et al., 1969; Kim and O'Neil, 1997) even though measured fractionations are comparable within analytical uncertainties in the temperature range 20–37 °C (Fig. 4). Blake et al. (1997), Lécuyer et al. (1999) and O'Neil et al. (2003) have shown that oxygen isotope exchange between dissolved phosphate and water is extremely slow. Indeed, according to the temperature dependence of the rate constant 'k' as determined by Lécuyer et al. (1999), the fraction of exchanged oxygen isotopes between phosphate and water is negligible for reaction times of 96 h and temperatures ranging from 10 °C to 37 °C. Consequently, comparison of oxygen isotope fractionation between HAP-bound carbonate and water with that of phosphate–water can only be made with oxygen isotope fractionation equations that were established empirically with apatites of biogenic origin. It is then observed that the oxygen isotope fractionation between apatite carbonate and phosphate (Kolodny et al., 1983) increases from about 7.5‰ up to 9.1‰ with the temperature decreasing from 37 °C to 10 °C (Fig. 5).

4. DISCUSSION

4.1. Did HAP-bound carbonate reach isotopic equilibrium during precipitation?

Podlesak et al. (2008) performed diet-controlled experiments on woodrats and measured oxygen isotopic fractionations between enamel carbonate and body water in the range 24.4–29.4‰. These values bracket the fractionation value determined during our experiments performed at 37 °C. Oxygen isotope fractionations that were measured between HAP carbonate and water are also close to those determined between calcite and water (O'Neil et al., 1969;

Table 1
Oxygen isotope compositions of carbonate ions in hydroxyapatites that were inorganically precipitated in waters of known isotopic compositions in the range 10–37 °C. Samples correspond to HAP precipitates obtained from distinct aqueous solutions, each HAP sample has been duplicated or triplicated (*n*) for the $\delta^{18}O$ analysis of apatite carbonate.

Sample	*n*	CO_3^{2-} (wt%)	$\delta^{18}O$ (CO_3^{2-}) (‰ V-SMOW)	$\delta^{18}O$ (H_2O) (‰ V-SMOW)	1000 ln α	*T* (°C)
HAP10-1	2	0.1	22.57	−10.09	32.46	10
HAP10-2	2	0.12	22.92	−10.09	32.80	10
HAP10-3	2	0.15	22.79	−10.09	32.68	10
HAP15-1	3	0.11	21.23	−10.07	31.13	15
HAP15-2	3	0.21	21.03	−10.04	30.90	15
HAP20-1	3	0.05	19.99	−9.96	29.80	20
HAP20-2	3	0.06	19.37	−9.94	29.17	20
HAP25-1	3	0.21	17.50	−10.46	27.86	25
HAP30-1	3	0.19	17.33	−9.81	27.04	30
HAP30-2	3	0.17	16.85	−9.77	26.53	30
HAP37-1	2	0.23	16.02	−9.30	25.24	37
HAP37-2	2	0.18	17.74	−6.89	24.50	37

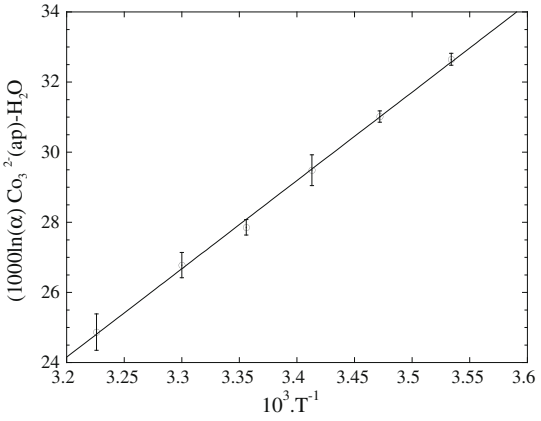

Fig. 3. Oxygen isotope fractionation equation between inorganic hydroxyapatite carbonate and water in the range 10–37 °C. $1000 \ln \alpha(CO_3^{2-}\text{–}H_2O) = 25.19\ (\pm 0.53)\cdot T^{-1} - 56.47\ (\pm 1.81)$ with $R^2 = 0.998$.

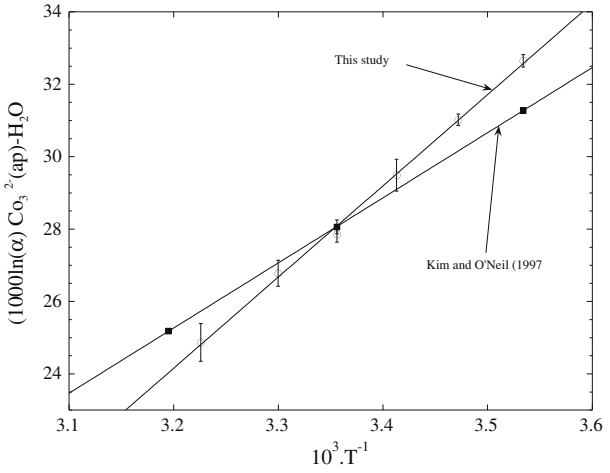

Fig. 4. Oxygen isotope fractionation equation between inorganic hydroxyapatite carbonate and water compared to the inorganic calcite–water equation (Kim and O'Neil, 1997).

Kim and O'Neil, 1997) for temperatures between 20 °C and 37 °C (isotopic differences do not exceed 0.5‰). However, the steeper slope observed for the fractionation equation between HAP carbonate and water is rather surprising (Fig. 3) when considering that equations determined for calcite, aragonite and HAP phosphate have similar slopes (O'Neil et al., 1969; Kolodny et al., 1983; Grossman and Ku, 1986). It must be also kept in mind that oxygen isotope fractionation between HAP-bound carbonate and water can be distinct from the fractionation between calcite and water considering the differences in chemistry and crystal lattice between the two minerals. However, we must question whether or not our experimental data reflect the oxygen isotope composition of natural carbonate-bearing HAP, taking into account that the amount of carbonate in experimental HAP is much lower than that of most biogenic apatites. Indeed, Koch et al. (1997) and Zazzo et al. (2004) reported CO_3^{2-} amounts ranging from 3.4 to 4.0 wt% for untreated enamel and enamel treated with acetic acid or sodium hypochlorite solutions. Experimental HAP crystals precipitated in this study contain only 0.05–0.23 wt‰ of CO_3^{2-}, which is

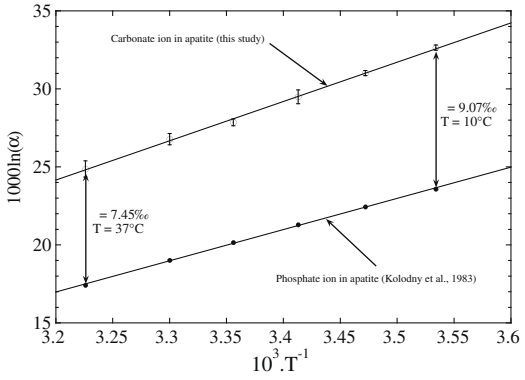

Fig. 5. Oxygen isotope fractionation equation between inorganic hydroxyapatite carbonate and water compared to the biogenic phosphate–water equation (Kolodny et al., 1983).

most likely the result of a high degree of crystallization in the absence of organic matrix. It has been documented that collagen-rich biogenic apatites such as bone and dentine have a poor crystallinity and a high carbonate content (LeGeros et al., 1967; Daculsi et al., 1997), thus at least partly explaining this difference in chemical composition. As observed in the case of divalent carbonates by Kim and O'Neil (1997), highly concentrated solutions or high rates of precipitation can generate 'non-equilibrium' minerals that are characterized by larger fractionation factors by as much as 2–3‰ associated with a poorer reproducibility. Similarly, Liang and Blake (2006, 2007) observed that apatite precipitates may be enriched in $P^{16}O_4$ relative to residual dissolved phosphate. Consequently, fractionation equations have a steeper slope than those attributed to 'equilibrium minerals'. However, several observations argue in favour of HAP precipitated near oxygen isotope equilibrium with the aqueous solution, which are (1) most crystals are well-crystallized as shown by XRD and IR-spectroscopy data, (2) the low solubility of HAP precludes the use of highly concentrated aqueous solutions, (3) fractionation values are independent of the water $\delta^{18}O$ at 37 °C (Table 1). Oxygen isotope equilibrium between precipitated HAP carbonate and water cannot be demonstrated, however, these first experimental data suggest that measured fractionations are close to those established between calcite and water in the range of temperature of most living ectothermic and endothermic animals.

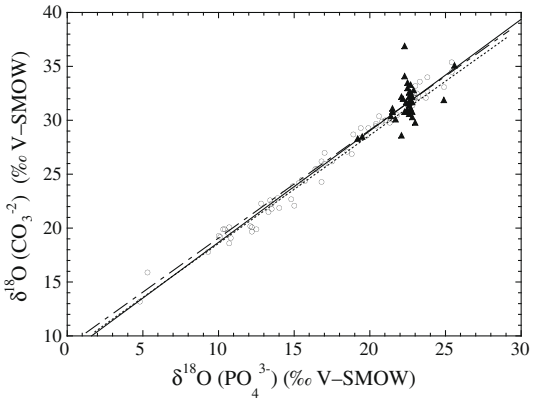

Fig. 6. $\delta^{18}O$ of apatite carbonate reported against $\delta^{18}O$ of apatite phosphate from teeth and bones of modern terrestrial mammals (open circles) and fish (filled triangles) that were compiled from Bryant et al. (1996), Iacumin et al. (1996), Shahack-Gross et al. (1999), Vennemann et al. (2001), Zazzo et al. (2004) and Martin et al. (2008). The intercept value of the regression line for modern mammals is an indicator of the $1000 \ln \alpha(CO_3^{2-}–PO_4^{3-})$ value recorded in these biogenic apatites for a temperature close to 37 °C. $\delta^{18}O(CO_3^{2-}) = 1.035(\pm0.017)\cdot\delta^{18}O(PO_4^{3-}) + 8.33$ (±0.30) with $R^2 = 0.983$. Dashed line: $1000 \ln \alpha(CO_3^{2-}–PO_4^{3-})$ by combining calcite and phosphate fractionation equations from Kim and O'Neil (1997) and Kolodny et al. (1983). Dotted line: $1000 \ln \alpha(CO_3^{2-}–PO_4^{3-})$ by combining fractionation equations from this study and the phosphate equation from Kolodny et al. (1983).

4.2. Oxygen isotope compositions of carbonate and phosphate in biogenic apatites

The dependence on temperature of the oxygen isotope fractionation between biogenic phosphate and water has been empirically determined several times and according to the Longinelli and Nuti (1973), Kolodny et al. (1983) and Lécuyer et al. (1996); $1000 \ln \alpha(PO_4^{3-}–H_2O)$ equals 17.4 ± 0.5‰ at 37 °C. Consequently, when using the fractionation equations experimentally determined for calcite by O'Neil et al. (1969) and Kim and O'Neil (1997), the oxygen isotope fractionation factor between carbonate (approximated by that of calcite–water) and phosphate in apatite from vertebrate bones and teeth lies between 7‰ and 8‰ over the studied range of temperatures (10–37 °C) because the slopes of these curves are close to each other. This estimate is in agreement with the result of calculations made by Bryant et al. (1996) who combined fractionation equations proposed by both Shemesh et al. (1988) and Zheng (1996) and which were based on measurements of natural samples and theoretical calculations, respectively. Measured oxygen isotope fractionation between HAP-bound carbonate (this study) and phosphate (Kolodny et al., 1983) is close to 7.5 at 37 °C (Fig. 5) and is in agreement with previous estimates presented above. However, an increasing oxygen isotope fractionation with decreasing temperature remains to be confirmed (Fig. 5).

A compilation of $\delta^{18}O$ values of both phosphate and carbonate (Fig. 6) from teeth and bones (Bryant et al., 1996; Iacumin et al., 1996; Zazzo et al., 2004) from modern mammals—which regulate body temperature close to 37 °C—confirms that both variables are linearly correlated with a slope close to 1 (1.03 ± 0.02) and an intercept of 8.3‰ that corresponds to a $1000 \ln \alpha(CO_3^{2-}–PO_4^{3-})$ value of 8.1‰. This fractionation factor is slightly higher or close to the fractionation factor expected to be in the range 7–8‰. It is noteworthy that the observed apparent oxygen isotope fractionation between carbonate and phosphate in apatite is more scattered in fish than in mammals (Fig. 6) as reported by Vennemann et al. (2001). These authors consider that the mean $\Delta_{carbonate–phosphate}$ value of 9.1‰ associated with a large standard deviation of 1.5‰ ($n = 44$) could reflect temperature of carbonate formation either higher or lower than that of phosphate, most of the analyzed fish having evolved in waters for which the temperature was in the range 12–23 °C (Vennemann et al., 2001).

Several mechanisms may be involved to explain the slight difference of oxygen isotope composition between carbonates from mammal apatite and inorganic HAP relative to the composition of the co-existing biogenic phosphate. Bryant et al. (1996) proposed that a difference in mineral stoichiometry could partly account for the observed relative slight ^{18}O-enrichment of carbonate in mammal apatite. Acid fractionation factors are indeed sensitive to mineral composition as reported by Friedman and O'Neil (1977). However, chemical compositions and crystallinity of HAP from mammal tooth or bone and from our low-temperature precipitates are close enough to exclude a significant influence on oxygen isotope fractionation factors. A second explanation could be a diachronism in the closure of oxygen isotope exchange between the carbonate–

water and phosphate–water systems with a diet-dependent body water of varying $\delta^{18}O$ value. However such a diachronism seems unlikely because of the large residence time of water in the studied mammals (Nagy and Peterson, 1988) which precludes short-time variations in the $\delta^{18}O$ of body water. Moreover, such a process should be responsible for a scattering of data but without modifying the mean value of 1000 ln $\alpha(CO_3^{2-}$–$PO_4^{3-})$. Scattering of data in Fig. 6 is high relative to the possible cumulative analytical uncertainties associated with the measurement of $\delta^{18}O$ values in both carbonate and phosphate components. Indeed, 1000 ln $\alpha(CO_3^{2-}$–$PO_4^{3-})$ values range from 7‰ to 10.5‰, independently of the methods used to analyze oxygen isotope compositions of apatite phosphate and carbonate. Such a data scattering could result from HAP carbonate precipitation out of isotopic equilibrium with body water. Precipitation of biogenic carbonate out of oxygen isotope equilibrium with ambient water (the so-called "vital effect") has been for example widely documented in brachiopods (Auclair et al., 2003), corals (Swart, 1983; McConnaughey, 1989a,b) and foraminifera (Zeebe, 1999). These isotopic disequilibria can result from high growth rates of the skeleton, varying amounts of metabolic CO_2 available during crystallization and variations in the extracellular pH at the site of mineralization.

Mineralization of bone and enamel from extracellular fluids is promoted by specialized cells (osteoblasts for bones, ameloblasts for enamel). Osteoblasts and ameloblasts are requisite for the synthesis of bone and enamel extracellular matrix production and of mineralized tissues (Robinson et al., 1979; Arnett, 2003). Bone extracellular matrix is composed of nearly 90% collagen (Lian, 2006), while non-collagen proteins comprise enamel extracellular matrix. Mineral accounts for up to 70% of bone weight and 95% of enamel. Since no predictable difference of 1000 ln $\alpha(CO_3^{2-}$–$PO_4^{3-})$ is observed between bone and enamel samples, it is unlikely that the composition of extracellular matrix or bonds between HAP and extracellular matrix will significantly affect the $\delta^{18}O$ value of HAP-bound carbonate. Regulation of pH and ionic conditions is essential to normal enamel growth and mineralization. The pH of extracellular fluid varies at different stages of the amelogenesis between 5.8 and 7.4 (Aoba and Moreno, 1987; Sasaki et al., 1991). Little is known about bone interstitial fluid composition, however, large pH variations of the extracellular fluid around neutral to acidic values are likely during bone turn-over. Bone mineralization occurs at pH around 7.1–7.4, however, acidification by osteoclasts is required for bone resorption (Fallon, 1984; Arnett and Spowage, 1996). These pH variations could be responsible for the 0–1‰ difference between the oxygen isotope composition of carbonate from inorganic apatite and carbonate from biogenic apatite formed under identical conditions.

5. CONCLUSIONS

Our experimental study demonstrates the temperature dependence of the oxygen isotope fractionation between HAP-bound carbonate and water, in contrast with previous studies in which no significant temperature dependence was reported. This result suggests the existence of a carbonate–phosphate temperature proxy in ectotherms or endotherms. Values of 1000 ln $\alpha(CO_3^{2-}$–$PO_4^{3-})$ at 37 °C are estimated to be in the range 7–8‰ by combining experimental fractionation equations for calcite–water and HAP-bound carbonate–water with empirical fractionations based on phosphate in biogenic apatites. This value is close to but slightly lower than the value of 8.1‰ deduced from a compilation of data obtained from modern mammals. This data set also shows a significant scattering independent of the analytical methods that were used. These isotopic differences could result either from out-of-equilibrium oxygen isotope fractionation or changes in pH of the extracellular fluid, both processes operating during the incorporation of the minor amounts of carbonate ions in the crystal lattice of the apatite. Despite the sensitive dependence on temperature of the isotopic fractionation between the carbonate component of biogenic apatite and water, the oxygen isotope composition of phosphate remains the most robust proxy of temperatures or water compositions considering the better knowledge of fractionation equations that were determined for aquatic ectotherms and terrestrial mammals.

However, the carbon isotope composition of the carbonate component of apatites is very useful for discussing diet and ecology of past vertebrates while oxygen isotope compositions may help to identify a diagenetic alteration as already shown by Iacumin et al. (1996) and Zazzo et al. (2004). A better understanding of the mechanisms that are responsible for the observed variations in the apparent fractionation factor between carbonate and phosphate could improve the interpretations of data obtained in the fossil record, especially if this isotopic fractionation is sensitive to changes in an animal's physiology such as growth rate or any metabolic perturbation. Future research should allow evaluating whether oxygen fractionation between synthetic HAP-bound carbonate and water differs or not from the fractionation between biogenic HAP-bound carbonate and water.

ACKNOWLEDGMENTS

The authors are grateful to Editor Boaz Luz, K.T. Uno and one anonymous reviewer for their constructive comments that contributed to improve the scientific content of this study. This study received grants from French CNRS and IUF.

REFERENCES

Amiot R., Lécuyer C., Escarguel G., Billon-Bruyat J.-P., Buffetaut E., Langlois C., Martin S., Martineau F. and Mazin J.-M. (2007) Oxygen isotope fractionation between crocodilian phosphate and water. *Palaeogeogr. Palaeoclimatol. Palaeoecol.* **243**, 412–420.

Aoba T. and Moreno E. C. (1987) The enamel fluid in the early secretory stage of porcine amelogenesis: chemical composition and saturation with respect to enamel mineral. *Calcif. Tissue Int.* **41**, 86–94.

Arnett T. (2003) Regulation of bone cell function by acid–base balance. *Proc. Nutr. Soc.* **62**, 511–520.

Arnett T. and Spowage M. (1996) Modulation of the resorptive activity of rat osteoclasts by small changes in extracellular pH near the physiological range. *Bone* **18**, 277–279.

Arppe L. L. and Karhu J. A. (2006) Implications for the late Pleistocene climate in Finland and adjacent areas from the isotopic composition of mammoth skeletal remains. *Palaeogeogr. Palaeoclimatol. Palaeoecol.* **231**, 322–330.

Auclair A.-C., Joachimski M. M. and Lécuyer C. (2003) Deciphering kinetic, metabolic, and environmental controls on stable isotope fractionations between seawater and the shell of *Terebretalia transversa* (Brachiopoda). *Chem. Geol.* **202**, 59–78.

Balasse M. (2002) Reconstructing dietary and environmental history from enamel isotopic analysis: time resolution of intra-tooth sequential sampling. *Int. J. Osteoarchaeol.* **12**, 155–165.

Balter V. and Lécuyer C. (2004) Determination of Sr and Ba partition coefficients between apatite and water from 5 °C to 60 °C: a potential new thermometer for aquatic paleoenvironments. *Geochim. Cosmochim. Acta* **68**, 423–432.

Blake R. E., O'Neil J. R. and Garcia G. A. (1997) Oxygen isotope systematics of biologically mediated reactions of phosphate: I. Microbial degradation of organophosphorus compounds. *Geochim. Cosmochim. Acta* **61**, 4411–4422.

Bocherens H., Mashkourb M., Billiou D., Pelléc E. and Mariotti A. (2001) A new approach for studying prehistoric herd management in arid areas: intra-tooth isotopic analyses of archaeological caprine from Iran. *C. R. Acad. Sci. (Paris)* **332**, 67–74.

Broecker W. S. and Peng T. H. (1982) *Tracers in the Sea*. Eldigio Press Lamont Doherty Geological Observatory, New York, 690p.

Bryant J. D., Luz B. and Froelich P. N. (1994) Oxygen isotopic composition of fossil horse tooth phosphate as a record of continental paleoclimate. *Palaeogeogr. Palaeoclimatol. Palaeoecol.* **107**, 303–313.

Bryant J. D., Koch P. L., Froelich P. N., Showers W. J. and Genna B. J. (1996) Oxygen isotope partitioning between phosphate and carbonate in mammalian apatite. *Geochim. Cosmochim. Acta* **60**, 5145–5148.

Cohn M. and Urey H. C. (1938) Oxygen exchange reactions of organic compounds and water. *J. Am. Chem. Soc.* **60**, 679–682.

Daculsi G., Bouler J. M. and LeGeros R. Z. (1997) Adaptive crystal formation in normal and pathological calcifications in synthetic calcium phosphate and related biomaterials. *Int. Rev. Cytol.* **172**, 129–191.

Daux V., Lécuyer C., Adam F., Martineau F. and Vimeux F. (2005) Oxygen isotope composition of human teeth and the record of climate changes in France (Lorraine) during the last 1700 years. *Clim. Change* **70**, 445–464.

Fallon M. D. (1984) Bone resorbing fluid from osteoclasts is acidic: an *in vitro* micropuncture study. In *Endocrine Control of Bone and Calcium Metabolism*, vol. 8A (eds. D. V. Cohn, T. Fujita, J. T. Potts Jr. and R. V. Talmage). Elsevier Science Publishers, Amsterdam, pp. 144–146.

Feranec R. S. and MacFadden B. J. (2000) Evolution of the grazing niche in Pleistocene mammals from Florida: evidence from stable isotopes. *Palaeogeogr. Palaeoclimatol. Palaeoecol.* **162**, 155–169.

Fricke H. C., Clyde W. C., O'Neil J. R. and Gingerich P. D. (1998) Evidence for rapid climate change in North America during the latest Paleocene thermal maximum: oxygen isotope compositions of biogenic phosphate from the Bighorn Basin (Wyoming). *Earth Planet. Sci. Lett.* **160**, 193–208.

Friedman I. and O'Neil J. R. (1977) Compilation of stable isotope fractionation factors of geochemical interest. In *Data of Geochemistry*, 6th ed. (ed. M. Fleischer). US Geological Survey Professional Paper 440 KK.

Gadbury C., Todd L., Jahren A. H. and Amundson R. (2000) Spatial and temporal variations in the isotopic composition of bison tooth enamel from the Early Holocene Hudson–Meng Bone Bed, Nebraska. *Palaeogeogr. Palaeoclimatol. Palaeoecol.* **157**, 79–93.

Grossman E. L. and Ku T.-L. (1986) Oxygen and carbon isotope fractionation in biogenic aragonite: temperature effects. *Chem. Geol., Isot. Geosci. Sect.* **59**, 59–74.

Hoppe K. A. (2006) Correlation between the oxygen isotope ratio of North American bison teeth and local waters: implication for paleoclimatic reconstructions. *Earth Planet. Sci. Lett.* **244**, 408–417.

Iacumin P., Cominotto D. and Longinelli A. (1996) A stable isotope study of mammal skeletal remains of mid-Pleistocene age, Arago cave, eastern Pyrenees, France. Evidence of taphonomic and diagenetic effects. *Palaeogeogr. Palaeoclimatol. Palaeoecol.* **126**, 151–160.

Jim S., Ambrose S. H. and Evershed R. P. (2004) Stable carbon isotopic evidence for differences in the dietary origin of bone cholesterol, collagen and apatite: implications for their use in palaeodietary reconstruction. *Geochim. Cosmochim. Acta* **68**, 61–72.

Joachimski M. M. and Buggisch W. (2002) Conodont apatite $\delta^{18}O$ signatures indicate climatic cooling as a trigger of the Late Devonian mass extinction. *Geology* **30**, 711–714.

Kaim W. and Schewderski B. (1994) *Bioinorganic chemistry: inorganic elements in the chemistry of life. An introduction and guide*. John Wiley and Sons, Chichester, 414p.

Kim S.-T. and O'Neil J. R. (1997) Equilibrium and nonequilibrium oxygen isotope effects in synthetic carbonates. *Geochim. Cosmochim. Acta* **61**, 3461–3475.

Koch P. L., Tuross N. and Fogel M. L. (1997) The effects of sample treatment and diagenesis on the isotopic integrity of carbonate in biogenic hydroxyapatite. *J. Archaeol. Sci.* **24**, 417–429.

Kocsis L., Vennemann T. W. and Fontignie D. (2007) Migration of sharks into freshwater systems during the Miocene and implications for Alpine paleoelevation. *Geology* **35**, 451–454.

Kohn M. J. (1996) Predicting animal $\delta^{18}O$: accounting for diet and physiological adaptation. *Geochim. Cosmochim. Acta* **60**, 4811–4829.

Kohn M. J. and Cerling T. E. (2002) Stable isotope compositions of biological apatite. In *Phosphates, Geochemical, Geobiological, and Materials Importance. Reviews in Mineralogy and Geochemistry*, vol. 48 (eds. M. J. Kohn, J. Rakovan and J. M. Hughes). Mineralogical Society of America, Washington, DC, pp. 455–488.

Kohn M. J., Schoeninger M. J. and Barker W. W. (1999) Altered states: effect of diagenesis on fossil tooth chemistry. *Geochim. Cosmochim. Acta* **63**, 2737–2747.

Kolodny Y. and Luz B. (1991) Oxygen isotopes in phosphates of fossil fish—Devonian to recent. In *Stable Isotope Geochemistry: A Tribute to Samuel Epstein* (eds. H. P. Taylor, J. R. O'Neil and I. R. Kaplan). The Geochemical Society, San Antonio, pp. 105–119.

Kolodny Y., Luz B. and Navon O. (1983) Oxygen isotope variations in phosphate of biogenic apatites: I. Fish bone apatite-rechecking the rules of the game. *Earth Planet. Sci. Lett.* **64**, 398–404.

Lécuyer C., Grandjean P. and Emig C. C. (1996) Determination of oxygen isotope fractionation between water and phosphate from living lingulids: potential application to palaeoenvironmental studies. *Palaeogeogr. Palaeoclimatol. Palaeoecol.* **126**, 101–108.

Lécuyer C., Grandjean P. and Sheppard S. M. F. (1999) Oxygen isotope exchange between dissolved phosphate and water at

temperatures ⩽135 °C: inorganic versus biological fractionations. *Geochim. Cosmochim. Acta* **63**, 855–862.

Lécuyer C., Bogey C., Garcia J.-P., Grandjean P., Barrat J.-A., Floquet M., Bardet N. and Pereda-Superbiola X. (2003) Stable isotope composition and rare earth element content of vertebrate remains from the Late Cretaceous of northern Spain (Laño): did the environmental record survive? *Palaeogeogr. Palaeoclimatol. Palaeoecol.* **193**, 457–471.

LeGeros R. Z. (1981) Apatites in biological systems. *Prog. Cryst. Growth Charact.* **4**, 1–45.

LeGeros R. Z., Trautz O. R., Legeros J. P., Klein E. and Shirra W. P. (1967) Apatite crystallites: effects of carbonate on morphology. *Science* **155**, 1409–1411.

LeGeros R. Z., Sakae T., Bautista C., Retino M. and LeGeros J. P. (1996) Magnesium and carbonate in enamel and synthetic apatites. *Adv. Dent. Res.* **10**, 225–231.

Lian J. B. (2006) Biology of bone mineralization. *Curr. Opin. Endocrinol. Diab.* **13**, 1–9.

Liang Y. and Blake R. E. (2006) Oxygen isotope composition of phosphate in organic compounds: isotope effects of extraction methods. *Org. Geochem.* **37**, 1263–1277.

Liang Y. and Blake R. E. (2007) Oxygen isotope fractionation between apatite and aqueous-phase phosphate: 20–45 °C. *Chem. Geol.* **238**, 121–133.

Longinelli A. (1965) Oxygen isotopic composition of orthophosphate from shells of living marine organisms. *Nature* **207**, 716–719.

Longinelli A. (1966) Ratios of oxygen-18:oxygen-16 in phosphate and carbonate from living and fossil marine organisms. *Nature* **211**, 923–927.

Longinelli A. (1984) Oxygen isotopes in mammal bone phosphate: a new tool for paleohydrological and paleoclimatological research? *Geochim. Cosmochim. Acta* **48**, 385–390.

Longinelli A. and Nuti S. (1968) Oxygen-isotope ratios in phosphate from marine organisms. *Science* **160**, 879–882.

Longinelli A. and Nuti S. (1973) Revised phosphate–water isotopic temperature scale. *Earth Planet. Sci. Lett.* **19**, 373–376.

Luz B. and Kolodny Y. (1985) Oxygen isotope variation in phosphate of biogenic apatites: IV. Mammal teeth and bones. *Earth Planet. Sci. Lett.* **75**, 29–36.

Martin C., Bentaleb I., Kaandorp R., Iacumin P. and Chatri K. (2008) Intra-tooth study of modern rhinoceros enamel $\delta^{18}O$: is the difference between phosphate and carbonate $\delta^{18}O$ a sound diagenetic test? *Palaeogeogr. Palaeoclimatol. Palaeoecol.* **266**, 183–189.

McConnaughey T. A. (1989a) ^{13}C and ^{18}O isotopic disequilibrium in biological carbonates: I. Patterns. *Geochim. Cosmochim. Acta* **53**, 151–162.

McConnaughey T. A. (1989b) ^{13}C and ^{18}O isotopic disequilibrium in biological carbonates: II. In vitro simulation of kinetic isotope effects. *Geochim. Cosmochim. Acta* **53**, 163–171.

Nagy K. A. and Peterson C. C. (1988) Scaling of water flux rate in animals. *Univ. Calif. Publ. Zool.* **120**, 1–172.

Okazaki M., Moriwaki Y., Aoba T., Doi Y., Takahasi J. and Kimura H. (1982) Crystallinity changes of CO_3-apatites in solutions at physiological pH. *Caries Res.* **16**, 308–314.

O'Neil J. R. (1986) Theoretical and experimental aspects of isotopic fractionation. In *Stable Isotopes in High Temperature Geological Processes. Reviews in Mineralogy*, vol. 16 (eds. J. W. Valley, H. P. Talylor Jr. and J. R. O'Neil). Mineralogical Society of America, Washington, DC, pp. 1–40.

O'Neil J. R., Clayton R. N. and Mayeda T. K. (1969) Oxygen isotope fractionation in divalent metal carbonates. *J. Chem. Phys.* **51**, 5547–5558.

O'Neil J. R., Vennemann T. W. and McKenzie W. F. (2003) Effects of speciation on equilibrium fractionations and rates of oxygen isotope exchange between $(PO_4)_{aq}$ and H_2O. *Geochim. Cosmochim. Acta* **67**, 3135–3144.

Passey B. H., Cerling T. E. and Levin N. E. (2007) Temperature dependence of oxygen isotope acid fractionation for modern and fossil tooth enamels. *Rapid Commun. Mass Spectrom.* **21**, 2853–2859.

Podlesak D. W., Torregrossa A.-M., Ehleringer J. R., Dearing M. D., Passey B. H. and Cerling T. E. (2008) Turnover of oxygen and hydrogen isotopes in the body water, CO_2, hair, and enamel of a small mammal. *Geochim. Cosmochim. Acta* **72**, 19–35.

Pucéat E., Lécuyer C., Sheppard S. M. F., Dromart G., Reboulet S. and Grandjean P. (2003) Thermal evolution of Cretaceous Tethyan marine waters inferred from oxygen isotope composition of fish tooth enamels. *Paleoceanography* **18**(2), 1029. doi:10.1029/2002PA000823.

Pucéat E., Reynard B. and Lécuyer C. (2004) Can crystallinity be used to determine the degree of chemical alteration of biogenic apatites? *Chem. Geol.* **205**, 83–97.

Robinson C., Briggs H. D., Atkinson P. J. and Weatherell J. A. (1979) Matrix and mineral changes in developing enamel. *J. Dent. Res.* **58**, 871–882.

Sasaki S., Takagi T. and Suzuki M. (1991) Cyclical changes in pH in bovine developing enamel as sequential bands. *Arch. Oral Biol.* **36**, 227–231.

Schuffert J. D., Kastner M., Emanuele G. and Jahnke R. A. (1990) Carbonate-ion substitution in francolite: a new equation. *Geochim. Cosmochim. Acta* **54**, 2323–2328.

Shahack-Gross R., Tchernov E. and Luz B. (1999) Oxygen isotopic composition of mammalian skeletal phosphate from the Natufian Period, Hayonim Cave, Israel: diagenesis and paleoclimate. *Geoarchaeology* **14**, 1–13.

Shemesh A. (1990) Crystallinity and diagenesis of sedimentary apatites. *Geochim. Cosmochim. Acta* **54**, 2433–2438.

Shemesh A., Kolodny Y. and Luz B. (1988) Isotope geochemistry of oxygen and carbon in phosphate and carbonate of phosphorite francolite. *Geochim. Cosmochim. Acta* **52**, 2565–2572.

Smith K. F., Sharp Z. D. and Brown J. H. (2002) Isotopic composition of carbon and oxygen in desert fauna: investigations into the effects of diet, physiology, and seasonality. *J. Arid Environ.* **52**, 419–430.

Stanton Thomas K. J. and Carlson S. J. (2004) Microscale $\delta^{18}O$ and $\delta^{13}C$ isotopic analysis of an ontogenetic series of the hadrosaurid dinosaur Edmontosaurus: implications for physiology and ecology. *Palaeogeogr. Palaeoclimatol. Palaeoecol.* **20**, 257–287.

Swart P. K. (1983) Carbon and oxygen isotope fractionation in scleractinian corals: a review. *Earth Sci. Rev.* **19**, 51–80.

Swart P. K., Burns S. J. and Leder J. J. (1991) Fractionation of the stable isotopes of oxygen and carbon in carbon dioxide during the reaction of calcite with phosphoric acid as a function of temperature and technique. *Chem. Geol.* **86**, 89–96.

Trotter J. A., Williams I. S., Barnes C. R., Lécuyer C. and Nicoll R. S. (2008) Did cooling oceans trigger Ordovician biodiversification? Evidence from conodont thermometry. *Science* **321**, 550–554.

Tütken T., Pfretzschnerb H.-U., Vennemann T. W., Sunc G. and Wang Y. D. (2004) Paleobiology and skeletochronology of Jurassic dinosaurs: implications from the histology and oxygen isotope compositions of bones. *Palaeogeogr. Palaeoclimatol. Palaeoecol.* **206**, 217–238.

Tütken T., Vennemann T. W., Janz H. and Heizmann E. P. J. (2006) Palaeoenvironment and palaeoclimate of the Middle Miocene lake in the Steinheim basin, SW Germany: a reconstruction from C, O, and Sr isotopes of fossil remains. *Palaeogeogr. Palaeoclimatol. Palaeoecol.* **241**, 457–491.

Vennemann T. W. and Hegner E. (1998) Oxygen, strontium, and neodymium isotope composition of fossil shark teeth as a proxy for the palaeoceanography and palaeoclimatology of the Miocene northern Alpine Paratethys. *Palaeogeogr. Palaeoclimatol. Palaeoecol.* **142**, 107–121.

Vennemann T. W., Hegner E., Cliff G. and Benz G. W. (2001) Isotopic composition of recent shark teeth as a proxy for environmental conditions. *Geochim. Cosmochim. Acta* **65**, 1583–1599.

Werner R. A. and Brand W. A. (2001) Referencing strategies and techniques in stable isotope ratio analysis. *Rapid Commun. Mass Spectrom.* **15**, 501–519.

Wright L. E. and Schwarcz H. P. (1998) Stable carbon and oxygen isotopes in Human tooth enamel: identifying breastfeeding and weaning in prehistory. *Am. J. Phys. Anthropol.* **106**, 1–18.

Zazzo A., Mariotti A., Lécuyer C. and Heintz E. (2002) Intra-tooth isotope variations in late Miocene bovid enamel from Afghanistan: paleobiological, taphonomical, and climatic implications. *Palaeogeogr. Palaeoclimatol. Palaeoecol.* **186**, 145–161.

Zazzo A., Lécuyer C., Sheppard S. M. F., Grandjean P. and Mariotti A. (2004) Diagenesis and the reconstruction of paleoenvironments: a method to restore original $\delta^{18}O$ values of carbonate and phosphate from fossil tooth enamel. *Geochim. Cosmochim. Acta* **68**, 2245–2258.

Zeebe R. E. (1999) An explanation of the effect of seawater carbonate concentration on foraminiferal oxygen isotopes. *Geochim. Cosmochim. Acta* **63**, 2001–2007.

Zeebe R. E. and Wolf-Gladrow D. (2001) CO_2 in seawater: equilibrium, kinetics, isotopes. In *Elsevier Oceanographic Series*, vol. 65 (ed. D. Halpern). Elsevier, Amsterdam, p. 346.

Zheng Y.-F. (1996) Oxygen isotope fractionations involving apatites: application to paleotemperature determination. *Chem. Geol.* **127**, 177–187.

Associate editor: Boaz Luz

Chemical Geology 332–333 (2012) 92–101

Contents lists available at SciVerse ScienceDirect

Chemical Geology

journal homepage: www.elsevier.com/locate/chemgeo

Carbon and oxygen isotope fractionations between aragonite and calcite of shells from modern molluscs

Christophe Lécuyer [a,*], Aurore Hutzler [b], Romain Amiot [a], Valérie Daux [c], Danièle Grosheny [d], Olga Otero [e], François Martineau [a], François Fourel [a], Vincent Balter [a], Bruno Reynard [a]

[a] Laboratoire de Géologie de Lyon, CNRS UMR 5276, Université Claude Bernard Lyon 1 et ENS Lyon, France
[b] Laboratoire CEREGE, CNRS UMR 6635, Europôle Méditerranéen de l'Arbois, Aix-en-Provence, France
[c] Laboratoire des Sciences du Climat et de l'Environnement/IPSL, UMR CEA/CNRS 1572, L'Orme des Merisiers, Bât. 701, CEA Saclay, 91191 Gif/Yvette Cedex, France
[d] Université de Strasbourg, EOST, CNRS UMR 7516, IPGS, 1 rue Blessig, 67084 Strasbourg, France
[e] Institut de Paléoprimatologie, Paléontologie humaine: Evolution et Paléoenvironnements, UMR CNRS 6046, INEE, Université de Poitiers, France

ARTICLE INFO

Article history:
Received 13 February 2012
Received in revised form 29 August 2012
Accepted 31 August 2012
Available online 18 September 2012

Editor: U. Brand

Keywords:
Aragonite
Calcite
Mollusc
Stable isotope
Isotopic fractionation

ABSTRACT

Carbon and oxygen isotope fractionations between calcite and aragonite were investigated by analyzing marine gastropods and bivalves that lived under temperate to tropical climates. Species that secrete both aragonite and calcite layers were studied to ensure similitude of changes in the isotopic composition of water, in diet, and in metabolic activity during shell growth. Aragonite and calcite layers from the adult parts of the shell were identified and mapped by using Raman spectroscopy. Powder samples were obtained by microdrilling under a stereo microscope. Thirty-six pairs of aragonite–calcite samples were obtained from ten gastropod and five bivalve species. Biogenic aragonite is ^{13}C-enriched by 0.95 ± 0.81‰ and ^{18}O-enriched by 0.37 ± 0.65‰ relative to co-existing biogenic calcite. Direction and magnitude of the carbon isotope fractionation are compatible with those already determined by using low-temperature experimental approaches. The observed oxygen isotope difference between biogenic aragonite and calcite is assigned to the difference (≈0.4‰) in the acid fractionation factor values that must be taken into account during digestion of carbonate polymorphs at 90 °C. It is concluded that biogenic calcium carbonate polymorphs precipitate close to, but not in isotopic equilibrium with seawater. Therefore, empirical oxygen isotope fractionation equations that were established on the basis of modern mollusc shells and ambient waters should be preferred for the calculation of aquatic paleotemperatures.

1. Introduction

Many aquatic invertebrates (molluscs, cephalopods, foraminifera, brachiopods) have exoskeletons made either of aragonite or calcite. This specificity results from the remarkable property of the extrapallial aqueous solution with its high Mg^{2+} content relative to Ca^{2+} (Wada and Fujinuki, 1976). It means that during shell crystallization, aragonite formation is expected because Mg^{2+} inhibits calcite precipitation (Berner, 1975; Davis et al., 2000). Takeuchi et al. (2008) have shown that Aspein, a protein occurring in the shell organic matrix of the oyster *Pinctada fucata*, is specifically involved in calcite formation within the prismatic layer. Carbon and oxygen isotope compositions of these two carbonate polymorphs constitute suitable proxies of water mass properties such as temperature, salinity and productivity. Consequently, the stable carbon and oxygen isotope compositions of fossil shells have been widely used in paleosalinity and paleotemperature reconstructions for some periods of the Phanerozoic (e.g. Krantz et al., 1987; Hendry and Kalin, 1997; Hendry et al., 2001; Malchus and Steuber, 2002; Schöne et al., 2004; Jones et al., 2005; Brigaud et al., 2008; Zakharov et al., 2011). Quantitative estimates of both temperature and carbon isotope composition of past water require a precise knowledge of the stable isotope fractionation equations for both calcium carbonate polymorphs.

To date, the issue of the direction and magnitude of carbon and oxygen isotope fractionations between aragonite and water ($\Delta^{13}C_{aragonite-water}$ and $\Delta^{18}O_{aragonite-water}$ values), and between calcite and water ($\Delta^{13}C_{calcite-water}$ and $\Delta^{18}O_{calcite-water}$ values) that would be precipitated in isotopic equilibrium remains controversial. Within the same water mass (i.e. of constant $\delta^{18}O$ value), carbon and oxygen isotope fractionations between shell-forming aragonite and calcite can be expressed as $\Delta^{13}C_{calcite-water}$ and $\Delta^{18}O_{calcite-water}$ values, respectively. Calcite was shown to be depleted in ^{18}O relative to aragonite by 0.5‰ to 0.8‰ from precipitation experiments (Tarutani et al., 1969; Kim and O'Neil, 1997; Kim et al., 2007b), semi-empirical calculations (Tarutani et al., 1969; Golyshev et al., 1981) and natural observations (e.g. Keith et al., 1964; Grossman and Ku, 1986; Barrera et al., 1994; Thorrold et al., 1997).

* Corresponding author.
E-mail address: clecuyer@univ-lyon1.fr (C. Lécuyer).

0009-2541/$ – see front matter © 2012 Elsevier B.V. All rights reserved.
http://dx.doi.org/10.1016/j.chemgeo.2012.08.034

Table 1
Stable oxygen isotope compositions and temperatures of waters where we sampled the studied modern molluscs. T of water: mean annual sea surface temperature. Seasonal T: mean seasonal temperature variation. Temperature data come from the NOAA (National Oceanographic Data Center) Data Center (Reynolds and Smith, 1995; Reynolds et al., 2002).

Location	Sampling period	cδ^{18}O of water (‰ V-SMOW)	T of water (°C)	Seasonal T (°C)	Mean water temperature of the four warmest months (°C)
Pointe Jean-Claude, Martinique	May 2002	0.55	29	±1	30±1
Tartane, Martinique	May 2002	1.2	29	±1	30±1
Saint-Pierre, Martinique	May 2002	1.1	29	±1	30±1
L'Etang Salé, Réunion	July 2002	0.4	25	±3	27±1
Antalya Bay, Turkey	September 2002	2.0	23	±4	25±2
Graclea Minoa Cap, Sicily	November 2005	1.5	19	±5	23±3
Magouëro, Brittany	July 2008	0.5	14	±5	16±2
Guidel, Brittany	January 2010	0.6	14	±5	16±2

Other studies suggest that calcite is ^{18}O-enriched with respect to aragonite from a few tenths of per mil up to 4.5‰, from field and laboratory observations (Epstein et al., 1953; Horibe and Oba, 1972), theoretical calculations based on the increment method (Zheng, 1999), and laboratory experiments (Zhou and Zheng, 2002, 2003).

Rubinson and Clayton (1969) calculated carbon isotope partition function ratios by extending Urey's (1947) and Bigeleisen and Mayer's (1947) theories, as described in studies published by O'Neil et al. (1969) and Tarutani et al. (1969). Computing outputs predicted a carbon isotope fractionation of 0.9‰ between aragonite and calcite. In conjunction with this theoretical approach, Rubinson and Clayton (1969) precipitated both phases from bicarbonate solutions by slow removal of carbon dioxide at 25 °C, and measured a mean carbon isotope fractionation factor of 1.8±0.2 (1000lnα). Turner (1982) obtained a similar equilibrium carbon isotope fractionation between aragonite and calcite of 1.4‰ by slowly precipitating both inorganic calcium carbonate polymorphs at 25 °C. According to Grossman and Ku (1986), ^{13}C-enrichment between aragonitic (*Hoeglundina elegans*) and calcitic (*Uvigerina* sp.) foraminifera increases from 1‰ to 2.5‰ with temperature decreasing from 25 °C to 0 °C. Romanek et al. (1992) measured, in the temperature range of 10 °C to 40 °C, a carbon isotope fractionation of 1.7±0.4‰ between synthetic aragonite and calcite precipitated by using an open-system chemostat technique.

No consensus can be inferred from literature data about the direction and magnitude of the oxygen isotope fractionation between calcite and aragonite, and carbon isotope fractionation is positive but of unknown amplitude. The comparison of data between the inorganic and biogenic calcium carbonate polymorphs is a difficult task because isotopic equilibrium during solid phase precipitation is not always achieved and cannot be easily demonstrated. In the natural environment, shells precipitate in waters whose temperature and isotopic compositions can vary enough to mask subtle differences in the isotopic compositions of both polymorphs that do not exceed a few tenths of per mil. Furthermore, the sampling of aragonitic and calcitic shells from molluscs living in close association does not ensure a record of the same water parameters (mean and seasonal temperatures, δ^{18}O of water) because of possible age differences and timing of shell mineralization among the studied population. They may also be biased by diet and metabolic differences between species.

In this study, the carbon and oxygen isotope compositions of aragonite and calcite layers of composite shells secreted by the same mollusc specimen were measured. Mapping of the mineral phases by Raman spectroscopy and in situ micro-drilling of the adjacent polymorphs were performed for obtaining samples that precipitated the closest possible in time. Temperature-dependent oxygen isotope fractionations between calcium carbonate polymorphs and their ambient water were explored from a dataset of molluscs living in the temperature range of 16±2 °C–30±1 °C. Finally, the data were used to discuss whether biogenic calcite and aragonite precipitated in isotopic equilibrium or not with ambient water.

2. Sampling and analytical techniques

2.1. Sampling strategy of modern mollusc shells

The seven bivalves and the twenty-nine gastropods were collected alive along with waters between years 2002 and 2008 (Table 1). Carbonate skeletons were cleaned within an ultrasonic bath to remove sedimentary matrix, then treated with H_2O_2 10% for 12 h to remove

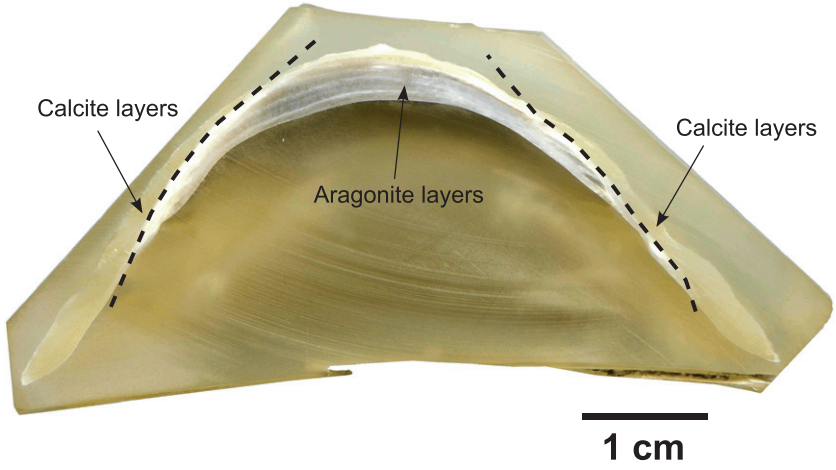

Fig. 1. Transversal section of a *Patella* shell (Guidel, Brittany, France) embedded in epoxy resin (yellow-green matrix). The outer pale pink layer is made of prismatic low-Mg calcite, the inner gray layer is made of aragonite.

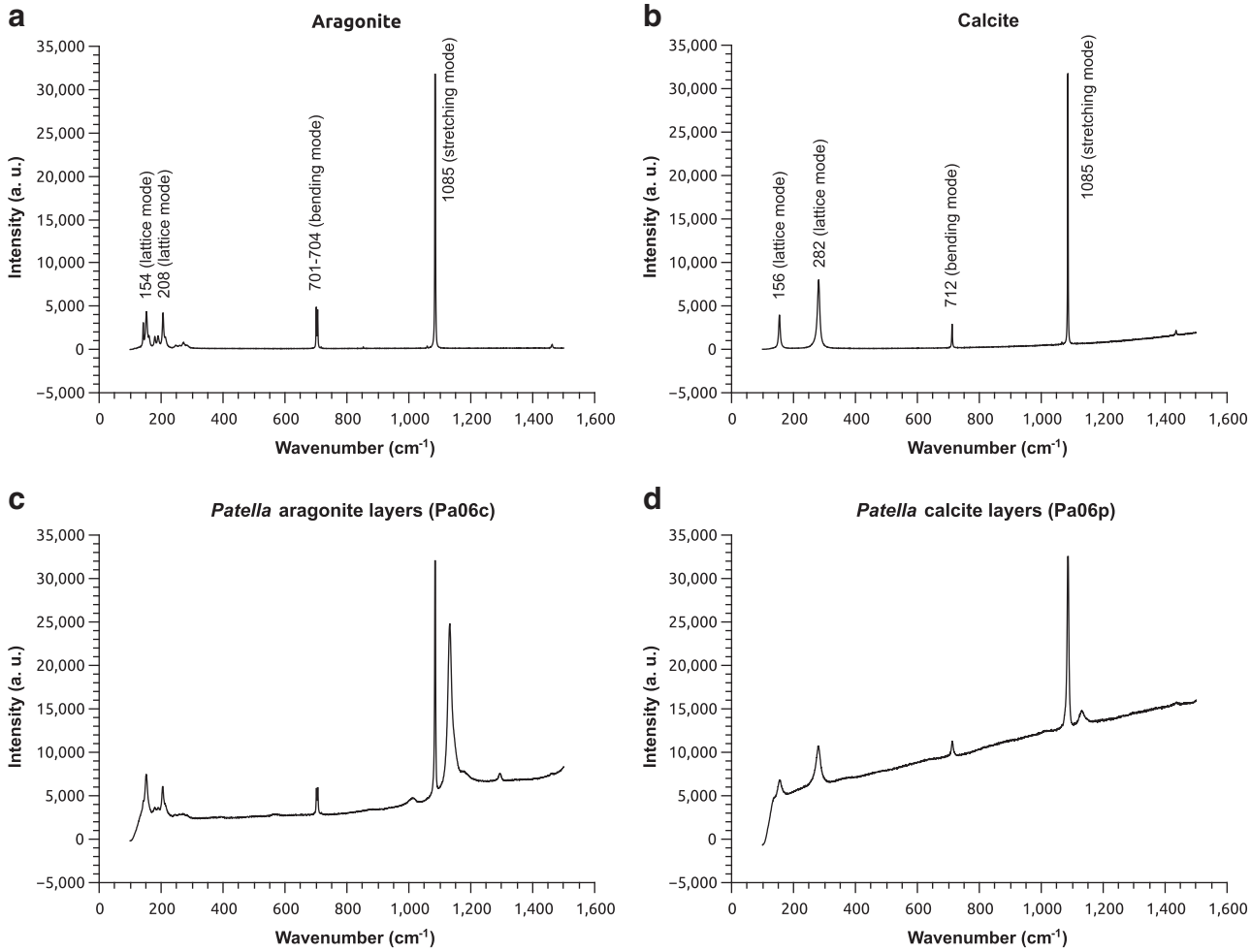

Fig. 2. Raman spectra of aragonite (c) and calcite (d) layers from a *Patella* shell (Guidel, Brittany, France) are compared to those obtained from reference materials (a and b).

organic matter. After washing with deionized water, the samples were dried at ambient temperature. Aragonite and calcite constituting the inner and outer layers of the selected bivalve and gastropod shells were identified using Raman spectroscopy. Mapped layers were then sampled under a stereo microscope and grounded into fine powder using a micro-driller. Three to five single grains of sample powders were then randomly analyzed using Raman spectroscopy in order to check for any possible contamination by adjacent layers during sampling. At least three Raman spectra were obtained on distinct spots of each grain, thus strongly reducing the probability that the grain was mineralogically heterogeneous.

2.2. Raman spectroscopy

Raman spectra were collected using a LabRam™ HR spectrometer and excitation provided by the 514.53 nm line of a Spectra-Physics™ Ar laser. Different parts of the shells were probed at the micrometer scale in backscattering geometry through an Olympus™ microscope. Laser power varied from 0.1 to 10 mW at the sample in order to prevent local heating and transformation especially for the absorbing black pigment-bearing parts of some shells. Recording times ranged from 1 to 10 min depending on laser power.

2.3. Carbon and oxygen isotope analyses of calcium carbonate

Stable isotope ratios were determined by using an auto sampler MultiPrep™ system coupled to a dual-inlet GV Isoprime™ isotope ratio mass spectrometer (IRMS). For each sample, an aliquot of about 100–200 μg of calcium carbonate was reacted with anhydrous oversaturated phosphoric acid at 90 °C for 20 min. In the first approximation, oxygen isotope ratios of both aragonite and calcite were calculated assuming an acid fractionation factor $1000\ln\alpha(CO_2\text{–}CaCO_3) = 8.1$. Differences between the acid fractionation factor values of the two calcium carbonate polymorphs are further discussed (see Section 4.1) considering determinations available in the literature. Isotopic compositions are quoted in the delta notation in ‰ relative to V-PDB. All sample measurements were triplicated and adjusted to the international reference NIST NBS19. External reproducibility is ±0.1‰ for $\delta^{18}O$ values and ±0.05 for $\delta^{13}C$ values (1σ).

2.4. Oxygen isotope analysis of water

The oxygen isotope ratios of waters surrounding the living molluscs were measured using an automated CO_2 equilibration technique developed by Horita et al. (1989). Aliquots of 400 μL of water were automatically equilibrated with CO_2 and analyzed using a MultiPrep™ system online with a GVI IsoPrime™ dual inlet IRMS. Reproducibility was typically ±0.03‰ (Table 1).

3. Results

3.1. Mineralogy of mollusc shells

All studied shells were analyzed for their mineralogy. Gastropods shells are constituted of an inner layer made entirely of aragonite whereas the outer prismatic layer is made of low-Mg calcite (Fig. 1). The two

Table 2
Stable carbon and oxygen isotope compositions of co-existing aragonite and calcite from modern molluscs. A: aragonite; C: low-Mg calcite.

Pair#	Sample code	Location	Water mass	Geographic coordinates	Class	Taxon	Mineral	$\delta^{13}C$ ‰ (PDB)	$\delta^{18}O$ ‰ (PDB)
1	Iso-J-1A*	Pointe Jean-Claude, Martinique	Central Atlantic Sea	14°36′43.74″N–60°52′40.32″O	Bivalvia	*Isognomon radiatus*	A	−0.34	−0.98
	Iso-J-1C*	Pointe Jean-Claude, Martinique	Central Atlantic Sea	14°36′43.74″N–60°52′40.32″O	Bivalvia	*Isognomon radiatus*	C	0.02	−0.81
2	Cra-J-1A*	Pointe Jean-Claude, Martinique	Central Atlantic Sea	14°36′43.74″N–60°52′40.32″O	Bivalvia	*Crassostrea virginica*	A	−2.14	−1.16
	Cra-J-1C*	Pointe Jean-Claude, Martinique	Central Atlantic Sea	14°36′43.74″N–60°52′40.32″O	Bivalvia	*Crassostrea virginica*	C	−2.42	−1.36
3	Ner-T-1A*	Tartane, Martinique	Central Atlantic Sea	14°45′30.45″N–60°55′15.10″O	Gastropoda	*Nerita tessellata*	A	2.79	−0.01
	Ner-T-1C*	Tartane, Martinique	Central Atlantic Sea	14°45′30.45″N–60°55′15.10″O	Gastropoda	*Nerita tessellata*	C	1.49	−0.03
4	Litra-St-A	Saint-Pierre, Martinique	Caribbean Sea	14°43′54.68″N–61°10′44.34″O	Gastropoda	*Litra* sp.	A	2.26	−0.69
	Litra-St-C	Saint-Pierre, Martinique	Caribbean Sea	14°43′54.68″N–61°10′44.34″O	Gastropoda	*Litra* sp.	C	1.62	−0.93
5	Ner-S-1A*	Saint-Pierre, Martinique	Caribbean Sea	14°43′54.68″N–61°10′44.34″O	Gastropoda	*Nerita tessellata*	A	2.08	−0.08
	Ner-S-1C*	Saint-Pierre, Martinique	Caribbean Sea	14°43′54.68″N–61°10′44.34″O	Gastropoda	*Nerita tessellata*	C	2.25	−0.25
6	C01i	Saint-Pierre, Martinique	Caribbean Sea	14°43′54.68″N–61°10′44.34″O	Gastropoda	*Citharium pica*	A	1.70	−2.05
	C01e	Saint-Pierre, Martinique	Caribbean Sea	14°43′54.68″N–61°10′44.34″O	Gastropoda	*Citharium pica*	C	1.48	−1.67
7	Ne02i2	Saint-Pierre, Martinique	Caribbean Sea	14°43′54.68″N–61°10′44.34″O	Gastropoda	*Nerita tessellata*	A	2.15	−1.17
	Ne02e2	Saint-Pierre, Martinique	Caribbean Sea	14°43′54.68″N–61°10′44.34″O	Gastropoda	*Nerita tessellata*	C	1.37	−2.11
8	Lima-E4-A2	L'Etang Salé, Réunion	Indian Ocean	21°15′22.09″S–55°19′22.24″E	Bivalvia	*Lima sowerbyi*	A	1.52	−1.04
	Lima-E4-C2	L'Etang Salé, Réunion	Indian Ocean	21°15′22.09″S–55°19′22.24″E	Bivalvia	*Lima sowerbyi*	C	−0.17	−1.81
9	Lima-E4-A1	L'Etang Salé, Réunion	Indian Ocean	21°15′22.09″S–55°19′22.24″E	Bivalvia	*Lima sowerbyi*	A	1.54	−0.55
	Lima-E4-C1	L'Etang Salé, Réunion	Indian Ocean	21°15′22.09″S–55°19′22.24″E	Bivalvia	*Lima sowerbyi*	C	0.24	−2.24
10	Spon-E4-A	L'Etang Salé, Réunion	Indian Ocean	21°15′22.09″S–55°19′22.24″E	Bivalvia	*Spondylus nicobaricus*	A	2.27	−0.62
	Spon-E4-C	L'Etang Salé, Réunion	Indian Ocean	21°15′22.09″S–55°19′22.24″E	Bivalvia	*Spondylus nicobaricus*	C	1.34	−1.70
11	Spon-E1-A	L'Etang Salé, Réunion	Indian Ocean	21°15′22.09″S–55°19′22.24″E	Bivalvia	*Spondylus nicobaricus*	A	1.66	0.70
	Spon-E1-C	L'Etang Salé, Réunion	Indian Ocean	21°15′22.09″S–55°19′22.24″E	Bivalvia	*Spondylus nicobaricus*	C	0.52	−0.88
12	NerB-E3-A	L'Etang Salé, Réunion	Indian Ocean	21°15′22.09″S–55°19′22.24″E	Gastropoda	*Nerita bisecta*	A	3.50	−0.33
	NerB-E3-C	L'Etang Salé, Réunion	Indian Ocean	21°15′22.09″S–55°19′22.24″E	Gastropoda	*Nerita bisecta*	C	1.84	−0.95
13	NerP-E3-A1	L'Etang Salé, Réunion	Indian Ocean	21°15′22.09″S–55°19′22.24″E	Gastropoda	*Nerita punctata*	A	3.43	−0.88
	NerP-E3-C1	L'Etang Salé, Réunion	Indian Ocean	21°15′22.09″S–55°19′22.24″E	Gastropoda	*Nerita punctata*	C	2.38	−0.80
14	NerP-E3-A2	L'Etang Salé, Réunion	Indian Ocean	21°15′22.09″S–55°19′22.24″E	Gastropoda	*Nerita punctata*	A	4.60	−0.49
	NerP-E3-C2	L'Etang Salé, Réunion	Indian Ocean	21°15′22.09″S–55°19′22.24″E	Gastropoda	*Nerita punctata*	C	2.23	−0.93
15	Pte-S2-A	Saint-Leu, Réunion	Indian Ocean	21°09′59.04″S–55°17′12.84″E	Bivalvia	*Pteria loweni*	A	2.88	−0.31
	Pte-S2-C	Saint-Leu, Réunion	Indian Ocean	21°09′59.04″S–55°17′12.84″E	Bivalvia	*Pteria loweni*	C	0.82	−0.95
16	NerAl-S2-A	Saint-Leu, Réunion	Indian Ocean	21°09′59.04″S–55°17′12.84″E	Gastropoda	*Nerita* cf. *albicilla*	A	1.97	−1.13
	NerAl-S2-C	Saint-Leu, Réunion	Indian Ocean	21°09′59.04″S–55°17′12.84″E	Gastropoda	*Nerita* cf. *albicilla*	C	0.44	−0.79
17	NerP-S3-A1	Saint-Leu, Réunion	Indian Ocean	21°09′59.04″S–55°17′12.84″E	Gastropoda	*Nerita punctata*	A	4.18	−0.33
	NerP-S3-C1	Saint-Leu, Réunion	Indian Ocean	21°09′59.04″S–55°17′12.84″E	Gastropoda	*Nerita punctata*	C	1.91	−1.51
18	NerB-S3-A1	Saint-Leu, Réunion	Indian Ocean	21°09′59.04″S–55°17′12.84″E	Gastropoda	*Nerita bisecta*	A	1.66	−0.23
	NerB-S3-C1	Saint-Leu, Réunion	Indian Ocean	21°09′59.04″S–55°17′12.84″E	Gastropoda	*Nerita bisecta*	C	1.01	−0.35
19	NerB-S3-A2	Saint-Leu, Réunion	Indian Ocean	21°09′59.04″S–55°17′12.84″E	Gastropoda	*Nerita bisecta*	A	2.89	−0.25
	NerB-S3-C2	Saint-Leu, Réunion	Indian Ocean	21°09′59.04″S–55°17′12.84″E	Gastropoda	*Nerita bisecta*	C	0.65	−0.91
20	NerP-S3-A2	Saint-Leu, Réunion	Indian Ocean	21°09′59.04″S–55°17′12.84″E	Gastropoda	*Nerita punctata*	A	3.53	−0.55
	NerP-S3-C2	Saint-Leu, Réunion	Indian Ocean	21°09′59.04″S–55°17′12.84″E	Gastropoda	*Nerita punctata*	C	1.96	−0.90
21	NerC-G1-A1	Grande-Anse, Réunion	Indian Ocean	21°22′18.57″S–55°32′49.21″E	Gastropoda	*Nerita chaeleon*	A	2.95	−0.53
	NerC-G1-C1	Grande-Anse, Réunion	Indian Ocean	21°22′18.57″S–55°32′49.21″E	Gastropoda	*Nerita chaeleon*	C	1.06	−0.95
22	NerC-G1-A2	Grande-Anse, Réunion	Indian Ocean	21°22′18.57″S–55°32′49.21″E	Gastropoda	*Nerita chamaeleon*	A	1.68	−0.69
	NerC-G1-C2	Grande-Anse, Réunion	Indian Ocean	21°22′18.57″S–55°32′49.21″E	Gastropoda	*Nerita chamaeleon*	C	0.28	−1.25
23	PatR-Tur-A	Antalya Bay, Turkey	Eastern Mediterranean Sea	36°35′07.12″N–30°35′03.10″E	Gastropoda	*Patella rustica*	A	1.05	1.31
	PatR-Tur-C	Antalya Bay, Turkey	Eastern Mediterranean Sea	36°35′07.12″N–30°35′03.10″E	Gastropoda	*Patella rustica*	C	0.83	0.91
24	PatR-Gr-A	Graclea Minoa Cap, Sicily	Western Mediterranean Sea	37°23′25.14″N–13°16′45.59″E	Gastropoda	*Patella rustica*	A	0.75	0.97
	PatR-Gr-C	Graclea Minoa Cap, Sicily	Western Mediterranean Sea	37°23′25.14″N–13°16′45.59″E	Gastropoda	*Patella rustica*	C	−0.77	0.30
25	PatV-M-A1	Magouëro, Brittany	North Atlantic Ocean	47°39′46.07″N–03°15′06.03″E	Gastropoda	*Patella vulgata*	A	−1.70	0.97
	PatV-M-C1	Magouëro, Brittany	North Atlantic Ocean	47°39′46.07″N–03°15′06.03″E	Gastropoda	*Patella vulgata*	C	−1.29	0.92
26	PatV-M-A2	Magouëro, Brittany	North Atlantic Ocean	47°39′46.07″N–03°15′06.03″E	Gastropoda	*Patella vulgata*	A	−0.28	0.93
	PatV-M-C2	Magouëro, Brittany	North Atlantic Ocean	47°39′46.07″N–03°15′06.03″E	Gastropoda	*Patella vulgata*	C	−1.24	0.77
27	Pa04c	Guidel, Brittany	North Atlantic Ocean	47°45′50.43″N–03°31′35.56″O	Gastropoda	*Patella vulgata*	A	1.23	0.09
	Pa04p	Guidel, Brittany	North Atlantic Ocean	47°45′50.43″N–03°31′35.56″O	Gastropoda	*Patella vulgata*	C	0.53	0.66
28	Pa02C	Guidel, Brittany	North Atlantic Ocean	47°45′50.43″N–03°31′35.56″O	Gastropoda	*Patella vulgata*	A	−0.21	0.08
	Pa02p	Guidel, Brittany	North Atlantic Ocean	47°45′50.43″N–03°31′35.56″O	Gastropoda	*Patella vulgata*	C	0.02	0.72
29	Pa06C	Guidel, Brittany	North Atlantic Ocean	47°45′50.43″N–03°31′35.56″O	Gastropoda	*Patella vulgata*	A	−0.50	1.14
	Pa06P	Guidel, Brittany	North Atlantic Ocean	47°45′50.43″N–03°31′35.56″O	Gastropoda	*Patella vulgata*	C	0.06	0.47
30	Pa08C	Guidel, Brittany	North Atlantic Ocean	47°45′50.43″N–03°31′35.56″O	Gastropoda	*Patella vulgata*	A	0.56	0.56
	Pa08P	Guidel, Brittany	North Atlantic Ocean	47°45′50.43″N–03°31′35.56″O	Gastropoda	*Patella vulgata*	C	0.62	0.96
31	Pa09C	Guidel, Brittany	North Atlantic Ocean	47°45′50.43″N–03°31′35.56″O	Gastropoda	*Patella vulgata*	A	0.67	1.35
	Pa09P	Guidel, Brittany	North Atlantic Ocean	47°45′50.43″N–03°31′35.56″O	Gastropoda	*Patella vulgata*	C	−0.70	1.15
32	Pa11C	Guidel, Brittany	North Atlantic Ocean	47°45′50.43″N–03°31′35.56″O	Gastropoda	*Patella vulgata*	A	0.30	0.99
	Pa11P	Guidel, Brittany	North Atlantic Ocean	47°45′50.43″N–03°31′35.56″O	Gastropoda	*Patella vulgata*	C	−0.43	0.94

Table 2 (*continued*)

Pair#	Sample code	Location	Water mass	Geographic coordinates	Class	Taxon	Mineral	$\delta^{13}C$ ‰ (PDB)	$\delta^{18}O$ ‰ (PDB)
33	Pa12C	Guidel, Brittany	North Atlantic Ocean	47°45′50.43″N–03°31′35.56″O	Gastropoda	*Patella vulgata*	A	0.60	1.62
	Pa12P	Guidel, Brittany	North Atlantic Ocean	47°45′50.43″N–03°31′35.56″O	Gastropoda	*Patella vulgata*	C	−0.63	0.77
34	Pa13C	Guidel, Brittany	North Atlantic Ocean	47°45′50.43″N–03°31′35.56″O	Gastropoda	*Patella vulgata*	A	−0.80	0.25
	Pa13P	Guidel, Brittany	North Atlantic Ocean	47°45′50.43″N–03°31′35.56″O	Gastropoda	*Patella vulgata*	C	−1.17	0.99
35	Pa18C	Guidel, Brittany	North Atlantic Ocean	47°45′50.43″N–03°31′35.56″O	Gastropoda	*Patella vulgata*	A	−1.39	0.96
	Pa18P	Guidel, Brittany	North Atlantic Ocean	47°45′50.43″N–03°31′35.56″O	Gastropoda	*Patella vulgata*	C	−1.70	1.25
36	Pa22C	Guidel, Brittany	North Atlantic Ocean	47°45′50.43″N–03°31′35.56″O	Gastropoda	*Patella vulgata*	A	0.08	2.27
	Pa22P	Guidel, Brittany	North Atlantic Ocean	47°45′50.43″N–03°31′35.56″O	Gastropoda	*Patella vulgata*	C	−1.54	0.16

polymorphs of $CaCO_3$ are readily identified from the low frequency part of the spectra (Fig. 2), and especially from the position and splitting of the symmetric bending mode, which occurs as a single peak at 712 cm^{-1} in calcite and as a doublet at 701–704 cm^{-1} in aragonite (e.g. Urmos et al., 1991; Gillet et al., 1993). High-Mg calcites can also be distinguished from low-Mg calcite from the much higher linewidths of their low frequency modes due to positional disorder enhanced by cationic substitution (Bischoff et al., 1985).

3.2. Oxygen isotope compositions and temperature of ambient waters

Mean water temperatures vary from 14 °C (Brittany, France) to 29 °C (Martinique, France) with the magnitude of seasonal variations increasing with latitude (Table 1) according to data retrieved from the NOAA (National Oceanographic Data Center) Data Center (Reynolds and Smith, 1995; Reynolds et al., 2002). Oxygen isotope compositions of sampled marine waters are ^{18}O-enriched relative to V-SMOW (Table 1). The mangrove water of Martinique Island, the open marine water of Réunion Island and the coastal marine waters of Brittany, France, have $\delta^{18}O$ values close to 0.5‰. The open marine waters of Martinique Island are slightly higher than 1‰ whereas the highest $\delta^{18}O$ values were obtained for the Mediterranean waters in Sicily (1.5‰) and in the bay of Antalya, Turkey (2.0‰).

3.3. Carbon and oxygen isotope compositions of aragonite–calcite pairs

3.3.1. Carbon and oxygen isotope differences between aragonite and calcite

Stable carbon and oxygen isotope ratios were measured in thirty-six pairs of aragonite (inner layer) and calcite (prismatic outer layer) obtained from shells of ten gastropod and five bivalve species (Table 2). The dataset reveals that biogenic aragonite is ^{13}C-enriched by 0.95 ± 0.81‰ and ^{18}O-enriched by $+0.37 \pm 0.65$‰ relative to co-existing biogenic calcite (Table 2). According to Shapiro–Wilk test, the $\Delta^{13}C_{aragonite-calcite}$ and $\Delta^{18}O_{aragonite-calcite}$ values (i.e. isotopic differences between the paired polymorphs) of gastropods and bivalves are normally distributed (for an alpha level of 0.1) and their mean values of 0.94 ± 0.82 and 1.00 ± 0.82‰, respectively, are comparable (Fig. 3a). Within the class of gastropods, however, the inter-species or inter-genus differences are significant. For instance, the mean $\Delta^{13}C_{aragonite-calcite}$ values of *Patella* and *Nerita*, are 0.55 ± 0.72 and 1.43 ± 0.72, respectively (Fig. 3b).

In the case of oxygen isotope ratios (Fig. 4a), the $\Delta^{18}O_{aragonite-calcite}$ values of studied bivalves are higher (0.83 ± 0.68) than those of analyzed gastropods (0.26 ± 0.60). Moreover, within the class of gastropods (Fig. 4b), *Nerita* has $\Delta^{18}O_{aragonite-calcite}$ values of 0.39 ± 0.42 themselves higher than those of *Patella* (0.18 ± 0.75).

Studied molluscs were sampled from locations spanning from tropical (Réunion and Martinique Islands) to marine warm temperate (Brittany peninsula, France) climatic belts. Neither carbon nor oxygen isotope differences between aragonite and calcite correlate with mean annual water temperature ($R^2 = 0.005$; p = not significant).

3.3.2. Oxygen isotope fractionation between mollusc shell and water

The dataset of this study was used for calculating the temperature--dependent oxygen isotope fractionation between the aragonite inner layer of mollusc shell and water (Fig. 5a). The results were compared to those already determined for aragonite-secreting molluscs (Grossman and Ku, 1986) and for synthetic aragonite (Kim et al., 2007b). For water temperatures higher than 23 °C, calculated isotopic fractionations match those obtained by computing the equation proposed by Grossman and Ku (1986) and are about 1‰ higher than those predicted by the equation experimentally-determined by Kim et al. (2007b). Below 23 °C, oxygen isotope fractionations are shifted towards lower values relative to the fractionation equation line of Grossman and Ku (1986). The five calculated fractionation values (corresponding to the five mean water temperatures reported in Table 1) show an apparent robust linear dependence to water temperature ($R^2 = 0.93$; n = 5; p = 0.02) but a lower slope (or 'temperature coefficient') value (-7.1 ± 1.1) than those close to −4 determined for biogenic aragonite (Grossman and Ku, 1986; Patterson et al., 1993; Thorrold et al., 1997; Radtke et al. 1998; White et al., 1999; Böhm et al., 2000; Lécuyer et al., 2004). It is also noteworthy that these observed fractionation values are up to 2.7‰ higher than those calculated with the equation determined by Zhou and Zheng (2003) for synthetic aragonite.

In the case of the calcite outer layer of the mollusc shells (Fig. 5B), oxygen isotope fractionation values deduced from this study are strongly correlated ($R^2 = 0.87$; N = 5; p = 0.05) to the water temperature and the slope (°C/‰ δ) of the fitting line is much lower (-6.5 ± 1.4) than those known for any divalent carbonate (O'Neil et al., 1969). For water temperature higher than 23 °C, these isotopic fractionations are higher than those expected from equations obtained for biogenic calcite (Anderson and Arthur, 1983) or slowly precipitated inorganic calcite (Kim and O'Neil, 1997). Below this threshold temperature value, fractionation values lie between the two equations determined by Anderson and Arthur (1983) and Kim and O'Neil (1997).

4. Discussion

4.1. Carbon and oxygen isotope fractionations between calcite and aragonite

The determination of the acid fractionation factors ($1000\ln\alpha_{CO_2-CaCO3}$) for aragonite and calcite has been refined by Kim and O'Neil (1997) and Kim et al. (2007a) since the first attempt made by Sharma and Clayton (1965). Mean differences between the $\delta^{18}O$ values of aragonite and calcite layers from a mollusc shell can be accounted for by a difference close to 0.4‰ in acid fractionation factors between the two polymorphs digested at 90 °C (Kim et al., 2007a). After correction of the acid fractionation factor, the mean $\Delta^{18}O_{aragonite-calcite}$ value of 0.37 ± 0.65 is reduced to -0.03 ± 0.65. A two-tailed Student's t-test reveals that there is a probability of 77% to have equal means (H_0) for the oxygen isotope compositions of aragonite and calcite (t = −0.3; CI from −0.25 to 0.19; n = 36; α = 0.05). Moreover, a two-tailed Welch's t-test rejects the null hypothesis that the $\Delta^{18}O_{aragonite-calcite}$ value of our population is equal to the admitted

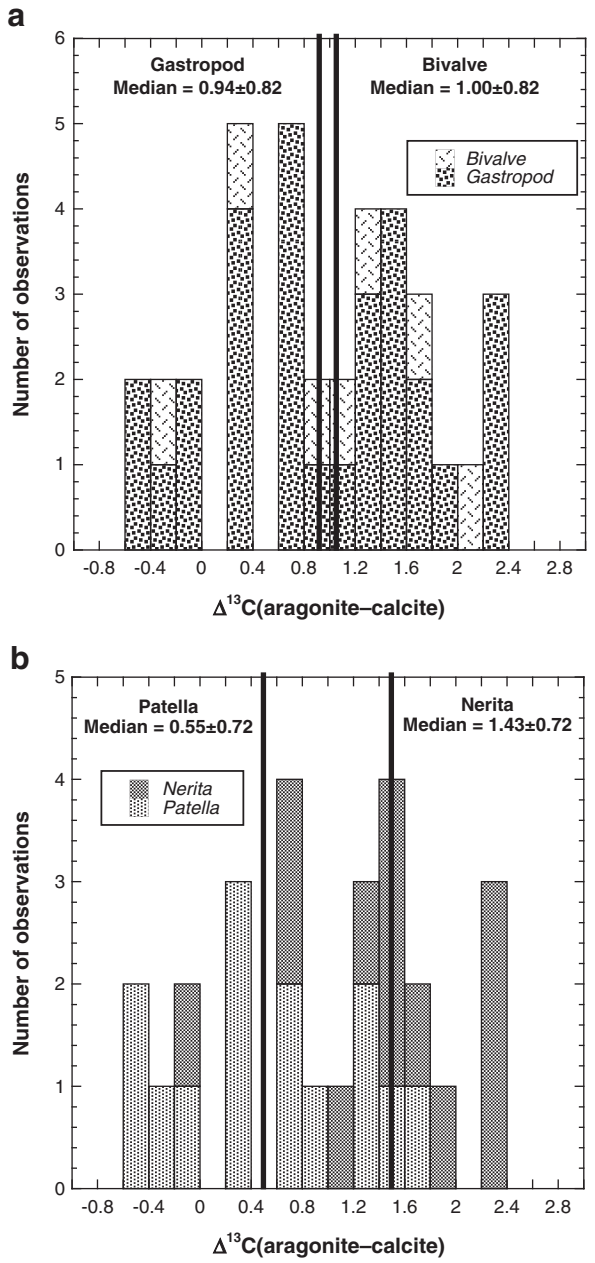

Fig. 3. Frequency histograms comparing the distribution of $\Delta^{13}C_{aragonite-calcite}$ values between gastropod and bivalve shells (a), and between *Patella* and *Nerita* gastropods (b).

theoretical fractionation value close to 0.7‰ ($t=-6.74$, CI from −0.95 to −0.51, $p=8.17\times10^{-8}$; $n=36$). Thus no sizable oxygen isotope fractionation is observed between co-existing aragonite and calcite layers secreted by the studied specimens of molluscs. This result confirms previous observations made on biogenic aragonite and calcite (e.g. Epstein et al., 1953; Keith et al., 1964) and is clearly at variance with conclusions inferred from most experimental (Tarutani et al., 1969; Kim and O'Neil, 1997; Kim et al., 2007b) and theoretical approaches (Tarutani et al., 1969; Golyshev et al., 1981).

The mean $\Delta^{13}C_{aragonite-calcite}$ value of 0.95 ± 0.81‰ is statistically different from zero according to a paired two-sample and two-tailed t-test ($t=7.04$, CI from 0.67 to 1.22, $p=3.35\times10^{-8}$; $n=36$). This value also needs to be compared with the lowest (0.9) and highest (1.8) fractionation values inferred respectively from the theoretical and experimental approaches performed by Rubinson and Clayton (1969). In the first case, the t-test indicates a high probability ($t=0.37$, CI from −0.22 to 0.32, $p=0.71$; $n=36$) for equal means (H_0) while in the second case it becomes small enough ($t=-6.29$, CI from −1.12 to −0.58, $p=3.22\times10^{-7}$; $n=36$) to suggest rejection of the null hypothesis. The isotopic data from the studied molluscs suggest that the ^{13}C-enrichment of aragonite relative to calcite does not exceed 1‰.

It cannot be excluded that sizable biases could result from the sampling of the aragonitic and calcitic layers of extant mollusc shells. There is some uncertainty regarding the synchronism of sampled parts of the shell; water temperatures and oxygen isotope composition could have been consequently different within a given aragonite–calcite pair. Diachronism could partly explain the large standard deviations

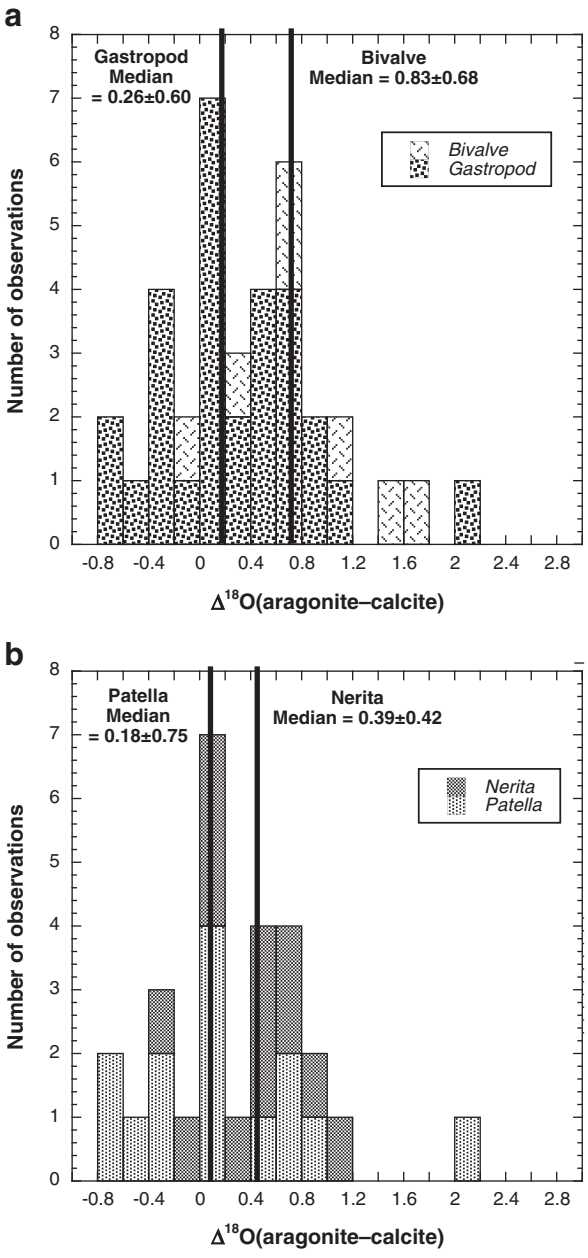

Fig. 4. Frequency histograms comparing the distribution of $\Delta^{18}O_{aragonite-calcite}$ values between gastropod and bivalve shells (a), and between *Patella* and *Nerita* gastropods (b).

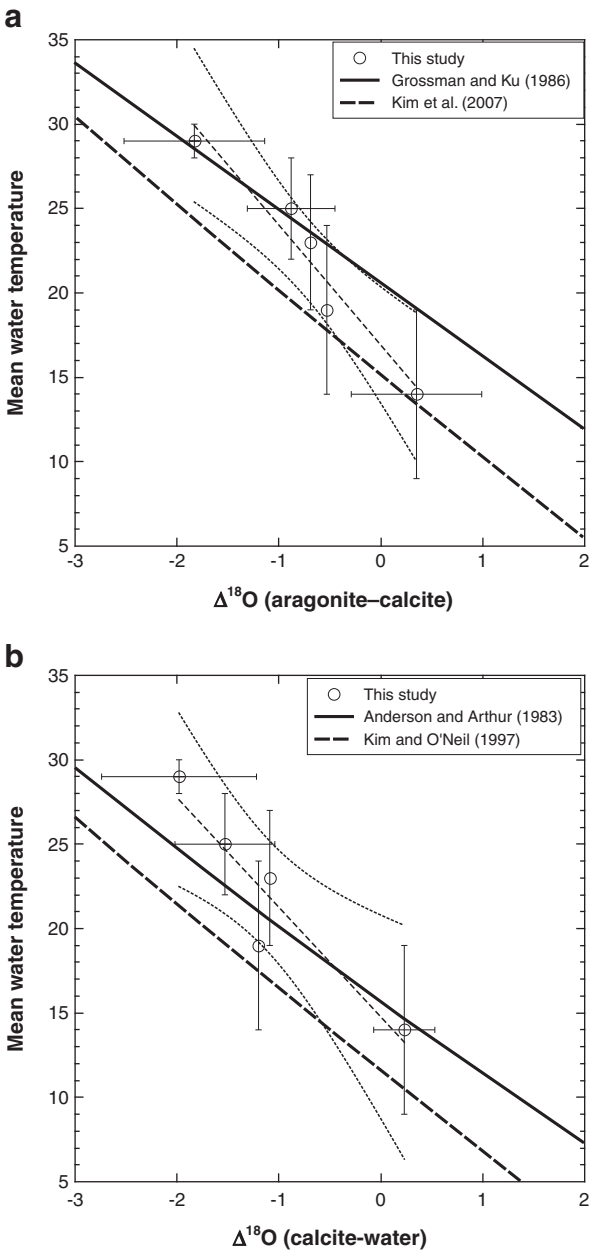

Fig. 5. Oxygen isotope fractionation ($\Delta^{18}O_{mineral-water}$) between aragonite–water (A) and calcite–water (B) as a function of the mean annual sea surface temperature. Data from the studied molluscs (8 locations but only 5 distinct temperatures, see Table 1) are compared to the isotopic fractionation equations published in the literature. (a): Plain bold line: mollusc data from Grossman and Ku (1986); dashed line: experimental data from inorganic aragonite (Kim et al., 2007b). (b): Plain bold line: mollusc data from Anderson and Arthur (1983); dashed line: experimental data from inorganic calcite (Kim and O'Neil, 1997). Errors bars on the y-axis represent the maximum seasonal variation of sea surface temperatures. Error bars on the x-axis represent the standard deviations (1σ) associated with the isotopic fractionation values. The linear regressions (dashed lines) are drawn along with associated bootstrapped 95% confidence interval belts (dotted lines). A: $t=-7.11$ (±1.08) $\Delta+16.91$ (±1.08); $R^2=0.93$. B: $t=-6.49$ (±1.42)$\Delta+14.76$ (±1.90); $R^2=0.87$.

associated with the $\Delta^{13}C_{aragonite-calcite}$ and $\Delta^{18}O_{aragonite-calcite}$ values (Table 2; Figs. 3 and 4).

Even though calcite from the studied shells is low-Mg calcite (i.e. <5 mol% $MgCO_3$), Mg^{2+} content is about one order higher in magnitude in the calcite shell than in the aragonite (Turekian and Armstrong, 1960; Amiel et al., 1973; Weber, 1973; Rosenthal and Katz, 1989; Bates and Brand, 1991). There is a sizable effect of the Mg content on the oxygen

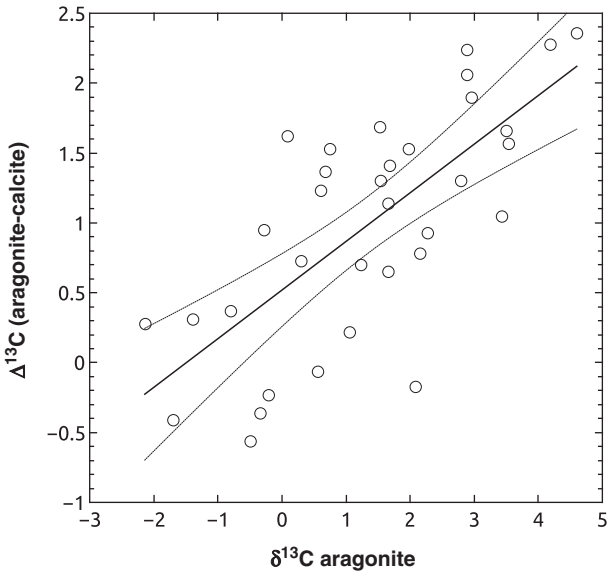

Fig. 6. Carbon isotope fractionation ($\Delta^{13}O_{aragonite-calcite}$) between aragonite and calcite as a function of the $\delta^{13}C$ value of aragonite for all the studied molluscs. The linear regression (plain line) is drawn along with associated bootstrapped 95% confidence interval belts (dotted lines). $\Delta^{13}C=0.35$ (±0.06) $\delta^{13}C+0.52$ (±0.13); $R^2=0.51$.

isotope fractionation between calcite and water (Tarutani et al., 1969; Jiménez-López et al., 2004; Brand et al., 2012) that was estimated to increase at a rate of 0.06 to 0.17 per mol% of $MgCO_3$ (Jiménez-López et al., 2004; Brand et al., 2012). Calcite of studied bivalves and gastropods contains no more than 2.5 mol% of $MgCO_3$ as estimated from literature data and Raman spectroscopy, which means that an additional uncertainty of about 0.3‰ may scramble the present estimation of the oxygen isotope fractionation between aragonite and calcite from molluscs.

Isotopic disequilibrium of small amplitude could take place during carbonate precipitation from the extrapallial fluid. This hypothesis is partly supported by the mean $\Delta^{13}C_{aragonite-calcite}$ and $\Delta^{18}O_{aragonite-calcite}$ values of studied mollusc shells that are lower than those observed during experiments or predicted by theoretical calculations (see aforementioned references). Moreover, $\Delta_{13}C_{aragonite-calcite}$ fractionation values are partly driven by the $\delta^{13}C$ value of aragonite as emphasized in Fig. 6 by the significant positive correlation between the two variables ($R^2=0.51$; $n=36$; $p=2.10^{-6}$).

Turner (1982) has experimentally demonstrated that the ^{13}C-enrichment of the calcium carbonate phase decreases with increasing precipitation rate. Owen et al. (2002) measured low $\delta^{13}C$ and $\delta^{18}O$ values of scallop calcite, compared with expected isotopic equilibrium, at shell growth exceeding 0.13 mm per day. Experiments performed by Kim and O'Neil (1997) reveal that out of equilibrium precipitation of calcite is responsible for higher calcite–water oxygen isotope fractionation values than those corresponding to equilibrium processes; these non-equilibrium calcite fractionation values mimic those known at equilibrium for the aragonite–water system. In the case of the $^{18}O/^{16}O$ ratios of carbonates, temperature dependence of both aragonite–water and calcite–water systems must be examined in order to test whether shell precipitation operates close or out of isotopic equilibrium.

4.2. Temperature-dependent oxygen isotope fractionation between mollusc shell and water

Shell growth rate depends on water temperature and varies among species (e.g. Storr et al., 1982). Adult parts of marine mollusc shells that slowly grew in water of nearly constant temperature have oxygen isotope

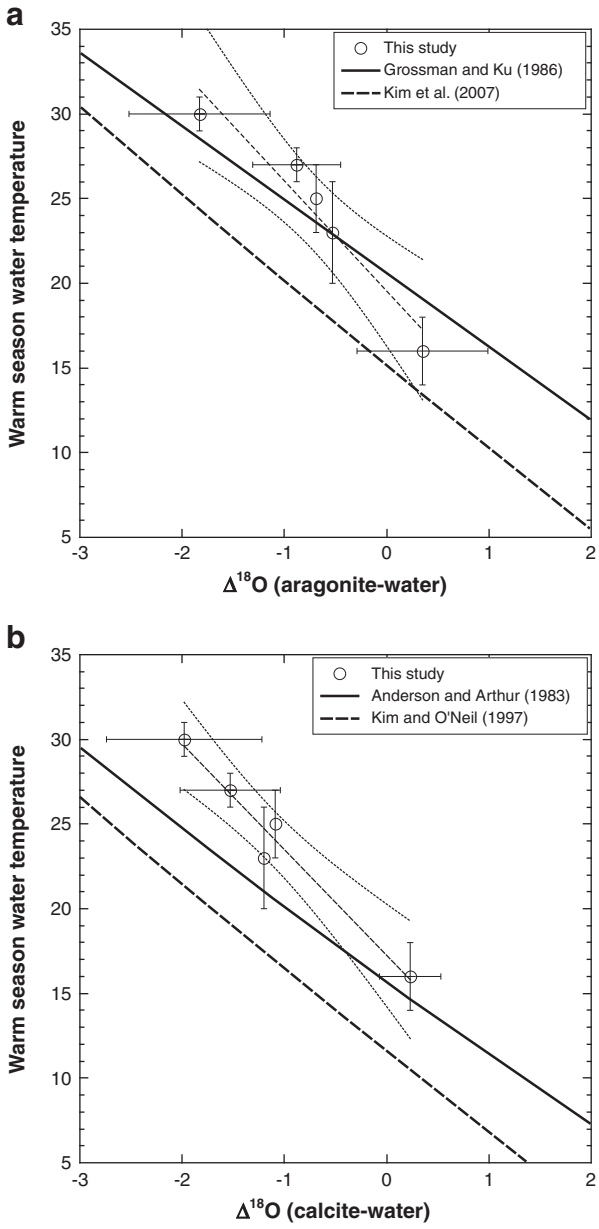

Fig. 7. Oxygen isotope fractionation ($\Delta^{18}O_{mineral-water}$) between aragonite–water (A) and calcite–water (B) as a function of the mean sea surface temperature of the fourth warmest months. Data from the studied molluscs are compared to isotopic fractionation equations published in the literature. (a): Plain bold line: mollusc data from Grossman and Ku (1986); dashed line: experimental data from inorganic aragonite (Kim et al., 2007b). (b): Plain bold line: mollusc data from Anderson and Arthur (1983); dashed line: experimental data from inorganic calcite (Kim and O'Neil, 1997). Errors bars on the y-axis represent the maximum variation in the sea surface temperature of the fourth warmest months. Error bars on the x-axis represent the standard deviations (1σ) associated with the isotopic fractionation values. The linear regressions (dashed lines) are drawn along with associated bootstrapped 95% confidence interval belts (dotted lines). A: $t = -6.50\ (\pm 1.02)\Delta + 19.54\ (\pm 1.02)$; $R^2 = 0.93$. B: $t = -6.24\ (\pm 0.71)\Delta + 17.25\ (\pm 0.95)$; $R^2 = 0.96$.

compositions strongly correlated with both temperature and $\delta^{18}O$ values of waters (e.g. Grossman and Ku, 1986; Owen et al., 2002; Kobashi and Grossman, 2003; Lécuyer et al., 2004). As can be observed in Fig. 5, $\Delta^{18}O_{aragonite-water}$ and $\Delta^{18}O_{calcite-water}$ are significantly correlated with water temperature, and Δ values match those measured by Grossman and Ku (1986) for samples that grew in water temperatures higher than or equal to 23 °C along with small seasonal variations (Fig. 5; Table 1). Here, there is no evidence for isotopic disequilibrium but the $\delta^{18}O$ values of biogenic aragonite and calcite sampled in temperate marine waters most likely record the warm seasons favorable to growth and reproduction instead of the mean annual temperatures. Better or similar correlations are indeed obtained between the Δ values and, for example, the mean temperature of the fourth warmest seasons (Fig. 7) even though expected values for the slope (≈−4 °C/‰ δ) are far from being reached (aragonite: slope = −6.5 ± 1.0 and $R^2 = 0.93$; calcite: slope = −6.2 ± 0.7 and $R^2 = 0.96$) despite high coefficients of determination for the two linear fits. Shell growth rate is species-dependent and related to several parameters such as water temperature and salinity, depth, turbidity, chemical composition of the sediment, food availability, predator activity, and period of reproduction (e.g. Borrero and Hilbish, 1988; Witbaard et al., 1999; Majoran et al., 2000; Schöne et al., 2005; Wanamaker et al., 2007). This complex multi-parameter relationship with shell growth rate is out of the scope of this study. Nevertheless, it emphasizes the challenge for determining temperature-dependent oxygen isotope fractionation between biogenic carbonate and water by using natural samples living in climatic belts characterized by high seasonality.

Tarutani et al. (1969) concluded, on the basis of available data obtained so far, that "in any case the differences in isotopic fractionation between inorganic and biogenic carbonates are very small, lending strong support to the interpretation that both sets of data represent a close approach to isotopic equilibrium between carbonate and water". However, as emphasized by Tremaine et al. (2011), equilibrium isotope fractionation factors between carbonate and water are not precisely known. In the framework of this study, it must be noted that even for aragonite and calcite that grew in warm waters (T ≥ 23 °C) under climate with weak seasonal variations (Equatorial, Tropical, Eastern Mediterranean), fractionation factors slightly differ from those inferred from inorganic carbonates slowly precipitated in dilute aqueous solutions (Kim and O'Neil, 1997; Kim et al., 2007b). Indeed, above the threshold temperature value close to 23 °C, $\Delta^{18}O_{aragonite-water}$ and $\Delta^{18}O_{calcite-water}$ values are about 1‰ higher than those determined by Kim et al. (2007b) and Kim and O'Neil (1997), respectively. The equation determined by Zhou and Zheng (2003) predicts aragonite–water fractionation values that are in full disagreement with those derived from natural samples, inorganic precipitates or theoretical calculations. It is noteworthy that the isotopic offset may reach 3.5‰, which corresponds to an unrealistic temperature difference close to 15 °C.

As discussed above, there is no statistical difference between the oxygen isotope compositions of aragonite and calcite layers formed by the studied molluscs. Moreover, significant isotopic offsets close to 1‰, which means an error of 4 °C in the temperature estimate, are identified between the $\Delta^{18}O_{aragonite-calcite}$ values for molluscs and those inferred from laboratory experiments. These combined results suggest that the oxygen isotope compositions of both biogenic calcium carbonate polymorphs precipitate close to but not in oxygen isotope equilibrium with the extrapallial fluid, itself known to have $\delta^{18}O$ values similar to those of ambient marine waters (Lécuyer et al., 2004). It is therefore emphasized that empirical oxygen isotope fractionation equations that were established on the basis of modern mollusc shells and ambient waters should be preferred for the calculation of aquatic paleotemperatures based on the $\delta^{18}O$ values of fossil molluscs.

5. Concluding remarks

Carbon and oxygen isotope fractionations between calcite and aragonite were investigated by analyzing shells of worldwide marine gastropods and bivalves that contain both carbonate polymorphs occurring as distinct layers. The most striking results are the following:

- Oxygen isotope compositions of shell calcium carbonate do not reflect the mean annual temperature of seawater, but rather most

likely that of the warm season. Only the $\delta^{18}O$ values of tropical and equatorial mollusc species constitute good proxies of the mean water temperature.

- Biogenic aragonite is ^{13}C-enriched by $0.95 \pm 0.81‰$ relative to co-existing biogenic calcite. Direction and magnitude of the carbon isotope fractionation are compatible with those already determined by using low-temperature experimental approaches. However, a lower magnitude in the isotopic fractionation as well as an associated higher standard deviation are observed in comparison to the expected values known for mechanism of precipitation at isotopic equilibrium.
- Biogenic aragonite is ^{18}O-enriched by $0.37 \pm 0.65‰$ relative to co-existing biogenic calcite. Most of the observed difference between the oxygen isotope compositions of biogenic aragonite and calcite is assigned to the difference ($\approx 0.4‰$) in the acid fractionation factors during the acid digestion of both polymorphs at 90 °C.
- Our results support a precipitation of both aragonite and calcite close to, but not in oxygen isotope equilibrium with the extrapallial fluid secreted by the mantle in the mollusc. Instead of experimentally or theoretically-determined isotope fractionation equations, those determined with data from modern molluscs should be privileged for estimating more accurately marine paleotemperatures deduced from the oxygen isotope compositions of fossil mollusc shells.

Acknowledgments

This study was funded by IUF granted to CL.

References

Amiel, A., Friedman, G.M., Miller, D.S., 1973. Distribution and nature of incorporation of trace elements in aragonite corals. Sedimentology 20, 47–64.

Anderson, T.F., Arthur, M.A., 1983. Stable isotopes of oxygen and carbon and their application to sedimentologic and paleoenvironmental problems. In: Arthur, M.A., Anderson, T.F., Kaplan, I.R., Veizer, J., Land, L.S. (Eds.), Stable Isotopes in Sedimentary Geology: SEPM Short Course, No.10, pp. 1–151.

Barrera, E., Tevesz, M.J.S., Carter, J.G., McCall, P.L., 1994. Oxygen and carbon isotopic composition and shell microstructure of the bivalve *Latermula elliptica* from Antarctica. Palaios 9, 275–287.

Bates, N.R., Brand, U., 1991. Environmental and physiological influences on isotopic and elemental compositions of brachiopod shell calcite: implications for the isotopic evolution of Paleozoic oceans. Chem. Geol. 94, 67–78.

Berner, R.A., 1975. The role of magnesium in the crystal growth of calcite and aragonite from sea water. Geochim. Cosmochim. Acta 39, 489–504.

Bigeleisen, J., Mayer, M.G., 1947. Calculations of equilibrium constants for isotopic exchange reactions. J. Chem. Phys. 15, 261–267.

Bischoff, W.D., Sharma, S.K., MacKenzie, F.T., 1985. Carbonate ion disorder in synthetic and biogenic magnesian calcites: a Raman spectral study. Am. Mineral. 70, 581–589.

Böhm, F., Joachimski, M.M., Dullo, W.-C., Eisenhauer, A., Lehnert, H., Reitner, J., Wörheide, G., 2000. Oxygen isotope fractionation in marine aragonite of coralline sponges. Geochim. Cosmochim. Acta 64, 1695–1703.

Borrero, F.J., Hilbish, T.J., 1988. Temporal variation in shell and soft tissue growth of the mussel *Geukensia demissa*. Mar. Ecol. Prog. Ser. 42, 9–15.

Brand, U., Azmy, K., Logan, A., Bitner, M.A., Durzi, B., Durzi, T., Zuschin, M., 2012. Oxygen isotopes & Mg content in brachiopod calcite: equilibrium fractionation and a new paleotemperature equation. V.M. Goldschmidt Conference, Montreal, June 2012: Session, 13a, p. 344.

Brigaud, B., Pucéat, E., Pellenard, P., Vincent, B., Joachimski, M.M., 2008. Climatic fluctuations and seasonality during the Late Jurassic (Ofordian–Early Kimmeridgian) inferred from $\delta^{18}O$ of Paris Basin oyster shells. Earth Planet. Sci. Lett. 273, 58–67.

Davis, K.J., Dove, P.M., De Yoreo, J.J., 2000. The role of Mg^{2+} as an impurity in calcite growth. Science 290, 1134–1137.

Epstein, S., Buchsbaum, R., Lowenstam, H.A., Urey, H.C., 1953. Revised carbonate–water isotopic temperature scale. Geol. Soc. Am. Bull. 64, 1315–1326.

Gillet, P., Biellmann, C., Reynard, B., McMillan, P.F., 1993. Raman spectroscopic studies of carbonates. Part 1: high-pressure and high-temperature behaviour of calcite, magnesite, dolomite, aragonite. Phys. Chem. Miner. 20, 1–18.

Golyshev, S.I., Padalko, N.L., Pechenkin, S.A., 1981. Fractionation of stable isotopes of carbon and oxygen in carbonate systems. Geochem. Int. 18, 85–99.

Grossman, E.L., Ku, T.-L., 1986. Oxygen and carbon isotope fractionation in biogenic aragonite: temperature effects. Chem. Geol. (Isotope Geosci. Sect.) 59, 59–74.

Hendry, J.P., Kalin, R.M., 1997. Are oxygen and carbon isotopes of mollusc shells reliable palaeosalinity indicators in marginal marine environments? A case study from the Middle Jurassic of England. J. Geol. Soc. Lond. 154, 321–333.

Hendry, J.P., Perkins, W.T., Bane, T., 2001. Short-term environmental change in a Jurassic lagoon deduced from geochemical trends in aragonite bivalve shells. Geol. Soc. Am. Bull. 113, 790–798.

Horibe, S., Oba, T., 1972. Temperature scales of aragonite–water and calcite–water systems. Fossils 23 (24), 69–79.

Horita, J., Ueda, A., Mizukami, K., Takatori, I., 1989. Automatic δD and $\delta^{18}O$ analyses of multi-water samples using H_2- and CO_2-water equilibration methods with a common equilibration set-up. Appl. Radiat. Isot. 40, 801–805.

Jiménez–López, C., Romanek, C.S., Huertas, F.J., Ohmoto, H., Caballero, E., 2004. Oxygen isotope fractionation in synthetic magnesian calcite. Geochim. Cosmochim. Acta 68, 3367–3377.

Jones, D.S., Quitmyer, I.R., Andrus, C.F.T., 2005. Oxygen isotopic evidence for greater seasonality in Holocene shells of *Donax variabilis* from Florida. Palaeogeogr. Palaeoclimatol. Palaeoecol. 58, 249–266.

Keith, M.L., Anderson, G.M., Eichler, R., 1964. Carbon and oxygen isotopic composition of mollusk shells from marine and fresh-water environments. Geochim. Cosmochim. Acta 28, 1757–1786.

Kim, S.-T., O'Neil, J.R., 1997. Equilibrium and nonequilibrium oxygen isotope effects in synthetic carbonates. Geochim. Cosmochim. Acta 61, 3461–3475.

Kim, S.-T., Mucci, A., Taylor, B.E., 2007a. Phosphoric acid fractionation factors for calcite and aragonite between 25 and 75 °C: revisited. Chem. Geol. 246, 135–146.

Kim, S.-T., O'Neil, J.R., Hillaire-Marcel, C., Mucci, A., 2007b. Oxygen isotope fractionation between synthetic aragonite and water: influence of temperature and Mg^{2+} concentration. Geochim. Cosmochim. Acta 71, 4704–4715.

Kobashi, T., Grossman, E., 2003. The oxygen isotopic record of seasonality in *Conus* shells and its application to understanding late middle Eocene (38 Ma) climate. Paleontolog. Res. 7, 343–355.

Krantz, D.E., Williams, D.F., Jones, D.S., 1987. Ecological and paleoenvironmental information using stable isotope profiles from living and fossil molluscs. Palaeogeogr. Palaeoclimatol. Palaeoecol. 58, 249–266.

Lécuyer, C., Reynard, B., Martineau, F., 2004. Stable isotope fractionation between mollusc shells and marine waters from Martinique Island. Chem. Geol. 213, 293–305.

Majoran, S., Agrenius, S., Kucera, M., 2000. The effect of temperature on shell size and growth rate in *Krithe praetexta praetexta* (Sars). Hydrobiologia 419, 141–148.

Malchus, N., Steuber, T., 2002. Stable isotope records (O, C) of Jurassic aragonitic shells from England and NW Poland: palaeoecologic and environmental implications. Geobios 35, 29–39.

O'Neil, J.R., Clayton, R.N., Mayeda, T.K., 1969. Oxygen isotope fractionation in divalent metal carbonates. J. Chem. Phys. 51, 5547–5558.

Owen, R., Kennedy, H., Richardson, C., 2002. Isotopic partitioning between scallop shell calcite and seawater: effect of shell growth rate. Geochim. Cosmochim. Acta 66, 1727–1737.

Patterson, W.P., Smith, G.R., Lohmann, K.C., 1993. Continental paleothermometry and seasonality using the isotopic composition of aragonitic otoliths of freshwater fishes. In: Swart, P.K., Lohmann, K.C., McKenzie, J., Savin, S. (Eds.), Climate Change in Continental Isotopic Records: Geophys. Monogr. Ser., vol. 78, pp. 191–202.

Radtke, R.L., Showers, W., Moksness, E., Lenz, P., 1998. Corrigendum: Environmental information stored in otoliths: insights from stable isotopes. Mar. Biol. 132, 347–348.

Reynolds, R.W., Smith, T.M., 1995. A high resolution global sea surface temperature climatology. J. Climate 8, 1571–1583.

Reynolds, R.W., Rayner, N.A., Smith, T.M., Stokes, D.C., Wang, W., 2002. An improved in situ and satellite SST analysis for climate. J. Climate 15, 1609–1625.

Romanek, C.S., Grossman, E.L., Morse, J.W., 1992. Carbon isotopic fractionation in synthetic aragonite and calcite: effects of temperature and precipitation rate. Geochim. Cosmochim. Acta 56, 419–430.

Rosenthal, Y., Katz, A., 1989. The applicability of trace elements in freshwater shells for paleogeochemical studies. Chem. Geol. 78, 65–76.

Rubinson, M., Clayton, R., 1969. Carbon-13 fractionation between aragonite and calcite. Geochim. Cosmochim. Acta 33, 997–1002.

Schöne, B.R., Castro, A.D.F., Fiebig, J., Houk, S.D., Oschmann, W., Kröncke, I., 2004. Sea surface water temperatures over the period 1884–1983 reconstructed from oxygen isotope ratios of a bivalve mollusk shell (*Arctica islandica*, southern North Sea). Palaeogeogr. Palaeoclimatol. Palaeoecol. 212, 215–232.

Schöne, B.R., Houk, S.D., Freyre Castro, A.D., Fiebig, J., Kröncke, I., Dreyer, W., Oschmann, W., 2005. Daily growth rates in shells of *Arctica islandica*: assessing subseasonal environmental controls on a long-lived bivalve mollusk. Palaios 20, 78–92.

Sharma, T., Clayton, R.N., 1965. Measurement of O^{18}/O^{16} ratios of total oxygen of carbonates. Geochim. Cosmochim. Acta 29, 1347–1353.

Storr, J.F., Costa, A.L., Prawel, D.A., 1982. Effects of temperature on calcium deposition in the hard-shell clam, *Merceneria merceneria*. J. Thermal Biol. 7, 57–61.

Takeuchi, T., Sarashina, I., Iijima, M., Endo, K., 2008. In vitro regulation of $CaCO_3$ crystal polymorphism by the highly acidic molluscan shell protein Aspein. FEBS Lett. 582, 591–596.

Tarutani, T., Clayton, R.N., Mayeda, T.K., 1969. The effect of polymorphism and magnesium substitution on oxygen isotope fractionation between calcium carbonate and water. Geochim. Cosmochim. Acta 33, 987–996.

Thorrold, S.R., Campana, S.E., Jones, C.M., Swart, P.K., 1997. Factors determining $\delta^{13}C$ and $\delta^{18}O$ fractionation in aragonitic otoliths of marine fish. Geochim. Cosmochim. Acta 61, 2909–2919.

Tremaine, D.M., Froelich, P.N., Wang, Y., 2011. Speleothem calcite farmed in situ: modern calibration of $\delta^{18}O$ and $\delta^{13}C$ paleoclimate proxies in a continuously-monitored natural cave system. Geochim. Cosmochim. Acta 75, 4929–4950.

Turekian, K.K., Armstrong, L., 1960. Magnesium, strontium and barium concentrations and calcite aragonite ratios of some recent molluscan shells. J. Mar. Res. 18, 133–151.

Turner, J.V., 1982. Kinetic fractionation of carbon-13 during calcium carbonate precipitation. Geochim. Cosmochim. Acta 46, 1183–1191.

Urey, H.C., 1947. The thermodynamic properties of isotopic substances. J. Chem. Soc. (Lond.) 562–581.

Urmos, J., Sharma, S.K., McKenzie, F.T., 1991. Characterization of some biogenic carbonates with Raman spectroscopy. Am. Mineral. 76, 641–646.

Wada, K., Fujinuki, T., 1976. Biomineralization in bivalve molluscs with emphasis on the chemical composition of the extrapallial fluid. In: Watanabe, N., Wilbur, K.M. (Eds.), The Mechanisms of Mineralization in the Invertebrates and Plants. University of South Carolina Press, Columbia, pp. 175–190.

Wanamaker Jr., A.D., Kreutz, K.J., Borns Jr., H.W., Introne, D.S., Feindel, S., Funder, S., Rawson, P.D., Barber, B.J., 2007. Experimental determination of salinity, temperature, growth, and metabolic effects on shell isotope chemistry of *Mytilus edulis* collected from Maine and Greenland. Paleoceanography 22, PA2217 http://dx.doi.org/10.1029/2006PA001352.

Weber, J.N., 1973. Incorporation of strontium into reef coral skeletal carbonate. Geochim. Cosmochim. Acta 37, 2173–2190.

White, R.M.P., Dennis, P.F., Atkinson, T.C., 1999. Experimental calibration and field investigation of the oxygen isotopic fractionation between biogenic aragonite and water. Rapid Commun. Mass Spectrom. 13, 1242–1247.

Witbaard, R., Duineveld, G.C.A., Wilde de, P.A.W.J., 1999. Geographic differences in growth rates of *Arctica islandica* (mollusca: Bivalvia) from the North Sea and adjacent waters. J. Mar. Biol. Assoc. U. K. 79, 907–915.

Zakharov, Y.D., Shigeta, Y., Nagendra, R., Safronova, P.P., Smyshlyaeva, O.P., Popov, A.M., Velivetskaya, T.A., Afanasyeva, T.B., 2011. Cretaceous climate oscillations in the southern palaeolatitudes: new stable isotope evidence from India and Madagascar. Cretaceous Res. 32, 623–645.

Zheng, Y.-F., 1999. Oxygen isotope fractionation in carbonate and sulfate minerals. Geochem. J. 33, 109–126.

Zhou, G.-T., Zheng, Y.-F., 2002. Kinetic mechanism of oxygen isotope disequilibrium in precipitated witherite and aragonite at low temperatures: an experimental study. Geochim. Cosmochim. Acta 66, 63–71.

Zhou, G.-T., Zheng, Y.-F., 2003. An experimental study of oxygen isotope fractionation between inorganically precipitated aragonite and water at low temperatures. Geochim. Cosmochim. Acta 67, 387–399.

Applied Geochemistry 27 (2012) 257–265

Contents lists available at SciVerse ScienceDirect

Applied Geochemistry

journal homepage: www.elsevier.com/locate/apgeochem

Semi-automatic determination of the carbon and oxygen stable isotope compositions of calcite and dolomite in natural mixtures

M. Baudrand [a], G. Aloisi [a,1], C. Lécuyer [a,*], F. Martineau [a], F. Fourel [a], G. Escarguel [a], M.-M. Blanc-Valleron [b], J.-M. Rouchy [b], V. Grossi [a]

[a] Université Lyon 1, CNRS, UMR 5276, Laboratoire de Géologie de Lyon, 2 rue Raphaël Dubois, F-69622 Villeurbanne, France
[b] Muséum National d'Histoire Naturelle, CNRS, UMR 7207, Paléobiodiversité et Paléoenvironnements, 57 rue Cuvier, CP 48, 75005 Paris, France

ARTICLE INFO

Article history:
Received 12 November 2010
Accepted 3 November 2011
Available online 12 November 2011
Editorial handling by R.S. Harmon

ABSTRACT

A semi-automatic, on-line method was developed to determine the $\delta^{13}C$ and $\delta^{18}O$ values of coexisting calcite and dolomite. An isotopic mass balance is used to calculate the compositions of dolomite after having measured that of calcite and of the "bulk" sample. The limit of validity of this method is established by performing isotopic measurements of artificial mixtures made of precisely weighted and isotopically-characterised dolomite and calcite. The accuracy and repeatability of the calculation of dolomite $\delta^{13}C$ and $\delta^{18}O$ are statistically determined with a Monte-Carlo procedure of error propagation. Stable isotope ratios are determined by using an automated MultiPrep™ system on-line with an isotope-ratio mass-spectrometer (IRMS). The reaction time and the temperature of reaction were optimised by comparing the results with the isotopic composition of known mixtures. The best results were obtained by phosphoric acid digestion after 20 min at 40 °C for calcite and 45 min at 90 °C for dolomite. This procedure allows an accurate determination of the isotopic ratios from small samples (300 μg). Application of this protocol to natural mixtures of calcite and dolomite requires the accurate determination of the relative abundance of calcite and dolomite by combining Mélières manocalcimetry (MMC) and X-ray diffractometry (XRD).

1. Introduction

Most sedimentary carbonate rocks have a complex diagenetic history which results in the formation of various assemblages of carbonate minerals (Bathurst, 1983). A common way of investigating the geochemical processes that produced those mineral assemblages is to measure the isotopic composition of carbonates for identifying the C sources (e.g. oceanic dissolved inorganic C, organic matter, CH_4) and for estimating the salinity and temperature of aqueous fluids that prevailed in the diagenetic environments (Fritz and Smith, 1970; Dworkin et al., 2005).

Measuring the isotopic composition of distinct carbonate phases (aragonite, calcite, dolomite) occurring in natural mixtures is not straightforward because the different phases cannot be physically separated in most cases, even though it must be noted that paramagnetic dolomite grains can be separated from calcite with a Frantz Isodynamic Separator (e.g. Sheppard and Schwarcz, 1970). Thus, the differential reactivity of $CaCO_3$ (aragonite and calcite) and $CaMg(CO_3)_2$ (dolomite) during acid digestion is used to selectively extract the CO_2 released by the two phases and to track the evolution of its isotopic composition. For example, for a given grain size and crystallinity, dolomite reacts more slowly than calcite (Epstein et al., 1964). Thus, the CO_2 produced after 20 min (Clayton et al., 1968), or 2 h (Al-Aasm et al., 1990) of reaction with phosphoric acid at 25 °C is considered to carry the isotopic signature of calcite. The isotopic signature of dolomite can be obtained by two alternative methods. Following the first reaction step during which the CO_2 produced is considered to come from calcite, the acid digestion is continued for 24 h to remove the remaining calcite while discarding the produced CO_2. Then, the remaining carbonate is further reacted with the same acid for 24 h at 50 °C; the CO_2 derived from this reaction step is then considered to carry the isotopic signature of dolomite (Al-Aasm et al., 1990). In a second procedure, the carbonate mixture is reacted with 1 N acetic acid for 20 min at 25 °C to remove calcite and the isotopic composition of dolomite is obtained from the CO_2 produced during a further treatment of 4 days with phosphoric acid at 25 °C (Pierre and Rouchy, 1990).

In this study, a semi-automatic method is presented to determine the C and O isotope compositions of sedimentary mixtures of calcite and dolomite. For some mixtures, it allows more repeatable and accurate measurements of small samples (300 μg required for the isotopic analyses) compared with the aforementioned conventional off-line methods. Following the determination of the relative proportions of calcite and dolomite by combining conventional Mélières ManoCalcimetry (MMC) and X-ray Diffractometry

* Corresponding author. Tel.: +33 (0)4 72 44 83 76.
E-mail address: Christophe.Lecuyer@univ-lyon1.fr (C. Lécuyer).
[1] Present address: Laboratoire d'Océanographie et du Climat, UPMC, Institut Pierre et Simon Laplace, CNRS, Paris, France.

0883-2927/$ - see front matter © 2011 Elsevier Ltd. All rights reserved.
doi:10.1016/j.apgeochem.2011.11.003

(XRD), the isotopic composition of calcite is measured with a MultiPrep™ automated system on-line with an IsoPrime™ isotope-ratio mass-spectrometer (IRMS). The isotopic composition of dolomite is then deduced from mass balance calculations after measuring the isotopic composition of the "bulk" sample (calcite + dolomite) with the MultiPrep™ system. A wide range of magmatic or metamorphic carbonate rocks (e.g. carbonatites, marbles) may contain mixed calcite and dolomite minerals and, as such, the potential utility of this new method may be extended beyond the research field of sedimentary geochemistry.

2. Material and methods

2.1. Calcite and dolomite end-members and standard mixtures

Time and temperature of reaction are parameters that need to be optimised in order to (1) minimize the contribution of dolomite when selectively digesting calcite and (2) achieve complete reaction when digesting the "bulk" sample. Optimisation of the above parameters was carried out by determining the isotopic composition of mixtures of well characterised calcite and dolomite "end-members" (Table 1), and by comparing the results with the theoretical isotopic compositions of the mixtures that were deduced from the isotopic compositions of the end-members and their mixing proportions (Table 2 and Section 3.1).

The choice of the end-members was based on their crystallographic properties and isotopic compositions (Table 1). The calcite end-member is from a 100% pure marble obtained from the Carrara Quarry (Italy). The dolomite end-member (98.9% dolomite, 1.1 wt.% silicates) was sampled in the vicinity of the Wadi Um Gheig on the Red Sea coast of Egypt (Aref, 1997). The sampling area is in the vicinity of ZnS and PbS deposits of hydrothermal origin (El Shazly, 1957). Associated with these hydrothermal deposits are diagenetic carbonates, such as the dolomite sample used for the dolomite end-member of the standard series, that formed via microbial transformation of evaporitic gypsum deposits of Miocene age (Aref, 1997). The degree of crystallinity can be qualitatively assessed based on the shape of X-ray diffraction peaks (Fig. 1). Very small crystallites are more imperfect than large ones, resulting in a broadening of the peaks as the crystallite size gets smaller. Crystallinity can affect the phosphoric reaction rate such that an increase in crystallinity, i.e. a decrease in surface area, results in a decrease in the rate of reaction. Thus, in the experiments, sensitive detection of cross-contamination results from the use of highly crystalline slower reacting calcite and a faster reacting poorly crystallised dolomite. The sensitivity to cross contamination increases with the difference in isotopic composition of the calcite and dolomite. In this case, $\Delta^{13}C = 9.9‰$ and $\Delta^{18}O = 3.0‰$ (Table 1). Conversely, the accuracy of the method decreases as isotopic compositions of calcite and dolomite approach one another. However, it can be easily tested by comparing the bulk rock analysis with the analysis of one phase.

The chemical composition of the dolomite end member was determined by X-ray Fluorescence. These data fit well with the XRD analyses (Table 1) in that only traces of elements typical of silicate minerals were detected (SiO_2 = 0.35 mol%, K_2O = 0.04 mol%, Al_2O_3 and Na_2O were below the detection limit). Given the trace amounts of Si present, the great majority of Ca (CaO = 49.69 mol%) and Mg (MgO = 49.26 mol%) can be safely ascribed to dolomite. Because the sum of the stoichiometric coefficients for divalent cations should add up to 1 in dolomite, a very small amount of cation substitution is possible in the end member dolomite. The XRF analyses detected traces of Mn (MnO = 0.49 mol%) and Fe_2O_3 (0.16 mol%), suggesting that very small amounts of these elements may be present in the dolomite lattice. In summary, the dolomite end member has a chemical formula very close to that of stoichiometric dolomite [Ca, $Mg(CO_3)_2$].

Table 2
Mineralogical and chemical compositions of the standard series.

Cal/Dol	MMC_{th}	$MMC_{det.}$	Δ_{MMC}	$XRD_{th.}$ cal	$XRD_{det.}$ cal	Δ_{XRD}
100/0	100.0	100.0	0	100	100	0
95/5	99.9	–	–	95.0	–	–
90/10	99.9	98.5	1.4	89.4	88.3	1.1
75/25	99.7	99.2	0.5	76.6	76.2	0.4
50/50	99.5	98.2	1.3	52.1	50.3	1.8
25/75	99.2	97.8	1.4	26.6	26.5	0.1
10/90	99.0	98.5	0.5	10.9	10.3	0.6
5/95	99.0	–	–	5.0	–	–
0/100	98.9	98.9	0	0	0	0

Cal/Dol = proportions of calcite and dolomite in the mixture; MMC_{th} = weighted carbonate content (±0.08%) corrected from dolomite purity and used as reference; MMC_{det} = carbonate content determined by MMC and corrected for temperature and pressure; Δ_{MMC} = difference between MMC_{th} and MMC_{det}; XRD_{th} cal = calcite content determined by weighing and corrected from dolomite purity; XRD_{det} cal = calcite content determined by MMC and XRD; Δ_{XRD} = difference between XRD_{th} cal and XRD_{det} cal.

The calcite and dolomite end-members were ground with an agate mortar and sieved between 50 μm and 100 μm. It is worth noting here that the real value of grinding and mixing is to physically free calcite from dolomite as much as possible. Sample homogenisation was performed by using a mini 'V-shape' mixer designed for powder–powder mixtures. Seven mixtures of the two end-members were prepared in variable proportions (Table 2). By mixing precisely weighed amounts of each end-member, it was possible to obtain an accurate determination of the carbonate content (±0.08%) for each mixture. The calcite and dolomite end-members together with the seven mixtures will be referred to hereafter as the "standard series".

2.2. Carbonate content and mineralogical composition

The carbonate content of the standard series was measured twice on 100 mg of powder using a Mélières manocalcimeter (MMC) apparatus derived from the carbonate bomb technique first described by Müller and Gastner (1971). The total carbonate content (in weight percent) was calculated from the volume of CO_2 evolved from the reaction of 100 mg of finely crushed sediment with 8 N HCl. The MMC apparatus was calibrated at 100% so that 1 mMol of CO_2 corresponded to 100 mg of calcite or aragonite. For dolomite, because of its different molecular weight, 100 mg did not correspond to 1 mMol of CO_2 and the values were corrected

Table 1
Calcite and dolomite end-members used for standard mixtures.

End-member	Composition (% mass)	Grain size (μm)	Crystallography	$\delta^{18}O$ (‰ PDB)	$\delta^{13}C$ (‰ PDB)	Origin
Calcite	100% $CaCO_3$	50–100	Marble (very well crystallised)	−1.8 ± 0.1	2.0 ± 0.1	Italy (Carrara Quarry)
Dolomite	98.9% [Ca, $Mg(CO_3)_2$] 1.1% of silicates	50–100	Diagenetic carbonate (poorly crystallised)	−4.8 ± 0.1	−7.9 ± 0.1	Egypt (wastes of Uhm Geigh ZnS mine)

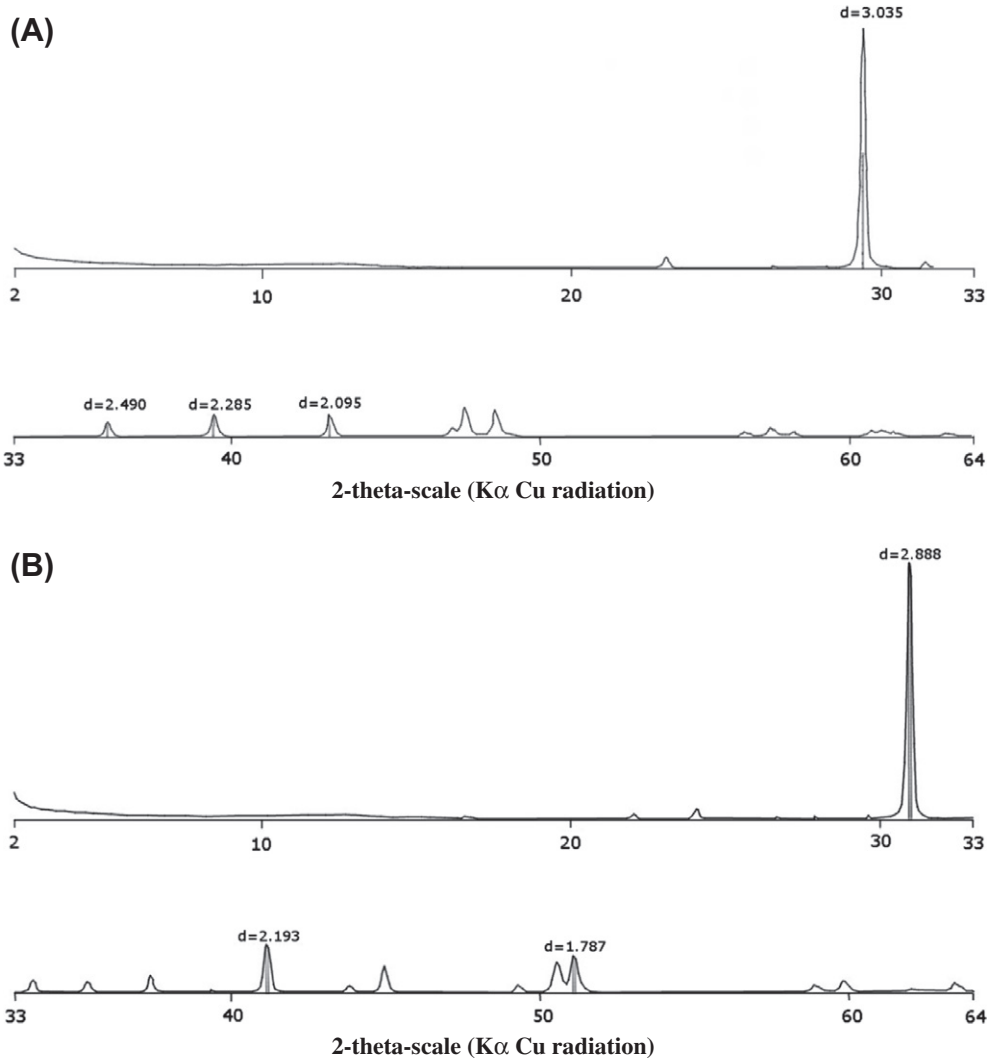

Fig. 1. Diffractograms of calcite (A) and dolomite (B) end-members. Vertical bars represent relative peak heights reported in standard diffractograms of calcite and dolomite. Peaks indicated by their *d*-values are the ones chosen in this work to determine calcite and dolomite concentrations.

(% dolomite = MMC/1.0855) to estimate the real weight percentages. The "bulk" mineralogy was determined by X-ray diffractometry using a Siemens D-500 instrument (Ni filtered Cu Kα radiation) scanning 2–64° (2θ) at a rate of 0.02° 2θ/s. About 600 mg of powdered sample was compacted in a plastic holder (2.4 cm in diameter and 2 mm in thickness) using a frosted glass. Attention was paid to the flatness of the sample surface in order to avoid preferred orientation. The MacDiff program by Rainer Petschik (servermac.geologie.unifrankfurt.de/Rainer.html) was used to quantify the relative proportions of calcite and dolomite in carbonate mixtures from X-ray diffractograms using the peak area method. The relative intensities were corrected using correction factors (I/Icor) from the PDF2 data base of the International Centre for Diffraction Data. Standard forms used are 05–0586 for calcite and 73–2324 for dolomite. Bish and Reynolds (1989) advised grinding samples to below 20 μm to optimise the repeatability of the analyses, while Walters et al. (1972) proposed an optimal size range between 5 and 44 μm. In the experiments, however, reproducible results were obtained using dolomite and calcite end-members sieved between 50 μm and 100 μm as well as below 20 μm. The carbonate content measured by MMC was then used to calculate absolute concentrations of calcite and dolomite in the sample from the relative concentrations obtained by XRD.

2.3. Isotopic measurements

Carbon and O isotope measurements were carried out with a MultiPrep™ automated system on-line with a Dual-Inlet Isoprime™ isotope ratio mass spectrometer at the Laboratoire Paléoenvironnements & Paléobiosphère (Université Lyon 1). The principle of this fully automated device is to react the carbonate phases with anhydrous H_3PO_4 at constant temperature to generate CO_2 according to the following acid–base reaction:

$$MeCO_3 + 2H_3PO_4 \rightarrow CO_2 + Me^{2+} + 2H_2PO_4^- + H_2O$$

where Me is an alkaline earth or a divalent transition metal cation.

One hundred wt.% H_3PO_4 was prepared in the standard way (Coplen et al., 1983). Before each batch of analyses, an aliquot of 5–6 mL of H_3PO_4 was outgassed for at least 24 h on a vacuum line. Each sample was ground to ca. 200 μm. The sample aliquot (typically 200–300 μg) was placed at the bottom of a V shape vial sealed with a rubber septum. The sample vials are then placed in a temperature regulated sample tray heated at 90 °C. From this stage all subsequent sample preparation is done automatically. The MultiPrep system is equipped with a double hole needle which allows the acid to be delivered to the vial and also to extract the CO_2 which has been generated during the reaction. First, the vial was

evacuated through the external needle connected to the MultiPrep vacuum system. Phosphoric acid was admitted to the vial through the inner needle using the acid pump. At this stage, the reaction starts, generating CO_2. During the 20 min reaction, the needle remained inside the valve. An external cold finger was maintained at −165 °C, constantly collecting the extracted CO_2. Once the reaction was completed, the external cold finger was heated to −70 °C to release the CO_2 without releasing water. The sample of CO_2 was automatically managed by the mass spectrometer inlet system according to its volume, and isotopically analyzed. Carrara marble was isotopically calibrated against NBS19 and NBS18.

Results are expressed in the usual δ notation in ‰ relative to V-PDB (Vienna–Pee Dee Belemnite) standard for both $\delta^{13}C$ and $\delta^{18}O$. The analytical uncertainty associated with the measurements of calcite and dolomite end-members was close to 0.1‰ for $\delta^{18}O$ and $\delta^{13}C$. During the course of acid digestion, the O isotope composition of reacting calcite in the carbonated mixtures was obtained by monitoring the evolution of the $\delta^{18}O$ value of the CO_2, which was corrected from the acid fractionation factor deduced from the isotopic composition of NBS-19 ($\delta^{18}O = -2.2‰$). The acid fractionation factor is also dependent on both mineralogy (Sharma and Clayton, 1965; Rosenbaum and Sheppard, 1986) and temperature (Swart et al., 1991). For instance, the O isotope composition of CO_2 released during H_3PO_4 digestion of calcite at 90 °C is 8.14‰ heavier than that of calcite, whereas the composition of CO_2 derived from dolomite is 8.95‰ heavier than that of dolomite (Böttcher, 1996; Das Sharma et al., 2002). The CO_2-calcite fractionation factor for the CO_2 released at 40 °C during the first 20 min was used and the residual amount of CO_2, deduced from mass balance calculation after the bulk analysis, was corrected from the fractionation factor between CO_2 and dolomite.

2.4. Acetic acid digestion of carbonated mixtures

The acetic acid digestion method of Pierre and Rouchy (1990) was modified for use with the MultiPrep™ system. The small amounts of sample required minimisation of loss during neutralisation and washing. Each calcite–dolomite mixture was thus reacted for 20 min with 1 N acetic acid according to the method of Pierre and Rouchy (1990), followed by washing and filtration. After drying at 60 °C, isotopic compositions were measured using the same procedure applied to "bulk" samples (see Section 3.2.2).

3. Results and discussion

3.1. Determination of mineral proportions based on XRD and MMC data

The carbonate content of the standard series deduced from the weights of calcite and dolomite is indicated in Table 2 (column MMC_{th}). Values lower than 100% for samples containing dolomite are due to the presence of 1.1 wt.% silicates in the dolomite end-member. Duplicate measurements of the carbonate content of the standard series were performed with the manocalcimeter (column MMC_{det} in Table 2); repeatability was better than 1 wt.%. The MMC measurements systematically underestimated (1.4 wt.% maximum) the carbonate content of mixtures prepared by accurate weighing. This small bias possibly results from the long reaction time needed for samples containing dolomite. The acid digestion (8 N HCl) of carbonates is strongly exothermic, and a long reaction time could result in cooling of the CO_2 released.

XRD analyses of the standard series were duplicated. The repeatability of the relative calcite–dolomite ratio was better than 1 wt.%. Compared to the standard diffractogram of calcite (form 05–0586), the diffractogram of the calcite end-member shows an over-diffraction of the main peak of calcite (d = 3.035 Å) of about 50 wt.% relative to the other calcite peaks (Fig. 1A). Thus, a large error (up to 14 wt.%) can occur if only the major peak of calcite is used to determine the relative abundance of calcite and dolomite; therefore, secondary peaks are also considered for the determination of the relative concentrations of calcite. The best results were obtained using the three calcite peaks: d = 2.490 Å, 2.285 Å and 2.095 Å, and the three peaks of dolomite: d = 2.888 Å, 2.193 Å and 1.787 Å. Thus, XRD diffractograms of samples must be compared to those available in standard forms in order to select the best combination of peaks to be used as a function of the sample crystallinity. This is a source of potential error during the isotopic analysis of whole-rock samples.

With this method, the difference between the relative abundance of calcite and dolomite in the samples deduced from accurate weighing ($XRD_{th\cdot cal}$) and that obtained by MMC and XRD ($XRD_{det\ cal}$) is smaller than 2 wt.% (Table 2) and does not show any relationship with the proportions of the end-members in the mixture.

The error propagation of the determination of each carbonate proportion by the combination of MMC and XRD is found to mainly depend on the error of the estimated peak areas. This error shows an inverse linear relationship with the peak area. The influence of the carbonate content in the sample is found to have only an indirect impact: when a sample has a low carbonate content, the peak areas are smaller, and errors on the peak areas, higher.

3.2. MultiPrep™ determination of the isotopic composition of calcite and dolomite in mixtures of both

3.2.1. Isotopic composition of calcite in calcite-dolomite mixtures

Phosphoric acid digestion tests were carried out on the calcite end-member at 90 °C, 80 °C, 70 °C, 45 °C, 40 °C and 30 °C with reaction times of 2, 3, 5, 10, 20, 25, 30 and 40 min (Fig. 2). Except for the first extractions (2–3 min), the $\delta^{13}C$ and $\delta^{18}O$ of the CO_2 produced by the calcite remained virtually unchanged with reaction time at any temperature. Some variations in $\delta^{18}O$ during initial stages of reaction were noted by Fritz and Fontes (1966), Walters et al. (1972) and Al-Aasm et al. (1990), but with virtually no systematic variations in $\delta^{13}C$ values. Al-Aasm et al. (1990) proposed that an increase in $\delta^{18}O$ values may be related to rapid reaction of fine calcite crystallites adhering to grain surfaces. In the present case, the maximum isotopic fractionation occurs for short reaction times and low temperatures. Reliable isotopic compositions of calcite are obtained for a reaction time of 5 min at 90 °C, and at least 20 min at 40 °C (Fig. 2). Isotopic fractionation was larger for both C and O at low temperatures for a same reaction time, and less of the calcite was digested when the reaction temperature was lower. This partial digestion could be mainly responsible for variations in isotopic fractionation with temperature (Al-Aasm et al., 1990).

The duration and temperature of reaction were optimised in order (1) to obtain a sufficiently high yield of calcite CO_2, and (2) to avoid large reaction times, which would have resulted in too much dolomite being dissolved. A temperature was preferred which results in a relatively short reaction time that minimises the dolomite contribution to the calcite signal. The optimal conditions are 20 min of H_3PO_4 digestion at 40 °C. However, when the standard series is analysed using these conditions, it is noted that the isotopic composition of the calcite CO_2 shifts towards the value of dolomite with increasing dolomite content in the mixture (Table 3, Fig. 3). This indicates that a small portion of the dolomite is reacting during acid digestion. For the 95/5 dolomite/calcite mixture, the C and O isotope compositions of calcite is then, respectively, 4.1‰ and 1.5‰ lower than the theoretical compositions computed from the isotopic composition of the end-members. The evolution of differences between the measured $\delta^{13}C$ and $\delta^{18}O$

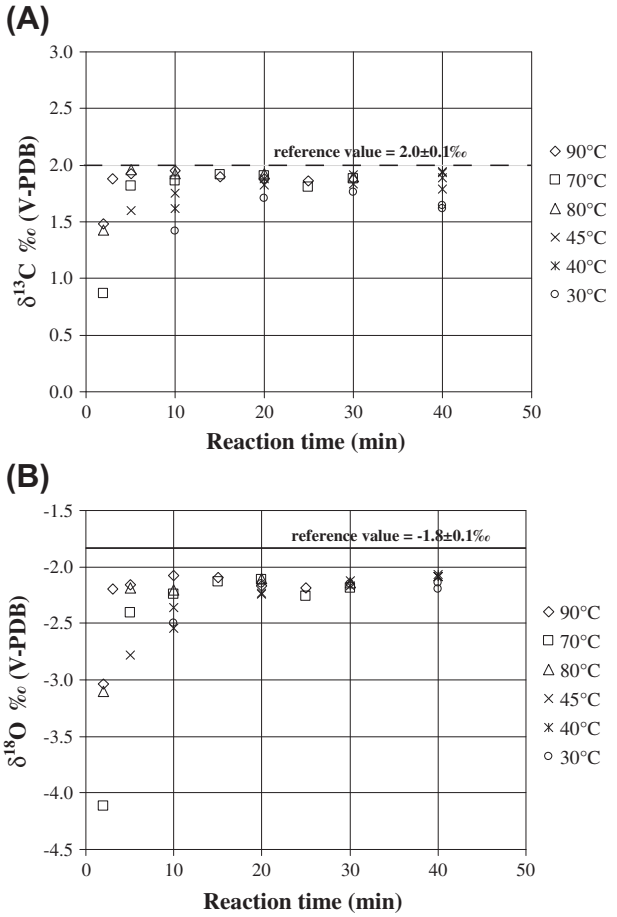

Fig. 2. Plot of $\delta^{13}C$ values of CO_2 (A) and $\delta^{18}O$ values of mineral (corrected for temperature fractionation) (B) during partial digestion of standard calcite with 100% H_3PO_4 for different temperatures as a function of the reaction time.

Table 3
Differences between calcite isotopic signatures determined by the present method (40 °C–20 min) and pure calcite end-member signature.

Cal/Dol	Manual method		This method	
	$\Delta^{13}C$ M	$\Delta^{18}O$ M	$\Delta^{13}C$ MP	$\Delta^{18}O$ MP
100/0	0.0	0.0	0.0	0.0
95/5	0.0	0.2	0.0	0.0
90/10	0.0	0.1	0.0	0.0
75/25	0.2	0.4	0.1	0.1
50/50	0.2	−0.1	0.3	0.1
25/75	0.7	0.1	0.9	0.3
10/90	1.9	0.6	2.5	0.9
5/95	4.3	2.3	4.1	1.5
0/100	9.9[a]	3.0[a]	9.9[a]	3.0[a]

$\Delta^{13}C$ M or $\Delta^{18}O$ M = difference between reference calcite isotopic signature (indicated for 100/0 mixture and $\delta^{13}C$ or $\delta^{18}O$ obtained with manual method (Al-Aasm et al., 1990); $\Delta^{13}C$ MP or $\Delta^{18}O$ MP = difference between reference dolomite isotopic signature and $\delta^{13}C$ or $\delta^{18}O$ obtained with this method.

[a] Not measured because protocol for calcite measurement does not allow dolomite measurements.

values and those of the calcite end-member can be modelled as exponential functions of the dolomite percentage in the mixture. This model is used for the Monte-Carlo procedure of the error propagation calculation on the $\delta^{13}C$ and $\delta^{18}O$ values of dolomite (Section 3.2.3). The repeatability of the direct isotopic measurements is better than 0.1‰.

In addition to the reaction conditions, the accuracy in the determination of the isotopic composition of calcite also depends on the

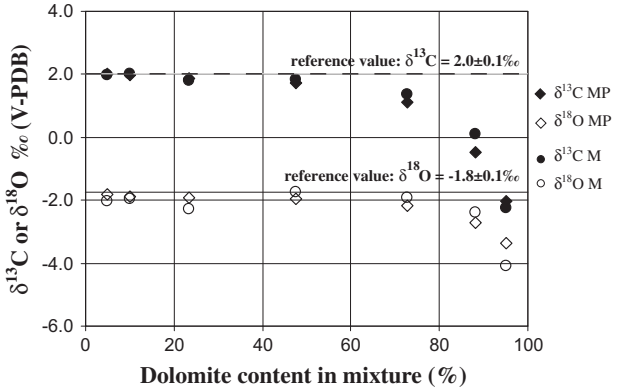

Fig. 3. Variation of the isotopic composition of calcite measured by the semi-automatic method (MP) and by the manual method (M) described by Al-Aasm et al. (1990) as a function of its concentration in calcite-dolomite mixtures. Reference values are given in Table 1.

difference between the isotopic compositions of the two carbonate pools. Here carbonates with $\delta^{13}C$ and $\delta^{18}O$ differences of 9.9‰ and 3.0‰, respectively, were used. A $\delta^{13}C$ difference large enough to be compared to those documented so far in sedimentary carbonates (Degens and Epstein, 1964; Fritz and Smith, 1970; Arenas et al., 1999; Bellanca et al., 2001) was selected. Nevertheless, for carbonate mixtures formed in diagenetic environments where anaerobic oxidation of CH_4 can result in a large fractionation of C isotopes (up to 50‰), the uncertainty might be larger.

Reaction rates can also be influenced by both the chemistry and grain size of the two carbonate pools. Whenever XRD analyses suggest that the chemical composition deviates significantly from the stoichiometric compositions of calcite and dolomite, the authors suggest performing a chemical analysis of the carbonates and adjusting the duration of the reaction to account for the effect of chemical composition on reaction rates. According to Böttcher (1996), the same reaction time is required for the complete H_3PO_4 digestion of a pure calcite and of a synthetic manganoan calcite ($Ca_{0.75}Mn_{0.25}CO_3$), but the reaction time needed for rhodochrosite is fourfold longer. Calcite and rhodochrosite having the same crystallographic space group (Trigonal–Hexagonal scalanohedral), it may be possible that Mn substitution has an influence on H_3PO_4 digestion rate if a large proportion is substituted. For substitution by other elements, the problem can become very complex because of crystallographic changes between two substitution end-members (with or without intermediate mineral) like the calcite–dolomite–magnesite partial solid solution. It is thus recommended to test the reaction time needed for H_3PO_4 digestion of any non-stoichiometric carbonate if its chemical and crystallographic properties are significantly altered. It is also advisable to use a powder sieved between 50 μm and 100 μm because grain size has an important impact on reaction rates (e.g. Fritz and Fontes, 1966; Clayton et al., 1968; Walters et al., 1972). For coarser powders, incomplete acid digestion could result in isotopic fractionation, whereas in the case of finer powders the rate of dolomite reaction would be higher, leading to a potential significant isotopic contamination of the co-existing calcite.

3.2.2. "Bulk" isotopic composition of calcite–dolomite mixtures

As dolomite reacts slower than calcite, the reaction temperature was set at 90 °C in order to achieve the complete acid digestion of calcite–dolomite mixtures as fast as possible. Expected isotopic compositions are calculated by using a mass balance equation combining carbonate contents and $\delta^{18}O$ and $\delta^{13}C$ values of end-members. The best fit is obtained for a reaction time of 45 min (Fig. 4) amongst a set of various reaction times (40, 45, 50 and

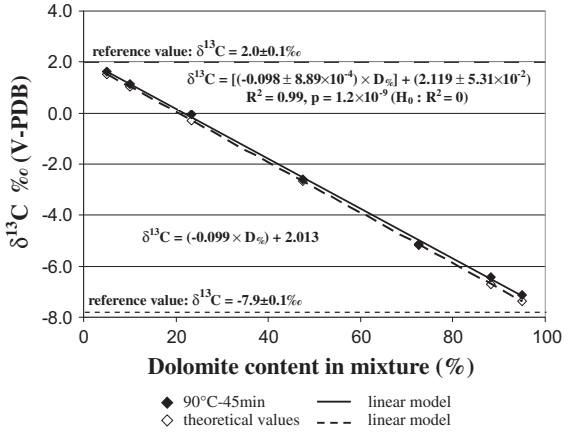

Fig. 4. Comparison between measured $\delta^{13}C_{bulk}$ values of the standard series (90 °C/45 min) and those calculated from $\delta^{13}C$ of end-members and known carbonate contents (reference values are given in Table 1). The two least-squares regression lines do not significantly differ from each other at the 95% confidence level based on Student's *t*-test comparisons of their slopes ($t = 1.185$, $d.f. = 5$, $p = 0.289$) and intercepts ($t = 1.994$, $d.f. = 5$, $p = 0.103$).

55 min). The empirical linear regression of the $\delta^{13}C$ "bulk" as a function of the dolomite content in the mixture obtained with this procedure is not statistically different from the theoretical fit calculated from end-member compositions and mixing proportions (Fig. 4). In any case, the difference from expected compositions (accuracy) is better than 0.1‰ and repeatability of measurements better than 0.1‰.

3.2.3. Calculated isotopic composition of dolomite in calcite–dolomite mixtures

Following the determination of the isotopic compositions of the calcite end-member and of the "bulk" calcite–dolomite mixture, the isotopic composition of the dolomite end-member can be calculated using the following isotopic mass balances:

$$(X_{cal} \times \delta^{13}C_{cal}) + (X_{dol} \times \delta^{13}C_{dol}) = \delta^{13}C_{bulk}$$

and

$$(X_{cal} \times \delta^{18}O_{cal}) + (X_{dol} \times \delta^{18}O_{dol}) = \delta^{18}O_{bulk}$$

with $X_{cal} + X_{dol} = 1$ and where $\delta^{13}C_{cal}$, $\delta^{13}C_{bulk}$, $\delta^{18}O_{cal}$ and $\delta^{18}O_{bulk}$ are the isotopic compositions of calcite and of the "bulk" carbonate mixture, and X_{cal} and X_{dol} are the weight proportions of calcite and dolomite in the mixtures determined from the MMC and XRD data. It is emphasised that the use of these equations depends on knowing that neither of the δ values for the two phases are identical or close to that condition. If, for example, $\delta^{13}C_{dol} = \delta^{13}C_{cal}$ then the system is indeterminate. It is also noteworthy that the errors will increase as the two δ values approach one another.

The global accuracy and uncertainty (SD) of this procedure results from the combined errors associated with (1) the measurements of the relative abundance of calcite and dolomite by MMC and XRD, (2) the determination of the isotopic compositions and (3) the cross-contamination between calcite and dolomite during selective acid digestion.

The accuracy of the $\delta^{13}C_{dol}$, and $\delta^{18}O_{dol}$ calculation mainly depends on the content of dolomite in the mixture. The calculated $\delta^{13}C_{dol}$ can be modelled as a logarithmical function of the dolomite content (Fig. 5A). The accuracy of $\delta^{18}O_{dol}$ calculation does not show any relationship with the dolomite content (Fig. 5B) but this may indicate that the difference between the two end-members $\delta^{18}O$ is not important enough to have a detectable influence.

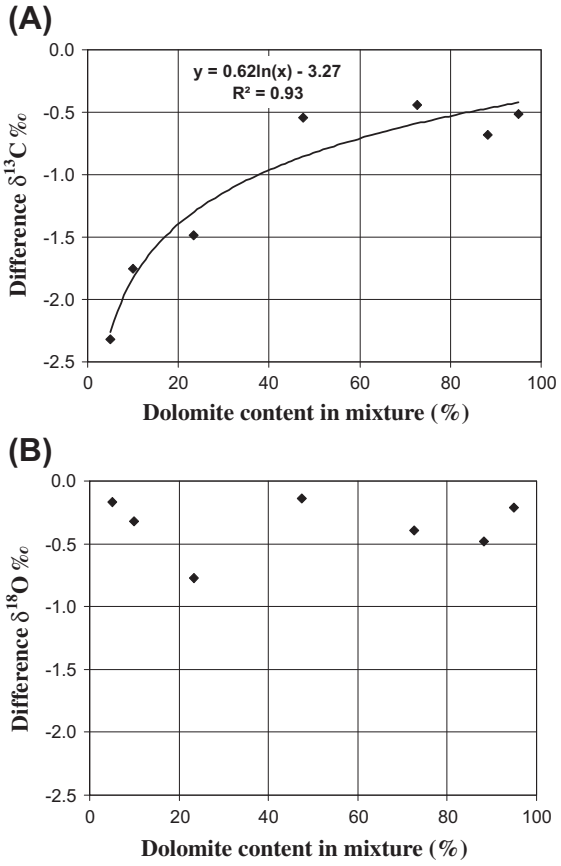

Fig. 5. Plot of the difference between reference $\delta^{13}C$ (A) and $\delta^{18}O$ (B) values of dolomite and calculated values of dolomite as a function of the dolomite percentage in the mixture.

By using a Monte-Carlo procedure of error propagation (a parametric bootstrap resampling, using 10^6 iterations) it was possible to integrate all errors and to quantify their respective influence on the SD associated with $\delta^{18}O_{dol}$ estimates. The SD-values calculated by this method (Fig. 6) are determined by combining: (1) a uniformly-distributed accuracy-term ($a \pm 0.1$‰ uniform random noise) with a normally-distributed repeatability-term (a Gaussian random noise with an assumed SD = 0.1‰) for both calcite and "bulk" isotopic compositions, (2) a normal 0.5% SD on the sample carbonate proportion, and (3) a normal SD on the sample calcite and dolomite proportion as measured from MMC and XRD peaks surface determination. The calculation of error propagation reveals that the driving parameter of the SD of the calculated $\delta^{13}C_{dol}$ and $\delta^{18}O_{dol}$ is the dolomite content of the mixture. Indeed, both propagated SD on $\delta^{13}C_{dol}$ and $\delta^{18}O_{dol}$ can be accurately modelled as a negative power function of the logit (i.e. natural log of the odds) of the dolomite content (=Log $(p_D/1 - p_D)$ where $p_D \in [0.05, 0.95]$ is the dolomite content in the sample), leading to the following empirical equations (Fig. 6; mean ±1 standard-deviation estimates given for both regression parameters):

$$\delta^{13}C_{dol} : SD = (14.161 \pm 1.179) \times (5.0 + \mathrm{Logit}(p_D))^{(-2.119 \pm 0.051)},$$
$$R^2 = 0.997 (p = 1.5 \times 10^{-7})$$

and

$$\delta^{18}O_{dol} : SD = (5.7 \pm 0.536) \times (4.285 + \mathrm{Logit}(p_D))^{(-1.981 \pm 0.0635)},$$
$$R^2 = 0.995 (p = 1.7 \times 10^{-6})$$

where the additive offset-constants (5.0 and 3.95, corresponding to p_D-values of 0.67% and 1.89%, respectively) have been determined

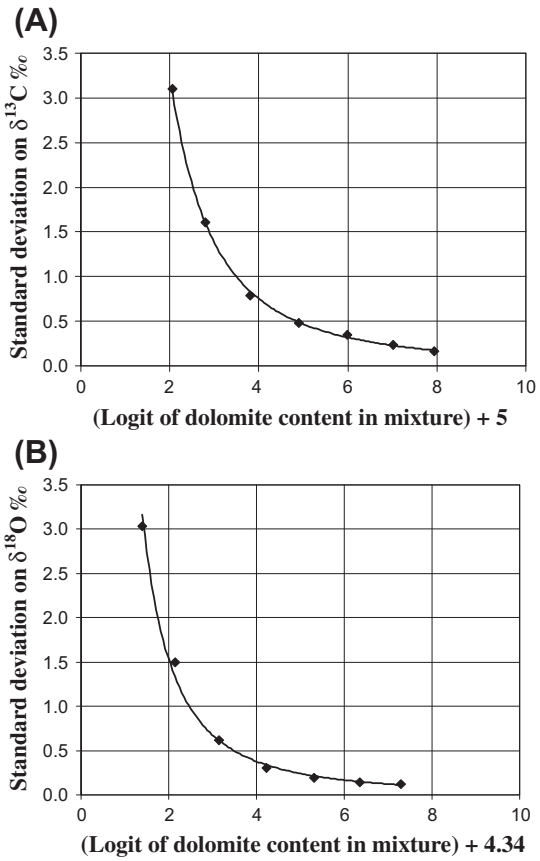

Fig. 6. Evolution of the error associated with $\delta^{13}C$ (A) and $\delta^{18}O$ (B) calculated values of dolomite as a function of the dolomite percentage in the mixture.

empirically in order to maximize the achieved correlation between the two variables, and the *p*-values test the null hypothesis of no power-relation between Logit(p_D) and SD.

The maximum computed SD (3.1‰ and 3.04‰ for $\delta^{13}C_{dol}$ and $\delta^{18}O_{dol}$, respectively) is obtained for a dolomite content of 5 wt.%. Although the model is able to predict the SD for smaller contents of dolomite, it is considered that 5 wt.% is the lower limit of applicability of this error model since the most reliable XRD detection limit was fixed at 5 wt.% (Bish and Reynolds, 1989). One parameter to mention is the comparison between operator's time needed for both automated and offline methods for carbonate isotopic analyses. For offline techniques it is estimated that, from weighing the sample to determining the isotopic ratios, 10 unknown samples can be analysed within 6 days with 3 days of 10–12 h for operator 1 to prepare the samples and 1 day for operator 2 to perform the mass spectrometer measurements in manual dual-inlet mode. As far as the semi-automated method is concerned, XRD determination has first to be considered which allows the analyses of 24 samples per day fully automated with less than 1 h per day of operator's time. Then for carbonate isotopic analyses performed with the MultiPrep system, 72 unknown samples can be analysed within 6 days with 1 h per day of one operator's time.

3.3. Comparison with the acetic acid method (AA) and the manual method (M)

3.3.1. Comparison of calcite isotopic signatures (manual method vs. this method)

Samples from the standard series were reacted off-line for 2 h at 25 °C following the method described in Al-Aasm et al. (1990), and the CO_2 derived from this reaction was considered to carry the calcite isotopic signature (Section 1). The $\delta^{13}C_{cal}$ and $\delta^{18}O_{cal}$ measured with this method were compared with the "calcite" isotopic signatures measured on the same mixtures with the new semi-automatic method (40 °C–20 min). As shown in Fig. 3, the determination of the C and O isotopic compositions of calcite with the new procedure is slightly more accurate than that obtained with the manual method. Moreover, the MultiPrep™ system is much faster as it allows preparing and analysing approximately 40 samples in 3 days, while the conventional off-line methods require approximately the same time for 10 times less samples.

3.3.2. Comparison of dolomite isotopic signatures (acetic acid method and manual method vs. this method)

The samples from the standard series described in the former section were further reacted (24 h at 50 °C after discarding the CO_2 released during 24 h at 25 °C) to obtain the "dolomite" ^{13}C and ^{18}O signatures which were compared with the calculated $\delta^{13}C$ and $\delta^{18}O$ values obtained with the present method. Despite the large SD values deduced from statistic Monte-Carlo error propagation calculation (Fig. 6), the present method yields a significantly better accuracy than the manual method for samples with low contents of dolomite (Fig. 7, Table 4). Moreover, a poor

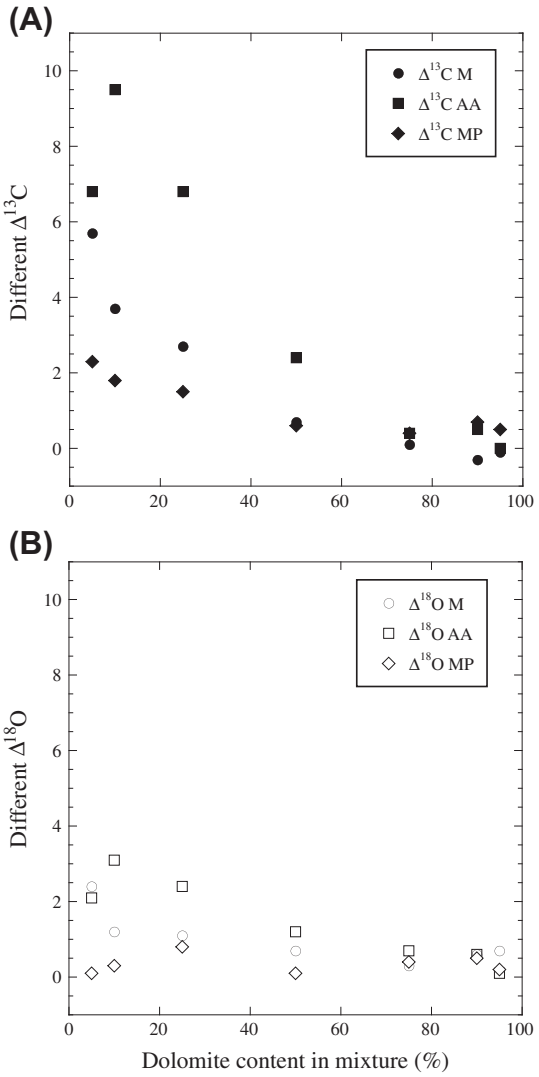

Fig. 7. Plot of $\delta^{13}C$ (A) and $\delta^{18}O$ (B) differences between real dolomite end-member isotopic signature and values determined using three methods: M = manual method (after Al-Aasm et al., 1990); AA = acetic acid method (modified after Pierre and Rouchy, 1990); MP = semi-automatic method.

Table 4
Dolomite isotopic signatures determined by the acetic acid method (Pierre and Rouchy, 1990), by the manual method (Al-Aasm et al., 1990) and by this semi-automatic method, and differences with pure dolomite end-member signature.

Cal/Dol	Manual method		Acetic acid method		This method	
	$\Delta^{13}C$ M	$\Delta^{18}O$ M	$\Delta^{13}C$ AA	$\Delta^{18}O$ AA	$\Delta^{13}C$ MP	$\Delta^{18}O$ MP
100/0	–	–	–	–	–	–
95/5	−2.2 ± 0.5	−2.4 ± 0.1	−2.1 ± 0.1	−3.3 ± 0.1	−5.6 ± 3.1	−4.7 ± 3.0
90/10	−4.2 ± 0.8	−3.6 ± 0.5	0.6 ± 0.1	−2.3 ± 0.1	−6.1 ± 1.6	−4.5 ± 1.4
75/25	−5.2 ± 0.2	−3.7 ± 0.2	−2.1 ± 0.1	−3.0 ± 0.1	−6.4 ± 0.8	−4.0 ± 0.6
50/50	−7.2 ± 0.6	−4.1 ± 0.2	−6.5 ± 0.1	−4.2 ± 0.1	−7.3 ± 0.5	−4.7 ± 0.3
25/75	−7.8 ± 0.1	−4.5 ± 0.1	−8.5 ± 0.1	−4.7 ± 0.1	−7.5 ± 0.4	−4.4 ± 0.2
10/90	−8.2 ± 0.1	−4.2 ± 0.1	−8.4 ± 0.1	−4.8 ± 0.1	−7.2 ± 0.2	−4.3 ± 0.1
5/95	−8.0 ± 0.1	−4.1 ± 0.1	−8.9 ± 0.1	−5.3 ± 0.1	−7.4 ± 0.2	−4.6 ± 0.1
0/100	−7.9 ± 0.1	−4.8 ± 0.1	−8.9 ± 0.1	−5.4 ± 0.1	−7.9 ± 0.1	−4.8 ± 0.1

repeatability in the $\delta^{13}C$ and $\delta^{18}O$ values of dolomite is noted with the manual method. This should be assigned to the step by step extraction procedure which operates out of equilibrium: indeed the first two steps of CO_2 sampling of the manual method are realised out of equilibrium for dolomite and an important kinetic fractionation occurs with partial digestion of a carbonate (as shown by Al-Aasm et al. (1990) and in Section 3.2.1).

The standard series was also treated with 1 N acetic acid for 20 min according to a protocol modified from Pierre and Rouchy (1990), Rouchy et al. (1998) and Pierre et al. (2000) (Section 2.3). As shown in Fig. 7 and Table 4, the determination of the C and O isotopic compositions of dolomite estimated with the present procedure is far more accurate than that obtained with acetic acid treatment for mixtures containing less than 50% dolomite (e.g. for a mixture with 10% of dolomite, the difference between computed $\delta^{13}C_{dol}$ and the $\delta^{13}C_{dol}$ expected for the end-member, is equal to 2 ± 2‰ with the present method vs. 9.7 ± 0.1‰ with the acetic acid method). This result must be compared to the standard deviation close to ±3‰ that was computed in Section 3.2.3 for a dolomite content of 5 wt.%. For mixtures with more than 50% of dolomite, both methods give comparable results.

The major advantage of the presented on-line method is to perform large series of small samples (300 μg) with a relative rapidity of the overall isotope determination (65 min). The main steps of the method are summarised in Fig. 8. However, it must be kept in mind that this method is mostly efficient for bi-modal samples with contrasting isotopic compositions and that contain at least 5 wt.% of dolomite. The off-line method allows the isotopic analysis of complex mineralogical matrices without limitation in sample size, however, this is a tedious and time-consuming technique (taking into account the maintenance of a vacuum system for the extraction and purification of gases) for analyzing large sample series.

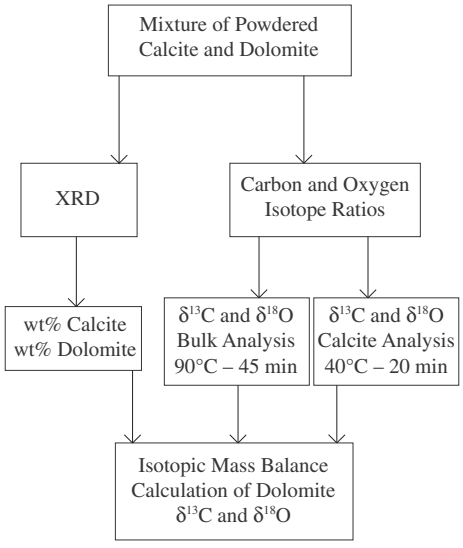

Fig. 8. Flow-chart summarising the step-by-step overview of the method to analyze calcite–dolomite mixtures in sediments.

4. Concluding remarks

The present method may allow an accurate estimation of the individual C and O isotopic compositions of calcite and dolomite present in natural mixtures of carbonates. The method relies heavily on the accurate quantification of the amounts of calcite and dolomite using X-ray diffraction. Even though the quantification procedure described in this study is adequate for artificial mixtures, a more reliable method (e.g. Rietveld refinement procedure; Mumme et al., 1996) might be preferred in some cases. It should also be kept in mind that many natural dolomites or dolomitised limestones are characterised by μm-scale intergrowths, therefore, sample crushing to produce particles which size is down to 100 μm cannot be used because it will result in composite aggregates of calcite and dolomite, which are unlikely to react in the same way as the artificial mixtures studied here. It is noteworthy that the reaction rate between dolomite and H_3PO_4 depends not only on grain size but also on the stoichiometry of the dolomite (Yui and Gong, 2003). The proposed method also shows limitations for the determination of the isotopic signature of dolomite in samples containing less than 5 wt.% dolomite. Appropriate analytical conditions need to be determined for specific groups of dolomites, the efficiency of the method is, therefore, well suited for the analysis of large sample series. It is emphasised that all isotopic measurements can be carried out using on-line methods which require smaller amounts of rock (300 μg of $CaCO_3$ vs. at least 100 mg) and short time analysis (65 min of reaction by sample vs. at least 4 days) compared with previously published off-line methods. It is considered that the present protocol can be applied to any natural sample pending some adjustments of analytical parameters to reach optimal results that depend on both physical and chemical properties of the studied rocks.

Acknowledgements

The authors thank J. Hoefs, S. Crowley, K. Huntington, B.E. Taylor and an anonymous reviewer for their constructive reviews that deeply improve the scientific quality of this study. This work was funded by the French National Research Agency (ANR) through the MICROCARB research project (Grant to GA) and by the Institut Universitaire de France (Grant to CL).

References

Al-Aasm, I.S., Taylor, B.E., South, B., 1990. Stable isotope analysis of multiple carbonates samples using selective acid extraction. Chem. Geol. 80, 119–125.

Aref, M.A.M., 1997. Evaporitic sedimentation and genesis of elemental sulphur at Um Reigha area, Red Sea Coast, Egypt. Egypt. J. Geol. 41/2A, 119–143.
Arenas, C., Alonso Zarza, A.M., Pardo, G., 1999. Dedolomitization and other early diagenetic processes in Miocene lacustrine deposits, Ebro Basin (Spain). Sed. Geol. 125, 23–45.
Bathurst, R.G.C., 1983. Carbonate sediments and their diagenesis. Developments in Sedimentology, vol. 12. Elsevier, New York, 660 pp.
Bellanca, A., Caruso, A., Ferruzza, G., Neri, R., Rouchy, J.M., Sprovieri, M., Blanc-Valleron, M.M., 2001. Transition from marine to hypersaline conditions in the Messinian Tripoli Formation from the marginal areas of the central Sicilian Basin. Sed. Geol. 140, 87–105.
Bish, D.L., Reynolds Jr., R.C., 1989. Sample preparation for X-Ray diffraction. In: Bish, D.L., Post, J.E., (Eds.), Modern Powder Diffraction. Rev. Min. Soc. Am. 20, 73–99.
Böttcher, M.E., 1996. $^{18}O/^{16}O$ and $^{13}C/^{12}C$ fractionation during the reaction of carbonates with phosphoric acid: effects of cationic substitution and reaction temperature. Isot. Environ. Health Stud. 32, 299–305.
Clayton, R.N., Jones, B.F., Berner, R.A., 1968. Isotope studies of dolomite formation under sedimentary conditions. Geochim. Cosmochim. Acta 32, 415–432.
Coplen, T.B., Kendall, C., Hoplle, J., 1983. Comparison of stable isotope reference samples. Nature 302, 236–238.
Das Sharma, S., Patil, D.J., Gopalan, K., 2002. Temperature dependence of oxygen isotope fractionation of CO2 from magnesite-phosphoric acid reaction. Geochim. Cosmochim. Acta 66, 589–593.
Degens, E.T., Epstein, S., 1964. Oxygen and carbon isotope ratios in coexisting calcites and dolomites from recent and ancient sediments. Geochim. Cosmochim. Acta 28, 23–44.
Dworkin, S.I., Nordt, L., Atchley, S., 2005. Determining terrestrial paleotemperatures using the oxygen isotopic composition of pedogenic carbonate. Earth Planet. Sci. Lett. 237, 56–68.
El Shazly, E.M., 1957. Classification of Egyptian mineral deposits. Egypt. J. Geol. 1, 1–20.
Epstein, S., Graf, D.L., Degens, E.T., 1964. Oxygen isotope studies on the origin of dolomites. In: Graig, H., Miller, S.L., Wasserburg, G.J. (Eds.), Isotopic and Cosmic Chemistry. North Holland Publishing Co., Amsterdam, pp. 169–180.
Fritz, P., Fontes, J.C., 1966. Fractionnement isotopique pendant l'attaque acide des carbonates naturels – Rôle de la granulométrie. C.R. Acad. Sci. Paris 263, 1345–1348.
Fritz, P., Smith, D.G.W., 1970. The isotopic composition of secondary dolomites. Geochim. Cosmochim. Acta 34, 1161–1173.
Müller, G., Gastner, M., 1971. The ''Karbonat-Bombe'', a simple device for the determination of the carbonate content in sediments, soils and other materials. Neues. Jahrb. Mineral. Monatsh. 10, 466–469.
Mumme, W.G., Tsambourakis, G., Madsen, I.C., Hill, R.J., 1996. Improved petrological modal analyses from X-ray powder diffraction data by use of the Rietveld method; Part II, Selected sedimentary rocks. J. Sed. Res. 66, 132–138.
Pierre, C., Rouchy, J.M., 1990. Sedimentary and diagenetic evolution of Messinian evaporites in the Tyrrhenian sea (ODP Leg 107, sites 652, 653 and 654): petrographic, mineralogical, and stable isotope records. In: Kastens K.A., Mascle J. (Eds.), Proc. Ocean Drill. Prog. Sci. Res. 107, 187–210.
Pierre, C., Rouchy, J.M., Gaudichet, A., 2000. Diagenesis in the gas hydrate sediments of the Blake Ridge: mineralogy and stable isotope compositions of the carbonate and sulfide minerals. In: Paull C.K., Matsumoto R., Wallace P.J. (Eds.), Proc. Ocean Drill. Prog. Sci. Res. 164, 139–146.
Rosenbaum, J., Sheppard, S., 1986. An isotopic study of siderites, dolomites and ankerites at high temperatures. Geochim. Cosmochim. Acta 50, 1147–1150.
Rouchy, J.M., Taberner, C., Blanc-Valleron, M.M., Sprovieri, R., Russel, M., Pierre, C., Di Stefano, E., Pueyo, J.J., Caruso, A., Dinarès-Turell, J., Gomis-Coll, E., Wolff, G.A., Cespuglio, G., Ditchfield, P., Pestrea, S., Combourieu-Nebout, N., Santisteban, C., Grimalt, J.O., 1998. Sedimentary and diagenetic markers of the restriction in a marine basin: the Lorca Basin (SE Spain) during Messinian. Sed. Geol. 121, 23–55.
Sharma, T., Clayton, R.N., 1965. Measurement of $^{18}O/^{16}O$ ratios of total oxygen from carbonates. Geochim. Cosmochim. Acta 29, 1347–1353.
Sheppard, S.M.F., Schwarcz, H.P., 1970. Fractionation of carbon and oxygen isotopes and magnesium between coexisting calcite and dolomite in metamorphic rocks. Contrib. Mineral. Petrol. 26, 161–198.
Swart, J.K., Burns, S.J., Leder, J.J., 1991. Fractionation of the stable isotopes of oxygen and carbon in carbon dioxide during the reaction of calcite with phosphoric acid as a function of temperature and technique. Chem. Geol. 86, 89–96.
Walters, L.J., Claypool, G.E., Choquette, P., 1972. Reaction rates and ^{18}O variation for carbonate-phosphoric acid preparation method. Geochim. Cosmochim. Acta 36, 129–140.
Yui, T.-F., Gong, S.-Y., 2003. Stoichiometry effect on stable isotope analysis of dolomite. Chem. Geol. 201, 359–368.

Carbon and oxygen isotope variability among foraminifera and ostracod carbonated shells

François Fourel[a,*], François Martineau[a], Christophe Lécuyer[a,#], Emoke Tóth [b], Agnes Görög[b], Gilles Escarguel[a] and Keith Hall[c]

[a] Laboratoire CNRS UMR 5125 "Paléoenvironnements & Paléobiosphère", Université Lyon 1, Campus de la Doua, F-69622 Villeurbanne, France.

[b] Department of Paleontology, University of Budapest, PO box 120, H-1518, Budapest, Hungary.

[c] Hall Analytical, Millbrook business centre, Floats Road Manchester, M23 9YG, United Kingdom.

also at Institut Universitaire de France

* corresponding author: francois.fourel@univ-lyon1.fr

Keywords: stable isotope, foraminifera, ostracod, heterogeneity, single shell analysis

Abstract – This study investigates the effect of biological and environmental inter-individual variability on the meaning of $\delta^{18}O$ and $\delta^{13}C$ values acquired on small carbonated shells. First we present data obtained with a MultiPrep automated carbonate system on small sample sizes of a homogeneous carbonate material: Carrara marble. This demonstrates the capacities of the analytical system to reliably run small amounts of carbonates even down to 10 µg. Then we present two data sets obtained on real fossil samples of various size (*sensu* number of individual organisms) calibrated against the NBS19 carbonate standard. Both datasets evidence a clear trend of between-biological sample standard deviation increase for both $\delta^{18}O$ and $\delta^{13}C$ measurements when the number of pooled specimens per sample decreases. According to the results obtained from a systematic study of a geologically homogeneous sample of coeval fossil *Elphidium* foraminifera, we estimate that there is 95% of chances to reach between-biological sample standard deviation values higher than 1.02‰ ($\delta^{18}O$) and 1.45‰ $\delta^{13}C$) based on single-cell measurements. Such values are one order of magnitude higher than the instrumental standard deviations associated with these stable isotope ratios. Conversely, a minimum of 35 ($\delta^{18}O$) and 44 ($\delta^{13}C$) pooled specimens of *Elphidium* appears necessary to reach a between-sample standard deviation ≤ 0.25‰ with a probability of 95%. Such biological intrinsic and irreducible variability between coeval individuals, and thus samples, clearly questions the interest for single-cell analyses, especially for paleoceanographic or paleoclimatic reconstruction purposes where secular oxygen and carbon isotope variations typically range between 0.5 and 1.5‰.

47 **1 – Introduction**

48

49 Stable oxygen isotope measurements of carbonated fossil shells were the pioneering
50 studies for determining the temperatures of past seawater (Urey, 1947; McRea, 1950; Epstein
51 et al., 1953). Many carbonate–secreting marine organisms are confined to marine platform
52 settings. Such environments are highly influenced by continental runoff and coastal oceanic
53 currents ultimately affecting, e.g., the depth gradients of temperature and salinity, and
54 photocline and nutricline depths. Coccoliths constitute a large fraction of the oceanic
55 nannoplankton since the Early Jurassic but their very small size (a few μm) still makes
56 difficult the isotopic analysis of fossils at the species, or at least genus level (but see, e.g.,
57 Stoll and Ziveri, 2002; Stoll and Shimizu, 2009; Fink et al., 2010). Foraminifera are also
58 unicellular organisms which size classically ranges from 40 μm up to ~1 mm; they appeared
59 during the early Paleozoic but benthic and planktonic forms invaded the deep and surface
60 oceans since the Cretaceous (Roth, 1989). The carbon and oxygen isotope compositions of
61 their shells have been widely used to reconstruct marine paleoproductivity and
62 paleotemperatures. For example, Shackleton (1967; 1986), Shackleton and Opdyke (1973)
63 and Shackleton et al. (1983) revealed the existence of a first–order long–term cooling of
64 Earth's surface since the Paleocene as well as the periodicity of the Quaternary
65 glacial-interglacial stages. Huber et al. (1995; 2002), Schmidt and Mysak (1996) and Jenkyns
66 et al. (2004) showed that the Cretaceous oceans about 100 My ago were much warmer than
67 today, especially at high latitudes in the absence of permanent polar ice caps. The occurrence
68 of foraminifera above and below the thermocline as well as from low to high latitudes led
69 many researchers to use their stable isotope compositions combined to Mg/Ca ratios as
70 proxies for both thermal structure of the oceans and volume of freshwater ice stored on the
71 continents (e.g. Billups and Schrag, 2003; Lea et al., 2006).

In the past two decades, increase in the sensitivity of dual-inlet isotope ratio mass spectrometers and their coupling to automated on–line preparation devices allowed the analysis of very small amounts of calcium carbonate, down to the 5–10 μg level. This instrumental improvement opened the field of analysis of single carbonate-secreting unicellular organisms such as foraminifera with weights ranging from a few tenths to hundreds micrograms for most of them. Consequently, many workers established carbon and oxygen isotopic seawater curves based on such single shell analysis techniques (e.g. Kelly et al., 1996; Price et al., 1998; Zachos et al., 2007). Nevertheless, inter-individual isotopic variability for both C and O has already been documented (Shuxi and Shackleton, 1990; Billups and Spero, 1995; Saraswati, 2004) and cannot be reduced only to analytical and instrumental accuracy. However, no convincing demonstration was made so far for identifying the environmental (temperature, $\delta^{18}O$ of water, productivity and $\delta^{13}O$ of DIC) and biological (physiology and phylogeny) drivers responsible for such isotopic differences between analyzed specimens. The knowledge of the amplitude of the inter-individual oxygen isotope variability is critical considering that most short- and long-term changes in the mean annual or seasonal temperature of surface waters did not exceed 5°C against up to 15°C for deep waters during the Phanerozoic (e.g. Shackleton, 1986; Zachos et al., 2001; 2003; Pucéat et al., 2003; Joachimski et al., 2009). Indeed, the slope of the oxygen isotope fractionation equation between calcium carbonate and water is slightly higher than 4, hence corresponding to the temperature amplitude recorded by 1‰ change in the $\delta^{18}O$ value of any aquatic carbonated shell. On the other hand, short-term changes in productivity as well as long-term variations in oxidation or burial of sedimentary organic matter typically produce variations of ±3‰ in the carbon isotope composition of seawater (Schidlowski, 1987).

Consequently, the aim of this study is to explore the amplitude of both carbon and oxygen isotopic variability as a function of sample size (i.e., number of individual shells

97 pooled in a sample). Selected targets were benthic foraminifera (*Elphidium* and *Ammonia*)
98 and ostracods (*Aurila*) since they have been extensively used for paleoenvironmental
99 reconstructions of aquatic environments (Holmes, 1996; Bauch et al., 2004).
100
101 **2 – Material and methods**
102
103 *2.1 Sample origin*
104
105 The studied fossil samples are derived from Sarmatian (Middle Miocene, 12.8-11.5
106 Ma) deposits of three boreholes (Perbál-5, Mány-17 and Mány-22) in the Zsámbék Basin,
107 Hungary that is located in the central part of the Pannonian Basin (Fig. 1 and 2). The lithology
108 of the Sarmatian deposits is heterogeneous: clays, clay marls, calcareous marls, sandstones
109 and limestones. The Sarmatian sequences are underlain by Badenian strata and overlain by
110 Pannonian or Pleistocene sediments.
111 For the analyses, very well preserved calcitic shells of foraminifera (*Elphidium*
112 *aculeatum, E. macellum* and *Ammonia beccarii*) and ostracods (*Aurila mehesi* and *A. notata*)
113 were selected (Fig. 3; see Görög (1992) and Tóth (2008) for detailed systematic descriptions
114 of the studied species). The fossil shells are derived from 102 layers of the boreholes (Fig. 2).
115
116 *2.2 Sample treatment*
117
118 For each core sample and both C and O investigations, about 100 g of air-dried
119 sediment was soaked in a dilute solution of hydrogen peroxide and then washed over a
120 column of sieves of diminishing mesh sizes to extract the carbonated shells (foraminifera and
121 ostracods). Then the shells were cleaned three times with deionized water in a ultrasonic bath

122 to remove the sedimentary matrix, and finally hand-picked under a stereomicroscope. In all
123 samples, the calcitic shells of foraminifera and ostracods preserved their original crystal
124 structure as it was proved by X-ray diffraction data (Tóth et al., 2010), therefore precluding
125 any diagenetic alteration of the pristine carbon and oxygen isotope compositions of the
126 studied fossils.
127
128 *2.3 Isotope ratio measurement*
129
130 Carbon and oxygen isotope ratio measurements have been performed with a MultiPrep
131 system on line with a dual Inlet IsoPrime™ Isotope Ratio Mass Spectrometer (IRMS). The
132 principle of the fully automated device is to react the calcium carbonates with anhydrous
133 phosphoric acid at 90°C to generate CO_2 according to the following acid–base reaction:
134 $CaCO_3 + H_3PO_4 \rightarrow CaHPO_4 + CO_2 + H_2O$.
135 Each sample is carefully ground into a powder with grain sizes around 200 μm. Then
136 the sample aliquot (typically 200-300 μg) is placed at the bottom of a V shape vial which is
137 then sealed with a rubber septum. The sample vials are then placed in a temperature regulated
138 sample tray heated at 90°C. From this stage all the sample preparation is done automatically.
139 The MultiPrep system is equipped with a double hole needle which allows the acid to be
140 delivered in the vial and also to extract the CO_2 which has been generated during the reaction.
141 First the vial is evacuated through the external needle connected to the MultiPrep vacuum
142 system. Then phosphoric acid is admitted in the vial through the inner needle using the acid
143 pump. At this stage the reaction starts and CO_2 is generated. The reaction time is 20 min and
144 during all this time the needle remains inside the valve. The external cold finger is maintained
145 at -165°C and the valve arrangement allows the CO_2 generated from the reaction to be
146 constantly extracted and trapped in the external cold finger. Once the reaction is completed

147 the external cold finger is heated at -70°C to release the CO_2 without releasing water. The
148 CO_2 pressure is read with a transducer located on the sample side of the IRMS Dual Inlet and
149 from this pressure reading the sample analysis strategy is decided. If the sample is big enough
150 it will be loaded in the dual inlet sample bellow and analyzed. If the sample is too small, it
151 will be trapped in the Dual Inlet cold finger and analyzed.
152
153 **3 – Results**
154
155 *3.1 – Background instrumental uncertainty*
156
157 Determination of the instrumental noise is a prerequisite to any quantification of the
158 carbon and oxygen isotopic variability between biological samples as a function of the
159 number of analyzed individuals per sample. Therefore three sets of measurements have been
160 performed on the international standard NBS–19 and an internal standard (Carrara Marble).
161 Both were routinely measured on a daily basis over 2 months. Instrumental standard
162 deviations associated with $\delta^{18}O$ and $\delta^{13}C$ measurements of "large" aliquots (~300 μg) of both
163 NBS–19 and Carrara marble are of 0.062‰ and 0.022‰ (NBS–19, n=49) (Table 1; Figure 4),
164 and of 0.069‰ and 0.036‰ (Carrara marble, n=30) (Table 2; Figure 5), respectively. These
165 comparable results allow concluding that both calcium carbonate matrices have the same
166 degree of isotopic homogeneity, and that the Carrara marble can be consequently used instead
167 of NBS–19 in order to evaluate the standard deviations associated with measurements of
168 natural samples of varying size.
169 Consequently, $\delta^{18}O$ and $\delta^{13}C$ standard deviations corresponding to the background
170 instrumental noise have been further estimated for a series of Carrara marble aliquots of
171 varying weight from 10 to 380 μg; the 29 performed measurements reveal that average

instrumental standard deviations associated with $\delta^{18}O$ and $\delta^{13}C$ are of 0.133‰ and 0.057‰, respectively (Table 3; Figure 6). It is worth noting here that the average instrumental standard deviations estimated for aliquots ranging from 10 to 60 μg (0.155‰ for $\delta^{18}O$, and 0.067‰ for $\delta^{13}C$) were larger than those obtained for aliquots ranging from 110 to 380 μg (0.093‰ for $\delta^{18}O$ and 0.035‰ for $\delta^{13}C$), illustrating the expected increase in instrumental uncertainty with decreasing quantity of analyzed material (Figure 6).

3.2 Inter-individual biological variability

Taking into account this background instrumental uncertainty, the following hypothesis was tested with natural microfossil samples of foraminifera (*Elphidium*; n=51 and *Ammonia*; n=16) and ostracods (*Aurila*; n=34): for a given sample weight, the between-biological sample isotopic variability should be independent on the number of individuals pooled in each analyzed sample. Table 4 and Figure 7 show that between-biological sample standard deviations related to $\delta^{18}O$ and $\delta^{13}C$ average empirical values increase up to 0.7‰ ($\delta^{18}O$) and 0.85‰ ($\delta^{13}C$) with the number of individuals decreasing most values being larger than the background instrumental standard deviations. Data were non-linearly least–square fitted with a power law, assuming that the standard deviation tends towards infinite values when the number of individuals per sample tends towards zero, whilst it should tend towards the background instrumental noise, i.e. the standard deviation defined by either large samples of NBS–19 or Carrara marble, when the number of individuals per sample becomes very large.

The quality of the fit being so weak when considering all three genera from various sample levels simultaneously (due to inter-sample and between-taxon isotopic differences), this approach was restricted to a taxonomically homogeneous pool of *Elphidium* foraminifera

197 extracted from the same, *Elphidium*-rich sample level from the Mány-17 borehole (Fig. 2),
198 from which sub–samples composed of 5, 10, 20, 30 and 40 individual shells (corresponding to
199 samples from 50 to 900 μg) were generated by randomly picking–up the fossils under a
200 stereomicroscope. Single-cell samples were not considered here due to their very small
201 weight (average individual shell weight: 16.5 ± 3.8 μg), involving relatively high associated
202 instrumental uncertainty when compared to the 5 to 40-cell samples, and thus biasing upward
203 the estimate of inter-biological sample variability effects. For each sub–sample size, four
204 distinct sub-samples have been made, allowing the computation of a between-biological
205 sample standard deviation (Table 5). Figure 8 shows that this standard deviation increases
206 with the number of individuals decreasing according to the following power laws (including
207 an additive constant which corresponds to the background instrumental standard deviation – a
208 value reached asymptotically when analyzing an "infinite" pool of individuals):
209
210 $$\text{SD of } \delta^{18}O = 0.133 + 34.268.N^{-2.485},\ R^2 = 0.83\ (p = 8.9.10^{-2})$$
211 $$\text{SD of } \delta^{13}C = 0.057 + 2.748.N^{-0.829},\ R^2 = 0.92\ (p = 9.8.10^{-3})$$
212
213 Where N is the number of individuals in the sample. According to the prediction
214 confidence interval belts associated to these equations, there is a probability of 95% (lower
215 bound of the 90% C.I. belt) to obtain between-biological sample standard deviations higher
216 than 1.02‰ and 1.45‰ for different $\delta^{18}O$ and $\delta^{13}C$ measurements of single specimens of
217 *Elphidium*, respectively. Such predicted inter-individual variability is about one order of
218 magnitude higher than the background instrumental uncertainty, indicating that a significant
219 amount of variability of eco-physiological origin is added when considering biological
220 organisms such as foraminifera.
221

4- Discussion

Isotopic studies of carbonated skeletons cannot escape the question of a possible diagenetic alteration that may potentially modify their pristine compositions. Selected foraminifera and ostracod samples from the Miocene deposits of Hungary have been already evaluated for their state of preservation as attested by the quality of their ultrastructure imaged by SEM techniques (Tóth et al., 2010). However, no definitive criterion is available in order to discard unambiguously alteration processes responsible for sizable changes in the post-depositional compositions of carbonated fossils. Nevertheless, on the basis of mass balance considerations, one can expect two isotopic patterns of water–mineral interactions that could operate within sedimentary deposits. The first one is the production of homogenized isotopic compositions of fossils in response to large volumes of aqueous fluids interacting with the hosting sediment; the second one, driven by low water–mineral ratios, should produce isotopic heterogeneities without any relation to the sample size (i.e., number of sampled individuals). These two scenari do not match the observed distribution of isotopic compositions in studied foraminifera and ostracod shells.

Carbon and oxygen isotope compositions of the studied carbonated fossil shells show unambiguously that empirical between-biological sample variability associated with $\delta^{18}O$ and $\delta^{13}C$ largely exceeds the background instrumental uncertainty and clearly relates to inter-individual variability (Fig. 7 and 8). This result clearly impacts interpretation of variations in both $\delta^{18}O$ and $\delta^{13}C$ values of marine carbonated microfossils as indicators of changing in ambient seawater temperature and productivity.

Indeed, in order to be able to detect subtle variations in seawater temperature based on $\delta^{18}O$ values, a minimum of 35 pooled specimens of *Elphidium* is necessary to reach a between-sample standard deviation $\leq 0.25‰$ with a probability of 95%, corresponding to an

247 estimated temperature uncertainty ≤ ±2°C at a 95% confidence level (Fig. 8). The analysis of
248 less than 3 pooled individual shells returns standard deviation values ≥ 0.25‰ in more than
249 95% of the sample cases, a value exceeding 1‰ (corresponding to an actual seawater
250 estimated temperature uncertainty of ±8°C at a 95% confidence level) when a single specimen
251 of *Elphidium* is analyzed. In such cases of large uncertainty, the detection of thermal events
252 such as changes in oceanic circulation or climatic events recorded by surface waters (whose
253 amplitudes rarely exceed 5°C as documented since the Mesozoic; Shackleton, 1986; Norris
254 and Röhl, 1999; Lécuyer et al., 2003; Pucéat et al., 2003; Joachimski et al., 2009) obviously
255 becomes problematic, if not impossible. The oxygen isotope composition of benthic
256 foraminifera such as *Elphidium* has been also extensively used as a proxy of variations in the
257 $\delta^{18}O$ of seawater as a consequence of changes in the continental ice volume. Once again, this
258 threshold of ~1‰ associated with the analysis of a single foraminifera shell constitutes a
259 "biological isotopic noise" in the same order of magnitude as the variation in the $\delta^{18}O$ of the
260 oceans resulting from ice cap growth during a glacial stage or a complete melting of existing
261 ice caps during a greenhouse interlude (Shackleton and Kennett, 1975; Billups and Schrag,
262 2003; Pekar and DeConto, 2006.

263 Concerning carbon isotope measurements, a minimum of 15 and 44 *elphidium*
264 individuals is required in order to reach between-sample standard deviations ≤ 0.5‰ and
265 ≤ 0.25‰, respectively (Fig. 8). The carbon isotope analysis of a single specimen generates a
266 standard deviation ≥ 1.45‰ in 95% of the sample cases; such threshold is comparable to
267 secular changes in the $\delta^{13}C$ values recorded in the marine carbonate deposits which are
268 interpreted either as variations in the primary production at time scales of about 50,000 yr, or
269 variations in the burial or oxidation rates of sedimentary organic matter at time scales of about
270 1 Myr (e.g. Magaritz et al., 1992; Kump and Arthur, 1999). However, this between-sample
271 standard deviation predicted for a single specimen analysis in a homogeneous taxonomical

and environmental/climatic context is significantly lower than some spectacular carbon isotope excursions recorded in sediments and which were interpreted as related to extreme events such as food chain rupture, volcanic paroxysm and large methane release by clathrates (e.g. Röhl et al., 2000; Pálfy et al., 2001; Hesselbo et al., 2002).

Contrasting the two relations inferred for $\delta^{18}O$ and $\delta^{13}C$, it is worth noting that the average observed values of inter-biological sample standard deviation in the 5-40 specimens and 50-900 μg sample weight ranges are slightly higher for $\delta^{13}C$ than for $\delta^{18}O$ measurements. Actually, based on the instrumental standard deviations as evidenced above, one should expect the reverse situation if such inter-biological sample standard deviations were the consequence of an analytical fractionation due to the instrument (the average instrumental error is ~2.3 times larger for $\delta^{18}O$ than for $\delta^{13}C$ based on 29 Carrara marble aliquots). Indeed, such result clearly points to the fact that the inter-biological sample variability evidenced here does originate in an inter-individual natural heterogeneity (i.e., biological variability) rather than in an instrumental fractionation spurious analytical effect.

Inter-individual $\delta^{18}O$ and $\delta^{13}C$ variations as evidenced here between specimens from the same foraminifera genus and fossil level are most likely resulting from eco-physiological intrinsic differences in metabolism (e.g., individual position within the autotrophy-heterotrophy gradient) and environmental conditions (e.g., depth–related changes in temperature and luminosity, and composition of dissolved inorganic carbon). In addition, such irreducible biological variability could be strongly, but artefactually enhanced by cryptic biological speciation events as increasingly evidenced in marine, planktic as well as benthic organisms (Knowlton, 1993; de Vargas et al., 1999, 2004; Irigoien et al., 2004; Chen and Hare, 2008; Darling and Wade, 2008). An efficient way to further exploring such possibility should be to independently perform the kind of analysis leading to Figure 8 on distinct morphological species showing contrasted cryptic diversity contexts (the higher the cryptic

297 diversity, the steeper the decreasing slope of the number of individuals *vs*. between-sample
298 standard deviation relation should be). The ongoing effort in developing morphometrical
299 recognition models of cryptic species (e.g., Morard et al. 2009) should allow solving this
300 problem in the future.
301
302 **5- Conclusion**
303
304 We have demonstrated in this paper that recent automated systems designed for the
305 analyses of $\delta^{13}C$ and $\delta^{18}O$ from carbonate samples are capable of measuring reliably small
306 quantities of pure calcite down to 5-10 µg with instrumental standard deviations close to
307 0.1‰. Such analytical accuracy opens up possibilities for the analysis of small microfossils
308 like foraminifera, especially for paleoclimate reconstruction purposes. Nevertheless, data
309 generated from small numbers of specimens (e.g., carbonated shells from single-cell
310 organisms) have to be considered with great caution. Indeed, our results show a general trend
311 to increase the between-biological sample standard deviation for both ^{13}C and ^{18}O
312 measurements when decreasing the number of specimen analysed. Based on a systematic
313 study performed on a homogeneous pool of *Elphidium* foraminifera, we estimate that there is
314 a probability of 95% to obtain between-biological sample standard deviations higher than
315 1.02‰ and 1.45‰ for $\delta^{18}O$ and $\delta^{13}C$ measurements of various single shells, respectively.
316 Such biological intrinsic and irreducible variability observed between coeval samples
317 clearly questions the interest for single-cell analyses. For instance, paleotemperature estimates
318 should not be done on single foraminifera $\delta^{18}O$ measurements.
319

320 **References**

321
322

323 Bauch, H.A., Erlenkeuser, H., Bauch, D., Mueller-Lupp, T., Taldenkova E., 2004. Stable
324 oxygen and carbon isotopes in modern benthic foraminifera from the Laptev Sea shelf:
325 implications for reconstructing proglacial and prof luvial environments in the Arctic.
326 Mar. Micropal. 5, 285–300.

327 Billups, K., Schrag D.P., 2003. Paleotemperatures and ice volume of the past 27 Myr revisited
328 with paired Mg/Ca and $^{18}O/^{16}O$ measurements on benthic foraminifera.
329 Paleoceanography 17(1), 1003, doi: 10.1029/2000PA000567.

330 Billups, K., Spero H.J. 1995. Relationship between shell size, thickness and stable isotopes in
331 individual planktonic foraminífera from two equatorial Atlantic cores. J. Foram. Res.
332 25, 24–37.

333 Chen, G., Hare, M.P., 2008. Cryptic ecological diversification of a planktonic estuarine
334 copepod, *Acartia tonsa*. Molecul. Ecol. 17, 1451–1468.

335 Darling, K.F., Wade, C.M., 2008. The genetic diversity of planktic foraminifera and the
336 global distribution of ribosomal RNA genotypes. Mar. Micropal. 67, 216–238.

337 Epstein, S., Buchsbaum, R., Lowenstam, H.A., Urey, H.C., 1953. Revised carbonate–water
338 isotopic temperature scale. Geol. Soc. Am. Bull. 64, 1315–1326.

339 Fink, C., Baumann, K.-H., Groeneveld, J., Steinke, S., 2010. Strontium/Calcium ratio, carbon
340 and oxygen stable isotopes in coccolith carbonate from different grain-size fractions in
341 South Atlantic surface sediments. Geobios, in press.

342 Görög, A., 1992. Sarmatian foraminifera of the Zsámbék Basin, Hungary. Annales
343 Universitatis Scientiarum Budapestinensis, sectio Geologica 29, 31–153.

344 Hesselbo, S.P., Robinson, S.A., Surlyk, F., Piasecki, S., 2002. Terrestrial and marine
345 extinction at the Triassic-Jurassic boundary synchronized with major carbon-cycle
346 perturbation: A link to initiation of massive volcanism? Geology 30, 251–254.

347 Holmes, J.A., 1996. Trace-element and stable-isotope geochemistry of non-marine ostracod
348 shells in Quaternary palaeoenvironmental reconstruction. J. Paleolimnol. 15, 223–235.

349 Huber, B.T., Norris, R.D., Macleod, K.G., 2002. Deep–sea paleotemperature record of
350 extreme warmth during the Cretaceous. Geology 30, 123–126.
351 Huber, B.T., Hodell, D.A., Hamilton, C.P., 1995. Mid- to Late Cretaceous climate of the
352 southern high latitudes: stable isotopic evidence for minimal equator-to-pole thermal
353 gradients. Geol. Soc. Am. Bull. 107, 1164–1191.
354 Irigoien, X., Huisman, J., Harris, R.P., 2004. Global biodiversity patterns of marine
355 phytoplankton and zooplankton. Nature 429, 863–867.
356 Jenkyns, H.C., Forster, A., Schouten, S., Damsté, J.S.S., 2004. High temperatures in the Late
357 Cretaceous Artic Ocean. Nature 432, 888–892.
358 Joachimski, M.M., Breisig, S., Buggisch, W., Talent, J.A., Mawson, R., Gereke, M., Morrow,
359 J.M., Day, J., Weddige, K., 2009. Devonian climate and reef evolution: insights from
360 oxygen isotopes in apatite. Earth. Planet. Sci. Lett. 284, 599-609.
361 Kelly, D.C., Bralower, T.J., Zachos, J.C., Silva, I.P., Thomas, E., 1996. Rapid diversification
362 of planktonic foraminífera in the tropical Pacific (ODP site 865) during the Late
363 Paleocene thermal maximum. Geology 24, 423–4126.
364 Knowlton, N., 1993. Sibling species in the sea. Ann. Rev. Ecol. Syst. 24, 189–216.
365 Kump, L.R., Arthur M.A., 1999. Interpreting carbon-isotope excursions: carbonates and
366 organic matter. Chem. Geol. 161, 181–198.

Lea, D.W., Pak, D.K., Belanger, C.L., Spero, H.J., Hall, M.A., Shackleton, N.J., 2006. Paleoclimate history of Galapagos surface waters over the last 135,000 yr. Quat. Sci. Rev. 25, 1152–1167.

Lécuyer, C., Picard, S., Garcia, J.-P., Sheppard, S.M.F., Grandjean, P., Dromart, G., 2003. Thermal evolution of Tethyan surface waters during the Midle-Late Jurassic: Evidence from $\delta^{18}O$ values of marine fish teeth. Paleoceanography 18(3), 1076, doi:10.1029/2002PA000863.

Magaritz, M., Krishnamurthy, R.V., Holser, W.T., 1992. Parallel trends in organic and inorganic carbon isotopes across the Permian/Triassic boundary. Am. J. Sci. 292, 727–739.

McRea, J.M.,,1950. On the isotopic chemistry of carbonates and a paleotemperature scale. J. Chem. Phys. 18, 849–857.

Morard, R., Quillévéré, F., Escarguel, G., Ujiie, Y., de Garidel-Thoron, T., Norris, R.D., de Vargas C., 2009. Morphological recognition of cryptic species in the planktonic foraminifer *Orbulina universa*. Mar. Micropal. 71, 148–165.

Norris, R.D., Röhl, U., 1999. Carbon cycling and chronology of climate warming during the Palaeocene/Eocene transition, Nature 401, 775–778.

Pálfy, J., Demény, A., Haas, J., Hetényi, M., Orchard, M., Veto, I., 2001. Carbon isotope anomaly and other geochemical changes at the Triassic-Jurassic boundary from a marine section in Hungary. Geology 29, 1047–1050.

Pekar, S.F., DeConto, R.M., 2006. High-resolution ice-volume estimates for the early Miocene: Evidence for a dynamic ice sheet in Antarctica. Palaeogeogr. Palaeoclimatol. Palaeoecol. 231, 101–109.

390 Price, G.D., Sellwood, B.W., Corfield, R.M., Clarke, L., Cartlidge J.E., 1998. Isotopic
391 evidence for palaeotemperatures and depth stratification of Middle Cretaceous
392 planktonic foraminífera from the Pacific Ocean. Geol. Mag. 135, 183–191.
393 Pucéat, E., Lécuyer, C., Sheppard, S.M.F., Dromart, G., Reboulet, S., Grandjean, P., 2003.
394 Thermal evolution of Cretaceous Tethyan marine waters inferred from oxygen isotope
395 composition of fish tooth enamels. Paleoceanography 18(2), 1029,
396 doi:10.1029/2002PA000823.

397 Röhl U., Bralower, T.J., Norris, R.D., Wefer, G., 2000. New chronology for the late
398 Paleocene thermal maximum and its environmental implications. Geology 28, 927–930.

399 Roth, P. H., 1989. Ocean circulation and calcareous nannoplankton evolution during the
400 Jurassic and Cretaceous. Palaeogeogr. Palaeoclimatol. Palaeoecol. 74, 111– 126.
401 Saraswati, P.K., 2004. Ontogenetic isotopic variation in foraminífera – Implications for
402 palaeo prox. Current Science 86, 858–860.
403 Schidlowski, M., 1987. Application of stable isotopes to early biochemical evolution on
404 Earth. Annu. Rev. Earth. Planet. Sci. 15: 47–72.
405 Schmidt, G.A., Mysak, L.A., 1996. Can increased poleward oceanic heat flux explain the
406 warm Cretaceous climate? Paleoceanography 11, 579–593.
407 Shackleton, N. J., Opdyke, N.D., 1973. Oxygen isotope and paleomagnetic stratigraphy of
408 equatorial Pacific core V28-2389: oxygen isotopes temperatures and ice volumes on a
409 10^5 and 10^6 year scale. Quat. Res. 3, 39–55.
410 Shackleton, N.J., 1967. Oxygen isotope analyses and Pleistocene temperatures reassessed.
411 Nature 215, 15–17.
412 Shackleton, N.J., 1986. Paleogene stable isotope events. Palaeogeogr. Palaeoclimatol.
413 Palaeoecolol. 57, 91–102.

414 Shackleton, N.J., Imbrie, J, Hall, M.A., 1983. Oxygen and carbon isotope record of East
415 Pacific core V19-30: Implications for the formation of deep water in the late
416 Pleistocene North Atlantic. Earth Planet. Sci. Lett. 65, 233–244.

417 Shackleton, N. J., 1986. Paleogene stable isotope events. Palaeogeogr. Palaeoclimatol.
418 Palaeoecolol. 57, 91–102.

419 Shackleton, N.J., Kennett, J.P., 1975. Paleotemperature history of the Cenozoic and initiation
420 of Antarctic glaciation: oxygen and carbon isotopic analyses in DSDP Sites 277, 279,
421 and 281. Init. Rep. Deep Sea Drill. Proj. 29, 743–755.

422 Shuxi, C., Shackleton, N.L., 1990. New technique for study on isotopic fractionation between
423 sea water and foraminiferal growing processes. Chin. J. Ocean. Limnol. 8, 299–305.

424 Stoll, H.M., Shimizu, N., 2009. Micropicking of nannofossils in preparation for analysis by
425 secondary ion mass spectrometry. Nature Protocol 4, 1038–1043.

426 Stoll, H.M., Ziveri, P., 2002. Separation of monospecific and restricted coccolith assemblages
427 from sediments using differential settling velocity. Mar. Micropal. 46, 209–221.

428 Tóth, E., 2008. Sarmatian (Middle Miocene) ostracod fauna from the Zsámbék Basin,
429 Hungary. Geol. Pann. 36, 101–51.

430 Tóth, E., Görög, A., Lécuyer, C., Moissette, P., Balter, V., Monostori, M., 2010.
431 Palaeoenvironmental reconstruction of the Sarmatian (Middle Miocene) Central
432 Paratethys based on palaeontological and geochemical analyses of foraminifera,
433 ostracods, gastropods and rodents. Geol. Mag. 147, 299–314.

434 Urey, H.C., 1947. The thermodynamic properties of isotopic substances. J. Chem. Soc.
435 London 1947, 562–587.

436 Vargas (de), C., Norris, R., Zaninetti, L., Gibb, S.W., Pawlowski J., 1999. Molecular evidence
437 of cryptic speciation in planktonic foraminifers and their relation to oceanic provinces.

Proc. Nat. Acad. Sci. U.S. 96, 2864–2868.

Vargas (de), C., Sáez, A.G., Medlin, L.K., Thierstein, H.R., 2004. Superspecies in the calcareous plankton. In: Thierstein, H.R., Young, J. (Eds.), Coccolithophores — from Molecular Processes to Global Impact. Springer-Verlag, Heidelberg, Germany, pp. 271–298.

Zachos, J.C., Bohaty, S.M., John, C.M., McCarren, H., Kelly, D.C., Nielsen, T., 2007. The Palaeocene–Eocene carbon isotope excursion: constraints from individual shell planktonic foraminifer records. Phil. Trans. R. Soc. 365, 1829–1842.

Zachos, J.C., Pagani, M., Sloan, L., Thomas, E., Billups, K. 2001. Trends, rhythms, and aberrations in global climate 65 Ma to Present. Science 292, 686–693.

Zachos, J.C., Wara, M.W., Bohaty, S.M., Delaney, M.L., Rose-Petrizzo, M., Brill, A., Bralower, T.J., Premoli-Silva, I., 2003. A transient rise in tropical sea surface temperature during the Paleocene-Eocene Thermal Maximum. Science 302, 1551–1554.

Tables:

Table 1: Carbon and oxygen isotope compositions of NBS19 aliquots over a period of six months. Sample weights vary from 280 to 390 μg. N.a.: not applicable (in case where only one measurement was performed).

Table 2: Carbon and oxygen isotope compositions of Carrara marble aliquots over a period of six months. Sample weights vary from 100 to 350 μg.

Table 3: Carbon and oxygen isotope compositions of Carrara marble aliquots which sample sizes range from 10 to 380 μg.

Table 4: Carbon and oxygen isotope compositions of Sarmatian foraminifera (*Elphidium*, *Ammonia)* and ostracod (*Aurila)* samples. Standard deviations were calculated from two replicates of each sample.

Table 5: Variations in carbon and oxygen isotope compositions of randomly generated sub–samples of Sarmatian *Elphidium* macellum from a homogeneous pool of *Elphidium* foraminifera extracted from the level 118.9 – 119.1m (samples M17-10 to M17-14) of Mány-17 borehole, Hungary.

Figures:

Figure 1: Geographical location of the studied fossils that were sampled from the Sarmatian (Middle Miocene, 12.8-11.5 Ma) deposits of three boreholes (Perbál-5, Mány-17 and Mány-22) in the Zsámbék Basin, Hungary.

Figure 2: Lithostratigraphic Sarmatian successions in the three boreholes and location of foraminifera and ostracod samples.

Figure 3: Foraminifera and ostracod species selecteded for stable carbon and oxygen isotope measurements. Scale bar=100 μm

(a) *Ammonia beccarii* (Linné). Dorsal side. Mány-22 borehole, depth 45-52.5 m.

(b) *Ammonia beccarii* (Linné). Ventral side. . Mány-22 borehole, depth 45-52.5 m.

(c) *Elphidium aculeatum* (d'Orbigny). Side view. Mány-17 borehole, depth 152.8-153 m.

(d) *Elphidium macellum* (Fichtel & Moll). Side view. Mány-22 borehole, depth 170-173 m.

(e) *Elphidium macellum* (Fichtel & Moll). Apertural view. Mány-22 borehole, depth 170-173 m.

(f) *Aurila mehesi* (Zalányi). RV. Mány-17 borehole, depth 168.7-171.2 m.

(g) *Aurila mehesi* (Zalányi). LV. Mány-17 borehole, depth 168.7-171.2 m.

(h) *Aurila notata* (Reuss). RV. Mány-22 borehole, depth 45-52.5 m.

(i) *Aurila notata* (Reuss). LV. Mány-22 borehole, depth 45-52.5 m.

Figure 4: Evolution of $\delta^{13}C$ and $\delta^{18}O$ values of NBS 19 reference calcite over a period of six months. Sample sizes vary from 280 to 390 μg.

499 Figure 5: Evolution of $\delta^{13}C$ and $\delta^{18}O$ values of Carrara marble over a period of six months.

500 Sample sizes vary from 100 to 350 μg.

501

Figure 6: Variations in $\delta^{13}C$ and $\delta^{18}O$ values as a function of sample weights (10 to 380 μg) of Carrara marble.

Figure 7: Variations in standard deviations of carbon and oxygen isotope measurements as a function of the number of individuals considering all three genera of foraminifera and ostracods from various levels in Sarmatian boreholes of Hungary (Fig. 2).

Figure 8: Variations in standard deviations of carbon and oxygen isotope measurements as a function of the number of individuals from the same pool of *Elphidium* foraminifera from the Mány-17 borehole (Fig. 2).

Table 1

NBS-19-#	$\delta^{13}C$ ‰ V–PDB	S.D.	$\delta^{18}O$ ‰ V–PDB	S.D.
NBS19-1	1.93	0.004	-2.33	0.011
NBS19-2	1.96	0.026	-2.16	0.185
NBS19-3	1.96	0.081	-2.16	0.239
NBS19-4	1.94	0.024	-2.26	0.100
NBS19-5	1.94	0.027	-2.15	0.222
NBS19-6	1.96	0.023	-2.23	0.041
NBS19-7	1.92	n.a.	-2.27	n.a.
NBS19-8	1.98	0.042	-2.14	0.092
NBS19-9	1.93	0.016	-2.22	0.058
NBS19-10	1.96	0.017	-2.15	0.094
NBS19-11	1.93	0.007	-2.30	0.027
NBS19-12	1.95	0.022	-2.23	0.050
NBS19-13	1.97	n.a.	-2.17	n.a.
NBS19-14	1.98	0.011	-2.12	0.013
NBS19-15	1.91	0.006	-2.18	0.131
NBS19-16	1.93	n.a.	-2.29	n.a.
NBS19-17	1.98	0.032	-2.12	0.125
NBS19-18	1.96	0.058	-2.22	0.081
NBS19-19	1.94	0.027	-2.17	0.134
NBS19-20	1.93	0.003	-2.33	0.017
NBS19-21	1.96	0.027	-2.15	0.068
NBS19-22	1.96	0.000	-2.12	0.046
NBS19-23	1.94	0.011	-2.24	0.019
NBS19-24	1.96	0.023	-2.16	0.047

NBS19-25	1.94	0.041	-2.26	0.132
NBS19-26	1.93	0.023	-2.24	0.055
NBS19-27	1.98	0.007	-2.11	0.002
NBS19-28	1.93	0.055	-2.21	0.194
NBS19-29	1.94	0.010	-2.26	0.021
NBS19-30	1.97	0.021	-2.14	0.038
NBS19-31	1.95	0.010	-2.20	0.005
NBS19-32	1.95	0.007	-2.20	0.006
NBS19-33	1.95	n.a.	-2.20	n.a.
NBS19-34	2.00	0.057	-2.31	0.139
NBS19-35	1.90	0.034	-2.08	0.154
NBS19-36	1.97	0.028	-2.21	0.107
NBS19-37	1.95	0.031	-2.22	0.041
NBS19-38	1.98	0.001	-2.16	0.034
NBS19-39	1.97	0.047	-2.15	0.212
NBS19-40	1.96	0.005	-2.20	0.039
NBS19-41	1.90	0.044	-2.28	0.101
NBS19-42	1.95	0.021	-2.20	0.063
NBS19-43	1.95	0.028	-2.20	0.121
NBS19-44	1.95	0.010	-2.20	0.087
NBS19-45	1.97	0.036	-2.25	0.087
NBS19-46	1.96	0.022	-2.16	0.094
NBS19-47	1.93	0.038	-2.17	0.124
NBS19-48	1.98	0.054	-2.11	0.123
NBS19-49	1.92	0.072	-2.30	0.181

Table 2

CM-#	$\delta^{13}C$ ‰ V–PDB	S.D.	$\delta^{18}O$ ‰ V–PDB	S.D.
CM1	1.993	0.044	-1.762	0.061
CM2	2.029	0.015	-1.962	0.079
CM3	2.082	0.017	-1.819	0.006
CM4	2.037	0.023	-1.836	0.051
CM5	2.054	0.072	-1.758	0.194
CM6	2.054	0.031	-1.846	0.010
CM7	1.987	0.023	-1.975	0.068
CM8	1.963	0.011	-2.056	0.026
CM9	1.987	0.032	-1.968	0.109
CM10	1.912	0.083	-2.016	0.180
CM12	1.944	0.044	-1.796	0.061
CM13	2.009	0.076	-1.846	0.043
CM14	1.997	0.080	-1.828	0.029
CM15	1.995	0.063	-1.917	0.101
CM16	2.067	0.024	-1.826	0.110
CM18	1.990	0.063	-1.884	0.114
CM20	2.043	0.037	-1.880	0.045
CM21	1.958	0.061	-1.865	0.088
CM22	2.032	0.030	-1.833	0.020
CM23	2.018	0.032	-1.849	0.052
CM24	2.029	0.052	-1.837	0.058
CM25	2.019	0.026	-1.848	0.085
CM26	2.034	0.030	-1.822	0.022
CM27	2.016	0.026	-1.861	0.021

CM28	2.028	0.056	-1.830	0.088
CM29	2.022	0.019	-1.853	0.053
CM30	2.029	0.024	-1.832	0.066
CM31	2.020	0.022	-1.852	0.044
CM32	2.028	0.025	-1.834	0.033
CM33	2.021	0.010	-1.851	0.027

Table 3

Sample Name	Weight (mg)	$\delta^{13}C$ ‰ V–PDB	$\delta^{18}O$ ‰ V–PDB
CM8	10	1.99	-1.90
CM15	10	2.07	-1.59
CM22	10	2.10	-1.58
CM23	10	1.99	-1.68
CM27	10	1.99	-1.64
CM28	10	1.91	-1.80
CM29	10	1.98	-1.56
CM7	30	1.90	-2.03
CM24	30	1.95	-1.76
CM25	40	2.07	-1.65
CM26	60	1.92	-1.88
CM4	110	2.04	-1.85
CM5	110	2.05	-1.80
CM14	110	2.05	-1.78
CM19	140	2.02	-1.85
CM20	140	1.98	-1.99
CM21	150	2.02	-1.93
CM6	160	2.07	-1.69
CM13	170	2.05	-1.86
CM12	180	2.01	-1.87
CM3	210	2.04	-1.96
CM2	260	2.03	-2.04
CM10	270	2.10	-1.82
CM11	270	2.08	-1.81

CM16	280	2.12	-1.71
CM17	280	2.05	-1.86
CM1	290	2.01	-1.99
CM9	290	2.06	-1.83
CM18	380	2.09	-1.84

Table 4

Sample #	Species	Weight (mg)	Individuals (n)	Mean $\delta^{13}C$ ‰ V–PDB	S.D.	Mean $\delta^{18}O$ ‰ V–PDB
PB-5-1	*Elphidium aculeatum*	300	10	-1.00	0.078	-1.07
PB-5-4	*Elphidium macellum*	300	15	-0.98	0.055	-1.69
PB-5-5	*Elphidium macellum*	290	14	0.39	0.252	-1.25
PB-5-7	*Elphidium aculeatum*	300	9	0.73	0.111	0.25
PB-5-8	*Elphidium macellum*	310	12	0.04	0.102	0.20
PB-5-17	*Elphidium macellum*	310	15	0.55	0.004	-0.52
PB-5-20	*Elphidium macellum*	300	8	0.77	0.111	-2.93
PB-5-21	*Elphidium macellum*	310	5	0.91	0.443	-2.53
PB-5-23	*Elphidium macellum*	310	14	1.10	0.069	-2.93
PB-5-25	*Elphidium macellum*	310	14	1.29	0.055	-2.35
PB-5-26	*Elphidium macellum*	310	6	0.55	0.260	-2.30
PB-5-28	*Elphidium aculeatum*	320	13	0.58	0.096	-2.34
PB-5-29	*Elphidium macellum*	310	7	1.54	0.040	-2.13
PB-5-33	*Elphidium macellum*	300	9	1.50	0.079	-1.68
PB-5-34	*Elphidium aculeatum*	310	5	1.80	0.040	-0.45
PB-5-36	*Elphidium macellum*	300	12	1.82	0.005	-1.73
PB-5-38	*Elphidium aculeatum*	310	16	0.48	0.073	-0.13
PB-5-46	*Elphidium hauerinum*	280	41	-0.16	0.021	-0.77
PB-5-47	*Elphidium macellum*	310	26	-0.69	n.a.	-1.92
PB-5-48	*Elphidium macellum*	280	35	-0.55	0.064	-1.87
PB-5-50	*Elphidium macellum*	310	18	-0.62	0.082	-2.58
PB-5-51	*Elphidium macellum*	300	25	-0.36	0.107	-1.59
PB-5-53	*Elphidium macellum*	300	26	0.13	0.123	-1.35
PB-5-54	*Elphidium macellum*	300	24	0.88	0.060	-1.62
PB-5-57	*Elphidium macellum*	290	33	-0.20	0.004	-0.53

M-17-2	*Elphidium macellum*	310	21	0.75	0.027	-2.47
M-17-4	*Elphidium macellum*	310	17	0.59	0.322	-1.00
M-17-6	*Elphidium aculeatum*	330	7	1.35	0.140	-1.43
M-17-8	*Elphidium aculeatum*	310	10	2.45	0.429	-1.00
M-17-11	*Elphidium macellum*	320	18	1.53	0.072	-1.09
M-17-13	*Elphidium aculeatum*	330	14	1.13	0.134	-0.59
M-17-14	*Elphidium aculeatum*	330	13	0.88	0.043	-0.73
M-17-16	*Elphidium macellum*	310	46	-0.08	0.029	-1.09
M-17-18	*Elphidium macellum*	310	21	1.38	0.263	-1.52
M-17-20	*Elphidium macellum*	310	12	-0.37	0.296	-1.20
M-17-22	*Elphidium macellum*	300	14	0.27	0.097	-2.22
M-17-24	*Elphidium macellum*	290	16	-0.59	0.027	-1.32
M-17-25	*Elphidium macellum*	320	27	-0.09	0.005	-2.24
M-17-26	*Elphidium macellum*	320	21	-0.40	0.039	-1.70
M-17-29	*Elphidium macellum*	320	10	1.08	0.034	-1.46
M-17-30	*Elphidium macellum*	290	27	0.38	0.043	-0.84
M-17-31	*Elphidium aculeatum*	300	21	-0.12	0.073	-1.13
M-17-32	*Elphidium macellum*	300	21	0.98	0.101	-1.48
M-17-34	*Elphidium macellum*	310	17	1.30	0.475	-3.21
M-17-36	*Elphidium macellum*	300	8	1.86	0.092	-2.83
M-17-37	*Elphidium macellum*	310	14	-0.98	0.145	-1.18
M-17-38	*Elphidium macellum*	290	11	1.92	0.006	-1.19
M-17-40	*Elphidium macellum*	290	13	0.58	0.210	-2.28
M-17-42	*Elphidium macellum*	310	10	1.04	0.316	-2.52
M-17-44	*Elphidium macellum*	310	13	1.11	0.229	-2.18
M-17-46	*Elphidium macellum*	320	28	0.49	0.348	-1.74
PB-5-6	*Ammonia becarii*	240	35	-0.72	0.167	-2.15
PB-5-11	*Ammonia becarii*	210	25	-0.09	0.003	-1.08

PB-5-13	*Ammonia becarii*	350	14	0.65	0.003	-2.49
PB-5-16	*Ammonia becarii*	320	1	0.36	0.099	-2.20
PB-5-31	*Ammonia becarii*	310	19	0.91	0.062	-2.90
PB-5-37	*Ammonia becarii*	290	25	0.67	0.072	-1.98
PB-5-42	*Ammonia becarii*	300	28	-0.13	0.071	-2.77
PB-5-43	*Ammonia becarii*	290	36	-0.33	0.084	-2.15
PB-5-44	*Ammonia becarii*	300	41	0.93	0.089	-2.05
PB-5-45	*Ammonia becarii*	300	44	-0.84	0.100	-1.09
PB-5-49	*Ammonia becarii*	310	52	-0.94	0.010	-2.46
PB-5-55	*Ammonia becarii*	300	15	1.14	0.085	-2.46
M-17-7	*Ammonia becarii*	300	11	1.09	0.034	-2.66
M-17-10	*Ammonia becarii*	320	33	0.51	0.118	-0.99
M-17-12	*Ammonia becarii*	330	23	0.91	0.046	-2.09
M-17-21	*Ammonia becarii*	310	35	0.47	0.271	-1.91
PB-5-2	*Aurila mehesi*	300	5	-2.86	0.127	-0.58
PB-5-3	*Aurila notata*	300	5	-5.13	0.741	-0.68
PB-5-9	*Aurila notata*	280	3	-6.01	0.327	-0.22
PB-5-10	*Aurila notata*	310	9	-6.11	0.090	-0.53
PB-5-12	*Aurila notata*	300	8	-3.29	0.156	-1.48
PB-5-15	*Aurila notata*	300	9	-4.87	0.296	-0.56
PB-5-18	*Aurila mehesi*	300	10	-4.24	0.293	-1.14
PB-5-19	*Aurila mehesi*	310	8	-2.76	0.323	-2.65
PB-5-22	*Aurila mehesi*	320	7	-2.45	0.085	-1.81
PB-5-24	*Aurila mehesi*	310	4	-0.50	0.009	-2.23
PB-5-27	*Aurila mehesi*	330	6	-2.37	0.388	-2.21
PB-5-30	*Aurila mehesi*	300	7	-2.23	0.217	-2.63
PB-5-32	*Aurila mehesi*	300	11	-1.93	0.113	-0.89
PB-5-35	*Aurila notata*	300	9	-1.79	0.113	-2.58

PB-5-39	*Aurila notata*	310	14	-5.21	0.073	-1.44
PB-5-40	*Aurila notata*	300	8	-4.36	0.028	-0.70
PB-5-41	*Aurila notata*	320	9	-3.84	0.053	-1.42
PB-5-52	*Aurila notata*	310	8	-3.57	0.180	-1.52
PB-5-56	*Aurila notata*	320	9	-3.39	0.439	-2.44
M-17-1	*Aurila mehesi*	290	10	-2.75	0.285	-1.82
M-17-3	*Aurila mehesi*	330	8	-2.65	0.082	-2.23
M-17-5	*Aurila mehesi*	320	8	-2.96	0.227	-1.27
M-17-9	*Aurila mehesi*	300	16	-2.91	0.300	-0.85
M-17-15	*Aurila notata*	290	14	-1.71	0.014	-1.79
M-17-17	*Aurila notata*	300	4	-4.97	0.447	-0.40
M-17-19	*Aurila notata*	300	4	-4.11	0.308	-0.43
M-17-23	*Aurila notata*	300	9	-5.03	0.020	-0.57
M-17-27	*Aurila notata*	310	8	-3.55	0.356	-1.45
M-17-28	*Aurila notata*	300	15	-3.38	0.040	-2.11
M-17-33	*Aurila notata*	320	17	-4.20	0.428	-1.81
M-17-39	*Aurila notata*	320	6	-3.61	0.221	-2.31
M-17-41	*Aurila notata*	330	9	-3.14	0.164	-2.70
M-17-43	*Aurila notata*	310	12	-4.20	0.099	-1.25
M-17-45	*Aurila notata*	300	10	-3.19	0.849	-2.03

Table 5

Sample #	Individuals (n)	Weight (mg)	$\delta^{13}C$ ‰ V–PDB	$\delta^{18}O$ ‰ V–PDB
Elphi M17_1	5	60	0.18	-2.11
Elphi M17_2	5	50	-0.66	-1.52
Elphi M17_3	5	50	-0.55	-1.93
Elphi M17_4	5	60	-1.72	-2.83
Elphi M17_5	10	130	0.33	-1.43
Elphi M17_6	10	140	-0.62	-1.75
Elphi M17_7	10	140	-0.21	-1.63
Elphi M17_8	10	160	-0.26	-1.66
Elphi M17_9	20	380	0.30	-1.69
Elphi M17_10	20	330	0.02	-1.43
Elphi M17_11	20	350	-0.50	-1.68
Elphi M17_12	20	330	-0.15	-1.88
Elphi M17_13	30	570	-0.11	-1.43
Elphi M17_14	30	540	0.27	-1.55
Elphi M17_15	30	610	-0.12	-1.79
Elphi M17_16	30	610	-0.33	-1.61
Elphi M17_17	40	710	-0.26	-1.47
Elphi M17_18	40	850	-0.34	-1.64
Elphi M17_19	40	790	-0.51	-1.74
Elphi M17_20	40	900	-0.13	-1.73

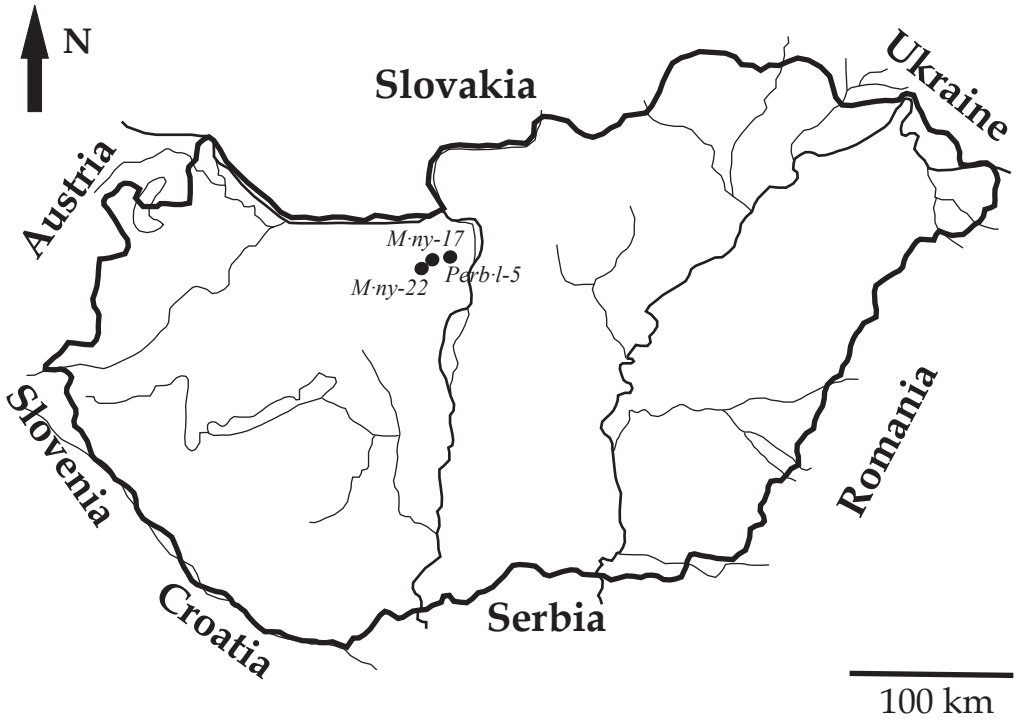
N
Slovakia
Ukraine
Austria
M·ny-17
Perb·l-5
M·ny-22
Slovenia
Romania
Croatia
Serbia
100 km

Figure 1

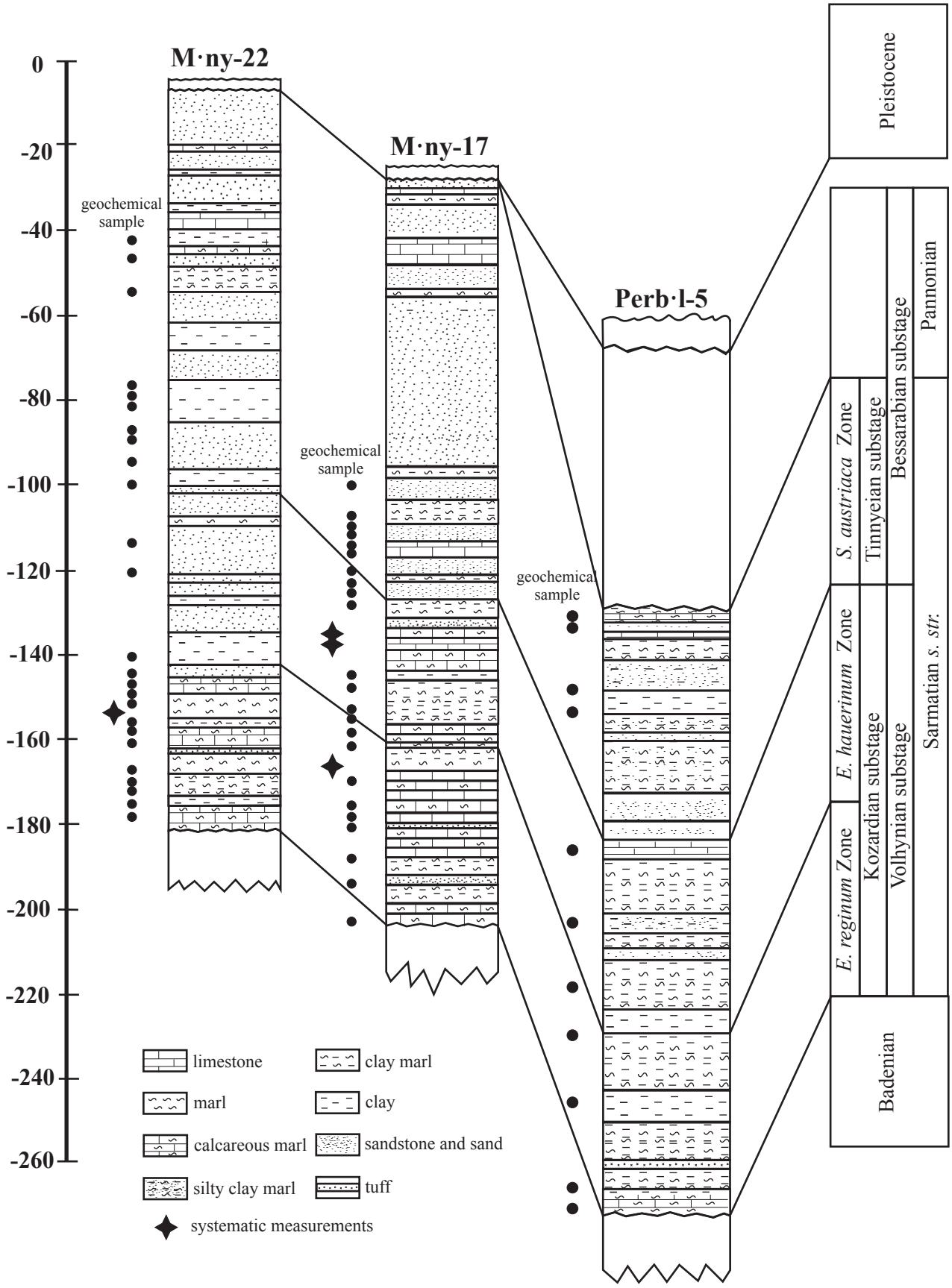
M·ny-22
M·ny-17
Perb·l-5
geochemical sample
geochemical sample
geochemical sample
0
-20
-40
-60
-80
-100
-120
-140
-160
-180
-200
-220
-240
-260
limestone
marl
calcareous marl
silty clay marl
clay marl
clay
sandstone and sand
tuff
systematic measurements
Pleistocene
Pannonian
Bessarabian substage
Tinyeian substage
S. austriaca Zone
E. hauerinum Zone
Kozardian substage
Volhynian substage
E. reginum Zone
Sarmatian s. str.
Badenian

Figure 2

Figure 3

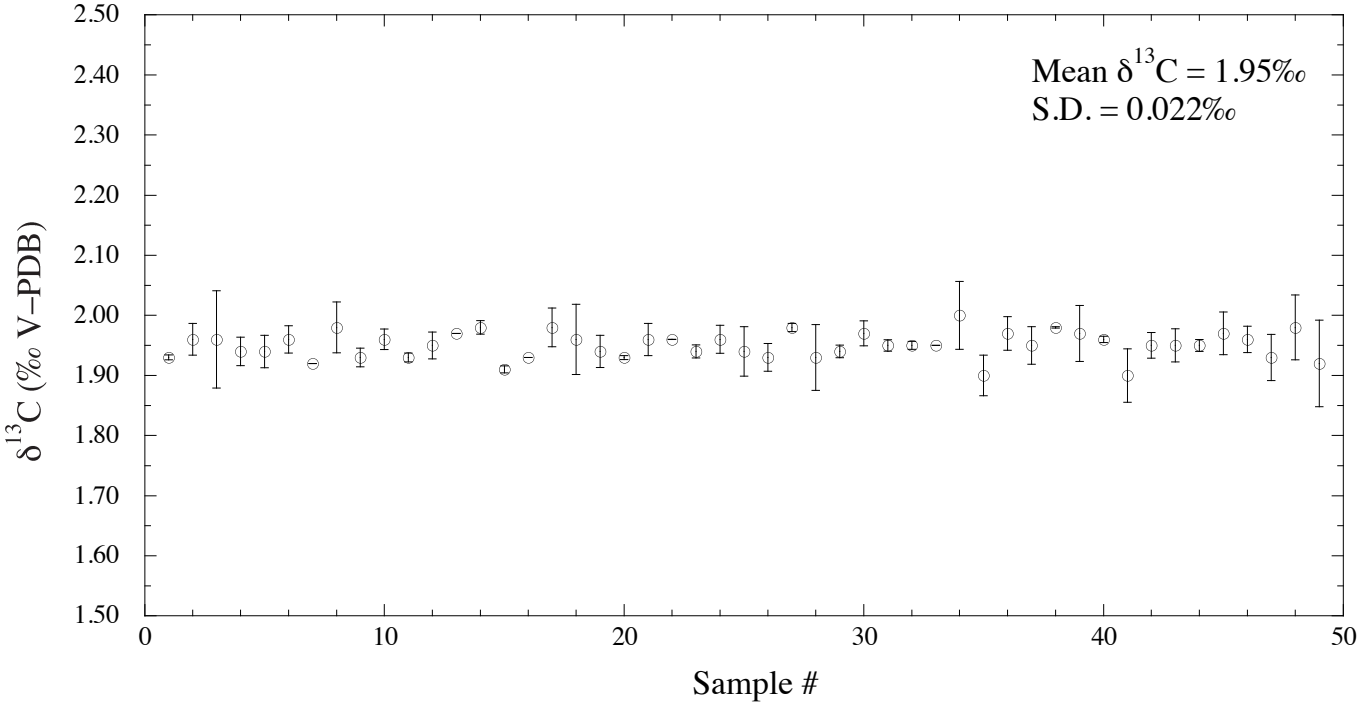
Mean δ13C = 1.95‰
S.D. = 0.022‰
δ13C (‰ V–PDB)
Sample #

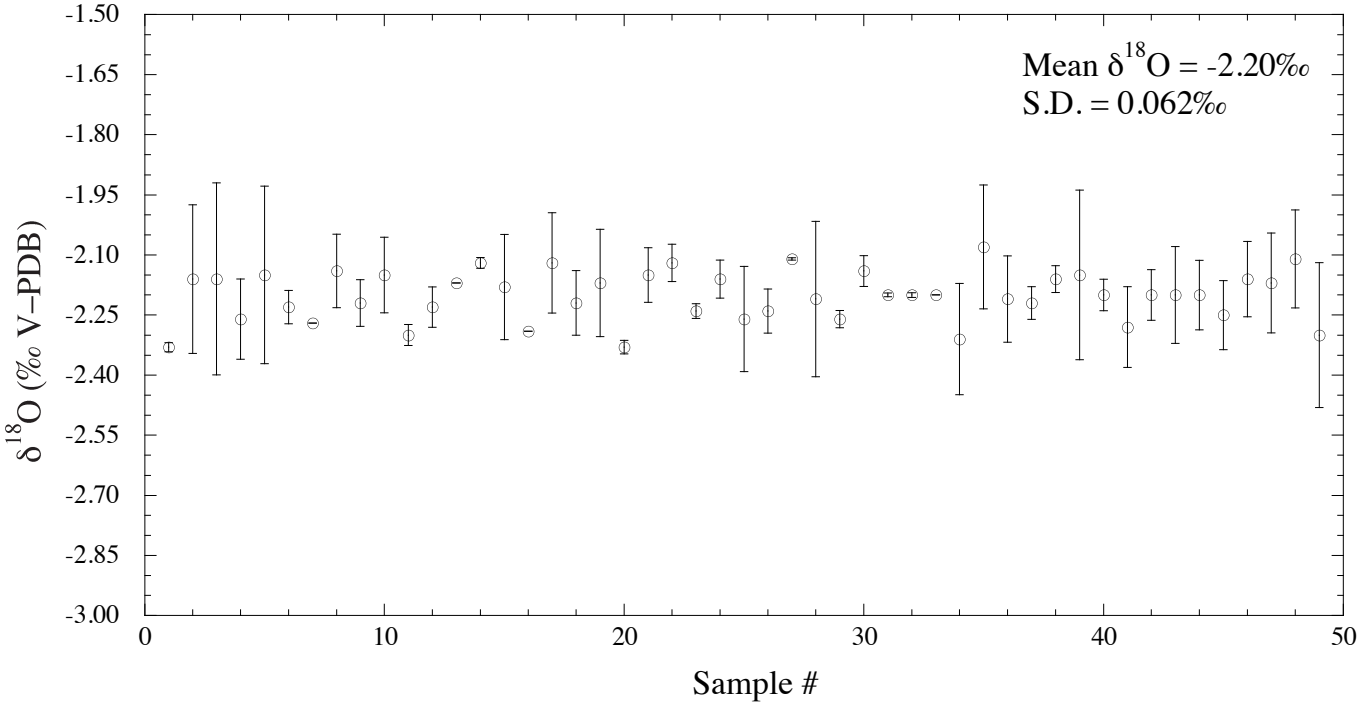
Mean δ18O = -2.20‰
S.D. = 0.062‰
δ18O (‰ V–PDB)
Sample #

Figure 4

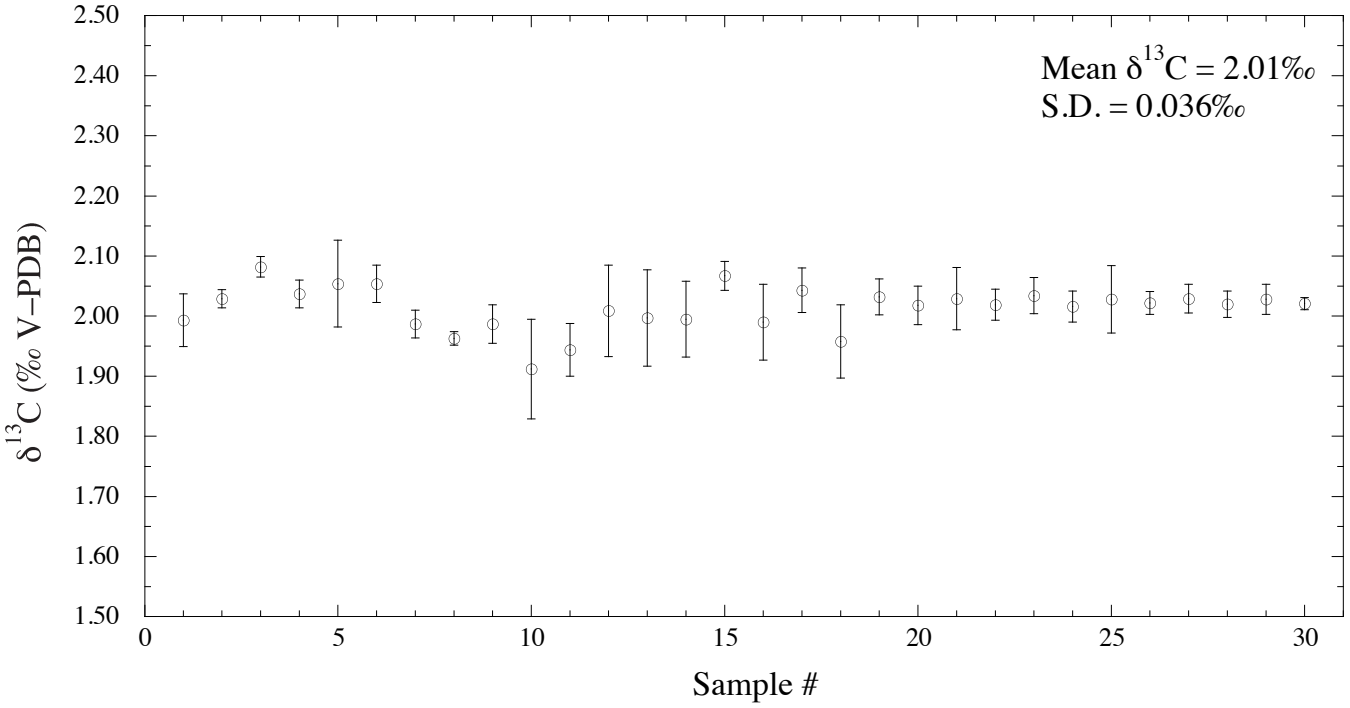
Mean δ13C = 2.01‰
S.D. = 0.036‰
δ13C (‰ V–PDB)
Sample #

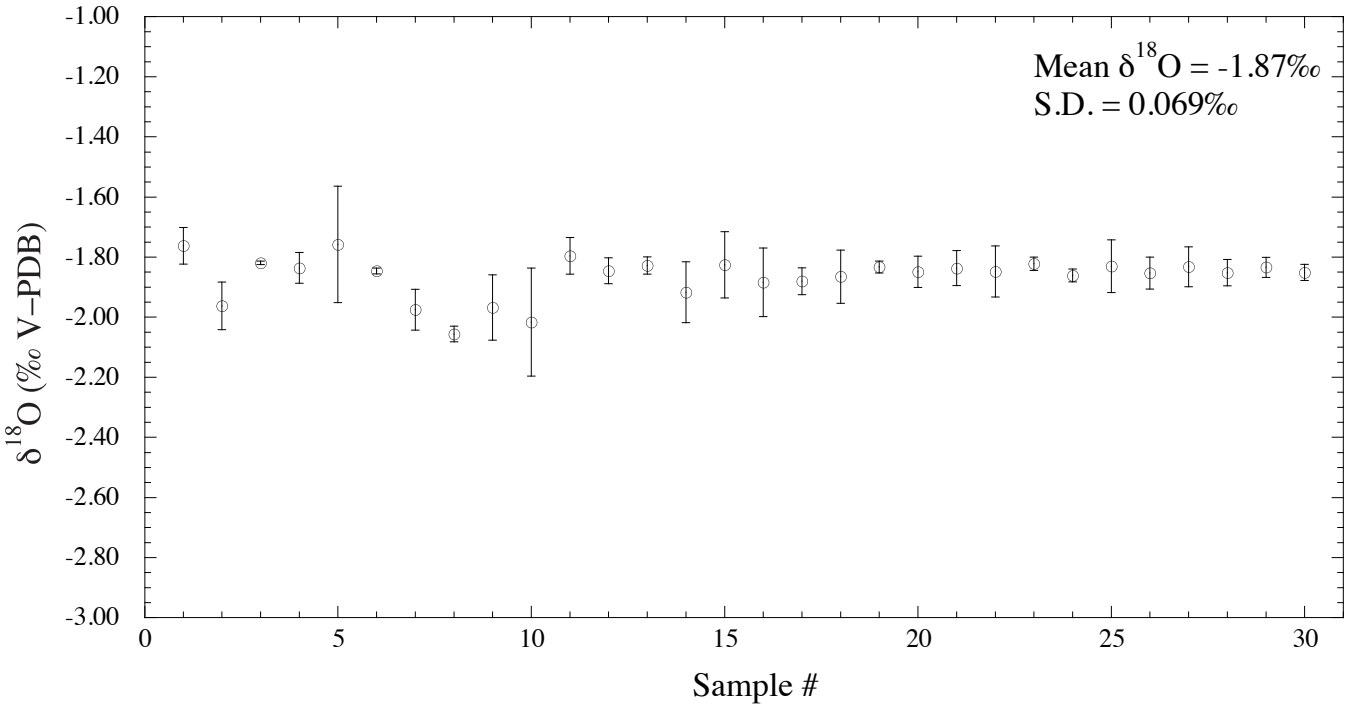
Mean δ18O = -1.87‰
S.D. = 0.069‰
δ18O (‰ V–PDB)
Sample #

Figure 5

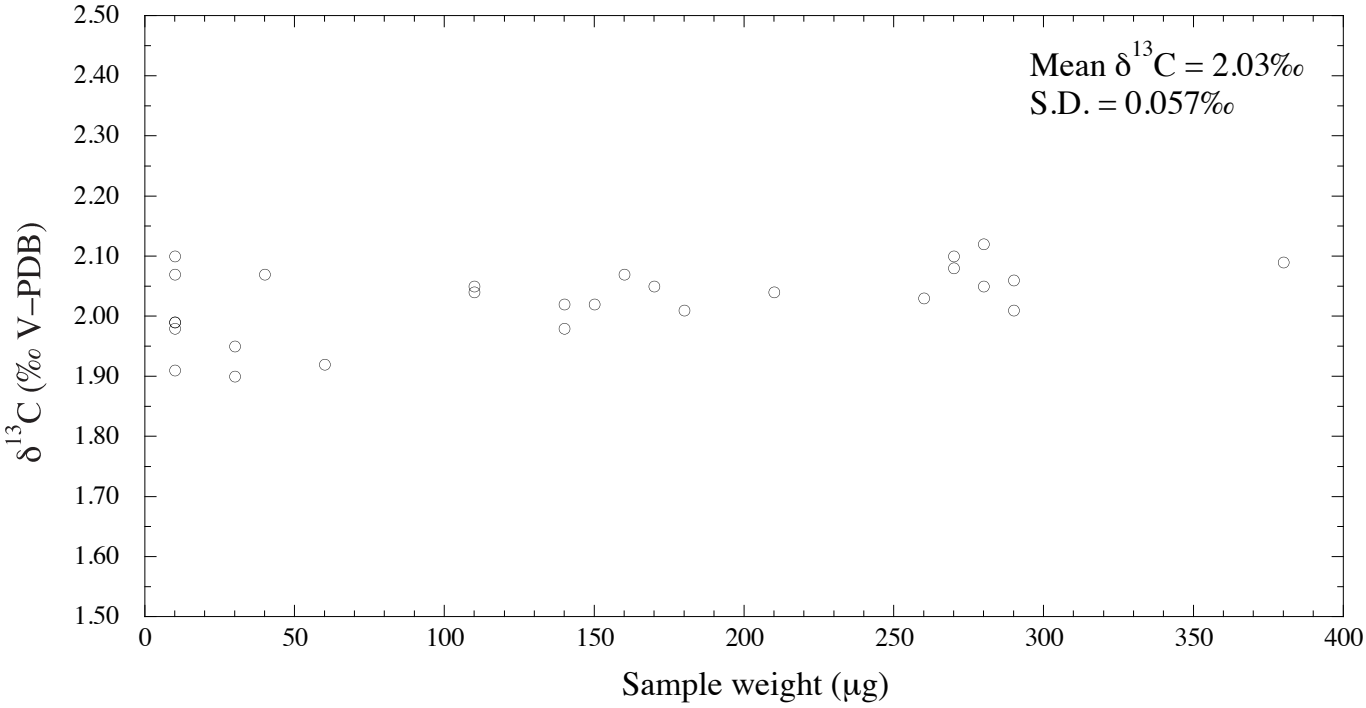
Mean δ13C = 2.03‰
S.D. = 0.057‰
δ13C (‰ V–PDB)
Sample weight (µg)

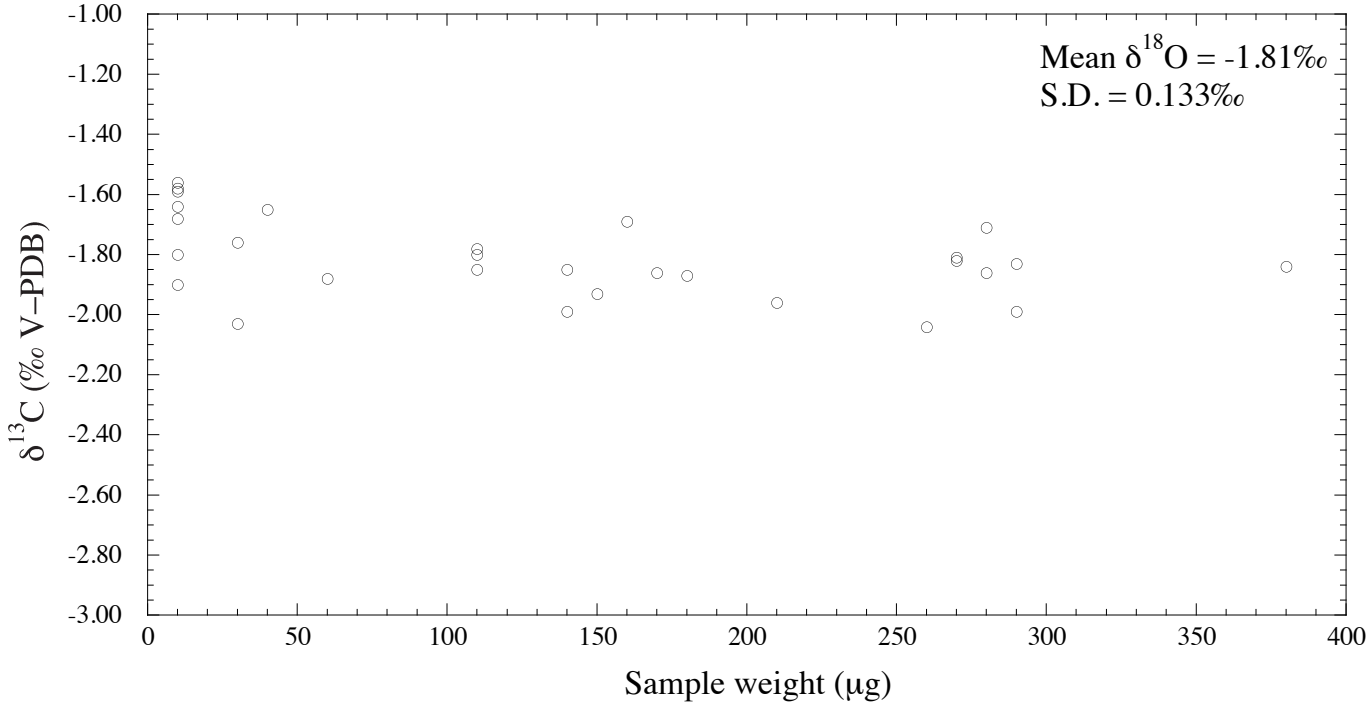
Mean δ18O = -1.81‰
S.D. = 0.133‰
δ13C (‰ V–PDB)
Sample weight (µg)

Figure 6

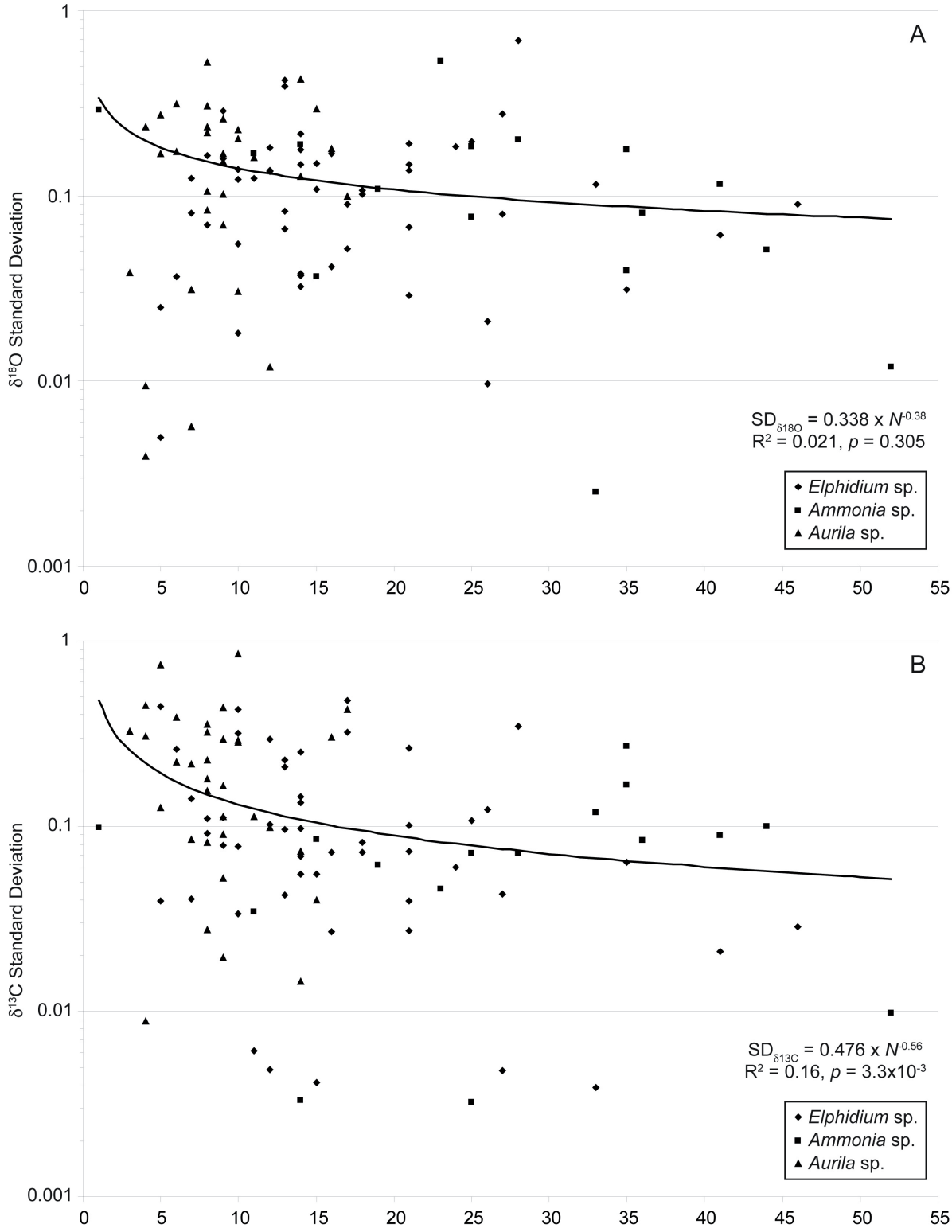
A
δ18O Standard Deviation
1
0.1
0.01
0.001
0
5
10
15
20
25
30
35
40
45
50
55
SD$_{\delta 18O}$ = 0.338 x $N^{-0.38}$
R^2 = 0.021, p = 0.305
Elphidium sp.
Ammonia sp.
Aurila sp.
B
δ13C Standard Deviation
1
0.1
0.01
0.001
0
5
10
15
20
25
30
35
40
45
50
55
SD$_{\delta 13C}$ = 0.476 x $N^{-0.56}$
R^2 = 0.16, p = 3.3x10^{-3}
Elphidium sp.
Ammonia sp.
Aurila sp.

Figure 7

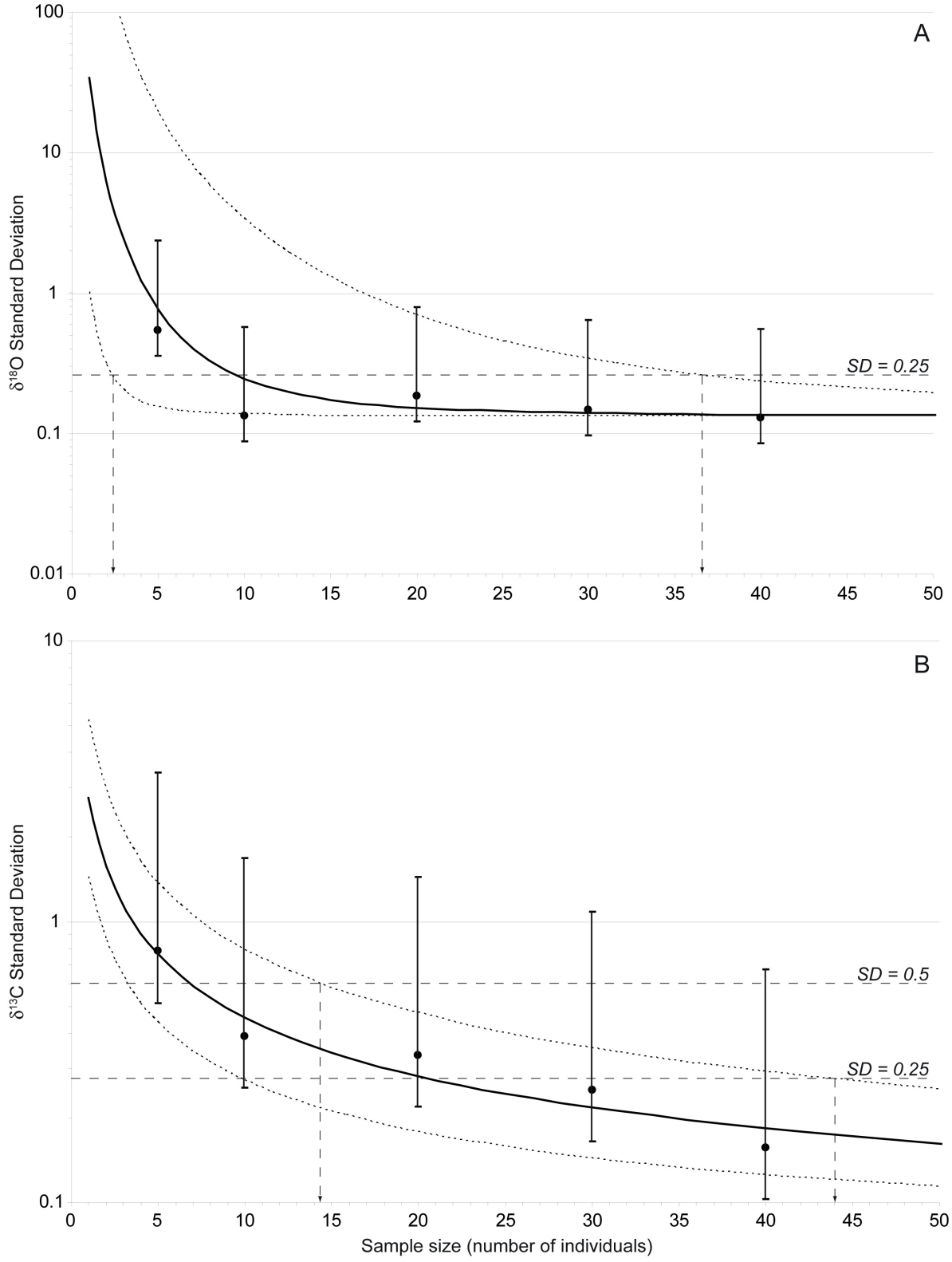
A
100
10
1
0.1
0.01
δ18O Standard Deviation
SD = 0.25
0
5
10
15
20
25
30
35
40
45
50
B
10
1
0.1
δ13C Standard Deviation
SD = 0.5
SD = 0.25
Sample size (number of individuals)

Figure 8

4.3/ Analyse des phosphates

Comme nous l'avons démontré dans les premiers chapitres de ce manuscrit, l'analyse isotopique des rapports $^{18}O/^{16}O$ sur des échantillons de phosphates provenant d'hydroxyapatites d'origine biogénique constitue une partie importante de notre travail de recherche. Toute amélioration intervenant sur cette technique représente donc un intérêt très significatif pour notre travail. Au-delà, depuis un certain nombre d'années, grâce à de tels travaux d'améliorations analytiques, les analyses isotopiques des phosphates deviennent plus accessibles à un plus grand nombre d'utilisateurs et ainsi permettent d'explorer de nouveaux champs d'investigation.

Dans la publication 4.7 nous avons reporté des travaux correspondant à la mise au point d'une méthode simple et rapide pour analyser les $\delta^{18}O_{PO4}$ sur des échantillons de phosphates d'argent en utilisant un analyseur élémentaire haute température en ligne en flux continu avec un spectromètre de masse de rapports isotopiques (EA-Py-CF-IRMS). Pour ce faire nous sommes partis du constat que s'il existait diverses techniques déjà publiées [54-58], plus ou moins complexes pour mesurer les $\delta^{18}O_{VSMOW}$ avec des analyseurs élémentaires en mode pyrolyse et en flux continu, il n'y avait pas de consensus général sur le système à adopter et particulièrement pour des molécules résistantes comme le phosphate d'argent Ag_3PO_4. La figure 4.5 illustre les différents systèmes de pyrolyse en flux continu utilisant la technique de l'analyse élémentaire en mode pyrolyse.

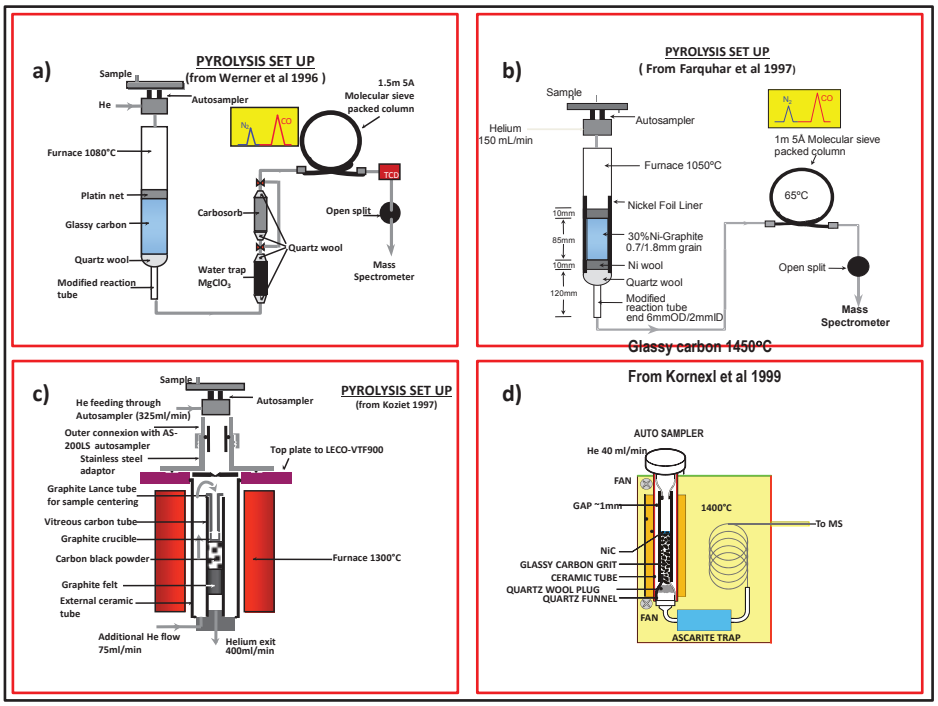

Figure 4.5 : Diverses techniques publiées pour l'analyse des rapports $^{18}O/^{16}O$ par analyse élémentaire en ligne en flux continu avec un IRMS. a) Werner et al 1996 [54] utilisent un four en quartz à base de glassy carbon chauffé à 1080°C en présence de nickel ; b) Farquhar et al. 1997 [55] utilisent un four en quartz tapissé d'une feuille de nickel rempli de graphite nickelé à 1050°C; c) Koziet 1997 [56] utilise un four en glassy carbon rempli de poudre de carbone à 1300°C; d) Kornexl et al. 1999 [57] utilisent un four en glassy carbon rempli de glassy carbon avec un niveau de graphite nickelé fonctionnant à 1400°C.

Le système de pyrolyse par analyseur élémentaire que nous avons mis au point est détaillé dans la figure 4.6. Il est basé sur un tube en céramique, à l'intérieur duquel on a mis des granules de glassy carbon, puis un niveau de graphite nickelé, le tout maintenu à une température de 1270°C.

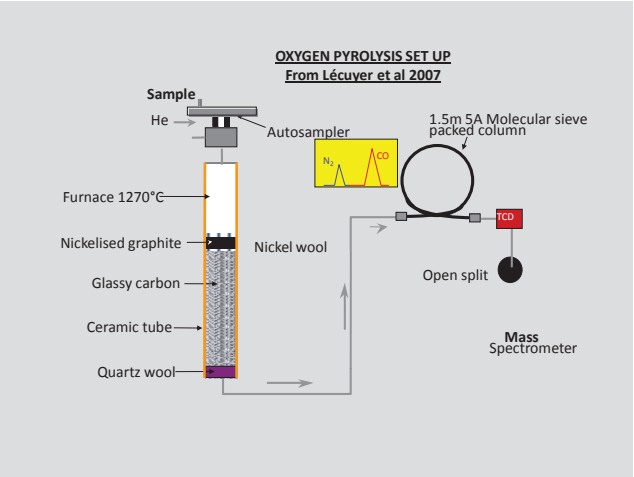

Figure 4.6 : Système de pyrolyse utilisé et décrit dans la publication 4.7 basé sur un four en céramique rempli de glassy carbon avec un niveau de carbone nickelé et maintenu à 1270°C.

Dans un premier temps nous nous sommes employés à fabriquer des standards de travail de phosphate d'argent selon le protocole décrit par Lécuyer et al. en 1999 [59] consistant à faire réagir du KH_2PO_4 avec des échantillons d'eau de rapports isotopiques variables en $^{18}O/^{16}O$. Ceci nous a permis d'obtenir une série d'échantillons de phosphates d'argent ayant une gamme de 13 ‰ de valeurs $\delta^{18}O_{VSMOW}$. Les rapports isotopiques des eaux ont été analysés avec le système AquaPrep décrit précédemment au paragraphe 4.1 et les analyses des phosphates d'argent ainsi générés effectuées par EA-Py-CF-IRMS ont été systématiquement comparées aux analyses faites sur les mêmes échantillons par les techniques classiques offline en dual inlet [60,61]. En plus de ces échantillons de phosphates synthétiques, nous avons également analysé une série de phosphate d'argent issus d'échantillons naturels dont les valeurs $\delta^{18}O_{VSMOW}$ étaient connues et présentaient une gamme répartie entre 12,8 ‰ et 29,9 ‰.

Nos résultats montrent que nous obtenons une répétabilité de 0,2 ‰ pour la mesure des $\delta^{18}O_{VSMOW}$ sur les phosphates d'argent avec la technique d'EA-Py-CF-IRMS. Ceci s'applique aussi bien aux analyses de phosphates synthétiques qu'aux analyses de phosphates

naturels. De plus cette technique nous permet de réduire la prise d'essai d'un facteur 10 par rapport aux analyses offline. La remarquable stabilité dans le temps de ces phosphates d'argent combinée avec la simplification procurée par cette technique d'analyse renforce l'argument en faveur de l'utilisation de ce matériaux afin de réaliser des standards internationaux différents de l'eau pour calibrer les analyses $^{18}O/^{16}O$.

La possibilité d'analyser les rapports $^{18}O/^{16}O$ des phosphates d'argent par EA-Py-CF-IRMS constitue déjà une avancée significative par rapport aux méthodes précédentes. Cependant nous avons poussé encore plus loin l'évolution de cette technique en participant à la mise au point d'un nouveau type d'analyseur élémentaire appliqué à ce type de mesure. Ce travail reporté dans la publication 4.8 est le fruit d'une collaboration avec la société Elementar GmbH basée à Hanau et de sa filière Elementar France. La principale différence entre le système Pyrocube que nous avons utilisé et les autres analyseurs élémentaires est qu'il n'utilise pas une colonne chromatographique pour séparer les divers gaz produits lors de la réaction de pyrolyse mais qu'il utilise un système de « purge and trap ». Comme nous l'avons décrit dans le paragraphe précédent il existe différentes méthodes de pyrolyse [54-58], mais aucun véritable consensus sur une méthode « universelle » de pyrolyse qui s'appliquerait à tous les types de matrices pour mesurer les rapports $^{18}O/^{16}O$. Un des paramètres fondamentaux contrôlant la qualité des analyses $^{18}O/^{16}O$ est la séparation chromatographique du pic de CO notamment par rapport au pic de N_2 [55,62]. C'est précisément ce que permet d'améliorer le système Pyrocube dont le schéma de fonctionnement est illustré sur la figure 4.7 et le principe de base décrit par Sieper et al. en 2010 [63].

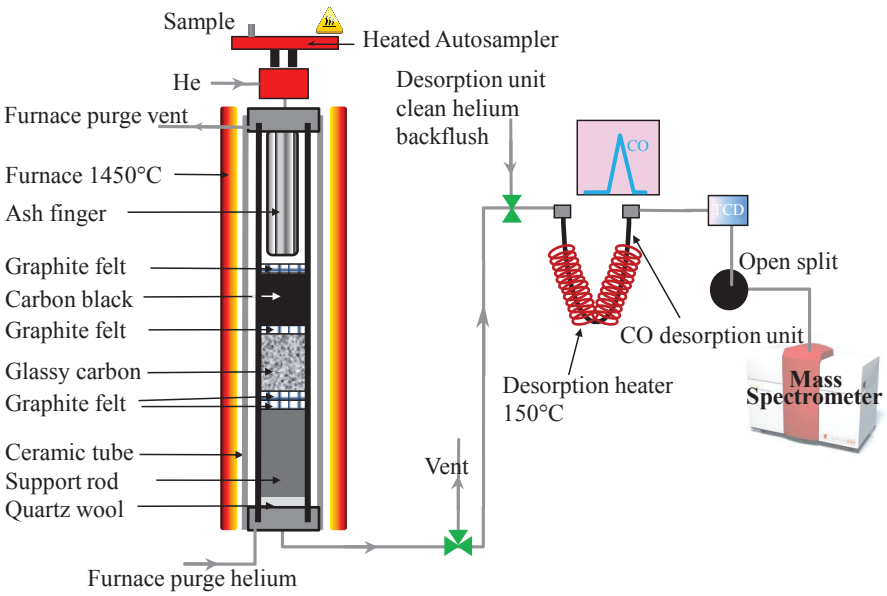

Figure 4.7 : Shéma de principe du fonctionnement du système Pyrocube en mode pyrolyse.

Le Pyrocube en mode pyrolyse est constitué d'un four à très haute température pouvant atteindre 1500°C. A l'intérieur de ce four on trouve un tube en céramique à l'intérieur duquel est placé un tube en glassy carbon. Entre ces deux fours circule un contre-courant d'hélium. Le tube en glassy carbon est rempli de matériaux carbonés avec des granules de glassy carbon ainsi que du noir de carbone. Le tout étant balayé par un flux d'hélium. Le piège du système « purge and trap » lui-même est situé en sortie du four. Le CO est piégé à température ambiante et libéré lorsque l'on chauffe le piège à 150°C. L'azote n'est pas piégé et passe directement vers le spectromètre de masse. Le Pyrocube est équipé de son propre système de détection constitué d'un « Thermal Conductivity Detector » (TCD). Une particularité du pyrocube est qu'il est équipé d'un système appelé « backflush » qui permet d'utiliser deux canaux différents d'hélium pour le piégeage et pour la libération du CO. Ceci fait que le CO entrant dans l'IRMS ne passe plus par le four de pyrolyse mais vient directement de

l'alimentation en hélium ce qui réduit de manière significative les opérations de maintenance de la source de l'IRMS. L'avantage principal du système Pyrocube pour ce type d'analyse est la qualité chromatographique du pic de CO à analyser dans l'IRMS. Ceci est illustré sur la figure 4.8.

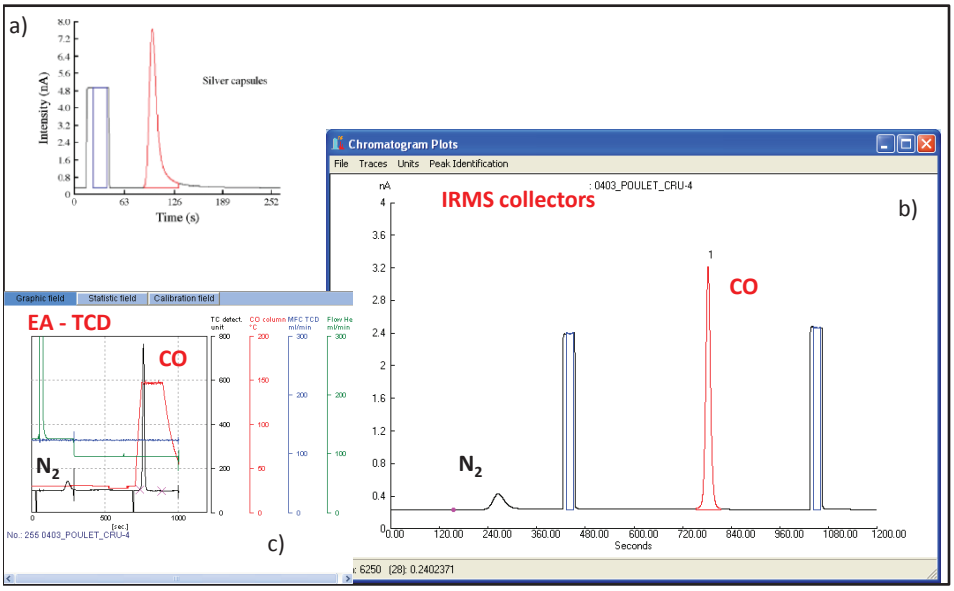

Figure 4.8 Comparaison de l'allure des traces de masse 28 des pics chromatographiques de CO entre un système utilisant une colonne chromatographique en a) et le système purge and trap du Pyrocube. c) représente l'allure du pic chromatographique enregistré sur le TCD du pyrocube simultanément à la trace du b).

Sur cette figure où l'on peut comparer en a) la trace isotopique de masse 28 d'un pic de CO provenant d'un système classique de séparation chromatographique sur colonne remplie et en b) et c) respectivement la trace isotopique de masse 28 et la trace TCD du pic provenant du système de piégeage du Pyrocube. Il est clair que le pic de CO provenant du Pyrocube présente une allure plus étroite et plus symétrique que celui issu d'un système chromatographique classique. Après une période de mise au point de ce nouveau système en

partant de notre expérience avec des systèmes plus classiques comme celui décrit au paragraphe précédent, nous nous sommes d'abord intéressés à l'analyse $^{18}O/^{16}O$ dans un même batch sur différents types d'échantillons déjà caractérisés pour leurs valeurs $\delta^{18}O_{SMOW}$ et représentant différents types de matrices : sulfates, nitrates, phosphates, vanilline, sucres. Nos résultats permettent de mettre en évidence que la technique d'EA-Py-CF-IRMS utilisant le Pyrocube et ses innovations technologiques permet d'obtenir des mesures $\delta^{18}O_{SMOW}$ précises et justes (1σ = 0,2 ‰) non seulement sur des matrices phosphatées, mais également sur différents types de matrices organiques ou inorganiques contenant de l'oxygène. Ceci pourrait être considéré comme une technique de référence pour l'analyse des rapports $^{18}O/^{16}O$ sur divers types d'échantillons avec la même configuration. Il s'agit là d'un point important car les analyses $^{18}O/^{16}O$ souffrent d'un manque de matériel de référence calibré autre que les eaux comme indiqué dans notre publication 4.7. Or cette étape est fondamentale pour le développement d'une nouvelle méthode d'analyse isotopique mais nécessite évidemment de pouvoir se servir d'un protocole unifié pour mesurer divers types d'échantillons et de matériaux de référence. Sur la figure 4.9 nous avons illustré le problème posé par la calibration des analyses $\delta^{18}O_{SMOW}$ des phosphates naturels avec les eaux de références classiquement utilisées : SMOW GISP et SLAP.

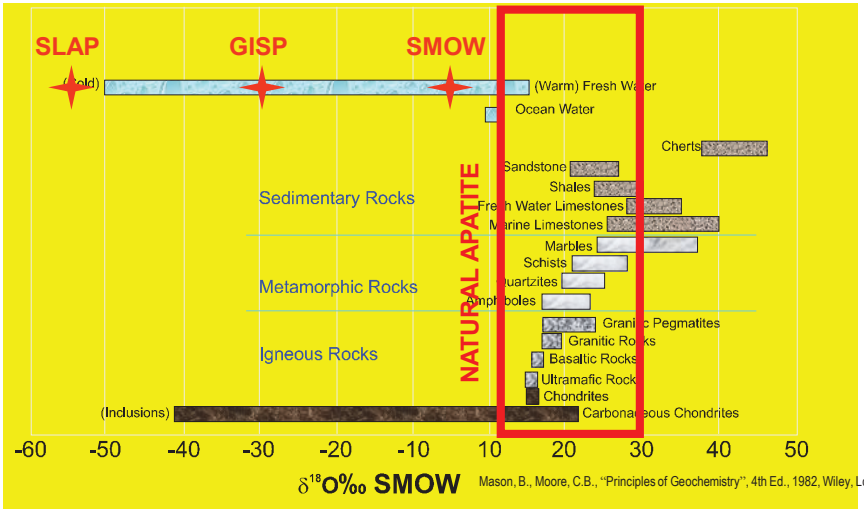

Figure 4.9: Report des données $\delta^{18}O_{SMOW}$ de différents constituants terrestres d'après B. Mason et al. [64], afin d'illustrer l'intérêt à utiliser dans le futur l'Ag_3PO_4 comme matériel de référence.

On voit bien sur cette figure le besoin d'obtenir d'autres matériaux de référence et il est évident que les qualités de stabilités dans le temps de l'Ag_3PO_4 combinées à la possibilité d'avoir maintenant une technique unifiée pour pouvoir mesurer dans un même batch des sucres ou des nitrates en les calibrant par rapport à un Ag_3PO_4 de référence revêt un intérêt croissant.

Les travaux effectués sur cette technique de l'EA-Py-CF-IRMS nous ont permis de faire évoluer de manière significative les analyses $^{18}O/^{16}O$ sur des matériaux solides. D'abord en rendant cette technique plus facile à mettre en œuvre que les méthodes dites «offline » ensuite en offrant une nouvelle technique permettant de réduire la prise d'essai donc rendant accessibles aux analyses $^{18}O/^{16}O$ de nouveaux sujets jusqu'alors difficile voire impossible à

analyser avec les méthodes conventionnelles. Nos travaux ont également permis de faire évoluer la réflexion sur le choix de futurs matériaux de référence pour la calibration des analyses $^{18}O/^{16}O$ sur des échantillons solides.

PUBLICATION 4.7
JOURNAL OF MASS SPECTROMETRY
J. Mass Spectrom. 2007; **42**: 36–41
Published online 6 December 2006 in Wiley InterScience
(www.interscience.wiley.com) DOI: 10.1002/jms.1130

JMS

High-precision determination of $^{18}O/^{16}O$ ratios of silver phosphate by EA-pyrolysis-IRMS continuous flow technique

Christophe Lécuyer,[1]*† François Fourel,[1] François Martineau,[1] Romain Amiot,[1] Aurélien Bernard,[1] Valérie Daux,[2]‡ Gilles Escarguel[1] and John Morrison[3]

[1] Laboratoire CNRS UMR 5125 'Paléoenvironnements & Paléobiosphère', Université Claude Bernard Lyon 1, Campus de la Doua, F-69622, Villeurbanne, France
[2] Laboratoire des Sciences du Climat et de l'Environnement, UMR CEA/CNRS 1572, L'Orme des Merisiers, Bât. 701, CEA Saclay, 91191 Gif/Yvette Cedex, France
[3] GV Instruments, Crewe Road, Wythenshawe, Manchester, M23 9BE, UK

Received 7 June 2006; Accepted 28 September 2006

A high-precision, and rapid on-line method for oxygen isotope analysis of silver phosphate is presented. The technique uses high-temperature elemental analyzer (EA)-pyrolysis interfaced in continuous flow (CF) mode to an isotopic ratio mass spectrometer (IRMS). Calibration curves were generated by synthesizing silver phosphate with a 13‰ spread in $\delta^{18}O$ values. Calibration materials were obtained by reacting dissolved potassium dihydrogen phosphate (KH_2PO_4) with water samples of various oxygen isotope compositions at 373 K. Validity of the method was tested by comparing the on-line results with those obtained by classical off-line sample preparation and dual inlet isotope measurement. In addition, silver phosphate precipitates were prepared from a collection of biogenic apatites with known $\delta^{18}O$ values ranging from 12.8 to 29.9‰ (V–SMOW). Reproducibility of ±0.2‰ was obtained by the EA-Py-CF-IRMS method for sample sizes in the range 400–500 μg. Both natural and synthetic samples are remarkably well correlated with conventional $^{18}O/^{16}O$ determinations. Silver phosphate is a very stable material and easy to degas and, thus, could be considered as a good candidate to become a reference material for the determination of $^{18}O/^{16}O$ ratios of phosphate by high-temperature pyrolysis.

KEYWORDS: phosphate; oxygen isotope; pyrolysis; continuous flow; biogenic apatite

INTRODUCTION

The oxygen isotope analysis of silver phosphate precipitated from biogenic phosphates opens up a large spectrum of paleoenvironmental applications[1–3] where elemental analyzer-pyrolysis-continuous flow-isotope ratio mass spectrometry techniques (EA-Py-CF-IRMS) play an important role[4,5] owing to their precision, speed of measurement and sensitivity. For example, intra-tooth micro sampling of continental hypsodont (continuous growth) vertebrates provides isotopic data used to calculate tooth growth rate, past seasonality and mean air temperatures.[6] Calibration curves and an adequate choice of reference material are required in order to compare EA-Py-CF-IRMS data with that obtained by conventional offline techniques such as the use of either fluorination,[7,8] or graphite reduction[9,10] of silver phosphate. To date, for EA-Py-CF-IRMS techniques, calibration curves have been generated by analyzing internal laboratory standards from various oxygen-bearing compounds (e.g. sucrose, silver nitrate, barium sulfate, potassium dihydrogen phosphate) presenting various degrees of chemical stability with time and which exhibit a large spread in $\delta^{18}O$ values as shown by Morrison[11] and Kornexl *et al.*[12] To produce the most accurate ^{18}O-phosphate calibration curves, we propose a method based on easily synthesized silver phosphate samples generated from water samples with different $\delta^{18}O$ values to avoid matrix effects and deterioration of the reference material with time.

*Correspondence to: Christophe Lécuyer, Laboratoire CNRS UMR 5125, 'Paléoenvironnements & Paléobiosphère', Université Claude Bernard Lyon 1, Campus de la Doua, F-69622 Villeurbanne, France.
E-mail: clecuyer@univ-lyon1.fr
†Also at Institut Universitaire de France, 103 Boulevard Saint-Michel, 75005 Paris, France.
‡Also at Université Paris 6, 4 place Jussieu, 75252 Paris Cedex 05, France.

EXPERIMENTAL

Analytical techniques

Synthesis of silver phosphate internal standards

Eleven samples of dissolved potassium dihydrogen phosphate (KH_2PO_4) were prepared to promote oxygen isotope exchange using double deionized water samples (DDWs) of various oxygen isotope compositions (Table 1). In each run,

Table 1. Oxygen isotope compositions of water samples that reacted with KH_2PO_4 to produce silver phosphate that were analyzed both by conventional offline and EA-Py-CF-IRMS techniques. Yields correspond to chemical recoveries during the precipitation of silver phosphate from dissolved KH_2PO_4. SD = Standard Deviation

Sample	Yield (wt%)	$\delta^{18}O$ (H_2O) AquaPrep	SD	$\delta^{18}O$ (PO_4) Offline method	SD 1σ	$\delta^{18}O$ (PO_4) Online method	SD 1σ
P1	95.8	−29.44	0.01	3.23	0.07	4.80	0.24
P2	89.9	−25.06	0.01	3.36	0.03	5.01	0.17
P3	92.4	−17.97	0.02	5.95	0.07	7.04	0.17
P4	93.2	−14.37	0.02	8.27	0.17	9.36	0.31
P5	91.7	−10.41	0.02	8.91	0.02	10.31	0.18
P6	93.5	−4.73	0.03	10.85	0.11	12.08	0.14
P7	93.5	−1.66	0.02	12.51	0.06	13.58	0.26
P8	94.3	0.42	0.01	13.53	0.05	14.56	0.13
P9	95.8	2.49	0.04	14.55	0.12	15.05	0.28
P10	93.6	5.29	0.03	15.77	0.11	16.45	0.27
P11	96.2	8.07	0.01	15.84	0.04	17.12	0.12

Table 2. Oxygen isotope compositions of silver phosphates obtained from biogenic apatites that were analyzed both by conventional off-line and EA-Py-CF-IRMS techniques. SD = Standard Deviation

Sample	Material	Reference	$\delta^{18}O$ (PO_4) offline	SD1σ	$\delta^{18}O$ (PO_4) online	SD 1σ
TH003	Turtle plate	Amiot *et al.*[16]	12.80	0.16	13.59	0.20
TH007b	Crocodile tooth	Unpublished	13.05	0.17	13.54	0.15
MA2	Human tooth	Daux *et al.*[15]	15.24	0.11	16.25	0.25
ES4	Lingulid shell	Lécuyer *et al.*[10]	15.93	0.19	15.91	0.08
TU005	Crocodile tooth	Amiot *et al.*[16]	16.40	0.14	17.49	0.15
DOM4	Human tooth	Daux *et al.*[15]	17.10	0.12	17.82	0.17
L1D	Fish tooth	Lécuyer *et al.*[17]	18.00	0.15	19.09	0.17
AST53	Fish tooth	Lécuyer *et al.*[17]	18.70	0.08	19.35	0.29
D36	Fish tooth	Lécuyer *et al.*[17]	18.90	0.13	19.84	0.11
TH006	Dinosaur tooth	Amiot *et al.*[16]	20.20	0.17	20.61	0.27
93362	Fish tooth	Lécuyer *et al.*[17]	20.30	0.15	20.75	0.09
D35	Fish tooth	Lécuyer *et al.*[17]	21.30	0.10	21.44	0.23
TC13400E	Bovidae tooth	Unpublished	23.90	0.14	24.02	0.38
REP8	Snake vertebrae	Lécuyer *et al.*[18]	29.85	0.05	28.99	0.19

50 mg of KH_2PO_4 was dissolved in 35 ml of deionized water. The resulting solutions had a concentration of 1000 mgl^{-1} (10.6 mM l^{-1}) of phosphate ions with a pH of 5 at ambient temperature; $H_2PO_4^-$ was the dominant phosphate species. The solutions were transferred into Ace Glass Pyrex tubes sealed with a threaded Teflon plug. These reaction tubes were placed in an oven for 7 days at 373 K. This protocol ensured sizable oxygen isotope exchange between dissolved phosphate and water according to Lécuyer *et al.*[13] Each sample of dissolved phosphate was quantitatively precipitated as silver phosphate.[14] Chemical recoveries ranged from 90 to 96 wt% (Table 1).

Synthesis of silver phosphate from natural apatites

Fourteen samples of modern or fossil biogenic apatites were selected for their large published range of $\delta^{18}O$ values,[15–19] except samples TH007b and TC13400E, (Table 2). The oxygen isotope compositions of these marine invertebrates (lingulids) and terrestrial or aquatic vertebrates (fish, reptiles, mammals) bound the isotopic range of biogenic apatites, which reflects variations in body or ambient temperature and oxygen isotope composition of ingested water and food. Silver phosphate was synthesized from all these samples according to a protocol adapted from the original method published by Crowson *et al*[14] and slightly modified by Lécuyer *et al.*[7] After dissolution of 15 to 30 mg of powdered apatite in 2 M HF at 25 °C for 24 h, the CaF_2 that precipitated was separated from the solution, which included the phosphate, by centrifugation. The CaF_2 precipitate was rinsed three times using DDW and the rinse water was added to the solution which was neutralized with a 2 M KOH solution. Cleaned Amberjet strong anion exchange resin (2 ml) was added to the neutralized solution in polypropylene tubes. The tubes were placed on a shaker table for 12 h to promote the ion exchange process. Excess solution was discarded and the resin was washed five times with DDW to remove the traces of ionic contaminants. To elute the phosphate ions quantitatively from the resin, 25–30 ml of 0.5 M NH_4NO_3 was added to bring the pH of the solution to 7.5–8.5, and the tubes were gently shaken for about 5 h. Silver phosphate was precipitated from the eluted solution. Following the method of Firsching,[20] the solution was placed

J. Mass Spectrom. 2007; **42**: 36–41
DOI: 10.1002/jms

in a 250-ml Erlenmeyer flask and about 1 ml of concentrated NH_4OH was added to raise the pH to 9–10. Fifteen milliliters of ammoniacal $AgNO_3$ solution was added to the flask. Upon heating this solution to 70 °C in a thermostatic bath, millimeter-sized yellow crystals of Ag_3PO_4 precipitated. The crystals of silver phosphate were collected on a Millipore filter, washed three times with DDW and air-dried at 50 °C.

Preparation of synthetic silver phosphate working standards

Water samples with $\delta^{18}O$ values varying from −29.4‰ to +8.1‰ (Table 1) were reacted with KH_2PO_4 with an initial $\delta^{18}O$ value of 11.7 ± 0.2‰. After 1 week of reaction at 373 K, we obtained a pool of eleven samples of about 145 mg of silver phosphate. Each sample was analyzed three times according to the off-line method described above providing a $\delta^{18}O$ value range from 3.2‰ to 16.1‰ (Table 1).

Water samples used to generate synthetic silver phosphates were calibrated for $\delta^{18}O$ values using an automated CO_2 equilibration technique developed by Horita *et al.*[21] Aliquots of 200 µl of water were automatically equilibrated with CO_2 and analyzed using a MultiPrep system on-line with a GVI IsoPrime dual inlet IRMS. Reproducibility was typically ±0.03‰ (Table 1).

$\delta^{18}O$ of silver phosphate

Data obtained with conventional techniques

The first set of oxygen isotope data was obtained by the following conventional off-line method. Aliquots of 8 mg of silver phosphate along with 0.5 mg of pure graphite were weighed into tin reaction capsules and loaded into quartz tubes and degassed for 30 min at 80 °C in vacuum. Silver phosphate was reduced to carbon dioxide at a temperature of 1100 °C following the protocol of Lécuyer *et al.*[10] adapted from O'Neil *et al.*[9] The CO_2 produced during this reaction was directly trapped in liquid nitrogen avoiding any kind of isotopic reaction with quartz at high temperature. The oxygen isotope ratio of the gas was measured with a VG Prism II mass spectrometer in dual inlet mode. The isotopic data represent averages of triplicate analyses and are presented with respect to the V–SMOW scale (Tables 1 and 2). The average standard deviation equals 0.11 ± 0.05‰ when combining both analyses of silver phosphates from synthetic and natural phosphates (Table 3). Silver phosphate precipitated from standard NBS120c (natural Miocene phosphorite from Florida) gave an average $\delta^{18}O$ value of 21.70 ± 0.10 ($n = 16$). Calibration of the 'graphite method' described above has been made with oxygen isotope measurements using fluorination. As this technique ensures a total conversion of apatite oxygen to carbon dioxide, any bias resulting from the so-called 'scale compression factor' (Vennemann *et al.*)[8] has been corrected by using two standards of distinct oxygen isotope composition. For NBS120c, we obtained a comparable mean $\delta^{18}O$ value of 21.70 ± 0.14‰ ($n = 21$). To bracket the isotopic range documented in this study, we analyzed the 'Durango apatite' which gave a mean $\delta^{18}O$ value of +9.45‰ ($n = 3$) by off-line pyrolysis against a value of +9.6‰ obtained by fluorination using BrF_5 reagent (C. France-Lanord, personnal communication).

Table 3. Correlation (unbiased R^2) between $\delta^{18}O$ mean values and standard deviations (SD), and mean expected $\delta^{18}O$ SD. For both 'synthetic' and 'natural' data sets, and off-line and online techniques, estimated $\delta^{18}O$ SD appear to be uncorrelated to their associated $\delta^{18}O$ mean values (significance level $\alpha > 0.05$ in all four cases after a Holm's correction of the individual p-values for limiting the overall experimental error rate)[22]. This relation remains insignificant after grouping the 'synthetic' and 'natural' data sets into a 'total' dataset, thus allowing the estimate of the expected $\delta^{18}O$ SD-values for the two analytical techniques

	Unbiased R^2 (p-value) [H_0: $R^2 = 0$; H_1: $R^2 \neq 0$]	Expected $\delta^{18}O$ SD ($\mu \pm 1\sigma$)
Synthetic – off-line method	0.031 ($p = 0.60$)	0.077 ± 0.045
Synthetic – on-line method	9.9×10^{-4} ($p = 0.93$)	0.206 ± 0.067
Natural – off-line method	0.396 ($p = 0.016$)	0.133 ± 0.038
Natural – on-line method	0.107 ($p = 0.25$)	0.195 ± 0.083
Total – off-line method	0.0699 ($p = 0.21$)	0.108 ± 0.049
Total – on-line method	0.0055 ($p = 0.73$)	0.200 ± 0.075

Data obtained with EA-Py-CF-IRMS technique

A second set of oxygen isotope data was obtained by averaging five measurements of aliquots of 400–500 µg of the same silver phosphate samples mixed with 500 mg of nickelized carbon and reduced to CO by high-temperature EA-pyrolysis using a EuroVector EuroEA3028-HT system interfaced in continuous flow (CF) mode to an IRMS (GVI IsoPrime). The samples were placed in silver foil capsules and loaded into the autosampler of the high-temperature elemental analyzer. Pyrolysis was performed at 1270 °C. The ceramic reaction tube was packed with glassy carbon in the presence of nickelized graphite to generate CO gas. CO from the sample was then transferred by He flow into the mass spectrometer. Reference CO was introduced through the IsoPrime dual inlet system. The $\delta^{18}O$ value of NBS120c was arbitrarily fixed at 21.7‰ for correction of instrumental mass fractionation during the CO isotopic analysis. The average standard deviation equals 0.20 ± 0.075‰ when combining both analyses of silver phosphates from synthetic and natural phosphates (Table 3). Aliquots of silver phosphates from NBS120c were analyzed several times a day in order to account for possible instrumental drift.

RESULT AND DISCUSSION

The measurement of oxygen isotopes by EA-Py-CF-IRMS is where most of our efforts were concentrated in this experiment. We started from the fundamental oxygen pyrolysis works reported by Werner *et al.*,[23] Farquhar *et al.*,[24] Koziet,[25] Bréas *et al.*,[26] and Kornexl *et al.*[12] and adapted them to our samples. All the measurements were done with a

J. Mass Spectrom. 2007; **42**: 36–41
DOI: 10.1002/jms

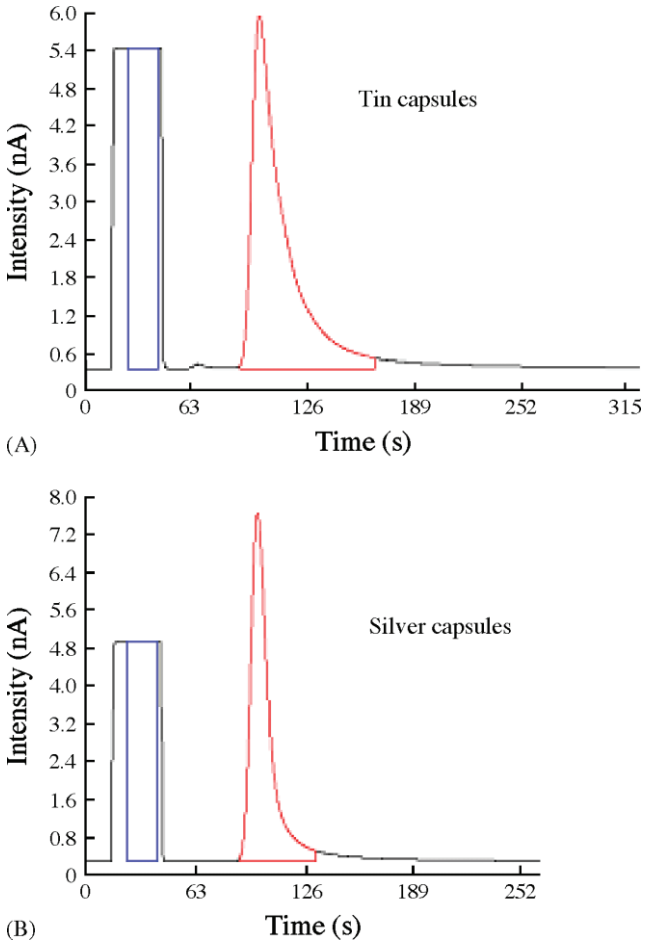

Figure 1. Mass 28 chromatograms corresponding to two Ag_3PO_4 samples prepared with a tin capsule (A) and with a silver capsule (B).

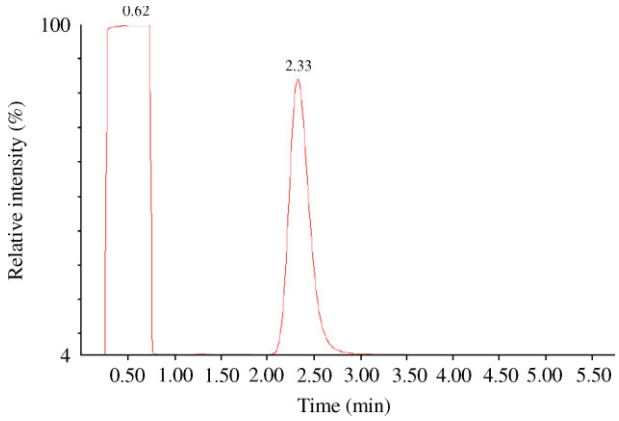

Figure 2. Typical mass 28 chromatogram obtained from Ag_3PO_4 sample with the optimized pyrolysis conditions. See the text for more explanations.

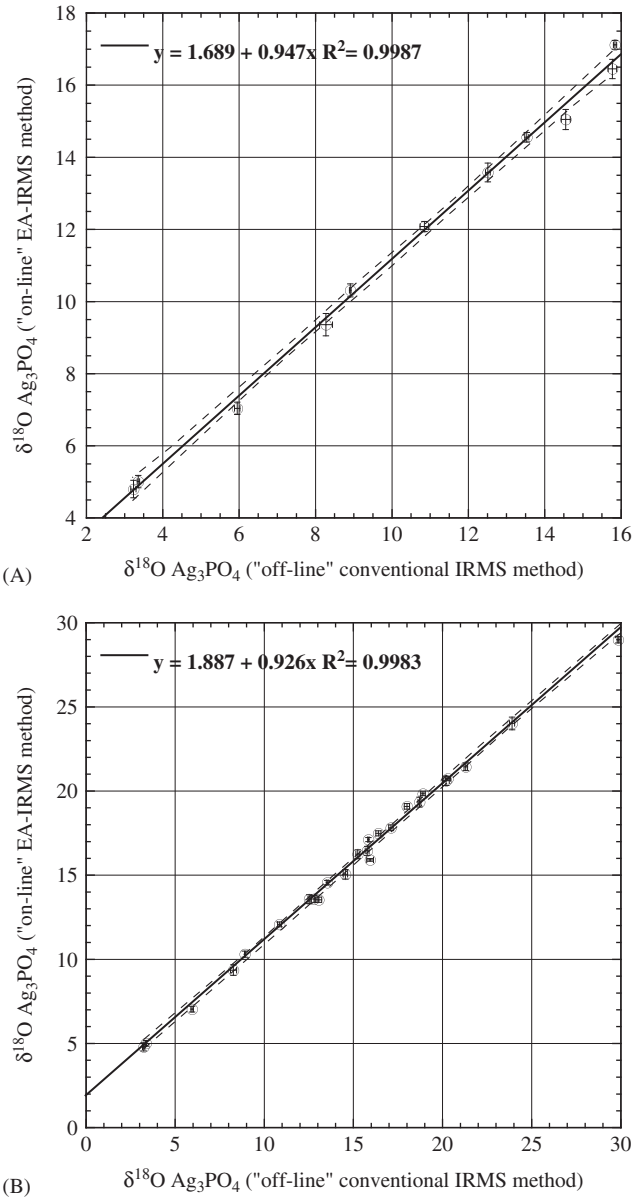

Figure 3. Linear relation between $\delta^{18}O_{SMOW}$ data obtained with EA-Py-CF-IRMS for Ag_3PO_4 samples *versus* $\delta^{18}O_{SMOW}$ data obtained with conventional offline techniques. (A) Synthetic Ag_3PO_4 samples only ($n = 11$): unbiased $R^2 = 0.9987$ [(99% CI: [0.9947; 0.9998])], Least-Squares model: $\delta^{18}O_{online} = (0.947 \times \delta^{18}O_{offline}) + 1.689$ (99% CI on the slope: [0.885; 0.986], 99% CI on the intercept: [1.271; 2.241]); (B) Both natural and synthetic Ag_3PO_4 samples ($n = 25$): unbiased $R^2 = 0.9985$ (99% CI: [0.9932; 0.9994]); Least-Squares model: $\delta^{18}O_{on-line} = (0.926 \times \delta^{18}O_{off-line}) + 1.889$ (99% CI on the slope: [0.916; 0.968], 99% CI on the intercept: [1.132; 2.059]). Dashed curves around the regression lines: 99% confidence belts on the predicted values; all confidence intervals (CI) estimated by a coupled parametric-nonparametric bootstrap with 10 000 iterations.

standard EuroVector EuroEA3028-HT elemental analyzer. On the basis of the results presented by Morrison,[11] we did not use a glassy carbon inner tube when pyrolyzing at a temperature of 1270 °C. In fact, we found that using the glassy carbon tube affected the shape of the chromatographic CO peak and increased the frequency of tube cleaning to remove the pyrolysis residues. We compared the results using silver capsules instead of tin capsules and noticed significant deterioration of chromatography while using tin (Fig. 1). It was therefore decided to use silver capsules for all the samples analyzed. Critically, we also noticed that

J. Mass Spectrom. 2007; **42**: 36–41
DOI: 10.1002/jms

reproducibility markedly improved by drying the samples at 70 °C overnight before placing them in the EA carousel. Following the discussion by Morison,[11] it was found that adding nickelized graphite to each silver capsule along with the silver phosphate sample (50 : 50) improved the reaction and lifetime of the reactor. Figure 2 shows an example of a typical chromatogram demonstrating a well-resolved and sharp CO peak. Throughout the experiments, we did not notice any significant intersample memory effect. It is recommended to replace the reactor tube after the analyses of about 300 consecutive samples.

We investigated whether the resulting 13‰ range in isotopic compositions for the eleven 'synthetic' silver phosphate samples could be used to intercalibrate the two analytical methods via a least-squares linear regression approach. A best fit line was computed between $\delta^{18}O_{SMOW}$ data obtained with EA-Py-CF-IRMS for synthetic Ag_3PO_4 samples as the dependent variable and $\delta^{18}O_{SMOW}$ data obtained with conventional offline techniques as the independent variable ($R^2 = 0.998$; Fig. 3(A)). The quality of the fit demonstrates that EA-Py-CF-IRMS is a suitable method for determining precise ($1\sigma = 0.2 \pm 0.075$‰) oxygen isotope compositions for small samples (≈400–500 μg) of silver phosphate. The results obtained on synthetic phosphates were confirmed by the measurements of silver phosphate obtained from the collection of biogenic apatites which lie on the regression line without deteriorating the quality of the fit with a R^2 of 0.9983 (Fig. 3(B)). We have repeated the conventional $\delta^{18}O$ procedure for sample REP8 with 8 years in between the two measurements and obtained two values at 29.85‰ and 29.79‰, which demonstrates that the silver phosphate is stable for at least 8 years and thus would be an appropriate reference material.

CONCLUSIONS

The two sets of data obtained in this study clearly demonstrate that EA-Py-CF-IRMS can be reliably used for the high-precision ($1\sigma = 0.2$‰) determination of $^{18}O/^{16}O$ ratios of phosphates. The protocol we have developed for the synthesis of silver phosphates offers a unique solution to the problem of generating working standards that are adapted to the analysis of biogenic apatites. The EA-Py-CF-IRMS setup we have used is significantly simpler than those previously published.[23–26] Pyrolysis performed below 1400 °C, without the need for a glassy carbon tube, makes this technique cheaper. Silver phosphate is easy to degas and maintains isotopic integrity for at least 8 years, which demonstrates that it is a good candidate for a reference material for the determination of $^{18}O/^{16}O$ ratios of phosphate by EA-Py-CF-IRMS.

Acknowledgements

The authors thank two anonymous reviewers who contributed to improve the scientific content of this work.

REFERENCES

1. Fricke HC, O'Neil JR. Inter- and intra-tooth variation in the oxygen isotope composition of mammalian tooth enamel phosphate: implications for palaeoclimatological and palaeobiological research. *Paleogeogr. Palaeoclimatol. Palaeoecol.* 1996; **126**: 91.
2. Fricke HC, Clyde WC, O'Neil JR, Gingerich PD. Evidence for rapid climate change in North America during the latest Paleocene thermal maximum: oxygen isotope compositions of biogenic phosphate from the Bighorn Basin (Wyoming). *Earth Planet. Sci. Lett.* 1998a; **160**: 193.
3. Fricke HC, Clyde WC, O'Neil JR, Gingerich PD. Intra-tooth variations in d18O (PO4) of mammalian tooth enamel as a record of seasonal variations in continental climate variables. *Geochim. Cosmochim. Acta* 1998b; **62**: 1839.
4. Joachimski MM, van Geldern R, Breisig S, Day J, Buggisch W. Oxygen isotope evolution of biogenic calcite and apatite during the middle and late Devonian. *Int. J. Earth Sci.* 2004; **93**: 542.
5. Joachimski MM, von Bitter PH, Buggisch W. Constraints on Pennsylvanian glacioeustatic sea-level changes using oxygen isotopes of conodont apatite. *Geology* 2006; **34**: 277.
6. Sharma S, Joachimski MM, Tobschall HJ, Singh IB, Tewari DP, Tewari R. Oxygen isotopes of bovid teeth as archives of paleoclimatic variations in archaeological deposits of the Ganga plain, India. *Q. Res.* 2004; **62**: 19.
7. Lécuyer C, Grandjean P, O'Neil JR, Capetta H, Martineau F. Thermal excursions in the ocean at the Cretaceous-Tertiary boundary (northern Morocco): the d18O record of phosphatic fish debris. *Paleogeogr. Palaeoclimatol. Palaeoecol.* 1993; **105**: 235.
8. Venneman TW, Fricke HC, Blake RE, O'Neil JR, Colman A. Oxygen isotope analysis of phosphates: a comparison of techniques for analysis of Ag3PO4. *Chem. Geol.* 2002; **185**: 321.
9. O'Neil JR, Roe LJ, Reinhard E, Blake RE. A rapid and precise method of oxygen isotope analyses of biogenic phosphate. *Isr. J. Earth Sci.* 1994; **43**: 203.
10. Lécuyer C, Grandjean P, Barrat J-A, Nolvak J, Emig C, Paris F, Robardet M. d18O and REE contents of phosphatic brachiopods: A comparison between modern and lower Paleozoic populations. *Geochim. Cosmochim. Acta* 1998; **62**: 2429.
11. Morrison J. A new high temperature EA-pyrolysis-IRMS solution to d18O analyses of phosphates. *Application Brief AB10*, Micromass, 1999.
12. Kornexl BE, Gehre M, Höfling R, Werner RA. On-line d18O measurements of organic and inorganic substances. *Rapid Commun. Mass Spectrom.* 1999; **13**: 1685.
13. Lecuyer C, Grandjean P, Sheppard SMF. Oxygen isotope exchange between dissolved phosphate and water at temperature <135 °C: Inorganic versus biological fractionations. *Geochim. Cosmochim. Acta* 1999; **63**: 855.
14. Crowson RA, Showers WJ, Wright EK, Hoering TC. A method for preparation of phosphate samples for oxygen isotope analysis. *Anal. Chem.* 1991; **63**: 2397.
15. Daux V, Lecuyer C, Adam F, Martineau F, Vimeux F. Oxygen isotope composition of human teeth and the record of climate changes in France (Lorraine) during the last 1700 years. *Clim. Change* 2005; **70**: 445.
16. Amiot R, Lécuyer C, Buffetaut E, Escarguel G, Fluteau F, Martineau F. Oxygen isotopes from biogenic apatites suggest widespread endothermy in Cretaceous dinosaurs. *Earth Pl. Sci. Let.* 2006; **246**: 41.
17. Lécuyer C, Picard S, Garcia JP, Sheppard SMF, Grandjean P, Dromart G. Thermal evolution of Tethyan surface waters during the middle-late Jurassic: Evidence from d18O values of marine fish teeth. *Paleoceanography* 2003; **18**: 1076, doi:10.1029/2002PA000863.
18. Lécuyer C, Grandjean P, Mazin J-M, de Buffrénil V. In *Secondary Adaptation to Life in Water II, University of Copenhagen (Denmark), Geologisk Museum, 13–17 September, ISBN 87-88114-22-8*, Hoch E and Brantsen AK (eds). University of Copenhagen: Copenhagen, Denmark, 1999; 33.
19. Zazzo A, Lécuyer C, Mariotti A. Experimentally-controlled carbon and oxygen isotopeexchange between bioapatites and water under inorganic and microbially-mediated conditions. *Geochim. Cosmochim. Acta* 2004; **68**: 1.

20. Firsching FH. Precipitation of silver phosphate from homogeneous solution. *Anal. Chem.* 1961; **33**: 873.
21. Horita J, Ueda A, Mizukami K, Takatori I. Automatic dD and d18O analyses of multi-water samples using H2- and CO2-water equilibtation methods with a common equilibration set-up. *Appl. Radiat. Isot.* 1989; **40**: 801.
22. Holm S. A simple sequentially rejective multiple test procedure. *Scand. J. Stat.* 1979; **6**: 65.
23. Werner RA, Kornexl BE, Rossman A, Schmidt HL. On-line determination of d18O values of organic substances. *Anal. Chim. Acta* 1996; **319**: 159.
24. Farquhar GD, Henry BK, Styles JM. A rapid on-line technique for determination of oxygen isotope composition of nitrogen-containing organic matter and water. *Rapid Commun. Mass Spectrom.* 1997; **11**: 1554.
25. Koziet J. Isotope ratio mass spectrometric method for the on-line determination of oxygen-18 in organic matter. *J. Mass Spectrom.* 1997; **32**: 103.
26. Bréas O, Guillou C, Reniero F, Sada E, Angerosa F. Oxygen-18 measurement by continuous flow pyrolysis/isotope ratio mass spectrometry of vegetable oils. *Rapid Commun. Mass Spectrom.* 1998; **12**: 188.

J. Mass Spectrom. 2007; **42**: 36–41
DOI: 10.1002/jms

Research Article

Rapid Communications in Mass Spectrometry

Received: 2 February 2011 Revised: 13 April 2011 Accepted: 13 April 2011 Published online in Wiley Online Library

Rapid Commun. Mass Spectrom. **2011**, *25*, 2691–2696
(wileyonlinelibrary.com) DOI: 10.1002/rcm.5056

$^{18}O/^{16}O$ ratio measurements of inorganic and organic materials by elemental analysis–pyrolysis–isotope ratio mass spectrometry continuous-flow techniques‡

François Fourel[1]*, François Martineau[1], Christophe Lécuyer[1†], Hans-Joachim Kupka[2], Lutz Lange[2], Charles Ojeimi[3] and Mike Seed[4]

[1]Laboratoire de Géologie de Lyon "Terre, Planètes Environnement", CNRS-UMR 5276 Université Claude Bernard Lyon 1, Ecole Normale Supérieure de Lyon Campus de la Doua, F-69622, Villeurbanne, France
[2]Elementar Analysensysteme GmbH, Donaustrasse 7, 63452 Hanau, Germany
[3]Elementar France 5, place Charles Beraudier 69, 428 Lyon Cedex 03, France
[4]Isoprime Ltd., Isoprime House Earl, Road, Cheadle Hulme, Cheadle SK8 6PT, UK

We have used a high-precision, easy, low-cost and rapid method of oxygen isotope analysis applied to various O-bearing matrices, organic and inorganic (sulfates, nitrates and phosphates), whose $^{18}O/^{16}O$ ratios had already been measured. It was first successfully applied to ^{18}O analyses of natural and synthetic phosphate samples. The technique uses high-temperature elemental analysis–pyrolysis (EA-pyrolysis) interfaced in continuous-flow mode to an isotope ratio mass spectrometry (IRMS) system. Using the same pyrolysis method we have been able to generate a single calibration curve for all those samples showing pyrolysis efficiencies independent of the type of matrix pyrolysed. We have also investigated this matrix-dependent pyrolysis issue using a newly developed pyrolysis technique involving 'purge-and-trap' chromatography. As previously stated, silver phosphate being a very stable material, weakly hygroscopic and easily synthesized with predictable $^{18}O/^{16}O$ values, could be considered as a good candidate to become a reference material for the determination of $^{18}O/^{16}O$ ratios by EA-pyrolysis-IRMS.

Continuous-flow pyrolysis techniques allow the determination of isotopic ratios for large series of small (a few hundreds of micrograms) samples. These methods have been applied to different types of organic or inorganic material although there is a recurrent problem regarding the adequate choice of pyrolysis technique as well as of the reference material for the calibration of the measurements.[1] One application in which a growing interest has recently been demonstrated is the oxygen isotope analysis of silver phosphate precipitated from biogenic phosphates, opening a large spectrum of paleoenvironmental applications that allow the reconstruction of variations in past seasonality, marine paleotemperatures and mean air temperatures.[2–7] Results obtained from Elemental Analyzer–Isotope Ratio Mass Spectrometry (EA-IRMS) techniques need to be compared with those obtained by conventional offline techniques, implying the use of either fluorination (Lécuyer *et al.*[8] and Vennemann *et al.*[9]) or graphite reduction of silver phosphate into CO_2 (O'Neil *et al.*[10] and Lécuyer *et al.*[11]). This comparison was described in Lécuyer *et al.*,[1] where, in order to avoid matrix effects, the method described was based only on silver phosphate samples. Unlike $^{13}C/^{12}C$, $^{15}N/^{14}N$ or $^{34}S/^{32}S$ EA-IRMS determinations where the protocols are well defined and very little variations are observed between laboratories, $^{18}O/^{16}O$ analyses present significant variations in the methods and no real consensus has yet been found (Brand *et al.*[12]), each group concentrating on its own application. In the early days of EA-pyrolysis, Koziet[13] focused on water and food samples looking at the effect of pyrolysis temperature before finally using 1300°C as the standard temperature.

Farquhar *et al.*[14] also looked at the oxygen pyrolysis of organic material using 1060°C as the optimum pyrolysis temperature while investigating the effect of CO-N_2 gas chromatographic separation. This separation of CO and N_2 is a key parameter as well as a significant limitation of this technique, as mentioned by Brand *et al.*[12] In the mass spectrometer, N_2 gas yields ions at *m/z* 28 and 29 whereas CO occurs at *m/z* 28 and 30. N_2 elutes first and must be totally eluted before CO is measured otherwise the mass30/mass28 ratio is interfered with. Kornexl *et al.*[15] suggested an alternative pyrolysis setup working at 1400°C and presented data obtained from both organic and inorganic oxygen-bearing samples. Bréas *et al.*[16] described a modified

* *Correspondence to:* F. Fourel, Laboratoire de Géologie de Lyon "Terre, Planètes Environnement", CNRS-UMR 5276 Université Claude Bernard Lyon 1, Ecole Normale Supérieure de Lyon, Campus de la Doua, F-69622 Villeurbanne, France.
E-mail: francois.fourel@univ-lyon1.fr
† Present address: Institut Universitaire de France, 103 Boulevard Saint-Michel, 75005 Paris, France.
‡ Presented at the 6th Congress of the French Society of Stable Isotopes (Société Française des Isotopes Stables, SFIS) held 26–29 October 2010 in Toulouse, France.

technique applied to food samples, operating at 1100°C as their optimized pyrolysis temperature. Saurer *et al.*[17] described their own pyrolysis setup dedicated to cellulose analysis and working at 1080°C. More recently, Revesz and Böhlke[18] compared various offline and online techniques for $\delta^{18}O$ determinations applied to nitrate analyses. The aim of this study was to develop a unified pyrolysis technique which could be applied to different types of samples from easily pyrolyzed organic matrices to more refractory samples like silver phosphates. This would allow the use of silver phosphate as a worldwide reference material for different pyrolysis applications.

Calibration curves have been set up by analyzing internal laboratory standards from various oxygen-bearing compounds (e.g. sucrose, silver nitrate, barium sulphate and potassium dihydrogen phosphate) with various degrees of chemical stability with time and which offer a range of spreads in the $\delta^{18}O$ values (Morrison[19]). One advantage of such a method is that it avoids the so-called 'matrix effect', allowing silver phosphate samples to be used as a reference material. Silver phosphate is an extremely valuable reference material as it can be easily synthesized in any laboratory worldwide and it shows virtually no deterioration with time.

EXPERIMENTAL

Offline conventional $\delta^{18}O$ analyses

The synthesis of silver phosphate as internal standards as well as from natural apatites is fully described in Lécuyer *et al.*[1] EA-pyrolysis-IRMS data were compared with a set of reference values that were obtained following a conventional offline method. Aliquots of 8 mg of silver phosphate were reduced to CO_2 in the presence of 0.5 mg of graphite at a temperature of 1100°C, following the protocol of Lécuyer *et al.*[11] adapted from O'Neil *et al.*[10] The oxygen isotope ratio of the gas was measured with a VG Prism II™ (IsoPrime Ltd., Cheadle Hulme, UK) isotope ratio mass spectrometer or an IsoPrime™ (IsoPrime Ltd.) isotope ratio mass spectrometer in dual-inlet mode. The $\delta^{18}O$ values reported have been calculated on the SLAP-SMOW scale following the procedures reported in Brand *et al.*[12] The average standard deviation is 0.11 ± 0.05‰ considering the analyses of silver phosphates from both synthetic and natural phosphates. Silver phosphate precipitated from standard NBS120c (Miocene phosphorite from Florida, USA) gave an average $\delta^{18}O$ value of 21.70 ± 0.10 ($n = 16$).

Conventional EA-pyrolysis-IRMS

EA-pyrolysis-IRMS data for silver phosphates were obtained by averaging five measurements of aliquots per sample. Between 400 and 500 µg of silver phosphate sample was mixed with 500 µg of nickelized carbon and reduced to CO by high-temperature EA-Pyrolysis using a EuroVector EuroEA3028-HT system (EuroVector SpA, Milan, Italy) interfaced to an IsoPrime isotope ratio mass spectrometer working in continuous-flow mode. The sample was placed in a silver foil capsule then loaded into the autosampler of the high-temperature elemental analyzer. Pyrolysis was performed at 1250°C. We used a ceramic reaction tube directly packed with glassy carbon, without any inner glassy carbon tube, in the presence of nickelized graphite to generate CO gas. The CO from the sample is then carried via a helium flow into the mass spectrometer. A reference CO sample is introduced through the reference gas injector system of the mass spectrometer. As mentioned above, the $\delta^{18}O$ value of NBS120c is fixed at 21.7‰ for correction of instrumental mass fractionation during the CO isotopic analysis. As was established by Lécuyer *et al.*,[1] the average standard deviation equals 0.20 ± 0.075‰ when combining the analyses of silver phosphates from both synthetic and natural phosphates. Aliquots of silver phosphates from NBS120c are analyzed every day, several times a day, in order to account for possible instrumental drift.

In addition to the silver phosphate samples, various O-bearing chemical matrices were pyrolysed under the same conditions and within the same analytical batches. The selected samples were sucrose (5 aliquots of 150 µg), saccarose (5 aliquots of 150 µg), vanillin (5 aliquots of 200 µg), barium sulfate (5 aliquots of 200 µg), and silver nitrate (5 aliquots of 200 µg). Reference values for other types of samples were provided by John Morrison (Nu Instruments Ltd., Wrexham, UK) from online continuous flow pyrolysis systems.

New 'purge-and-trap' high-temperature EA-pyrolysis-IRMS

The system used, called varioPYROcube, was recently developed by Elementar GmbH (Hanau, Germany). This system had already been used for the elemental and isotopic analysis of organic compounds (Sieper *et al.*[20]), but it had not yet been tested for the oxygen isotope analysis of phosphate samples. The general set up is shown in Fig. 1, consisting of a carbon-based reactor filled with a layer of glassy carbon chips and a layer of carbon black inside a glassy carbon tube. To prevent damage to the glassy carbon tube from contact with oxygen, this tube is placed inside a ceramic tube which is heated to 1450°C. The gap between the glassy carbon tube and the ceramics is flushed with helium, which is not used as carrier gas, but instead sent to vent. Due to diffusion of ambient air through the ceramics at higher temperature, this gas could be contaminated with oxygen and might lead to higher background in the mass spectrometer. Another novel feature of the system described by Sieper *et al.*[20] is the separation of the gaseous pyrolysis products by the use of a temperature-controlled 'purge-and-trap' chromatography device instead of a packed GC column as in the previously described system. In that configuration, during the pyrolysis step, the EA carrier gas helium flow is set to 'straight' mode. In that mode, N_2 is not trapped and flows into the system whereas CO is trapped into a selective desorption column. Once the pyrolysis step is finished, the helium flow is set to 'backflush' mode, allowing clean helium to flow through the desorption trap to avoid any effect to the mass spectrometer from nitrogen-containing species which decompose very slowly. The CO desorption unit is then heated up to 150°C and the trapped CO is desorbed and enters the thermal conductivity detector (TCD) where the signal is detected as a focused peak. The rest of the system is similar to the previously described EA setup.[20]

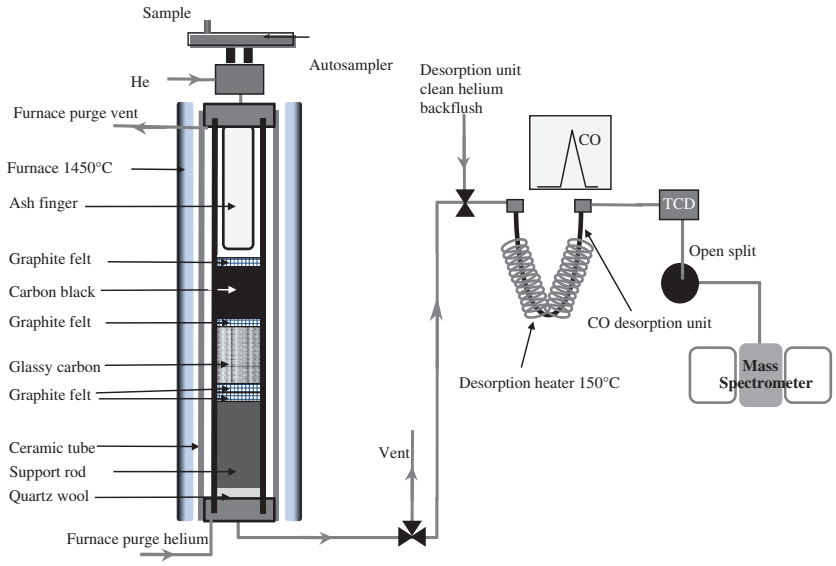

Figure 1. Oxygen pyrolysis setup for the 'purge-and-trap' varioPYROcube system derived from Sieper *et al.*[20] Pyrolysis temperature is set at 1450°C and desorption temperature is set at 150°C. Gas separation is ensured by the desorption unit. No GC packed column is used in this configuration.

DISCUSSION

Conventional EA-pyrolysis-IRMS

The optimization of the pyrolysis setup is fully described in Lécuyer *et al.*[1] Despite analyzing samples with different matrices, we did not modify the pyrolysis conditions and we pyrolyzed all the samples within the same analytical batches. All the measurements were carried out with a standard EuroVector EuroEA3028-HT elemental analyzer. As already mentioned, there was no need for a glassy carbon tube inside the ceramic tubes when pyrolysing at 1250°C. The samples were also outgassed at 70°C overnight before placing them in the EA carousel to avoid contamination by atmospheric water. Finally, in order to improve both the reaction and the lifetime of the reactor, nickelized graphite was added inside the silver capsules in a 1:1 proportion with respect to the silver phosphate samples.

Based on this protocol, we investigated whether the large range of isotopic compositions of various organic and inorganic matrices could allow us to intercalibrate the two methods by a

Table 1. Oxygen isotope compositions of silver phosphates (EPO 1, EPO5, EPO11, NBS120C), sucrose (ANU Sucr), vanillin (MV1), barium sulfate ($BaSO_4$) and silver nitrate ($AgNO_3$) that were analyzed in two runs by conventional EA–pyrolysis–IRMS continuous flow techniques. ref. values = reference $\delta^{18}O$ values for those samples. SD = standard deviation

RUN 1 Sample	$\delta^{18}O_{VSMOW}$ measured	SD	N	$\delta^{18}O_{VSMOW}$ ref. values
NBS120C	21.70 ‰	0.19 ‰	5	21.7 ‰
EPO1	5.03 ‰	0.43 ‰	3	3.2 ‰
EPO5	10.09 ‰	0.17 ‰	4	8.9 ‰
EPO11	16.67 ‰	0.15 ‰	3	15.8 ‰
ANU Sucr	34.73 ‰	0.25 ‰	3	36.4 ‰
MV1	10.83 ‰	0.25 ‰	3	9.5 ‰
$BaSO_4$	12.41 ‰	0.18 ‰	4	12.0 ‰
$AgNO_3$	18.93 ‰	0.23 ‰	3	19.6 ‰
RUN 2 Sample	$\delta^{18}O_{VSMOW}$ measured	SD	N	$\delta^{18}O_{VSMOW}$ ref. values
NBS120C	21.70 ‰	0.27 ‰	6	21.7 ‰
EPO1	5.10 ‰	0.41 ‰	6	3.2 ‰
EPO5	10.86 ‰	0.22 ‰	6	8.9 ‰
EPO11	17.92 ‰	0.15 ‰	5	15.8 ‰
ANU Sucr	35.16 ‰	0.44 ‰	5	36.4 ‰
MV1			5	
$BaSO_4$	14.08 ‰	0.65 ‰	5	12.0 ‰
$AgNO_3$	18.99 ‰	0.30 ‰	5	19.6 ‰

linear regression of data. This experiment was performed twice and the results of both runs are summarized in Table 1 and Fig. 2. The quality of the best fit ($R^2 = 0.9950$) demonstrates that high-temperature EA–pyrolysis–IRMS should be a suitable method for precisely determining ($1\sigma = 0.29 \pm 0.14$‰) the oxygen isotope compositions of relatively small samples (≈ 400–500 µg) of silver phosphate and of sucrose (≈ 150 µg) using the same calibration curve.

New 'purge-and-trap' high-temperature EA-pyrolysis-IRMS setup

The instrumental setup was derived from that described by Sieper *et al.*[20] We first investigated the treatment of the background signal, and concluded that it was necessary to use a blank subtraction subroutine in order to correct the data. This was because in any conventional system using GC column separation, any blank entering the system will be taken into account as a constant background dealt with during peak integration. Working with a 'purge-and-trap' system means that the blank gas is trapped into the desorption unit and released with the sample CO gas. It is therefore necessary to subtract this signal from that of the sample. Based on the experience of Sieper *et al.*,[20] we investigated different pyrolysis temperatures as well as different desorption temperatures to optimize the pyrolysis conditions for silver phosphate samples The best results were obtained by using a pyrolysis temperature of 1450°C and a CO desorption temperature of 150°C. Using these optimized conditions, we tested both reproducibility and accuracy for the oxygen isotope ratios of silver phosphates generated from biogenic apatites that we had already analyzed by conventional offline methods (Table 2). The measured values using the EA-pyrolysis method are in good agreement with the expected offline values, the average difference being 0.1‰. Another parameter tested with this device was the silver phosphate sample size. The accuracy of measurements is preserved for a silver phosphate sample size higher than 300 µg (Table 3). Below that threshold it seems that the data quality begins to deteriorate. Based on those preliminary

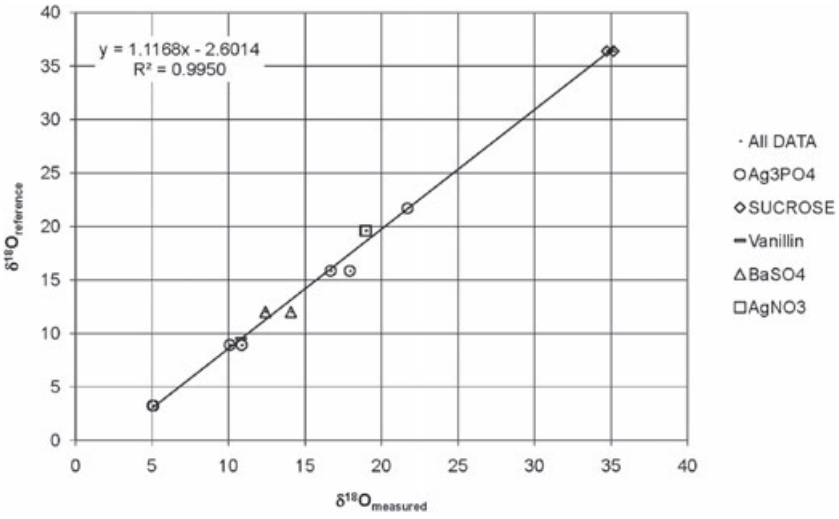

Figure 2. $\delta^{18}O_{VSMOW}$ values measured with conventional EA-pyrolysis-IRMS method described in Lécuyer *et al.*[1] plotted against reference $\delta^{18}O_{VSMOW}$ values for various organic and inorganic samples.

Table 2. Oxygen isotope compositions of silver phosphates obtained from biogenic apatites that were analyzed both by conventional off–line and new 'purge-and-trap' EA–pyrolysis–IRMS techniques. ref. values = reference $\delta^{18}O$ values for those samples. SD = standard deviation

Sample Name -	$\delta^{18}O_{VSMOW}$ measured	SD -	N -	$\delta^{18}O_{VSMOW}$ ref. values
NBS120c	21.70‰	0.17‰	5	21.7‰
CLR5	18.07‰	0.41‰	4	17.84‰
CLR6	18.02‰	0.41‰	3	18.05‰
CLR7	18.58‰	0.33‰	4	18.3‰
CL08	22.42‰	0.27‰	4	22.29‰
CL12	21.37‰	0.43‰	5	21.03‰
FC3 01	20.73‰	0.16‰	3	20.55‰
FC3 03	20.46‰	0.24‰	4	20.49‰
6-75-5	6.92‰	0.25‰	5	6.94‰
3-75-5	8.80‰	0.28‰	5	8.71‰
LI125-0-05	−9.48‰	0.26‰	5	−9.61‰

results we carried out an experiment where we mixed various matrices within the same batch using the same calibrated material as in the experiment described above. Sucrose, vanillin, $BaSO_4$ and $AgNO_3$ were then pyrolyzed alongside our silver phosphate samples (Table 4; Fig. 3). Once again, the quality of the best fit ($R^2 = 0.997$) obtained between

Table 3. Oxygen isotope compositions of various amounts of silver phosphates obtained from NBS120c that were analyzed with the new 'purge-and-trap' EA–pyrolysis–IRMS techniques. Sample amounts vary from 100 to 700 µg. SD = standard deviation. N = number of data points. AVERall = average calculated from all the analysed samples. AVER. 300-700 = average calculated with samples having masses between 300 and 700 µg

Sample weight (µg)	$\delta^{18}O_{VSMOW}$ measured	SD	N
100	21.20‰	0.80‰	7
300	21.87‰	0.24‰	8
500	21.89‰	0.26‰	7
700	21.80‰	0.22‰	8
	AVERall	SD	N
	21.70‰	0.50‰	30
	AVER. 300-700	SD	N
	21.85‰	0.23‰	23

Table 4. Oxygen isotope compositions (‰) of silver phosphates (EPO 1, EPO5, EPO11, NBS120C), sucrose (ANU Sucr), vanillin (MV1), barium sulfate ($BaSO_4$) and silver nitrate ($AgNO_3$) that were analyzed by the new 'purge-and-trap' EA–pyrolysis–IRMS techniques. ref. values = reference $\delta^{18}O$ values for those samples. SD = standard deviation (‰)

Sample	$\delta^{18}O_{VSMOW}$ measured	SD	N	$\delta^{18}O_{VSMOW}$ ref. values
NBS120C	21.70	0.10‰	5	21.70
SUCROSE	35.55	0.21	4	36.40
SACCHAROSE	27.96	0.04	5	27.90
VANILIN	9.01	0.22	4	9.50
BASO4	11.14	0.42	4	12.00
AGNO3	20.34	0.28	4	19.60
EPO2	3.29	0.24	4	3.36
EPO5	8.83	0.29	6	8.91
EPO11	15.79	0.23	6	15.84

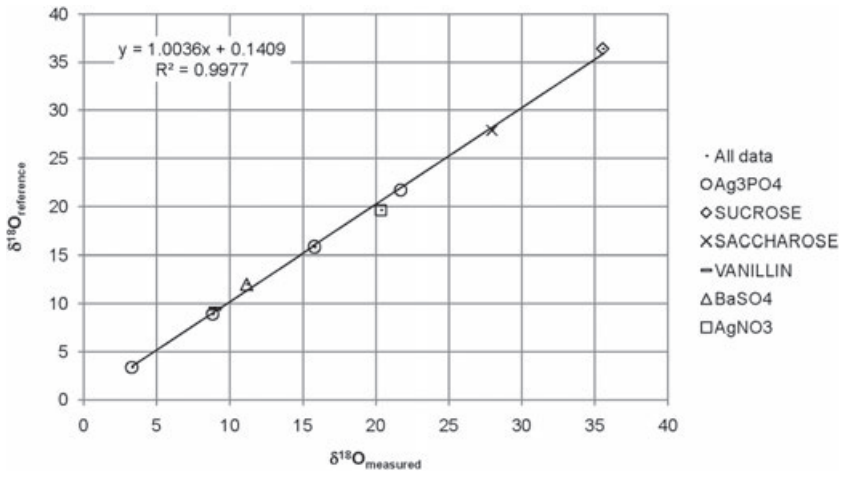

Figure 3. $\delta^{18}O_{VSMOW}$ values measured with the new EA-Pyrolysis-IRMS method using 'purge-and-trap' technology plotted against reference $\delta^{18}O_{VSMOW}$ values for various organic and inorganic samples.

measured values and reference values ($3‰ < \delta^{18}O < 35‰$) emphasizes the performance of this pyrolysis method. The reference values had been determined independently by other methods or in different laboratories for those samples. A key parameter is the slope of the regression line of 1.0036 that is very close to unity; this is an advantage for this technique over the conventional EA–pyrolysis–IRMS technique.

CONCLUSIONS

The data obtained through this study confirm that the EA–pyrolysis methods have the potential to be reliably used for the high-precision ($1\sigma = 0.2‰$) determination of $^{18}O/^{16}O$ ratios not only of phosphates, but also various oxygen-bearing organic and inorganic compounds. The new procedure, using a 'purge-and-trap' varioPYROcube elemental analyzer, is able to generate robust data in terms of accuracy and precision, taking also into account that the various caveats related to the chromatographic separation of gases, as described by Farquhar *et al.*,[14] are avoided. The lack of a universal calibration material has been a major drawback to the development of the oxygen pyrolysis technique. The protocol developed by Lécuyer *et al.*[1] for the synthesis of silver phosphates offers a unique solution to the generation of Ag_3PO_4 working standards in a large range of isotopic compositions, which can be adapted to various applications. Silver phosphate is very stable with time and only weakly hygroscopic. It thus could be considered as a top candidate as a reference material for the determination of $^{18}O/^{16}O$ ratios by high-temperature pyrolysis.

REFERENCES

[1] C. Lécuyer, F. Fourel, F. Martineau, R. Amiot, A. Bernard, V. Daux, G. Escarguel, J. Morrison. High-precision determination of $^{18}O/^{16}O$ ratios of silver phosphate by EA-pyrolysis-IRMS continuous flow technique. *J. Mass Spectrom.* **2007**, *42*, 36.
[2] H. C. Fricke, J. R. O'Neil, N. Lynnerup. Oxygen isotope composition of human tooth enamel from medieval Greenland: linking climate and society. *Geology* **1995**, *23*, 869.
[3] H. C. Fricke, J. R. O'Neil. Inter- and intra-tooth variation in the oxygen isotope composition of mammalian tooth enamel phosphate: implications for the palaeoclimatological and palaeobiological research. *Palaeogeogr. Palaeoclimatol. Palaeoecol.* **1996**, *126*, 91.
[4] H. C. Fricke, W. C. Clyde, J. R. O'Neil, P. D. Gingerich. Evidence for rapid climate change in North America during the latest Paleocene thermal maximum: oxygen isotope compositions of biogenic phosphate from the Bighorn Basin (Wyoming). *Earth Planet. Sci. Lett.* **1998**, *160*, 193.
[5] H. C. Fricke, W. C. Clyde, J. R. O'Neil, P. D. Gingerich. Intra-tooth variations in $\delta^{18}O$ (PO_4) of mammalian tooth enamel as a record of seasonal variations in continental climate variables. *Geochim. Cosmochim. Acta* **1998**, *62*, 1839.
[6] M. M. Joachimski, R. van Geldern, S. Breisig, J. Day, W. Buggisch. Oxygen isotope evolution of biogenic calcite and apatite during the Middle and Late Devonian. *Int. J. Earth Sci.* **2004**, *93*, 542.
[7] S. Sharma, M. M. Joachimski, H. J. Tobschall, I. B. Singh, D. P. Tewari, R. Tewari. Oxygen isotopes of bovid teeth as archives of paleoclimatic variations in archaeological deposits of the Ganga plain, India. *Quartenary Research* **2004**, *62*, 19.
[8] C. Lécuyer, P. Grandjean, J. R. O'Neil, H. Capetta, F. Martineau. Thermal excursions in the ocean at the Cretaceous-Tertiary boundary (northern Morocco): $\delta^{18}O$ record of phosphatic fish debris *Paleogeogr. Paleoclimatol. Paleoecol.* **1993**, *105*, 235.
[9] T. W. Venneman, H. C. Fricke, R. E. Blake, J. R. O'Neil, A. Colman. Oxygen isotope analysis of phosphates: a comparison of techniques for analysis of Ag_3PO_4. *Chem. Geol.* **2002**, *185*, 321.
[10] J. R. O'Neil, L. J. Roe, E. Reinhard, R. E. Blake. A rapid and precise method of oxygen isotope analysis of biogenic phosphates. *Isr. J. Earth Sci.* **1994**, *43*, 203.
[11] C. Lécuyer, P. Grandjean, J.-A. Barrat, J. Nolvak, C. Emig, F. Paris, M. Robardet. $\delta^{18}O$ and REE contents of phosphatic brachiopods: a comparison between modern and lower Paleozoic populations. *Geochim. Cosmochim. Acta* **1998**, *62*, 2429.
[12] W. A. Brand, T. B. Coplen, A. T. Aerts-Bijma, J. K. Böhlke, M. Gehre, H. Geilmann, M. Gröning, H. G. Jansen, H. A. J. Meijer, S. J. Mroczkowski, H. Qi, K. Soergel, H. Stuart-Williams, S. M. Weise, R. A. Werner. Comprehensive inter-laboratory calibration of reference materials for $\delta^{18}O$ versus VSMOW using various on-line high-temperature conversion techniques. *Rapid Commun. Mass Spectrom.* **2009**, *23*, 999.
[13] J. Koziet. Isotope ratio mass spectrometric method for the online determination of oxygen-18 in organic matter. *J. Mass Spectrom.* **1997**, *32*, 103.
[14] G. D. Farquhar, B. K. Henry, J. M. Styles. A rapid on-line technique for determination of oxygen isotope composition of nitrogen-containing organic matter and water. *Rapid Commun. Mass Spectrom.* **1997**, *11*, 1554.
[15] B. E. Kornexl, M. Gehre, R. Höfling, R. A. Werner. On-line $\delta^{18}O$ measurements of organic and inorganic substances. *Rapid Commun. Mass Spectrom.* **1999**, *13*, 1685.
[16] O. Bréas, C. Guillou, F. Reniero, E. Sada, F. Angerosa. Oxygen-18 measurement by continuous flow pyrolysis/isotope ratio mass spectrometry of vegetable oils. *Rapid Commun. Mass Spectrom.* **1998**, *12*, 188.
[17] M. Saurer, I. Robertson, R. Siegwolf, M. Leuenberger. Oxygen isotope analysis of cellulose: an interlaboratory comparison. *Anal. Chem.* **1998**, *70*, 2074.
[18] K. Revesz, J. K. Böhlke. Comparison of $\delta^{18}O$ measurements in nitrate by different combustion techniques. *Anal. Chem.* **2002**, *74*, 5410.
[19] J. Morrison. A new high temperature EA-pyrolysis-IRMS solution to $\delta^{18}O$ analyses of phosphates. *Application Brief AB10 Micromass*, **1999**.
[20] H. P. Sieper, H. J. Kupka, L. Lange, A. Roßmann, N. Tanz, H. L. Schmidt. Essential methodological improvements in the oxygen isotope ratio analysis of N-containing organic compounds. *Rapid Commun. Mass Spectrom.* **2010**, *24*, 2849.

4.4/ Analyses isotopiques du soufre

Comme cela a été très bien décrit par Bernhard Mayer and Roy Krouse dans le chapitre 26 du Handbook : "Stable Isotope Analytical Techniques" 2004 [65], les analyses isotopiques du soufre ont longtemps souffert de leur degré élevé de complexité en comparaison des analyses de l'azote ou du carbone. Au-delà des difficultés technologiques impliquées dans la préparation des échantillons, le soufre présente la particularité d'apparaître naturellement sous un grand nombre d'espèces aussi bien organiques qu'inorganiques. De plus, il est présent naturellement avec des degrés de valence variant de -2 à +6. Le soufre présente naturellement quatre isotopes stables, ^{32}S (95.02%), ^{33}S (0,75%), ^{34}S (4,21%) et ^{36}S (0,02%). Compte tenu des difficultés analytiques et des fractionnements naturels des isotopes du soufre les mesures les plus communes sont celles du rapport $^{34}S/^{32}S$.

Pendant longtemps, la seule méthode pratique de mesurer les isotopes du soufre était de transformer le soufre de l'échantillon en gaz SF_6 et de mesurer ce gaz SF_6 dans un spectromètre de masse ayant une géométrie compatible avec cette espèce gazeuse afin de pouvoir mesurer les rapports des masses 148/146. Le développement des spectromètres de masse « benchtop » ayant une capacité limitée aux masses proches de 70 amu interdisait donc la détermination des rapports isotopiques du soufre. C'est l'utilisation des analyseurs élémentaires utilisant SO_2 comme espèce gazeuse qui a permis un développement beaucoup plus important des analyses isotopiques du soufre [66].

A l'état naturel le cycle du soufre présente un haut degré de complexité comme le montre ce shéma synthétique (P. Wynn communication personnelle, d'après Wynn et al 2008 [67]) avec des niveaux de fractionnements très variables.

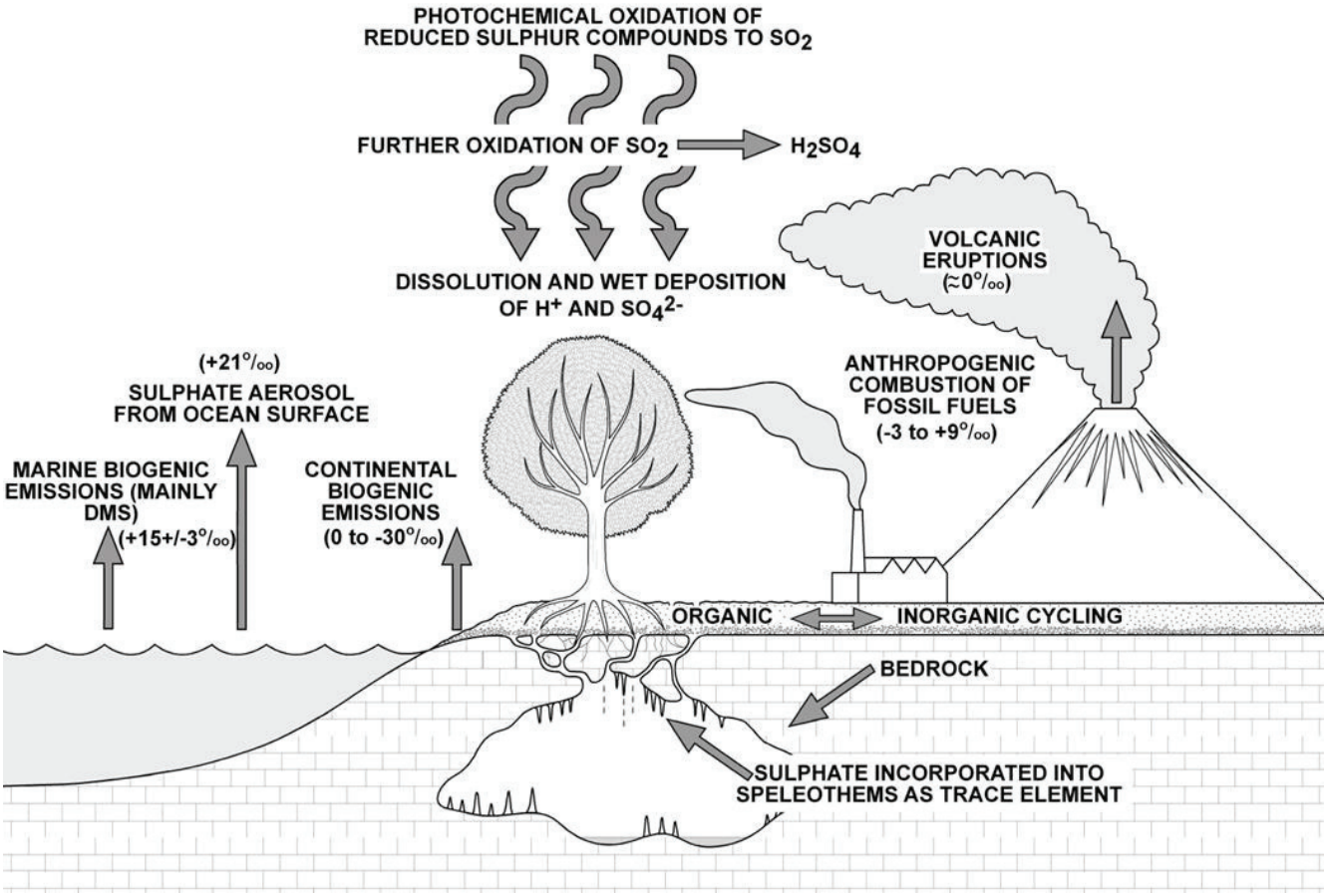

Figure 4.10 : D'après Wynn et al. 2008 [67] : Représentation schématique du cycle du soufre illustrant la complexité des divers fractionnements isotopiques pouvant intervenir durant ce cycle.

Ceci permet, une fois dépassée la limitation technique d'avoir accès à un outil unique produisant des informations différentes, et donc complémentaires des analyses isotopiques des éléments N et C. Comme nous l'avons déjà discuté dans le chapitre 1 les analyses isotopiques $\delta^{13}C$, $\delta^{15}N$ et $\delta^{34}S$ sont accessibles par EA-IRMS en mode combustion depuis le milieu des années 90, en général elle se font en deux étapes successives, une analyse pour déterminer les signatures $\delta^{13}C$ et $\delta^{15}N$, puis une seconde série d'analyses pour le $\delta^{34}S$, utilisant généralement une configuration de réacteurs de combustion/réduction différente dans l'analyseur élémentaire. La possibilité d'obtenir simultanément, sur la même aliquote d'échantillon, les

trois signatures isotopiques ainsi que les concentrations en N, C et S sur des temps d'analyse de 12 à 15 minutes représente donc un pas en avant significatif dans l'évolution des techniques isotopiques pour l'analyse des isotopes stables et particulièrement pour l'approche multi-isotopique qui tend à se développer dans de nombreux domaines.

Là encore, la technique « purge and trap » caractéristique du système PyroCube décrite dans le paragraphe précédent a été évaluée puis utilisée en mode combustion pour les analyses isotopiques $\delta^{34}S_{CDT}$. Nous avons détaillé dans le chapitre 2 l'intérêt des analyses isotopiques dans le domaine des reconstructions paléoenvironnementales. Il se trouve que les compositions isotopiques en soufre $^{34}S/^{32}S$ des minéraux phosphatés tels que par exemple l'hydroxyapatite n'ont jamais été utilisées dans ce domaine. Les tests préliminaires effectués avec le système « purge and trap » en mode combustion, et en particulier la qualité des analyses obtenues nous ont poussé à adapter cette technique à la caractérisation isotopique en $\delta^{34}S_{CDT}$ de deux phosphorites naturelles déjà certifiées en composition : BCR32, NBS120c [68,69] . Le but étant de pouvoir utiliser ces deux matériaux de référence pour calibrer ce type d'analyse sur des échantillons qui, comme le BCR32 et leNBS120c présentent des concentrations en soufre très faibles (respectivement 0,37 %poids et 0,74 %poids).

Le principe de fonctionnement du système Pyrocube en mode combustion NCS est illustré dans la figure 4.11.

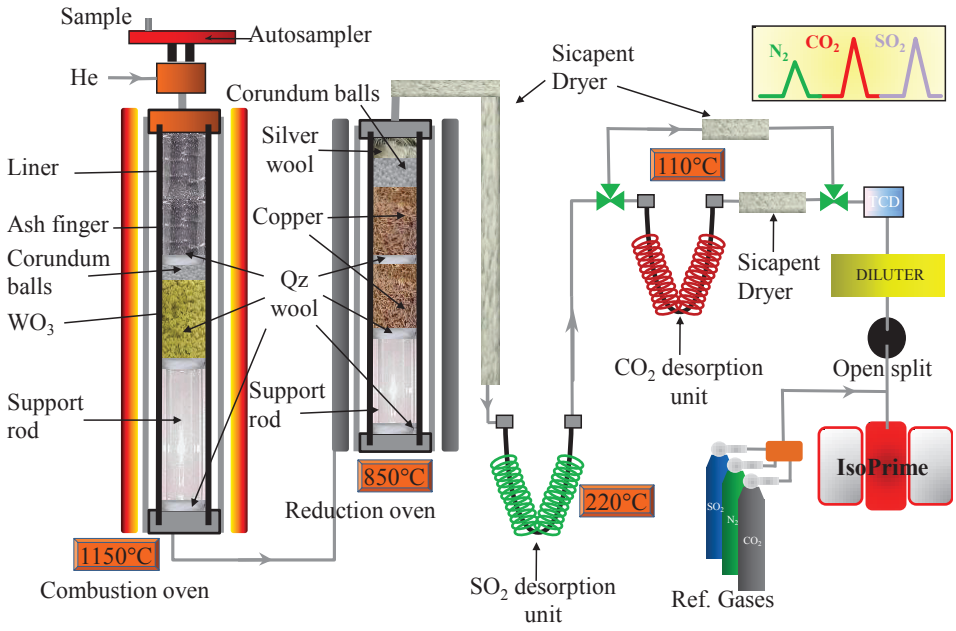

Figure 4.11 : Schéma de principe du fonctionnement du système Pyrocube en mode combustion NCS.

Dans cette configuration, le système est constitué d'un four de combustion basé sur un tube de quartz rempli de granules d'oxyde de tungstène maintenu à une température de 1150°C et d'un four de réduction rempli de cuivre et maintenu à une température de 850°C. Le tout étant balayé par un flux d'hélium dans lequel on introduit de l'oxygène au moment de la combustion de l'échantillon. Au-delà du four de réduction on a placé un piège à eau avant le système de « purge and trap » proprement dit. Dans ce système « purge and trap

» nous avons un piège à SO_2 opérant à température ambiante et libérant le gaz lorsqu'il est chauffé à 220°C et un piège à CO_2 opérant à température ambiante et libérant le gaz lorsqu'il est chauffé à 110°C. L'azote lorsqu'il y en a n'est pas piégé et passe directement. Ensuite le TCD du Pyrocube permet de mesurer les concentrations des divers gaz issus de la combustion, puis l'open-split permet l'admission des gaz à analyser dans l'IRMS. Comme pour les mesures simultanées N, C précédemment évoquées dans le chapitre 3, l'adjonction

d'un système de dilution permet d'une part de compenser les différences de concentrations des divers gaz à analyser ou d'autre part, lorsque cela est nécessaire de diluer un gaz en excès qui risquerait de perturber la source avant l'arrivée de gaz à analyser. Comme dans le cas de la pyrolyse évoquée dans le paragraphe 4.3 l'avantage primordial de la technique du « purge and trap » est de pouvoir choisir le temps de rétention des pics de gaz analyte et donc ainsi la séparation entre les différentes espèces gazeuses ce qui n'est évidemment pas le cas lorsqu'on utilise une colonne chromatographique dans un système EA-IRMS classique (voir figure 4.13).

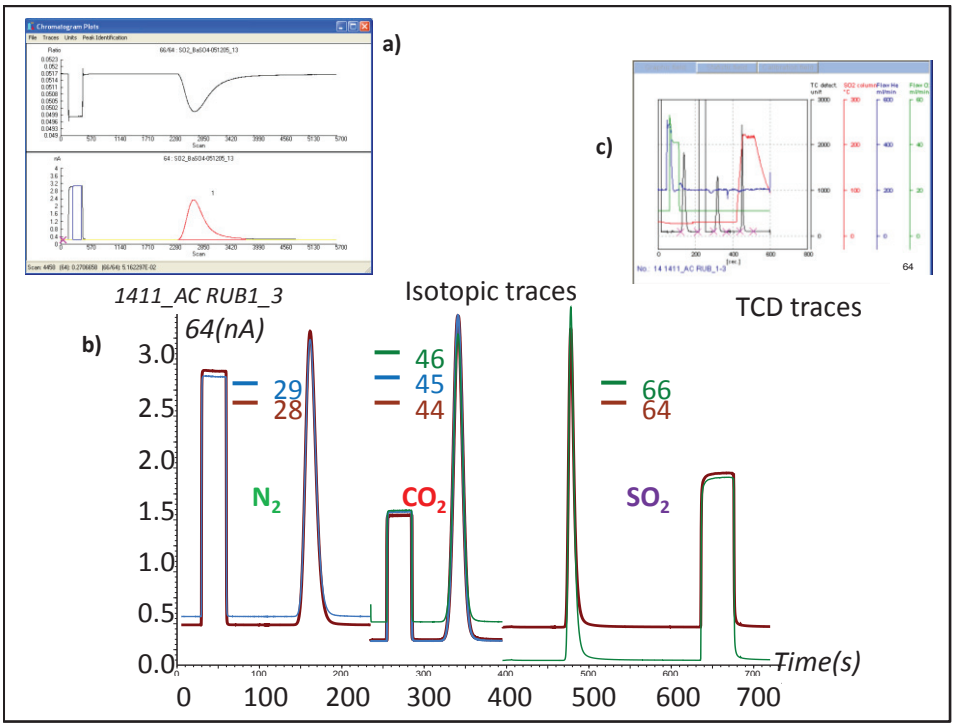

Figure 4.12 Comparaison de l'allure des traces de masses 64, 66 des pics chromatographiques de SO_2 entre un système utilisant une colonne chromatographique en a) et le système purge and trap du Pyrocube en b. c) représente l'allure du pic chromatographique enregistré sur le TCD du Pyrocube simultanément à la trace du b). L'échantillon analysé est un acide rubéanique référence de travail (Ac.Rub.1 $C_2H_4N_2S_2$) contenant à la fois N, C et S pour illustrer la qualité de la séparation entre les différents gaz N_2, CO_2 et SO_2 pouvant être générés lors de la combustion.

De plus, là encore, comme dans le cas du gaz CO et même peut-être encore plus dans le cas du SO_2, lors de la séparation sur colonne chromatographique, le pic de SO_2 a une tendance à montrer un phénomène de « tailing », c'est-à-dire un retour différé à la ligne de base, bien connu en chromatographie, qui rend l'intégration plus délicate lors du calcul des rapports isotopiques. Ce phénomène de « tailing » est absent lorsqu'on utilise le système « purge and trap » ce qui facilite l'intégration pour le calcul des rapports isotopiques et donc améliore la répétabilité. Ceci est illustré sur la figure 4.12 où l'on a utilisé un chromatogramme Pyrocube réalisé sur un acide rubéanique utilisé comme référence de travail (Ac.Rub.1 $C_2H_4N_2S_2$) contenant à la fois N, C et S pour illustrer la qualité de la séparation entre les différents gaz N_2, CO_2 et SO_2 et le peu d'influence des autres gaz sur la chromatographie du pic de SO_2. De fait, les gaz issus de la combustion étant piégés sur des colonnes spécifiques différentes, les abondances relatives des uns par rapport aux autres ont peu d'impact sur la qualité du pic de SO_2 à analyser. Ceci ouvre la porte à des limites de détection potentielles inférieures à ce que l'on observe en EA-IRMS classique. Les résultats reportés dans la publication 4.9 démontrent tout d'abord l'efficacité de la combustion du système utilisé puisque des rendements de combustion ont été calculés à partir de matériaux connus sur les données des traces TCD et ont été évalués à 99,1% (SD=1,7 ; N=11) et 101,2% (SD=2 ; N=15) respectivement pour le standard IAEA-S1 [70-72] et le standard de travail Ac. Rub.1.

Ensuite nous avons calibré les valeurs $\delta^{34}S_{CDT}$ des deux phosphorites naturelles BCR32 et NBS120c (voir figure 4.13) en les mesurant avec des références internationales : IAEA-S1[70-73](Ag_2S: $\delta^{34}S_{CDT}$ = -0,3‰), IAEA-S2[70,71](Ag_2S: $\delta^{34}S_{CDT}$ = 22,7‰), IAEA-S3[70,71] (Ag_2S: $\delta^{34}S_{CDT}$ = -32,3‰), IAEA-S4[73,74](soufre minéral S: $\delta^{34}S_{CDT}$ = 16,9‰), IAEA-SO5[75] ($BaSO_4$: $\delta^{34}S_{CDT}$ = 0,5‰), IAEA-SO6[75] ($BaSO_4$: $\delta^{34}S_{CDT}$ = -34,1‰), et NBS127[75,76]($BaSO_4$: $\delta^{34}S_{CDT}$ = 20,3‰).

Figure 4.13 : Phosphorites naturelles calibrées en $\delta^{34}S_{CDT}$ dans cette étude.

Cela nous permet de proposer les valeurs suivantes :

BCR32 $\delta^{34}S_{CDT}$ = 18,2 ‰ (SD = 0,3 : N=23)

NBS120c $\delta^{34}S_{CDT}$ = 18,3 ‰ (SD = 0,4 : N=20).

Encore une fois il convient de souligner que ces valeurs ont été obtenues sur des échantillons contenant respectivement 0,72 %poids et 0,47 %poids de soufre ce qui a nécessité des prises d'essais de 5mg et 8mg respectivement pour le BCR32 et le NBS120c correspondant à des quantités de soufre de l'ordre de 30 µg. Le but de cette étude était de caractériser les deux phosphorites précitées, aussi nous n'avons pas poussé plus loin la recherche de la quantité minimale de S nécessaire à une analyse $\delta^{34}S_{CDT}$ fiable par cette technique. Mais les résultats que nous avons obtenus nous laissent à penser qu'il est possible d'aller encore plus loin dans la réduction de la prise d'essai, probablement jusqu'à 0,2 %poids.

Les résultats de cette étude constituent la première étape d'un nouveau champ d'investigation pour les analyses $^{34}S/^{32}S$ appliquées aux reconstructions paléoenvironnementales et fournira désormais à la communauté scientifique un nouvel outil isotopique complémentaire de ceux déjà évoqués dans ce manuscrit.

Le dernier article présenté dans ce travail sous la forme de la publication 4.10 concerne également les analyses isotopiques du soufre au moyen du système Pyrocube en mode combustion qui vient d'être évoqué ci-dessus. Cette fois nous nous sommes intéressés plus particulièrement à la capacité de ce système de répondre aux besoins grandissants d'analyses multi-isotopiques sur des échantillons de tailles réduites et donc nécessitant l'analyse simultanée des trois signatures isotopiques $\delta^{15}N_{AIR}$, $\delta^{13}C_{PDB}$ et $\delta^{34}S_{CDT}$.

La configuration utilisée ici est la même que pour la publication 4.9. Nous sommes partis de la constatation que la détermination simultanée, sur la même prise d'essai des valeurs $\delta^{15}N_{AIR}$, $\delta^{13}C_{PDB}$ et $\delta^{34}S_{CDT}$ ainsi que des valeurs de %N, %C, %S pourrait s'avérer fondamentale pour retracer par exemple l'origine de la matière organique [77], les conditions d'oxydo-réduction des environnements marins ou terrestres accueillant des organismes vivants [78], des processus métaboliques [79], des régimes alimentaires sur des humains ou des animaux [80] ou bien même retracer la structure de chaînes trophiques [81]. Les premiers résultats de cette étude représentent l'analyse simultanée des trois signatures isotopiques NCS sur un mélange entre notre standard de travail NC constitué par de l'acide aspartique calibré par rapport aux standards internationaux déjà cités : IAEA-N1, IAEA-N2, IAEA-CH6, IAEA7, IAEA-C3 et IAEA-C4 et le standard IAEA-S1 déjà mentionné dans l'article précédent. Nous avons montré que la technique purge and trap dans ce cas fournit des valeurs précises et répétables lorsque les trois signatures sont mesurées simultanément, sans différence significative avec les mesures obtenues séparément. Lors de cette première phase également, comme il n'existe pas encore de matériel de référence calibré pour les trois signatures isotopiques N, C, S nous avons calibré notre standard de travail Ac. Rub.1 déjà mentionné. Cela nous a permis de proposer les valeurs suivantes pour cet échantillon :

Ac. Rub.1 :

$\delta^{15}N_{AIR}$ = -2,43 ‰ (SD = 0.13 ; N = 15)

$\delta^{13}C_{PDB}$ = -35,73 ‰ (SD = 0,10 ; N = 15)

$\delta^{34}S_{CDT}$ = 3,8 ‰ (SD = 0,2 ; N = 15)

Ensuite, afin de véritablement tester le potentiel de cette technique pour la mesure des $\delta^{34}S$ nous avons entrepris de mesurer la plupart des standards de soufre disponibles (voir figure 4.14) à savoir : : IAEA-S1[70-73](Ag_2S: $\delta^{34}S_{CDT}$ = -0,3 ‰), IAEA-S2[70,71](Ag_2S: $\delta^{34}S_{CDT}$ = 22,7 ‰), IAEA-S3[70,71] (Ag_2S: $\delta^{34}S_{CDT}$ = -32,3 ‰), IAEA-S4[73,74](soufre minéral S: $\delta^{34}S_{CDT}$ = 16,9 ‰), IAEA-SO5[75] ($BaSO_4$: $\delta^{34}S_{CDT}$ = 0,5 ‰), IAEA-SO6[75] ($BaSO_4$: $\delta^{34}S_{CDT}$ = -34,1 ‰), et NBS127[75,76]($BaSO_4$: $\delta^{34}S_{CDT}$ = 20,3 ‰).

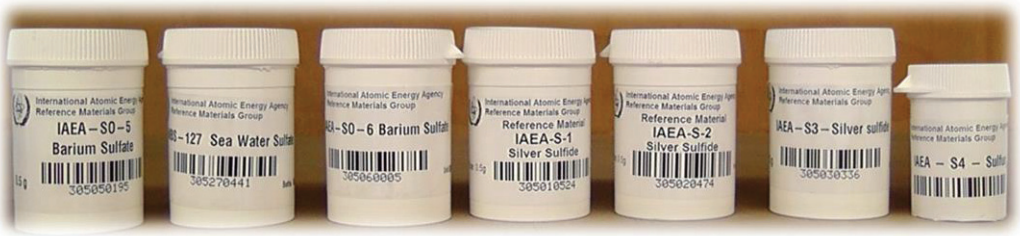

Figure 4.14 : Matériaux de référence utilisés lors de notre étude.

Nous présentons dans cet article deux jeux de données pour la calibration isotopique, l'un organisé en fonction des types de matrices à analyser et l'autre en fonction des valeurs isotopiques de référence. Lorsque l'on reporte les valeurs mesurées en fonction des valeurs admises on obtient deux droites de régression de type y = a.x + b. Les facteurs σ_{reg} des erreurs standards sur les régressions sont respectivement de 0,37 ‰ (N = 51) et 0,48 ‰ (N = 40). Il est à noter que cela représente des valeurs extrêmes car nous avons volontairement poussé les limites de la technique. En temps normal, de telles différences de matrices ou de valeurs isotopiques ne seraient pas utilisées au sein d'un même batch d'analyses. En plus des matériaux de référence précités, nous avons également placé dans les batchs des aliquotes de

nos standards de travail Ac. Rub.1 et acide Aspartique (AA) ainsi que deux autres échantillons de sphalérite calibrés en $\delta^{34}S_{CDT}$ fournis par Stanislaw Halas de l'université de Lublin en Pologne [82]. Si l'on utilise les droites de calibration ainsi générées pour calculer les $\delta^{34}S_{CDT}$ de tous ces échantillons et qu'on les compare avec les valeurs admises, on obtient un très bon accord entre les deux (aux environs de 0.2-0.4‰). Au-delà des analyses $\delta^{34}S_{CDT}$, on constate également que sur les deux standards de travail calibrés en $\delta^{15}N_{AIR}$ et $\delta^{13}C_{PDB}$ les valeurs obtenues sont très proches des valeurs admises, ce qui démontre que l'analyse simultanée n'est en aucun cas un compromis par rapport aux analyses individuelles. Enfin, et c'est également un point important de cette technique, l'utilisation de la trace TCD pour mesurer les concentrations en N, C et S de ces échantillons fournit des résultats très proches également des valeurs attendues, ce qui n'est pas toujours le cas lorsqu'on utilise les traces isotopiques pour de telles déterminations, notamment pour les échantillons nécessitant l'emploi d'un système de dilution.

Ainsi cette étude confirme le potentiel de la technique « purge and trap » en ce qui concerne les déterminations simultanées des valeurs $\delta^{15}N_{AIR}$ et $\delta^{13}C_{PDB}$ et $\delta^{34}S_{CDT}$ ainsi que des concentrations en N, C et S . Ceci constitue un nouvel outil pour les études multi-isotopiques où la quantité d'échantillon disponible est limitée comme par exemple l'étude de paléo régimes alimentaires de nos ancêtres à partir de restes de momies [83].

Ainsi, après avoir mis en évidence l'intérêt de la technique du « purge and trap » en mode pyrolyse dans le paragraphe précédent, nous avons développé un nouvel outil isotopique permettant d'ouvrir de nouvelles possibilités en ce qui concerne les analyses isotopiques du soufre ainsi que les analyses multi isotopiques de l'azote du carbone et du soufre.

References Chapitre 4

(1) S. Epstein S. & T.K. Mayeda (1953). *Geochim. Cosmochim. Acta,* **4**: 213–224.

(2) J. Horita (1988) *Chem. Geol.,* **72**: 89–94.

(3) J. Horita (1989) *Chem. Geol.,* **79** : 107–112.

(4) J. Horita J., A. Ueda, K. Mizukami & I. Takatori (1989) *Apl. Radiat. Isot.,* **40**: 801-805.

(5) T.B. Coplen, J.D. Wildman, J. Chen (1991) *Anal. Chem.,* **63**: 910–912.

(6) H. Taube (1954) *J. Chem. Phys.,* **58**: 523-528.

(7) H. Craig & L.I. Gordon (1965) *In: Stable Isotopes in Oceanographic Studies and Paleotemperatures, E. Tongiorgi (Ed.), Lab. Geol. Nucl.,* 9-130.

(8) J.R. O'Neil & L.H. Adami (1969) *J. Phys. Chem.,* **73**: 1553-1558.

(9) A.H. Truesdell (1974) *Earth Planet. Sci. Lett*., **23**: 387-396.

(10) Z. Sofer & J.R. Gat (1972) *Earth Planet. Sci. Lett*., **15**: 232-238.

(11) K. Kazahaya (1986) *Ph.D. dissertation, Tokyo Inst. Techn.,* pp. 185.

(12) J.R. O'Neil & A.H. Truesdell (1991) *In: Stable Isotope Geochemistry: A Tribute to Samuel Epstein, H.P. Taylor, J.R. O'Neil and I.R. Kaplan (Eds), The Geochemical Society, Special Publication n° 3,* 17-25.

(13) S.M. Fortier (1994) *Chem. Geol.,* **116**: 155-162.

(14) C. Bourg, M. Stievenard & J. Jouzel J. (2001) *Chem. Geol*., **173** : 331-337

(15) H.C. Urey (1947) *J. Chem. Soc. London*, 562–587.

(16) J.M. McRea (1950) *J. Chem. Phys.,* **18**: 849–857.

(17) S. Epstein, R. Buchsbaum, H.A. Lowenstam & H.C. Urey (1953) *Geol. Soc. Am. Bull.,* **64**: 1315–1326.

(18) R.Z. LeGeros (1981) *Prog. Cryst. Growth Charact*., **4**, 1-45.

(19) M. Okazaki, Y. Moriwaki, T. Aoba, Y. Doi, J. Takahasi & H. Kimura (1982) *Caries Res*., **16**: 308-314.

(20) J.D. Schuffert, M. Kastner, G. Emanuele & R.A. Jahnke (1990) *Geochim. Cosmochim Acta,* **54**: 2323-2328.

(21) R.Z. LeGeros, T. Sakae, C. Bautista, M. Retino and J.P. LeGeros (1996) *Adv. Dent. Res.,* **10**: 225-231.

(22) J.D. Bryant, P.L. Koch, P.N. Froelich, W.J. Showers & B.J. Genna (1996) *Geochim. Cosmochim Acta,* **60**: 5145-5148.

(23) P. Iacumin, D. Cominotto & A. Longinelli (1996) *Palaeogeogr. Palaeoclimatol. Palaeoecol*., **126**: 151-160.

(24) R.S. Feranec & B.J. Mc Faden (2000) *Palaeogeogr. Palaeoclimatol. Palaeoecol*., **162**: 155-169.

(25) C. Gadbury, L. Todd, A.H. Jahren & R. Amundson (2000) *Palaeogeogr. Palaeoclimatol. Palaeoecol*., **157**: 79-93.

(26) H. Bocherens, M. Mashkourb, D. Billiou, E. Péllec & A. Mariotti (2001) *C. R. Acad. Sci. (Paris),* **332**: 67-74.

(27) M. Balassa (2002) *Int. J. Ostreoarchaeol.,* **12**: 155-165.

(28) K.J. Stanton Thomas & S.J. Carlson (2004) *Palaeogeogr. Palaeoclimatol. Palaeoecol*., **20**: 257-287.

(29) L.L. Arppe & J.A. Kahru (2006) *Palaeogeogr. Palaeoclimatol. Palaeoecol*., **231**: 322-330.

(30) A. Zazzo, A. Mariotti, C. Lécuyer & E. Heintz (2002) *Palaeogeogr. Palaeoclimatol. Palaeoecol*., **186**: 145-161.

(31) C. Lécuyer, C. Bogey, J.P. Garcia P. Grandjean, J.A. Barrat, M. Floquet, N. Bardet & X. Pereda-Superbiola (2003) *Palaeogeogr. Palaeoclimatol. Palaeoecol*., **193**: 457-471.

(32) T. Tütken, H.U. Pfretzschnerb, T.W. Venneman, G. Sunc & Y.D. Wang (2004) *Palaeogeogr. Palaeoclimatol. Palaeoecol*., **206**: 217-238.

(33) J.R. O'Neil, R.N. Clayton & T.K. Mayeda (1969) *J. Chem Phys*., **51**: 5547-5558.

(34) S.T. Kim & J.R. O'Neil (1997) *Geochim. Cosmochim. Acta*, **61**: 3461-3475.

(35) K. Wada & T. Fujinuki (1976) *In Watanabe N. Wilbur K.M. Eds. The Mechanisms of Mineralistaion in the Invertebrates and Plants University of South Carolina Press, Columbia*, 175-190.

(36) D.E. Krantz, D.F. Williams & D.S. Jones (1987) *Palaeogeogr. Palaeoclimatol. Palaeoecol*., **58**: 249-266.

(37) Y.D. Zakharov, Y. Shigeta, R. Nagendra, P.P. Sofonova, O.P. Smyshlyaeva, A.M. popov, T.A. Velivetskaya & T.B. Afanasyeva (2011) Cretaceous Res., 32, 623-645.

(38) R.G.C Bathurst (1983) *Developments in Sedimentology*, *vol. 12. Elsevier, New York,* 1-660.

(39) P. Fritz, D.G.W Smith. (1970) *Geochim. Cosmochim. Acta*, **34**: 1161-1173.

(40) S.I. Dworkin, L. Nordt, S. Atchley, (2005) *Earth Planet. Sci. Lett*., **237**: 56-68.

(41) S. Epstein, D.L. Graf & E.T. Degens (1964) *In: Graig, H., Miller, S.L., Wasserburg, G.J., (Eds.), Isotopic and Cosmic Chemistry. North Holland Publishing Co., Amsterdam,* 169-180.

(42) R.N. Clayton, B.F. Jones & R.A. Berner (1968) *Geochim. Cosmochim. Acta*, **32**: 415-432.

(43) I.S. Al Aasm, B.E. Taylor & B. South (1990) *Chem. Geol.,* **80**: 119-125.

(44) N.J. Shackleton (1967) *Nature*, **215**: 15-17.

(45) N.J. Shackleton (1986) *Palaeogeogr. Palaeoclimatol. Palaeoecolol.*, **57**: 91-102.

(46) N.J. Shackleton & N.D. Opdyke (1973) *Quat. Res.,* **3**: 39-55

(47) N.J. Shackleton, J. Imbrie & M.A. Hall (1983) *Earth Planet. Sci. Lett*., **65**: 233-244.

(48) D.C. Kelly, T.J. Bralower, J.C. Zachos, I.P. Silva & E. Thomas (1996) *Geology*, **24**: 423–4126.

(49) G.D. Price, B.W. Sellwood, R.M. Corfield, L. Clarke & J.E. Cartlidge (1998) *Geol. Mag.,* **135**: 183–191.

(50) J.C. Zachos, S.M. Bohaty, C.M. John, H. McCarren, D.C. Kelly & T. Nielsen (2007) *Trans. R. Soc.,* **365**: 1829–1842.

(51) C. Shuxi & N.L. Shackleton (1990) *Chin. J. Ocean. Limnol.,* **8**: 299–305.

(52) K. Billups & H.J. Spero (1995) J. *Foram. Res.,* **25**: 24–37.

(53) P.K. Saraswati (2004) *Current Science*, **86**: 858–860.

(54) R.A. Werner, B.E. Kornexl, A. Rossman & H. L. Schmidt (1996) *Anal. Chim. Acta*, **319**, 159-164.

(55) G.D. Farquhar, B.K. Henry & J.M. Styles (1997) *Rapid Commun. Mass Spectrom.,* **11**, 1554.

(56) J. Koziet (1997) *J. Mass Spectrom.,* **32**: 103-108.

(57) B.E Kornexl, M. Gehre, R. Höfling & R.A.Werner (1999) *Rapid Comm. Mass Spectrometry*, **13**: 1685-1693.

(58) O. Bréas, C. Guillou, F. Reniero, E. Sada & F. Angerosa (1998) *Rapid Commun. Mass Spectrom*., **12**: 188-192.

(59) C. Lecuyer, P. Grandjean & S.M.F. Sheppard (1999) *Geochem. Cosmochem. Acta*, **63**: 855-862.

(60) J.R. O'Neil, L.J. Roe, E. Reinhard & R.E. Blake (1994) *Isr. J. Earth Sci.,* **43**: 203–212

(61) C. Lécuyer, P. Grandjean, J.-A.Barrat, J. Nolvak, C. Emig, F. Paris & M. Robardet (1998) *Geochim. Cosmochim. Acta*, **62**: 2429-2436.

(62) W.A. Brand, T.B. Coplen, A.T. Aerts-Bijma, J.K. Böhlke, M. Gehre, H. Geilmann, M. Gröning, H.G. Jansen, H.A. J. Meijer, S.J. Mroczkowski, H. Qi, K. Soergel, H. Stuart-Williams, S.M. Weise & R. A. Werner. (2009) *Rapid Commun.Mass Spectrom*., **23**: 999.

(63) H.P. Sieper, H.J. Kupka, L. Lange, A. Roßmann, N. Tanz & H.L. Schmidt (2010) *Rapid Commun. Mass Spectrom.,* **24**: 2849–2858

(64) B. Mason & C.B. Moore (1982) *"Principles of Geochemistry", 4th Ed., , Wiley*, *London.*

(65) B. Mayer & R.H. Krouse (2004) *Handbook of Isotope Analytical Techniques, Volume1, Chapter 26*, **26**: 538.

(66) A. Giesemann, H.J. Jaeger, A.L. Norman, H.R. Krouse & W. Brandt (1994) *Analytical Chemistry*, **66**: 2816.

(67) P.M. Wynn, I.J. Fairchild, A. Baker, S. Frisia, A. Borsato, J. Maldini & F. Mc Dermot (2008) *Geochim. Cosmochim. Acta*, **72**: 2465-2477.

(68) Community Bureau of Reference-BCR. (1982) *Certified reference material certificate of analyses for BCR n°32. Commission of the European communities report n°541*.

(69) National Bureau of Standards-NBS. (1988) *Certificate of analysis for standard Reference Material 120c. U.S. department of commerce report*.

(70) B.W. Robinson (1993) *Sulphur isotope standards. Proceedings of a consultants' meeting held in Vienna, 1-3. Dec IAEA-TECDOC-825*: 39-45.

(71) W. Stichler, R. Gonfiantini & K. Rozanski (1995) *Reference and intercomparison materials for stable isotopes of light elements. Proceedings of a consultants' meeting held in Vienna, 1 - 3. Dec. 1993. IAEA-TECDOC-825*: 7-11.

(72) T.B. Coplen & H.R. Krouse (1998) *Nature*, **392**: 32.

(73) R.W. Carmody & R.R. Seal II (1999) *Chem. Geol.,* **153 1-4**: 289-295.

(74) H.P. Qi & T.B. Coplen (2003) *Chem. Geol.,* **199 1-2**: 183-187.

(75) S. Halas & J. Szaran (2001) *Rapid Commun. Mass Spectrom*, **15 17**: 1618-1620.

(76) G. Hut (1987) *Consultants' group meeting on stable isotope reference samples for geochemical and hydrological investigations, 16-18 Sep. 1985. Report to the Director General, INTERNATIONAL ATOMIC ENERGY AGENCY, Vienna*.

(77) M.J. Mitchell, H.R. Krouse, B. Mayer, A.C. Stam & Y. Zhang (1998) *In: Kendall C., Mc Donnell JJ (eds) Isotope tracers in catchment hydrology. Elsevier Amsterdam*: 489.

(78) P.M. Wynn, A. Borsato, A. Baker, S. Frisia, R. Miorandi & I.J. Fairchild (2013) *Biogeochemistry*, **114**: 255.

(79) N. Tanz & H. Schmidt (2010) *J. Agric. Food Chem*., **58**: 3139.

(80) O. Nehlich, B.T. Fuller, M. Jay, A. Mora, R.A. Nicholson, C.I. Smith & M.P. Richards (2011) *Geochim. Cosmochim. Acta*, **75**: 4963.

(81) M.P. Richards, B.T. Fuller, M. Sponheimer, T. Robinson & L. Ayliffe (2003) *Int. J. Osteoarchaeol.*, **13**: 37.

(82) T. Ding, S. Valkiers, H. Kipphardt, P. De Bièvre, P.D.P. Taylor, R. Gonfiantini & R. Krouse (2001) *Geochim. Cosmochim. Acta*, **65**: 2433-2437.

(83) A. Touzeau, R. Amiot, J. Blichert-Toft, J.P. Flandrois, F. Fourel, V. Grossi, F. Martineau, P. Richardin & C. Lécuyer (2014) *Journ. of Archaeol. Sci.,* **46** : 114-124.

GEOSTANDARDS and GEOANALYTICAL RESEARCH

Measurement of $^{34}S/^{32}S$ Ratios of NBS 120c and BCR 32 Phosphorites Using Purge and Trap EA-IRMS Technology

François **Fourel** (1)*, François **Martineau** (1), Magali **Seris** (1) and Christophe **Lécuyer** (1, 2)

(1) Laboratoire de Géologie de Lyon "Terre-Planète Environnement", CNRS-UMR 5276 Université Claude Bernard Lyon 1, Ecole Normale Supérieure de Lyon, Campus de la Doua, F-69622, Villeurbanne, France

(2) Institut Universitaire de France, Xxxxx, Xxxxx

* Corresponding author. e-mail: Francois.Fourel@univ-lyon1.fr

Measurements of sulfur stable isotope ratios ($^{34}S/^{32}S$) have suffered from technical difficulties in analysing low-S materials reducing their use despite their undeniable scientific interest. The measurement of $^{34}S/^{32}S$ ratios is a powerful tool for deciphering problems such as determining the sources of environmental pollutants, to detect adulteration, tracking the evolution of the redox state of the oceans and quantifying the role of the bacterial activity in sulfide minerals genesis. We have used a high-precision method of sulfur isotope determination using a new type of elemental analyser based on 'purge and trap' technology. This new technique demonstrates the high quality of $^{34}S/^{32}S$ measurements for samples with S concentrations lower than 1% *m/m*. International calibrated references of diverse sulfur-bearing materials were used to calibrate two low (< 1%)-S-bearing phosphorites used as compositional reference material for future use as isotopic references: BCR 32 and NBS 120c. $\delta^{34}S_{CDT}$ values of, respectively, 18.2‰ (1*s* = 0.3; *n* = 23) and 18.3‰ (1*s* = 0.4; *n* = 20) are proposed for these. Calibration of both phosphorites with international reference materials led to calculation of a mean standard error close to 0.4‰. The demonstration of a capability to reliably measure S isotope ratios in low-S phosphate minerals or rocks opens up new fields of palaeoenvironmental reconstructions.

Keywords: sulfur, isotope, continuous flow analysis, analytical calibration, rock reference materials.

Les mesures des rapports isotopiques du soufre ($^{34}S/^{32}S$) ont souffert de difficultés techniques pour l'analyse des matériaux ayant de faibles concentrations en S réduisant ainsi leur utilisation malgré leur indéniable intérêt scientifique. La mesure des rapports $^{34}S/^{32}S$ est un outil performant pour résoudre des problèmes tels que déterminer les sources de polluants environnementaux, pour détecter certaines adultérations, suivre les conditions d'oxydo-réduction des océans et quantifier le rôle de l'activité bactérienne dans la genèse des minéraux contenant du soufre. Nous avons utilisé une méthode de haute précision pour l'analyse des rapports isotopiques du soufre en utilisant un nouveau type d'analyseur élémentaire basé sur la technique du « purge and trap ». Cette nouvelle technique démontre la grande qualité des mesures $^{34}S/^{32}S$ pour des échantillons ayant des concentrations en S inférieures à 1% m/m. Des références internationales constituées de divers matériaux soufrés ont été utilisées pour calibrer deux phosphorites contenant de faibles teneurs en soufre (< 1%) considérées comme des références compositionnelles afin de pouvoir les utiliser comme références isotopiques : BCR 32 et NBS 120c. Des valeurs isotopiques de respectivement 18.2‰ (1s = 0.3; n = 23) et 18.3‰ (1s = 0.4; n = 20) sont ainsi proposées. La calibration de ces deux phosphorites avec des materiaux de référence internationaux nous a permis de calculer une erreur standard moyenne proche de 0.4‰. La démonstration de la possibilité de mesurer de manière fiable les rapports isotopiques du soufre dans des roches ou minéraux pauvres en soufre ouvre de nouveaux champs d'investigation pour les reconstructions paléo-environnementales.

Mots-clés : soufre, isotope, combustion, analyseur élémentaire, palaeoenvironment.

Received 04 Dec 13 – Accepted 06 Apr 14

doi: 10.1111/j.1751-908X.2014.00297.x

Preston and Owens (1985) have been the pioneers in the stable isotope measurements of compounds in continuous flow mode using an elemental analyser (EA) coupled to an isotopic ratio mass spectrometer (IRMS). At that time, the EA was configured in combustion mode, and only $^{13}C/^{12}C$ ratios were measured although Preston and Owens (1985) identified the future possibility of measuring other isotopic ratios such as $^{15}N/^{14}N$ ratios with such a system using a chromatographic packed column to separate the compounds. Simultaneous analyses of both $^{13}C/^{12}C$ and $^{15}N/^{14}N$ were also made available (Fry *et al.* 1992) with some limitations for the high C/N ratios. In the mid-1990s, determinations of sulfur isotope ratios became available to EA-IRMS users by analysing SO_2 as a gas species (Giesemann *et al.* 1994) using a chromatographic separation of the gases. In this study, we report the use of an EA system recently made accessible to IRMS studies based on a different principle that separates gases and is referenced as a 'purge and trap' technology (Sieper *et al.* 2010, Fourel *et al.* 2011).

A key factor is that purge and trap technology generates high-quality SO_2 chromatographic peaks even for samples with low-S concentrations (< 1% *m/m*), which constitutes a significant advance over the conventional packed GC column-based chromatographic system and improves the quality of the isotopic data calculated from chromatographic peaks.

After preliminary work to demonstrate that the system could generate robust $\delta^{34}S_{CDT}$ data alongside $\delta^{13}C_{PDB}$ and $\delta^{15}N_{AIR}$ determinations, we tested this capacity for high-quality $\delta^{34}S_{CDT}$ determinations to tackle new fields of investigations that have proved analytically difficult up to this point. There has been increased interest in the application of stable isotopes to the understanding of phosphate tissue metabolism in fossil vertebrates. The advance of deriving silver phosphate from biogenic phosphate has opened the possibility of applying oxygen isotopes to a large spectrum of palaeoenvironmental applications including, for example, the reconstruction of variations in past seasonality, marine palaeotemperatures and mean air temperatures (e.g., Fricke *et al.* 1995, 1998, Joachimski *et al.* 2004, Sharma *et al.* 2004). Besides oxygen isotope determinations of the phosphate radical itself, minor amounts of carbonate occur naturally in the crystal lattice of apatites (LeGeros 1981, LeGeros *et al.* 1996), and both carbon and oxygen isotope ratios have been investigated as valuable targets for palaeoclimatic reconstructions and diet estimates of extinct vertebrates (e.g., Cerling and Harris 1999, Cerling *et al.* 2003, Ehleringer 2005, Zazzo *et al.* 2005).

Sulfur isotope compositions from phosphatic minerals (e.g., hydroxyapatite) have not been used in the field of palaeoenvironment reconstructions. The quality of the sulfur isotope data obtained using the new purge and trap technology led us to apply this technique to the natural phosphorites BCR 32 and NBS 120c (Community Bureau of Reference 1982, National Bureau of Standards 1988) with the aim of determining sulfur isotopic ratios of the reference materials even though both have S concentrations below 1% *m/m* (0.37 and 0.74% *m/m* of S for NBS 120c and BCR 32, respectively). We show that without any prior wet chemistry, the new technique presented here allows the determination of high-precision $\delta^{34}S_{CDT}$ values for large aliquots (≈ 5–8 mg) of both BCR 32 and NBS 120c phosphorites. These can now be further used as reference materials for the determination of $\delta^{34}S_{CDT}$ values of phosphatic minerals such as sedimentary, hydrothermal or magmatic apatites.

Analytical techniques

New 'purge and trap' high-temperature EA-pyrolysis-IRMS

The system used, called VarioPYROcube, was developed by Elementar GmbH (Elementar Analysensysteme GmbH, Hanau, Germany) and recently made available online with IRMS instruments. This system has been investigated in pyrolysis mode for elemental and oxygen isotopic determination in organic and inorganic compounds (Sieper *et al.* 2010, Fourel *et al.* 2011).

The general set-up is shown in Figure 1. As in most conventional EA-IRMS systems, this one used helium as a carrier gas and consisted of a combustion tube followed by a reduction tube. The combustion tube was filled with tungsten oxide to ensure full conversion of sulfur into SO_2 gas and was heated to 1150 °C. Besides the tungsten oxide, an oxygen injection system allowed the introduction of an oxygen gas pulse with the sample injection. The volume and timing of this oxygen injection was user defined and could be optimised for different types of matrices. The reduction tube was filled with copper pellets and held at 850 °C. A chemical water trap using a SICAPENT™ dryer followed the reduction oven and each trap.

The original purge and trap system lies after the PyroCube water trap. Nitrogen gas is not trapped and goes straight through this unit. A CO_2 trap operating at room temperature in trapping mode can then be used to analyse $^{13}C/^{12}C$ ratios by heating to 110 °C to release trapped CO_2. Before the CO_2 trap, a SO_2 trap operates at room

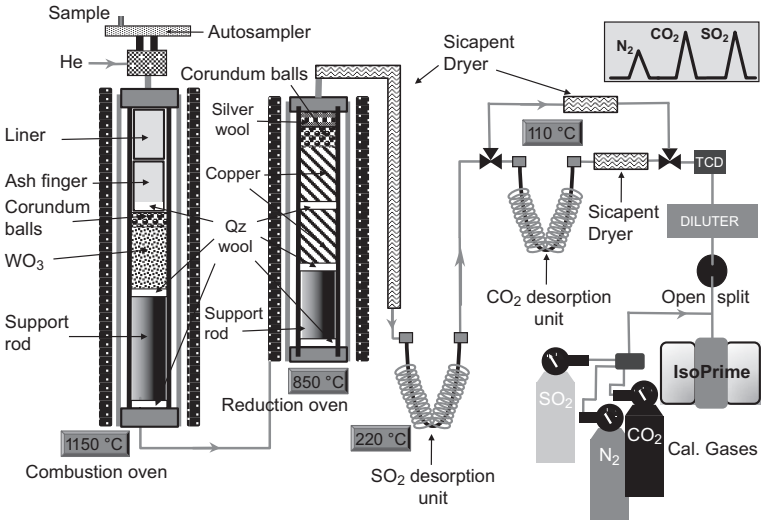

Figure 1. Combustion set-up for the 'purge and trap' varioPYROcube system. Combustion temperature was set at 1150 °C, reduction temperature was set at 850 °C, CO_2 desorption temperature was set at 850 °C and desorption temperature for SO_2 was set at 220 °C. Gas separation was ensured by the desorption unit. No GC packed column was used in this configuration.

temperature in trapping mode and at 220 °C in release mode to desorb the trapped SO_2. All analytical gases pass through a thermal conductivity detector (TCD) used to determine N, C and S abundances. The EA system is connected online via an open split device to an IsoPrime IRMS system with a diluting system to allow high C/S ratio samples. For the reference materials NBS 120c and BCR 32, the CO_2 peak is diluted to avoid any interference with the SO_2 peak. Alternatively, the CO_2 and SO_2 desorption traps can be programmed at appropriate timings. This is another advantage of the purge and trap system over conventional packed GC column separation.

One key parameter for obtaining good quality data in continuous flow isotopic determinations is the shape of the peak of analyte gas generated by the continuous flow preparation system entering the IRMS. This is true for all gas species (Sacks *et al.* 2003), but it is even more critical for SO_2, which requires special care to improve peak symmetry as well as to minimise peak tailing (Yun *et al.* 2005).

Dealing with chromatographic separation, nonsymmetrical peaks with large tailing are considered to be more difficult to integrate. For concentration determinations using thermal conductivity detectors (TCD) or Flame Ionisation Detectors (FID), one chromatographic trace is integrated and calculation algorithms have been developed to overcome those difficulties. In the case of isotopic ratio determinations, we face at least two or more isotopic chromatographic traces integrated simultaneously; therefore, higher is the degree of complexity and more critical is the quality of the chromatographic peak.

In the case of CO, one advantage of the purge and trap technology identified by Sieper *et al.* (2010) and Fourel *et al.* (2011) was the possibility of generating narrow and symmetrical peaks prior to gas introduction into the source of the IRMS system. Generating symmetrical and narrow SO_2 peaks with the PyroCube system was then carefully investigated.

Results and Discussion

Peak quality and calculation of S concentrations

When EA and IRMS methods have been carefully synchronised, the optimisation procedure for sample combustion follows the same strategy as in conventional EA-IRMS and can then deliver isotopic traces for SO_2 gas species like the one shown in Figure 2. It is important to point out here the quality of the SO_2 peak shape despite the low concentration of S in the original matrix as reported for the $^{18}O/^{16}O$ analyses in pyrolysis mode (Fourel *et al.* 2011): purge and trap systems generate chromatographic peaks that are sharp, symmetrical, showing no tailing and are well separated from one another.

Sulfur concentrations of 0.47% *m/m* (1*s* = 0.05) and 0.72% *m/m* (1*s* = 0.09) were calculated from TCD for NBS 120c and BCR 32 (Table 1), respectively, and compare well

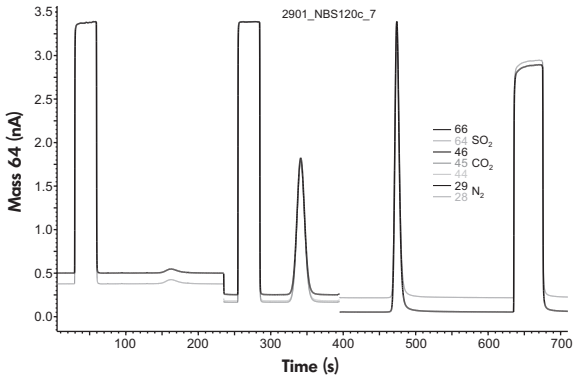

Figure 2. Isotopic chromatogram measured with the IRMS system showing the high quality of the SO_2 peak from an aliquot of 8 mg of NBS 120c as well as the efficient peak separation that allowed clean 64 ($^{32}S^{16}O_2$) and 66 ($^{34}S^{16}O_2$) isotopic traces. It is important to notice the efficient baseline separation between the unwanted gas species such as N_2 and CO_2.

with those proposed (noncertified) for NBS 120c (0.37%) and certified for BCR 32 (0.74%) using either gravimetry after acid oxidant dissolution (average value obtained from ten laboratories) or reduction to S^{2-} and titration with mercuric solution (measurements made in one laboratory). In the framework of this study, it was emphasised that elemental concentrations determined using the TCD traces were preferred over the isotopic traces as is the usual practice with EA-IRMS systems. Indeed, in the case of multi-elemental analyses, at least one or more gas species have to go through a diluting system prior to introduction into the source of the IRMS system; therefore, the integrated isotopic trace is modified compared to the total peak area generated from the combustion step. This potential pitfall can be overcome by using careful calibration procedures; however, a direct integration of the TCD trace is a simple and safe option.

Determination of $\delta^{34}S_{CDT}$ values for NBS 120c and BCR 32

The PyroCube coupled to an IsoPrime IRMS was operated to evaluate its potential in the measurements of $\delta^{34}S_{CDT}$ values from natural sedimentary rocks used as two compositional references, which are the BCR 32 (Moroccan phosphorite; Community Bureau of Reference BCR certificate 1982) and NBS 120c (Florida phosphorite National Bureau of Standards NBS certificate 1988). Both of them contain about 33% *m/m* of P_2O_5. Like most phosphatic minerals (apatite) or rocks (phosphorites), they contain low amounts of S (below 1%). Thus, the use of large aliquots of samples is required for the determination of $^{34}S/^{32}S$ ratios, being 5 mg and 8 mg for BCR 32 and NBS 120c, respectively, and corresponding to about 30 μg of S. This is compatible with the dynamic range for $^{34}S/^{32}S$ analyses with this EA-IRMS configuration.

First, in order to evaluate the ability of such an apparatus to reliably combust compounds for sulfur isotopic determinations, samples bearing both organic and inorganic sulfur were mixed within the same analytical run with different sample masses. IAEA-S1 (silver sulfide Ag_2S) and one of our working reference materials Ac.Rub.1 (rubeanic acid $C_2H_4N_2S_2$) were selected to test the quality of the combustion yields. Sample amounts correspond to a 30–350 μg range of S concentrations for which theoretical combustion yields were calculated on the basis of their chemical formulae. The data calculated from the TCD records led us to calculate yields of 99.1% (1*s* = 1.7; *n* = 11) and 101.2% (1*s* = 2.0; *n* = 15) for IAEA-S1 and Ac.Rub.1, respectively. This test demonstrates the capacity of this apparatus to combust quantitatively a diverse range of S-bearing samples into SO_2 and also revealed the linearity of such combustion yields, which is an important parameter in the analysis of samples with low concentrations.

Three batches of isotopic measurements were performed using international reference materials to calculate

Table 1.
Sulfur concentration determinations from TCD data for phosphorite materials NBS120c and BCR32 from three analytical batches

Sample	Mean S (%)	*s*	*N*
BCR 32 batch#1	0.74	0.06	10
BCR 32 batch#2	0.71	0.07	10
BCR 32 batch#3	0.71	0.13	10
NBS 120c batch#1	0.52	0.03	10
NBS 120c batch#2	0.41	0.02	10
NBS 120c batch#3	0.47	0.02	10

s, standard deviation; *N*, number of aliquots analysed.

the $\delta^{34}S_{CDT}$ of BCR 32 and NBS 120c. The reference materials (Table 2) were selected in order to offer isotopic values that bracket the expected values for the phosphorite samples. These international reference materials are IAEA-S1 (silver sulfide Ag_2S) with a $\delta^{34}S_{CDT}$ of -0.3‰, IAEA-S2 (silver sulfide Ag_2S) with a $\delta^{34}S_{CDT}$ of 22.7‰, IAEA-S3 (silver sulfide Ag_2S) with a $\delta^{34}S_{CDT}$ of -32.3‰, IAEA-S4 (mineral sulfur S) with a $\delta^{34}S_{CDT}$ of 16.9‰, IAEA-SO5 (barium sulfate $BaSO_4$) with a $\delta^{34}S_{CDT}$ of 0.5‰, IAEA-SO6 (barium sulfate $BaSO_4$) with a $\delta^{34}S_{CDT}$ of -34.1‰ and NBS127 (barium sulfate $BaSO_4$) with a $\delta^{34}S_{CDT}$ of 20.3‰ (IAEA TECDOC-825 1995).

Sulfur isotopic data were obtained for three batches of measurements for each phosphorite material (Table 2). During the measurement of sulfur isotopic ratios as SO_2, an analytical bias may interfere with the measured ratios due to the different isotopomers related to the existence of ^{16}O, ^{17}O and ^{18}O (Mayer and Krouse 2004). The systematic isotopic measurements of reference-calibrated material along with unknown samples are one method of calibration that is also used to account for oxygen corrections when determining sulfur isotopes as SO_2 (Mayer and Krouse 2004). This technique was used here to determine the $\delta^{34}S_{CDT}$ values of both BCR 32 and NBS 120c. Three regression lines were

Table 2.
δ^{34}SCDT calibration for NBS 120c and BCR 32. Calibrated reference materials used were IAEA-S1, IAEA-S2, IAES-S3, IAEA-S4, IAEA-SO5, IAEA-SO6 and NBS 127

Batch#1 RM	**$\delta^{34}S_{AVE}$**	***s***	***N***	**$\delta^{34}S_{REF}$**
NBS 127	18.8	0.3	4	20.3
IAEA-SO5	-0.2	0.1	5	0.5
IAEA-SO6	-34.2	0.2	5	-34.1
IAEA-S1	-1.2	0.1	4	-0.3
IAEA-S2	20	0.3	4	22.7
IAEA-S3	-32.5	0.1	5	-32.3
IAEA-S4	14.7	0.1	5	16.9
Batch#1 Sample	**$\delta^{34}S_{AVE}$**	***s***	***N***	
BCR 32	18	0.2	7	
NBS 120c	18.3	0.5	6	
Batch#2 RM	**$\delta^{34}S_{AVE}$**	***s***	***N***	**$\delta^{34}S_{REF}$**
NBS 127	16.3	0.1	5	20.3
IAEA-SO5	-3	0.1	5	0.5
IAEA-SO6	-35.9	0.1	5	-34.1
IAEA-S1	-4	0.1	4	-0.3
IAEA-S2	17.3	0.2	5	22.7
IAEA-S3	-34.4	0.2	5	-32.3
IAEA-S4	12.1	0.1	5	16.9
Batch#2 Sample	**$\delta^{34}S_{AVE}$**	***s***	***N***	
BCR 32	18.2	0.4	8	
NBS 120c	18.3	0.2	8	
Batch#3 RM	**$\delta^{34}S_{AVE}$**	***s***	***N***	**$\delta^{34}S_{REF}$**
NBS 127	18.8	0.3	4	20.3
IAEA-SO5	-0.2	0.1	5	0.5
IAEA-SO6	-34.2	0.2	5	-34.1
IAEA-S1	-1.2	0.1	4	-0.3
IAEA-S2	20	0.3	4	22.7
IAEA-S3	-32.5	0.1	5	-32.3
IAEA-S4	14.7	0.1	5	16.9
Batch#3 Sample	**$\delta^{34}S_{AVE}$**	***s***	***N***	
BCR 32	18.2	0.3	8	
NBS 120c	18.3	0.5	6	
MEAN Sample	**$\delta^{34}S_{AVE}$**	***s***	***N***	
BCR 32	18.2	0.3	23	
NBS 120c	18.3	0.4	20	

Weight (mg) is the average aliquot weight in milligrams.
s, standard deviation; *N*, number of aliquots analysed.

computed between the certified values of the international reference materials and the raw measurements corresponding to the three successive batches of measurements (Figure 3). Using this calibration equation (Figure 3), we have been able to propose a mean $\delta^{34}S_{CDT}$ value of 18.2‰ (1*s* = 0.3; *n* = 23) for BCR 32 and a mean $\delta^{34}S_{CDT}$ value of 18.3‰ (1*s* = 0.4; *n* = 20) for NBS 120c. In the range of sulfur isotope ratios investigated in Figure 3, the three regression lines corresponding to the three batches of measurements

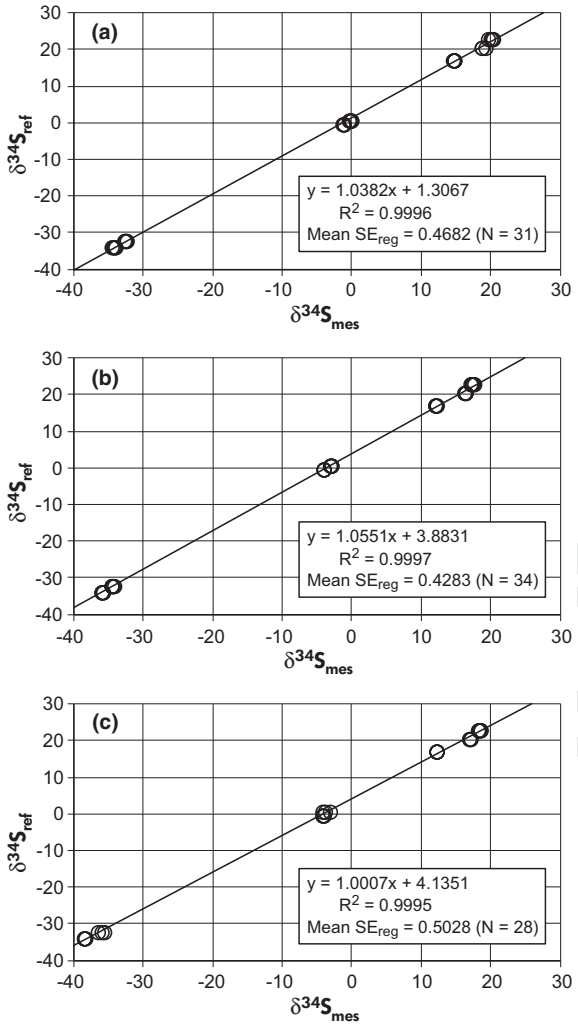

Figure 3. $\delta^{34}S_{CDT}$ calibration batches for NBS 120c and BCR 32 characterisation. Batch#1, Batch#2 and Batch#3 were performed separately and are reported, respectively, in (a), (b) and (c). $\delta^{34}S_{mes}$ is the raw value measured against the SO_2 calibration gas, and $\delta^{34}S_{ref}$ is the admitted value for each calibrated reference material supplied with each calibration certificate. Regression parameters are expressed as y = (slope)*x + (intercept) for each batch; mean SE_{reg} is the mean standard error of the regression for each batch. *N* is the number of data points.

allowed the calculation of a mean standard error (SE) between 0.4 and 0.5‰ for values of *n* between 28 and 34.

Conclusions

The results we are reporting in this study illustrate the capacities of the PyroCube system online with an IRMS instrument to reliably measure $\delta^{34}S_{CDT}$ values of phosphorite rocks (BCR 32 and NBS 120c) with low-S concentrations (0.4–0.7% *m/m*), although relatively large aliquots (5–8 mg) are required to ensure satisfactory precision (SE = 0.4‰). We propose BCR 32 and NBS 120c as potential isotopic reference materials in the framework of any further studies of the determination of sulfur isotope compositions of biogenic apatites. Repeated measurements of both phosphorites and calibration against international reference materials provide the following $\delta^{34}S_{CDT}$ values: 18.2‰ (1*s* = 0.3; *n* = 23) for BCR 32 and 18.3‰ (1*s* = 0.4; *n* = 20) for NBS 120c. The results of this study are the first step to open up a new field of investigation using the scientific potential of sulfur isotope compositions of biogenic apatites. For example, sulfur isotope ratios of biogenic apatites, possibly in combination with oxygen and strontium isotope ratios, could be used to help deciphering the marine versus freshwater environments of some extinct vertebrate species (e.g., turtles, crocodiles) for which the living aquatic environment remains an open question in the literature.

References

Cerling T.E. and Harris J.M. (1999)
Carbon isotope fractionation between diet and bioapatite in ungulate mammals and implications for ecological and palaeoecological studies. **Oecologia**, **120**, 347–363.

Cerling T.E., Harris J.M. and Passey B.H. (2003)
Diets of East African Bovidae based on stable isotope analysis. **Journal of Mammalogy**, **84**, 456–470.

Community Bureau of Reference (1982)
Certified reference material certificate of analyses for BCR No. 32. **Commission of the European Communities, Report No. 541.**

Ehleringer J.R. (2005)
The influence of atmospheric CO_2, temperature, and water on the abundance of C3/C4 taxa. **In: Ehleringer J.R., Cerling T.E. and Dearing M.D. (eds), A history of atmospheric CO2 and its effects on plants, animals, and ecosystems. Springer (New York, USA)**, 214–231.

Fourel F., Martineau F., Lecuyer C., Kupka H.J., Lange L., Ojeimi C. and Seed M. (2011)
$^{18}O/^{16}O$ ratio measurements of inorganic and organic materials by elemental analysis–Pyrolysis–isotope ratio mass spectrometry continuous flow techniques. **Rapid Communications in Mass Spectrometry**, **25**, 2691–2696.

references

Fricke H.C., O'Neil J.R. and Lynnerup N. (1995)
Oxygen isotope composition of human tooth enamel from medieval Greenland: linking climate and society. **Geology**, **23**, 869–872.

Fricke H.C., Clyde W.C. and O'Neil J.R. (1998)
Intra-tooth variations in $\delta^{18}O$ (PO_4) of mammalian tooth enamel as a record of seasonal variations in continental climate variables. **Geochimica et Cosmochimica Acta**, **62**, 1839–1850.

Fry B., Brand W., Mersch F.J., Tholke K. and Garritt R. (1992)
Automated analysis system for coupled $\delta^{13}C$ and $\delta^{15}N$ measurements. **Analytical Chemistry**, **64**, 288–291.

Giesemann A., Jaeger H.J., Norman A.L., Krouse H.R. and Brandt W. (1994)
Online sulfur-isotope determination using an elemental analyser coupled to a mass spectrometer. **Analytical Chemistry**, **66**, 2816–2819.

IAEA Vienna (1995)
TECDOC-825. Reference and intercomparison materials for stable isotopes of light elements. **Proceedings of a consultants meeting held in Vienna,** 1–3 December 1993.

Joachimski M.M., van Geldern R., Breisig S., Buggisch W. and Day J. (2004)
Oxygen isotope evolution of biogenic calcite and apatite during the Middle and Late Devonian. **International Journal of Earth Sciences**, **93**, 542–553.

LeGeros R.Z. (1981)
Apatites in biological systems. **Progress in Crystal Growth and Characterization of Materials**, **4**, 1–45.

LeGeros R.Z., Sakae T., Bautista C., Retino M. and LeGeros J.P. (1996)
Magnesium and carbonate in enamel and synthetic apatites. **Advances in Dental Research**, **10**, 225–231.

Mayer B. and Krouse R.H. (2004)
Procedures for sulfur isotope abundance studies. **Handbook of isotope analytical techniques, Volume 1, Chapter 26. Elsevier** (??????), 538–???.

National Bureau of Standards (1988)
Certificate of analysis for standard reference material 120c. **U.S. Department of Commerce report** (?????).

Preston T. and Owens N.J.P. (1985)
Preliminary ^{13}C measurements using a gas chromatograph interfaced to an isotope ratio mass spectrometer. **Biomedical Mass Spectrometry, 12-9**, 510–???.

Sacks G.L., Wolyniak C.J. and Brenna J.T. (2003)
Analysis of quantization error in high precision continuous-flow isotope ratio mass spectrometry. **Journal of Chromatography A**, **1020**, 273–282.

Sharma S., Joachimski M.M., Tobschall H.J., Singh I.B., Tewari D.P. and Tewari R. (2004)
Oxygen isotopes of bovid teeth as archives of palaeoclimatic variations in archaeological deposits of the Ganga plain, India. **Quaternary Research**, **62**, 19–28.

Sieper H.P., Kupka H.J., Lange L., Roßmann A., Tanz N. and Schmidt H.L. (2010)
Essential methodological improvements in the oxygen isotope ratio analysis of N-containing organic compounds. **Rapid Communications in Mass Spectrometry**, **24**, 2849–2858.

Yun M., Mayer B. and Taylor S.W. (2005)
$\delta^{34}S$ measurements on organic materials by continuous flow isotope ratio mass spectrometry. **Rapid Communications in Mass Spectrometry**, **19**, 1429–1436.

Zazzo A., Balasse M. and Patterson W. (2005)
High-resolution $\delta^{13}C$ intratooth profiles in bovine enamel: implications for mineralization pattern and isotopic attenuation. **Geochimica et Cosmochimica Acta**, **69**, 3631–3642.

PUBLICATION 4.10

Simultaneous N, C, S stable isotope analyses using new purge and trap EA-IRMS technology.

Journal:	*Rapid Communications in Mass Spectrometry*
Manuscript ID:	RCM-14-0170.R1
Wiley - Manuscript type:	Research Article
Date Submitted by the Author:	11-Jul-2014
Complete List of Authors:	fourel, francois; CNRS-UMR5276, LGL-TPE Universite Lyon1 martineau, francois; CNRS, Sciences de la Terre Seris, Magali; UMR5276-Universite Claude Bernard Lyon1, LGL-TPE Lecuyer, Christophe; CNRS-UMR5276, LGL-TPE Universite Lyon1; Institut Universitaire de France,
Keywords:	carbon, nitrogen, sulfur, isotope, combustion, elemental-analyser
Abstract:	RATIONALE: We have used a high–precision, easy and rapid method of simultaneous analysis of carbon ($^{13}C/^{12}C$), nitrogen ($^{15}N/^{14}N$) and sulfur ($^{34}S/^{32}S$) isotope ratios as well as elemental concentrations using a new type of elemental analyzer. This new technique provides multiple isotopic signatures on smaller sample aliquots with high precisions especially for sulfur determinations. METHOD: The technique described here is Isotopic Ratio Mass Spectrometry (IRMS) on line in continuous flow mode with an Elemental Analyzer (EA) based on "purge and trap" technology rather than conventional packed-GC gas separation. Emphasis is put on the efficiency of the system to reliably combust sulfur–bearing compounds of both organic and inorganic origin with high conversion yields. RESULTS: High quality of $^{34}S/^{32}S$ determinations is illustrated using various international reference materials. Working NCS calibrated material has been selected and characterized as well in order to fully use the capacities of the system in future work. CONCLUSIONS: The possibilities of such a system to reliably measure S isotopes as well as N and C within the same aliquot of sample opens up new fields of investigation in many domains where multi-isotopic approaches are required.

Simultaneous N, C, S stable isotope analyses using new purge and trap EA-IRMS technology.

François Fourel[1,*], François Martineau[1], Magali Seris[1] and Christophe Lécuyer[1,#]

[1]Laboratoire de Géologie de Lyon "Terre, Planètes Environnement", CNRS UMR 5276, Université Claude Bernard Lyon 1, Ecole Normale Supérieure de Lyon, Campus de la Doua, F-69622 Villeurbanne, France.

*Corresponding author

#also at Institut Universitaire de France

Abstract

RATIONALE: We have used a high–precision, easy and rapid method of simultaneous analysis of carbon ($^{13}C/^{12}C$), nitrogen ($^{15}N/^{14}N$) and sulfur ($^{34}S/^{32}S$) isotope ratios as well as elemental concentrations using a new type of elemental analyzer. This new technique provides multiple isotopic signatures on smaller sample aliquots with high precisions especially for sulfur determinations.

METHOD: The technique described here is Isotopic Ratio Mass Spectrometry (IRMS) on line in continuous flow mode with an Elemental Analyzer (EA) based on “purge and trap” technology rather than conventional packed-GC gas separation. Emphasis is put on the efficiency of the system to reliably combust sulfur–bearing compounds of both organic and inorganic origin with high conversion yields.

RESULTS: High quality of $^{34}S/^{32}S$ determinations is illustrated using various international reference materials. Working NCS calibrated material has been selected and characterized as well in order to fully use the capacities of the system in future work.

CONCLUSIONS: The possibilities of such a system to reliably measure S isotopes as well as N and C within the same aliquot of sample opens up new fields of investigation in many domains where multi-isotopic approaches are required.

Keywords: carbon, nitrogen, sulfur, isotope, combustion, elemental-analyser

Introduction

The development of continuous flow techniques for Isotope Ratio Mass Spectrometry determinations started with the connection on line between an Elemental Analyzer (EA) and an IRMS system (Preston and Owens 1985 [1]). In these early days combustion mode only was available to configure the Elemental Analyzer for isotopic analyses and $^{13}C/^{12}C$ ratios only were measured although Preston and Owens (1985) already mentioned the future possibility of measuring both $^{13}C/^{12}C$ and $^{15}N/^{14}N$ ratios simultaneously with such a system using a chromatographic packed column to separate the compounds to analyze. Those preliminary investigations were done on planktonic material where carbon concentration was an order of magnitude higher than nitrogen which was a true limitation. This was soon realised [2] with some limitations for the high C/N ratios. In the mid 90's, sulfur isotope measurements became available to the EA-IRMS users by analysing SO_2 as the gas species for organic matter[3] . Those techniques were all based on a chromatographic separation of the gases to analyze. Nowadays in most EA-IRMS systems available, N and C isotopic compositions are accessible from the same aliquot of sample using chromium oxide and cobaltous oxide as oxidising agents, but for S isotopes analyses, the oxidising agent used is tungstic oxide. The packed GC columns traditionally used for N_2-CO_2 separation are also different in length and packing from the GC columns used to isolate the SO_2 peak. Those differences in analytical setups make it difficult to measure C, N and S isotope ratios from the same sample aliquot. We report in this study the use of an EA system recently made accessible to IRMS studies, and which is based on a principle of gas separation called "purge and trap" [4,5] allowing the simultaneous determination of C, N, S stable isotope ratios and concentrations from the same aliquot of sample in less than 12 minutes. Such a triple determination of isotopic ratios performed on the same sample aliquot has potential power applications in the fields of Earth sciences, archaeology, biochemistry or ecology. Indeed, the C, N and S isotopic signatures of organic compounds are useful to track the origin of organic matter[6], the redox conditions of the environment of aquatic and terrestrial living organisms[7], metabolic pathways[8], diets and palaeodiets of humans or animals[9] as well as the structure of trophic chains[10]. The aim of this study was to compare the quality of the data obtained when measuring the three gas species simultaneously from the same sample aliquot compared to the data obtained when those species are measured separately. Special emphasis was put on the

$^{34}S/^{32}S$ data as simultaneous analyses for $^{13}C/^{12}C$ and $^{15}N/^{14}N$ has now become a well established technique.

Combustion operating parameters were optimised in order to improve the peak shape quality especially that for SO_2, which is generally a concern for conventional EA-IRMS analysis when using packed GC columns. Timing for CO_2 and SO_2 release as well as trap release temperature were tested to define the best operating conditions. Moreover, combustion yields were monitored for both organic and inorganic sulfur compounds. These were calculated from data provided by the EA Thermal Conductivity Detector (TCD) and optimized by tuning both furnace temperature and time of reaction. Once this step has been achieved, reproducibility of N–C–S isotopic measurements was explored. Until now, no multi-isotopic reference calibrated material is available to test simultaneous isotopic analyses. Thus we calibrated our own multi isotope laboratory reference material by using our N–C laboratory standard aspartic acid ($C_4H_7NO_4$) calibrated against reference calibrated material such as IAEA C3, IAEA-C4, IAEA-CH6, IAEA-CH7, IAEA-N1, IAEA-N2, USGS-25 mixed with NBS127 (barium sulfate $BaSO_4$) standard calibrated for $\delta^{34}S_{CDT}$ determinations. This allowed us to check that there was no difference in analytical performances for precision and accuracy between separate isotopic determinations for N, C and S separately or simultaneous measurements of all isotopic signatures from one single aliquot of the same mixed elements. Finally, the accuracy of measured $^{34}S/^{32}S$ ratios was established by measuring the available international standards (mean standard error: sigma ≈ 0.4‰ for n ≥30).

Analytical techniques

"Purge and trap" High Temperature EA-pyrolysis-IRMS

The system used, called VarioPyroCube, was developed by Elementar GmbH (Elementar Analysensysteme GmbH, Donaustrasse 7, 63452 Hanau, Germany) and recently made available online with IRMS instruments. This system had already been widely investigated in pyrolysis mode for the elemental and isotopic analysis of organic and inorganic compounds [4,5] , but it had not yet been fully investigated for sulfur isotopic analyses and especially for both organic and inorganic sulfur samples. Moreover, the unique capacity for the system to determine simultaneously $^{13}C/^{12}C$, $^{15}N/^{14}N$ and $^{34}S/^{32}S$ isotopic ratios had not been

evaluated yet.

The general setup of the instrument is illustrated in figure 1. Like in most conventional EA-IRMS systems this instrument operates with helium as a carrier gas and consists of a combustion tube followed by a reduction tube. The combustion tube is filled with tungstic oxide in order to ensure full conversion of sulfur into SO_2 gas. The combustion tube is kept at 1150°C. Besides the tungstic oxide, an oxygen injection system allows the introduction of an oxygen gas pulse with the sample injection. The volume and timing of this oxygen injection is user-defined and can then be optimized for different types of chemical compounds. The reduction tube is filled with copper pellets and held at 850°C. A chemical water trap, which operates using a SICAPENT^{TM} dryer, follows the reduction tube.

Nitrogen gas is not trapped and goes straight through the system towards the Thermal Conductivity Detector (TCD) located before the exit of the PyroCube system. For CO_2 and SO_2 gases, after the water trap, lies the purge and trap original system of the PyroCube. The CO_2 trap operates at room temperature in trapping mode and can then be heated at 110°C to release the trapped CO_2 that is used to analyze $^{13}C/^{12}C$ ratios. Next to the CO_2 trap lies a SO_2 trap operating at room temperature in trapping mode and which can be heated at 220°C in order to release the trapped SO_2 that is used to analyze $^{34}S/^{32}S$ ratios. All analytical gas pass through the TCD that is used to determine N, C and S abundances. The EA system is then connected online via an open split device to an IsoPrime mass spectrometer system. The sample line is equipped with a programmable dilution system supplied by IsoPrime UK Ltd (Isoprime House Earl Road Cheadle Hulme Cheadle SK8 6PT, UK) in order to dilute the CO_2,N_2 or SO_2 gases generated from the combustion of the chemical compounds that could be present in too high concentrations, therefore generating a saturation of the amplifiers. More recent mass spectrometers are now equipped with larger dynamic range head amplifier which reduces the systematic need for this dilution step. In parallel to this sample line, a second helium line is connected to the source of the mass spectrometer to carry the three calibration gases that are CO_2, N_2 and SO_2.

Results and Discussion

NCS analyses

The optimization of the PyroCube system in order to properly measure C, N and S stable isotope ratios as well as relative abundances within the same run requires a precise coordination between both Elemental Analyzer and IRMS, which are both controlled by their own processing software running in parallel on the same computer. In order to measure beam sizes compatible with the dynamic range of the mass spectrometer and depending on the chemical composition of the samples to analyze, we used a diluting system. We used the IsoPrime UK Ltd diluter, which can be programmed through the software method to specifically adjust the intensity of one gas species without inducing significant isotopic fractionation for the studied isotope ratios. Once both EA and IRMS computer programs have been fully synchronized, the optimization procedure for sample combustion follows the same strategy as in conventional EA-IRMS techniques. In that case, the instrument is able to deliver isotopic traces for all analyzed gas species like the one shown in Figure 2, with a special emphasis on the quality of the SO_2 peak shape. As it was already mentioned for $^{18}O/^{16}O$ analyses in pyrolysis mode by Fourel et al. 2011[5], 'purge and trap' devices generate chromatographic peaks that are sharp, symmetrical and devoid of the so-called 'peak tails', which are critical during the acquisition of isotopic ratios for gases extracted from the EA system.

The first experiment reported here deals with the capacity of the system to measure simultaneously the $\delta^{13}C$, $\delta^{15}N$ and $\delta^{34}S$ values of the same sample aliquot. Up to now there has been no reference calibrated material available for multi-isotopic analyses. In order to evaluate the quality of these simultaneous isotopic measurements, samples of aspartic acid (an amino acid of chemical formula $C_4H_7NO_4$), were mixed with samples of barium sulfate used as a calibration chemical compound for sulfur isotopic measurements (Table 1). The aspartic acid has been used as an internal laboratory N and C calibration material, and was previously calibrated against several international reference materials (IAEA-N1, IAEA-N2, IAEA-CH6, IAEA-CH-7, IAEA-C3 and IAEA-C4). The main purpose of this test was to show that the isotopic reproducibility for the three isotopic ratios measured simultaneously compares well with the conventional individual determinations of $\delta^{13}C$, $\delta^{15}N$ and $\delta^{34}S$ values (Table 1). Before, during and following the measurements of aliquots from our test mixtures, the two laboratory standards were also analyzed separately showing no significant differences between the values obtained as individual samples or mixed together.

Calibration of $^{34}S/^{32}S$ ratios along with those obtained for C and N

If the combined analysis of C and N stable isotope ratios using the EA-IMRS technology is now a well-established technique, the possibility to add the analysis of S isotopic ratios on the same sample aliquot is of significant interest when researchers are facing limited amounts of chemical compounds to analyze. Here we focus on the quality of $\delta^{34}S$ values obtained using such an analytical protocol. One critical aspect is the complete combustion of S, either of organic or inorganic origin, into SO_2; it has been tested through a first set of aliquot measurements of IAEA-S1 silver sulfide (corresponding to a range of 35–350 μg of S) mixed with rubeanic acid also called dithiooxamide of chemical formula $C_2H_4N_2S_2$. Figure 3 reports the total S amounts calculated from the sample weight versus the S area measured from the PyroCube TCD. These results show that the decomposition of sulfur into SO_2 from both organic and inorganic compounds provides high combustion yields for S (calculated yields from TCD data and theoretical S contents from both samples range between 96 and 105 wt %) over the wide range of sample amounts considered.

As we mentioned earlier, there is no calibrated reference material for the simultaneous determination of $\delta^{13}C_{PDB}$ and $\delta^{15}N_{AIR}$. In order to calibrate a batch of samples, aliquots of $\delta^{15}N_{AIR}$ calibrated material must be added to a $\delta^{13}C_{PDB}$ calibrated material. With three isotopic signatures to measure simultaneously, using individual reference calibrated material for the three isotopic species requires a sample versus standard ratio which is not convenient. We then decided to calibrate a working standard for $\delta^{34}S_{CDT}$, $\delta^{13}C_{PDB}$ and $\delta^{15}N_{AIR}$ determinations. We analyzed the three isotopic ratios in aliquots of rubeanic acid along with the calibrated reference materials for different sample experiments over one month. The results of this calibration process are reported in Table 2. As an indication, we also reported the C, N and S concentrations measured with the TCD traces from the elemental analyzer. As this rubeanic acid is not a calibrated material, the reference values for concentrations have been calculated from the chemical formula of rubeanic acid. As far as the isotopic data are concerned for the three gas species the quality of the data is close to what is generally admitted for the same isotopic signature run individually for the same type of sample. For

the concentration data, the results obtained are very close to the expected values with reproducibility close to what is achieved with conventional elemental analyzers.

In order to fully evaluate the performances of the purge and trap technology for sulfur analyses we decided to setup a third set of isotopic measurements that was devoted to most of the available international reference materials IAEA-S1[11,12,13] (silver sulfide Ag_2S) with a $\delta^{34}S_{CDT}$ of -0.3‰, IAEA-S2[11,12] (silver sulfide Ag_2S) with a $\delta^{34}S_{CDT}$ of 22.7‰, IAEA-S3[11,12] (silver sulfide Ag_2S) with a $\delta^{34}S_{CDT}$ of -32.3‰, IAEA-S4[14.15] (mineral sulfur S) with a $\delta^{34}S_{CDT}$ of 16.9‰, IAEA-SO5[16] (barium sulfate $BaSO_4$) with a $\delta^{34}S_{CDT}$ of 0.5‰, IAEA-SO6[16] (barium sulfate $BaSO_4$) with a $\delta^{34}S_{CDT}$ of -34.1‰, and NBS127[16.17] (barium sulfate $BaSO_4$) with a $\delta^{34}S_{CDT}$ of 20.3‰ (IAEA TECDOC-825 1995) in order to check the accuracy of the analyses over a wide range of sulfur isotopic ratios (Table 3 and Figure 4). In Figure 4 are reported the values of the international standards measured in the same analytical experiment from two different runs. In the framework of run#1, samples were grouped by rank of isotopic value, while in run#2 they were sorted according to their matrix chemical composition. This is usually not what isotope scientists would do for day-to-day analyses. However, the rather extreme conditions of this test were considered as significant enough to evaluate such a new technique. Results reported in Table 3 show differences within the uncertainties of the technique between the measured isotopic compositions obtained for both run#1 and run#2. These two experiments were designed according to a way of calibration commonly used to account for oxygen corrections when analyzing sulfur isotopes as SO_2 [18]. In the large investigated range of sulfur isotope compositions of various chemical matrices, linear regressions between raw and true isotopic measurements led to obtain calibration lines (R^2 = 0.999) that predict mean standard errors of these regression lines close to 0.4‰ associated with the determination of $\delta^{34}S$ values. The regression parameters from figure 4 are expressed as y = (slope)*x + (intercept) for each experiment, σ_{reg} is the mean standard error of the regression for each batch and is respectively 0.37‰ (N=51) and 0.48‰ (N=40) for run#1 and run#2, respectively, where N is the number of data.

Furthermore, in Table 3 we have also reported $\delta^{15}N$ and $\delta^{13}C$ values obtained from our laboratory working calibrated material aspartic acid (AA), which is used for day-to-day N and C isotopic

measurements, as well as our rubeanic N, C, S working reference material. We have also added to the batch of measurements the $\delta^{34}S_{CDT}$ calibrated samples of sphalerite (ZnS-1 and ZnS-2) supplied by Stanislaw Halas (Maria Curie-Sklodowska University in Lublin, Poland) and which had been previously calibrated by Ding T. et al. 2001[19]. Table 3 shows good agreement within the uncertainties of the method between the measured and admitted values (especially for $\delta^{34}S_{CDT}$ analyses) for those calibrated working standards which were analyzed as samples along with reference materials characterized by a large range of $\delta^{34}S_{CDT}$ values. What we specify as "admitted values" are the isotopic values from secondary working standards calibrated against reference calibrated material. It is worthy to note that the simultaneous determination of multiple isotopic compositions of organic and inorganic compounds, which here does not generate any deterioration of the analytical performance of the instrument, is usually a major drawback for conventional EA-IRMS analyses using conventional packed column GC separation. Although this has not been fully investigated, it must be noted that matrices with various C/S ratios do not seem to influence the performance of the instrument, even though the chemical composition of analyzed compounds is usually a critical parameter when using conventional EA systems based on chromatographic separation. As a comparison, reproducibility specifications for individual analyses of $\delta^{13}C$, $\delta^{15}N$ and $\delta^{34}S_{CDT}$ supplied by manufacturers are generally estimated respectively at 0.10‰, 0.45‰ and 0.20‰. Those specifications are usually given for natural abundance organic samples with low C:N and C:S ratios.

When purge and trap technology is used for gas separation, one of the main analytical concern compared to gas chromatographic separation is intersample memory effect. In order to evaluate this aspect we have reported in figure 5 a classical plot to quantify the potential carry over from one sample to another. Within the same experiment where several aliquots of the same samples are analyzed and several samples with different isotopic contents are analysed one after the other. We have plotted on the X axis the absolute value of the difference between the average isotopic ratio for sample N and the average isotopic ratio for sample N-1 versus on the Y axis the absolute value for the difference between the isotopic ratio of aliquot 1 and the isotopic ratio of aliquot 3 for sample N. We have done this plot for one experiment where we measured samples with different $^{13}C/^{12}C$ ratios (figure 3 a). We have also reported this plot for two batches

where we measured samples with different $^{34}S/^{32}S$ ratios. One experiment was done in which analyzed samples were sorted by expected $^{34}S/^{32}S$ ratios while samples were sorted by type of matrix in the second one. Any significant memory effect should generate positive correlations on those plots. What we can see from figure 3 is that no memory effect could be identified with this technique. As nitrogen is not going through any trap we did not apply the same test to $^{15}N/^{14}N$ analyses.

NCS concentrations

The Vario Pyrocube is equipped with a Thermal Conductivity Detector (TCD) allowing the determinations of N, C and S concentrations within each analyzed sample. In the past, most determinations of elemental concentrations by EA-IRMS techniques were based on the areas of the major peaks from isotopic traces that are generally able to provide good quality compositional data. In the case of simultaneous determinations of multi–element relative abundances, the main drawback encountered is related to the input of several gas species through a dilution system in order to measure the isotopic ratios. This technique introduces an uncertainty that can be avoided when using directly the EA TCD data. Relative abundances of C, N and S in rubeanic acid ($C_2H_4N_2S_2$), aspartic acid ($C_4H_7NO_4$), sphalerite (ZnS), silver sulfide (Ag_2S), native sulfur (S), barium sulfate ($BaSO_4$) from calibration runs #1 and #2 are averaged and reported in Table 4. Despite the various S concentrations and chemical compositions of hosting organic and inorganic compounds, compositional data are characterized by acceptable reproducibility and accuracy both better than 1 wt%.

Conclusions

The results reported in this study demonstrate the capacities of the PyroCube Elemental Analyzer coupled online with an IRMS instrument to determine simultaneously $\delta^{13}C$, $\delta^{15}N$ and $\delta^{34}S$ values from the same sample aliquot with high–levels of precision for the three isotopic systems (±0.2‰; ±0.2‰; ±0.4‰; respectively). Besides the acquisition of the stable isotope ratios, the quantification of N, C and S relative

abundances directly from the EA-TCD prevents uncertainties associated with the use of any dilution system. This instrument opens up new possibilities for a multi-isotopic analysis of both organic and inorganic compounds without increasing either the analytical time or cost. For example, fields of application of such a method concerns the detection of food product alteration or the identification of organic matter sources, especially in cases where sample sizes are very limited. As far as sulfur isotopic analyses are concerned, this versatile system has demonstrated its capacities to reliably determine $\delta^{34}S$ values both in terms of precision and accuracy.

References

1. T. Preston, N. J. P. Owens. Preliminary ^{13}C measurements using a gas ghromatograph gnterfaced to an isotope ratio mass spectrometer. *Biomedical. Mass Spectrom.* **1985,** *12-9*, 510.
2. B. Fry, W. Brand, F. J. Mersch, K. Tholke, R. Garritt. Automated analyses system for coupled $\delta^{13}C$ and $\delta^{15}N$ measurement. *Anal. Chem.* **1992**, *64*, 288.
3. A. Giesemann, H. J. Jaeger, A. L. Norman, H. R. Krouse, W. Brandt. On-line sulfur-isotope determination using an elemental analyser coupled to a mass spectrometer. *Anal. Chem*. **1994**, *66*, 2816.
4. H. P. Sieper, H. J. Kupka, L. Lange, A. Roßmann, N. Tanz , H. L. Schmidt. Essential methodological improvements in the oxygen isotope ratio analysis of N-containing organic compounds. *Rapid Commun. Mass Spectrom.* **2010**, *24*, 2849.
5. F. Fourel, F. Martineau, C. Lécuyer, H. J. Kupka, L. Lange, C. Ojeimi, M. Seed. $^{18}O/^{16}O$ ratio measurements of inorganic and organic materials by EA–Pyrolysis–IRMS continuous flow techniques. *Rapid Commun. Mass Spectrom*. **2011**, *25*, 2691.
6. M. J. Mitchell, H. R. Krouse, B. Mayer, A. C. Stam, Y. Zhang. Use of stable isotopes in evaluating sulphur biogeochemistry of forest ecosystems. *In: Kendall C., Mc Donnell JJ (eds) Isotope tracers in catchment hydrology. Elsevier Amsterdam*, **1998,** 489.
7. P. M. Wynn, A. Borsato, A. Baker, S. Frisia, R. Miorandi, I. J. Fairchild. Biogeochemical cycling of sulphur in karst and transfer into speleothem archives at Grotta di Ernesto, Italy. *Biogeochemistry* **2013**, *114*, 255.
8. N. Tanz, H. Schmidt. $\delta^{34}S$ value measurements in food origin assignments and sulfur isotope fractionation in plants and animals. *J. Agric. Food Chem*. **2010**, *58*, 3139.
9. O. Nehlich, B. T. Fuller, M. Jay, A. Mora, R. A. Nicholson, C. I. Smith, M. P. Richards. Application of sulphur isotope ratios to examine weaning patterns and freshwater fish consumption in Roman Oxfordshire, UK. *Geochim. Cosmochim. Acta* **2011**, *75*, 4963.
10. M. P. Richards, B. T. Fuller, M. Sponheimer, T. Robinson, L. Ayliffe. Sulphur isotopes in palaeodietary studies: a review and results from a controlled feeding experiment. *Int. J. Osteoarchaeol.* **2003**, *13*, 37.
11. B. W. Robinson. Sulphur isotope standards. *Proceedings of a consultants' meeting held in Vienna, 1-3. Dec. 1993. IAEA-TECDOC-825*, **1995,** 39.
12. W. Stichler, R. Gonfiantini, K. Rozanski. Reference and intercomparison materials for stable isotopes of light elements. *Proceedings of a consultants' meeting held in Vienna, 1 - 3. Dec. 1993. IAEA-TECDOC-825*, **1995**, 7.
13. T. B. Coplen, H. R. Krouse. Sulphur isotope data consistency improved. *Nature* **1998**, *392,* 32.
14. R. W. Carmody, R. R. Seal II. Evaluation of the sulfur isotopic composition and homogeneity of the Soufre de Lacq reference material. *Chem. Geol.* **1999**, *153 1-4,* 289.

15. H. P. Qi, T. B. Coplen. Evaluation of the $^{34}S/^{32}S$ ratio of Soufre de Lacq elemental sulfur isotopic reference material by continuous flow isotope-ratio mass spectrometry. *Chem. Geol.* **2003**, *199 1-2,* 183.

16. S. Halas, J. Szaran. Improved thermal decomposition of sulfates to SO_2 and mass spectrometric determinations of $\delta^{34}S$ of IAEA-SO-5, IAEA-SO-6 and NBS-127 sulfate standards. *Rapid Commun. Mass Spectrom.* **2001**, *15 17*, 1618.

17. G. Hut. Consultants' group meeting on stable isotope reference samples for geochemical and hydrological investigations, 16-18 Sep. 1985. *Report to the Director General, INTERNATIONAL ATOMIC ENERGY AGENCY, Vienna*, **1987**.

18. B. Mayer and R. H. Krouse. Procedures for sulfur isotope abundance studies., *Handbook of Isotope Analytical Techniques, Volume1, **Chapter 26**,* **2004,** *26,* 538.

19. T. Ding, S. Valkiers, H. Kipphardt, P. De Bièvre, P. D. P. Taylor, R. Gonfiantini, R. Krouse. Calibrated sulfur isotope abundance ratios of three IAEA sulfur isotope reference materials and V-CDT with a reassessment of the atomic weight of sulfur. *Geochim. Cosmochim. Acta* **2001**, *65,* 2433.

Table caption

Table 1: Reproducibility for $\delta^{13}C_{VPDB}$(‰), $\delta^{15}N_{AIR}$(‰) and $\delta^{34}S_{CDT}$(‰) values simultaneously determined from working laboratory calibration material (WS Mixture = aspartic acid $C_4H_7NO_4$ mixed with NBS127 barium sulfate $BaSO_4$ in proportion 2:1) used for N and C determinations and used for S determinations mixed together. Weight (mg) is the average aliquot weight in milligrams. SD = standard deviation. N = number of aliquots analyzed. "REF values" are the admitted values for aspartic acid and barium sulfate calibrated samples.

Table 2: Characterisation of our NCS working standard rubeanic acid for $\delta^{13}C_{VPDB}$(‰), $\delta^{15}N_{AIR}$(‰) and $\delta^{34}S_{CDT}$(‰) isotopic ratios (Rub. Ac. Isot. Rat.). The calibration runs have been done using aspartic acid working standard, IAEA-S1 and IAEA-NBS127. Three calibration analytical batches were executed over a period of one month. Concentrations (Rub. Ac. Conc.) for N (W%N), C (W%C) and S (W%S) have also been measured from the Pyrocube Thermal Conductivity Detector data (TCD) recorded simultaneously with the isotopic ratios. The indicated theoretical concentrations (Theor. Conc.) of N (W%N), C (W%C) and S (W%S) have been calculated from the rubeanic acid chemical formula.

Table 3: $\delta^{34}S_{CDT}$(‰) calibration runs using Reference Calibrated Material (RCM) IAEA-S1, IAEA-S2, IAES-S3, IAEA-S4, IAEA-SO5, IAEA-SO6 and NBS127. Results for working standards (WS) calibrated against those RCM are indicated. AA = aspartic acid, Ac Rub = rubeanic acid, ZnS1 and ZnS2 = Sphalerite. Ref. = admitted values for RCM material. Adm. = admitted values for calibrated working standards (WS) which are not RCM. W(mg) = sample weight in milligrams. SD = standard deviation. N = number of aliquots analyzed. For IAEA-S4 SO_2 peak was diluted before introduction in the mass spectrometer. For AA, the CO_2 peak was diluted before introduction in the mass spectrometer. For Ac. Rub. Both SO_2 and CO_2 peaks were diluted before introduction in the mass spectrometer.

Table 4: NCS compositional data calculated from the Vario Pyrocube Thermal Conductivity Detector (TCD) data. Theor. = theoretical concentration from chemical formula of each compound. Mes. = measured value. SD = standard deviation. N = number of aliquots analyzed.

Table 1:

	Weight (mg)	$\delta^{34}S_{AVE}$	$SD_{\delta^{34}S}$	N	$\delta^{15}N_{AVE}$	$SD_{\delta^{15}N}$	N	$\delta^{13}C_{AVE}$	$SD_{\delta^{13}C}$	N
WS Mixture	0.300	20.2	0.2	12	-6.49	0.18	16	-24.80	0.12	16
REF Value	-	20.3	0.4	-	-6.46	0.20	-	-24.83	0.11	-

Table 2:

	Weight (mg)	$\delta^{34}S_{AVE}$	$SD_{\delta^{34}S}$	N	$\delta^{15}N_{AVE}$	$SD_{\delta^{15}N}$	N	$\delta^{13}C_{AVE}$	$SD_{\delta^{13}C}$	N
Rub.Ac. Isot. Rat.	0.150	3.8	0.2	15	-2.43	0.13	15	-35.73	0.10	15

	Weight (mg)	W%S	$SD_{\%S}$	N	W%N	$SD_{\%N}$	N	W%C	$SD_{\%C}$	N
Rub.Ac. Conc.	0.150	54.8	1.1	15	23.8	0.6	15	20.9	0.5	15
Theor. Conc.	0.150	53.3	-	-	23.3	-	-	20.0	-	-

Table 3:

RUN 1 RCM	W (mg)	$\delta^{34}S_{CDT}$	$SD_{\delta^{34}S}$	N	$\delta^{34}S_{CDT}$ Ref.
NBS127	0.20	20.6	0.1	6	20.3
IAEA-SO5	0.20	0.5	0.2	5	0.5
IAEA-SO6	0.20	-33.9	0.3	6	-34.1
IAEA-S1	0.30	-0.5	0.3	7	-0.3
IAEA-S2	0.30	22.2	0.1	5	22.7
IAEA-S3	0.30	-32.4	0.2	6	-32.3
IAEA-S4	0.20	16.5	0.1	5	16.9

RUN 1 WS	W (mg)	$\delta^{34}S_{CDT}$	$SD_{\delta^{34}S}$	N	$\delta^{34}S_{CDT}$ Adm.	$\delta^{15}N_{AIR}$	$SD_{\delta^{15}N}$	N	$\delta^{15}N_{AIR}$ Adm.	$\delta^{13}C_{PDB}$	$SD_{\delta^{13}C}$	N	$\delta^{13}C_{PDB}$ Adm.
ZnS1	0.15	-0.7	0.1	6	-0.3								
ZnS2	0.15	-32.6	0.2	7	-32.3								
Ac Rub	0.50	3.6	0.2	8	3.8	-2.31	0.20	10	-2.43	-35.81	0.22	9	-35.73
AA	0.50	-	-	-	-	-6.36	0.20	12	-6.46	-24.85	0.09	10	-24.83

RUN 2 RCM	W (mg)	$\delta^{34}S_{CDT}$	$SD_{\delta^{34}S}$	N	$\delta^{34}S_{CDT}$ Ref.
NBS127	0.20	20.8	0.2	7	20.3
IAEA-SO5	0.20	0.4	0.3	5	0.5
IAEA-SO6	0.20	-33.9	0.1	6	-34.1
IAEA-S1	0.30	-1.3	0.1	7	-0.3
IAEA-S2	0.30	23.2	0.1	6	22.7
IAEA-S3	0.30	-32.1	0.2	5	-32.3
IAEA-S4	0.20	16.8	0.1	7	16.9

RUN 2 WS	W (mg)	$\delta^{34}S_{CDT}$	$SD_{\delta^{34}S}$	N	$\delta^{34}S_{CDT}$ Adm.	$\delta^{15}N_{AIR}$	$SD_{\delta^{15}N}$	N	$\delta^{15}N_{AIR}$ Adm.	$\delta^{13}C_{PDB}$	$SD_{\delta^{13}C}$	N	$\delta^{13}C_{PDB}$ Adm.
ZnS1	0.15	-0.4	0.2	6	-0.3								
ZnS2	0.15	-32.2	0.2	6	-32.3								
Ac Rub	0.50	3.8	0.3	5	3.8	-2.51	0.21	10	-2.43	-35.48	0.19	10	-35.73
AA	0.50	-	-	-	-	-6.51	0.18	10	-6.46	-24.91	0.12	10	-24.83

Table 4:

SAMPLE	%Smes	SD	N	%S theor.	%Nmes	SD	N	%N theor.	%Cmes	SD	N	%C theor.
NBS127	15.3	1.2	10	15.0								
IAEA-SO5	15.8	0.5	10	15.0								
IAEA-SO6	15.2	0.8	10	15.0								
IAEA-S1	15.0	0.2	10	15.0								
IAEA-S2	15.6	0.3	10	15.0								
IAEA-S3	15.1	0.4	10	15.0								
IAEA-S4	100.9	2.2	10	100.0								
ZnS-1	32.9	0.8	10	33.0								
ZnS-2	25.7	1.0	10	33.0								
AA	-	-	-	-	10.4	0.3	10	10.5	36.2	0.1	10	36.1
Ac Rub	53.2	1.6	10	53.3	23.3	0.6	10		19.9	0.3	10	20

Figure captions

Figure 1: NCS combustion set up for the "purge and trap" VarioPyroCube system. Combustion temperature is set at 1150 °C, reduction temperature is set at 850°C, CO_2 desorption temperature is set at 850°C and desorption temperature for SO_2 is set at 220 °C. Gas separation is ensured by the desorption unit. No GC packed column is used in this configuration.

Figure 2: Isotopic chromatogram measured with the IRMS system showing the high quality of the SO_2 peak from an aliquot of 500 µg of rubeanic acid ($C_2H_4N_2S_2$) as well as the efficient peak separation that allows clean 64 ($^{32}S^{16}O_2$) and 66 ($^{34}S^{16}O_2$) isotopic traces. CO_2 and SO_2 peaks are diluted with an automated diluter located between the Pyrocube and the IRMS system. It is important to notice the efficient baseline separation between the unwanted gas species like N_2 and CO_2.

Figure 3: Combustion yields for S combustion as measured with the PyroCube Thermal Conductivity Detector (TCD) for both organic rubeanic acid (= triangles) and inorganic sulfur-bearing (barium sulfate = circles) samples. Sulfur amounts range from 40 to 400 µg. S area = SO_2 peak area measured from the Pyrocube TCD (mV. s). S amount (mg) = amount of S calculated from the sample weight and the percentage (wt %) of S in the sample.

Figure 4: $\delta^{34}S_{CDT}$(‰) calibration Runs#1 and #2 using international reference material isotopically characterised for $\delta^{34}S$(‰) values. Run#1 and Run#2 were performed separately and are reported respectively in a) and b). $\delta^{34}S_{mes}$(‰) is the raw value measured against the SO_2 calibration gas and $\delta^{34}S_{ref}$ is the admitted value for each calibrated reference material

supplied with each calibration certificate. Regression parameters are expressed as y = (slope)*x + (intercept) for each batch, σ_{reg} is the mean standard error of the regression for each batch. N is the number of data points. Reference Calibrated Material used are IAEA-S1, IAEA-S2, IAES-S3, IAEA-S4, IAEA-SO5, IAEA-SO6 and NBS127.

Figure 5: Memory effect test: The X axis represents the absolute value of the difference between the average isotopic ratio for sample N and the average isotopic ratio for sample N-1 versus on the Y axis the absolute value for the difference between the isotopic ratio of aliquot 1 (al1) and the isotopic ratio of aliquot 3 (al3) for sample N. a) Memory effect plot for one experiment in which we measured samples with different $^{13}C/^{12}C$ values. b) Memory effect plot for two batches in which we measured samples with different $^{34}S/^{32}S$ ratios. Circles and plain line: experiment with samples analysed sorted by expected $^{34}S/^{32}S$ values. Triangles and dotted line experiment with samples sorted by type of matrix.

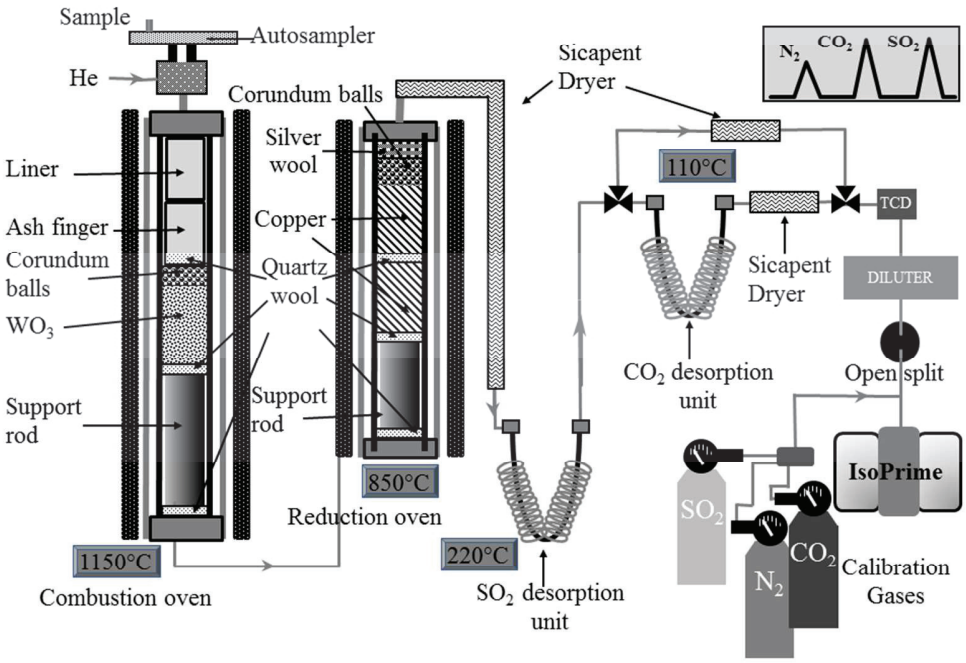

Figure 1
254x190mm (96 x 96 DPI)

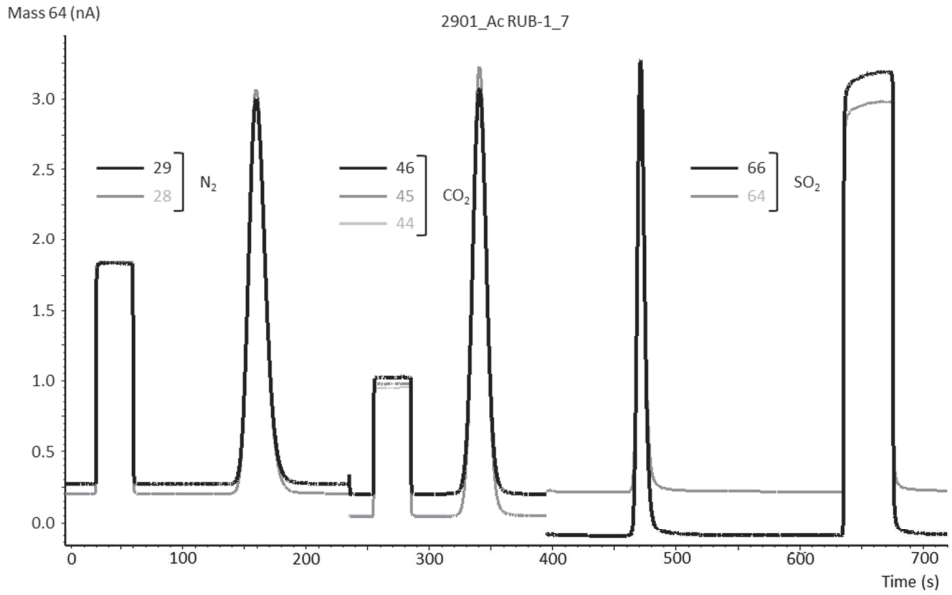

Figure 2
275x190mm (96 x 96 DPI)

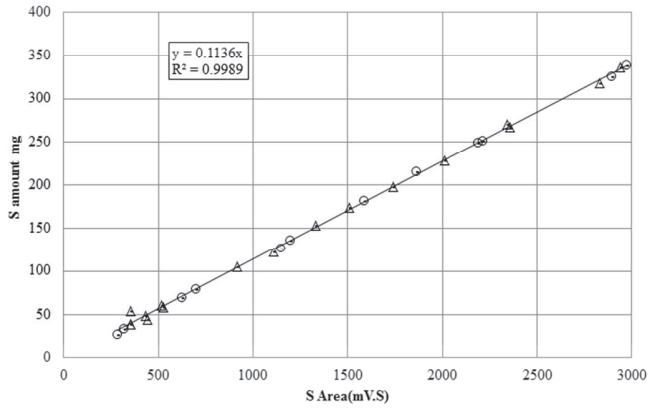

Figure 3
275x190mm (96 x 96 DPI)

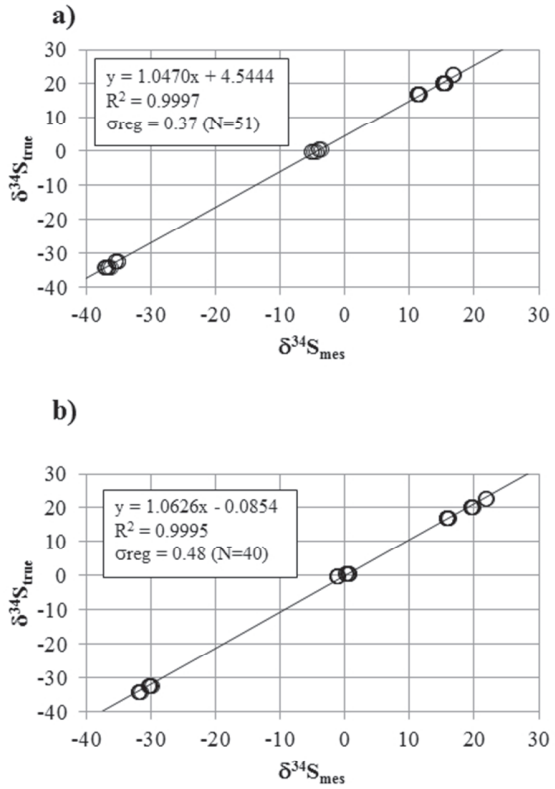

Figure 4
190x254mm (96 x 96 DPI)

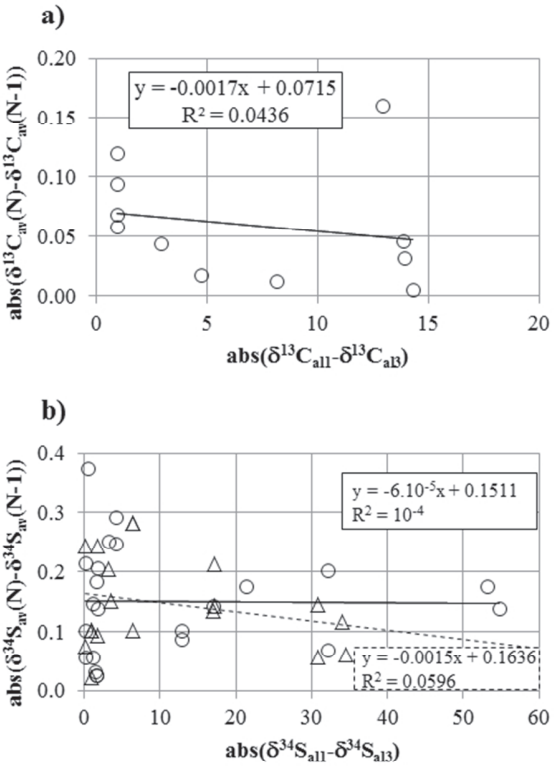

Figure 5
190x254mm (96 x 96 DPI)

« On ne fait jamais attention à ce qui a été fait ; on ne voit que ce qui reste à faire. »

Marie Curie

CONCLUSION

Tout au long de ce travail, nous avons essayé de montrer l'imbrication étroite entre l'évolution technique des systèmes de mesure et la réponse à apporter à d'importantes questions scientifique fondée sur la spectrométrie de masse de rapports isotopiques. Nous avons commencé dans le chapitre 1, comme il se doit, par un rappel historique de l'évolution de cette méthodologie assez récente puisque tout juste centenaire. Puis nous avons illustré dans le chapitre 2 l'importance de ces techniques aujourd'hui tout d'abord dans le domaine des études paléo-environnementales qui constitue l'une des spécialités de notre laboratoire. Nous avons démontré ainsi l'utilité de l'analyse isotopique afin de quantifier des phénomènes appréciés auparavant que par des données qualitatives. Ensuite, dans le chapitre 3 nous avons souligné l'apport des analyses isotopiques afin de mieux caractériser et quantifier des phénomènes physiologiques sur des organismes actuels ou fossiles. Nous avons pour cela dû déborder de notre terrain d'investigation paléontologique traditionnel et aller chercher des applications au moyen de collaborations avec nos collègues biologistes de l'UCBL.

Puis dans le chapitre 4, après avoir démontré ainsi l'utilisation croissante des techniques isotopiques dans notre domaine, nous avons montré comment il était possible de faire évoluer ces techniques isotopiques afin de pouvoir répondre à des questions scientifiques toujours plus ardues. Nous avons fait cela aussi bien sur des techniques déjà existantes que nous avons contribué à améliorer (paragraphes 4.1, 4.2), que sur de nouvelles techniques que nous avons développées en relation avec les industriels de l'instrumentation scientifique (paragraphes 4.3, 4.4).

Bien évidemment, il reste de nombreuses questions à aborder et de nombreuses évolutions techniques futures pour nous permettre d'y répondre. La réduction de la prise d'essai, les techniques dites de « clumped isotopes » qui n'ont pas été abordées ici ; les analyses isotopiques du chlore et du brome ; les analyses isotopiques du silicium, sans parler des nouvelles méthodes IRMS utilisant le LASER ou bien de la possibilité de connecter en ligne des systèmes de chromatographie liquide de type HPLC à un IRMS.

Mais notre propos était de toujours associer étroitement évolution technologique et question scientifique sans que l'un ne prenne le pas sur l'autre et notamment que l'évolution technologique ne constitue pas simplement un exercice de style. Nous espérons avoir pu contribuer de manière significative à l'évolution du domaine fascinant des techniques isotopiques dont il ne fait aucun doute que le champ d'investigation ne peut que s'accroître.

Titre en anglais : Improvements of geochemical tools for palaeoenvironment investigations.

Résumé en anglais:

THe history of stable isotopes began in 1913 with the work of Frederick Soddy. Since then, analytical techniques in that domain have been in constant evolution, providing answers to more and more elaborated scientific questions and spreading into various application fields where their tracing abilities have become extremely useful today.

This work first describes the evolution of those analytical techniques through time and especially the fundamental step forward with continuous flow techniques especially through elemental analysis.

For the second part we illustrate the importance of stable isotope analyses for paleoenvironmental reconstructions to better understand the climatic history of the Earth and its inhabitants from different periods. This is mainly based on $^{18}O/^{16}O$ analyses from phosphatic or carbonaceous matrices.

The third part is dedicated to the use of stable isotopes as tracers of various fundamental metabolic pathways from both fossil and actual samples. For this latter case we have used the capacity of stable isotopes to be used at natural abundance as well as artificially labelled. We have used $^{18}O/^{16}O$ isotopic signatures from phosphatic samples as well as $^{13}C/^{12}C$ and $^{15}N/^{14}N$ from organic matter.

The fourth part is dedicated to analytical developments covering several domains. First we investigated D/H and $^{18}O/^{16}O$ measurements from waters. We are proposing new correction parameters for isotopic measurements from waters with salinity higher than sea water. Then we have dealt with $^{13}C/^{12}C$ and $^{18}O/^{16}O$ isotopic analyses from carbonates and we suggest new parameters to constrain oxygen isotopic fractionation between carbonates from apatite and water as well as carbon and oxygen isotopic fractionation between calcite and aragonite from actual living organisms. We have also developed a new semi-automated technique to measure carbon and oxygen isotopic signatures from calcite and dolomite mixtures with various proportions. Then we have attempted to quantify the natural and instrumental variability of oxygen and carbon isotopic analyses from microfossils. An important part of this analytical work has been dedicated to $^{18}O/^{16}O$ isotopic analyses from biogenic phosphate material. In collaboration with instrument manufacturers we have developed a new system to improve both quality and automation of those measurements as well as reduce the aliquot sizes in order to get access to smaller samples. Eventually we have developed sulfur isotopic analyses in collaboration with instrument manufacturers to evaluate the capacities of a new analytical setup to generate reliable N, C, S multi- isotopic analyses.

Last, we summarize the contribution of this work to the evolution of stable isotope techniques and we try to evaluate the future fields of investigation for those techniques just over one hundred years old.